VASCULAR BIOLOGY, HAEMOSTASIS AND EXTRACELLULAR NUCLEIC ACIDS IN VASCULAR DISEASES AND IMMUNITY. A TRIBUTE TO KLAUS T. PREISSNER

EDITED BY: Ritva Tikkanen, Silvia Fischer and Carl P. Blobel
PUBLISHED IN: Frontiers in Physiology, Frontiers in Medicine and Frontiers in Cell and Developmental Biology

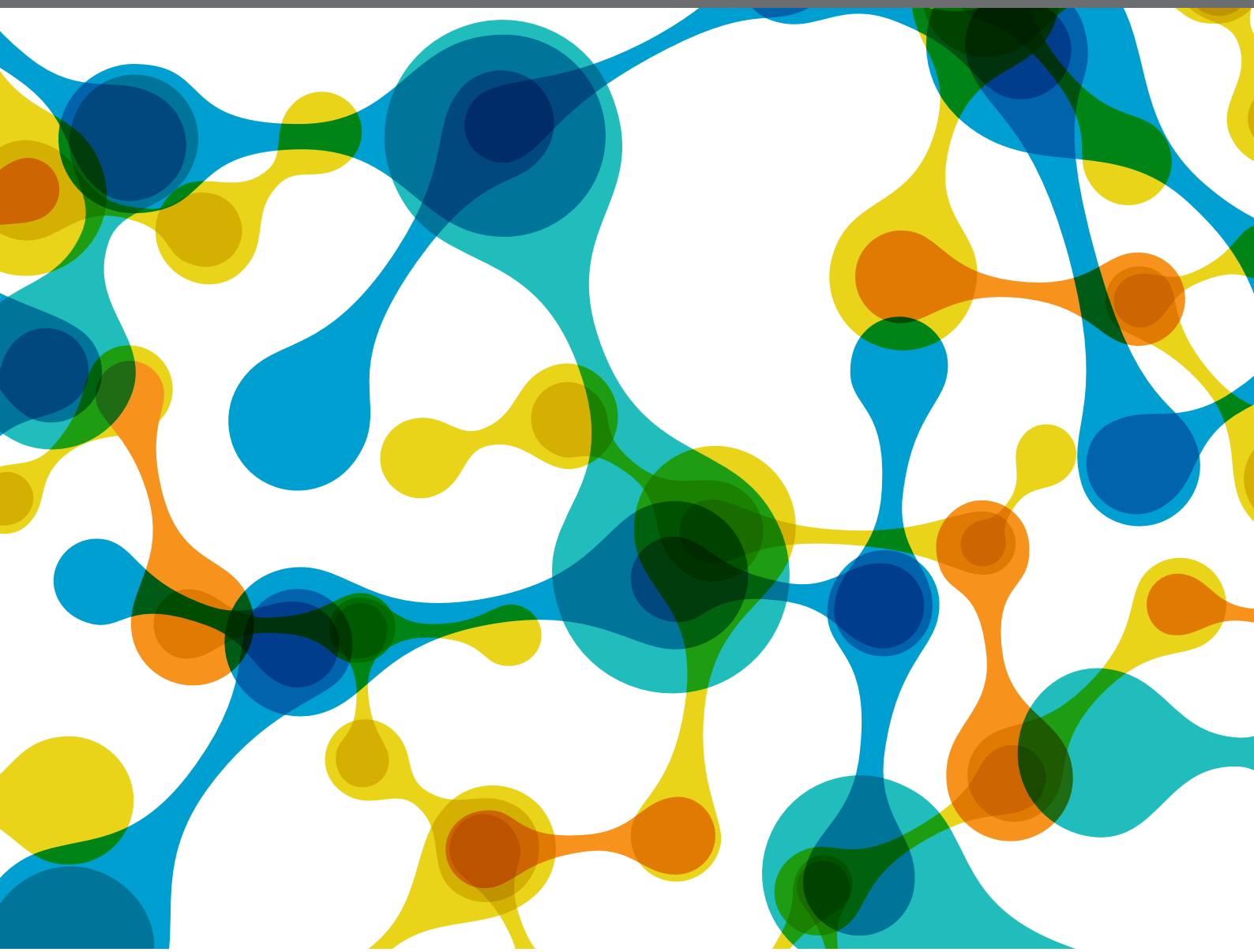

frontiers Research Topics

frontiers

ISSN 1664-8714
ISBN 978-2-88974-204-2
DOI 10.3389/978-2-88974-204-2

About Frontiers

Frontiers is more than just an open-access publisher of scholarly articles: it is a pioneering approach to the world of academia, radically improving the way scholarly research is managed. The grand vision of Frontiers is a world where all people have an equal opportunity to seek, share and generate knowledge. Frontiers provides immediate and permanent online open access to all its publications, but this alone is not enough to realize our grand goals.

Frontiers Journal Series

The Frontiers Journal Series is a multi-tier and interdisciplinary set of open-access, online journals, promising a paradigm shift from the current review, selection and dissemination processes in academic publishing. All Frontiers journals are driven by researchers for researchers; therefore, they constitute a service to the scholarly community. At the same time, the Frontiers Journal Series operates on a revolutionary invention, the tiered publishing system, initially addressing specific communities of scholars, and gradually climbing up to broader public understanding, thus serving the interests of the lay society, too.

Dedication to Quality

Each Frontiers article is a landmark of the highest quality, thanks to genuinely collaborative interactions between authors and review editors, who include some of the world's best academicians. Research must be certified by peers before entering a stream of knowledge that may eventually reach the public - and shape society; therefore, Frontiers only applies the most rigorous and unbiased reviews.
Frontiers revolutionizes research publishing by freely delivering the most outstanding research, evaluated with no bias from both the academic and social point of view. By applying the most advanced information technologies, Frontiers is catapulting scholarly publishing into a new generation.

What are Frontiers Research Topics?

Frontiers Research Topics are very popular trademarks of the Frontiers Journals Series: they are collections of at least ten articles, all centered on a particular subject. With their unique mix of varied contributions from Original Research to Review Articles, Frontiers Research Topics unify the most influential researchers, the latest key findings and historical advances in a hot research area! Find out more on how to host your own Frontiers Research Topic or contribute to one as an author by contacting the Frontiers Editorial Office: frontiersin.org/about/contact

VASCULAR BIOLOGY, HAEMOSTASIS AND EXTRACELLULAR NUCLEIC ACIDS IN VASCULAR DISEASES AND IMMUNITY. A TRIBUTE TO KLAUS T. PREISSNER

Topic Editors:
Ritva Tikkanen, University of Giessen, Germany
Silvia Fischer, University of Giessen, Germany
Carl P. Blobel, Hospital for Special Surgery, United States

Topic Editor Prof. Ritva Tikkanen Receives Research Funding From Neurogene Inc. and GC Pharma for Studies Unrelated to the Subject. Topic Editor Prof. Carl Blobel is Co-Inventor on a Patent Describing a Method of Identifying Agents for Combination With Inhibitors of iRhoms. He and the Hospital for Special Surgery (New York, USA) are Investigating Suitable Approaches to Identify iRhom Inhibitors, and are Co-Founders of a Small Company Called SciRhom in Munich to Pursue These Efforts. Topic Editor Dr. Sylvia Fischer Declares no Competing Interests With Regards to the Research Topic Subject.

Citation: Tikkanen, R., Fischer, S., Blobel, C. P., eds. (2022). Vascular Biology, Haemostasis and Extracellular Nucleic Acids in Vascular Diseases and Immunity. A Tribute to Klaus T. Preissner. Lausanne: Frontiers Media SA.
doi: 10.3389/978-2-88974-204-2

Table of Contents

05 ***Differential Role for Activating FcγRIII in Neointima Formation After Arterial Injury and Diet-Induced Chronic Atherosclerosis in* Apolipoprotein E-*Deficient Mice***
Yaw Asare, Janine Koehncke, Jaco Selle, Sakine Simsekyilmaz, Joachim Jankowski, Gansuvd Shagdarsuren, Johannes E. Gessner, Jürgen Bernhagen and Erdenechimeg Shagdarsuren

16 ***Expression of Chitotriosidase in Macrophages Modulates Atherosclerotic Plaque Formation in Hyperlipidemic Mice***
Jonathan Yap, Sara McCurdy, Martin Alcala, Jason Irei, Jan Garo, Whitney Regan, Bog-Hieu Lee, Shiro Kitamoto and William A. Boisvert

31 ***Small Things Matter: Relevance of MicroRNAs in Cardiovascular Disease***
Linsey J. F. Peters, Erik A. L. Biessen, Mathias Hohl, Christian Weber, Emiel P. C. van der Vorst and Donato Santovito

45 ***Antiplatelet Activity of Tussilagone via Inhibition of the GPVI Downstream Signaling Pathway in Platelets***
Jing Zhou, Ru-Ping Yang, Wei Song, Hui-Min Xu and Yong-Hui Wang

55 ***Impact of Von Willebrand Factor on Bacterial Pathogenesis***
Michael Steinert, Isabell Ramming and Simone Bergmann

63 ***Endothelial Ribonuclease 1 in Cardiovascular and Systemic Inflammation***
Katrin Bedenbender and Bernd T. Schmeck

74 ***p38 and Casein Kinase 2 Mediate Ribonuclease 1 Repression in Inflamed Human Endothelial Cells via Promoter Remodeling Through Nucleosome Remodeling and Deacetylase Complex***
Katrin Bedenbender, Isabell Beinborn, Evelyn Vollmeister and Bernd Schmeck

90 ***RNase A Treatment Interferes With Leukocyte Recruitment, Neutrophil Extracellular Trap Formation, and Angiogenesis in Ischemic Muscle Tissue***
Manuel Lasch, Konda Kumaraswami, Simona Nasiscionyte, Susanna Kircher, Dominic van den Heuvel, Sarah Meister, Hellen Ishikawa-Ankerhold and Elisabeth Deindl

102 ***Neutrophil Extracellular Traps Induce MCP-1 at the Culprit Site in ST-Segment Elevation Myocardial Infarction***
Thomas M. Hofbauer, Anna S. Ondracek, Andreas Mangold, Thomas Scherz, Johanna Nechvile, Veronika Seidl, Christine Brostjan and Irene M. Lang

115 ***Brahma-Related Gene 1 Deficiency in Endothelial Cells Ameliorates Vascular Inflammatory Responses in Mice***
Yuanyuan Zhang, Huidi Wang, Mingzi Song, Tongchang Xu, Xuyang Chen, Tianfa Li and Teng Wu

128 ***The Role of Complement in Myocardial Infarction Reperfusion Injury: An Underappreciated Therapeutic Target***
Carl-Wilhelm Vogel

135 ***Autoregulatory "Multitasking" at Endothelial Cell Junctions by Junction-Associated Intermittent Lamellipodia Controls Barrier Properties***
Jochen Seebach, Nadine Klusmeier and Hans Schnittler

146 ***RNase A Inhibits Formation of Neutrophil Extracellular Traps in Subarachnoid Hemorrhage***
Anton Früh, Katharina Tielking, Felix Schoknecht, Shuheng Liu, Ulf C. Schneider, Silvia Fischer, Peter Vajkoczy and Ran Xu

frontiers in Physiology

ORIGINAL RESEARCH
published: 17 June 2020
doi: 10.3389/fphys.2020.00673

Differential Role for Activating FcγRIII in Neointima Formation After Arterial Injury and Diet-Induced Chronic Atherosclerosis in *Apolipoprotein E*-Deficient Mice

Yaw Asare[1,2†‡], Janine Koehncke[2†], Jaco Selle[2,3], Sakine Simsekyilmaz[2], Joachim Jankowski[2,4], Gansuvd Shagdarsuren[5], Johannes E. Gessner[6], Jürgen Bernhagen[7,8*‡] and Erdenechimeg Shagdarsuren[2,9*‡]*

[1] Institute for Stroke and Dementia Research (ISD), LMU University Hospital, Ludwig Maximilian University of Munich (LMU), Munich, Germany, [2] Institute for Molecular Cardiovascular Research (IMCAR), University Hospital, RWTH Aachen University, Aachen, Germany, [3] Translational Experimental Pediatrics – Experimental Pulmonology, Department of Pediatric and Adolescent Medicine, University of Cologne, Cologne, Germany, [4] Experimental Vascular Pathology, Cardiovascular Research Institute Maastricht (CARIM), Maastricht University, Maastricht, Netherlands, [5] Department of Nephrology, School of Medicine, Mongolian National University of Medical Sciences, Ulaanbaatar, Mongolia, [6] Molecular Immunology Research Unit, Clinical Department of Immunology and Rheumatology, Hannover Medical School, Hanover, Germany, [7] Vascular Biology, Institute for Stroke and Dementia Research (ISD), LMU University Hospital, Ludwig Maximilian University of Munich (LMU), Munich, Germany, [8] Munich Heart Alliance, Munich, Germany, [9] Institute for Transplantation Diagnostics and Cell Therapeutics, University Hospital and Medical Faculty, Heinrich Heine University Düsseldorf, Düsseldorf, Germany

OPEN ACCESS

Edited by:
Ritva Tikkanen,
University of Giessen, Germany

Reviewed by:
Alex Bobik,
Baker Heart and Diabetes Institute, Australia
Ilze Bot,
Leiden University, Netherlands

***Correspondence:**
Yaw Asare
yaw.asare@med.uni-muenchen.de
Jürgen Bernhagen
juergen.bernhagen@med.uni-muenchen.de
Erdenechimeg Shagdarsuren
erdenechimeg.guenther@med.uni-duesseldorf.de

†These authors have contributed equally to this work

‡These authors share senior authorship

Specialty section:
This article was submitted to Vascular Physiology, a section of the journal Frontiers in Physiology

Received: 30 March 2020
Accepted: 26 May 2020
Published: 17 June 2020

Citation:
Asare Y, Koehncke J, Selle J, Simsekyilmaz S, Jankowski J, Shagdarsuren G, Gessner JE, Bernhagen J and Shagdarsuren E (2020) Differential Role for Activating Fcγ RIII in Neointima Formation After Arterial Injury and Diet-Induced Chronic Atherosclerosis in Apolipoprotein E-Deficient Mice. Front. Physiol. 11:673. doi: 10.3389/fphys.2020.00673

Atherogenesis and arterial remodeling following mechanical injury are driven by inflammation and mononuclear cell infiltration. The binding of immune complexes (ICs) to immunoglobulin (Ig)-Fc gamma receptors (FcγRs) on most innate and adaptive immune cells induces a variety of inflammatory responses that promote atherogenesis. Here, we studied the role of FcγRIII in neointima formation after arterial injury in atherosclerosis-prone mice and compared the outcome and mechanism to that of FcγRIII in diet-induced "chronic" atherosclerosis. *Fcγrlll*$^{-/-}$*/Apoe*$^{-/-}$ and control *Apoe*$^{-/-}$ mice were subjected to wire-induced endothelial denudation of the carotid artery while on high-fat diet (HFD). *Fcγrlll* deficiency mitigated neointimal plaque formation and lesional macrophage accumulation, and enhanced neointimal vascular smooth muscle cell (VSMC) numbers. This went along with a reduced expression of tumor necrosis factor-α (TNF-α), monocyte chemoattractant protein-1 (MCP-1/CCL2), and vascular cell adhesion molecule-1 (VCAM-1) in the neointimal lesions. Interestingly, in a chronic model of diet-induced atherosclerosis, we unraveled a dichotomic role of FcγRIII in an early versus advanced stage of the disease. While *Fcγrlll* deficiency conferred atheroprotection in the early stage, it promoted atherosclerosis in advanced stages. To this end, *Fcγrlll* deficiency attenuated pro-inflammatory responses in early atherosclerosis but promoted these events in advanced stages. Analysis of the mechanism(s) underlying the athero-promoting effect of *Fcγrlll* deficiency in late-stage atherosclerosis revealed increased serum levels of anti-oxidized-LDL immunoglobulins IgG2c and IgG2b. This was paralleled by enhanced lesional accumulation of IgGs without affecting levels of complement-activated products C5a or C5ar1, FcγRII, and

FcγRIV. Moreover, *Fcγrlll*-deficient macrophages expressed more *Fcγrll*, *Tnf-α,* and *Il-1β* mRNA when exposed to IgG1 or oxLDL-IgG1 ICs *in vitro*, and peripheral CD4+ and CD8+ T-cell levels were altered. Collectively, our data suggest that deficiency of activating *FcγRIII* limits neointima formation after arterial injury in atherosclerosis-prone mice as well as early stage chronic atherosclerosis, but augments late-stage atherosclerosis suggesting a dual role of FcγRIII in atherogenic inflammation.

Keywords: Fc gamma receptors, atherosclerosis, inflammation, neointima formation, hyperlipidemia, cytokine, complement

INTRODUCTION

As a chronic and progressive inflammatory condition of the arterial vessel wall, atherosclerosis is initiated by the recruitment of inflammatory cells and the accumulation of oxidized low density lipoproteins (oxLDL) that jointly drive the progression of atherosclerotic plaque development (Bernhagen et al., 2007; Weber and Noels, 2011; Libby et al., 2013). Previous studies suggest that oxLDL can induce autoimmune responses as evidenced by the presence of anti-oxLDL antibodies in mouse and human atherosclerotic lesions (Salonen et al., 1992; Erkkila et al., 2000). Hence, atherosclerosis has also been viewed as an autoimmune or immune complex disease (Nilsson and Hansson, 2008).

Immunoglobulin-Fc gamma receptors (FcγRs) play an important role in the clearance of immune complexes (ICs) (Nimmerjahn and Ravetch, 2008). Accumulating data also indicate the involvement of FcγRs in inflammatory diseases mediated by ICs (Meyer et al., 1998; Baudino et al., 2008). FcγRs are important cell-surface receptors on hematopoietic cells and are able to specifically bind to immunoglobulin G (IgG). This binding capacity induces a variety of biological responses like inflammatory cell activation, phagocytosis and antibody-dependent cellular cytotoxicity as well as maintenance of immunoglobulin homeostasis (Nimmerjahn and Ravetch, 2008). Four different classes of FcγRs are present in mice: FcγRI, FcγRII, FcγRIII, and FcγRIV. These receptors are classified as "activating" (FcγRI, III, and VI) and "inhibiting" (FcγRII) receptors. In spite of their differences (activating versus inhibiting), FcγRs generally play a crucial role in the clearance of IC-containing oxidized LDL. Serum LDL-IC concentrations in patients with coronary heart disease were found to be higher than those in healthy individuals (Wang et al., 2003), and the cholesterol content of circulating ICs (CICs) correlated with the presence and severity of atherosclerosis (Burut et al., 2010). Furthermore, binding of oxLDL-IC to FcγR on macrophages can activate a variety of pro-inflammatory cell responses. These include the release of inflammatory molecules such as Tnf-α and the complement component C5a, as well as the transformation of macrophages into foam cells, an important hallmark mechanism of atherosclerosis (Kiener et al., 1995).

The complement anaphylatoxin C5a is a well-described pro-inflammatory molecule, whose effect is conveyed by binding to the C5a receptors C5aR1 and C5aR2 that are expressed on immune and vascular cells (Siciliano and Rollins, 1990). Recent studies indicate that C5a may play an important role in the regulation of FcγR-dependent responses as well as in the synergistic regulation of both C5aR1 and FcγRs. IC-induced activation of FcγRIII leads to local formation of C5a, which causes further activation of C5aR1 and up-regulation of FcγRIII (Baumann et al., 2000). These intertwined processes are generally considered necessary for cell activation and inflammatory immune responses. However, the pathogenic significance of activating FcγRIII for local C5a production and its interaction with the C5a/C5aR1-axis as well as co-regulation of C5aR1/FcγR have not been explored in atherosclerosis. Although the functional role of both FcγR common chain and FcγRIII in diet-induced atherosclerotic plaque formation in hyperlipidemic mice has been amply studied (Hernandez-Vargas et al., 2006; Kelly et al., 2010; Ng et al., 2011; Zhu et al., 2014), their specific roles in different stages of atherosclerosis have not been scrutinized. Moreover, the effect of FcγRIII on accelerated atherosclerosis after arterial injury is unexplored.

Therefore, here we studied the role of FcγRIII in neointima formation after mechanical arterial injury in comparison with its role in chronic high-fat diet-induced atherosclerosis, and determined the effects of the cooperative role of FcγRIII/C5aR1 in atherosclerotic vascular inflammation.

MATERIALS AND METHODS

Mice

C57BL/6J *FcγrIII*-deficient mice ($Fc\gamma rIII^{-/-}$) were crossed with atherosclerosis-prone C57BL/6J *Apoe*-deficient mice ($Apoe^{-/-}$) to generate $Fc\gamma rIII^{-/-}/Apoe^{-/-}$. The knockout for both genes was confirmed using genotyping PCR. Eight-week-old female $Fc\gamma rIII^{-/-}/Apoe^{-/-}$ and corresponding control $Apoe^{-/-}$ mice received a high-fat diet (HFD; 21% fat, 0.15% cholesterol and 19.5% casein (Sniff, Soest, Germany) for 4 weeks to induce early atherosclerosis or for 12 and 24 weeks to study effects in late-stage atherosclerosis. Wire-induced endothelial-denudation of the carotid artery was performed in mice receiving HFD for 1 week before and 4 weeks after surgery (n = 10 for each group). All animal experiments were approved by local authorities (Landesamt für Natur, Umwelt und Verbraucherschutz (LANUV), Nordrhein-Westfalen, Germany) and complied with the German animal protection law.

Tissue Preparation

Mice were euthanized using an overdose of Ketamine (500 mg/kg)/Xylazine (50 mg/kg) and perfused with sterile

phosphate-buffered saline (PBS). For RNA isolation, tissue and organs were snap-frozen in liquid nitrogen and stored at −80°C. For immunohistochemical staining, tissues and organs were either fixed in 4% paraformaldehyde (PFA) and embedded in paraffin or used for cryosectioning. Aortas were placed in 4% PFA overnight, cut longitudinally and the adventitia was removed before *en face* staining.

Determination of Atherosclerotic Lesions

The extent of atherosclerosis was assessed on aortic roots and on thoracoabdominal aortas by staining for lipid deposition with oil-red-O (ORO) staining (Sigma-Aldrich, Deisenhofen, Germany) and quantified by computerized image analysis (Diskus Software, Hilgers, Königswinter, Germany) and Leica Qwin Imaging software (Leica Ltd., Cambridge, United Kingdom). Briefly, atherosclerotic lesion areas were measured on a constant number of 5-μm transversal sections through the heart and aortic roots. For each aortic root, the average of ORO-stained areas from six sections separated by 50 μm from each other was calculated. The thoracoabdominal aorta was opened longitudinally along the ventral midline, and lesion areas in *en face* preparations were stained with ORO. The percentage of lipid deposition was calculated by dividing the stained area by the total thoracoabdominal aortic surface. For analysis of carotid arteries, 4-μm transversal serial sections from the paraffin-embedded carotid arteries were collected on glass slides. Within a standardized distance (0–360 μm) from the bifurcation, carotid artery sections (10 sections per mouse; each separated 40 μm apart) were stained using Movat's pentachrome stain. The areas of lumen, neointima (between lumen and internal elastic lamina), media (between internal and external elastic laminae) and area within the external elastic lamina (aEEL) were measured by planimetry using Diskus Software (Hilgers). For each mouse, data from these 10 sections were averaged to represent neointima formation along this standardized distance.

Histological and Immunohistological Analysis

Serial sections of the aortic roots and carotid arteries were analyzed for their cellular composition by quantitative immunohistochemistry. Immunofluorescence staining was performed using antibodies against CD3 (MCA1477, AbD Serotec, Cologne, Germany), CD45R/B220 (553085, BD Bioscience, Heidelberg, Germany), myeloperoxidase (MPO, RB-373-A, Neomarkers, Freemont, CA, United States), C5aR1 (CD88, ab59390, Abcam, Cambridge, United Kingdom), α-SMA (M0851, Dako, Hamburg, Germany), Mac-2 (CL8942AP, CEDARLANE, Burlington, ON, Canada), VCAM-1, MCP-1/CCL2, and TNF-α (all from Santa Cruz, Santa Cruz, CA, United States), CD19 (clone 6D5, MCA1439, BioRad) and FITC- or Cy3-conjugated secondary antibody (Jackson ImmunoResearch, Ely, United Kingdom). Nuclei were co-stained with 4′, 6-diamidino-2-phenylindol (DAPI). Proliferating cells were determined using the Ki-67 marker (M7249, DakoCytomation) and apoptotic cells using TUNEL-staining Kit (Roche). Immunoglobulins were detected using anti-IgG (AI-9200, Vector Laboratories, Burlingame, CA, United States) and anti-IgM (sc-2075, Santa Cruz) antibodies and visualized by avidin-biotin-complex method. Lipid deposits were stained with Nile Red and Oil-red-O (Sigma-Aldrich). Collagen contents were analyzed using Gomori Trichrome staining. Images were recorded with a Leica DMLB fluorescence microscope and a charge-coupled device camera. Analysis of images was performed using Diskus analysis software (Hilgers) with the exception of Nile Red stainings, which were analyzed using Image J software (National Institute of Health).

RNA Extraction and cDNA Synthesis

Aorta tissues were homogenized in RLT buffer (Qiagen, Hilde, Germany) using Homogenator (Qiagen) and stainless-steel beads (74104, Qiagen). Macrophages were disrupted in RLT buffer + 1% β-mercapto-ethanol. Total RNA was purified using RNeasy spin column kit (Qiagen) and the concentration was determined by measuring the absorbance at 260 nm using a Nanodrop spectrophotometer (GE Healthcare, Freiburg, Germany). Equal concentrations (1 μg) were transcribed into cDNA using the High Capacity cDNA Reverse Transcription Kit (Applied Biosystems, Heidelberg, Germany) according to manufacturer's protocols.

Real-Time PCR

Gene expression was determined by real-time PCR with primers for mouse *Tnf*-α, *Il-1*β, *Tgf*-β, *Il-6, Il-10, Il-4* (Sigma) and *C5ar1, Fcgr3a, Fcgr2b* (Biorad, Munich, Germany) in a thermal cycler 7900HT (Applied Biosystems). The expression of target genes was calculated by the ΔΔCt method and normalized to GAPDH. All RT-PCR reactions were carried out in duplicate. A preparation without template served as a negative control.

ELISA

Plasma was obtained from blood that was centrifuged at 3000 *g* for 20 min. Immunoglobulin titers against oxidized low-density lipoprotein (oxLDL) and malondialdehyde-oxidized (MDA-LDL) in plasma were measured using sandwich ELISA. 96-well ELISA plates (Nunc, Dreieich, Germany) were coated overnight at 4°C with 10 μg/μl oxidized LDL or MDA-LDL. After washing with PBST, plasma dilutions of 1:100 were added and incubated for 2 h at RT. Detection occurred for 1 h at RT with mouse anti-IgG (sc-2005), anti-IgM (sc-2064), anti-IgA (sc-3791), anti-IgG2a (sc-2061), anti-IgG2b (sc-2062), and anti-IgG3 (sc-2063) antibodies (Santa Cruz) labeled with horseradish peroxidase (HRP). Substrate was added and chemiluminescence was measured at 450 nm using an ELISA reader (Tecan, Männedorf, Switzerland). The C5a plasma titer was determined using a C5a detection Kit (ELM-ccC5a-001, Raybiotech, Peachtree Corners, GA, United States). Total Plasma cholesterol and triglyceride levels were quantified using enzymatic assays (Analyticon, 4046 and 5052, Lichtenfels, Germany) according to the manufacturer's protocol. Plasma levels of IL-10 (88-7105-8), IL-6 (88-7064-88) and Tnf-α (88-7324-88, Bioscience, Würzburg, Germany) were determined by using ELISA kits.

Flow Cytometry

Cells were isolated from spleen and lymph nodes and a single-cell suspension was prepared and filtered over MACS pre-separation filter (Miltenyi, Bergisch Gladbach, Germany). Thereafter, cells were treated with erythrocyte lysis buffer (0.155 M NH_4Cl, 10 mM $NaHCO_3$). Cell suspensions were carefully washed and stained with FACS staining buffer and combinations of antibodies against T and B cells: FITC-anti-CD3, APC-anti-CD4, PE-Cy7-anti-CD8, PE-anti-CD25, Per-CP-Cy5.5-anti-CD19 and APC-Cy7-anti-CD45. For regulatory T cells: PerCP-Cy5.5-anti-CD3, FITC-anti-CD4, PE-anti-CD25, APC-Cy7-anti-CD45 and APC-anti-Foxp3. All antibodies were obtained from eBioscience (Vienna, Austria) and were incubated for 60 min on ice. Mouse regulatory T-cell staining kit (eBioscience) was used for permeabilization and fixation of cells for intracellular staining of Foxp3. At least 100.000 gated cells were acquired, after appropriate fluorescence compensation, and analyzed in a FACSCanto II using FACSDiva software (BD Biosciences). Final analysis was performed using FlowJo software (Tree Star Inc.).

OxLDL and Immune Complex Preparation

To prepare oxLDL, human plasma LDL (437644, Calbiochem, Heidelberg, Germany) was diluted with sterile PBS to a final concentration of 1.5 mg/ml and incubated with copper sulfate (5 μM) at 37°C for 4 h (mild oxidation) or overnight (heavy oxidation). The reaction was stopped using 25 μl EDTA (5 mM), and oxidized LDL (oxLDL) was purified using PD10 desalting columns (GE healthcare). Final elution was done in 3.5 ml sterile PBS and oxLDL preparations stored at 4°C in the dark. The concentration was determined using Bradford assay. Malondialdehyde (MDA)-LDL from human plasma was purchased from Hölzel (Cologne, Germany). ICs were produced by incubating oxLDL (30 μg/ml) and mouse anti-oxLDL-IgG1 (OB40, University of Graz; 100 μg/ml) in sterile PBS at 4°C overnight. The concentration was determined using Lowry assay.

Isolation and Stimulation of Macrophages

Bone marrow-derived macrophages (BMDMs) were isolated from femur and tibia of $Apoe^{-/-}$ and $FcγrIII^{-/-}/Apoe^{-/-}$ mice as already established (Asare et al., 2017). Briefly, bones were isolated, cut open with a sterile scissor and flushed with ice-cold sterile PBS using a syringe with a 27-G needle. The bone marrow was filtered through a 40 μm cell strainer (Greiner) and collected in a 50 ml falcon. The cells were then centrifuged at 1200 rpm for 5 min, resuspended in culture medium (RPMI 1640 + L-Glucose, 10 mM HEPES, 10% FCS, 100 U/ml Gentamycin, 15% LCM) and plated in 15 cm bacterial plastic plates (Greiner). After 7 days of differentiation, the macrophages were used for stimulation experiments. The cells were transferred into 6-well plates (Greiner, Frickenhausen, Germany), cultured overnight without LCM and synchronized for 2 h without FCS. The stimulation of macrophages was done by adding 10 μg/ml and 50 μg/ml oxidized LDL, IgG or ICs for 6 h at 37°C; unstimulated macrophages served as control. RNA was isolated, reverse transcribed and used for RT-PCR.

Statistical Analysis

All statistical analysis was performed using GraphPad Prism 5 (GraphPad software Inc.). All data are given as means ± SEM and were analyzed for normality by the Kolmogorov–Smirnov test or D'Agostino and Pearson omnibus test and then by the 2-tailed Student *t* test or two-way ANOVA with Bonferroni post-test as appropriate. $P < 0.05$ was considered statistically significant.

RESULTS

FcγrIII Deficiency Limits Neointima Expansion in Atherosclerosis-Prone Mice

To study the effect of *FcγrIII* deficiency in neointima formation after arterial injury, $FcγrIII^{-/-}/Apoe^{-/-}$ and control $Apoe^{-/-}$ mice received an HFD 1 week before and 4 weeks after endothelial denudation of the left common carotid artery. *FcγrIII* deficiency attenuated neointimal plaque formation when compared to control mice, whereas the medial area was unaltered (**Figures 1A,B**). Analysis of the cellular composition in the neointimal plaques and medial area revealed significantly reduced Mac-2^+ macrophages (**Figures 1C,D** and **Supplementary Figure S1A**) and an increase in α-SMA^+ vascular smooth muscle cell (VSMC) numbers whereas medial VSMC numbers were not affected (**Figures 1E,F** and **Supplementary Figure S1B**) in *FcγrIII*-deficient mice. Also, the neointimal collagen content and IgG area did not differ between control $Apoe^{-/-}$ and *FcγrIII*-deficient mice (**Supplementary Figures S1C,D**). Furthermore, injury-induced Tnf-$α^+$ cells were reduced in *FcγrIII*-deficient neointimal plaques (**Figure 1G**) and this went along with reduced expression levels of downstream adhesion molecules and chemokines. Specifically, we found significantly lower numbers of cells expressing Mcp-1/Ccl2 and Vcam-1 upon *FcγrIII* deficiency compared to control mice (**Figures 1H–J**), consistent with the limited expansion of the neointima observed in *FcγrIII*-deficient mice. Collectively, these data indicate that FcγRIII promotes pro-inflammatory responses in the vasculature to accelerate neointima formation after arterial injury.

Dichotomic Role of FcγRIII in Chronic Atherosclerosis

We next compared the observed effect of FcγRIII in neointimal lesion formation with that in a model of early atherosclerosis, i.e., $FcγrIII^{-/-}/Apoe^{-/-}$ versus $Apoe^{-/-}$ mice on a 4-week HFD in the absence of mechanic injury. In line with previous reports (Zhu et al., 2014), *FcγrIII* deficiency conferred atheroprotection in early stages of the disease and limited the expression of inflammatory cytokines and adhesion molecules (**Supplementary Figures S2A–E**).

We also studied the role of FcγRIII in intermediate and late-stage atherosclerosis in atherogenic mice receiving an HFD for 12 and 24 weeks, respectively. The analysis revealed an

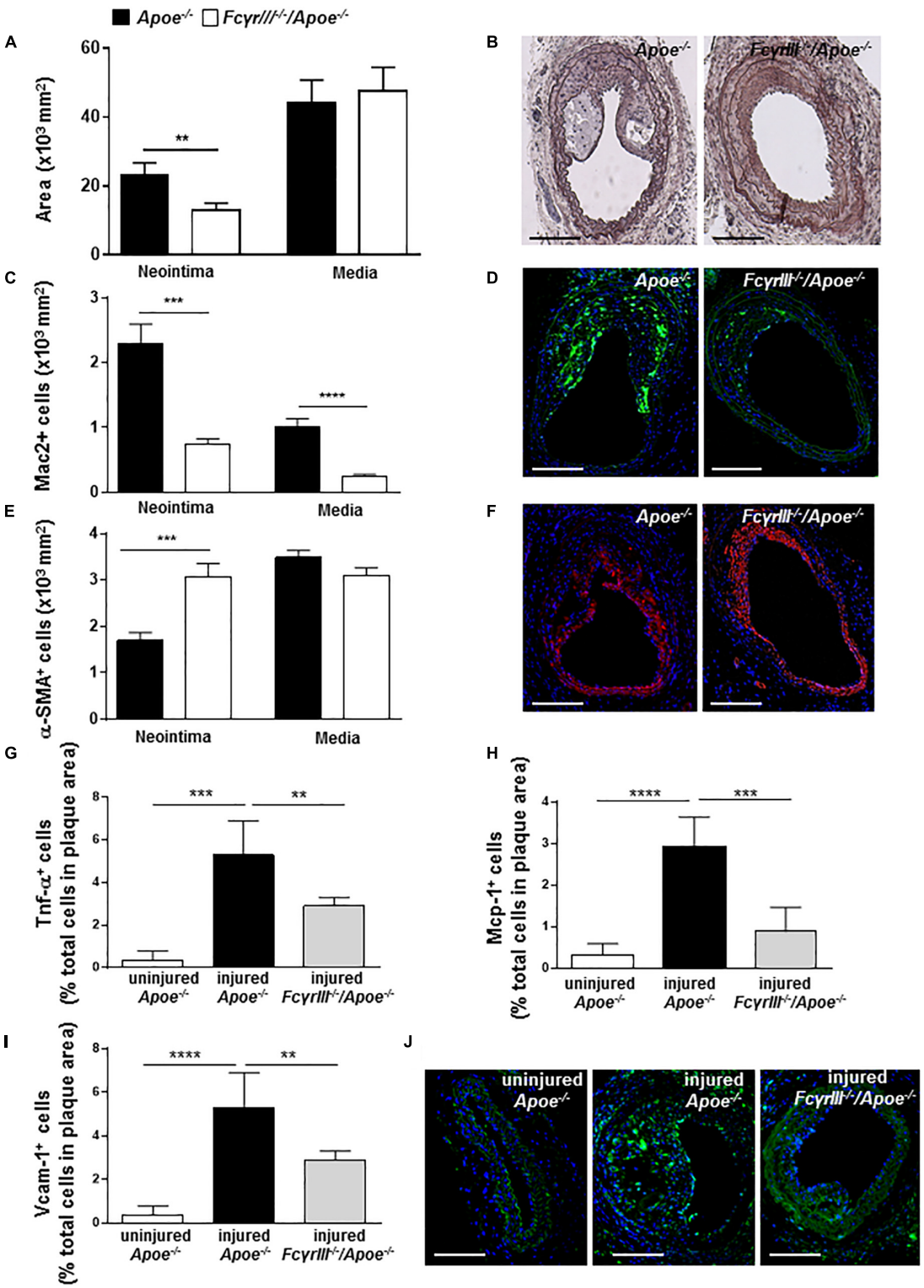

FIGURE 1 | *Fcγrlll* deficiency limits neointima expansion in atherosclerosis-prone mice. **(A)** Quantification of neointimal and medial area in *Fcγrlll*$^{-/-}$/*Apoe*$^{-/-}$ and *Apoe*$^{-/-}$ mice 4 weeks after wire-induced injury in carotid arteries. **(B)** Representative images of Movat's pentachrome staining. Scale bars 200 μm. **(C)** Quantification of neointimal and medial Mac2^{+} macrophages and **(D)** representative immunofluorescence images for Mac-2 (green). **(E)** Quantification of neointimal and medial α-SMA^{+} smooth muscle cells and **(F)** representative α-SMA staining (red). Scale bars 200 μm. Cell nuclei are in blue. **(G)** Quantification of neointimal Tnf-α^{+}, **(H)** Mcp-1^{+}, and **(I)** Vcam-1^{+} cells. **(J)** Representative immunofluorescence images for Vcam-1 (green) are shown. Graphs represent the mean ± SEM (n = 6–7 mice per group). 2-tailed t-test, *Fcγrlll*$^{-/-}$/*Apoe*$^{-/-}$ vs. *Apoe*$^{-/-}$ mice. $^{**}p < 0.01$, $^{***}p < 0.001$, $^{****}p < 0.0001$.

unexpected and previously unrecognized phenotype, in which *FcγrIII* deficiency promoted atherosclerosis in the aorta at both 12 and 24 weeks of HFD as determined by *en face* staining (**Figures 2A,B**). *FcγrIII* deficiency also led to an atheropromoting effect in aortic root in mice receiving a 12-week HFD regimen, while no effect was seen in aortic root after 24 weeks of HFD (**Figures 2C,D**). To further explore this unexpected finding, serial sections of the aortic roots were analyzed by quantitative immunohistochemistry to determine the cellular plaque composition. Lesional Mac-2$^+$ macrophages were significantly decreased in *FcγrIII*$^{-/-}$/*Apoe*$^{-/-}$ compared to control *Apoe*$^{-/-}$ mice after both 12 and 24 weeks of HFD (**Figures 2E,F**), but this went along with an increased necrotic core size (**Supplementary Figure S3**). Similarly, α-SMA+ VSMC content was significantly reduced after 12 but not 24 weeks of HFD (**Figures 2G,H**). Lesional total T lymphocyte (CD3$^+$) and MPO$^+$ neutrophil content as well as Ki-67$^+$ proliferative and TUNEL$^+$ apoptotic cells did not differ between both groups (**Supplementary Table S1**) and neither did the expression of C5a, *C5ar1*, *FcγRII*, and *FcγRIV* (**Supplementary Figures S4A–F**). However, while there are technical limitations regarding the reliable quantification of lesional T-cell subsets, *FcγrIII* deficiency led to altered splenic and lymph node CD4+, CD8+, and FoxP3+ T-cell subset levels as measured by flow cytometry (**Supplementary Figures S5A–D**). Together, these data indicate that *FcγrIII* deficiency has a dichotomic role in chronic atherosclerosis of hyperlipidemic atherogenic mice, attenuating early lesion formation but augmenting intermediate-late-stage atherosclerosis.

FcγrIII Deficiency Enhances the Accumulation of Immunoglobulins in Intermediate-to-Advanced Atherosclerotic Lesions

Fc gamma receptor aggregation mediates inflammatory responses induced by autoantibodies and ICs (Ben Mkaddem et al., 2019) and the progression of atherosclerosis is characterized by the presence of disease-promoting autoantibodies against modified LDL (Shoenfeld et al., 2004). To investigate whether anti-oxidized low-density lipoprotein (oxLDL) and anti-malondialdehyde-oxidized (MDA-LDL) antibodies may explain the observed increased plaque size in *FcγrIII*$^{-/-}$/*Apoe*$^{-/-}$ mice in intermediate-late-stage atherosclerosis, we measured serum levels of anti-oxLDL and anti-MDA-LDL IgM, IgA, and IgG antibody subtypes. At 12 weeks of HFD, the levels of circulating IgG, IgG2a, and IgG2b anti-oxLDL antibodies were significantly increased in *FcγrIII*$^{-/-}$/*Apoe*$^{-/-}$ mice compared to control mice (**Figure 3A**), whereas only a trend for increased IgG (subtype) levels was noted after 24 weeks of HFD (**Figure 3B**). IgA and IgM titers showed no significant differences between both groups at both intervals of HFD. Analysis of anti-MDA-LDL antibodies revealed significantly enhanced IgG and IgG1 titer in *FcγRIII*$^{-/-}$/*Apoe*$^{-/-}$ mice after 12 weeks of HFD compared to *Apoe*$^{-/-}$ mice (**Figure 3C**). After 24 weeks of HFD, the anti-MDA-LDL IgG1 titer was increased in *FcγrIII*$^{-/-}$/*Apoe*$^{-/-}$ mice compared to *Apoe*$^{-/-}$ mice. Differences for all other anti-MDA-LDL Ig subtypes did not reach significance at either time interval (**Figure 3D**). To more directly examine the functional consequences of elevated circulating Ig antibody subtypes following *FcγrIII* deficiency on atherosclerotic lesion formation, serial sections of aortic roots were analyzed by quantitative immunohistochemistry for an accumulation of IgG and IgM whole fractions. Our analysis revealed significantly increased IgG concentrations in the lesions of *FcγrIII*$^{-/-}$/*Apoe*$^{-/-}$ mice at both time points of HFD (**Figures 3E,F**), whereas IgM content did not differ between groups (**Figures 3G,H**). Given that plaque IgG-type antibodies are generally considered to be atherogenic, while IgMs predominantly exhibit atheroprotective activity (Schmitz et al., 2018; Sage et al., 2019), these findings suggest the need of FcγRIII for clearance of pro-atherogenic ICs against modified lipoproteins, and may at least partly explain the exacerbated atherosclerotic lesion formation observed upon *FcγrIII* deficiency.

FcγrIII Deficiency Induces Pro-inflammatory Profile in Macrophages

Based on the reported role of FcγRIII in regulating the decision between pro- and anti-inflammatory responses by inducing ITAM or inhibitory ITAM (ITAMi) signaling (Aloulou et al., 2012), we determined the phenotype of macrophages in *FcγrIII*$^{-/-}$/*Apoe*$^{-/-}$ mice. BMDMs were stimulated with two different concentrations of oxidized LDL, anti-oxLDL-IgG1, and soluble ICs for 6 h. Analysis of gene expression revealed an increase of *Tnf*-α, *Il-1*β, *iNOS, and FcγrII* upon *FcγrIII* deficiency, while the expression of *Arginase-1*, *Tgf*-β, *Il-10,* and *C5ar1* did not differ in both groups (**Figures 4A–D** and **Supplementary Figures S6A–D**). Of note, quantification of pro-inflammatory gene expression in the atherosclerotic lesions showed increased lesional *Tnf*-α and *Il-1*β levels in *FcγrIII*-deficient mice (**Figures 4E,F**). Collectively, these findings indicate that *FcγrIII* deficiency enhances pro-inflammatory responses in the bone marrow-derived compartment of the vasculature to promote advanced atherosclerosis.

DISCUSSION

Our study investigated the role of activating FcγRIII in neointima expansion after arterial injury and in diet-induced chronic atherosclerosis in *Apolipoprotein E*-deficient hypercholesterolemic mice, comparing the phenotype in early versus intermediate-to-late stages. Using a wire injury-based accelerated atherosclerosis model, we demonstrate that *FcγrIII* deficiency reduces neointimal plaque size and macrophage content and induces a stable plaque phenotype with an increased VSMC compartment, which was paralleled by reductions in proinflammatory cytokine TNF-α, the chemokine MCP-1/CCL2, and the atherogenic adhesion molecule VCAM-1 in the vasculature. The lesion-lowering protective effect of *FcγrIII* deficiency was mirrored in a model of diet-induced "early" atherogenesis. In contrast, in a diet-induced model

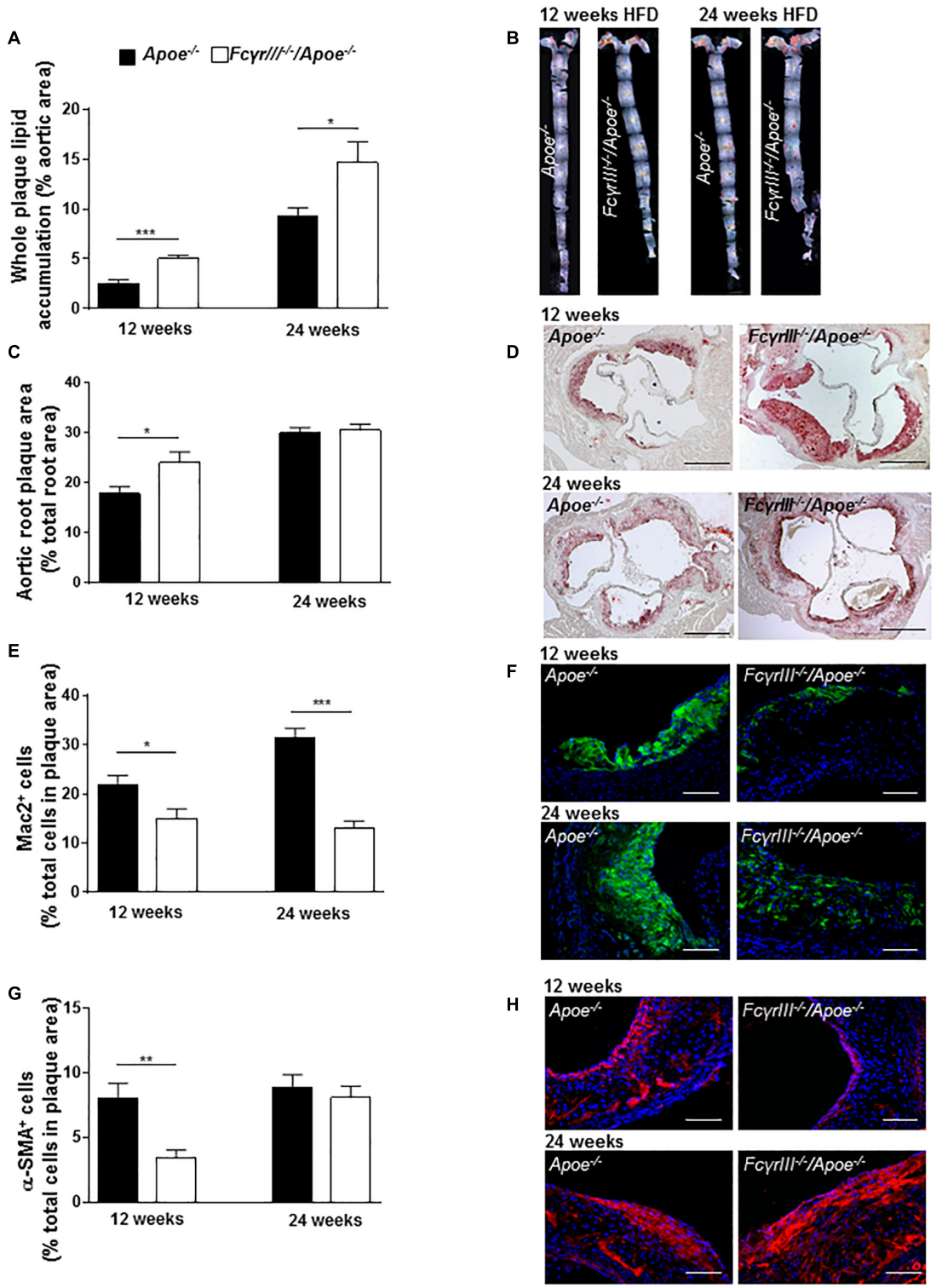

FIGURE 2 | Dichotomic role of FcγRIII in chronic atherosclerosis. **(A–H)** *FcγrIII*$^{-/-}$ *Apoe*$^{-/-}$, and *Apoe*$^{-/-}$ mice received HFD for 12 and 24 weeks. **(A)** Quantification of lesion size in whole aorta (n = 6–9 mice per group). **(B)** Representative image of en face stained whole aorta lesions. **(C)** Quantification of lesion sizes in aortic root (n = 10–12 mice per group). **(D)** Representative image of Oil-Red-O stained aortic root lesion. Scale bar 500 μm. **(E)** Quantification of Mac-2 + macrophages (green). **(F)** Representative Mac-2 immunostaining (green). **(G)** Quantification of α-SMA smooth muscle cells. **(H)** Representative α-SMA immunostaining (red). Magnification × 40; scale bar 100 μm; and (n = 10 mice per group). Graphs represent mean ± SEM. 2-tailed t-test, $^{*}p < 0.05$, $^{**}p < 0.01$, $^{***}p < 0.001$.

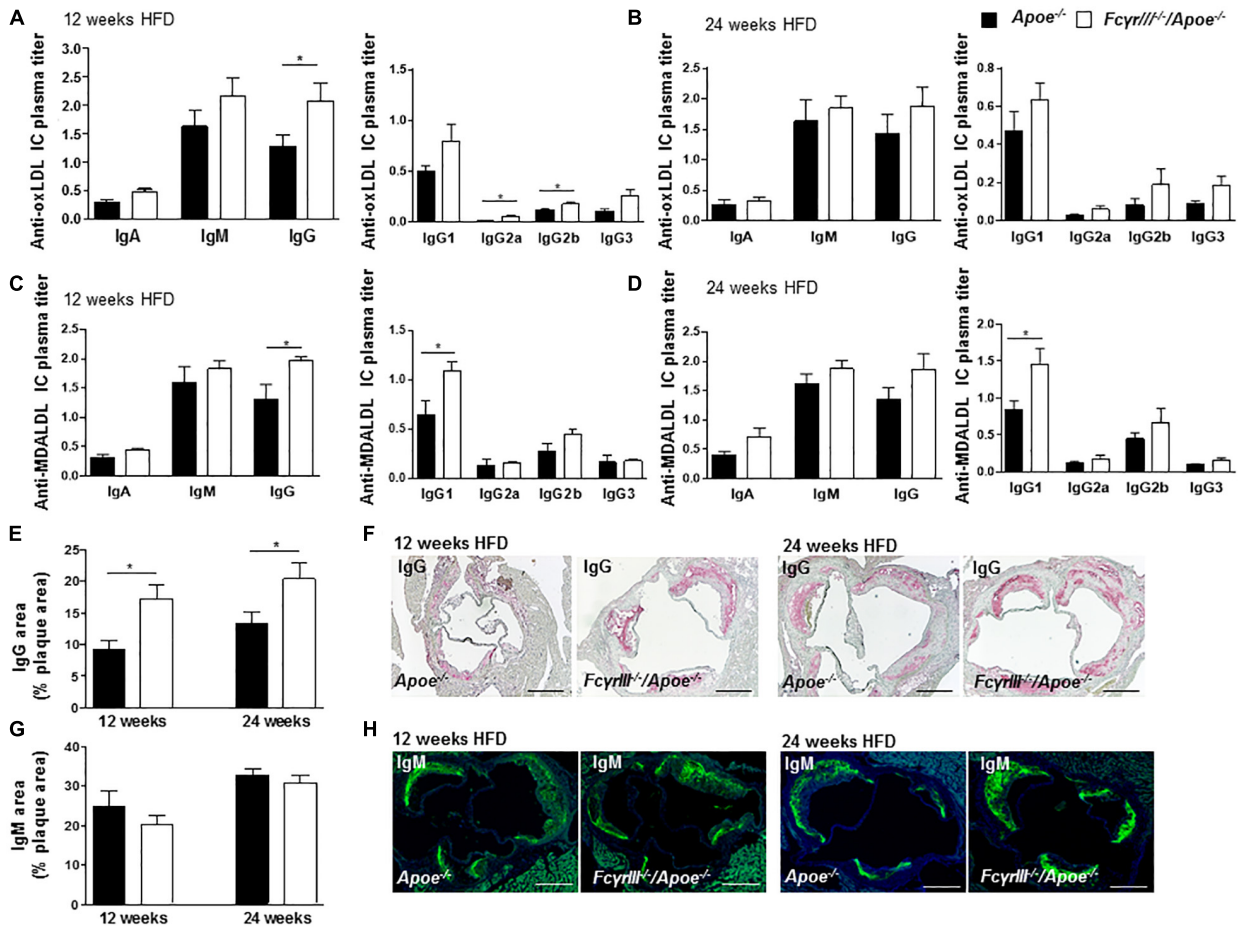

FIGURE 3 | *Fcγrlll* deficiency enhances the accumulation of immunoglobulins in intermediate-to-advanced atherosclerotic lesions. **(A–H)** *Fcγrlll*$^{-/-}$*Apoe*$^{-/-}$, and *Apoe*$^{-/-}$ mice received HFD for 12- and 24-weeks. **(A,B)** Quantification of anti-oxLDL IgA, IgM, IgG, and IgG subtypes IgG2a, IgG2b, and IgG3 in plasma from mice fed HFD for 12 weeks **(A)** and for 24 weeks **(B)**. **(C,D)** Quantification of plasma levels of anti-MDA-LDL in mice fed HFD for 12 weeks **(C)** and for 24 weeks **(D)**. **(E)** Quantification of accumulated IgG antibodies in aortic root lesions. **(F)** Representative IgG staining. **(G)** Quantification of accumulated IgM antibodies in aortic root lesions. **(H)** Representative IgM staining. Scale bar 500 μm. Graphs represent mean ± SEM (n = 6). 2-tailed t-test, $^*p < 0.05$.

of "advanced" atherosclerosis, *FcγrIII* deficiency exacerbated atherosclerotic plaque formation after 12 and 24 weeks of HFD. This was accompanied by lesional accumulation of IgG-type immunoglobulins and elevated serum autoantibodies against modified-LDL and lipid levels. Of note, these unexpected atheropromoting effects of *FcγrIII* deficiency were independent of the cooperativity between the C5a/C5aR1 and FcγRIII/FcγRII axis; hence supporting their independent role in the pathogenesis of a different disease context.

Neointima formation after endothelial denudation is driven by intima exposure, platelet adhesion, activation of inflammatory genes, and increased leukocyte trafficking into the injured vessel wall. To restore the integrity of the artery, phenotypically changed VSMCs accumulate in the intimal layer to maintain vascular stability. Likewise, the extent of macrophage infiltration is a strong determinant of neointimal lesion size (Schober and Weber, 2005). Hence, inhibiting genes that regulate leukocyte trafficking including Mac-1, VCAM-1, and MCP-1/CCL2 has generally resulted in reduced neointimal mass, indicating a decisive role of inflammation in neointimal formation (Shah, 2003). Our data indicating a protective role of *FcγrIII* deficiency in neointima formation after arterial injury is attributable to the reduction of lesional inflammatory cells and VCAM-1, MCP-1/CCL2, and TNF-α levels.

Our findings that *FcγrIII* deficiency exacerbates intermediate-to-late-stage atherosclerosis at first sight contradicts previously reported data, according to which *FcγrIII* deficiency attenuated atherosclerotic plaque formation (Kelly et al., 2010; Zhu et al., 2014). In *FcγrIII*$^{-/-}$*/Ldlr*$^{-/-}$ mice, Kelly et al. (2010) observed fewer lesions after 24 weeks of HFD. While it is difficult to reconcile these findings, it is worth noting that *Apoe*$^{-/-}$ mice on HFD develop extensive late-stage atherosclerosis with different characteristics than the corresponding *Ldlr*$^{-/-}$ mice receiving HFD for the same duration (Veniant et al., 2001). Notwithstanding their limitations and differences, both models have been instrumental in identifying specific pathways that can be targeted for atheroprotection in humans (Gleissner, 2016). Using 5-week-old *FcγrIII*$^{-/-}$*/Apoe*$^{-/-}$ mice fed an HFD for

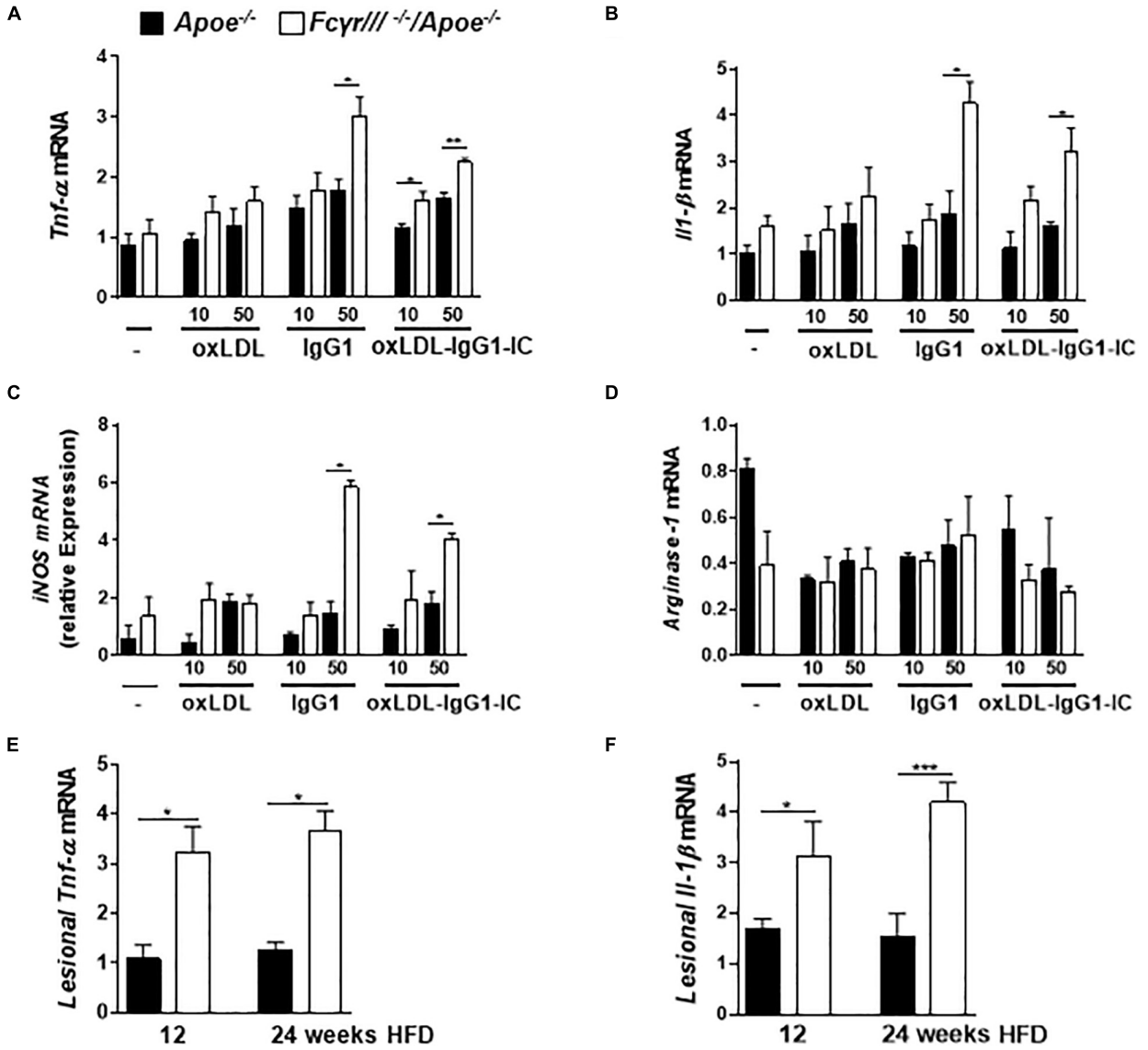

FIGURE 4 | *FcγrIII* deficiency induces pro-inflammatory profile in macrophages. **(A–D)** BMDMs from *FcγrIII*$^{-/-}$/*Apoe*$^{-/-}$, and *Apoe* $^{-/-}$ mice were stimulated with varying concentrations of oxidized LDL, IgG1 and oxLDL-IgG1 immune complexes (IC) for 6 h. Quantification of *Tnf*-α **(A)**, *Il-1*β **(B)**, *iNOS* **(C)**, and Arginase-1 **(D)** mRNA levels. $n = 3$ independent experiments. **(E,F)** *FcγRIII*$^{-/-}$/*Apoe*$^{-/-}$, and *Apoe* $^{-/-}$ mice received HFD for 12- and 24- weeks. Quantification of lesional *Tnf*-α **(E)** and *Il-1*β **(F)** in aortic tissues. $n = 6$ mice per group. Graphs represent the mean ± SEM. two-tailed *t*-test, *FcγrIII*$^{-/-}$/*Apoe*$^{-/-}$ vs. *Apoe*$^{-/-}$ mice, $^{*}p < 0.05$, $^{**}p < 0.01$, $^{***}p < 0.001$.

10 weeks, Zhu et al. (2014) reported a reduced lesion size accompanied by a decreased foam cell content. These conditions are closer to the conditions used in our 12-week HFD model of intermediate stage atherosclerosis, but differences still apply. In fact, HFD in our intermediate model of *FcγrIII*$^{-/-}$/*Apoe*$^{-/-}$ mice was not started until the age of 8 weeks and the applied diet in our model was 2 weeks longer. The model applied by Zhu et al. (2014) may thus be closer to our 4-week HFD model of early atherosclerosis. Indeed, in this model, we found *FcγrIII* deficiency to confer atheroprotection in 8-week-old mice. In conjunction, the data by Kelly, Zhu and colleagues and the data in our current study indicate a Janus-faced role of FcγRIII in atherosclerosis, exhibiting a pro-atherogenic role in early atherosclerosis and/or younger mice, whereas this effect appears to be overcompensated by a FcγRIII-mediated athero-protective mechanisms in more advanced stages of the disease. Whether the alterations in splenic and lymph node T cells that we observed in our study upon *FcγrIII* deficiency contribute to this effect is unclear and clearly needs future scrutiny. The decrease in FoxP3+ Tregs in the 12-week HFD model could support this notion, but Tregs were found to be elevated in *FcγrIII*$^{-/-}$/*Apoe*$^{-/-}$ mice at 24 weeks of HFD, and the analysis of CD4+ and CD8+ subsets provided a complex picture as well.

Autoantibodies are produced against oxidized LDL, but whether the titer of anti-oxLDL autoantibodies serves as a marker for atherosclerosis progression is still a unclear (Shoenfeld et al., 2004). Anti-oxLDL IgGs are known to be pro-atherogenic by forming IC with oxLDL (Mallavia et al., 2013), which bind to FcγR and lead to a pro-inflammatory cell response by macrophage activation. Anti-oxLDL IgM antibodies have been suggested to play a protective role in atherosclerosis (Faria-Neto et al., 2006) and ICs block the oxLDL uptake by macrophages. We found that the IgM anti-oxLDL response remained unchanged in plasma of *FcγrIII*-deficient mice, whereas the IgG anti-oxLDL antibodies were increased. Further analysis revealed an increase in the IgG2a/b response accompanied by a slight increase in IgG1, suggesting a pro-inflammatory effect of ICs in lesion progression. Additionally, clinical studies have shown that IgG antibodies directed against another form of modified LDL, MDA-LDL, correlate with cardiovascular diseases (Salonen et al., 1992). We observed an increased IgG and IgG1 response in plasma upon *FcγrIII* deficiency, indicating a role for anti-MDA-LDL antibodies in the progression of lesion formation. Furthermore, autoantibodies against oxLDL have been detected in atherosclerotic lesions (Shoenfeld et al., 2004) and plaques are known to contain large amounts of IgM and IgG (Yla-Herttuala et al., 1994). This could be a result of diffusion as well as deposition of Igs and ICs from the circulation into the intima (Burut et al., 2010). In our current study, we found an increased accumulation of IgG in *FcγRIII*-deficient lesions, while IgM deposition did not differ between both groups. Hence, indicating that deficiency of *FcγrIII* is accompanied by a defective clearance of anti-oxLDL ICs leading to lesional accumulation of IgG.

Our study also offers a mechanistic explanation for the observed dichotomy. Monomeric IgG1 and oxLDL-IgG1 IC-triggered cytokine production is enhanced in *FcγrIII*-deficient macrophages, insinuating an anti-inflammatory role for FcγRIII, at least in this experimental paradigm. Likewise, in a mouse model of obstructed kidney, an anti-inflammatory effect of FcγRIII was seen in IVIg (intravenous immunoglobulin) and 2.4G2 F(ab)2 (anti-FcγRIII/II antibody)-treated mice (Aloulou et al., 2012). On the other hand, a decrease in TNF-α was found after MDA-LDL-IC incubation of CD16 siRNA-transfected macrophages (Zhu et al., 2014) and bone marrow-transplanted *Fcrγ-chain*-deficient mice (Mallavia et al., 2013). ICs used in these studies consisted of all types of IgG, whereas we used mouse IgG1 which, similar to IVIg, was shown to control the inflammatory response by ITAMi (Aloulou et al., 2012). In addition, FcγRIII is the only activating receptor that is able to bind to IgG1 and small ICs can mimic the response mediated by IVIg (Siragam et al., 2005). Although previous studies have proven that even at high concentrations of IgG1, FcγRIII is the mediating receptor in *FcγrII*-deficient models (Siragam et al., 2006; Aloulou et al., 2012), we cannot completely exclude possible effects from FcγRII or paired FcγRII/FcγRIII complexes. Moreover, dual activating and inhibitory effects of FcγRIII, depending on the degree of aggregation of its natural ligand IgG, have been described (Pinheiro da Silva et al., 2007).

In summary, we present evidence for a protective effect of *FcγrIII* deficiency in neointima expansion and in early atherosclerosis. This is attributable to reduced pro-inflammatory responses in the vasculature. However, in advanced atherosclerosis *FcγrIII* deficiency augments lesion formation, at least in part through enhanced accumulation of Igs in the atherosclerotic lesions. It will be intriguing to identify the triggers of this Ig-mediated response in the future. Gaining a better insight into *FcγRIII* function in atherosclerosis will provide valuable information for the rational design of anti-atherosclerotic therapeutics.

DATA AVAILABILITY STATEMENT

The raw data supporting the conclusions of this article will be made available by the authors, without undue reservation, to any qualified researcher. Requests to access the datasets should be directed to yaw.asare@med.uni-muenchen.de.

ETHICS STATEMENT

The animal study was reviewed and approved by the Landesamt für Natur, Umwelt und Verbraucherschutz (LANUV), Nordrhein-Westfalen, Germany.

AUTHOR CONTRIBUTIONS

JK, YA, JS, and SS performed the experiments and analyzed the data. ES and YA planned and supervised the experiments. ES, YA, and JB wrote the manuscript. YA, ES, JB, JJ, GS, and JG edited and revised the manuscript. All authors contributed to the article and approved the submitted version.

FUNDING

This work was supported by the Else-Kröner-Fresenius-Stiftung (2011_A88) to ES, by the Deutsche Forschungsgemeinschaft (DFG) grant GU1221/3-1 to ES, SFB1123-A3 to JB, and SFB1123-B3 to YA, and by DFG under Germany's Excellence Strategy within the framework of the Munich Cluster for Systems Neurology (EXC 2145 SyNergy – ID 390857198) to JB. YA also received funding from the FöFoLe program of Ludwig Maximilian University of Munich (LMU) Munich (FöFoLe 921) and the Friedrich Baur Stiftung. JJ was supported by grants from Deutsche Forschungsgemeinschaft (DFG) (SFB TRR 219; C-04, S-03).

ACKNOWLEDGMENTS

We thank R. Soltan, Y. Kong, and M. Garbe for excellent technical assistance.

SUPPLEMENTARY MATERIAL

The Supplementary Material for this article can be found online at: https://www.frontiersin.org/articles/10.3389/fphys.2020.00673/full#supplementary-material

REFERENCES

Aloulou, M., Ben Mkaddem, S., Biarnes-Pelicot, M., Boussetta, T., Souchet, H., Rossato, E., et al. (2012). IgG1 and IVIg induce inhibitory ITAM signaling through FcgammaRIII controlling inflammatory responses. *Blood* 119, 3084–3096. doi: 10.1182/blood-2011-08-376046

Asare, Y., Ommer, M., Azombo, F. A., Alampour-Rajabi, S., Sternkopf, M., Sanati, M., et al. (2017). Inhibition of atherogenesis by the COP9 signalosome subunit 5 in vivo. *Proc. Natl. Acad. Sci. U.S.A.* 114, E2766–E2775. doi: 10.1073/pnas.1618411114

Baudino, L., Nimmerjahn, F., Azeredo da Silveira, S., Martinez-Soria, E., Saito, T., Carroll, M., et al. (2008). Differential contribution of three activating IgG Fc receptors (FcgammaRI, FcgammaRIII, and FcgammaRIV) to IgG2a- and IgG2b-induced autoimmune hemolytic anemia in mice. *J. Immunol.* 180, 1948–1953. doi: 10.4049/jimmunol.180.3.1948

Baumann, U., Kohl, J., Tschernig, T., Schwerter-Strumpf, K., Verbeek, J. S., Schmidt, R. E., et al. (2000). A codominant role of Fc gamma RI/III and C5aR in the reverse Arthus reaction. *J. Immunol.* 164, 1065–1070. doi: 10.4049/jimmunol.164.2.1065

Ben Mkaddem, S., Benhamou, M., and Monteiro, R. C. (2019). Understanding Fc Receptor involvement in inflammatory diseases: from mechanisms to new therapeutic tools. *Front. Immunol.* 10:811. doi: 10.3389/fimmu.2019.00811

Bernhagen, J., Krohn, R., Lue, H., Gregory, J. L., Zernecke, A., Koenen, R. R., et al. (2007). MIF is a noncognate ligand of CXC chemokine receptors in inflammatory and atherogenic cell recruitment. *Nat. Med.* 13, 587–596. doi: 10.1038/nm1567

Burut, D. F., Karim, Y., and Ferns, G. A. (2010). The role of immune complexes in atherogenesis. *Angiology* 61, 679–689. doi: 10.1177/0003319710366124

Erkkila, A. T., Narvanen, O., Lehto, S., Uusitupa, M. I., and Yla-Herttuala, S. (2000). Autoantibodies against oxidized low-density lipoprotein and cardiolipin in patients with coronary heart disease. *Arterioscler. Thromb. Vasc. Biol.* 20, 204–209. doi: 10.1161/01.atv.20.1.204

Faria-Neto, J. R., Chyu, K. Y., Li, X., Dimayuga, P. C., Ferreira, C., Yano, J., et al. (2006). Passive immunization with monoclonal IgM antibodies against phosphorylcholine reduces accelerated vein graft atherosclerosis in apolipoprotein E-null mice. *Atherosclerosis* 189, 83–90. doi: 10.1016/j.atherosclerosis.2005.11.033

Gleissner, C. A. (2016). Translational atherosclerosis research: from experimental models to coronary artery disease in humans. *Atherosclerosis* 248, 110–116. doi: 10.1016/j.atherosclerosis.2016.03.013

Hernandez-Vargas, P., Ortiz-Munoz, G., Lopez-Franco, O., Suzuki, Y., Gallego-Delgado, J., Sanjuan, G., et al. (2006). Fcgamma receptor deficiency confers protection against atherosclerosis in apolipoprotein E knockout mice. *Circ. Res.* 99, 1188–1196. doi: 10.1161/01.RES.0000250556.07796.6c

Kelly, J. A., Griffin, M. E., Fava, R. A., Wood, S. G., Bessette, K. A., Miller, E. R., et al. (2010). Inhibition of arterial lesion progression in CD16-deficient mice: evidence for altered immunity and the role of IL-10. *Cardiovasc. Res.* 85, 224–231. doi: 10.1093/cvr/cvp300

Kiener, P. A., Rankin, B. M., Davis, P. M., Yocum, S. A., Warr, G. A., and Grove, R. I. (1995). Immune complexes of LDL induce atherogenic responses in human monocytic cells. *Arterioscler. Thromb. Vasc. Biol.* 15, 990–999. doi: 10.1161/01.atv.15.7.990

Libby, P., Lichtman, A. H., and Hansson, G. K. (2013). Immune effector mechanisms implicated in atherosclerosis: from mice to humans. *Immunity* 38, 1092–1104. doi: 10.1016/j.immuni.2013.06.009

Mallavia, B., Oguiza, A., Lopez-Franco, O., Recio, C., Ortiz-Munoz, G., Lazaro, I., et al. (2013). Gene Deficiency in Activating Fcgamma receptors influences the macrophage phenotypic balance and reduces atherosclerosis in mice. *PLoS One* 8:e66754. doi: 10.1371/journal.pone.0066754

Meyer, D., Schiller, C., Westermann, J., Izui, S., Hazenbos, W. L., Verbeek, J. S., et al. (1998). FcgammaRIII (CD16)-deficient mice show IgG isotype-dependent protection to experimental autoimmune hemolytic anemia. *Blood* 92, 3997–4002. doi: 10.1182/blood.v92.11.3997.423k52_3997_4002

Ng, H. P., Burris, R. L., and Nagarajan, S. (2011). Attenuated atherosclerotic lesions in apoE-Fcgamma-chain-deficient hyperlipidemic mouse model is associated with inhibition of Th17 cells and promotion of regulatory T cells. *J. Immunol.* 187, 6082–6093. doi: 10.4049/jimmunol.1004133

Nilsson, J., and Hansson, G. K. (2008). Autoimmunity in atherosclerosis: a protective response losing control? *J. Intern. Med.* 263, 464–478. doi: 10.1111/j.1365-2796.2008.01945.xJIM1945

Nimmerjahn, F., and Ravetch, J. V. (2008). Fcgamma receptors as regulators of immune responses. *Nat. Rev. Immunol.* 8, 34–47. doi: 10.1038/nri2206

Pinheiro da Silva, F., Aloulou, M., Skurnik, D., Benhamou, M., Andremont, A., Velasco, I. T., et al. (2007). CD16 promotes *Escherichia coli* sepsis through an FcR gamma inhibitory pathway that prevents phagocytosis and facilitates inflammation. *Nat. Med.* 13, 1368–1374. doi: 10.1038/nm1665

Sage, A. P., Tsiantoulas, D., Binder, C. J., and Mallat, Z. (2019). The role of B cells in atherosclerosis. *Nat. Rev. Cardiol.* 16, 180–196. doi: 10.1038/s41569-018-0106-9

Salonen, J. T., Yla-Herttuala, S., Yamamoto, R., Butler, S., Korpela, H., Salonen, R., et al. (1992). Autoantibody against oxidised LDL and progression of carotid atherosclerosis. *Lancet* 339, 883–887. doi: 10.1016/0140-6736(92)90926-t

Schmitz, C., Noels, H., El Bounkari, O., Straussfeld, E., Megens, R. T. A., Sternkopf, M., et al. (2018). Mif-deficiency favors an atheroprotective autoantibody phenotype in atherosclerosis. *FASEB J.* 32, 4428–4443. doi: 10.1096/fj.201800058R

Schober, A., and Weber, C. (2005). Mechanisms of monocyte recruitment in vascular repair after injury. *Antioxid. Redox Signal.* 7, 1249–1257. doi: 10.1089/ars.2005.7.1249

Shah, P. K. (2003). Inflammation, neointimal hyperplasia, and restenosis: as the leukocytes roll, the arteries thicken. *Circulation* 107, 2175–2177. doi: 10.1161/01.cir.0000069943.41206.bd

Shoenfeld, Y., Wu, R., Dearing, L. D., and Matsuura, E. (2004). Are anti-oxidized low-density lipoprotein antibodies pathogenic or protective? *Circulation* 110, 2552–2558. doi: 10.1161/01.CIR.0000143225.07377.EA

Siciliano, S. J., and Rollins, T. E. (1990). Springer MS. *Interaction between the C*5a receptor and Gi in both the membrane-bound and detergent-solubilized states. *J. Biol. Chem.* 265, 19568–19574.

Siragam, V., Brinc, D., Crow, A. R., Song, S., Freedman, J., and Lazarus, A. H. (2005). Can antibodies with specificity for soluble antigens mimic the therapeutic effects of intravenous IgG in the treatment of autoimmune disease? *J. Clin. Invest.* 115, 155–160. doi: 10.1172/JCI22753

Siragam, V., Crow, A. R., Brinc, D., Song, S., Freedman, J., and Lazarus, A. H. (2006). Intravenous immunoglobulin ameliorates ITP via activating Fc gamma receptors on dendritic cells. *Nat. Med.* 12, 688–692. doi: 10.1038/nm1416

Veniant, M. M., Withycombe, S., and Young, S. G. (2001). Lipoprotein size and atherosclerosis susceptibility in Apoe(-/-) and Ldlr(-/-) mice. *Arterioscler. Thromb. Vasc. Biol.* 21, 1567–1570. doi: 10.1161/hq1001.097780

Wang, J., Qiang, H., Zhang, C., Liu, X., Chen, D., and Wang, S. (2003). Detection of IgG-bound lipoprotein(a) immune complexes in patients with coronary heart disease. *Clin. Chim. Acta* 327, 115–122. doi: 10.1016/s0009-8981(02)00342-x

Weber, C., and Noels, H. (2011). Atherosclerosis: current pathogenesis and therapeutic options. *Nat. Med.* 17, 1410–1422. doi: 10.1038/nm.2538

Yla-Herttuala, S., Palinski, W., Butler, S. W., Picard, S., Steinberg, D., and Witztum, J. L. (1994). Rabbit and human atherosclerotic lesions contain IgG that recognizes epitopes of oxidized LDL. *Arterioscler Thromb* 14, 32–40. doi: 10.1161/01.atv.14.1.32

Zhu, X., Ng, H. P., Lai, Y. C., Craigo, J. K., Nagilla, P. S., Raghani, P., et al. (2014). Scavenger receptor function of mouse Fcgamma receptor III contributes to progression of atherosclerosis in apolipoprotein E hyperlipidemic mice. *J. Immunol.* 193, 2483–2495. doi: 10.4049/jimmunol.1303075

Conflict of Interest: The authors declare that the research was conducted in the absence of any commercial or financial relationships that could be construed as a potential conflict of interest.

frontiers in Physiology

ORIGINAL RESEARCH
published: 23 June 2020
doi: 10.3389/fphys.2020.00714

Expression of Chitotriosidase in Macrophages Modulates Atherosclerotic Plaque Formation in Hyperlipidemic Mice

Jonathan Yap[1], Sara McCurdy[1], Martin Alcala[2], Jason Irei[1], Jan Garo[1], Whitney Regan[1], Bog-Hieu Lee[3], Shiro Kitamoto[4] and William A. Boisvert[1]**

[1] Center for Cardiovascular Research, John A. Burns School of Medicine, University of Hawaii, Honolulu, HI, United States,
[2] Department of Chemistry and Biochemistry, Facultad de Farmacia, Universidad CEU San Pablo, Madrid, Spain,
[3] Department of Food and Nutrition, School of Food Science and Technology, Chung-Ang University, Seoul, South Korea,
[4] Departments of Cardiovascular Medicine and Advanced Therapeutics for Cardiovascular Diseases, Graduate School of Medical Sciences, Kyushu University, Fukuoka, Japan

Objective: To determine whether overexpression of the chitin degrading enzyme, chitotriosidase (CHIT1), modulates macrophage function and ameliorates atherosclerosis.

Approach and Results: Using a mouse model that conditionally overexpresses CHIT1 in macrophages (CHIT1-Tg) crossbred with the *Ldlr*$^{-/-}$ mouse provided us with a means to investigate the effects of CHIT1 overexpression in the context of atherosclerosis. *In vitro*, CHIT1 overexpression by murine macrophages enhanced protein expression of IL-4, IL-8, and G-CSF by BMDM upon stimulation with a combination of lipopolysaccharide (LPS) and interferon-γ (IFN-γ). Phosphorylation of ERK1/2 and Akt was also down regulated when exposed to the same inflammatory stimuli. Hyperlipidemic, *Ldlr*$^{-/-}$-CHIT1-Tg (CHIT1-OE) mice were fed a high-fat diet for 12 weeks in order to study CHIT1 overexpression in atherosclerosis. Although plaque size and lesion area were not affected by CHIT1 overexpression *in vivo*, the content of hyaluronic acid (HA) and collagen within atherosclerotic plaques of CHIT1-OE mice was significantly greater. Localization of both ECM components was markedly different between groups.

Conclusions: These data demonstrate that CHIT1 alters cytokine expression and signaling pathways of classically activated macrophages. *In vivo*, CHIT1 modifies ECM distribution and content in atherosclerotic plaques, both of which are important therapeutic targets.

Keywords: atherosclerosis, macrophage, chitotriosidase, hyaluronic acid, collagen

OPEN ACCESS

Edited by:
Ritva Tikkanen,
University of Giessen, Germany

Reviewed by:
Matti Sakari Jauhiainen,
Minerva Foundation Institute for Medical Research, Finland
Antti Saraste,
University of Turku, Finland

***Correspondence:**
Bog-Hieu Lee
lbheelb@cau.ac.kr
William A. Boisvert
wab@hawaii.edu

Specialty section:
This article was submitted to Vascular Physiology, a section of the journal Frontiers in Physiology

Received: *16 March 2020*
Accepted: *29 May 2020*
Published: *23 June 2020*

Citation:
Yap J, McCurdy S, Alcala M, Irei J, Garo J, Regan W, Lee B-H, Kitamoto S and Boisvert WA (2020) Expression of Chitotriosidase in Macrophages Modulates Atherosclerotic Plaque Formation in Hyperlipidemic Mice. Front. Physiol. 11:714. doi: 10.3389/fphys.2020.00714

INTRODUCTION

Chitin is among the most abundant biopolymers in nature, second only to cellulose. It is a linear polysaccharide made up of repeating *N*-acetyl-D-glucosamine (GlcNAC) monomers. Chitin functions as the primary structural component in the exoskeleton of arthropods, and is produced by mollusks, crustaceans, fungi, and nematodes as well (Tharanathan and Kittur, 2003). Endogenous

chitin is not present in vertebrates and is, in fact, recognized by macrophage TLRs as a pathogen associated molecular pattern (PAMP). Like most mammalian chitinases, Chitotriosidase (CHIT1) is a member of the glycosyl-hydrolase enzymatic family 18 (GH18). Cleavage of substrate is achieved through hydrolysis of β(1→4) glycosidic bonds. There are two major isoforms of CHIT1 that arise from post-translational modification. In macrophages, CHIT1 is initially synthesized as a 50 kDa protein. This isoform is either secreted in response to an inflammatory stimulus or packaged in lysosomes and lysosome-related organelles (LRO) where the acidic environment within is believed to promote cleavage into a still fully enzymatically active 39 kDa isoform (Renkema et al., 1995, 1997).

Several different reports have described elevated serum CHIT1 activity in atherosclerotic patients and animals (Artieda et al., 2003; Fach et al., 2004; Karadag et al., 2008). Previously published data from our group showed that CHIT1 inhibition using a chitinase inhibitor, allosamidin, promotes atherosclerosis in ApoE$^{-/-}$ mice (Kitamoto et al., 2013). Pretreatment of bone marrow-derived macrophages (BMDM) *in vitro* with allosamidin and subsequent stimulation with IFN-γ significantly upregulated pro-inflammatory mediators associated with M1 macrophage polarization such as MCP-1, TNF-α, iNOS, IL-6, IL-12, and IL-1β when compared to IFN-γ treatment alone. *In vivo*, ApoE$^{-/-}$ mice fed a Western diet for 6 weeks and administered allosamidin via a surgically implanted pump, exhibited significantly greater lesion area in the aortic arch compared to vehicle control. Moreover, we found that lesion area was also significantly larger in the aortic sinus, and that macrophage deposition was also significantly greater.

Because we observed an exacerbation of atherosclerosis by inhibiting CHIT1, we sought to examine if overexpression of CHIT1 in macrophages may exhibit possible athero-protective properties. Our findings demonstrate that CHIT1 overexpression *in vitro* augmented the transcription and expression of cytokines and chemokines associated with atherosclerosis. We also observed differences in plaque morphology between atherosclerotic mice overexpressing CHIT1 compared to littermate controls. Given these findings and given that chitin does not exist in atherosclerotic plaques, further exploration of the non-traditional role of CHIT1 in plaque macrophages may be warranted and may indeed provide novel insight into macrophage behavior and atherosclerotic plaque morphology.

MATERIALS AND METHODS

Mouse Strains

Wild-type C57BL/6 mice and LDLR null mice generated on a C57BL/6 background animal were purchased from Jackson Laboratories (Bar Harbor, Maine). CHIT1-OE mice were developed in cooperation with Kyushu University and Riken research Institute (Saitama, Japan). Briefly, the transgene depicted in **Figure 1A** was microinjected into fertilized mouse embryos.

To confirm successful transgene insertion, PCR and gel electrophoresis was used to detect the presence of primer sequences specific to the CHIT1 and EGFP sections of the transgene (**Figure 1B**). Ldlr$^{-/-}$ mice were crossbred with the CHIT1-Tg mice to produce Ldlr$^{-/-}$-CHIT1-Tg animals, which overexpress CHIT1 and are prone to atherosclerosis. Given that the EGFP stop sequence is flanked by loxp sites (floxed), we employed a Cre-lox method of overexpression. For our experiments, floxed Ldlr$^{-/-}$-CHIT1-Tg mice were used as littermate controls. Experimental animals were produced by breeding Ldlr$^{-/-}$-CHIT1-Tg mice with LysM-CRE mice, in which Cre-recombinase is under transcriptional control of the lysozyme promoter. Because lysozyme is constitutively produced by macrophages, the resultant animals overexpress CHIT1 as the floxed EGFP/β-globin, poly-A stop sequence is excised. Thus, the genetic characterization of our experimental mouse models can be described as follows: ldlr$^{-/-}$- CHIT1-Tg-LysM^{Cre} (CHIT1-OE) Mice between 8 and 12 weeks of age were used for isolation of bone marrow derived macrophages. Male CHIT1-OE mice between 8 and 10 weeks were utilized for the in vivo atherosclerosis study. At 8–10 weeks of age, animal subjects were placed on HFD containing 15.8% (wt/wt) fat and 1.25% cholesterol (wt/wt) (diet 94059; Harlan Teklad Laboratories, Indianapolis, IN, United States) for 12 weeks to induce atherosclerosis. All animal studies and protocols were approved by the University of Hawaii Institutional Animal Care and Use Committee.

Bone Marrow-Derived Macrophage Cell Isolation and *in vitro* Cell Culture

Experimental and control mice were sacrificed by CO_2 asphyxiation at 8–10 weeks of age. 70% EtOH was sprayed on the animals to disinfect the skin. Each femur and tibia was surgically removed under a biosafety hood. Using a 30-gauge needle, the marrow within the exposed bones were flushed out with ice cold PBS into a 50-mL falcon tube while on ice. The isolated bone marrow was broken up by vigorous pipetting with a 10-mL pipette. It was then passed through a 40-μm cell strainer into a 50-mL falcon tube, and centrifuged at 1,300 RPM (≈300 × *g*) for 5 min to form a pellet. PBS was aspirated and the remaining pellet was resuspended in BMDM differentiation medium (DMEM/F12, [Gibco], 10% FBS, 20% L929 conditioned medium, and 1% pen/strep [Gibco]). Cell viability was determined by staining a 10 μL sample of cells in suspension with trypan blue. Cells were cultured at a density of 1×10^6 cells per mL and plated in 15-cm tissue-culture treated plates (Corning) with 25 mL of medium. 5–10 mL of media was added to the plate every other day for 7 days. Differentiated macrophages adherent to the plate were detached using non-enzymatic Cell Stripper solution (Gibco). The cells were then counted and re-plated as specified in each experiment.

Preparation of Lysates From Cells and Tissues

RIPA buffer (10 mM Tris-Cl [pH 7.6], 1 mM EDTA, 1% Triton X-100, 0.1% sodium deoxycholate, 0.1% SDS, 140 mM NaCl) and 1X Halt protease and phosphatase inhibitor cocktails (Thermo Fisher) was used in preparation of lysates. Adherent cells in

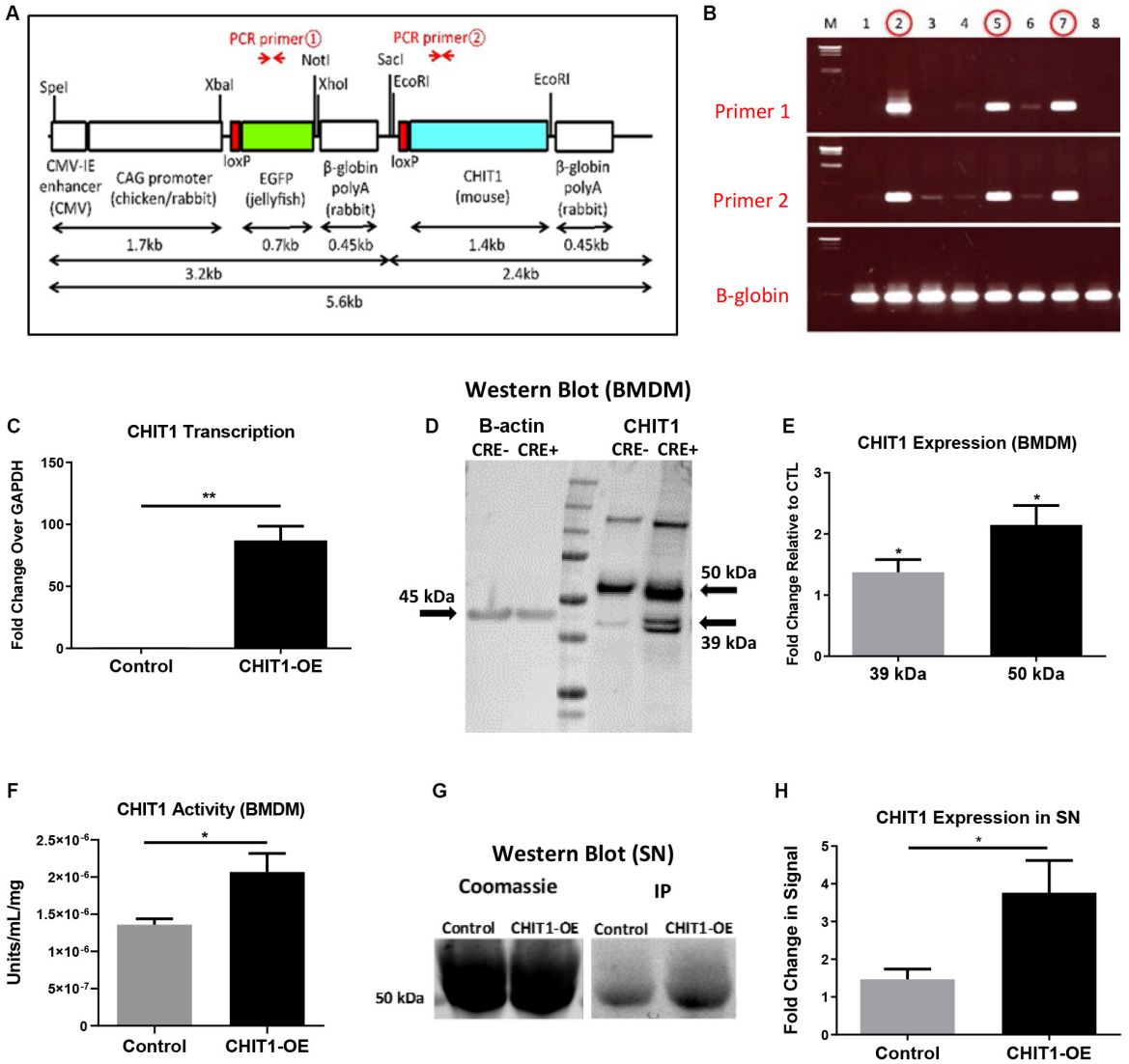

FIGURE 1 | (A) The transgene was designed with an EGFP stop sequence (green) that is removed in the presence of Cre recombinase. When Cre recombinase is expressed in lysozyme producing cells, the CHIT1 gene (blue) is constitutively expressed by macrophages. **(B)** Results from genotyping F0 mice indicate the presence of both primers and confirm transgene insertion. B-globin gene was used as internal control. **(C)** Transcription of CHIT1 mRNA was quantified using qPCR. cDNA was isolated from control and CHIT1-OE BMDM ($P = 0.0059$). **(D)** Western blot imaging of CHIT1 protein expression. Both the 50 kDa and 39–42 kDa isoforms were significantly increased in BMDM from CHIT1-OE mice compared to controls ($P = 0.0245$ and 0.0168 respectively). **(E)** Membranes after Western blot were imaged using Licor Odyssey CLx and analyzed with image studio software measurements reflect the fold change in florescence intensity. **(F)** CHIT1 activity was analyzed in BMDM from control (Cre-) and CHIT1-OE (Cre+). Liberated 4-MU emission was measured with a plate reader to determine enzymatic activity ($P = 0.0305$. **(G)** immunoprecipitation was performed on supernatants of BMDM harvested from CHIT1-OE mice and control animals. Coomassie staining of the membrane was used as a total protein control ($P = 0.0330$). **(H)** Analysis of Western blot images with image studio software showed a significant increase in CHIT1 protein expression. $N = 3$; $^*P<0.05$; $^{**}P<0.01$.

6-well plates were washed with PBS which was then aspirated from each well before adding 100 μL of ice cold lysis buffer with protease/phosphatase inhibitor cocktails (diluted 1:1,000) (Roche). Plates were kept on ice for 15 min before scraping the wells with a cell scraper and transferring the lysates to 1.5 ml Eppendorf tubes on ice. Samples were then sonicated by pulsing 10 times with a probe sonicator (Thermo Fisher) at power level 2.5, and centrifuged at 400 × *g* for 5 min at 4°C. Lysates were transferred to a new Eppendorf tube and the pelleted cell debris was discarded. Pierce BCA protein assay kit (Thermo Fisher) was used to determine protein concentrations of lysates in a 1:10 dilution of samples.

Polyacrylamide Gel Electrophoresis and Western Blot Transfer

Precast NuPAGE® Novex® 4–12% Bis-Tris Mini or Midi protein gels (Invitrogen) with 12 or 20-lanes respectively, were used in

conjunction with the appropriate mini or midi electrophoresis gel box. 4× SDS loading buffer (0.1 M Tris-HCl pH 6.8, 0.7% SDS, 33% glycerol, 0.01% bromophenol blue, 8% β-mercaptoethanol) was added to 10–20 μg of protein and this mixture was heated and maintained at 95°C for 5 min. Samples were loaded into each lane and 4 μL of Li-cor 1-color protein marker was added as a size reference latter. Gels were run in 1X NuPAGE® MES SDS Running Buffer (Invitrogen) at a constant voltage of 150 V until the loading dye has completely migrated to the bottom of the gel. The gel is removed from its casing and placed on a low florescence PVDF membrane that has been activated in 100% methanol and immersed in 1× Efficient™ Western Transfer Buffer (G-Biosciences® #786-019) with 20% methanol for 5 min. The gel and membrane together were placed between sheets of filter paper soaked in transfer buffer, and compressed tightly within the transfer cassette. The transfer cassette was placed in the transfer chamber along with an ice pack and stir Rod. The chamber was then put on ice. Protein was transferred to the membrane after running for 1 h at 100 V.

Membrane Incubation With Antibodies and Scanning

The membranes were blocked in 1:1 Li-cor blocking buffer and PBS for 1 h with gentle agitation on an orbital shaker. The blocked membranes were incubated with primary antibodies (**Table 1**) diluted in Li-cor blocking buffer at room temperature for 1 h or at 4°C overnight. Membranes were subsequently washed three times with 0.1% Tween20 in PBS. Secondary antibodies diluted in Li-cor blocking buffer were incubated with membranes at room temperature for 1 h in the dark. After washing three times for 5 min each with 0.1% PBST, membranes were scanned with a Li-cor Odyssey infrared scanner and images were analyzed with Li-cor Image Studio (Li-cor Biosciences).

Reverse Transcriptase Quantitative PCR (RT-qPCR)

Total RNA was extracted by adding 500 μL–1 mL TRIzol reagent (Life Technologies) to each sample in a 1.5 mL Eppendorf tube. The sample was then vortexed until completely dissolved and chloroform was added to TRIzol in a 20% v/v ratio, and inverted vigorously to mix. The samples were centrifuged at 12,400 RPM for 15 min in a pre-cooled centrifuge at 4°C. Once phase separation occurs, the aqueous fraction was carefully pipetted into a separate tube and combined with an equal volume of nuclease-free, 70% ethanol. Samples were mixed thoroughly and put through RNA purification columns provided in the Qiagen RNeasy RNA extraction kit. DNA digest was performed, on-column, for 15 min at room temperature. After the appropriate wash steps, columns were allowed to completely dry. Elution of RNA from the columns was performed using 30–50 μL nuclease-free water. RNA concentration and quality was determined with a NanoDrop 2000. RNA was used immediately for RT-qPCR or stored at −80°C. 1 μg of total RNA per sample would be used to transcribe cDNA using the qScript cDNA synthesis kit (Quanta Biosciences). 80 μL of nuclease-free water was added to each cDNA sample, bringing the total volume to 100 μL. In performing the RT-qPCR, 4 μL of cDNA was added to each well along with a master mix of 12.5 μL SYBR Green 2X master mix containing ROX (Roche), 0.5 μL of both forward and reverse primers (10 μM), and 7 μL of nuclease-free water. 10 μL of the reaction mixture was pipetted in triplicate to a 384-well qPCR plate and analyzed with an Applied Biosystems 7900HT Fast Real-Time PCR System.

Cytokine Array

The Proteome Profiler Array: Mouse Chemokine Array Kit (R&D) was used to determine relative levels of 40 different mouse Cytokines and Chemokines. Cell lysates were prepared by rinsing BMDM cultures with PBS and then adding 100–150 μL of lysis buffer to each well. The cells and lysis buffer are incubated for 30 min before harvesting with a cell scraper. Protein concentration was determined using BCA assay. 2 mL of array buffer 6 (blocking buffer) is added to each well and the pre-blotted, nitrocellulose membranes that were provided in the kit are added to the wells. The membranes were incubated for 1 h at room temperature. 15 μL of reconstituted Mouse Cytokine Array Panel A Detection Antibody Cocktail was added to each sample containing 100 μg total protein. The wells were emptied of Array Buffer 6 and the samples/antibody mixtures were added to the wells and allowed to incubate overnight at 2–8°C on a rocking platform shaker. Each membrane was washed and then 2 mL of IRDye 800CW Streptavidin (LI-COR, Catalog #926-32230) diluted 1:2,000 using the Array Buffer 6 was added to each well of the dish. After incubating for 30 min at room temperature, each membrane was removed and images were collected with an Odyssey CLx imaging system.

Blood Collection and Sacrifice of Study Animals

Blood from each mouse was collected at the start and end point of the study using a submandibular bleeding technique. A portion of the whole blood collected was centrifuged at 1,500 × *g* for 15 min to achieve plasma separation. Plasma samples were used to measure lipid levels. At the study's conclusion, animals were euthanized by CO_2 asphyxiation and total blood was collected through cardiac puncture of the left ventricle. Each mouse was perfused with ice cold PBS followed by 4% PFA/5% sucrose. The hearts and aortas were removed and analyzed as described below.

Analysis of Serum Cholesterol and Triglyceride Levels

At the end of the atherosclerosis study blood cholesterol and triglyceride measurements were gathered from serum samples of all mice in each group. A fluorometric assay kit (Cayman Chemical) was used to determine total cholesterol. Samples were diluted 1:200 with assay buffer in duplicates prepared in a 96-well plate. Serum samples were also analyzed for triglyceride levels. A colorimetric assay (Cayman Chemical) allowed for the measurement of fluorescence or absorbance using a SpectraMax Microplate Reader. Standard curves were derived from standard solutions provided in the kit.

Analysis of Lesion Area of Whole Aortas and Aortic Root Cryosections

Upon dissection of the animal, adventitial fat was cleared away from aorta and branching arteries. The entire aorta was then cut open longitudinally, excised, and pinned to a wax lined dissecting tray. Oil-Red-O Stock (ORO) solution was prepared with 1 g of ORO powder (Sigma-Aldrich) dissolved in 300 mL of 99% isopropanol. A working solution of the stain was prepared fresh by mixing 180 mL of stock solution with 120 mL Milipore water. The solution was allowed to equilibrate for 1 h before filtration with Whatman filter paper into a clean glass bottle. 60% isopropanol was used to wash the pinned aortas which were then completely submerged in ORO working solution for 15 min. The aortas were washed with 60% isopropanol until the stain was no longer visibly being removed (3–4 washes). Aortas were photographed and the images were analyzed to measure plaque area using the ImageJ software.

Fixed hearts were collected from the study mice and mounted in Optimal Cutting Temperature (OCT) compound (Tissue-Tek) which were then frozen at −80°C. Embedded hearts were sectioned in a sagittal orientation through the aortic valve were all three leaflets are visible. Cryo-sectioning was achieved with a cryostat and serial sections of 10 μm increments were made, and five representative sections were selected from each mouse. These sections would be used to visualize lesion area as represented with ORO staining. Newly prepared cross-sections were incubated in PBS for 5 min and then air dried. They were dipped 10 X in 60% isopropanol and then stained with fresh ORO working solution for 15 min. The staining solution was removed and the slides were again dipped 10 X in isopropanol and washed for 5 min under running tap water. Slides were covered using mounting media (Sigma-Aldrich) and dried overnight. Photos were taken of the sections at 5× zoom and the ORO stained area was quantified using ImageJ and represented as a percentage of total aortic area.

Immunohistochemical Staining of Aortic Root Cryosections

Immunohistochemical (IHC) staining was used to characterize and quantify CHIT1 expression, macrophage populations, necrotic core area, ECM deposition, and collagen formation in WT and CHIT1-OE mouse, aortic cryosections. Slides with mounted cryosections were prepared for IHC by fixing in ice cold, 100% acetone for 1 min and then washed with PBS using dip-style glass chamber. Tissue sections were circled with a PAP pen and then washed with PBS-Tween. Antigen retrieval was carried out using 0.05% trypsin/0.1% calcium chloride solution (trypsin/CA). Slides were incubated with trypsin CA in a humidified chamber at 37°C for 15 min, and allowed to cool at room temperature for 10 min. Antigen retrieval solution was removed and slides were washed three times with PBS-Tween. 0.1% Triton X-100 was then applied for 20 min, removed, and slides were washed again with PBS-Tween.

Hydrogen peroxide block was performed by adding enough 3% hydrogen peroxide to cover each section and incubate until bubbles can no longer be observed emanating from the tissue. Slides were then rinsed with PBS and placed in a dip chamber containing PBS for 2 min. Sections were blocked with 5% donkey serum dissolved in 2% BSA with 1X PBS. Slides were incubated in block solution for 1 h at room temperature.

Primary antibodies (**Table 1**) for CHIT1 (Santa Cruz Biotechnology) and macrophages (MOMA-2, Abcam) were added to the sections and allowed to incubate overnight at 4°C. Sections were washed with PBS-Tween followed by addition of the horseradish peroxidase (HRP), conjugated secondary antibody. Slides were incubated in a dark humidified chamber for 1 h at room temperature. Sections were washed with PBS-Tween and kept wet until mounted. One drop of reagent a was diluted in 1 mL of distilled water as described in the AEC staining kit instructions (Invitrogen). One drop of reagent be and reagent C were then added and the solution was kept away from light and incubated with the cryosections for 30 min (or until color development is satisfactory). Slides were then rinsed with distilled water. Mayer's hematoxylin counter stain was applied using a dip chamber for no more than 10 s. The slide was then washed and rinsed under running tap water for 5 min. Next, the slides were put into a dip chamber containing Scott's Bluing solution for 30 s and dipped once in tap water to wash. Dako fluorescent mounting media was added to the top of each section, which was then covered with a coverslip and stored at 4°C.

Visualization of hyaluronic acid was achieved using biotinylated hyaluronic acid binding protein (BHABP, EMD/Millipore/Calbiochem). After acetone fix, hydrogen peroxide block, and blocking (2% BSA in 1X PBS), streptavidin/biotin blocking was performed according to the instructions provided by the kit (Vector Laboratories): incubate section with Avadin D solution for 15 min at room temperature rinse with PBS-Tween, next incubate section with biotin solution for 15 min at room temperature and rinse again with PBS-Tween. BHABP was diluted 1:100 in blocking solution and applied to sections. These were allowed to incubate at room temperature for 1 h. BHABP was aspirated away and slides were washed 3X with PBS. The streptavidin-conjugated HRP was then applied to the cells for 1 h at room temperature before washing 3X with PBS. AEC chromogen and Mayer's hematoxylin counter stain was added as described above.

Hyaluronidase negative controls sections were prepared in the same way as sample sections. However, no detection stain was

TABLE 1 | List of antibodies used in Western Blot and IHC.

Name	Product number	Company	Dilution
CHIT1	sc-271460	Santa Cruz Biotechnology	1:500
MOMA	sc-59332	Santa Cruz Biotechnology	1:500
β-actin	ABT264	Sigma	1:2,000
ERK1/2	9102	Cell signaling	1:1,000
pERK1/2 (Thr202/Tyr204)	9101	Cell signaling	1:1,000
pAKT (Ser473)	4060	Cell signaling	1:1,000
PIκB-α (Ser32)	2859	Cell signaling	1:1,000
IRDye 800CW	925-32213	Licor	1:10,000
IRDye 800CW	926-32214	Licor	1:10,000
IRDye 680CW	926-68072	Licor	1:10,000

added. Instead, cryosections were incubated with hyaluronidase (StemCell Technologies) for 2 h at room temperature.

Picro-Sirius Red staining was used to visualize collagen in the aortic root. Cryosections were acetone fixed and trypsin/CA antigen retrieval was applied. As described in the instruction manual (Abcam), Picro-Sirius red solution was added to completely cover the section, and incubated for 60 min. The slide was rinsed with two changes of acetic acid solution, and then rinsed once in absolute alcohol. The cryosections were then dehydrated into changes of absolute alcohol and the slide was mounted in resinous mounting media.

Statistical Analysis

A minimum of three biological replicates run in duplicate or triplicate were analyzed for *in vitro* experiments as indicated. All Data are represented as the average of biological replicates ± SEM. Quantification in each cryosection was carried out by acquiring five images from representative regions of the aortic sinus. Images were analyzed using ImageJ. Statistical analysis was performed using GraphPad Prism 8 software. To determine significance, unpaired, two-tailed Welsh's *t*-test was performed when comparing experimental and control groups. $^{*}P < 0.05$, $^{**}P < 0.005$, $^{***}P < 0.0005$, $^{****}P < 0.0001$.

RESULTS

Validation of CHIT1 Overexpression

Initial experiments were performed to confirm CHIT1 overexpression in BMDM harvested from CHIT1-OE mice. As mentioned above, CHIT1-Tg mice were crossbred with $ldlr^{-/-}$ mice, thereby providing us with an atherosclerotic, CHIT1 overexpressing mouse model. Moreover, CHIT1 overexpression is achieved using the Cre-Lox system whereby the removal of a LoxP-flanked stop sequence allows for conditional overexpression of CHIT1 in lysozyme producing macrophages (**Figure 1A**). Conditional overexpression with LysMCre is made possible because the Cre recombinase gene is inserted after the promoter of the LysM gene and as lysozyme is constitutively expressed so too is Cre recombinase, and with that CHIT1.

CHIT1 Overexpression in Macrophages

To verify the overexpression of CHIT1 in macrophages, BMDM were harvested from both experimental and littermate control animals. Isolated RNA was analyzed with "quantitative" PCR (qPCR). We found that CHIT1 transcription was not affected in control BMDM as the transcript detected was similar to our internal control, GADPH (**Figure 1C**). CHIT1 transcription was significantly increased in CHIT1-OE BMDM when compared to control BMDM. Cell lysates were prepared from BMDM and visualized using Western blot analysis. **Figures 1D,E** show protein expression was enhanced in CHIT1-OE BMDM as evidenced by the presence of one distinct band at 50 kDa and one at 39 kDa (per company's description of CHIT1 antibody, double bands are a result of disulfide bonds) which are characteristic of the predicted molecular weight of both CHIT1 isoforms. The 39 kDa isoform of CHIT1 is a product of the post-translational modification of the 50 kDa isoform and was only visible in CHIT1-OE BMDM. We determined that CHIT1 enzymatic activity is elevated in both cell lysates and the supernatant of CHIT1-OE BMDM as exhibited by the cleavage of 4-MU-conjugated substrates (**Figure 1F**). Due to the fact that only the 50 kDa isoform of CHIT1 is secreted while the 39 kDa isoform is sequestered in specialized vesicles, we analyzed the supernatant of macrophage cell cultures for the presence of CHIT1. As expected, we found that the 50 kDa, secreted isoform of CHIT1 was robustly expressed in the supernatant of CHIT1-OE BMDM (**Figures 1G,H**). $N = 3$.

Overexpression of CHIT1 Modulates Cytokine Expression in Macrophages

In order to better understand the effects of CHIT1 overexpression on cytokine expression by macrophages, a cytokine antibody array was performed using nitrocellulose membranes spotted with capture antibodies for a variety of cytokines and chemokines. Given that CHIT1 is highly expressed by activated macrophages, the classic combination of IFN-γ and LPS was used to stimulate macrophages by a TLR-2 and TLR-4 respectively. The assay analyzed cell lysates prepared from BMDM, treated with 20 ng/mL IFN-γ + 100 ng/mL LPS (TR). Under these conditions, macrophages are polarized toward an inflammatory phenotype which is reflective of the atherosclerotic plaque environment. Membranes were incubated with cell lysates from both CHIT1-OE BMDM (CRE+) and control BMDM (CRE-) for 8 h prior to application of biotin-labeled detection antibodies. Results in **Figures 2A–C** showed a significant up regulation of G-CSF, the anti-inflammatory cytokine IL-4, and KC (the murine homolog of IL-8) which is involved in immune cell recruitment, macrophage phagocytosis, parasitic invasion defense, and is expressed during both M1 and M2 inflammatory conditions, $N = 3$.

Inflammatory Signaling Pathways Are Inhibited by CHIT1 Overexpression

Phosphorylation is a fundamental component of intracellular signal transduction. To further explore the cell signaling potential of CHIT1, we treated both CHIT1-OE (CRE+) and control BMDM (CRE-) with 20 ng/mL IFN-γ + 100 ng/mL LPS for 0, 0.5, and 1 h. Cell lysates were prepared and analyzed via Western blot for specific phosphorylated signaling molecules: ERK 1/2, Akt, and IκB (**Figure 3A**). Although not significant between groups or across time points, CHIT1-OE and control BMDM both exhibit increases in pERK 1/2, pAkt, and pIκB at the 0-h time point. This effect, however, was exaggerated in experimental BMDM when compared to controls. pERK1/2 and pAkt was significantly down regulated after 1 and 0.5 h periods, respectively, upon incubation with pro-inflammatory stimuli (**Figures 3B,C**). Thus, depicting a decrease in phosphorylated signaling in these pathways. This is consistent with diminished transcription of pro-inflammatory cytokines that we observed. Values were quantified from Western blot using densitometric analysis with the Licor Odessey CLx and ImageStudio software. ERK1/2 and β-actin were used as experimental controls, $N = 3$.

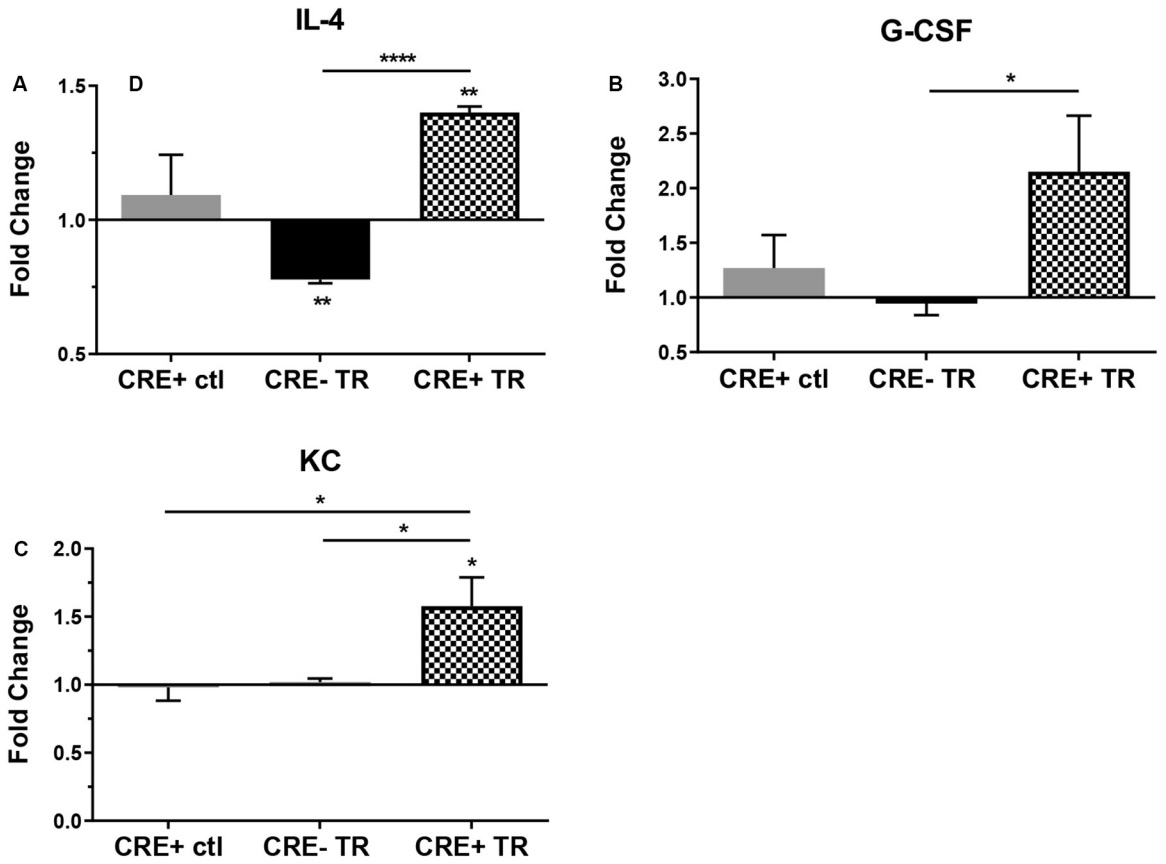

FIGURE 2 | Protein expression in CHIT1-OE BMDM and control BMDM was measured with a mouse cytokine array. Cell lysates were prepared from experimental and control BMDM which were untreated or exposed to 20 ng/mL IFN-γ + 100 ng/mL LPS for 8 h To induce pro-inflammatory activation. Between groups, treated BMDM exhibited a significant increase in protein expression between groups of **(A)** IL-4 ($P<0.0001$), **(B)** G-CSF($P = 0.0497$), and **(C)** KC ($P = 0.0426$). $N = 3$ biological replicates, each run in duplicate. Values represent fold change in florescence. $^{*}P<0.05$, $^{****}P<0.0001$.

Characterization of Mice Before and After HFD

Upon termination of the HFD regimen, blood was collected from all study mice in each group prior to being euthanized. Serum cholesterol and triglyceride levels were subsequently measured with fluorometric and colorimetric analysis (**Figures 4A,B**). No statistically significant difference in cholesterol or triglycerides was detected between experimental and control groups. Measurement of body weight before and after 12 weeks of HFD was also conducted (**Figure 4C**) and revealed significant weight gain in both post-HFD groups, although no differences observed between groups, $N = 28$ (14 per group).

CHIT1 Is Highly Expressed in Atherosclerotic Plaques of CHIT1-OE Mice Post-HFD

Given the importance of macrophages in every stage of atherosclerosis and the fact that CHIT1 is among the most abundantly expressed proteins by activated macrophages, we wished to investigate the presence of CHIT1 in the plaques of our control mice. We also wanted to determine how much more CHIT1 expression was achieved in the lesion of the *CHIT1-OE* mice compared to the control mice. We stained serial cryosections prepared at a thickness of 10 μm of the aortic sinus with a murine CHIT1 antibody (**Figure 5A**). Ensuing 24 h of incubation, a secondary HRP conjugated chromogen was applied and CHIT1 was visualized using light microscopy. The staining revealed significantly more robust expression of CHIT1 in the atherosclerotic plaques of CHIT1-OE mice in comparison to littermate controls (**Figure 5B**). CHIT1 staining was quantified using ImageJ software and expressed as the CHIT1 stained area as a percentage of the total plaque area, $N = 7$.

Macrophage Content in Atherosclerotic Plaques Is Unaffected by CHIT1 Overexpression

Macrophages play multifaceted roles in the development of atherosclerosis. Recruitment and accumulation of macrophages is associated with increased plaque size and weakening of the fibrous cap. We sought to determine whether CHIT1 overexpression in $Ldlr^{-/-}$ mice alters macrophage accumulation in atherosclerotic plaques. To this end, slides were prepared

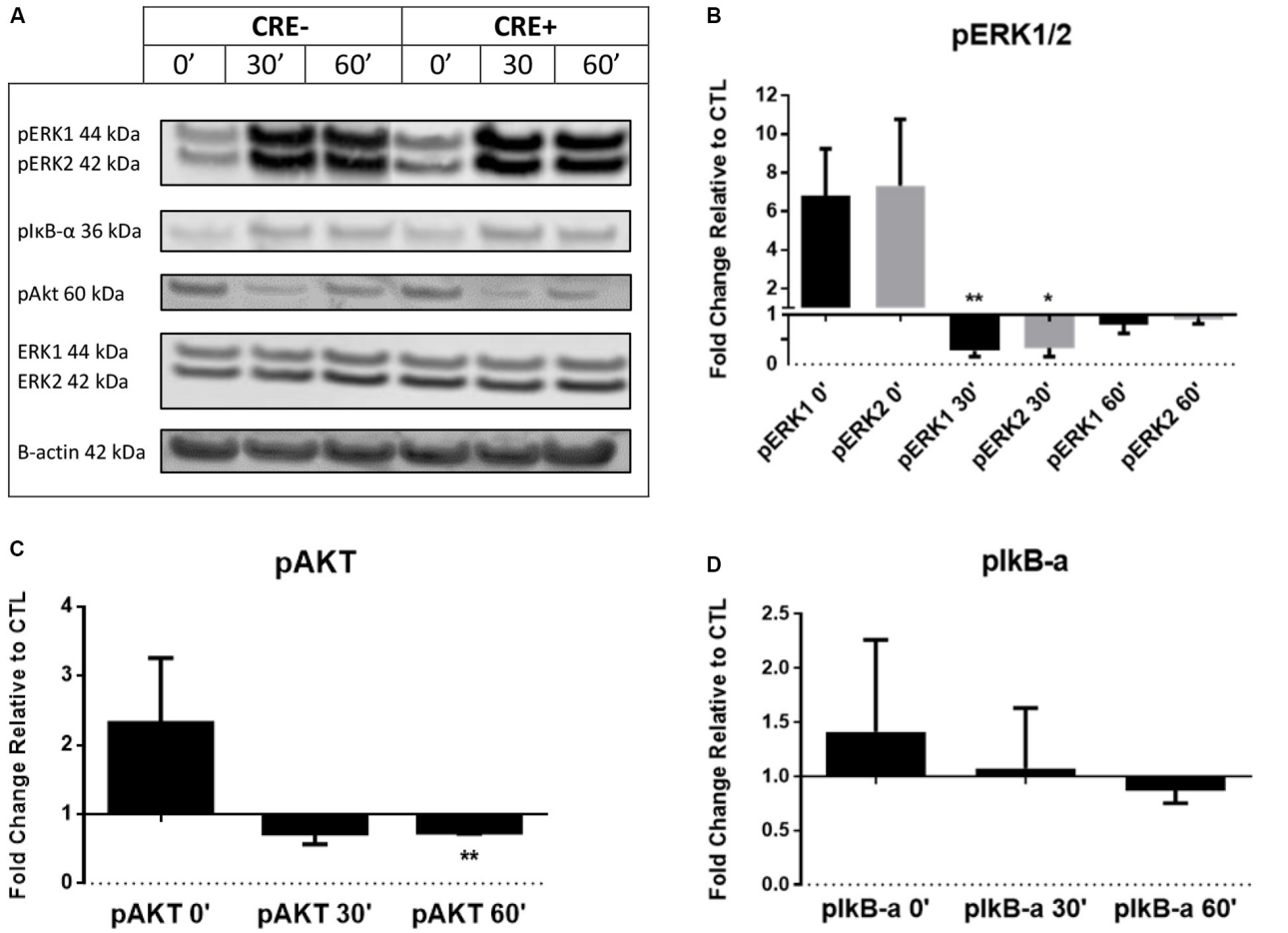

FIGURE 3 | BMDM from CHIT1-OE mice and control animals were treated with 20 ng/mL IFN-γ + 100 ng/mL LPS for 0, 0.5, and 1 h. **(A)** Cell lysates were incubated with florescent antibodies for phosphorylated signaling molecules and expression of phosphorylated proteins was analyzed by Western blotting. Florescence intensity was measured using the Licor Odyssey cLx. All bars represent fold change in densitometric, florescence intensity between CHIT1-OE BMDM and control BMDM. Florescence signal from Western blot of phosphorylated proteins: pIκB-α, pAkt, and pERK1/2 was normalized to control protein and then compared between groups. **(B)** Exposure to pro-inflammatory stimuli significantly depressed pERK1 and pERK2 signaling in CHIT1-OE BMDM after 0.5 h ($P = 0.0085$ and 0.0219 respectively). **(C)** pAkt signaling was significantly different between groups after 1 h when compared to control BMDM ($P = 0.0020$). **(D)** No significant results were obtained in protein expression of pIκB-α. $N = 3$, $^{*}P<0.05$, $^{**}P<0.01$.

from serial cryosections of the aortic sinus at 10 μm increments. **Figure 5C** depicts samples from each group that were incubated for 24 h with MOMA primary antibody and then and HRP conjugated chromogen was applied. MOMA is a macrophage specific stain and therefore, it was utilized to determine macrophage content and plaques. No significant difference was observed between groups after analyzing percent MOMA stained area relative to total plaque area (**Figure 5D**), $N = 7$.

CHIT1 Overexpression in Atherosclerotic Mice Does Not Affect Plaque Area

Areas of the cardiovascular system that are subject to high flow volumes and shear stress for vulnerable regions for the development of atherosclerotic plaque. The aortic sinus, aortic arch, and abdominal aorta are widely accepted as being indicative of atherosclerosis *in vivo*. In an effort to determine the effects of CHIT1 overexpression in $Ldlr^{-/-}$ mice, mouse hearts were perfused with 4% PFA/5% sucrose before being removed from the animal. Serial cryosections were prepared at a thickness of 10 μm. Samples from both groups were stained with ORO (**Figure 6A**). Plaque area was not significantly different in CHIT1-OE mice compared to littermate controls and quantification was performed using ImageJ software and measurements are represented as the percentage of stained area in relation to total sinus area. No significant differences in the area of ORO-stained lesion were observed between the control and the overexpressing mice (**Figure 6C**), $N = 14$.

To further analyze plaque content *in vivo* we also quantified plaque accumulation in the whole aorta. This was accomplished by cleaning and excision of the entire aorta from the aortic arch to the iliac bifurcation. An incision was made longitudinally along the length of the aorta such that it could be separated, pinned, and stained with ORO for 30 min (**Figure 6B**). Plaque

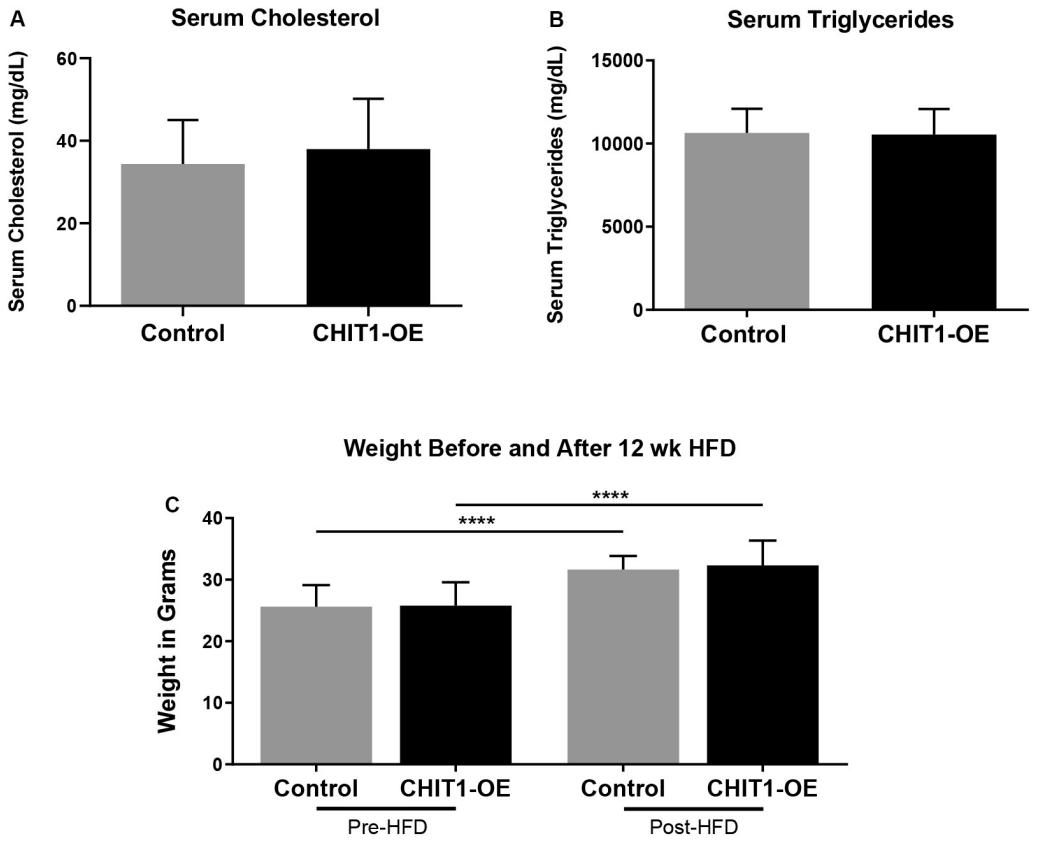

FIGURE 4 | (A,B) Measurements of serum cholesterol and triglyceride were taken after 12 weeks of HFD. Colorimetric and fluorometric analysis revealed no significant difference between control mice and CHIT1-OE mice. **(C)** Animals were weighed before and after initiation of HFD, which showed significant weight gain within groups over the 12 week period. However, animal weights were not significantly different when compared between CHIT1-OE and control groups ($P < 0.0001$). $N = 24$ (12 per group), $^{****}P < 0.0001$.

aggregation was measured with ImageJ software and results are represented as percentage of stained area in relation to total aortic area (**Figure 6D**). As with the aortic sinus lesions, there were no significant differences in the extent of lesion development on the inner surfaces of the aortas between the 2 groups (**Figure 5D**), $N = 14$.

CHIT1 Overexpression Alters ECM Content in the Aortic Sinus of *Ldlr*$^{-/-}$ Mice

At sacrifice, mice were perfused with PBS followed by 4% PFA/5% sucrose. The hearts were collected and embedded in OCT compound to be frozen and cryosectioned at a thickness of 10 μm. Serial sections were made at the aortic sinus where three valve leaflets were visible. The heart sections were stained for hyaluronic acid (HA) using a biotinylated hyaluronic acid binding protein (BHABP) and collagen using picrosirius red.

Our data show that the pattern of collagen and HA accumulation had observational differences in distribution between CHIT1-OE mice and littermate controls (**Figures 7A,C**). We found that collagen distribution in plaques from CHIT1-OE mice was most prevalent on the luminal aspect of atherosclerotic plaques and could be found encircling necrotic cores. Picrosirius red staining was significantly more abundant and saturated in CHIT1-OE mice. We also observed necrotic cores being densely surrounded by collagen fibers in aortic sinus sections from CHIT1-OE mice. These characteristics of collagen were not seen in littermate controls. From our *in vivo* analysis, we also determined that HA expression was generally limited to the periphery of atherosclerotic plaques in control mice, while in CHIT1-OE mice HA staining could be seen within almost all aspects of the plaque. Most notably, HA staining colocalized with necrotic regions of the atherosclerotic plaque in CHIT1-OE mice. Stained cryosections were analyzed using ImageJ software to quantify the area of HA and collagen deposition as a percentage of overall plaque area (**Figures 7B,D**). Both HA and collagen were significantly more abundant in CHIT1-OE mice. $N = 7$.

DISCUSSION

In previously published work, we reported that CHIT1 mRNA was present in atherosclerotic lesions within the descending aorta of cynomolgus monkeys. CHIT1 mRNA expression was also closely correlated with macrophage infiltration in

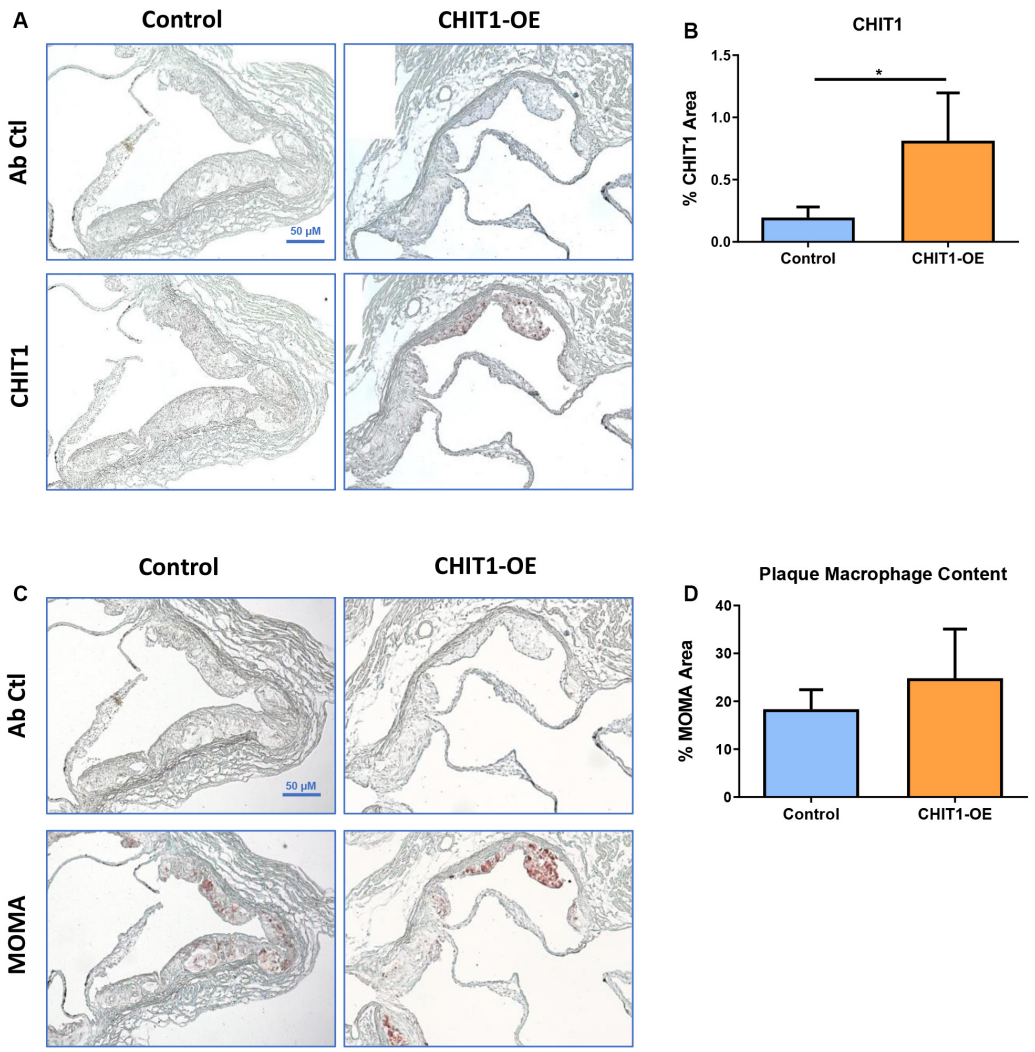

FIGURE 5 | (A) Cryosections of the aortic sinus from both CHIT1-OE mice and littermate controls after 12 weeks of HFD were stained with biotinylated antibodies against CHIT1. **(B)** Immunohistological staining for CHIT1 revealed significantly enhanced CHIT1 expression in the atherosclerotic plaques of CHIT1-OE mice when compared to control animals. Quantification represents stained area as a percentage of total plaque area ($P = 0.0101$). **(C)** Serial cryosections of the aortic sinuswere also stained with MOMA to determine macrophage content. **(D)** Analysis of stained area versus % total plaque area. Measurement with ImageJ software showed no significant differences in macrophage content between experimental and control animals ($P = 0.1982$). $N = 7$ per group, $^{*}P < 0.05$.

atherosclerotic plaques of abdominal aortas. Our research further demonstrated that inhibition of CHIT1 with allosamidin promoted atherosclerosis in hyperlipidemic mice (Kitamoto et al., 2013). Here we show *In vitro* evidence using CHIT1-OE macrophages that overexpression of CHIT1 modulates cytokine expression in an anti-inflammatory and migratory manner when subjected to an inflammatory stimulus of IFN-γ with LPS. A non-resolving inflammatory response promotes the development of atherosclerosis through continuous recruitment and activation of immune cells, perhaps most importantly, macrophages. As CHIT1 is abundantly produced by activated macrophages, it is likely that it's expression contributes to anti-inflammatory cell functions. In developing a $Ldl^{-/-}$- CHIT1-OE mouse model we were able to conduct an *in vivo* mouse study to investigate the effects of CHIT1 overexpression in an atherosclerotic animal model. While we were unable to observe significant differences in macrophage content or lesion size, we found significant alterations in plaque morphology. The accumulation and distribution of HA and collagen allude to a possible interaction between CHIT1 and the ECM.

Dysregulation of the innate immune response drives atherogenesis, and the resultant stages of atherosclerosis are largely attributable to the recruitment and infiltration of monocytes into the intimal layer of the vessel wall. Interestingly, we found protein expression of the chemotactic cytokine KC (the murine homolog of IL-8) is significantly upregulated in CHIT1-OE macrophages when treated with inflammatory stimuli. KC and its receptor CXCR2 are secreted by activated macrophages and play a significant role in immune cell trafficking and infiltration of the vessel wall. In an effort to

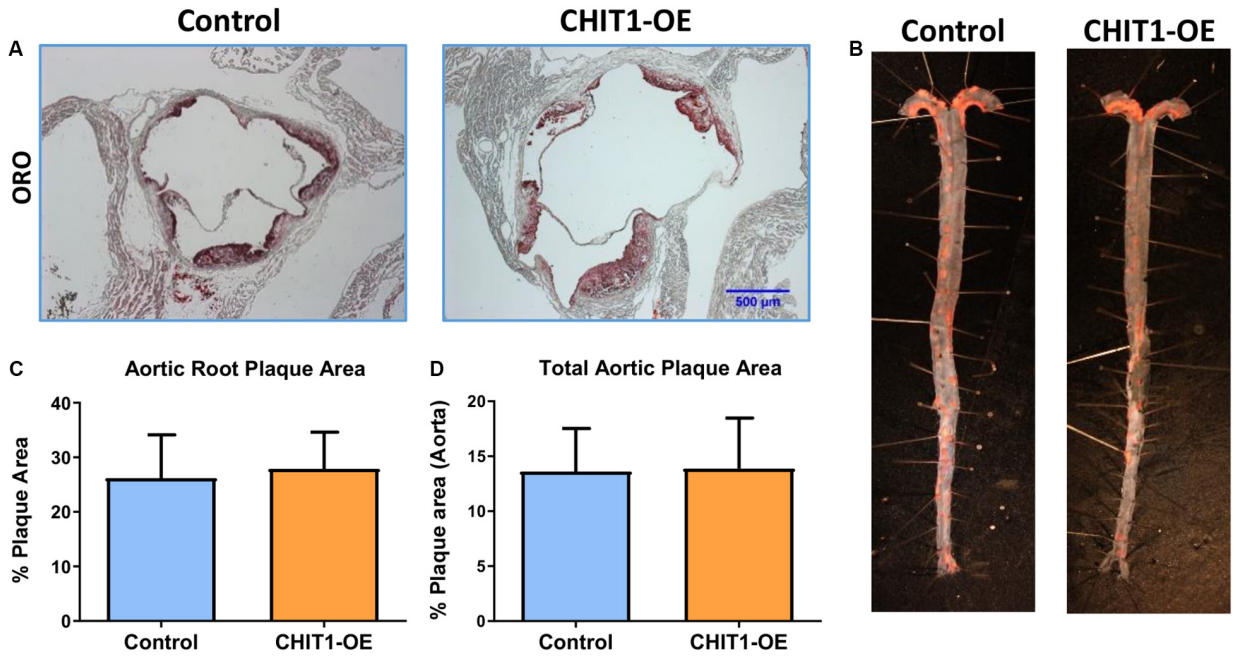

FIGURE 6 | (A) Cryosections of the aortic sinus from both CHIT1-OE (CRE+) mice and littermate controls (CRE-) after 12 weeks of HFD were stained with Oil-Red-O to determine plaque size. **(C)** Analysis of plaque area is represented as a function of % total area. Measurement with ImageJ software showed no significant differences in plaque size between experimental and control animals (P = 0.5399). **(B)** Whole aortas were removed from both CHIT1-OE and control mice after 12 weeks of HFD. The specimens were pinned and stained with Oil-Red-O. **(D)** No difference was observed between groups upon quantification of plaque area as a percentage of total aortic area (P = 0.8731). N = 14 per group.

elucidate the mechanism of KC/CXCR2 in atherosclerosis, Boisvert et al. utilized LDLR$^{-/-}$, atherosclerosis-prone mice with KC/GRO-α$^{-/-}$ and CXCR2$^{-/-}$ mice to demonstrate that overexpression of KC/GRO-α and CXCR2 are essential to macrophage accumulation into atherosclerotic lesions. Results also revealed that KC/GRO-α and CXCR2 do not play a critical role in macrophage recruitment into early atherosclerotic lesions (Boisvert et al., 2006). While it is generally accepted that KC participates in development of atherosclerosis, other studies suggest a putative role of IL-8/KC in smooth muscle cell proliferation and recruitment as well as angiogenesis (Yue et al., 1994; Boisvert et al., 1998; Simonini et al., 2000). IL-8 was shown to be a potent macrophage-derived mediator of angiogenesis. Human recombinant IL-8 was administered in the rat cornea where it induced proliferation and chemotaxis of human umbilical vein endothelial cells. Also, blockade of IL-8 by antibodies decreased angiogenic activity of inflamed human rheumatoid synovial tissue macrophages (Koch et al., 1992). Such findings suggest that IL-8 may be involved in tissue repair and wound healing.

IL-4 is a cytokine associated with alternative macrophage activation which potentiates Th2 inflammatory processes. We have demonstrated that IL-4 protein expression is significantly upregulated in CHIT1-OE BMDM. Experimental evidence demonstrates that IL-4 signaling involves SOCS1 to induce M2 macrophage polarization while inhibiting SOCS3 signaling and negatively regulating M1 polarization (Whyte et al., 2011; Qin et al., 2012). IL-4 activation of alveolar macrophages has been shown to promote wound healing in the long after Helmand invasion or during gut inflammation in mice (Bosurgi et al., 2017). And in the context of atherosclerosis, IL-4 attenuated atherosclerosis in several different mouse models (George et al., 2000; King et al., 2002; Davenport and Tipping, 2003). Given that IL-4 and IL-13 signaling includes a pathway requiring both cytokines, and the putative interactions of CHIT1 with IL-13, it is foreseeable that CHIT1 can participate in IL-4/IL-13 signal transduction.

A definitive role for macrophage-derived granulocyte colony stimulating factor (G-CSF) in atherosclerosis has yet to be established. However, several studies suggest protective roles for G-CSF in atherosclerotic animal models. We observed a significant increase in protein expression of G-CSF in BMDM harvested from CHIT1-OE mice compared to WT controls. Experiments with human peripheral blood mononuclear cells (PBMC) illustrated that G-CSF post-transcriptionally inhibits TNF-α secretion from PBMC. Suppression of TNF-α secretion was accomplished without affecting mRNA expression (Kitabayashi et al., 1995). G-CSF also promotes generation of type-1 regulatory T cells (Treg) that secrete the anti-inflammatory cytokine IL-10, and TGF-β1 which is associated with tissue repair, wound healing, and fibrosis (Rutella et al., 2004). Several studies have described a protective role for G-CSF in atherosclerotic mouse and rabbit models. Daily treatment of ApoE deficient mice with G-CSF for 9 weeks resulted in less atheromatous plaque area and a decrease in macrophage infiltration into atherosclerotic lesions. The authors

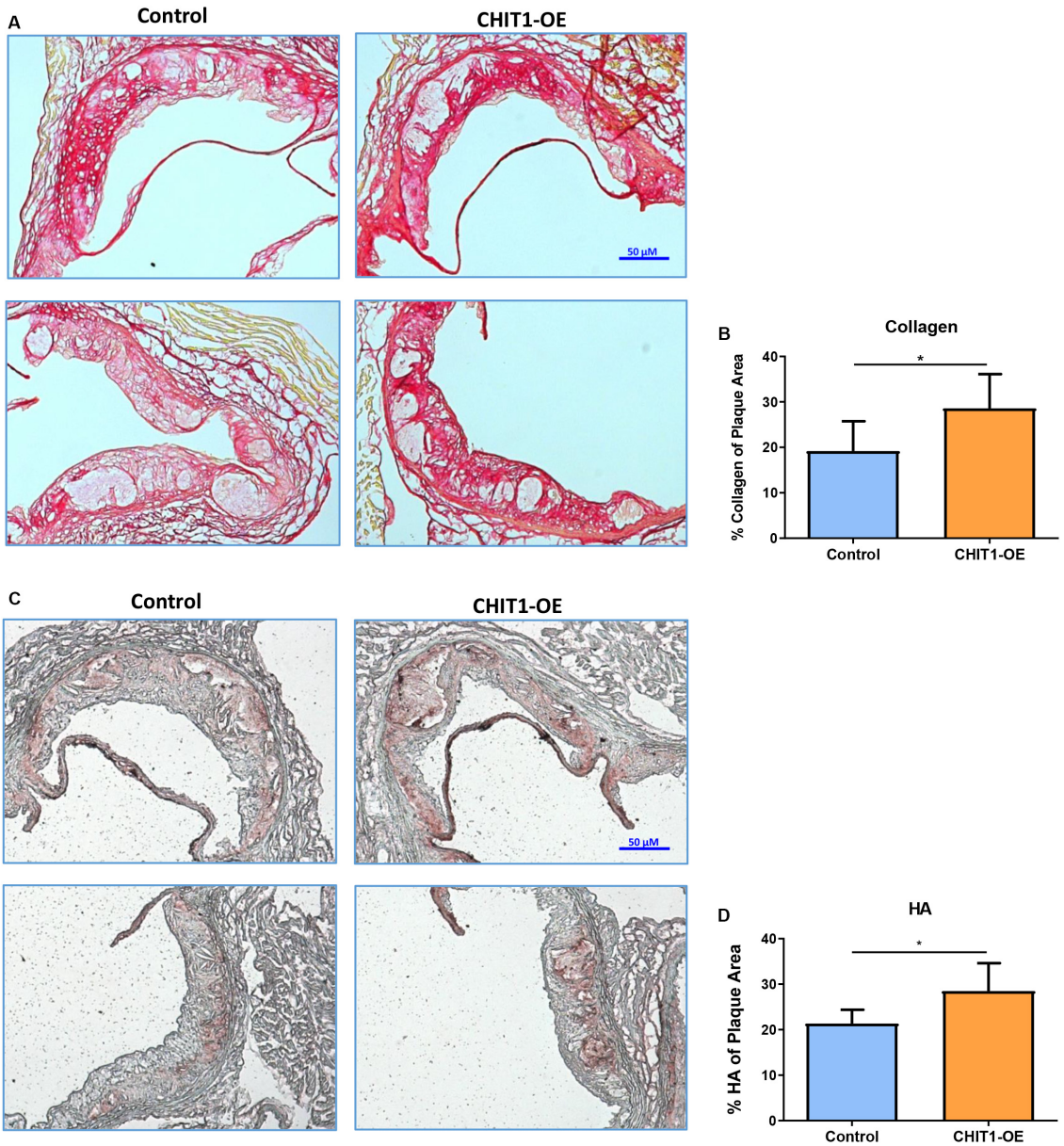

FIGURE 7 | (A) Cryosections of the aortic sinus from both CHIT1-OE mice and littermate controls after 12 weeks of HFD were stained with picrosirius red to visualize type I collagen. While collagen appears unorganized and lightly stained, especially on the luminal aspect of necrotic cores in control sections, collagen observed in CHIT1-OE mice presented a more organized "lattice" appearance and was distributed around necrotic cores and specifically on the luminal aspect. **(B)** Quantification of picrosirius red as a percentage of total plaque area exhibited significantly more collagen deposition in CHIT1-OE mice compared to littermate controls ($P = 0.0289$). **(C)** HA stained with BHABP can be seen localized in the periphery of the aortic sinus in control cryosections, whereas HA appears throughout the plaque and within the necrotic cores of CHIT1-OE. HA is extensively visible in plaques of CHIT1-OE mice. Interestingly, HA appears to accumulate within the acellular necrotic core regions. **(D)** Analysis of BHABP staining revealed significantly greater HA content in the aortic sinus of CHIT1-OE mice compared to littermate controls ($P = 0.0370$). $^*P < 0.05$, $N = 7$ per group.

also observed decreased serum cholesterol and LDL, which is suggestive of lipid-related effects of G-CSF (Sinha et al., 2014). In hyperlipidemic and cholesterol fed rabbit models, G-CSF administration prevented progression of atherosclerotic lesions and vascular stenosis, while encouraging plaque stability and reendothelialization. Moreover, it was shown that an appropriate dosage of G-CSF was required for these protective effects to manifest most efficiently (Hasegawa et al., 2006; Matsumoto et al., 2010).

To extend our understanding of the inflammatory mechanisms affected by CHIT1 overexpression, we investigated inflammatory signaling pathways associated with atherosclerosis. Our data revealed significant decrease in pERK1/2 protein expression in BMDM from CHIT1-OE mice compared to

littermate controls when exposed to IFN-γ + LPS after 30 min *in vitro*. We also observed that Akt signaling was suppressed in CHIT1-OE BMDM after 60 min of treatment with the same inflammatory stimuli *in vitro*. The ERK1/2 signaling pathway is critical to the expression and secretion of various downstream effectors that mediate inflammation. Experimental evidence demonstrates that LPS stimulation of murine peritoneal macrophages activated ERK1/2 signaling, causing the subsequent induction of TNF-α secretion (Dumitru et al., 2000). IFN-γ stimulation of this pathway in human macrophages induced alterations in the expression of several key genes implicated in the progression of atherosclerosis, such as MCP-1 (Li et al., 2010). Akt signaling has various roles in macrophage function. Deficiency of Akt mediated signal transduction elicits M2 macrophage polarization and negative regulation of the TLR4 signaling pathway (Taganov et al., 2006; Chassin et al., 2010; Li et al., 2015). In relation to atherosclerosis, Zhai et al. (2014) found that inhibition of Akt signaling depressed autophagy *in vitro*, and atherosclerotic mouse models exhibited enhanced plaque stability as well as diminished inflammatory response was promoted by Akt/mTOR-mediated autophagy. As it pertains to ECM content, both ERK1/2 and Akt signaling are involved in the turnover of HA and collagen. The hyaluronic acid receptor (CD44) is a macrophage cell surface receptor responsible for the recognition and phagocytosis of HA. Activation of ERK1/2 and Akt signaling pathways by CD44 results in degradation of HA by hyaluronidase (Culty et al., 1992; Stern and Jedrzejas, 2006; Vachon et al., 2006). Activation of these pathways has also been shown to enhance collagen degradation by matrix metalloproteinases (Cho et al., 2008).

The ECM is an important component for a wide array of cellular functions. In the cardiovascular system, ECM interactions serve as a cell signaling platform and maintain structural integrity of the heart and vasculature. Changes in ECM content related to atherosclerosis has been implicated in fibrous cap formation and plaque stability. Our results demonstrate a significant increase in key ECM components: hyaluronic acid (HA) and collagen in the plaques *CHIT1-OE* mice when compared to littermate controls. HA is a large, hydrophilic glycosaminoglycan (GAG) that is integral to wound healing and tissue remodeling (Litwiniuk et al., 2016). HA catabolism is carried out by enzymes known as hyaluronidases (Hyal) which hydrolyze β(1-4) glycosidic bonds between the alternating moieties of D-glucoronic acid and *N*-acetyl-D-glucosamine. Cleavage of these linkages results in a polydisperse range of HA chain length (Stern and Jedrzejas, 2006). Hyal1 is found in the heart and its expression is dependent on activation of the CD44, cell surface receptor and the subsequent initiation of ERK1/2 and Akt signaling (Gee et al., 2002; Vachon et al., 2006; Harada and Takahashi, 2007; Misra et al., 2015). Degradation of HA by hyaluronidases is upregulated in unstable atherosclerotic plaques, while the formation of a pericellular HA matrix supports smooth muscle cell proliferation and migration possibly enhancing plaque stability (Evanko et al., 1999; Bot et al., 2010). It should be noted that no endogenous substrate for CHIT1 has been identified in vertebrates. However, studies have demonstrated that the DG42 gene in Xenopus and mouse models produces chitin-oligosaccharides as a precursor to HA chains (Meyer and Kreil, 1996; Semino et al., 1996). Also, due to the structural similarity of HA to its native substrate; chitin, the CHIT1 binding domain is capable of interactions with HA (Ujita et al., 2003; Crasson et al., 2017). It may be possible that chitin interactions with HA prevent its degradation, thereby promoting plaque stability.

Like HA, collagen contributes to the mechanical strength of atheromatous plaques. Collagen comprises up to 60% of the total plaque protein and engages a multitude of cell functions. Modulation of macrophage behavior, smooth muscle cell proliferation/migration, and plaque reinforcement exemplify the variety of functions and cell types that collagen can influence (Koyama et al., 1996; Rocnik et al., 1998; Wesley et al., 1998). CHIT1 has also been implicated in collagen production as evidenced by fibrotic diseases in the liver and lungs. Interstitial lung disease with pulmonary fibrosis is representative of pulmonary systemic sclerosis. CHIT1$^{-/-}$ murine models demonstrate reduced fibrosis, and *in vitro* studies showed that CHIT1 interactions with TGF-β1 augment the expression of both TGF-β 1 and 2 receptors and subsequent TGF-β-induced ERK activation (Lee et al., 2012). Human Kupffer cells were also implemented to investigate the role of CHIT1 in nonalcoholic steatohepatitis. This data highlighted the ability of CHIT1 to activate hepatic stellate cells which, in turn, results in the overproduction of collagen and ultimately hepatic fibrosis (Malaguarnera et al., 2006). Collagen degradation occurs by the action of matrix metalloproteinases (MMP) and several studies have demonstrated the presence and proteolytic activity of MMPs in vulnerable atherosclerotic plaques (Newby, 2008; Newby et al., 2009; Jabłońska-Trypuć et al., 2016).

In our assessment of plaque morphology, despite having no difference in macrophage content or size, collagen and hyaluronic acid deposition was markedly different between experimental and control animals. *CHIT1-OE* mice displayed hyaluronic acid staining throughout the plaque and around necrotic cores, whereas aortic sections from control mice showed accumulation of hyaluronic acid around the periphery of the vessel. Collagen staining revealed substantial accumulation on the luminal aspect of necrotic cores in CHIT1-OE animals. In contrast, collagen distribution in control animals did not show any particular patterning in atherosclerotic plaques. Taken together, overexpression of CHIT1 by macrophages augments ECM biosynthesis and organization in such a way that enhances plaque stability in ldlr$^{-/-}$ mouse models.

The data presented here suggest a novel, nonenzymatic role for CHIT1 in inflammation and atherosclerosis. Results generated from this work demonstrate that, *in vitro,* CHIT1 modulates macrophage transcription and protein expression of chemokines and cytokines that are central to inflammation and atherosclerosis. We also provide evidence of alterations in macrophage cells signaling pathways. And lastly, analysis of aortic sinus cryosections exhibit significant differences in prevalence of HA and collagen as well as localized distribution between control mice and *CHIT1-OE* mice. As mentioned before, various studies have demonstrated nonenzymatic interactions involving CHIT1, inflammation, and tissue repair. Given our

results, it is possible that CHIT1 influences macrophage behavior in such a way that is atheroprotective in mitigating inflammation and enhancing plaque stability.

LIMITATIONS

Although we have described a putative role for CHIT1 as it pertains to plaque stability, our experimentation did not include several key aspects that could further validate our findings. For example, future studies should focus on interaction between CHIT1 and HA (both structurally and metabolically), quantifying fibrous cap thickness and smooth muscle cell content, a measure of plaque vulnerability/stability index, and histological examination of other organs that are prone to fibrosis.

DATA AVAILABILITY STATEMENT

All datasets generated for this study are included in the article/supplementary material.

ETHICS STATEMENT

The animal study was reviewed and approved by the University of Hawaii IACUC.

AUTHOR CONTRIBUTIONS

JY, SM, SK, B-HL, and WB contributed to the conception and design of the study. MA and SK contributed to biochemical analysis of samples. JY, SM, WR, JG, and JI contributed to the design and application of experimental procedures. SM and SK contributed to statistical analysis. JY wrote the first draft of the manuscript. SM, SK, and WB wrote sections of the manuscript. All authors contributed to manuscript revisions, read, and approved the submitted version.

FUNDING

This research was supported by the Chung-Ang University Research Grants in 2019, and by American Heart Association grant 16GRNT30810007 to WB. JY was supported by NIH grant 1F31HL139082.

ACKNOWLEDGMENTS

We thank Monica Montgomery for her excellent technical support. Parts of this manuscript were adapted from my original dissertation produced and published in conjunction with the University of Hawaii at Manoa (Yap, 2019).

REFERENCES

Artieda, M., Cenarro, A., Gañán, I., Jericó, C., Gonzalvo, M., Casado, I., et al. (2003). Serum chitotriosidase activity is increased in subjects with Atherosclerosis Disease. *Arterioscler. Thromb. Vasc. Biol.* 23, 1645–1652. doi: 10.1161/01.atv.0000089329.09061.07

Boisvert, W. A., Rose, K. A., Johnson, M. E., Fuentes, S. A., Lira, L. K., Curtiss, R. A., et al. (2006). Up-regulated expression of the CXCR2 ligand KC/GRO-alpha in atherosclerotic lesions plays a central role in macrophage accumulation and lesion progression. *Am. J. Pathol.* 168, 1385–1395. doi: 10.2353/ajpath.2006.040748

Boisvert, W. A., Santiago, L. K., Curtiss, L., and Terkeltaub, R. (1998). A leukocyte homologue of the IL-8 receptor CXCR-2 mediates the accumulation of macrophages in atherosclerotic lesions of LDL receptor-deficient mice. *J. Clin. Invest.* 101, 353–363. doi: 10.1172/jci1195

Bosurgi, L., Cao, M., Cabeza-Cabrerizo, A., Tucci, L. D., Hughes, Y., Kong, J. S., et al. (2017). Macrophage function in tissue repair and remodeling requires IL-4 or IL-13 with apoptotic cells. *Science* 356:1072. doi: 10.1126/science.aai8132

Bot, P. T., Pasterkamp, M.-J., Goumans, C., Strijder, F. L., Moll, J.-P., De Vries, S. T., et al. (2010). Hyaluronic acid metabolism is increased in unstable plaques. *Eur. J. Clin. Invest.* 40, 818–827. doi: 10.1111/j.1365-2362.2010.02326.x

Chassin, C., Kocur, J., Pott, C. U., Duerr, D., Gutle, M., and Lotz, P. (2010). miR-146a mediates protective innate immune tolerance in the neonate intestine. *Cell Host Microbe* 8, 358–368. doi: 10.1016/j.chom.2010.09.005

Cho, S. J., Chae, B. K., Shin, H. K., Kim, R., and Kim, A. (2008). Akt- and MAPK-mediated activation and secretion of MMP-9 into stroma in breast cancer cells upon heregulin treatment. *Mol. Med. Rep.* 1, 83–88.

Crasson, O., Courtade, R. R., Léonard, F. L., Aachmann, F., Legrand, R., Parente, D., et al. (2017). Human chitotriosidase: catalytic domain or carbohydrate binding module, who's leading HCHT's biological function. *Sci. Rep.* 7: 2768.

Culty, M., Nguyen, H., and Underhill, C. B. (1992). The hyaluronan receptor (CD44) participates in the uptake and degradation of hyaluronan. *J. Cell Biol.* 116, 1055–1062. doi: 10.1083/jcb.116.4.1055

Davenport, P., and Tipping, P. G. (2003). The role of interleukin-4 and interleukin-12 in the progression of atherosclerosis in apolipoprotein E-deficient mice. *Am J. Pathol.* 163, 1117–1125. doi: 10.1016/s0002-9440(10)63471-2

Dumitru, C. D., Ceci, C., Tsatsanis, D., Kontoyiannis, K., Stamatakis, J.-H., Lin, C., et al. (2000). TNF-α induction by LPS Is regulated posttranscriptionally via a Tpl2/ERK-dependent pathway. *Cell* 103:1071–1083.

Evanko, S. P., Angello, J., and Thomas, N. (1999). Formation of hyaluronan- and versican-rich pericellular matrix is required for proliferation and migration of vascular smooth muscle cells. *Arterioscler. Thromb. Vasc. Biol.* 19, 1004–1013. doi: 10.1161/01.atv.19.4.1004

Fach, E. M., Garulacan, J., Gao, Q., Xiao, S. M., Storm, Y. P., Dubaquie, S. A., et al. (2004). In vitro biomarker discovery for atherosclerosis by proteomics. *Mol Cell Proteomics* 3, 1200–1210.

Gee, K., Lim, W., Ma, D., Nandan, F., Diaz-Mitoma, M., and Kozlowski, P. (2002). Differential regulation of CD44 expression by lipopolysaccharide (LPS) and TNF-α in human monocytic cells: distinct involvement of c-Jun N-Terminal Kinase in LPS-Induced CD44 Expression. *J. Immunol.* 169, 5660–5672. doi: 10.4049/jimmunol.169.10.5660

George, J., Shoenfeld, B., Gilburd, A., Afek, A., Shaish, H., and Harats, D. (2000). Requisite role for interleukin-4 in the acceleration of fatty streaks induced by heat shock protein 65 or Mycobacterium tuberculosis. *Circ. Res.* 86, 1203–1210. doi: 10.1161/01.res.86.12.1203

Harada, H., and Takahashi, M. (2007). CD44-dependent intracellular and extracellular catabolism of hyaluronic acid by hyaluronidase-1 and -2. *J. Biol Chem.* 282, 5597–5607. doi: 10.1074/jbc.m608358200

Hasegawa, H., Takano, M., Ohtsuka, K., Ueda, Y., Niitsuma, Y., Qin, H., et al. (2006). G-CSF prevents the progression of atherosclerosis and neointimal formation in rabbits. *Biochem. Biophys. Res. Commun.* 344, 370–376. doi: 10.1016/j.bbrc.2006.03.081

Jabłońska-Trypuć, A., Matejczyk, M., and Rosochacki, S. (2016s). Matrix metalloproteinases (MMPs), the main extracellular matrix (ECM) enzymes in collagen degradation, as a target for anticancer drugs. *J. Enzyme. Inhib. Med. Chem.* 31, 177–183. doi: 10.3109/14756366.2016.1161620

Karadag, B., Kucur, F. K., Isman, M., Hacibekiroglu, M., and Vural, V. A. (2008). Serum chitotriosidase activity in patients with coronary artery disease. *Circ. J.* 72, 71–75. doi: 10.1253/circj.72.71

King, V. L., Szilvassy, S., and Daugherty, A. (2002). Interleukin-4 deficiency decreases atherosclerotic lesion formation in a site-specific manner in female LDL receptor-/- mice. *Arterioscler. Thromb. Vasc. Biol.* 22, 456–461. doi: 10.1161/hq0302.104905

Kitabayashi, A., Hirokawa, Y., Hatano, M., Lee, J., Kuroki, H., and Niitsu, P. (1995). Granulocyte colony-stimulating factor downregulates allogeneic immune responses by posttranscriptional inhibition of tumor necrosis factor-alpha production. *Blood* 86, 2220–2227. doi: 10.1182/blood.v86.6.2220.bloodjournal8662220

Kitamoto, S., Egashira, T., Ichiki, X., Han, S., McCurdy, S., Sakuda, K., et al. (2013). Chitinase inhibition promotes atherosclerosis in hyperlipidemic mice. *Am. J. Pathol.* 183, 313–325. doi: 10.1016/j.ajpath.2013.04.003

Koch, A. E., Polverini, S. L., Kunkel, L. A., Harlow, L. A., DiPietro, V. M., Elner, S. G., et al. (1992). Interleukin-8 as a macrophage-derived mediator of angiogenesis. *Science* 258, 1798–1801. doi: 10.1126/science.1281554

Koyama, H., Raines, K. E., Bornfeldt, J. M., Roberts, M., and Ross, R. (1996). Fibrillar collagen inhibits arterial smooth muscle proliferation through regulation of Cdk2 inhibitors. *Cell* 87, 1069–1078. doi: 10.1016/s0092-8674(00)81801-2

Lee, C. G., Herzog, F., Ahangari, Y., Zhou, M., Gulati, C.-M., Lee, X., et al. (2012). Chitinase 1 is a biomarker for and therapeutic target in scleroderma-associated interstitial lung disease that augments TGF-β1 signaling. *J. Immunol.* 189, 2635–2644. doi: 10.4049/jimmunol.1201115

Li, N., McLaren, D. R., Michael, M., Clement, C. A., Fielding, M., and Ramji, D. (2010). ERK is integral to the IFN-γ–mediated activation of STAT1, the expression of key genes implicated in atherosclerosis, and the uptake of modified lipoproteins by human macrophages. *J. Immunol.* 185, 3041–3081.

Li, Y., Zhao, B., Shi, S., Ma, Z., Xu, Y., Ge, Y., et al. (2015). Functions of miR-146a and miR-222 in tumor-associated macrophages in breast cancer. *Sci. Rep.* 5:18648.

Litwiniuk, M., Krejner, M. S., Speyrer, A. R., Gauto, A., and Grzela, T. (2016). Hyaluronic acid in inflammation and tissue regeneration. *Wounds* 28, 78–88.

Malaguarnera, L., Di Rosa, A. M., Zambito, N., dell'Ombra, F., Nicoletti, K., and Malaguarnera, M. (2006). Chitotriosidase gene expression in Kupffer cells from patients with non-alcoholic fatty liver disease. *Gut* 55, 1313–1320. doi: 10.1136/gut.2005.075697

Matsumoto, T., Watanabe, T., Ueno, A., Tsunemi, B., Hatano, Y., Kusumi, M., et al. (2010). Appropriate doses of granulocyte-colony stimulating factor reduced atherosclerotic plaque formation and increased plaque stability in cholesterol-fed rabbits. *J. Atheroscler. Thromb.* 17, 84–96. doi: 10.5551/jat.2279

Meyer, M. F., and Kreil, G. (1996). Cells expressing the DG42 gene from early Xenopus embryos synthesize hyaluronan. *Proc. Natl. Acad. Sci. U.S.A.* 93, 4543–4547. doi: 10.1073/pnas.93.10.4543

Misra, S., Hascall, R. R., Markwald, C., and Ghatak, S. (2015). Interactions between hyaluronan and its receptors (CD44, RHAMM) regulate the activities of inflammation and cancer. *Front. Immunol.* 6:201. doi: 10.3389/fimmu.2015.00201

Newby, A. C. (2008). Metalloproteinase expression in monocytes and macrophages and its relationship to atherosclerotic plaque instability. *Arterioscler. Thromb. Vasc. Biol.* 28, 2108–2114. doi: 10.1161/atvbaha.108.173898

Newby, A. C., George, Y., Ismail, J. L., Johnson, G. B., Sala-Newby, R., and Thomas, A. C. (2009). Vulnerable atherosclerotic plaque metalloproteinases and foam cell phenotypes. *Thromb. Haemost.* 101, 1006–1011. doi: 10.1160/th08-07-0469

Qin, H., Holdbrooks, Y., Liu, S. L., Reynolds, L. L., Yanagisawa, P., and Benveniste, E. N. (2012). SOCS3 deficiency promotes M1 macrophage polarization and inflammation. *J. Immunol.* 189, 3439–3448. doi: 10.4049/jimmunol.1201168

Renkema, G. H., Boot, A., Strijland, W. E., Donker-Koopman, L., van den Berg, A. O., and Muijsers, R. (1997). Synthesis, sorting, and processing into distinct isoforms of human macrophage chitotriosidase. *Eur. J. Biochem.* 244, 279–285. doi: 10.1111/j.1432-1033.1997.00279.x

Renkema, G. H., Boot, A. O., Muijsers, W. E., Donker-Koopman, L., and Aerts, J. M. (1995). Purification and characterization of human chitotriosidase, a novel member of the chitinase family of proteins. *J. Biol. Chem.* 270, 2198–2202. doi: 10.1074/jbc.270.5.2198

Rocnik, E. F., Chan, B. M., and Pickering, J. G. (1998). Evidence for a role of collagen synthesis in arterial smooth muscle cell migration. *J. Clin. Invest.* 101, 1889–1898. doi: 10.1172/jci1025

Rutella, S., Bonanno, L., Pierelli, A., Mariotti, E., Capoluongo, A. M., Contemi, F., et al. (2004). Granulocyte colony-stimulating factor promotes the generation of regulatory DC through induction of IL-10 and IFN-α. *Eur. J. Immunol.* 34, 1291–1302. doi: 10.1002/eji.200324651

Semino, C. E., Specht, A., Raimondi, B., and Robbins, P. W. (1996). Homologs of the Xenopus developmental gene DG42 are present in zebrafish and mouse and are involved in the synthesis of Nod-like chitin oligosaccharides during early embryogenesis. *Proc. Natl. Acad. Sci. U.S.A.* 93, 4548–4553. doi: 10.1073/pnas.93.10.4548

Simonini, A., Moscucci, W. M., Muller David, R., Bates Eric, D., Pagani Francis, D., and Burdick, M. (2000). IL-8 Is an angiogenic factor in human coronary atherectomy tissue. *Circulation* 101, 1519–1526. doi: 10.1161/01.cir.101.13.1519

Sinha, S. K., Mishra, S., Nagwani, S., and Rajavashisth, T. (2014). Effects of G-CSF on serum cholesterol and development of atherosclerotic plaque in apolipoprotein E-deficient mice. *Int. J. Clin. Exp. Med.*7, 1979–1989.

Stern, R., and Jedrzejas, M. (2006). Hyaluronidases: their genomics, structures, and mechanisms of action. *Chem. Rev.* 106, 818–839. doi: 10.1021/cr050247k

Taganov, K. D., Boldin, K.-J., Chang, M., and Baltimore, D. (2006). NF-κB-dependent induction of microRNA miR-146, an inhibitor targeted to signaling proteins of innate immune responses. *Proc. Natl. Acad. Sci. U.S.A.* 103:12481. doi: 10.1073/pnas.0605298103

Tharanathan, R. N., and Kittur, F. S. (2003). Chitin–the undisputed biomolecule of great potential. *Crit. Rev. Food Sci. Nutr.* 43, 61–87. doi: 10.1080/10408690390826455

Ujita, M., Sakai, K., Hamazaki, M., Yoneda, S., Isomura, D., and Hara, A. (2003). Carbohydrate binding specificity of the recombinant chitin-binding domain of human macrophage chitinase. *Biosci. Biotechnol. Biochem.* 67, 2402–2407. doi: 10.1271/bbb.67.2402

Vachon, E., Martin, J., Plumb, V., Kwok, R. W., Vandivier, M., Glogauer, A., et al. (2006). CD44 is a phagocytic receptor. *Blood* 107, 4149–4158. doi: 10.1182/blood-2005-09-3808

Wesley, R. B., Meng, D., Godin, L., and Galis, S. (1998). Extracellular matrix modulates macrophage functions characteristic to atheroma: collagen type I enhances acquisition of resident macrophage traits by human peripheral blood monocytes in vitro. *Arterioscler. Thromb. Vasc. Biol.* 18, 432–440. doi: 10.1161/01.atv.18.3.432

Whyte, C. S., Bishop, D., Rückerl, S., Gaspar-Pereira, R. N., Barker, J. E., Allen, A. J., et al. (2011). Suppressor of cytokine signaling (SOCS)1 is a key determinant of differential macrophage activation and function. *J. Leukoc. Biol.* 90, 845–854. doi: 10.1189/jlb.1110644

Yap, J. (2019). *Overexpression of Chitotriosidase-1 Modulates Macrophage Function and Alters Plaque Morphology in Hyperlipidemic Mice. 2019*. Ann Arbor, MI: University of Hawai'i at Manoa, 89.

Yue, T. L., Wang, C. P., Sung, B., Olson, P. J., McKenna, J. L., Gu, P., et al. (1994). Interleukin-8. A mitogen and chemoattractant for vascular smooth muscle cells. *Circ. Res.* 75, 1–7. doi: 10.1161/01.res.75.1.1

Zhai, C., Cheng, H., Mujahid, H., Wang, J., Kong, Y., Yin, J., et al. (2014). Selective inhibition of PI3K/Akt/mTOR signaling pathway regulates autophagy of macrophage and vulnerability of atherosclerotic plaque. *PLoS One* 9:e90563. doi: 10.1371/journal.pone.0090563

Conflict of Interest: The authors declare that the research was conducted in the absence of any commercial or financial relationships that could be construed as a potential conflict of interest.

frontiers in Physiology

REVIEW
published: 07 July 2020
doi: 10.3389/fphys.2020.00793

Small Things Matter: Relevance of MicroRNAs in Cardiovascular Disease

Linsey J. F. Peters[1,2,3,4], Erik A. L. Biessen[1,2], Mathias Hohl[5], Christian Weber[4,6,7,8†], Emiel P. C. van der Vorst[1,2,3,4,6†] and Donato Santovito[4,6†]*

[1] Institute for Molecular Cardiovascular Research, RWTH Aachen University, Aachen, Germany, [2] Department of Pathology, Cardiovascular Research Institute Maastricht, Maastricht University Medical Centre, Maastricht, Netherlands, [3] Interdisciplinary Center for Clinical Research, RWTH Aachen University, Aachen, Germany, [4] German Centre for Cardiovascular Research, Partner Site Munich Heart Alliance, Munich, Germany, [5] Klinik für Innere Medizin III, Universität des Saarlandes, Homburg, Germany, [6] Institute for Cardiovascular Prevention, Ludwig-Maximilians-University Munich, Munich, Germany, [7] Department of Biochemistry, Cardiovascular Research Institute Maastricht, Maastricht University Medical Centre, Maastricht, Netherlands, [8] Munich Cluster for Systems Neurology, Munich, Germany

OPEN ACCESS

Edited by:
Silvia Fischer, University of Giessen, Germany

Reviewed by:
Christoph Lipps, University Hospital of Giessen and Marburg, Germany
Kerstin Troidl, Max Planck Institute for Heart and Lung Research, Germany

***Correspondence:**
Christian Weber
Christian.Weber@med.uni-muenchen.de

†*These authors share last authorship*

Specialty section:
This article was submitted to Vascular Physiology, a section of the journal Frontiers in Physiology

Received: *28 April 2020*
Accepted: *15 June 2020*
Published: *07 July 2020*

Citation:
Peters LJF, Biessen EAL, Hohl M, Weber C, van der Vorst EPC and Santovito D (2020) Small Things Matter: Relevance of MicroRNAs in Cardiovascular Disease. Front. Physiol. 11:793. doi: 10.3389/fphys.2020.00793

MicroRNAs (miRNAs) are short sequences of non-coding RNA that play an important role in the regulation of gene expression and thereby in many physiological and pathological processes. Furthermore, miRNAs are released in the extracellular space, for example in vesicles, and are detectable in various biological fluids, such as serum, plasma, and urine. Over the last years, it has been shown that miRNAs are crucial in the development of several cardiovascular diseases (CVDs). This review discusses the (patho)physiological implications of miRNAs in CVD, ranging from cardiovascular risk factors (i.e., hypertension, diabetes, dyslipidemia), to atherosclerosis, myocardial infarction, and cardiac remodeling. Moreover, the intriguing possibility of their use as disease-specific diagnostic and prognostic biomarkers for human CVDs will be discussed in detail. Finally, as several approaches have been developed to alter miRNA expression and function (i.e., mimics, antagomirs, and target-site blockers), we will highlight the miRNAs with the most promising therapeutic potential that may represent suitable candidates for therapeutic intervention in future translational studies and ultimately in clinical trials. All in all, this review gives a comprehensive overview of the most relevant miRNAs in CVD and discusses their potential use as biomarkers and even therapeutic targets.

Keywords: microRNAs, cardiovascular diseases, cardiovascular risk factors, atherosclerosis, myocardial infarction, cardiac remodeling, therapy, biomarker

INTRODUCTION

MicroRNAs (miRNAs) are short sequences (∼22 nucleotides) of endogenous non-coding RNA that emerged as a class of negative post-transcriptional regulators of gene expression. Hundreds of different miRNAs have been identified in humans with many of them showing highly conserved sequences and preferential target transcripts across species (Kozomara and Griffiths-Jones, 2014). The post-transcriptional regulation mediated by miRNAs takes place in the RNA-induced silencing

complex (RISC), a macromolecular complex where miRNAs loaded into the protein Argonaute-2 (AGO2) interact with the 3′untranslated region (3′UTR) of target RNAs. This interaction allows the recruitment of multiple additional proteins (e.g., TNRC6, PABPC) which favor decay of target RNAs or inhibition of their translation, hence realizing the negative regulation of gene expression (Bartel, 2018). Additionally, some specific miRNAs (e.g., miR-126-5p) have recently been shown to operate also through uncanonical mechanisms which contribute to their ultimate effects on cellular homeostasis and function (Dragomir et al., 2018; Santovito et al., 2020a). As a class, miRNAs are able to regulate the expression of multiple effectors playing crucial roles in developmental processes as well as in human diseases. Interestingly, miRNAs are also released in the extracellular space, for example in vesicles (i.e., exosomes, microparticles, apoptotic bodies), as also reviewed by Davidson et al. (2019), and can be bound to carrier proteins such as AGO2, or associated to plasma lipoproteins (Arroyo et al., 2011; Vickers et al., 2011; Loyer et al., 2014b). Mechanisms for selective sorting and release of miRNAs (especially in exosomes) are under investigation and involves the raft-like regions in vesicular membranes, the sumoylation of RNA-binding proteins, the secretive autophagy and the LC3-conjugation machinery (Villarroya-Beltri et al., 2013; Janas et al., 2015; Leidal et al., 2020). Extracellular miRNAs can convey messages into recipient cells, thus realizing a paracrine (and possibly endocrine) intercellular communication system (Valadi et al., 2007; Zernecke et al., 2009; Zhang et al., 2017). Noteworthy, extracellular miRNAs are detectable in human biological fluids such as serum, plasma, urine, and tears with peculiar changes in their expression associated with multiple diseases and regulated by treatments. The stability of circulating miRNAs and their regulation in pathological conditions raised the intriguing possibility of their use as disease and prognostic biomarkers for human diseases (Zampetaki et al., 2012a; Hayes et al., 2014; Santovito and Weber, 2017; Tielking et al., 2019). The relevance of miRNAs in the cardiovascular system was suggested by evidence that deletion of *Dicer*, the rate-limiting enzyme for maturation of miRNAs, in mice resulted in embryonic death due to defective angiogenesis and subsequent hemorrhages (Yang et al., 2005). Starting from this early evidence, multiple studies have confirmed the expression of miRNAs in human cardiac and vascular tissues and provided strong evidence on the role of miRNAs in the development and progression of multiple cardiovascular diseases (CVDs). Here, we will discuss the (patho)physiological implication of miRNAs in cardiovascular risk factors, atherosclerosis, cardiac remodeling, and myocardial infarction. Additionally, miRNAs are of course also being studied in other CVDs, such as myocarditis and arrhythmia. However, this review will not focus on these pathologies, as they have already been extensively reviewed elsewhere (Bátkai and Thum, 2012; Tijsen et al., 2012; Kim, 2013; Santulli et al., 2014; Marques and Charchar, 2015; Hijmans et al., 2018). Moreover, we will review the potential application of miRNAs as biomarker and therapeutic targets. As recent years enormous amounts of studies have focused on miRNAs in the discussed topics, we will only highlight the most relevant miRNAs that have been described in multiple studies or seem highly promising for clinical applications.

CARDIOVASCULAR RISK FACTORS

Clinical and pre-clinical studies highlight the influence of miRNAs in the complex pathways underlying medical conditions (i.e., dyslipidemia, diabetes, hypertension) which increase the risk of cardiovascular events (**Figure 1**).

Pathology

Genome-wide association studies revealed an intriguing association between abnormalities of plasma lipids and 69 miRNAs that regulate the expression of key genes in lipoprotein metabolism (Wagschal et al., 2015). Among them, miR-148a-3p is predominantly expressed in the liver and controls, at post-transcriptional level, the expression and function of low-density lipoprotein (LDL)-receptor and ATP-binding cassette transporter A1 (ABCA1) (Goedeke et al., 2015). Similarly, miR-223-3p regulates both cholesterol synthesis via the repression of 3-hydroxy-3-methylglutaryl-CoA synthase 1 (HMGCS1) and methylsterol mono-oxygenase 1 (SC4MOL) as well as cholesterol efflux through regulation of scavenger receptor class B type 1 (SR-B1) and ABCA1 (Vickers et al., 2014). In addition, miR-30c-5p affects *de novo* lipid biosynthesis in the liver and the release of ApoB-containing lipoproteins, probably through the regulation of expression and function of lysophosphatidylglycerol acyltransferase 1 (LPGAT1) and microsomal triglyceride transfer protein (MTTP), respectively (Soh et al., 2013). Finally, strong evidence on the regulatory role of miRNAs in reverse cholesterol transport and high-density lipoproteins (HDL) metabolism is accumulating, as extensively reviewed elsewhere (Canfran-Duque et al., 2016).

Besides lipid metabolism, miRNAs also regulate glucose metabolism and are thereby involved in the pathophysiology of diabetes. Conditional Dicer knock-out in the pancreas ($Pdx^{Cre}Dicer^{fl/fl}$) impedes the formation of Langerhans islets and differentiation of insulin-producing β-cells (Lynn et al., 2007). Highly expressed in the β-cell, miR-375-3p controls insulin synthesis under hyperglycemia conditions and prevents its release (Poy et al., 2004; El Ouaamari et al., 2008). Interestingly, higher miR-375-3p expression is observed in β-cells of patients with type 2 diabetes, thereby suggesting its relevance in this human disease (Zhao et al., 2010). Insulin sensitivity is also regulated by miRNAs as for example the let-7 miRNA-family participates in pathways leading to impaired insulin sensitivity in the skeletal muscle. This effect is mediated by targeting insulin receptor substrate (IRS)-2 and insulin-like growth factor (IGF)-1 receptor and antagonizing let-7 by RNA-interference or transgenic overexpression of two negative modulators of let-7 biogenesis (Lin28a and Lin28b) improved insulin sensitivity and glucose homeostasis (Frost and Olson, 2011; Zhu et al., 2011). On the other hand, the miR-103/-107 family is up-regulated in the liver of obese mice and governs hepatic insulin sensitivity. Indeed, overexpression of miR-107 increases hepatic gluconeogenesis, resulting in hyperinsulinemia

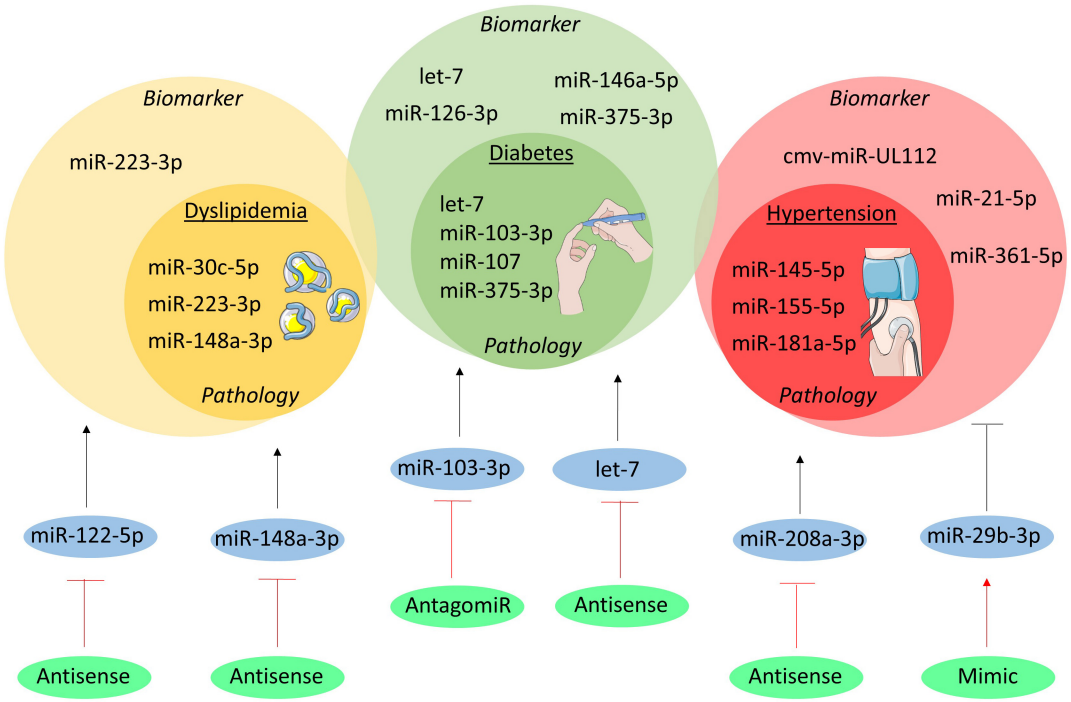

FIGURE 1 | MicroRNAs in cardiovascular risk factors. The miRNAs involved in the pathogenesis of dyslipidemia, diabetes and hypertension are shown in the inner yellow, green, and red circles, respectively. In the outer circles the miRNAs are listed which have been studied as biomarker. Moreover, the therapeutically targeted miRNAs are shown in blue circles and their initial effect on the cardiovascular risk factors is depicted as a black, stimulatory or inhibitory arrow. The green circles indicate the method of intervention and their effect on the miRNA is visualized as a red, stimulatory or inhibitory arrow.

and hyper-glycemia, while treatment with an antagomir against miR-103-3p improves glycemic tolerance, insulin sensitivity, and decreases both subcutaneous and visceral adipose tissue in mice (Trajkovski et al., 2011).

Finally, miRNAs participate in the regulation of blood pressure and development of hypertension by affecting the renin-angiotensin axis. Indeed, a single-nucleotide-polymorphism (rs5186) disrupts the binding site for miR-155-5p in the type 1 angiotensin II receptor (AGTR1) mRNA and is associated with increased risk for hypertension (Bonnardeaux et al., 1994; Sethupathy et al., 2007). The expression of AGTR1 is higher in young hypertensive patients carrying the mutant allele, directly correlated with arterial blood pressure, and inversely correlated with miR-155-5p expression in blood mononuclear cells (Ceolotto et al., 2011). Being hosted on chromosome 21, miR-155-5p could also contribute to the lower blood pressure in patients with Down syndrome (Sethupathy et al., 2007). Additionally, miR-181a-5p regulates the expression of renin *in vitro*, it is downregulated in a murine model of neurogenic hypertension and in the renal cortex of hypertensive patients, and inversely correlated with higher renin mRNA expression (Marques et al., 2011; Jackson et al., 2013). Finally, miR-145-5p regulates angiotensin-converting enzyme (ACE) in vascular smooth muscle cells (VSMCs) and *in vivo* deficiency results in hypotension and impaired vascular reactivity (Boettger et al., 2009). Additionally, changes in miR-145 expression were found in hypertensive patients in blood mononuclear cells and in carotid atherosclerotic plaques (Santovito et al., 2013; Kontaraki et al., 2014). Overall, the role of miRNAs in the regulation of lipid and glucose metabolism and vascular reactivity has been associated with important implications for the development of pathological abnormalities, like hypertension, diabetes and atherosclerosis.

Biomarker

Dyslipidemia and diabetes are diagnosed by routine blood tests. Nonetheless, alterations identified in circulating miRNAs could contribute to a better characterization of the patients and unveil new molecular pathways. For examples, miR-223-3p does not only control hepatic cholesterol and lipoproteins metabolism, but is also loaded into HDL to be released in conditions of hypercholesterolemia as shown in patients with familial hypercholesterolemia (Vickers et al., 2011). However, diabetes is among the most investigated diseases in regards of circulating miRNAs. Among the miRNAs affected in their circulating levels, there are those involved in the above-mentioned mechanisms of insulin release and sensitivity (i.e., miR-375-3p, the let-7 family), those involved in inflammation (e.g., miR-146a-5p), and those influencing endothelial biology such as miR-126-3p (Zampetaki et al., 2010; Kong et al., 2011; Santovito et al., 2014). This finding further supports the existence of profound crosstalk between diabetes, endothelial (dys)function, and atherosclerosis. Finally, anti-diabetic treatment could promote a (partial) reversion of the abnormalities in circulating miRNAs, hence highlighting their

possible use to monitor therapeutic efficacy (Ortega et al., 2014; Santovito et al., 2014).

Hypertension has been associated with anomalies of circulating miRNAs. Although not essential for diagnostic purposes, circulating miRNAs may own additive prognostic value. For example, whole blood expression of miR-361-5p could discriminate patients affected by salt-sensitive vs. salt-resistant hypertension, thus possibly supporting the clinical decision of the appropriate anti-hypertensive treatment (Qi et al., 2017). Moreover, higher plasma levels of miR-21-5p positively correlated with carotid intima-media thickness in hypertensive patients, nominating this miRNA as a non-invasive marker of carotid atherosclerosis in these patients (Cengiz et al., 2015). Finally, an intriguing study showed an increase of circulating cmv-miR-UL112, a miRNA encoded by the human cytomegalovirus, in patients with hypertension (together with changes of endogenous miR-296-5p and let-7e-5p), thus proposing a link between cytomegalovirus infection and hypertension that mandate additional experimental proof (Li et al., 2011).

Therapeutic Potential

Therapeutic modulation of miRNAs affects serum lipoproteins in experimental studies. A remarkable evidence is provided by a clinical trial employing anti-sense interference of miR-122-5p (known as Miravirsen). Although this was a phase 2 clinical trial investigating safety and efficacy of miR-122-5p inhibition for Hepatitis C, treatment resulted in a dose-dependent decrease of serum total cholesterol levels (Janssen et al., 2013). The underlying mechanisms are not yet fully elucidated, although experiments in animal models identified 3-hydroxy-3-methylglutaryl-CoA reductase (HMGCR), the key enzyme for intracellular cholesterol biosynthesis, and MTTP, which transfers triglycerides onto ApoB during very low-density lipoprotein (VLDL) biogenesis, as two relevant targets (Esau et al., 2006; Tsai et al., 2012). Therapeutic modulation of other miRNAs to improve lipid and glucose metabolism has also been tested in animal models. For example, inhibition of miR-148a-3p by antisense nucleotides resulted in lower LDL cholesterol and higher HDL cholesterol in serum, reflecting the upregulation of hepatic LDL-receptor and ABCA1 (Goedeke et al., 2015). Moreover, inhibition of miR-103-3p by antagomir resulted in lower plasma glucose and improved insulin resistance in liver and adipose tissue of obese mice (Trajkovski et al., 2011). Similarly, systemic administration of an antisense nucleotide targeting the whole let-7 family prevented impaired glucose tolerance in obese mice by improving hepatic and muscular insulin sensitivity (Frost and Olson, 2011). These data designate miR-103-3p and let-7 as possible therapeutic targets in diabetes.

Finally, miRNAs have been experimentally tested as therapeutic agents in hypertension and related organ damages. Systemic administration of antisense nucleotides against miR-208a-3p blunted cardiac stress and consequent pathological hypertrophy in hypertensive rats (Dickinson et al., 2013). Moreover, treatment with miR-29b-3p after Angiotensin II-induced hypertension improved the progressive impairment of cardiac function and reverted histological markers of hypertensive cardiopathy in mice (Zhang et al., 2014). These studies unveil the therapeutic potential of miRNAs in hypertension and its complications.

ATHEROSCLEROSIS

Atherosclerosis is the main underlying cause of many CVDs. It is a chronic inflammatory disease of the arterial walls that eventually determine vessel stenosis and acute occlusion by atherothrombosis. The pathophysiological mechanisms leading to atherosclerosis progression are numerous and complex as reviewed elsewhere (Weber and Noels, 2011).

Pathology

Endothelial Cells

Several lines of evidence show the involvement of miRNAs in all stages of atherosclerosis (**Figure 2**). Amongst the most expressed miRNAs in endothelial cells (ECs), especially the miR-126 duplex plays a crucial role in regulating endothelial function. In contrast to most of the miRNAs, the precursor of miR-126 gives rise to two stable mature miRNA strands (miR-126-3p and miR-126-5p) which both coordinate atheroprotective functions. Indeed, miR-126-3p can regulate angiogenesis and reduces inflammatory leukocyte adhesion to ECs by repressing targets such as the vascular cell adhesion molecule-1 (VCAM-1) (Fish et al., 2008; Harris et al., 2008). On the other hand, miR-126-5p not only promotes the proliferative capacity by targeting delta-like 1 (Dlk1), a negative regulator of the NOTCH1 pathway (Schober et al., 2014), but also protects ECs from apoptotic cell death through an uncanonical mechanism. Indeed, high shear stress promotes nuclear localization of miR-126-5p by a pathway involving the activation of autophagy and the RNA-binding protein Mex3a (Dragomir et al., 2018; Santovito et al., 2020a). Nuclear miR-126-5p acts as an aptamer by directly binding to the effector caspase-3, inhibiting its catalytical activity, and protecting ECs from apoptosis (Santovito et al., 2020a). Besides the intracellular role, the guide strand of miR-126 (miR-126-3p) is released via apoptotic bodies and mediates a paracrine signaling regulating CXCL12 release (Zernecke et al., 2009). The relevance of the cell-specific contribution of CXCL12 and its receptor CXCR4 in the progression of atherosclerosis has been extensively proven (van der Vorst et al., 2015; Doring et al., 2017, 2019), thus further linking the miR-126 duplex to atherosclerosis development.

Besides the miR-126 duplex, other EC-related miRNAs have been demonstrated to play a role in atherosclerosis. Studies involving a murine model of conditional deletion of *Dicer* in ECs ($Cdh5^{Cre}Dicer^{fl/fl}$) revealed a detrimental role for miR-103-3p in atherosclerosis. Indeed, miR-103-3p promotes endothelial inflammation by targeting Kruppel-like factor 4 (KLF4) and inhibits EC proliferation and promotes DNA damage through targeting of lncWDR59 in areas of disturbed shear stress (Hartmann et al., 2016; Natarelli et al., 2018). Silencing of *Dicer* also associated with higher expression of KLF2, an effect mediated by miR-92a-3p (Wu et al., 2011), a miRNA upregulated in atheroprone vascular areas, to promote

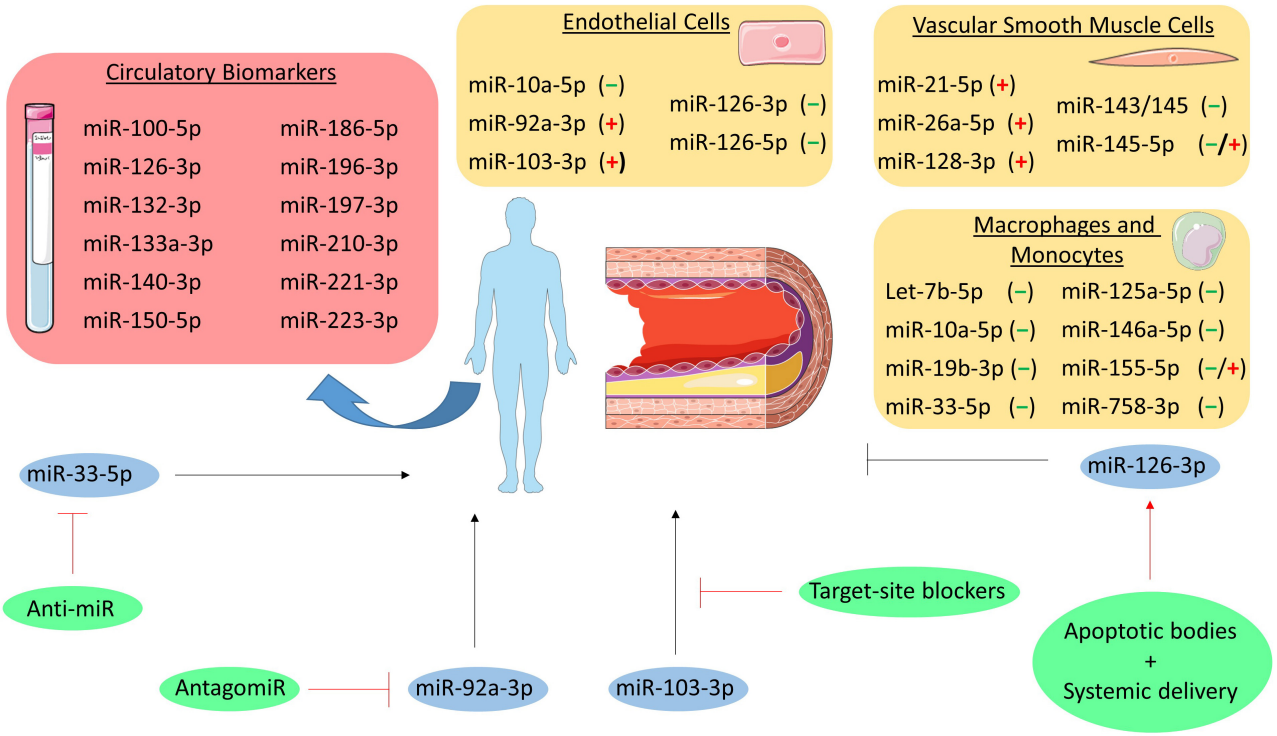

FIGURE 2 | MicroRNAs in atherosclerosis. MiRNAs involved in the pathogenesis of atherosclerosis are grouped per cell type (i.e., endothelial cells, vascular smooth muscle cells, and macrophages and monocytes). The (–), (+), and (–/+) indicate that the miRNA is either atheroprotective, pro-atherogenic or both, respectively. Additionally, circulatory biomarker miRNAs are listed in the red box. Furthermore, the miRNAs that have been studied as therapeutic target are depicted in blue circles and their initial effect on atherosclerosis is shown as a black, stimulatory or inhibitory arrow. The therapeutic intervention is shown in green circles and the effect on the miRNA is depicted as a red, stimulatory or inhibitory arrow.

endothelial activation and atherosclerosis progression (Loyer et al., 2014a). Furthermore, miR-92a-3p can be released in extracellular vesicles, thereby driving an atheroprone phenotype in recipient macrophages by targeting KLF4 (Chang et al., 2019) and regulating ECs angiogenic ability through a thrombospondin 1 (THBS1)-dependent mechanism (Liu et al., 2019). In contrast, miR-10a-5p is downregulated in atherosusceptible areas to foster IκB/NF-κB-mediated infiammation by repressing MAP3K7 and β-TRC (Fang et al., 2010).

Smooth Muscle Cells

Besides their role in ECs, miRNAs expressed in VSMCs also contribute to atherosclerosis and arterial remodeling. As one of the most enriched, the miR-143/-145 cluster acts as a phenotypical regulator of VSMCs. These miRNAs prevent proliferation and acquisition of a pro-atherosclerotic synthetic phenotype, with the effects being mediated by multiple targets such as KLF4, KLF5, and ACE (Boettger et al., 2009; Cheng et al., 2009; Cordes et al., 2009). Interestingly, this miRNA cluster is involved in an atheroprotective intercellular crosstalk between VSMCs and ECs. While miR-143/-145 produced in ECs favors the acquisition of an atheroprotective phenotype of VSMCs (reduced proliferation and dedifferentiation) upon vesicle-mediated transfer (Hergenreider et al., 2012), miR-143/-145 is also transferred from VSMCs to nearby ECs via tunneling nanotubes and contributes to stabilization of the endothelium (Hergenreider et al., 2012; Climent et al., 2015). Finally, a circular RNA (namely *circ_Lrp6*) acts as a natural sponge for miR-145-5p dampening its activity (Hall et al., 2019), highlighting a further regulatory layer for miR-145-5p activities. However, the ultimate relevance of miR-145-5p in atherosclerosis requires additional investigations as beneficial effects were observed by local vascular overexpression (Lovren et al., 2012; Hall et al., 2019) as well as by genetic deletion (Xin et al., 2009; Sala et al., 2014). Other miRNAs also contribute to VSMCs phenotype: miR-128-3p regulates methylation of the *Myh11* gene (crucial for the contractile phenotype) by targeting KLF4, thus preventing dedifferentiation (Farina et al., 2020); miR-21-5p promotes VSMCs proliferation and neointima formation thought repressing phosphatase and tensin homolog (PTEN) expression (Ji et al., 2007); miR-26a-5p facilitates VSMCs proliferation and migration affecting the TGF-β pathway (Leeper et al., 2011).

Monocytes and Macrophages

Monocytes and macrophages also express miRNAs that are involved in atherosclerosis development. Genetic deletion of *Dicer* in macrophages ($LysM^{Cre}Dicer^{fl/fl}$) exacerbated atherosclerosis by enhancing inflammatory activation and favoring formation of foam cells due to an impaired mitochondrial fatty acid metabolism (Wei et al., 2018). The

metabolic effects were reversed by re-expression of miR-10a-5p and let-7b-5p with consequent repression of *Lcor* (Wei et al., 2018). miR-155-5p, which is enriched in hematopoietic cells, is involved in atherosclerosis featuring opposite roles during early and advanced stages of the disease. Its expression in macrophages increases during atherogenesis and, while it suppresses early lesion formation by inhibiting macrophage proliferation, it promotes inflammatory activation and reduces efferocytosis at advanced stages (Donners et al., 2012; Nazari-Jahantigh et al., 2012; Du et al., 2014; Wei et al., 2015). Moreover, miR-146a-5p induced by inflammatory stimuli participates to resolution of inflammation by restraining inflammatory cytokines expression, reducing oxidized LDL (oxLDL) uptake, and protecting against atherosclerosis (Taganov et al., 2006).

Macrophage cholesterol uptake and efflux is also regulated by miRNAs. The uptake of oxidized lipoprotein is inhibited *in vitro* by miR-125a-5p and miR-155-5p by down-regulating the scavenger receptors CD68 and LOX1 (Chen et al., 2009; Huang et al., 2010). However, the cholesterol efflux pathways are the most affected by miRNA regulation. Cholesterol efflux first requires conversion of cholesteryl esters (stored in lipid droplets) into free cholesterol mediated by neutral cholesteryl ester hydroxylases or by autophagy. This latter process is repressed by miR-155-5p in macrophages and could contribute to reduced cholesterol efflux upon lipid (over)loading (Du et al., 2014). Free cholesterol is then transferred to apolipoprotein A1 or mature HDL by the synergic action of ABCA1 and ABCG1, respectively. In macrophages, these transporters are strongly regulated by multiple miRNAs such as miR-33-5p, miR-758-3p, and miR-19b-3p (Najafi-Shoushtari et al., 2010; Rayner et al., 2010; Ramirez et al., 2011; Lv et al., 2014). Interestingly, inflammatory stimuli (e.g., lipopolysaccharide) upregulate the expression of miR-33-5p in macrophages which stimulates an inflammatory phenotype (Ouimet et al., 2015), suggesting an additional link between lipid homeostasis and inflammation status. Unlike mice, humans express two miR-33 homologs (miR-33a-5p and miR-33b-5p) that exhibit a different regulation. Indeed, while miR-33a-5p is not affected (or slightly downregulated), miR-33b-5p is upregulated in atherosclerotic plaques from hypercholesterolemic patients and is paralleled by a lower translation rate of the ABCA1 protein (Mandolini et al., 2015). The presence of two miR-33 homologs should be considered while translating murine findings into a human disease.

Biomarker

Atherosclerotic plaque disruption underlies the development of acute ischemic syndromes and identification of vulnerable plaques is an unmet need in medical research. Studies performed on human unstable atherosclerotic plaques revealed peculiar changes in the expression profiles of miRNAs, including miR-100-5p, miR-127-3p, miR-133a-3p, miR-210-3p, miR-221-3p (Cipollone et al., 2011; Maitrias et al., 2015; Eken et al., 2017). These studies allowed the investigation of regulated targets and pathways influencing the mechanisms of plaque destabilization, however miRNAs analysis in atherosclerotic lesions may have limited application in clinical practice. Interestingly, the circulating levels of some of these miRNAs (i.e., miR-100-5p, miR-133a-3p, miR-210-3p, miR-221-3p) are also altered in patients with vulnerable carotid or coronary atherosclerotic plaques (Tsai et al., 2013; Wang et al., 2013; Soeki et al., 2015; Eken et al., 2017), suggesting their role as possible biomarkers to identify patients with vulnerable plaques. However, independent cohorts should be analyzed with standardized analytical procedures to properly validate the findings, assess diagnostic performance, and prove clinical utility.

Circulating miRNAs have also been tested for their ability to predict cardiovascular events. As one of the miRNAs regulated in vulnerable plaques (Cipollone et al., 2011; Maitrias et al., 2015), high plasma miR-133a-3p levels were associated with a higher risk of cardiovascular events in a prospective study in patients with familiar hypercholesterolemia with a follow-up of 8 years (Escate et al., 2020). Furthermore, a prospective population-based survey unveiled the association of miR-126-3p, miR-197-3p, and miR-223-3p with the incidence of myocardial infarction over a 10-year follow-up period (Zampetaki et al., 2012b). Finally, higher miR-19b-3p, miR-132-3p, miR-140-3p, miR-150-5p, miR-186-5p levels were linked to a high degree of cardiovascular deaths in the following 4 years in patients with coronary artery disease (Karakas et al., 2017).

Therapeutic Potential

Systemic and local administration of mimics, antagomirs, and target-site blockers was employed in animal models to explore the therapeutic potential of miRNA modulation *in vivo*. For example, delivery of miR-126-3p via apoptotic bodies as well as systemic treatment with the miR-126-5p mimic reduced atherosclerotic lesion formation in mice (Zernecke et al., 2009; Schober et al., 2014), hence supporting the beneficial role of the miR-126 duplex in vascular homeostasis. On the other hand, beneficial effects were observed by the inhibition of endothelial miRNAs with detrimental functions. Indeed, inhibition of miR-92a-3p by injection of an antagomir (Loyer et al., 2014a) or disruption of the interactions between miR-103-3p and its proatherogenic targets (Hartmann et al., 2016; Natarelli et al., 2018) reduced atherosclerosis and improved the lesion phenotype.

The inhibition of miR-33-5p was also extensively investigated, as cholesterol efflux and reverse transport represent an intriguing therapeutic opportunity for atherosclerosis regression. In mice, short-term (4 weeks) anti-miR-33 treatment increased cholesterol efflux from lesional macrophages and promotes regression of atherosclerosis (Rayner et al., 2011). However, long-term treatment (14 weeks) was not associated with beneficial effects on atherosclerosis (Marquart et al., 2013). A possible explanation is the concomitant hepatic overexpression of genes regulating fatty acid synthesis (e.g., acetyl-CoA carboxylase) with consequent increased plasma triglyceride levels and liver steatosis (Goedeke et al., 2014). Notably, long-term treatment of non-human primates, which express both miR-33 homologs, did not cause liver toxicity (Rottiers et al., 2013). It is therefore

possible that the lack of miR-33b in rodents does not allow the complete evaluation of underlying mechanisms in murine models. In example, lower miR-33b-5p expression in human atherosclerotic plaques is observed after treatment with rosuvastatin (Santovito et al., 2020b), possibly contributing to anti-atherosclerotic properties of this molecule. Therefore, miR-33 represents a promising target for atherosclerosis, although further investigations are required to verify safety and efficacy in primates.

MYOCARDIAL INFARCTION

Myocardial infarction (MI) is characterized by the necrosis of myocytes followed by extracellular matrix (ECM) deposition by activated cardiac fibroblasts and consequent scar formation. This pathology is defined as cardiomyocyte death due to prolonged ischemia mostly caused by coronary artery disease.

PATHOLOGY

Myocardial infarction usually involves different types of cell death including necrosis and apoptosis, which are regulated amongst others by miRNAs (**Figure 3**; Higashi et al., 2015; Wang J.X. et al., 2015). Both pro- and anti-apoptotic miRNAs have been identified regarding apoptosis, such as miR-93-5p, miR-138-5p, and miR-320-3p. miR-93-5p was found to be anti-apoptotic in cardiomyocytes by targeting PTEN in mice with ischemia/reperfusion (I/R) injury (Ke et al., 2016). Additionally, in an *in vitro* study miR-138-5p protects cardiac myoblasts against hypoxia-induced apoptosis via the MLK3/JNK/c-jun pathway (He et al., 2013). In contrast, miR-320-3p targets IGF-1 and thereby promotes apoptosis in cardiomyocytes (Song et al., 2016).

Additionally, miRNAs like miR-103a-3p, miR-107, miR-155-5p, and miR-30b-5p are either anti- or pro-necrotic in cardiac disorders (Liu et al., 2011; Wang K. et al., 2015,b). For example, miR-103a-3p and miR-107 induce necrosis in cardiomyocytes by targeting Fas-associated protein with death domain (FADD) (Wang J.X. et al., 2015). In contrast, miR-30b-5p inhibits necrosis through targeting cyclophilin D, which usually promotes necrosis. Interestingly, enhanced expression of miR-30b-5p in the heart reduced necrosis and MI size following I/R injury (Wang K. et al., 2015). Likewise, overexpression of miR-155-5p in cardiomyocyte progenitor cells attenuates necrosis by targeting receptor interacting protein 1 (RIP1) (Liu et al., 2011).

Biomarker

In MI, cardiac troponins are used as the golden standard diagnostic biomarkers. Although the measurement of troponin levels is a sensitive test, it is not specific for MI as for example myocarditis can also alter troponin levels (Halushka et al., 2019). Therefore, the opportunity for miRNAs as biomarker lies in its potential to discriminate true MI from other diseases, which have similar classical biomarker profiles as MI. A number of miRNAs have been explored in the context of MI, such as miR-1a-3p, miR-133a-3p, and miR-499a-5p. miR-1a-3p, miR-133a-3p, and miR-499a-5p levels were all elevated in MI patients, but were not more specific as compared to troponin (Ai et al., 2010; Wang et al., 2010). In contrast, it was found that 93% of 510 patients suffering from MI were tested positive for miR-499a-5p, while only 88% tested positive for troponin (Devaux et al., 2012). Therefore, it seems that miRNAs still have some additional value on top of troponins.

Therapeutic Potential

The inability of cardiomyocytes to replicate and regenerate the lost contractile tissue raises the need for novel therapies, as the current ones fail to restore this replication-potential. Interestingly, one very recent study investigated the therapeutic potential of miR-199a-5p in pigs. This miRNA was administered in pigs through an adeno-associated viral vector directly after MI was induced, which resulted in improved contractility, increased muscle mass and reduced scar formation one month after MI and miR-199a-5p delivery. However, despite these improvements a longer, uncontrolled expression of this miRNA resulted in sudden death of 7 out of 10 pigs indicating that the dosage of this potential treatment has to be tightly controlled (Gabisonia et al., 2019). Furthermore, miR-92a-3p inhibition on MI recovery in mice was investigated. The mice were injected with an antagomir at 0, 2, 4, 7, and 9 days after MI was induced, after which cardiac function was determined at day 14. Improved heart function and reduced infarction size could be observed in antagomir injected mice compared to the control injected mice (Bonauer et al., 2009).

CARDIAC REMODELING

Cardiac remodeling is generally defined as molecular and cellular changes clinically manifested as changes in heart shape, size and function caused by cardiac load or injury (Cohn et al., 2000). Cardiac hypertrophy and fibrosis are part of this pathology. In cardiac hypertrophy, myocyte death increases the contractile load on neighboring myocytes, which leads to increased myocyte size. As a maladaptive response to the impaired heart performance, cardiac myofibroblasts deposit an excessive amount of excessive ECM in the interstitium, thereby further enhancing cardiac stiffness and dysfunction (Westermann et al., 2011).

Pathology

miR-133a-3p, miR-1a-3p, miR-27b-3p, and miR-208a-3p are one of the many miRNAs involved in hypertrophy (**Figure 4**). miR-133a-3p levels in cardiomyocytes significantly decrease in animal models of hypertrophy and in patients with hypertrophic cardiomyopathy as compared to healthy controls. Moreover, overexpression of this miRNA resulted in preserved cardiac function, whilst inhibition resulted in increased hypertrophy, further associating and even causally linking miR-133a-3p to hypertrophy (Carè et al., 2007). Just like miR-133a-3p, miR-1a-3p has a high abundance in cardiomyocytes and has a lower expression in heart failure patients (Elia et al., 2009). More interestingly, restoration of miR-1a-3p gene expression seems to reverse pressure-induced cardiac hypertrophy in rats

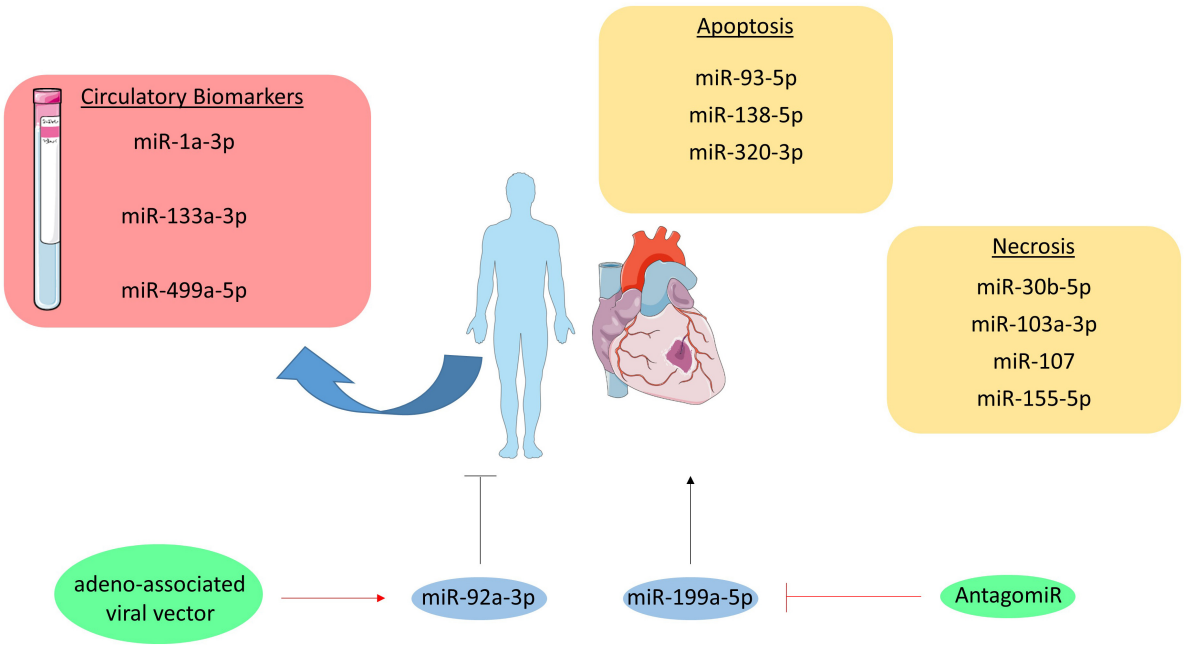

FIGURE 3 | MicroRNAs in myocardial infarction. MiRNAs involved in the pathogenesis of myocardial infarction are grouped per cell death type (i.e., apoptosis and necrosis). Moreover, the circulatory miRNAs studies as biomarker are listed in the red box. Furthermore, the therapeutically targeted miRNAs are visualized in blue circles and their initial effect on myocardial infarction is shown as a black, stimulatory or inhibitory arrow. The therapeutic intervention is depicted in green circles and their effect on the targeted miRNA is shown as a red, stimulatory or inhibitory arrow.

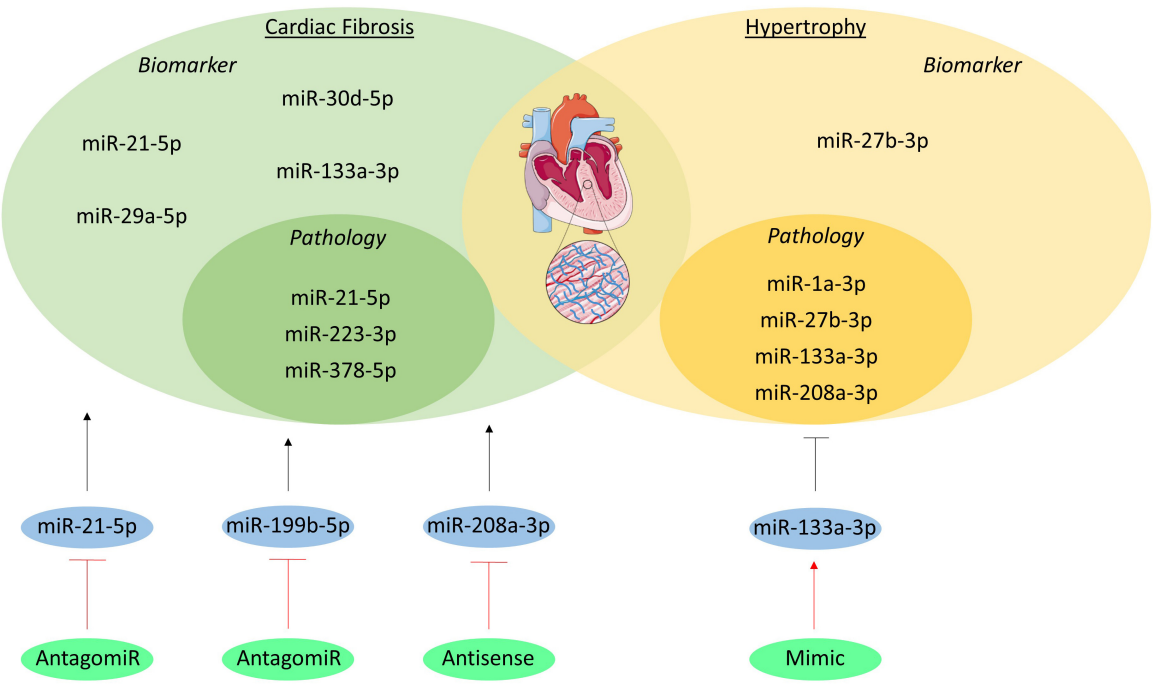

FIGURE 4 | MicroRNAs in cardiac remodeling. The miRNAs involved in the pathogenesis of cardiac fibrosis and hypertrophy are visualized in the inner green and yellow circles, respectively. The miRNAs which have been studied as biomarker are listed in the outer circles. Additionally, the miRNAs studied as therapeutic are shown in blue circles and their initial effect on the pathologies is visualized as a black, stimulatory or inhibitory arrow. The method of intervention is depicted in the green circles and their effect on the miRNA target is shown as a red, stimulatory or inhibitory arrow.

(Karakikes et al., 2013). miR-27b-3p has also been shown to be involved in hypertrophy development. *In vivo* silencing of this miRNA with an antagomiR resulted in attenuation of cardiac hypertrophy and dysfunction in mice with heart failure, suggesting that miR-27b-3p promotes cardiac hypertrophy and dysfunction (Wang et al., 2012). miR-208a-3p is also expressed in high levels in healthy cardiomyocytes, where it regulates the balance between the two myosin heavy chains (MHC) isotypes, i.e., α- and β-MHC. This miRNA induces a shift towards the β-MHC isotype, which reduces contractility and is known to be a maladaptive response to cardiac stress (Krenz and Robbins, 2004; Callis et al., 2009).

Several miRNAs have been studied regarding cardiac fibrosis, including miR-21-5p, miR-378-5p, and miR-223-3p. miR-21-5p levels are elevated in cardiac fibroblasts of fibrotic mouse hearts and in heart failure patients (van Rooij et al., 2006). This miRNA also stimulates ECM deposition in mice with increased afterload and myocardial ischemia, which are some of the underlying causes of cardiac remodeling (Thum et al., 2008; Roy et al., 2009). Furthermore, miR-378-5p has been shown to be secreted by cardiomyocytes as a consequence of mechanical stress and it inhibits excessive cardiac fibrosis in an extracellular vesicles-dependent secretory manner (Yuan et al., 2018). Lastly, overexpression of miR-223-3p leads to increased proliferation, differentiation and migration of cardiac fibroblasts and *in vivo* inhibition leads to alleviated cardiac fibrosis (Liu et al., 2018).

Biomarker

MiRNAs might serve as new serological biomarkers for a precise detection of cardiac remodeling. miR-27b-3p serum levels were measured through stem-loop RT-PCR in 200 hypertensive patients with left ventricular hypertrophy (LVH), 100 hypertensive patients without LVH, and 100 healthy volunteers. Results showed that miR-27b-3p serum levels were significantly higher in the patients with LVH compared to both the hypertensive and healthy subjects without LVH (Wang et al., 2017).

Although cardiac tissue biopsy analysis has been the golden standard for the diagnosis of cardiac fibrosis, circulating biomarkers have been studied to develop a more non-invasive approach (Richards, 2017). Biomarker potential of miRNAs have been well established in myocardial fibrosis, including miR-21-5p, miR-29a-5p, miR-30d-5p, and miR-133a-3p. These were measured in the plasma of left ventricular non-compaction (LVNC) patients both with and without myocardial fibrosis diagnosed with cardiac magnetic resonance with late gadolinium enhancement (LGE), where LGE positivity reflects the presence of fibrosis. Four miRNAs were significantly upregulated in LVNC patient with fibrosis as compared to LVNC patients without fibrosis, suggesting that these miRNAs could be used as biomarkers for detecting fibrosis in the clinic (Szemraj-Rogucka et al., 2019).

Therapeutic Potential

Cardiac remodeling evokes downregulation of specific miRNAs in the heart; overexpression of these miRNAs is sufficient to induce hypertrophy (van Rooij et al., 2006), creating the opportunity to identify novel targets for miRNA-based therapies. A first *in vivo* study regarding miRNA-based therapies implanted osmotic minipumps in mice for a continues delivery of an antagomir targeting miR-133a-3p. This inhibition of miR-133a-3p resulted in marked and sustained hypertrophy compared to saline infused mice, suggesting an artificial overexpression of miR-133a-3p might have therapeutic value for hypertrophy (Carè et al., 2007). Another study used an antagomir targeting miR-21-5p into mice that underwent a transverse aortic constriction (TAC) operation to induce pressure overload of the left ventricle or into sham operated mice. Silencing miR-21-5p in TAC operated mice resulted in reduced interstitial fibrosis in the heart and attenuated cardiac dysfunction as compared to their controls (Thum et al., 2008). Moreover, *in vivo* inhibition of miR-199b-5p in mice and miR-208a-3p in rats inhibited cardiac remodeling and improved heart function (da Costa Martins et al., 2010; Montgomery Rusty et al., 2011).

THE ROAD TOWARD CLINICAL APPLICATION: CURRENT LIMITATIONS AND FUTURE CHALLENGES

As described in the previous chapters, circulating miRNAs hold promising diagnostic and prognostic potential in CVDs. Yet, further work is necessary to address some aspects that currently limit their use in clinical routine. A large core of evidence derives from monocentric case-control studies, and external validation in large prospective cohorts is often missing. Moreover, anomalies of circulating miRNAs also associate with several non-CVDs (e.g., cancer, inflammatory diseases) as well as concomitant treatments (Hayes et al., 2014; Tielking et al., 2019). However, it is particularly complex to take all these variables into account in studies on circulating miRNAs and appropriate multivariate analyses are sometimes missing or inconclusive, especially in small cohorts. Importantly, there is a relevant lack of standardization in methods and analytical workflows. The most commonly used technique for measuring circulating miRNAs is qPCR with its inherent limitations raised by the lack of unequivocally accepted normalization strategies. Several approaches have been pursued ranging from the use of a synthetic spike-in (e.g., cel-miR-39), to the identification of sets of endogenous miRNAs with the lowest variance among samples, to applying an average of cycle thresholds (Zampetaki et al., 2012a; Halushka et al., 2019). Other techniques have also been applied such as droplet digital PCR, chip-based digital PCR, and RNA-sequencing. However, the disparities in methods and analytical workflows make it difficult to merge results from multiple studies (e.g., meta-analyses). Therefore, all these aspects warrant an urgent need for a consensus. This represents a keystone for proceeding with validation of diagnostic and prognostic performances in multicentric prospective cohorts with the final aim to establish their role in improving risk stratification of patients with CVDs.

Finally, in the light of their pathophysiological relevance, it was a logical consequence to imagine miRNAs as novel

therapeutic entities for clinical application. To date, clinical trials (phase 1 and 2) provided proof-of-principle evidence that modulation of miRNAs is feasible in humans (e.g., miravirsen, a miR-122-5p inhibitor) (Janssen et al., 2013). On the other hand, the premature halt of some trials on other miRNA-based therapeutics (i.e., miR-34 mimics) reflects the existence of limiting aspects to overcome. In particular, a single miRNA could target multiple genes and those genes are expressed and regulated in a cell- and tissue-dependent manner, thus evolving the notion of "off-target effects" to an unprecedented complexity, compared to standard drugs. Therefore, tissue-specific delivery is crucial to minimize side effects due to off-targeting of transcripts in other cells types (as in the case of anti-miR-33, see section "Therapeutic Potential"). Although systemic administration can easily reach therapeutic concentrations of miRNAs in organs such as liver and kidney, the delivery in other tissues (e.g., arteries) requires carefully engineered carriers. They include nanoparticles coated with appropriate antigens recognized by receptors unambiguously expressed on targeted cells. However, nanoparticles display low efficiencies in cell internalization and in the release of miRNAs inhibitors in the cytoplasm (1–2%) (Gilleron et al., 2013) thus fostering research to develop new and more effective strategies. In this context, bacterially derived minicells coupled with antibodies against cell-specific markers has been effectively employed for tissue-specific delivery of miR-16 mimics in patients with mesothelioma (van Zandwijk et al., 2017) and may extend the portfolio of cell-specific delivery systems. Another relevant aspect is the influence of chemical modifications of nucleotides on the efficacy and safety of the miRNA-based compounds. Indeed, specific chemistries (e.g., 2′O-methyl nucleotides, Locked Nucleic Acids) are applied to anti-miRNA oligonucleotides to enhance the resistance to serum nucleases, the affinity to their targets, and the pharmacokinetic profile. However, some modifications might influence both the strength of miRNA inhibition and the efficacy of cellular uptake. Moreover, these changes could induce sequence-independent toxicity mainly observed for high doses of oligonucleotides which include inhibition of the coagulation, activation of the complement cascade and activation of immune response by triggering both innate and adaptive arms (Li and Rana, 2014). These findings demand for additional efforts to improve the pharmacodynamic and pharmacokinetic profiles that, together with advanced delivery system, would increase the therapeutic windows of miRNA-based therapeutics. These and other limitations are extensively discussed elsewhere (van Rooij et al., 2012; Li and Rana, 2014; Zhou et al., 2018) and represent exciting challenges for future research to hopefully move this new class of drug from bench to bedside.

CONCLUDING REMARKS

Overall, miRNAs play an important role in several cardiovascular risk factors and in the pathophysiology of atherosclerosis, cardiac remodeling and MI. These molecules also showed great potential as both biomarkers and therapeutic targets in all of these pathologies, although further research and especially clinical validation is still required. MiRNAs can be a valuable addition to the currently used biomarkers, to further fine-tune diagnostics and come one step closer to the optimal scenario being personalized medicine. In order to use miRNAs in the clinic it is essential that the most promising candidates are further validated in a clinical setting and in different patient cohorts. The use of miRNA targeting as therapeutic strategy is still in its infancy. Pre-clinical studies show very promising results, although most studies are only performed in rodent models so far. It will be very interesting to further study this therapeutic approach in a more translatable setting in order to perform more clinical trials studying the efficacy and safety of these treatments. All in all, it has been extensively demonstrated that miRNAs play an important role in several cardiovascular pathologies and initial studies show great promise for the use of miRNA as biomarkers and even therapeutic targets in the future.

AUTHOR CONTRIBUTIONS

LP, EV, and DS contributed to the literature research and writing of the manuscript. EB, MH, and CW contributed to writing of the manuscript and made critical revisions. All authors contributed to the article and approved the submitted version.

FUNDING

The authors' research is supported by a grant from the Interdisciplinary Center for Clinical Research within the faculty of Medicine at the RWTH Aachen University, the DZHK (German Centre for Cardiovascular Research) and the BMBF (German Ministry of Education and Research), and NWO-ZonMw Veni (91619053) to EV; by the Deutsche Forschungsgemeinschaft (DFG) (TRR267-A2 and SFB1123 TP A1) and by the European Research Council (AdG°692511) to CW; and by the DFG (SFB TRR219-M02) to MH.

ACKNOWLEDGMENTS

All illustrations are made with the help of SMART Servier Medical Art (https://smart.servier.com/). CW is a Van de Laar professor of atherosclerosis.

REFERENCES

Ai, J., Zhang, R., Li, Y., Pu, J., Lu, Y., Jiao, J., et al. (2010). Circulating microRNA-1 as a potential novel biomarker for acute myocardial infarction. *Biochem. Biophys. Res. Commun.* 391, 73–77. doi: 10.1016/j.bbrc.2009.11.005

Arroyo, J. D., Chevillet, J. R., Kroh, E. M., Ruf, I. K., Pritchard, C. C., Gibson, D. F., et al. (2011). Argonaute2 complexes carry a population

of circulating microRNAs independent of vesicles in human plasma. *Proc. Natl. Acad. Sci. U.S.A.* 108, 5003–5008. doi: 10.1073/pnas.1019055108

Bartel, D. P. (2018). Metazoan microRNAs. *Cell* 173, 20–51. doi: 10.1016/j.cell.2018.03.006

Bátkai, S., and Thum, T. (2012). MicroRNAs in hypertension: mechanisms and therapeutic targets. *Curr. Hypertens. Rep.* 14, 79–87. doi: 10.1007/s11906-011-0235-6

Boettger, T., Beetz, N., Kostin, S., Schneider, J., Kruger, M., Hein, L., et al. (2009). Acquisition of the contractile phenotype by murine arterial smooth muscle cells depends on the mir143/145 gene cluster. *J. Clin. Invest.* 119, 2634–2647. doi: 10.1172/JCI38864

Bonauer, A., Carmona, G., Iwasaki, M., Mione, M., Koyanagi, M., Fischer, A., et al. (2009). MicroRNA-92a controls angiogenesis and functional recovery of ischemic tissues in mice. *Science* 324, 1710–1713. doi: 10.1126/science.1174381

Bonnardeaux, A., Davies, E., Jeunemaitre, X., Fery, I., Charru, A., Clauser, E., et al. (1994). Angiotensin II type 1 receptor gene polymorphisms in human essential hypertension. *Hypertension* 24, 63–69. doi: 10.1161/01.hyp.24.1.63

Callis, T. E., Pandya, K., Seok, H. Y., Tang, R.-H., Tatsuguchi, M., Huang, Z.-P., et al. (2009). MicroRNA-208a is a regulator of cardiac hypertrophy and conduction in mice. *J. Clin. Invest.* 119, 2772–2786. doi: 10.1172/JCI36154

Canfran-Duque, A., Lin, C. S., Goedeke, L., Suarez, Y., and Fernandez-Hernando, C. (2016). Micro-RNAs and high-density lipoprotein metabolism. *Arterioscler. Thromb. Vasc. Biol.* 36, 1076–1084. doi: 10.1161/ATVBAHA.116.307028

Carè, A., Catalucci, D., Felicetti, F., Bonci, D., Addario, A., Gallo, P., et al. (2007). MicroRNA-133 controls cardiac hypertrophy. *Nat. Med.* 13, 613–618.

Cengiz, M., Yavuzer, S., Kilickiran Avci, B., Yuruyen, M., Yavuzer, H., Dikici, S. A., et al. (2015). Circulating miR-21 and eNOS in subclinical atherosclerosis in patients with hypertension. *Clin. Exp. Hypertens.* 37, 643–649. doi: 10.3109/10641963.2015.1036064

Ceolotto, G., Papparella, I., Bortoluzzi, A., Strapazzon, G., Ragazzo, F., Bratti, P., et al. (2011). Interplay between miR-155, AT1R A1166C polymorphism, and AT1R expression in young untreated hypertensives. *Am. J. Hypertens.* 24, 241–246. doi: 10.1038/ajh.2010.211

Chang, Y. J., Li, Y. S., Wu, C. C., Wang, K. C., Huang, T. C., Chen, Z., et al. (2019). Extracellular MicroRNA-92a mediates endothelial cell-macrophage communication. *Arterioscler. Thromb. Vasc. Biol.* 39, 2492–2504. doi: 10.1161/atvbaha.119.312707

Chen, T., Huang, Z., Wang, L., Wang, Y., Wu, F., Meng, S., et al. (2009). MicroRNA-125a-5p partly regulates the inflammatory response, lipid uptake, and ORP9 expression in oxLDL-stimulated monocyte/macrophages. *Cardiovasc. Res.* 83, 131–139. doi: 10.1093/cvr/cvp121

Cheng, Y., Liu, X., Yang, J., Lin, Y., Xu, D. Z., Lu, Q., et al. (2009). MicroRNA-145, a novel smooth muscle cell phenotypic marker and modulator, controls vascular neointimal lesion formation. *Circ. Res.* 105, 158–166. doi: 10.1161/CIRCRESAHA.109.197517

Cipollone, F., Felicioni, L., Sarzani, R., Ucchino, S., Spigonardo, F., Mandolini, C., et al. (2011). A unique microRNA signature associated with plaque instability in humans. *Stroke* 42, 2556–2563. doi: 10.1161/STROKEAHA.110.597575

Climent, M., Quintavalle, M., Miragoli, M., Chen, J., Condorelli, G., and Elia, L. (2015). TGFbeta triggers miR-143/145 transfer from smooth muscle cells to endothelial cells, thereby modulating vessel stabilization. *Circ. Res.* 116, 1753–1764. doi: 10.1161/circresaha.116.305178

Cohn, J. N., Ferrari, R., and Sharpe, N. (2000). Cardiac remodeling—concepts and clinical implications: a consensus paper from an international forum on cardiac remodeling. *J. Am. Coll. Cardiol.* 35, 569–582. doi: 10.1016/s0735-1097(99)00630-0

Cordes, K. R., Sheehy, N. T., White, M. P., Berry, E. C., Morton, S. U., Muth, A. N., et al. (2009). miR-145 and miR-143 regulate smooth muscle cell fate and plasticity. *Nature* 460, 705–710. doi: 10.1038/nature08195

da Costa Martins, P. A., Salic, K., Gladka, M. M., Armand, A.-S., Leptidis, S., el Azzouzi, H., et al. (2010). MicroRNA-199b targets the nuclear kinase Dyrk1a in an auto-amplification loop promoting calcineurin/NFAT signalling. *Nat. Cell Biol.* 12, 1220–1227. doi: 10.1038/ncb2126

Davidson, S. M., Andreadou, I., Barile, L., Birnbaum, Y., Cabrera-Fuentes, H. A., Cohen, M. V., et al. (2019). Circulating blood cells and extracellular vesicles in acute cardioprotection. *Cardiovasc. Res.* 115, 1156–1166. doi: 10.1093/cvr/cvy314

Devaux, Y., Vausort, M., Goretti, E., Nazarov, P. V., Azuaje, F., Gilson, G., et al. (2012). Use of circulating MicroRNAs to diagnose acute myocardial infarction. *Clin. Chem.* 58, 559–567. doi: 10.1373/clinchem.2011.173823

Dickinson, B. A., Semus, H. M., Montgomery, R. L., Stack, C., Latimer, P. A., Lewton, S. M., et al. (2013). Plasma microRNAs serve as biomarkers of therapeutic efficacy and disease progression in hypertension-induced heart failure. *Eur. J. Heart Fail.* 15, 650–659. doi: 10.1093/eurjhf/hft018

Donners, M. M., Wolfs, I. M., Stoger, L. J., van der Vorst, E. P., Pottgens, C. C., Heymans, S., et al. (2012). Hematopoietic miR155 deficiency enhances atherosclerosis and decreases plaque stability in hyperlipidemic mice. *PLoS One* 7:e35877. doi: 10.1371/journal.pone.0035877

Doring, Y., Noels, H., van der Vorst, E. P. C., Neideck, C., Egea, V., Drechsler, M., et al. (2017). Vascular CXCR4 limits atherosclerosis by maintaining arterial integrity: evidence from mouse and human studies. *Circulation* 136, 388–403. doi: 10.1161/circulationaha.117.027646

Doring, Y., van der Vorst, E. P. C., Duchene, J., Jansen, Y., Gencer, S., Bidzhekov, K., et al. (2019). CXCL12 derived from endothelial cells promotes atherosclerosis to drive coronary artery disease. *Circulation* 139, 1338–1340. doi: 10.1161/circulationaha.118.037953

Dragomir, M. P., Knutsen, E., and Calin, G. A. (2018). SnapShot: unconventional miRNA functions. *Cell* 174, 1038–1038.e1. doi: 10.1016/j.cell.2018.07.040

Du, F., Yu, F., Wang, Y., Hui, Y., Carnevale, K., Fu, M., et al. (2014). MicroRNA-155 deficiency results in decreased macrophage inflammation and attenuated atherogenesis in apolipoprotein E-deficient mice. *Arterioscler. Thromb. Vasc. Biol.* 34, 759–767. doi: 10.1161/atvbaha.113.302701

Eken, S. M., Jin, H., Chernogubova, E., Li, Y., Simon, N., Sun, C., et al. (2017). MicroRNA-210 enhances fibrous cap stability in advanced atherosclerotic lesions. *Circ. Res.* 120, 633–644. doi: 10.1161/CIRCRESAHA.116.309318

El Ouaamari, A., Baroukh, N., Martens, G. A., Lebrun, P., Pipeleers, D., and van Obberghen, E. (2008). miR-375 targets 3'-phosphoinositide-dependent protein kinase-1 and regulates glucose-induced biological responses in pancreatic beta-cells. *Diabetes Metab. Res. Rev.* 57, 2708–2717. doi: 10.2337/db07-1614

Elia, L., Contu, R., Quintavalle, M., Varrone, F., Chimenti, C., Russo, M. A., et al. (2009). Reciprocal regulation of microRNA-1 and insulin-like growth factor-1 signal transduction cascade in cardiac and skeletal muscle in physiological and pathological conditions. *Circulation* 120, 2377–2385. doi: 10.1161/CIRCULATIONAHA.109.879429

Esau, C., Davis, S., Murray, S. F., Yu, X. X., Pandey, S. K., Pear, M., et al. (2006). miR-122 regulation of lipid metabolism revealed by in vivo antisense targeting. *Cell Metab.* 3, 87–98. doi: 10.1016/j.cmet.2006.01.005

Escate, R., Padro, T., Suades, R., Camino, S., Muniz, O., Diaz-Diaz, J. L., et al. (2020). High miR-133a levels in the circulation anticipates presentation of clinical events in familial hypercholesterolemia patients. *Cardiovasc. Res.* doi: 10.1093/cvr/cvaa039 [Epub ahead of print].

Fang, Y., Shi, C., Manduchi, E., Civelek, M., and Davies, P. F. (2010). MicroRNA-10a regulation of proinflammatory phenotype in athero-susceptible endothelium in vivo and in vitro. *Proc. Natl. Acad. Sci. U.S.A.* 107, 13450–13455. doi: 10.1073/pnas.1002120107

Farina, F. M., Hall, I. F., Serio, S., Zani, S. M., Climent, M., Salvarani, N., et al. (2020). miR-128-3p is a novel regulator of vascular smooth muscle cell phenotypic switch and vascular diseases. *Circ. Res.* 126, e120–e135. doi: 10.1161/circresaha.120.316489

Fish, J. E., Santoro, M. M., Morton, S. U., Yu, S., Yeh, R. F., Wythe, J. D., et al. (2008). miR-126 regulates angiogenic signaling and vascular integrity. *Dev. Cell* 15, 272–284. doi: 10.1016/j.devcel.2008.07.008

Frost, R. J., and Olson, E. N. (2011). Control of glucose homeostasis and insulin sensitivity by the Let-7 family of microRNAs. *Proc. Natl. Acad. Sci. U.S.A.* 108, 21075–21080. doi: 10.1073/pnas.1118922109

Gabisonia, K., Prosdocimo, G., Aquaro, G. D., Carlucci, L., Zentilin, L., Secco, I., et al. (2019). MicroRNA therapy stimulates uncontrolled cardiac repair after myocardial infarction in pigs. *Nature* 569, 418–422. doi: 10.1038/s41586-019-1191-6

Gilleron, J., Querbes, W., Zeigerer, A., Borodovsky, A., Marsico, G., Schubert, U., et al. (2013). Image-based analysis of lipid nanoparticle-mediated siRNA delivery, intracellular trafficking and endosomal escape. *Nat. Biotechnol.* 31, 638–646. doi: 10.1038/nbt.2612

Goedeke, L., Rotllan, N., Canfran-Duque, A., Aranda, J. F., Ramirez, C. M., Araldi, E., et al. (2015). MicroRNA-148a regulates LDL receptor and ABCA1 expression to control circulating lipoprotein levels. *Nat. Med.* 21, 1280–1289. doi: 10.1038/nm.3949

Goedeke, L., Salerno, A., Ramirez, C. M., Guo, L., Allen, R. M., Yin, X., et al. (2014). Long-term therapeutic silencing of miR-33 increases circulating triglyceride levels and hepatic lipid accumulation in mice. *EMBO Mol. Med.* 6, 1133–1141. doi: 10.15252/emmm.201404046

Hall, I. F., Climent, M., Quintavalle, M., Farina, F. M., Schorn, T., Zani, S., et al. (2019). Circ_Lrp6, a circular RNA enriched in vascular smooth muscle cells, acts as a sponge regulating miRNA-145 function. *Circ. Res.* 124, 498–510. doi: 10.1161/circresaha.118.314240

Halushka, P. V., Goodwin, A. J., and Halushka, M. K. (2019). Opportunities for microRNAs in the crowded field of cardiovascular biomarkers. *Annu. Rev. Pathol. Mech. Dis.* 14, 211–238. doi: 10.1146/annurev-pathmechdis-012418-012827

Harris, T. A., Yamakuchi, M., Ferlito, M., Mendell, J. T., and Lowenstein, C. J. (2008). MicroRNA-126 regulates endothelial expression of vascular cell adhesion molecule 1. *Proc. Natl. Acad. Sci. U.S.A.* 105, 1516–1521. doi: 10.1073/pnas.0707493105

Hartmann, P., Zhou, Z., Natarelli, L., Wei, Y., Nazari-Jahantigh, M., Zhu, M., et al. (2016). Endothelial dicer promotes atherosclerosis and vascular inflammation by miRNA-103-mediated suppression of KLF4. *Nat. Commun.* 7:10521. doi: 10.1038/ncomms10521

Hayes, J., Peruzzi, P. P., and Lawler, S. (2014). MicroRNAs in cancer: biomarkers, functions and therapy. *Trends Mol. Med.* 20, 460–469. doi: 10.1016/j.molmed.2014.06.005

He, S., Liu, P., Jian, Z., Li, J., Zhu, Y., Feng, Z., et al. (2013). miR-138 protects cardiomyocytes from hypoxia-induced apoptosis via MLK3/JNK/c-jun pathway. *Biochem. Biophys. Res. Commun.* 441, 763–769. doi: 10.1016/j.bbrc.2013.10.151

Hergenreider, E., Heydt, S., Treguer, K., Boettger, T., Horrevoets, A. J., Zeiher, A. M., et al. (2012). Atheroprotective communication between endothelial cells and smooth muscle cells through miRNAs. *Nat. Cell Biol.* 14, 249–256. doi: 10.1038/ncb2441

Higashi, K., Yamada, Y., Minatoguchi, S., Baba, S., Iwasa, M., Kanamori, H., et al. (2015). MicroRNA-145 repairs infarcted myocardium by accelerating cardiomyocyte autophagy. *Am. J. Physiol. Heart Circ. Physiol.* 309, H1813–H1826. doi: 10.1152/ajpheart.00709.2014

Hijmans, J. G., Diehl, K. J., Bammert, T. D., Kavlich, P. J., Lincenberg, G. M., Greiner, J. J., et al. (2018). Association between hypertension and circulating vascular-related microRNAs. *J. Hum. Hypertens.* 32, 440–447. doi: 10.1038/s41371-018-0061-2

Huang, R. S., Hu, G. Q., Lin, B., Lin, Z. Y., and Sun, C. C. (2010). MicroRNA-155 silencing enhances inflammatory response and lipid uptake in oxidized low-density lipoprotein-stimulated human THP-1 macrophages. *J. Invest. Med.* 58, 961–967. doi: 10.231/JIM.0b013e3181ff46d7

Jackson, K. L., Marques, F. Z., Watson, A. M., Palma-Rigo, K., Nguyen-Huu, T. P., Morris, B. J., et al. (2013). A novel interaction between sympathetic overactivity and aberrant regulation of renin by miR-181a in BPH/2J genetically hypertensive mice. *Hypertension* 62, 775–781. doi: 10.1161/HYPERTENSIONAHA.113.01701

Janas, T., Janas, M. M., Sapon, K., and Janas, T. (2015). Mechanisms of RNA loading into exosomes. *FEBS Lett.* 589, 1391–1398. doi: 10.1016/j.febslet.2015.04.036

Janssen, H. L., Reesink, H. W., Lawitz, E. J., Zeuzem, S., Rodriguez-Torres, M., Patel, K., et al. (2013). Treatment of HCV infection by targeting microRNA. *N. Engl. J. Med.* 368, 1685–1694. doi: 10.1056/NEJMoa1209026

Ji, R., Cheng, Y., Yue, J., Yang, J., Liu, X., Chen, H., et al. (2007). MicroRNA expression signature and antisense-mediated depletion reveal an essential role of MicroRNA in vascular neointimal lesion formation. *Circ. Res.* 100, 1579–1588. doi: 10.1161/circresaha.106.141986

Karakas, M., Schulte, C., Appelbaum, S., Ojeda, F., Lackner, K. J., Munzel, T., et al. (2017). Circulating microRNAs strongly predict cardiovascular death in patients with coronary artery disease-results from the large AtheroGene study. *Eur. Heart J.* 38, 516–523. doi: 10.1093/eurheartj/ehw250

Karakikes, I., Chaanine Antoine, H., Kang, S., Mukete Bertrand, N., Jeong, D., Zhang, S., et al. (2013). Therapeutic cardiac-targeted delivery of miR-1 reverses pressure overload–induced cardiac hypertrophy and attenuates pathological remodeling. *J. Am. Heart Assoc.* 2:e000078. doi: 10.1161/JAHA.113.000078

Ke, Z.-P., Xu, P., Shi, Y., and Gao, A.-M. (2016). MicroRNA-93 inhibits ischemia-reperfusion induced cardiomyocyte apoptosis by targeting PTEN. *Oncotarget* 7, 28796–28805. doi: 10.18632/oncotarget.8941

Kim, G. H. (2013). MicroRNA regulation of cardiac conduction and arrhythmias. *Transl. Res.* 161, 381–392. doi: 10.1016/j.trsl.2012.12.004

Kong, L., Zhu, J., Han, W., Jiang, X., Xu, M., Zhao, Y., et al. (2011). Significance of serum microRNAs in pre-diabetes and newly diagnosed type 2 diabetes: a clinical study. *Acta Diabetol.* 48, 61–69. doi: 10.1007/s00592-010-0226-0

Kontaraki, J. E., Marketou, M. E., Zacharis, E. A., Parthenakis, F. I., and Vardas, P. E. (2014). Differential expression of vascular smooth muscle-modulating microRNAs in human peripheral blood mononuclear cells: novel targets in essential hypertension. *J. Hum. Hypertens.* 28, 510–516. doi: 10.1038/jhh.2013.117

Kozomara, A., and Griffiths-Jones, S. (2014). miRBase: annotating high confidence microRNAs using deep sequencing data. *Nucleic Acids Res.* 42, D68–D73. doi: 10.1093/nar/gkt1181

Krenz, M., and Robbins, J. (2004). Impact of beta-myosin heavy chain expression on cardiac function during stress. *J. Am. Coll. Cardiol.* 44, 2390–2397. doi: 10.1016/j.jacc.2004.09.044

Leeper, N. J., Raiesdana, A., Kojima, Y., Chun, H. J., Azuma, J., Maegdefessel, L., et al. (2011). MicroRNA-26a is a novel regulator of vascular smooth muscle cell function. *J. Cell. Physiol.* 226, 1035–1043. doi: 10.1002/jcp.22422

Leidal, A. M., Huang, H. H., Marsh, T., Solvik, T., Zhang, D., Ye, J., et al. (2020). The LC3-conjugation machinery specifies the loading of RNA-binding proteins into extracellular vesicles. *Nat. Cell Biol.* 22, 187–199. doi: 10.1038/s41556-019-0450-y

Li, S., Zhu, J., Zhang, W., Chen, Y., Zhang, K., Popescu, L. M., et al. (2011). Signature microRNA expression profile of essential hypertension and its novel link to human cytomegalovirus infection. *Circulation* 124, 175–184. doi: 10.1161/CIRCULATIONAHA.110.012237

Li, Z., and Rana, T. M. (2014). Therapeutic targeting of microRNAs: current status and future challenges. *Nat. Rev. Drug Discov.* 13, 622–638. doi: 10.1038/nrd4359

Liu, J., van Mil, A., Vrijsen, K., Zhao, J., Gao, L., Metz, C. H. G., et al. (2011). MicroRNA-155 prevents necrotic cell death in human cardiomyocyte progenitor cells via targeting RIP1. *J. Cell Mol. Med.* 15, 1474–1482. doi: 10.1111/j.1582-4934.2010.01104.x

Liu, X., Xu, Y., Deng, Y., and Li, H. (2018). MicroRNA-223 regulates cardiac fibrosis after myocardial infarction by targeting RASA1. *Cell. Physiol. Biochem.* 46, 1439–1454. doi: 10.1159/000489185

Liu, Y., Li, Q., Hosen, M. R., Zietzer, A., Flender, A., Levermann, P., et al. (2019). Atherosclerotic conditions promote the packaging of functional microRNA-92a-3p into endothelial microvesicles. *Circ. Res.* 124, 575–587. doi: 10.1161/circresaha.118.314010

Lovren, F., Pan, Y., Quan, A., Singh, K. K., Shukla, P. C., Gupta, N., et al. (2012). MicroRNA-145 targeted therapy reduces atherosclerosis. *Circulation* 126(11 Suppl. 1), S81–S90. doi: 10.1161/circulationaha.111.084186

Loyer, X., Potteaux, S., Vion, A. C., Guerin, C. L., Boulkroun, S., Rautou, P. E., et al. (2014a). Inhibition of microRNA-92a prevents endothelial dysfunction and atherosclerosis in mice. *Circ. Res.* 114, 434–443. doi: 10.1161/circresaha.114.302213

Loyer, X., Vion, A. C., Tedgui, A., and Boulanger, C. M. (2014b). Microvesicles as cell-cell messengers in cardiovascular diseases. *Circ. Res.* 114, 345–353. doi: 10.1161/circresaha.113.300858

Lv, Y. C., Tang, Y. Y., Peng, J., Zhao, G. J., Yang, J., Yao, F., et al. (2014). MicroRNA-19b promotes macrophage cholesterol accumulation and aortic atherosclerosis by targeting ATP-binding cassette transporter A1. *Atherosclerosis* 236, 215–226. doi: 10.1016/j.atherosclerosis.2014.07.005

Lynn, F. C., Skewes-Cox, P., Kosaka, Y., McManus, M. T., Harfe, B. D., and German, M. S. (2007). MicroRNA expression is required for pancreatic islet cell genesis in the mouse. *Diabetes Metab. Res. Rev.* 56, 2938–2945. doi: 10.2337/db07-0175

Maitrias, P., Metzinger-Le Meuth, V., Massy, Z. A., M'Baya-Moutoula, E., Reix, T., Caus, T., et al. (2015). MicroRNA deregulation in symptomatic carotid plaque. *J. Vasc. Surg.* 62, 1245–1250.e1. doi: 10.1016/j.jvs.2015.06.136

Mandolini, C., Santovito, D., Marcantonio, P., Buttitta, F., Bucci, M., Ucchino, S., et al. (2015). Identification of microRNAs 758 and 33b as potential modulators of ABCA1 expression in human atherosclerotic plaques. *Nutr. Metab. Cardiovasc. Dis.* 25, 202–209. doi: 10.1016/j.numecd.2014.09.005

Marquart, T. J., Wu, J., Lusis, A. J., and Baldan, A. (2013). Anti-miR-33 therapy does not alter the progression of atherosclerosis in low-density lipoprotein receptor-deficient mice. *Arterioscler. Thromb. Vasc. Biol.* 33, 455–458. doi: 10.1161/ATVBAHA.112.300639

Marques, F. Z., Campain, A. E., Tomaszewski, M., Zukowska-Szczechowska, E., Yang, Y. H., Charchar, F. J., et al. (2011). Gene expression profiling reveals renin mRNA overexpression in human hypertensive kidneys and a role for microRNAs. *Hypertension* 58, 1093–1098. doi: 10.1161/HYPERTENSIONAHA.111.180729

Marques, F. Z., and Charchar, F. J. (2015). "microRNAs in essential hypertension and blood pressure regulation," in *microRNA: Medical Evidence: From Molecular Biology to Clinical Practice*, ed. G. Santulli (Cham: Springer International Publishing), 215–235. doi: 10.1007/978-3-319-22671-2_11

Montgomery Rusty, L., Hullinger Thomas, G., Semus Hillary, M., Dickinson Brent, A., Seto Anita, G., Lynch Joshua, M., et al. (2011). Therapeutic inhibition of miR-208a improves cardiac function and survival during heart failure. *Circulation* 124, 1537–1547. doi: 10.1161/CIRCULATIONAHA.111.030932

Najafi-Shoushtari, S. H., Kristo, F., Li, Y., Shioda, T., Cohen, D. E., Gerszten, R. E., et al. (2010). MicroRNA-33 and the SREBP host genes cooperate to control cholesterol homeostasis. *Science* 328, 1566–1569. doi: 10.1126/science.1189123

Natarelli, L., Geissler, C., Csaba, G., Wei, Y., Zhu, M., di Francesco, A., et al. (2018). miR-103 promotes endothelial maladaptation by targeting lncWDR59. *Nat. Commun.* 9:2645. doi: 10.1038/s41467-018-05065-z

Nazari-Jahantigh, M., Wei, Y., Noels, H., Akhtar, S., Zhou, Z., Koenen, R. R., et al. (2012). MicroRNA-155 promotes atherosclerosis by repressing Bcl6 in macrophages. *J. Clin. Invest.* 122, 4190–4202. doi: 10.1172/jci61716

Ortega, F. J., Mercader, J. M., Moreno-Navarrete, J. M., Rovira, O., Guerra, E., Esteve, E., et al. (2014). Profiling of circulating microRNAs reveals common microRNAs linked to type 2 diabetes that change with insulin sensitization. *Diabetes Care* 37, 1375–1383. doi: 10.2337/dc13-1847

Ouimet, M., Ediriweera, H. N., Gundra, U. M., Sheedy, F. J., Ramkhelawon, B., Hutchison, S. B., et al. (2015). MicroRNA-33-dependent regulation of macrophage metabolism directs immune cell polarization in atherosclerosis. *J. Clin. Invest.* 125, 4334–4348. doi: 10.1172/jci81676

Poy, M. N., Eliasson, L., Krutzfeldt, J., Kuwajima, S., Ma, X., Macdonald, P. E., et al. (2004). A pancreatic islet-specific microRNA regulates insulin secretion. *Nature* 432, 226–230. doi: 10.1038/nature03076

Qi, H., Liu, Z., Liu, B., Cao, H., Sun, W., Yan, Y., et al. (2017). micro-RNA screening and prediction model construction for diagnosis of salt-sensitive essential hypertension. *Medicine* 96:e6417. doi: 10.1097/MD.0000000000006417

Ramirez, C. M., Davalos, A., Goedeke, L., Salerno, A. G., Warrier, N., Cirera-Salinas, D., et al. (2011). MicroRNA-758 regulates cholesterol efflux through posttranscriptional repression of ATP-binding cassette transporter A1. *Arterioscler. Thromb. Vasc. Biol.* 31, 2707–2714. doi: 10.1161/atvbaha.111.232066

Rayner, K. J., Sheedy, F. J., Esau, C. C., Hussain, F. N., Temel, R. E., Parathath, S., et al. (2011). Antagonism of miR-33 in mice promotes reverse cholesterol transport and regression of atherosclerosis. *J. Clin. Invest.* 121, 2921–2931. doi: 10.1172/JCI57275

Rayner, K. J., Suarez, Y., Davalos, A., Parathath, S., Fitzgerald, M. L., Tamehiro, N., et al. (2010). MiR-33 contributes to the regulation of cholesterol homeostasis. *Science* 328, 1570–1573. doi: 10.1126/science.1189862

Richards, A. M. (2017). Circulating biomarkers of cardiac fibrosis. *Circ. Heart Fail.* 10:e003936. doi: 10.1161/CIRCHEARTFAILURE.117.003936

Rottiers, V., Obad, S., Petri, A., McGarrah, R., Lindholm, M. W., Black, J. C., et al. (2013). Pharmacological inhibition of a microRNA family in nonhuman primates by a seed-targeting 8-mer antimiR. *Sci. Transl. Med.* 5:212ra162. doi: 10.1126/scitranslmed.3006840

Roy, S., Khanna, S., Hussain, S.-R. A., Biswas, S., Azad, A., Rink, C., et al. (2009). MicroRNA expression in response to murine myocardial infarction: miR-21 regulates fibroblast metalloprotease-2 via phosphatase and tensin homologue. *Cardiovasc. Res.* 82, 21–29. doi: 10.1093/cvr/cvp015

Sala, F., Aranda, J. F., Rotllan, N., Ramirez, C. M., Aryal, B., Elia, L., et al. (2014). MiR-143/145 deficiency attenuates the progression of atherosclerosis in Ldlr-/-mice. *Thromb. Haemost.* 112, 796–802. doi: 10.1160/th13-11-0905

Santovito, D., De Nardis, V., Marcantonio, P., Mandolini, C., Paganelli, C., Vitale, E., et al. (2014). Plasma exosome microRNA profiling unravels a new potential modulator of adiponectin pathway in diabetes: effect of glycemic control. *J. Clin. Endocrinol. Metab.* 99, E1681–E1685.

Santovito, D., Egea, V., Bidzhekov, K., Natarelli, L., Mourão, A., Blanchet, X., et al. (2020a). Non-canonical inhibition of caspase-3 by a nuclear microRNA confers endothelial protection by autophagy in atherosclerosis. *Sci. Transl. Med.* 12:eeaz2294. doi: 10.1126/scitranslmed.aaz2294

Santovito, D., Marcantonio, P., Mastroiacovo, D., Natarelli, L., Mandolini, C., De Nardis, V., et al. (2020b). High dose rosuvastatin increases ABCA1 transporter in human atherosclerotic plaques in a cholesterol-independent fashion. *Int. J. Cardiol.* 299, 249–253. doi: 10.1016/j.ijcard.2019.07.094

Santovito, D., Mandolini, C., Marcantonio, P., De Nardis, V., Bucci, M., Paganelli, C., et al. (2013). Overexpression of microRNA-145 in atherosclerotic plaques from hypertensive patients. *Expert Opin. Ther. Targets* 17, 217–223. doi: 10.1517/14728222.2013.745512

Santovito, D., and Weber, C. (2017). Zooming in on microRNAs for refining cardiovascular risk prediction in secondary prevention. *Eur. Heart J.* 38, 524–528. doi: 10.1093/eurheartj/ehw259

Santulli, G., Iaccarino, G., De Luca, N., Trimarco, B., and Condorelli, G. (2014). Atrial fibrillation and microRNAs. *Front. Physiol.* 5:15. doi: 10.3389/fphys.2014.00015

Schober, A., Nazari-Jahantigh, M., Wei, Y., Bidzhekov, K., Gremse, F., Grommes, J., et al. (2014). MicroRNA-126-5p promotes endothelial proliferation and limits atherosclerosis by suppressing Dlk1. *Nat. Med.* 20, 368–376. doi: 10.1038/nm.3487

Sethupathy, P., Borel, C., Gagnebin, M., Grant, G. R., Deutsch, S., Elton, T. S., et al. (2007). Human microRNA-155 on chromosome 21 differentially interacts with its polymorphic target in the AGTR1 3' untranslated region: a mechanism for functional single-nucleotide polymorphisms related to phenotypes. *Am. J. Hum. Genet.* 81, 405–413. doi: 10.1086/519979

Soeki, T., Yamaguchi, K., Niki, T., Uematsu, E., Bando, S., Matsuura, T., et al. (2015). Plasma microRNA-100 is associated with coronary plaque vulnerability. *Circ. J.* 79, 413–418. doi: 10.1253/circj.cj-14-0958

Soh, J., Iqbal, J., Queiroz, J., Fernandez-Hernando, C., and Hussain, M. M. (2013). MicroRNA-30c reduces hyperlipidemia and atherosclerosis in mice by decreasing lipid synthesis and lipoprotein secretion. *Nat. Med.* 19, 892–900. doi: 10.1038/nm.3200

Song, C.-L., Liu, B., Diao, H.-Y., Shi, Y.-F., Zhang, J.-C., Li, Y.-X., et al. (2016). Down-regulation of microRNA-320 suppresses cardiomyocyte apoptosis and protects against myocardial ischemia and reperfusion injury by targeting IGF-1. *Oncotarget* 7, 39740–39757. doi: 10.18632/oncotarget.9240

Szemraj-Rogucka, Z. M., Szemraj, J., Masiarek, K., and Majos, A. (2019). Circulating microRNAs as biomarkers for myocardial fibrosis in patients with left ventricular non-compaction cardiomyopathy. *Arch. Med. Sci.* 15, 376–384. doi: 10.5114/aoms.2019.82919

Taganov, K. D., Boldin, M. P., Chang, K. J., and Baltimore, D. (2006). NF-kappaB-dependent induction of microRNA miR-146, an inhibitor targeted to signaling proteins of innate immune responses. *Proc. Natl. Acad. Sci. U.S.A.* 103, 12481–12486. doi: 10.1073/pnas.0605298103

Thum, T., Gross, C., Fiedler, J., Fischer, T., Kissler, S., Bussen, M., et al. (2008). MicroRNA-21 contributes to myocardial disease by stimulating MAP kinase signalling in fibroblasts. *Nature* 456, 980–984. doi: 10.1038/nature07511

Tielking, K., Fischer, S., Preissner, K. T., Vajkoczy, P., and Xu, R. (2019). Extracellular RNA in central nervous system pathologies. *Front. Mol. Neurosci.* 12:254. doi: 10.3389/fnmol.2019.00254

Tijsen, A. J., Pinto, Y. M., and Creemers, E. E. (2012). Circulating microRNAs as diagnostic biomarkers for cardiovascular diseases. *Am. J. Physiol. Heart Circ. Physiol.* 303, H1085–H1095. doi: 10.1152/ajpheart.00191.2012

Trajkovski, M., Hausser, J., Soutschek, J., Bhat, B., Akin, A., Zavolan, M., et al. (2011). MicroRNAs 103 and 107 regulate insulin sensitivity. *Nature* 474, 649–653. doi: 10.1038/nature10112

Tsai, P. C., Liao, Y. C., Wang, Y. S., Lin, H. F., Lin, R. T., and Juo, S. H. (2013). Serum microRNA-21 and microRNA-221 as potential biomarkers for cerebrovascular disease. *J. Vasc. Res.* 50, 346–354. doi: 10.1159/000351767

Tsai, W. C., Hsu, S. D., Hsu, C. S., Lai, T. C., Chen, S. J., Shen, R., et al. (2012). MicroRNA-122 plays a critical role in liver homeostasis and hepatocarcinogenesis. *J. Clin. Invest.* 122, 2884–2897. doi: 10.1172/JCI63455

Valadi, H., Ekstrom, K., Bossios, A., Sjostrand, M., Lee, J. J., and Lotvall, J. O. (2007). Exosome-mediated transfer of mRNAs and microRNAs is a novel mechanism of genetic exchange between cells. *Nat. Cell Biol.* 9, 654–659. doi: 10.1038/ncb1596

van der Vorst, E. P., Doring, Y., and Weber, C. (2015). MIF and CXCL12 in cardiovascular diseases: functional differences and similarities. *Front. Immunol.* 6:373. doi: 10.3389/fimmu.2015.00373

van Rooij, E., Purcell, A. L., and Levin, A. A. (2012). Developing microRNA therapeutics. *Circ. Res.* 110, 496–507. doi: 10.1161/CIRCRESAHA.111.247916

van Rooij, E., Sutherland, L. B., Liu, N., Williams, A. H., McAnally, J., Gerard, R. D., et al. (2006). A signature pattern of stress-responsive microRNAs that can evoke cardiac hypertrophy and heart failure. *Proc. Natl. Acad. Sci. U.S.A.* 103, 18255–18260. doi: 10.1073/pnas.0608791103

van Zandwijk, N., Pavlakis, N., Kao, S. C., Linton, A., Boyer, M. J., Clarke, S., et al. (2017). Safety and activity of microRNA-loaded minicells in patients with recurrent malignant pleural mesothelioma: a first-in-man, phase 1, open-label, dose-escalation study. *Lancet Oncol.* 18, 1386–1396. doi: 10.1016/s1470-2045(17)30621-6

Vickers, K. C., Landstreet, S. R., Levin, M. G., Shoucri, B. M., Toth, C. L., Taylor, R. C., et al. (2014). MicroRNA-223 coordinates cholesterol homeostasis. *Proc. Natl. Acad. Sci. U.S.A.* 111, 14518–14523. doi: 10.1073/pnas.1215767111

Vickers, K. C., Palmisano, B. T., Shoucri, B. M., Shamburek, R. D., and Remaley, A. T. (2011). MicroRNAs are transported in plasma and delivered to recipient cells by high-density lipoproteins. *Nat. Cell Biol.* 13, 423–433. doi: 10.1038/ncb2210

Villarroya-Beltri, C., Gutierrez-Vazquez, C., Sanchez-Cabo, F., Perez-Hernandez, D., Vazquez, J., Martin-Cofreces, N., et al. (2013). Sumoylated hnRNPA2B1 controls the sorting of miRNAs into exosomes through binding to specific motifs. *Nat. Commun.* 4:2980. doi: 10.1038/ncomms3980

Wagschal, A., Najafi-Shoushtari, S. H., Wang, L., Goedeke, L., Sinha, S., deLemos, A. S., et al. (2015). Genome-wide identification of microRNAs regulating cholesterol and triglyceride homeostasis. *Nat. Med.* 21, 1290–1297. doi: 10.1038/nm.3980

Wang, F., Long, G., Zhao, C., Li, H., Chaugai, S., Wang, Y., et al. (2013). Plasma microRNA-133a is a new marker for both acute myocardial infarction and underlying coronary artery stenosis. *J. Transl. Med.* 11:222. doi: 10.1186/1479-5876-11-222

Wang, G. K., Zhu, J. Q., Zhang, J. T., Li, Q., Li, Y., He, J., et al. (2010). Circulating microRNA: a novel potential biomarker for early diagnosis of acute myocardial infarction in humans. *Eur. Heart J.* 31, 659–666. doi: 10.1093/eurheartj/ehq013

Wang, J., Song, Y., Zhang, Y., Xiao, H., Sun, Q., Hou, N., et al. (2012). Cardiomyocyte overexpression of miR-27b induces cardiac hypertrophy and dysfunction in mice. *Cell Res.* 22, 516–527. doi: 10.1038/cr.2011.132

Wang, J.-X., Zhang, X.-J., Li, Q., Wang, K., Wang, Y., Jiao, J.-Q., et al. (2015). MicroRNA-103/107 regulate programmed necrosis and myocardial ischemia/reperfusion injury through targeting FADD. *Circ. Res.* 117, 352–363. doi: 10.1161/CIRCRESAHA.117.305781

Wang, K., An, T., Zhou, L. Y., Liu, C. Y., Zhang, X. J., Feng, C., et al. (2015). E2F1-regulated miR-30b suppresses cyclophilin D and protects heart from ischemia/reperfusion injury and necrotic cell death. *Cell Death Differ.* 22, 743–754. doi: 10.1038/cdd.2014.165

Wang, Y., Chen, S., Gao, Y., and Zhang, S. (2017). Serum MicroRNA-27b as a screening biomarker for left ventricular hypertrophy. *Tex. Heart Inst. J.* 44, 385–389. doi: 10.14503/thij-16-5955

Weber, C., and Noels, H. (2011). Atherosclerosis: current pathogenesis and therapeutic options. *Nat. Med.* 17, 1410–1422. doi: 10.1038/nm.2538

Wei, Y., Corbalan-Campos, J., Gurung, R., Natarelli, L., Zhu, M., Exner, N., et al. (2018). Dicer in macrophages prevents atherosclerosis by promoting mitochondrial oxidative metabolism. *Circulation* 138, 2007–2020. doi: 10.1161/circulationaha.117.031589

Wei, Y., Zhu, M., Corbalan-Campos, J., Heyll, K., Weber, C., and Schober, A. (2015). Regulation of Csf1r and Bcl6 in macrophages mediates the stage-specific effects of microRNA-155 on atherosclerosis. *Arterioscler. Thromb. Vasc. Biol.* 35, 796–803. doi: 10.1161/atvbaha.114.304723

Westermann, D., Lindner, D., Kasner, M., Zietsch, C., Savvatis, K., Escher, F., et al. (2011). Cardiac inflammation contributes to changes in the extracellular matrix in patients with heart failure and normal ejection fraction. *Circ. Heart Fail.* 4, 44–52. doi: 10.1161/CIRCHEARTFAILURE.109.931451

Wu, W., Xiao, H., Laguna-Fernandez, A., Villarreal, G. Jr., Wang, K. C., Geary, G. G., et al. (2011). Flow-dependent regulation of kruppel-like factor 2 is mediated by MicroRNA-92a. *Circulation* 124, 633–641. doi: 10.1161/circulationaha.110.005108

Xin, M., Small, E. M., Sutherland, L. B., Qi, X., McAnally, J., Plato, C. F., et al. (2009). MicroRNAs miR-143 and miR-145 modulate cytoskeletal dynamics and responsiveness of smooth muscle cells to injury. *Genes Dev.* 23, 2166–2178. doi: 10.1101/gad.1842409

Yang, W. J., Yang, D. D., Na, S., Sandusky, G. E., Zhang, Q., and Zhao, G. (2005). Dicer is required for embryonic angiogenesis during mouse development. *J. Biol. Chem.* 280, 9330–9335. doi: 10.1074/jbc.m413394200

Yuan, J., Liu, H., Gao, W., Zhang, L., Ye, Y., Yuan, L., et al. (2018). MicroRNA-378 suppresses myocardial fibrosis through a paracrine mechanism at the early stage of cardiac hypertrophy following mechanical stress. *Theranostics* 8, 2565–2582. doi: 10.7150/thno.22878

Zampetaki, A., Kiechl, S., Drozdov, I., Willeit, P., Mayr, U., Prokopi, M., et al. (2010). Plasma microRNA profiling reveals loss of endothelial miR-126 and other microRNAs in type 2 diabetes. *Circ. Res.* 107, 810–817. doi: 10.1161/CIRCRESAHA.110.226357

Zampetaki, A., Willeit, P., Drozdov, I., Kiechl, S., and Mayr, M. (2012a). Profiling of circulating microRNAs: from single biomarkers to re-wired networks. *Cardiovasc. Res.* 93, 555–562. doi: 10.1093/cvr/cvr266

Zampetaki, A., Willeit, P., Tilling, L., Drozdov, I., Prokopi, M., Renard, J. M., et al. (2012b). Prospective study on circulating MicroRNAs and risk of myocardial infarction. *J. Am. Coll. Cardiol.* 60, 290–299. doi: 10.1016/j.jacc.2012.03.056

Zernecke, A., Bidzhekov, K., Noels, H., Shagdarsuren, E., Gan, L., Denecke, B., et al. (2009). Delivery of microRNA-126 by apoptotic bodies induces CXCL12-dependent vascular protection. *Sci. Signal.* 2:ra81. doi: 10.1126/scisignal.2000610

Zhang, Y., Huang, X. R., Wei, L. H., Chung, A. C., Yu, C. M., and Lan, H. Y. (2014). miR-29b as a therapeutic agent for angiotensin II-induced cardiac fibrosis by targeting TGF-beta/Smad3 signaling. *Mol. Ther.* 22, 974–985. doi: 10.1038/mt.2014.25

Zhang, Y., Kim, M. S., Jia, B., Yan, J., Zuniga-Hertz, J. P., Han, C., et al. (2017). Hypothalamic stem cells control ageing speed partly through exosomal miRNAs. *Nature* 548, 52–57. doi: 10.1038/nature23282

Zhao, H., Guan, J., Lee, H. M., Sui, Y., He, L., Siu, J. J., et al. (2010). Up-regulated pancreatic tissue microRNA-375 associates with human type 2 diabetes through beta-cell deficit and islet amyloid deposition. *Pancreas* 39, 843–846. doi: 10.1097/MPA.0b013e3181d12613

Zhou, S. S., Jin, J. P., Wang, J. Q., Zhang, Z. G., Freedman, J. H., Zheng, Y., et al. (2018). miRNAS in cardiovascular diseases: potential biomarkers, therapeutic targets and challenges. *Acta Pharmacol. Sin.* 39, 1073–1084. doi: 10.1038/aps.2018.30

Zhu, H., Shyh-Chang, N., Segre, A. V., Shinoda, G., Shah, S. P., Einhorn, W. S., et al. (2011). The Lin28/let-7 axis regulates glucose metabolism. *Cell* 147, 81–94. doi: 10.1016/j.cell.2011.08.033

Conflict of Interest: The authors declare that the research was conducted in the absence of any commercial or financial relationships that could be construed as a potential conflict of interest.

frontiers in Medicine

ORIGINAL RESEARCH
published: 29 July 2020
doi: 10.3389/fmed.2020.00380

Antiplatelet Activity of Tussilagone via Inhibition of the GPVI Downstream Signaling Pathway in Platelets

Jing Zhou[1], *Ru-Ping Yang*[2]*, *Wei Song*[3]*, *Hui-Min Xu*[4] *and Yong-Hui Wang*[1]

[1] Department of Pharmacy, Zhumadian Central Hospital, Zhumadian, China, [2] Department of Pharmacy, Xiangyang Central Hospital, Affiliated Hospital of Hubei University of Arts and Science, Xiangyang, China, [3] Department of Pharmacy, Renmin Hospital, Wuhan University, Wuhan, China, [4] Department of Pharmacy, Second Affiliated Hospital, Zhejiang University School of Medicine, Hangzhou, China

Tussilagone is a sesquiterpenoid extracted from *Tussilago farfara* and is used as an oriental medicine for asthma and bronchitis. Although previous studies have shown that tussilagone has an inhibitory effect on platelet aggregation, no studies have been performed to investigate its precise effect on platelets, and the underlying mechanism remains unclear. In the present study, we showed that tussilagone inhibited platelet aggregation induced by collagen, thrombin and ADP, as well as platelet release induced by collagen and thrombin, in mice. Tussilagone decreased P-selectin expression and αIIbβ3 activation (JON/A binding) in activated platelets, which indicated that tussilagone inhibited platelet activation. Moreover, tussilagone suppressed platelet spreading on fibrinogen and clot retraction. The levels of phosphorylated Syk, PLCγ2, Akt, GSK3β, and MAPK (ERK1/2 and P38) and molecules associated with GPVI downstream signaling were downregulated in the presence of tussilagone. In addition, tussilagone prolonged the occlusion time in a mouse model of $FeCl_3$-induced carotid artery thrombosis and had no effect on mouse tail bleeding time. These results indicate that tussilagone inhibits platelet function *in vitro* and *in vivo* and that the underlying mechanism involves the Syk/PLCγ2-PKC/MAPK and PI3K-Akt-GSK3β signaling pathways downstream of GPVI. This research suggests that tussilagone is a potential candidate antiplatelet drug for the prevention of thrombosis.

Keywords: tussilagone, sesquiterpenoid, antiplatelet, thrombosis, glycoprotein VI pathway

OPEN ACCESS

Edited by:
Ritva Tikkanen,
University of Giessen, Germany

Reviewed by:
Christine Shu Mei Lee,
Anzac Research Institute, Australia
Ilaria Canobbio,
University of Pavia, Italy

***Correspondence:**
Ru-Ping Yang
yangruping666@126.com
Wei Song
lianzi87@126.com

Specialty section:
This article was submitted to Hematology, a section of the journal Frontiers in Medicine

Received: *25 March 2020*
Accepted: *19 June 2020*
Published: *29 July 2020*

Citation:
Zhou J, Yang R-P, Song W, Xu H-M and Wang Y-H (2020) Antiplatelet Activity of Tussilagone via Inhibition of the GPVI Downstream Signaling Pathway in Platelets. Front. Med. 7:380. doi: 10.3389/fmed.2020.00380

INTRODUCTION

Platelets play important roles in hemostasis, thrombosis, inflammation, immunity, tumor metastasis and cardiovascular diseases, such as heart failure, ischemic stroke, and acute coronary syndrome (1–6). Platelets are activated by a variety of receptor-mediated stimulants, such as collagen, thrombin, ADP and thromboxane A2 (TxA2), which promotes a signaling cascade within platelets, resulting in platelet deformation, release of granular substances, and synthesis of thromboxane to promote the formation of thrombus (2). Antiplatelet therapy is still paramount to the management of these diseases.

Recent studies highlighted the importance of platelet glycoprotein (GP) VI receptor, widely known as the major receptor for collagen, and also binds to laminins, immobilized fibrinogen and fibrin (7, 8). Binding of GPVI to collagen induces tyrosine phosphorylation of the immune-receptor tyrosine-based activation motif (ITAM) in the cytoplasmic tail of the FcRγ chain, leading to a tyrosine phosphorylation-regulated cascade that involves Syk and PLCγ2 (9). Platelet GPVI represents an attractive new target because it is only expressed on platelets and megakaryocytes. In addition, GPVI blockade has been demonstrated to have efficient antithrombotic potential and show beneficial effects in other diseases (10).

At present, antiplatelet therapy mainly targets signaling pathways in platelets, such as TXA2 synthesis, adenosine diphosphate (ADP)-mediated signaling, cAMP, and integrin αIIbβ3-mediated signaling pathways (11). Although current antiplatelet agents are commonly used in clinical practice, their limitations still need to be addressed. The main severe and relatively common side effect of antiplatelet therapy is a higher risk of hemorrhage, for example, gastrointestinal bleeding and intracranial and intracerebral hemorrhage (12, 13). Another limitation affecting the efficiency of many antiplatelet drugs is genetic differences in the ability to metabolize prodrugs, such as clopidogrel, acquired anaphylaxis (heparin and aspirin) and drug resistance (aspirin) (14, 15). Thus, there is a need to develop novel platelet inhibitors with better efficacy and safety.

A multitude of traditional Chinese medicines (TCMs) are thought to promote blood circulation and remove blood stasis (16–18). Sesquiterpenoids extracted from the rhizomes of *Curcuma zedoaria* have been reported to have antiplatelet effects (19). Tussilagone, a sesquiterpene, can be extracted from the flower buds of the TCM *Tussilago farfara* L. (*T. farfara*) and used as an index of chemical extraction of *T. farfara*. Recent studies have shown that tussilagone has anti-inflammatory activity (20–22), inhibits dendritic cell function (23), suppresses the production and gene expression of MUC5AC mucin (24), and suppresses angiogenesis (25). Tussilagone has also been previously reported to have an inhibitory effect on rabbit platelet aggregation (26). However, to date, there have been no other reports on the effects of tussilagone on platelets. In this study, we investigated the effects of tussilagone on platelet function and arterial thrombosis and elucidated the possible underlying mechanism of these effects.

MATERIALS AND METHODS

Reagents and Chemicals

Tussilagone (**Figure 1**) was obtained from Chengdu Preferred Bio-tech Co., Ltd. (Sichuan, China). Dimethylsulfoxide (DMSO), ethylenediamine tetraacetic acid (EDTA), bovine serum albumin (BSA), adenosine diphosphate (ADP), thrombin, prostaglandin E1 (PGE_1), and phalloidin tetramethylrhodamine isothiocyanate (phalloidin-TRITC) were purchased from Sigma Chemicals (St. Louis, MO, USA). Collagen (Type I, from equine tendons suspended in an isotonic glucose solution of pH 2.7) and luciferin-luciferase were purchased from Chrono-Log Corp. (Havertown, PA, USA). Antibodies against phospho-Akt (Ser473), phospho-GSK3β (Ser9), phospho-p38 (Thr180/Tyr182), phospho-ERK1/2 (Tyr202/204), and phospho-$PLC\gamma_2$ (Tyr1217) were purchased from Cell Signaling (Beverly, MA, USA). Antibodies against phospho-Syk (Tyr525/526) were purchased from ABclonal Technology (Wuhan, Hubei, China). Anti-AKT, anti-GSK3β, anti-Syk, anti-p38, anti-ERK1/2, anti-$PLC\gamma_2$, anti-GAPDH and HRP-conjugated goat anti–rabbit IgG antibodies were obtained from Santa Cruz Biotechnology (Santa Cruz, CA, USA). A FITC-conjugated anti-CD62P antibody was obtained from BD Biosciences (San Jose, CA, USA). A PE-conjugated anti-αIIbβ3 antibody (JON/A) (M023-2) was obtained from Emfret Analytics (Eibelstadt, Germany). Protease and phosphatase inhibitor cocktails were purchased from EMD Millipore Chemicals (Billerica, MA, USA). The ECL Western blotting detection reagent was purchased from Pierce Chemical Co. (Rockford, IL, USA).

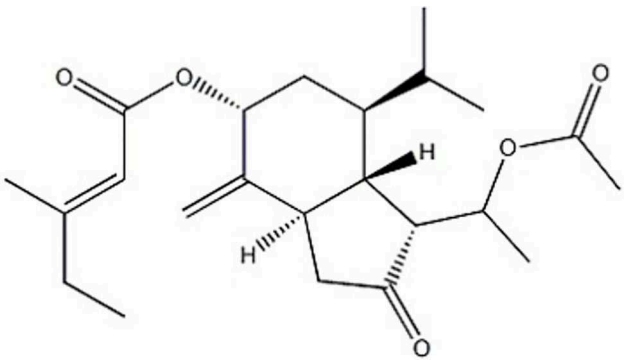

FIGURE 1 | Chemical structure of tussilagone.

Animals

Male ICR mice (weight, 18–25 g; age, 8 weeks) purchased from Hubei Experimental Animal Research Center (Wuhan, Hubei, China) were housed in a specific pathogen-free environment under standard laboratory conditions: relative humidity of 55–65%, temperature of 22–24°C, 12-h dark/light cycle (lights on at 7:00; lights off at 19:00). The mice were provided free access to food and water and acclimated for at least 1 week before the experiment. All experimental protocols and animal care procedures were carried out according to the relevant guidelines and were approved by the Ethics Committee for Experimental Animals at Zhumadian Central Hospital.

To investigate the effect of tussilagone on platelets *in vivo*, mice were separated into two groups ($n = 8$ per group). The tussilagone mice were orally administered tussilagone (10 mg/kg) daily (25), while the control mice received the same dose of corn oil. After 7 days, the mice were used for ferric chloride-induced carotid injury experiments, a tail bleeding time assay and an *ex vivo* platelet aggregation test.

Mouse Platelet Isolation and Preparation

Washed mouse platelets and platelet-rich plasma (PRP) were prepared as described previously (27). Briefly, after mice were anesthetized with urethane by intraperitoneal injection, whole blood was drawn from the inferior vena cava into a syringe containing 3.8% sodium citrate (9:1, v/v). PRP was obtained by removing red blood cells after centrifuging the whole blood for 15 min at 150 × g. By centrifuging blood samples that contained almost no platelets at 800 × g for 15 min, the supernatant was obtained as the platelet-poor plasma (PPP) fraction. The PPP was used as a reference solution and diluent in the aggregation assay. Blood (2–3 mL) was diluted with Tyrode's buffer (137 mM NaCl, 13.8 mM $NaHCO_3$, 5.5 mM glucose, 2.5 mM KCl, 20 mM HEPES, and 0.36 mM NaH_2PO_4, pH 7.4) containing 1 μM PGE1 and centrifuged at 160 × g for 15 min at room temperature to obtain platelets. The platelets were washed twice softly with Tyrode's buffer containing 1 μM PGE1 and 1 mM EDTA. The pelleted platelets were resuspended in Tyrode's buffer (3.0×10^8/mL) and incubated for 30 min at 37°C prior to stimulation.

Platelet Aggregation and ATP Release Assays

Platelet aggregation and ATP release assays were performed as described previously (28) by using an aggregometer (Chrono-Log Corp., Havertown, PA, USA). Briefly, washed platelet suspensions or PRP (3×10^8/mL) was placed *in silicon*ized glass cuvettes at 37°C with a stir speed of 1,000 rev/min in the aggregometer. Before stimulation with different agonists, the washed platelets and PRP were preincubated with 0.4% DMSO (vehicle) or different concentrations of tussilagone (10, 20, or 40 μM) for 5 min at 37°C. $CaCl_2$ (final concentration of 1 mM) was added prior to agonist stimulation. When the platelets were stimulated with agonist, platelet ATP release was measured using luciferin-luciferase reagent. The aggregation and ATP release results were recorded by Aggregolink software. The data are presented as actual traces, and the aggregation and ATP release of untreated platelets (vehicle) were set as 100%. Aggregation was assessed turbidimetrically and expressed as the percent change in light transmission.

Clot Retraction

A total of 500 μL of washed platelet suspension (3.0×10^8/mL) containing 400 μg/mL fibrinogen and 1 mM $CaCl_2$ was stimulated with 5 μL of thrombin (20 U/mL) to initiate clot retraction at 37°C. Clot retraction was monitored by taking photographs at the indicated time points using a digital camera (Nikon D90, Japan).

Platelet Spreading

Washed platelets (3.0×10^7/mL) were incubated with different concentrations of Tussilagone (10, 20, or 40 μM) or vehicle (0.4% DMSO) for 5 min and permitted to spread on coverglasses coated with fibrinogen (25 μg/mL) or BSA for 45 min at 37°C in 24-well plates. Then, PBS was used to wash the coverglasses twice after the platelet suspension was removed. The adherent platelets were fixed with 2% paraformaldehyde, permeabilized with 0.1% Triton, and stained with fluorescein-labeled phalloidin. A fluorescence microscope (Nikon TE-2000S, Japan) was used to obtain images, and ImageJ software (NIH, USA) was used to calculate the platelet spreading area.

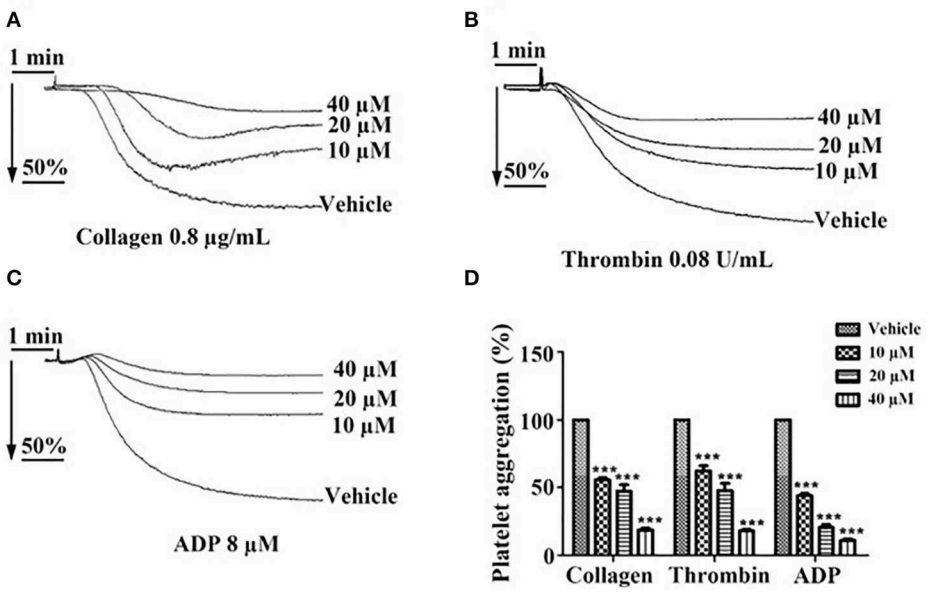

FIGURE 2 | Inhibitory effect of tussilagone on platelet aggregation induced by different agonists. Preincubated with different concentrations of tussilagone (10, 20, or 40 μM) or vehicle for 5 min, platelet aggregation of washed platelets induced by **(A)** collagen (0.8 μg/mL) or **(B)** thrombin (0.08 U/mL) and platelet aggregation of PRP (3.0×10^8/mL) induced by **(C)** ADP (8 μM). **(D)** The aggregation (%) were quantified. One-way ANOVA was used for analysis. The data are presented as the mean ± SEM ($n = 4$). ***$p < 0.001$, vs. vehicle.

Flow Cytometry Analysis

A FITC-conjugated anti-CD62P antibody or PE-labeled anti-αIIbβ3 antibody (JON/A) was added to washed platelets (5.0×10^7/mL) pretreated with different concentrations of Tussilagone (10, 20, or 40 μM) or vehicle (0.4% DMSO) for 5 min at 37°C, and the platelets were incubated for 15 min at room temperature in the dark. Then, the samples were analyzed by flow cytometry (BD Biosciences, CA).

Western Blotting

Resting washed platelets (3.0×10^8/mL) or platelets stimulated with the agonist after being preincubated with tussilagone or vehicle for 5 min were lysed with the same volume of 2× lysis buffer (300 mM NaCl, 20 mM EGTA, 2% Triton X-100, 30 mM HEPES, 0.2 mM $MgCl_2$, 2× protease inhibitor cocktail and 2× phosphatase inhibitor cocktail). The protein concentration was quantified by a BCA assay. We subjected the samples to electrophoresis on a 10% SDS polyacrylamide gel (SDS-PAGE) and transferred them to polyvinylidene difuoride (PVDF) membranes. The membranes were blocked with 5% skim milk for 1 h at room temperature before incubated with the corresponding antibodies. Then, the membranes were incubated with appropriate HRP-conjugated secondary antibodies for 1 h at room temperature. The blots were developed using a chemical luminescence imaging system (DNR Bio-imaging Systems) and analyzed by ImageJ.

Ferric Chloride-Induced ($FeCl_3$) Carotid Injury

A carotid thrombosis model was established as previously described (28). After anesthetization by intraperitoneal injection of urethane, the left common carotid artery was exposed. Blood flow was continuously monitored using a perivascular flow probe (Transonic, UK) connected to a TS420 flow meter (Transonic, UK). A 2-mm strip of filter paper saturated with 12% $FeCl_3$ was applied to the carotid artery surface for 3 min. Blood flow was monitored for 30 min or until the absence of blood for 1 min after removal of the filter paper. Occlusion was defined as the time required for > 90% loss of the initial blood volume.

Tail Bleeding Assay

The mice were anesthetized, and a 3-mm segment of the tail tip was amputated with a scalpel. Tail bleeding was monitored by gently absorbing the blood with filter paper at 30-s intervals without touching the wound site. The bleeding time was defined as the time required for bleeding to stop for more than 1 min or 30 min.

Statistical Analysis

We analyzed the data using GraphPad Software 6.0 (Graph Pad, USA). All data were normally distributed and expressed as the means ± standard errors of the mean (SEMs). Data were analyzed by Two-tailed unpaired Student's *t*-test or one-way ANOVA followed by Tukey's multiple comparison test. $P < 0.05$ were considered statistically significant.

RESULTS

Tussilagone Inhibits Platelet Aggregation

Incubation of washed platelets or PRP with tussilagone (10, 20, or 40 μM) for 5 min led to a concentration-dependent inhibitory effect on platelet aggregation induced by collagen (0.8 μg/mL) (55.7 ± 1.5, 47.3 ± 4.7, and 18.7 ± 1.3%, respectively), thrombin (0.08 U/mL) (62.3 ± 3.8, 47.7 ± 5.5, and 18.0 ± 1.2%, respectively) and ADP (8 μM) (44.0 ± 1.5, 20.7 ± 2.2, and 11.0 ± 1.2%, respectively) (**Figure 2**).

Tussilagone Inhibits Platelet Granule Secretion and Platelet Activation

To investigate whether tussilagone has an effect on platelet granule secretion, washed platelets were preincubated with different concentrations of tussilagone and then stimulated with collagen (0.8 μg/mL) or thrombin (0.08 U/mL). The results showed that tussilagone (10, 20, or 40 μM) had a significant inhibitory effect on platelet ATP release induced by collagen (61.2 ± 2.3, 44.0 ± 4.5, and 24.7 ± 2.3%, respectively) and thrombin (60.0 ± 2.9, 41.7 ± 2.0, and 27.3 ± 1.8%, respectively) (**Figures 3A,B**). Then, we examined the effect of tussilagone on platelet activation. Washed platelets were preincubated with tussilagone before stimulation with thrombin (0.2 U/mL) and P-selectin expression and αIIbβ3 activation (JON/A binding) were detected by flow cytometry. We found that tussilagone also inhibited platelet P-selectin expression and JON/A binding (**Figures 3C,D**).

Tussilagone Suppresses Platelet Spreading on Fibrinogen and Clot Retraction

Platelet spreading on fibrinogen was investigated after preincubation with tussilagone (10, 20, or 40 μM). Compared to that in the vehicle group, the formation of filopodia and lamellipodia by platelets, as well as the area of single adherent platelets and relative surface coverage area were reduced in the tussilagone-treated group in a dose-dependent manner (**Figures 4A,B**). In addition, in the presence of tussilagone, especially at the high dose, clot retraction was also significantly suppressed (**Figures 4C,D**).

Tussilagone Negatively Affects Collagen-Induced Intracellular Signaling in Platelets

To investigate how tussilagone inhibits platelet function, we examined signaling molecules in platelets after collagen stimulation. Western blotting results showed that the levels of Syk, PLCγ2, Akt, and GSK3β, as well as the phosphorylation of mitogen-activated protein kinase (MAPK) family members (ERK1/2 and P38), were decreased by tussilagone (40 μM) (**Figure 5**). These findings indicate that tussilagone negatively regulates GPVI signaling in platelets.

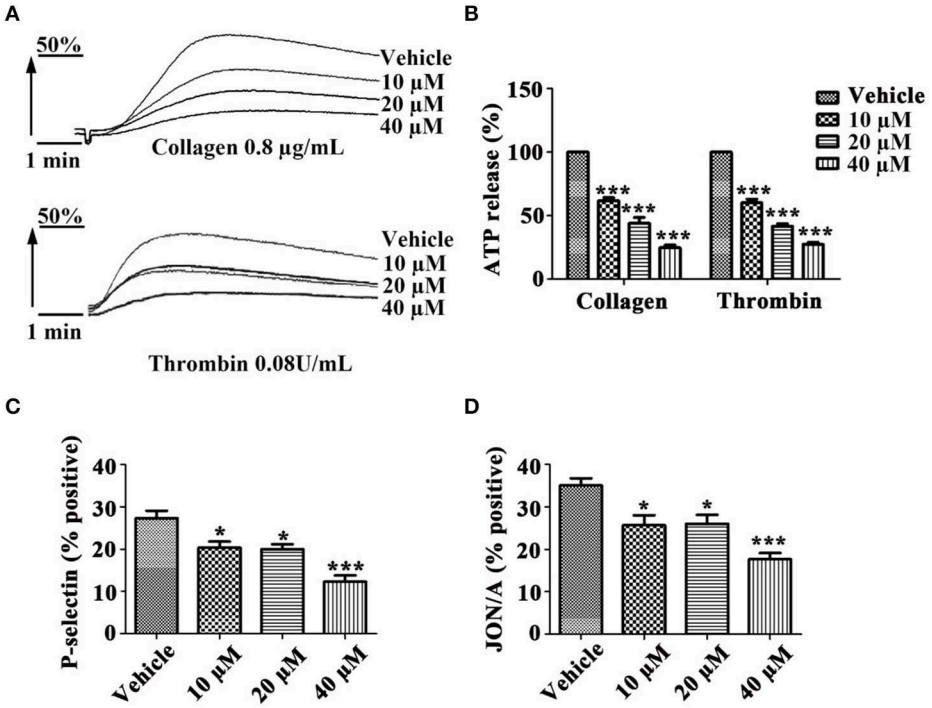

FIGURE 3 | Tussilagone inhibits platelet ATP release, P-selectin expression and αIIbβ3 activation. **(A)** Representative traces of platelet ATP release induced by collagen (0.8 μg/mL) or thrombin (0.08 U/mL) were recorded. **(B)** Quantification of ATP release. **(C)** Platelet P-selectin expression and **(D)** αIIbβ3 activation (JON/A binding) were detected by flow cytometry after platelet activation. Washed platelets (5.0×10^7/mL) were preincubated with different concentrations of tussilagone (10 μM, 20 μM, or 40 μM) or vehicle for 5 min at 37°C and stimulated with thrombin (0.2 U/mL) in the presence of a FITC-conjugated anti-CD62P antibody or a PE-conjugated JON/A antibody. The data are presented as the mean ± SEM ($n = 4$). One-way ANOVA was used for data analysis. *$p < 0.05$ and ***$p < 0.001$ vs. vehicle.

Tussilagone Inhibits Platelet Function and Thrombosis *in vivo*

To determine the inhibitory effect of tussilagone on platelets *in vivo*, mice were given tussilagone orally for 7 days, while the control mice were given corn oil. The occlusion time of the carotid artery and tail bleeding time were measured. Compared with control $FeCl_3$-induced carotid injury model mice, $FeCl_3$-induced carotid injury model mice treated with tussilagone (10 mg/kg) exhibited prolonged thrombotic occlusion time (**Figure 6A**). The tail bleeding time assay showed that compared to control, tussilagone had no effect on tail bleeding time (**Figure 6B**). In addition, compared to those from control mice, washed platelets from tussilagone-treated mice showed decreased aggregation induced by collagen (**Figures 6C,D**). These results indicate that tussilagone inhibits platelet function *in vivo* without affecting bleeding time.

DISCUSSION

Tussilagone is a component extracted from the flower buds of *Tussilago farfara* L. (Kuan dong hua) and is used as a traditional oriental medicine for asthma and bronchitis. Tussilagone was shown to have an effect on hemodynamics and platelet aggregation as early as 1987 (26, 29). However, to date, no further studies on the effects of tussilagone on platelets have been conducted. In the present study, we found that tussilagone at concentrations of 10, 20, and 40 μM inhibited platelet aggregation induced by collagen, thrombin and ADP; platelet ATP release induced by collagen, thrombin; P-selectin expression and αIIbβ3 activation in activated platelets; platelet spreading; and clot retraction. In addition, tussilagone reduced the formation of thrombus in a carotid artery model induced by $FeCl_3$ and did not affect tail bleeding time. Mechanistically, tussilagone decreased the phosphorylation of molecules involved in the Syk/PLCγ2-PKC/MAPK and PI3K-Akt-GSK3β signaling pathways downstream of GPVI.

Platelet aggregation contributes to thrombosis and growth. When the endothelial cell monolayer is breached, collagen fibrils within the vessel wall become exposed to the circulation to form a complex with von Willebrand factor (vWF). Platelets are captured when the glycoprotein (GP) Ibα on the platelet surface binds to vWF, which is essential for platelet activation (30). Platelet aggregate formation is dependent on the local generation or release of soluble agonists, such as ADP, α-thrombin and thromboxane A2 (TXA2), which are of particular importance in the process that converts αIIbβ3 into a high-affinity receptor for soluble adhesive proteins (31). Tussilagone

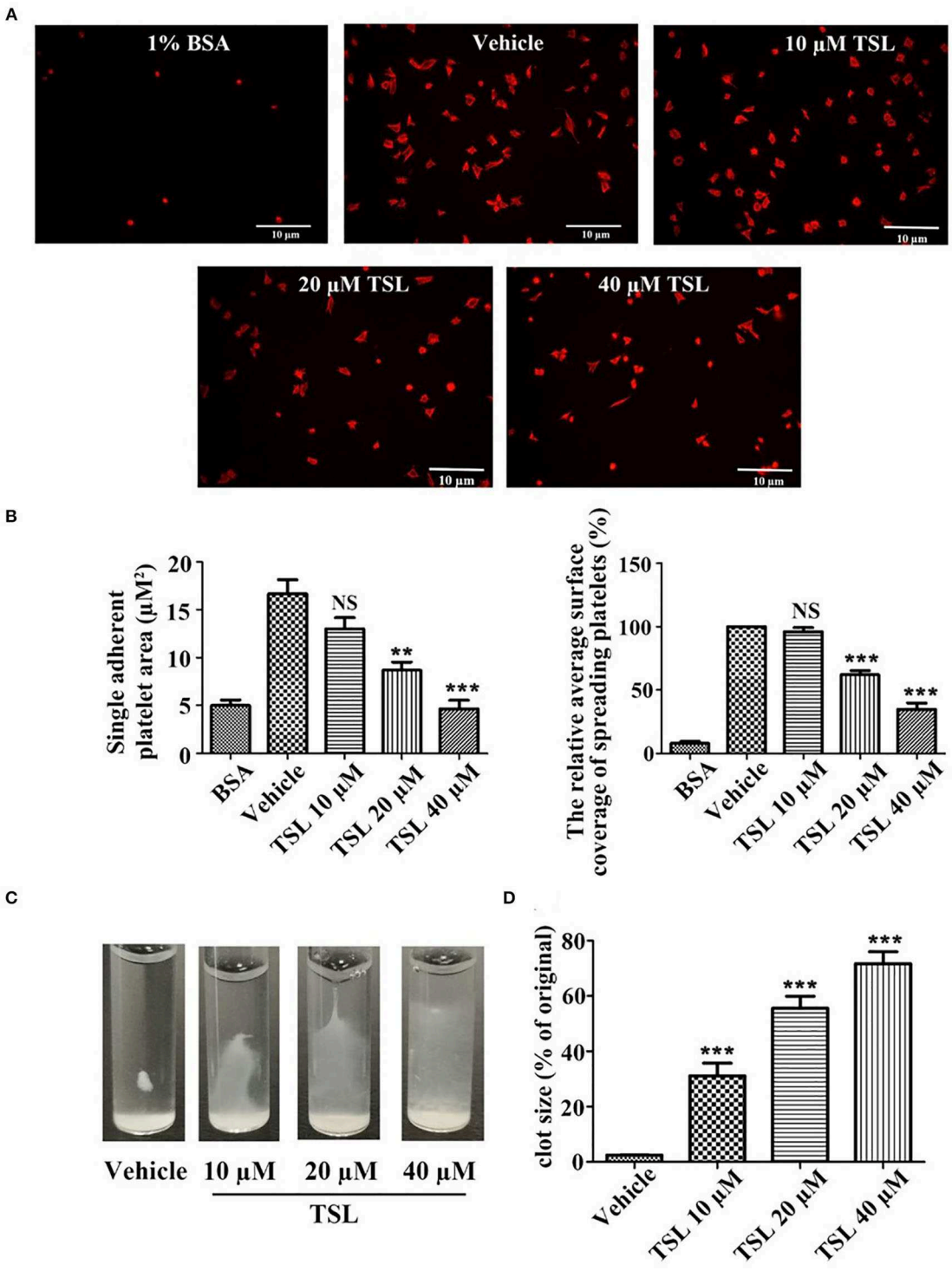

FIGURE 4 | Tussilagone suppresses platelet spreading on fibrinogen-coated surfaces and clot retraction. **(A)** Representative images of platelet spreading on BSA- or fibrinogen-coated surfaces. Washed platelets (2.0×10^7/mL) were preincubated with vehicle or different concentrations of tussilagone (10, 20, or 40 μM) for 5 min at 37°C before being allowed to spread on coated glass. **(B)** The area covered by single adherent platelets (left) and the relative average coverage area of spreading platelets (the values were normalized to vehicle, which was set as 100%) (right) were quantified. **(C)** Representative images of clot retraction were taken 15 min later. **(D)** Summary data of clot retraction were presented. The data are presented as the mean ± SEM ($n = 4$). One-way ANOVA was used for data analysis. $^{**}p < 0.01$, $^{***}p < 0.001$, NS, not significant, vs. vehicle. TSL, tussilagone.

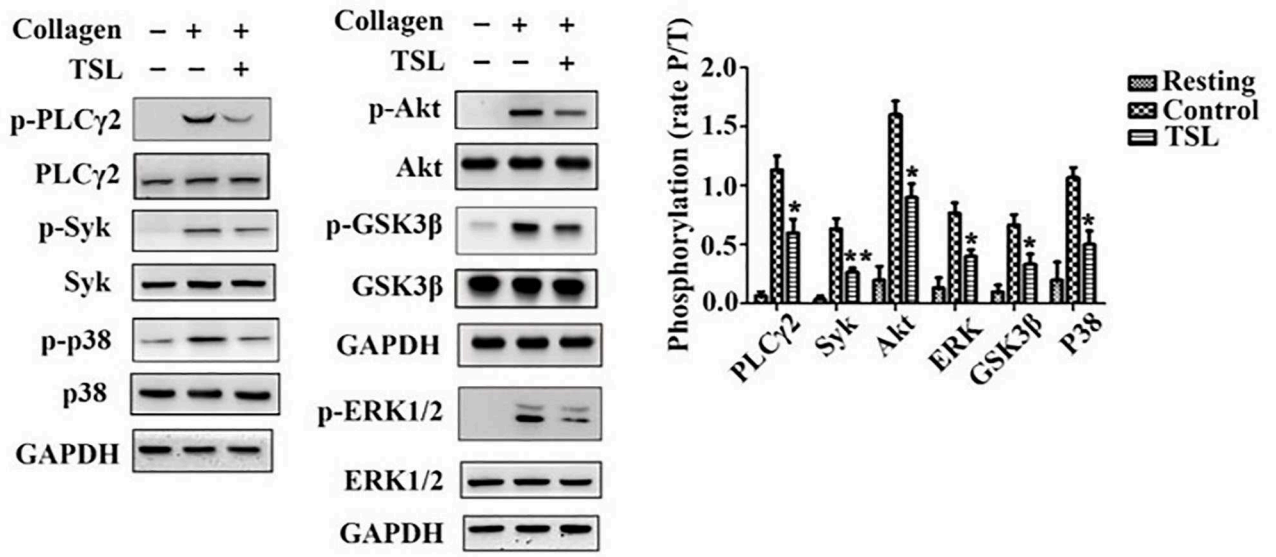

FIGURE 5 | Tussilagone inhibits collagen-induced intracellular signaling in platelets. Washed platelets (3.0×10^8/mL) were preincubated with vehicle or tussilagone (40 μM) for 5 min at 37°C before being stimulated with collagen (0.8 μg/mL) with stirring at 1,000 rpm in an aggregometer at 37°C and then lysed to analyze signaling molecules by Western blotting. Representative blots are shown, and the levels of PLCγ2, Syk, Akt, GSK3β, p38, and ERK1/2 phosphorylation were determined. The data are presented as the mean ± SEM ($n = 4$). One-way ANOVA was used for data analysis. *$p < 0.05$ and **$p < 0.01$ vs. vehicle. TSL, tussilagone.

had a strong inhibitory effect on collagen-, thrombin- and ADP-induced platelet aggregation in a concentration-dependent manner (**Figure 1**). These results led us to further investigate the effect of tussilagone on platelets.

Molecules stored in specific granules are released when platelets are activated, and this is an important step for hemostasis, thrombosis, and other pathophysiological processes (32). There are three main granules: α-granules, dense granules and lysosomes contained in platelets (33). α-Granules are unique to platelets, and they are the most abundant platelet granules and contain many proteins, such as P-selectin, fibrinogen, and vWF. Dense granules are rich in ADP, ATP and 5-HT (34). When platelet activation occurs, ATP is released from dense granules, intracellular P-selectin is released from α-granules and exposed to the platelet membrane and conformational changes in integrin αIIbβ3 occur (35). Tussilagone not only inhibited platelet ATP release induced by collagen and thrombin (**Figures 3A,B**) but also suppressed platelet P-selectin expression and αIIbβ3 activation (JON/A binding) stimulated by thrombin (**Figures 3C,D**). These results suggest that tussilagone has an inhibitory effect on platelet activation.

Integrin αIIbβ3, as a platelet-abundant specific adhesive receptor, initiates outside-in signaling and plays a complex pivotal role in platelet physiology, such as spreading, adhesion, aggregation, clot formation and clot retraction (36). All these processes accelerate stable thrombus formation (37). Tussilagone also had an inhibitory effect on platelet spreading (**Figures 4A,B**) and clot retraction (**Figures 4C,D**). This indicates that tussilagone can inhibit outside-in signaling in platelets.

To study the underlying molecular mechanism of the antiplatelet function of tussilagone, we focused on GPVI signaling stimulated by collagen. Collagen binds to GPVI, leading to the Src kinase-dependent phosphorylation of the two conserved tyrosines, the binding of the tandem SH2 domains of Syk and the initiation of a signaling cascade that activates PLCγ2. Activated PLCγ2 induces the formation of the second messengers inositol 1,4,5-trisphosphate (IP3) and 1,2-diacylglycerol (DAG), resulting in the mobilization of intracellular Ca^{2+} stores and the activation of PKC/MAPK (ERK1/2, P38, JNK), respectively (38). Furthermore, MAPK ERK1/2, p38, and JNK1 in platelets are also activated by other stimuli, such as thrombin, vWF and ADP, and contribute to hemostasis and thrombosis (39). In addition, the stimulation of the PI3K/Akt pathway by GPVI-mediated platelet activation and integrin engagement play important roles in thrombus formation and stabilization (40). Moreover, GSK3β has been found in platelets and acts as an Akt effector to regulate platelet activation (41). The phosphorylation of GSK3β by Akt is related to decreased GSK3β activity, which leads to negative regulation of platelet function and thrombosis (42). Our data showed that tussilagone decreased the phosphorylation of Syk, PLCγ2, MAPK (P38 and ERK1/2), Akt and its substrate GSK3β downstream of collagen-induced GPVI signaling (**Figure 5**).

To further explore the inhibitory effect of tussilagone on platelets *in vivo*, mice were orally administered tussilagone for 7 days to evaluate acute thrombus formation following $FeCl_3$-induced injury of the carotid artery. Our study showed that tussilagone markedly prolonged the occlusion

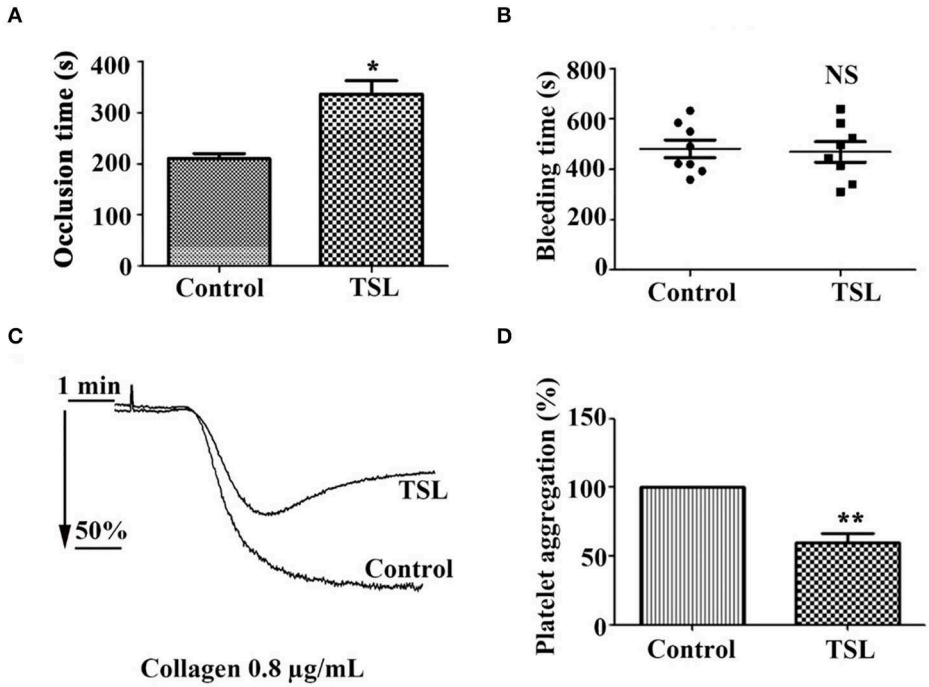

FIGURE 6 | Tussilagone inhibits thrombosis *in vivo*. **(A)** Vascular occlusion times were compared between vehicle- and tussilagone-treated mice after $FeCl_3$-induced injury of the carotid artery. The occlusion time represents the amount of time required to form an occlusive thrombus as described in the Materials and Methods. **(B)** The effect of tussilagone on bleeding time. The bleeding time from tail transection to complete cessation of bleeding was recorded. There were eight mice per group for **(A,B)**. **(C)** Representative traces of platelet aggregation induced by collagen (0.8 μg/mL) in control mice and tussilagone-treated mice. **(D)** The aggregation (%) was quantified, and the aggregation of control mice was taken as 100% ($n = 4$). The data are presented as the mean ± SEM. Two-tailed unpaired Student's *t*-test was used for data analysis. $^*p < 0.05$, $^{**}p < 0.01$, NS, not significant, vs. control. TSL, tussilagone.

time (**Figure 6A**). In addition, collagen-induced platelet aggregation was reduced in tussilagone-treated mice compared to control mice (**Figures 6C,D**), which was consistent with the inhibitory effect of tussilagone on platelet aggregation *in vitro*. In view of the multitarget and multilevel characteristics of traditional Chinese medicines, antiplatelet effects have been widely explored (43). However, certain ingredients with antiplatelet effects, such as atractylodes lactone compounds (44) and miltirone (28), have been reported to cause side effects associated with bleeding. Therefore, it is important to find safe and effective antiplatelet agents. Fortunately, we found that tussilagone had no effect on tail bleeding time in mice (**Figure 6B**). These results indicate that tussilagone inhibits platelet function *in vivo* without affecting bleeding.

In conclusion, our results showed that tussilagone inhibited platelet aggregation, granule release, αIIbβ3 activation, platelet spreading on fibrinogen and clot retraction. In addition, tussilagone also inhibited thrombosis in a $FeCl_3$-induced carotid artery model and had no effect on bleeding time. These results illustrate that tussilagone has a potent inhibitory effect on platelet function *in vitro* and *in vivo*. The underlying mechanism is possibly the inhibition of the Syk-PLCγ2-PKC/MAPK and PI3K-Akt-GSK3β pathways downstream of GPVI signaling cascades. The research suggests that tussilagone has the potential to be developed as a new antiplatelet candidate for the prevention of thrombotic disorders.

DATA AVAILABILITY STATEMENT

The raw data supporting the conclusions of this article will be made available by the authors, without undue reservation, to any qualified researcher.

ETHICS STATEMENT

The animal study was reviewed and approved by Ethics Committee for Experimental Animals of Zhumadian Central Hospital.

AUTHOR CONTRIBUTIONS

WS and R-PY contributed to the conception, design of the study, and critically revised the article. JZ, H-MX, and Y-HW acquired the data. Y-HW performed the statistical analysis. JZ and H-MX wrote the first draft of the manuscript. All authors contributed to manuscript revision and read and approved the submitted version.

FUNDING

This work was supported by the National Natural Science Foundation of China (81703479 to H-MX).

ACKNOWLEDGMENTS

We thank Zhumadian Central Hospital for funding this research and Prof. Zhang-Yin Ming for critical reading of the manuscript.

REFERENCES

1. Dovizio M, Alberti S, Guillem-Llobat P, Patrignani P. Role of platelets in inflammation and cancer: novel therapeutic strategies. *Basic Clin Pharmacol Toxicol.* (2014) 114:118–27. doi: 10.1111/bcpt.12156
2. McManus DD, Freedman JE. MicroRNAs in platelet function and cardiovascular disease. *Nat Rev Cardiol.* (2015) 12:711–7. doi: 10.1038/nrcardio.2015.101
3. Koupenova M, Kehrel BE, Corkrey HA, Freedman JE. Thrombosis and platelets: an update. *Eur Heart J.* (2017) 38:785–91. doi: 10.1093/eurheartj/ehw550
4. Michael H. Normal platelet function. *Cancer Metastasis Rev.* (2017) 36:195–8. doi: 10.1007/s10555-017-9677-x
5. Koupenova M, Clancy L, Corkrey HA, Freedman JE. Circulating platelets as mediators of immunity, inflammation, and thrombosis. *Circ Res.* (2018) 122:337–51. doi: 10.1161/CIRCRESAHA.117.310795
6. Schlesinger M. Role of platelets and platelet receptors in cancer metastasis. *J Hematol Oncol.* (2018) 11:125. doi: 10.1186/s13045-018-0669-2
7. Gawaz M. Novel Ligands for Platelet Glycoprotein VI. *Thromb Haemost.* (2018) 118:435–6. doi: 10.1055/s-0038-1635080
8. Mangin PH, Onselaer MB, Receveur N, Le Lay N, Hardy AT, Wilson C, et al. Immobilized fibrinogen activates human platelets through glycoprotein VI. *Haematologica.* (2018) 103:898–907. doi: 10.3324/haematol.2017.182972
9. Watson SP, Poulter NS, Pollitt AY, Owen DM, Gardiner EE, Andrews RK, et al. Clustering of glycoprotein VI (GPVI) dimers upon adhesion to collagen as a mechanism to regulate GPVI signaling in platelets. *J Thromb Haemost.* (2017) 15:549–64. doi: 10.1111/jth.13613
10. Jamasbi J, Ayabe K, Goto S, Nieswandt B, Peter K, Siess W. Platelet receptors as therapeutic targets: past, present and future. *Thromb Haemost.* (2017) 117:1249–57. doi: 10.1160/TH16-12-0911
11. Yeung J, Holinstat M. Newer agents in antiplatelet therapy: a review. *J Blood Med.* (2012) 3:33–42. doi: 10.2147/JBM.S25421
12. Khan NI, Siddiqui FM, Goldstein JN, Cox M, Xian Y, Matsouaka RA, et al. Association between previous use of antiplatelet therapy and intracerebral hemorrhage outcomes. *Stroke.* (2017) 48:1810–7. doi: 10.1161/STROKEAHA.117.016290
13. Pannach S, Goetze J, Marten S, Schreier T, Tittl L, Beyer-Westendorf J. Management and outcome of gastrointestinal bleeding in patients taking oral anticoagulants or antiplatelet drugs. *J Gastroenterol.* (2017) 52:1211–20. doi: 10.1007/s00535-017-1320-7
14. Rozalski M, Boncler M, Luzak B, Watala C. Genetic factors underlying differential blood platelet sensitivity to inhibitors. *Pharmacol Rep.* (2005) 57:1–13.
15. Zhong WP, Wu H, Chen JY, Li XX, Lin HM, Zhang B, et al. Genomewide association study identifies novel genetic loci that modify antiplatelet effects and pharmacokinetics of clopidogrel. *Clin Pharmacol Ther.* (2017) 101:791–802. doi: 10.1002/cpt.589
16. Liu Y, Yin H, Chen K. Platelet proteomics and its advanced application for research of blood stasis syndrome and activated blood circulation herbs of Chinese medicine. *Sci China Life Sci.* (2013) 56:1000–6. doi: 10.1007/s11427-013-4551-8
17. Choleva M, Boulougouri V, Panara A, Panagopoulou E, Chiou A, Thomaidis NS, et al. Evaluation of anti-platelet activity of grape pomace extracts. *Food Funct.* (2019) 10:8069–80. doi: 10.1039/C9FO02138H
18. Jafari Azad B, Daneshzad E, Meysamie AP, Koohdani F. Chronic and acute effects of cocoa products intake on arterial stiffness and platelet count and function: a systematic review and dose-response Meta-analysis of randomized clinical trials. *Crit Rev Food Sci Nutr.* (2020). doi: 10.1080/10408398.2020.1750343. [Epub ahead of print].
19. Chen JJ, Tsai TH, Liao HR, Chen LC, Kuo YH, Sung PJ, et al. New sesquiterpenoids and anti-platelet aggregation constituents from the rhizomes of curcuma zedoaria. *Molecules.* (2016) 21:1385. doi: 10.3390/molecules21101385
20. Hwangbo C, Lee HS, Park J, Choe J, Lee JH. The anti-inflammatory effect of tussilagone, from Tussilago farfara, is mediated by the induction of heme oxygenase-1 in murine macrophages. *Int Immunopharmacol.* (2009) 9:1578–84. doi: 10.1016/j.intimp.2009.09.016
21. Kim YK, Yeo MG, Oh BK, Kim HY, Yang HJ, Cho SS, et al. Tussilagone inhibits the inflammatory response and improves survival in CLP-induced septic mice. *Int J Mol Sci.* (2017) 18:2744. doi: 10.3390/ijms18122744
22. Cheon HJ, Nam SH, Kim JK. Tussilagone, a major active component in Tussilago farfara, ameliorates inflammatory responses in dextran sulphate sodium-induced murine colitis. *Chem Biol Interact.* (2018) 294:74–80. doi: 10.1016/j.cbi.2018.08.022
23. Park Y, Ryu HS, Lee HK, Kim JS, Yun J, Kang JS, et al. Tussilagone inhibits dendritic cell functions via induction of heme oxygenase-1. *Int Immunopharmacol.* (2014) 22:400–8. doi: 10.1016/j.intimp.2014.07.023
24. Choi BS, Kim YJ, Yoon YP, Lee HJ, Lee CJ. Tussilagone suppressed the production and gene expression of MUC5AC mucin via regulating nuclear factor-kappa B signaling pathway in airway epithelial cells. *Korean J Physiol Pharmacol.* (2018) 22:671–7. doi: 10.4196/kjpp.2018.22.6.671
25. Li J, Peng J, Zhao S, Zhong Y, Wang Y, Hu J, et al. Tussilagone suppresses angiogenesis by inhibiting the VEGFR2 signaling pathway. *Front Pharmacol.* (2019) 10:764. doi: 10.3389/fphar.2019.00764
26. Hwang SB, Chang MN, Garcia ML, Han QQ, Huang L, King VF, et al. L-652,469–a dual receptor antagonist of platelet activating factor and dihydropyridines from Tussilago farfara L. *Eur J Pharmacol.* (1987) 141:269–81. doi: 10.1016/0014-2999(87)90272-X
27. Liu G, Xie W, He AD, Da XW, Liang ML, Yao GQ, et al. Antiplatelet activity of chrysin via inhibiting platelet alphaIIbbeta3-mediated signaling pathway. *Mol Nutr Food Res.* (2016) 60:1984–93. doi: 10.1002/mnfr.201500801
28. Song W, Ma YY, Miao S, Yang RP, Zhu Y, Shu D, et al. Pharmacological actions of miltirone in the modulation of platelet function. *Acta Pharmacol Sin.* (2019) 40:199–207. doi: 10.1038/s41401-018-0010-1
29. Li YP, Wang YM. The effects of tussilagone on the hemodynamics of conscious dogs and dogs during hemorrhagic shock. *Yao Xue Xue Bao.* (1987) 22:486–90.
30. Brass L. Understanding and evaluating platelet function. *Hemat Am Soc Hematol Educ Program.* (2010) 2010:387–96. doi: 10.1182/asheducation-2010.1.387
31. Ruggeri ZM, Jackson SP. Platelet thrombus formation in flowing blood. In: Michelson AD, editor. *Platelets, 3rd edition.* Cambridge: Elsevier Inc., (2013). p. 399–423. doi: 10.1016/B978-0-12-387837-3.00020-1
32. Papapanagiotou A, Daskalakis G, Siasos G, Gargalionis A, Papavassiliou AG. The role of platelets in cardiovascular disease: molecular mechanisms. *Curr Pharm Des.* (2016) 22:4493–505. doi: 10.2174/1381612822666160607064118
33. Rendu F, Brohard-Bohn B. The platelet release reaction: granules' constituents, secretion and functions. *Platelets.* (2001) 12:261–73. doi: 10.1080/09537100120068170
34. Flaumenhaft R. Platelet secretion. In: Michelson AD, editor. *Platelet. 3rd edition*. Cambridge: Academic Press. (2013). p. 343–66. doi: 10.1016/B978-0-12-387837-3.00018-3
35. Berny-Lang MA, Frelinger AL, Barnard MR, Michelson AD. Flow cytometry. In: Michelson, AD, editor. *Platelets, 3rd edition.* Cambridge: Elsevier Inc. (2013). p. 581–602. doi: 10.1016/B978-0-12-387837-3.00029-8
36. Gao W, Shi P, Chen X, Zhang L, Liu J, Fan X, et al. Clathrin-mediated integrin alphaIIbbeta3 trafficking controls platelet spreading. *Platelets.* (2018) 29:610–21. doi: 10.1080/09537104.2017.1353682

37. Jackson SP, Nesbitt WS, Kulkarni S. Signaling events underlying thrombus formation. *J Thromb Haemost.* (2003) 1:1602–12. doi: 10.1046/j.1538-7836.2003.00267.x
38. Rayes J, Watson SP, Nieswandt B. Functional significance of the platelet immune receptors GPVI and CLEC-2. *J Clin Invest.* (2019) 129:12–23. doi: 10.1172/JCI122955
39. Adam F, Kauskot A, Rosa JP, Bryckaert M. Mitogen-activated protein kinases in hemostasis and thrombosis. *J Thromb Haemost.* (2008) 6:2007–16. doi: 10.1111/j.1538-7836.2008.03169.x
40. Guidetti GF, Canobbio I, Torti M. PI3K/Akt in platelet integrin signaling and implications in thrombosis. *Adv Biol Regul.* (2015) 59:36–52. doi: 10.1016/j.jbior.2015.06.001
41. Barry FA, Graham GJ, Fry MJ, Gibbins JM. Regulation of glycogen synthase kinase 3 in human platelets: a possible role in platelet function? *FEBS Lett.* (2003) 553:173–8. doi: 10.1016/S0014-5793(03)01015-9
42. Li D, August S, Woulfe DS. GSK3beta is a negative regulator of platelet function and thrombosis. *Blood.* (2008) 111:3522–30. doi: 10.1182/blood-2007-09-111518
43. Tsai HH, Lin HW, Lu YH, Chen YL, Mahady GB. A review of potential harmful interactions between anticoagulant/antiplatelet agents and Chinese herbal medicines. *PLoS ONE.* (2013) 8:e64255. doi: 10.1371/journal.pone.0064255
44. Chen Y, Yang W, Guo L, Wu X, Zhang T, Liu J, et al. Atractylodes lactone compounds inhibit platelet activation. *Platelets.* (2017) 28:194–202. doi: 10.1080/09537104.2016.1209477

Conflict of Interest: The authors declare that the research was conducted in the absence of any commercial or financial relationships that could be construed as a potential conflict of interest.

frontiers in Medicine

MINI REVIEW
published: 03 September 2020
doi: 10.3389/fmed.2020.00543

Impact of Von Willebrand Factor on Bacterial Pathogenesis

Michael Steinert[1,2], *Isabell Ramming*[1] *and Simone Bergmann*[1]*

[1] *Institut für Mikrobiologie, Technische Universität Braunschweig, Braunschweig, Germany,* [2] *Department of Infection Biology, Helmholtz Center for Infection Diseases, Braunschweig, Germany*

Von Willebrand factor (VWF) is a mechano-sensitive protein with crucial functions in normal hemostasis, which are strongly dependant on the shear-stress mediated defolding and multimerization of VWF in the blood stream. Apart from bleeding disorders, higher plasma levels of VWF are often associated with a higher risk of cardiovascular diseases. Herein, the disease symptoms are attributed to the inflammatory response of the activated endothelium and share high similarities to the reaction of the host vasculature to systemic infections caused by pathogenic bacteria such as *Staphylococcus aureus* and *Streptococcus pneumoniae*. The bacteria recruit circulating VWF, and by binding to immobilized VWF on activated endothelial cells in blood flow, they interfere with the physiological functions of VWF, including platelet recruitment and coagulation. Several bacterial VWF binding proteins have been identified and further characterized by biochemical analyses. Moreover, the development of a combination of sophisticated cell culture systems simulating shear stress levels of the blood flow with microscopic visualization also provided valuable insights into the interaction mechanism between bacteria and VWF-strings. *In vivo* studies using mouse models of bacterial infection and zebrafish larvae provided evidence that the interaction between bacteria and VWF promotes bacterial attachment, coagulation, and thrombus formation, and thereby contributes to the pathophysiology of severe infectious diseases such as infective endocarditis and bacterial sepsis. This mini-review summarizes the current knowledge of the interaction between bacteria and the mechano-responsive VWF, and corresponding pathophysiological disease symptoms.

Keywords: von Willebrand, *Staphylococcus areus*, *Streptococcus pneumoniae*, microfluidic, sepsis

OPEN ACCESS

Edited by:
Silvia Fischer,
University of Giessen, Germany

Reviewed by:
Volker Huck,
University Medical Center Hamburg-Eppendorf, Germany
Jonas Emsley,
University of Nottingham, United Kingdom

***Correspondence:**
Simone Bergmann
simone.bergmann@tu-bs.de

Specialty section:
This article was submitted to Hematology, a section of the journal Frontiers in Medicine

Received: *28 May 2020*
Accepted: *30 July 2020*
Published: *03 September 2020*

Citation:
Steinert M, Ramming I and Bergmann S (2020) Impact of Von Willebrand Factor on Bacterial Pathogenesis. Front. Med. 7:543. doi: 10.3389/fmed.2020.00543

INTRODUCTION

Vascular hemostasis is a live-saving mechanism, which balances coagulation, thrombogenesis, and fibrinolysis in response to vascular injuries and inflammatory processes. Key element of the hemostasis are the Weibel Palade bodies (WPBs), which represent defense vesicles, constitutively produced by the endothelium of the vessel walls. The vesicles are filled with vasoactive substances, immune defense modulators, and proteins involved in coagulation (1, 2). In addition to megakaryocytes, endothelial WPBs are the main source of Von Willebrand factor (VWF). This glycoprotein mediates platelet activation, anchorage of thrombocytes to the subendothelial collagen, and induction of plasma haemostasis via factor VIII (3, 4). Moreover, VWF promotes cell migration in angiogenesis via interaction with different cell surface receptors and induction of

signaling pathways (5). The high importance of VWF for balanced hemostasis is conveyed by the appearance of bleeding disorders such as the von Willebrand disease caused by an inherited quantitative or functional VWF deficiency (3).

VWF constantly circulates in the bloodstream at concentrations between 8 and 14.0 μg/mL (3, 6). But, vasoactive hormones such as epinephrine and vasopressin as well as the plasma proteins thrombin, histamine, and numerous other mediators of inflammation and/or thrombosis induce the release of VWF in response to vascular injury or inflammatory stimuli. The released VWF increases the plasma levels of this protein, and some proportion of VWF is temporarily retained on the cell surface and binds to collagen of the exposed subendothelial matrix (7, 8). This subendothelial immobilization is also significantly strengthened by the endothelial glycocalyx in a heparanase-sensitive manner (9). VWF is a mechano-sensitive protein, which responds to shear stress-mediated forces by conformational changes.

Shear stress is defined as the force exerted by the blood flow on blood vessel walls. This stress generates a response in the vascular wall, characterized by release of endothelial mediators, which in turn stimulate structural remodeling through activation of gene expression and protein synthesis (10). The shear stress-derived conformational changes of VWF are crucial for the biological function of VWF in hemostasis. Upon exposition to the shear forces in the bloodstream, the immobilized VWF unfolds to large protein strings, thereby exposing further functionally important binding sites (7, 11, 12). In particular, the defolded A1 binding site mediates adhesion of platelets and recruits them via binding to the platelet glycoprotein GP?bα (11, 13, 14). This VWF-platelet interaction finally results in a factor VIII-induced fibrin-incorporation and in stabilization of generated thrombi.

Elevated VWF-levels are directly associated with cardiovascular diseases (CD) of high-risk groups such as the elderly and diabetes patients (15). Alongside with tissue plasminogen activator (t-PA), and D-dimer of fibrinogen, VWF is characterized as one out of three biomarkers directly associated with atherosclerotic lesions and coronary heart disease (16, 17). This unveils the thrombus-generating activity of elevated VWF-concentrations as one of the dominant causative factors for coronary heart disease (18).

In addition to the role of VWF in CD, VWF serves as a ligand binding site for bacteria, which cause live-threatening local and systemic infection diseases, such as *Staphylococcus aureus* and *Streptococcus pneumoniae* (19, 20). *S. aureus* is a human pathogenic bacterium causing, among others, infective endocarditis and heart valve prosthetic infection (21, 22). In this respect, shear-force-mediated adhesion of staphylococci to VWF is directly associated with coagulation and typical disease symptoms (23, 24). Similarly, *S. pneumoniae*, a commensal colonizing the upper respiratory epithelium and a major cause of community-acquired pneumoniae in elderly and immunocompromised patients (25, 26), has also been recurringly isolated from heart valve endocardium of patients suffering from subacute endocarditis (27, 28). Furthermore, an increasing amount of clinical case studies report that up to one-third of patients suffer from major adverse cardiac effects (MACE) and vascular impairments within months and even years after recovering from severe pneumococcal infections such as pneumoniae and septicemiae (29–31). The observation of similarities between the association of CD with VWF-release, and symptoms induced by bacterial infections initiated an increasing need to develop infection models and sophisticated visualization techniques in the last decade. With these models, the pathomechanistical function of some crucial bacterial virulence factors in VWF-mediated disease progression could be deciphered.

BACTERIAL BINDING TO VWF UNDER SHEAR FLOW

The release of VWF from endothelial WPBs is induced by host-derived hormones such as epinephrine and histamine and other plasma factors and is also triggered by pathogenic bacteria (32). For example, in 1991, Sporn et al. were the first to observe that the intracellular pathogen *Rickettsia rickettsii*, the main cause of the Rocky Mountain spotted fever, induces the release of VWF out of WPB of cultured endothelial cells [(33), **Table 1**]. Moreover, in our previous studies, we demonstrated that luminal VWF secretion from WPB of human lung endothelial cells is significantly increased in response to pneumococcal adherence and the cytotoxic effects of the pneumococcus toxin pneumolysin (45). These results strongly suggest that *in vivo*, the interaction between circulating bacteria in the bloodstream and the endothelial vasculature might directly lead to elevated VWF plasma levels.

In this respect, the scientific question was raised whether the released VWF is directly subverted by the bacteria for their own benefit, i.e., as a binding site at the host endothelium, for platelet aggregation, or interference with the host coagulation. Indeed, Herrmann et al. were the first to demonstrate the binding of *S. aureus* bacteria to VWF coated surfaces and VWF in suspension (46). A short time later, a heparin-sensitive bacterial binding to soluble VWF was also reported for coagulase-negative *Staphylococcus* species, often associated with infections of prosthetic devices [(40), **Table 1**].

Bacterial adhesion to the vascular endothelium is of high importance for the pathology of blood-born infections, since this promotes bacterial settlement, induces inflammatory responses, and facilitates bacterial transmigration and dissemination into deeper tissue sites. It became obvious that blood-flow induced conformational changes of the VWF molecule, which are crucial for the physiological function of VWF in the bloodstream, might also be of high relevance for VWF-mediated bacterial adhesion. For a long time, it remained a technically challenging task to unreveal details of the bacterial interaction with the mechano-sensitive VWF under shear stress condition. But meanwhile, a variety of model systems have been established that enable the simulation of different physiological shear stress situations including sophisticated visualization techniques [for review, please refer to Bergmann and Steinert (47)]. The first experimental studies on the binding of multimerized VWF to platelets were performed with "Cone-and-Plate" viscometers

TABLE 1 | Bacterial VWF-binding proteins and function in adhesion and infectious diseases.

Species	VWF binding factor	Function of VWF binding	References
Staphylococcus aureus	SPA	Bacterial attachment to VWF strings in flow and collagen-rich subendothelium via catch bond mechanisms	(19, 34–36)
	VWbp	Flow-independent VWF binding of bacteria, coagulase activity, activation of host prothrombin, induction of fibrin formation, involved in pneumonia progression	(37–39)
Coagulase-negative Staphylococci	N.D.	Binding of soluble VWF to *S. epidermidis, S. haemolyticus,* and *S. hominis*	(40)
Staphylococcus lugdunensis	VWFbl	Attachment to endothelium under flow, adherence to cardiac valves and induction of endocarditis	(41, 42)
Streptococcus pneumoniae	enolase	Mediating adherence to endothelium and bacterial aggregation in blood	(20)
Rickettsia rickettsii	N.D.	Induction of VWF release	(33)
Helicobacter pylori	N.D.	Increase in VWF plasma levels, Induction of platelet aggregation	(43, 44)

(N.D, not determined).

in combination with flow cytometric quantifications (48). Viscometer-generated shear stress application was also combined with ristocetin-incubation of VWF. Ristocetin is an antibiotic produced by *Amycolatopsis lurida,* and is still used as the Gold standard in diagnostics of von Willebrand-disease (49). Ristocetin binds to VWF in a shear-stress-independent manner, thereby inducing the exposure of the VWF-mediated platelet binding site for thrombocyte recruitment and aggregation (49). Following the objective to quantitatively analyse the specific protein ligand-interaction with VWF under a defined medium flow, several surface-coating technologies have been established that create so-called "functionalized surfaces." For example, Mascari and Ross have quantified the detachment of staphylococci from collagen in real–time using a parallel plate flow chamber combined with phase-contrast video–microscopy and digital image processing (50). The results provided evidence that staphylococci adhere directly to multimerized VWF strings and attach to collagen of the exposed subendothelium in blood-borne infections (34).

In addition to the biochemical interaction studies, several *in vivo* mouse infection models employing *vwf* gene-deficient mice and platelet-depleted mice enable evaluation and monitoring of systemic consequences associated with hemostatic processes. The *in vivo* analyses revealed that *S. aureus* bacteria directly attach to cell-bound VWF of the endothelial vasculature (23, 51). Moreover, visualization of bacterial mouse infection via *intravital* microscopy confirmed that bacteria, which attached to VWF strings, resist shear stress-mediated clearance by the blood flow [(19), **Figure 1**]. Deeper insight into the pathophysiological consequences of the pneumococcus interaction with VWF was also provided by infection analyses using zebrafish larvae. *Danio rerio* serves as a suitable *in vivo* model, sharing high morphologic and functional similarity to the human endothelial tissue and both, intrinsic and extrinsic coagulation pathways (52–54). Microscopic real-time visualization of larval infection confirmed the recruitment of endothelial-derived VWF to circulating pneumococci and VWF-mediated attachment to the endothelial vessel walls (20).

BACTERIAL VWF BINDING PROTEINS AND BINDING MECHANISMS

The bacterial interaction with components of the hemostasis *in vivo* augurs the presence of specific bacterial surface proteins, which mediate binding to VWF. The protein A (SPA) of *S. aureus* was identified as a bacterial VWF-binding protein. SPA elicits binding activities to both, the soluble and the surface-immobilized VWF [(35), **Table 1**]. Six years later, the VWF binding sites of protein A were narrowed down to the IgG-binding domain (55). Using single-molecule atomic force microscopy (AFM), Viela et al. further demonstrated that VWF binds very tightly to SPA via a force-sensitive catch bond mechanism, which involves force-induced structural changes in the SPA domains (36, 56). Meanwhile, protein similarities led to the assumption that several bacterial virulence factors may use this binding mechanism to resist clearance by high shear stress during infections (57).

In addition to SPA, a second staphylococcal VWF binding protein (VWbp) with coagulase activity was identified from a phage display-library screen in 2002 [(37, 38), **Table 1**]. Studies using functionalized surface-technology revealed that in contrast to SPA, VWbp appears to be of significant relevance for VWF recruitment rather than under static conditions (58). Likewise, pneumococci bind VWF under static conditions, and also recruit globular circulating VWF via the surface-exposed enolase [(20), **Table 1**]. This protein also mediates binding of pneumococci to plasminogen and to extracellular nucleic acids, which both promotes bacterial attachment to epithelial and endothelial cells (59). Moreover, similar to the staphylococcal VWbp, the VWF binding site for the pneumococcal enolase is located within the defolded A1 domain of VWF (19, 20, 60). All bacterial VWF-binding proteins identified so far are listed in **Table 1**.

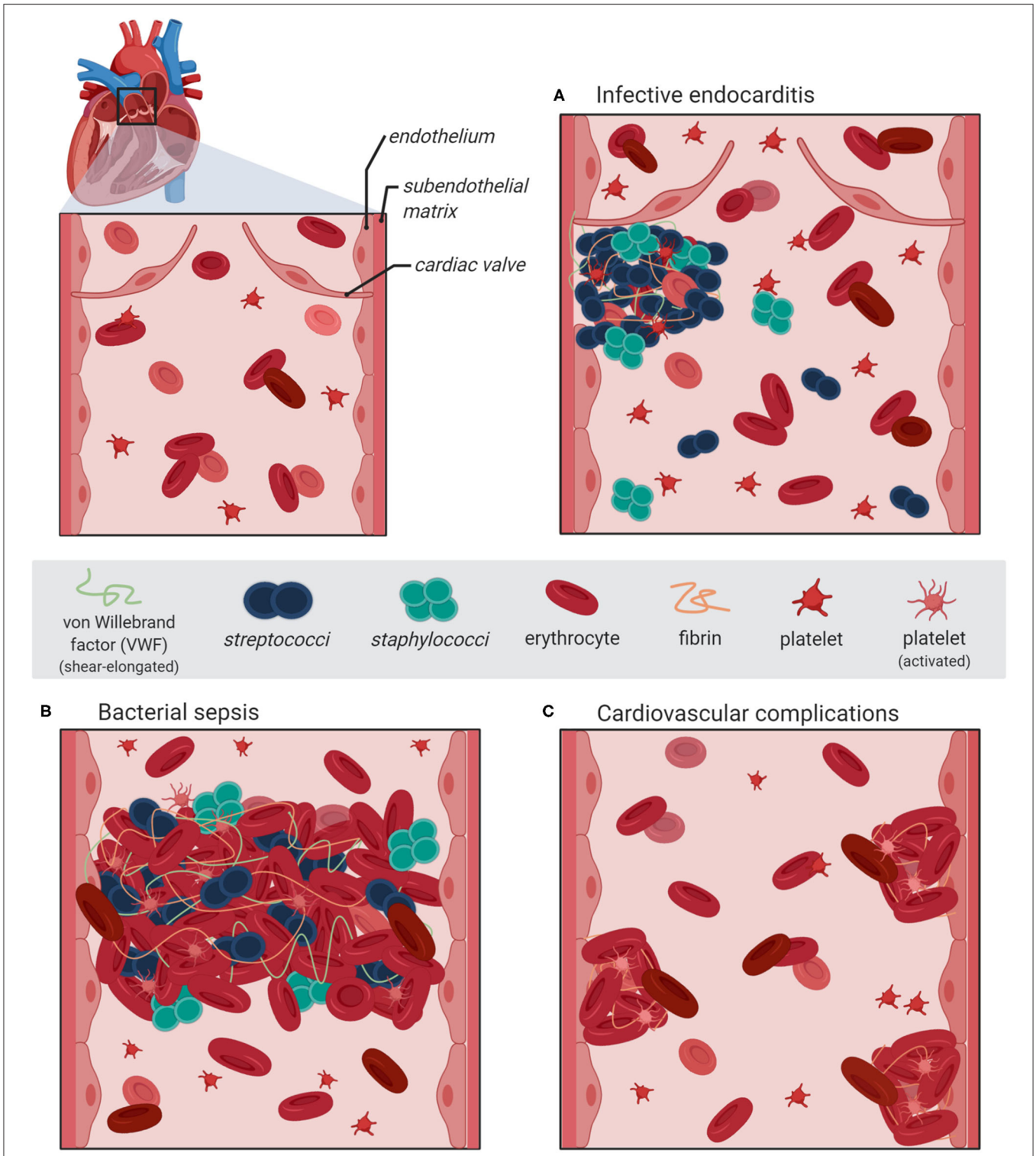

FIGURE 1 | Schematic illustration of bacterial vascular infections and diseases associated with VWF-mediated adhesion of *S. aureus* and *S. pneumoniae* to activated endothelium. The section at the upper left represents a magnification of the heart pulmonary arerty with the artrioventricular valve. **(A)** An infective endocarditis is associated with VWF-mediated bacterial attachment to the activated valve endocard leading to the formation of inflammation-inducing bacterial vegetations containing platelets and fibrin. **(B)** During sepsis, bacterial adhesion to the inflamed vasculature is promoted via elongated VWF strings and induces the formation thrombi, which might lead to occlusions of the microvasculature. **(C)** Severe systemic bacterial infections are accompanied with recurring endothel activation leading to a longterm dysbalanced hemostasis, which increases the risk of cardiovascular complications such as major adverse cardiac effects. The figure was generated using bioRender Software.

In addition to the analyses of perfused VWF protein-coated, functionalized surfaces, the group of Schneider et al. established an air pressure-driven, unidirectional, and continuous pump system manufactured by the company ibidi® (19). In contrast to the formerly described flow systems that are employed to analyse protein-protein-interactions under shear stress conditions, the ibidi® pump technology enables sterile long term cultivation of VWF-producing endothelial cells, which can be incubated with bacteria and microscopically analyzed in real-time. As a result, this air-driven microfluidic pump device enabled the analyses of staphylococcal interaction with VWF on endothelial cell surfaces under shear stress conditions (19) and was also used to establish a pneumococcus cell culture infection model of primary endothelial cells in flow (20, 61). With this system, the attachment of pneumococci to multimerized VWF strings on the endothelial cell surface was successfully visualized and quantitatively evaluated. In accordance with the VWF binding characteristics of *S. aureus,* VWF binding to pneumococci is heparin-sensitive and depends on the amount of polysaccharide capsule expression (20). It is of note that pneumococcal attachment to VWF strings is also characterized by remarkable bond stability for longer time periods even at high shear flow parameters, which might be promoted by a concerted action of several additional, yet unidentified VWF-binding proteins (20). In addition, results of surface plasmon resonance binding studies and cell culture infections studies in flow revealed that the pneumococcus enolase interacts with both, globular circulating VWF and with VWF strings with comparable avidity. Based on the observation that multi adhesive proteins such as the bacterial enolase are already detected on the surface of various bacterial species, it can be assumed that the bacterial interaction with VWF is part of a general mechanism with pivotal relevance for pathophysiology.

EFFECT OF STAPHYLOCOCCAL AND STREPTOCOCCAL INTERACTION WITH VWF ON COAGULATION AND VASCULAR DISEASES

As summarized in **Table 1**, VWF binding to bacteria has only been studied to detail for staphylococci and streptococci. Taking clinical symptoms into account, different functional aspects of the bacterial interaction with VWF can be directly or indirectly correlated with at least three severe infection diseases: infective endocarditis, bacterial sepsis, and cardiovascular complications.

Infective endocarditis is regarded as a paradigm of bacterial diseases associated with vascular inflammation and VWF-interaction (24). Most of the acute infective endocarditis are caused by *S. aureus* and are associated with up to 100% mortality rate if left untreated (21, 22). Compared to that, infective endocarditis caused by *S. pneumoniae* is rare but no less severe (27, 28). Infection of the heart valves is initiated by the attachment of circulating bacteria to the endocardium and the formation of bacterial vegetations, which are embedded in fibrin and platelets (**Figure 1A**). During disease progress, the vegetations induce further inflammatory processes, which result in ulceration, rupture, and necrosis of the valve cusps (62, 63). Experimental shear stress determination using native porcine aortic valve models revealed that even in a healthy human vasculature, the systolic shear stress at the heart valve leaflet can reach up to 21.3 dyn/cm^2 at the aortic site and up to 92 dyn/cm^2 at the ventricular site (64, 65). Similar to the activation of specific proinflammatory and procoagulant protein expression patterns of endothelial cells, the hemodynamic forces also promote the activation of endocardial Notch-dependent signaling pathways in the endocardial cells of the atrio-ventricular valve (66). The observed magnitude of shear stress is sensed by the mechano-responsive VWF and induces stretching and multimerization of VWF proteins. Thereby, VWF displays crucial binding sites for bacterial surface adhesins and mediates bacterial attachment to the heart valve. In line with this, visualization of staphylococcal mouse infection via 3D confocal microscopy confirmed the adhesion of fluorescent *S. aureus* to murine aortic valves (23). The mouse infection studies further demonstrated that following valve damage, VWF and fibrin are both deposited on the damaged valve endocardium and serve as attachment sites for *S. aureus* [(23, 51), **Figure 1A**]. Moreover, endothelial cell culture infections and *intravital* microscopy of bacterial mouse infection confirmed that staphylococci and pneumococci resist shear stress-mediated clearance by the blood flow by binding to VWF strings at the endothelial vessel walls (19, 20, 51). Following disease progress, the VWF-mediated bacterial attachment also promotes the recruitment of large amounts of platelets, capturing *S. aureus* to the valve surface [(23, 24, 67, 68), **Figures 1A,B**]. The observation that among the staphylococci, only *S. aureus* and *S. lugdunensis* are able to bind VWF might, in part, explain why these bacteria are more effective in causing endocarditis than other staphylococci (41).

Bacterial VWF binding is also involved in the formation of large platelet aggregates within the blood circulation. In this respect, the formation of bacterial-induced platelet aggregates and the depletion of clotting factors from blood represents a crucial pathomechanism, which is directly attributed to disease symptoms typical for bacterial sepsis. For example, staphylococcal sepsis is associated with an increase in coagulation activity and an enhanced thrombosis (**Figure 1B**; **Table 1**). It is assumed that the *Staphylococcus*-induced dysregulated activation of systemic thrombosis leads to thrombotic microangiopathy, which is associated with an accelerated fibrinolysis and bleeding tendency, referred to as disseminated intravascular coagulation [DIC, (69)]. Moreover, this bacterial mechanism is also assumed to directly induce the formation of abscesses [(39, 70–73), **Figure 1B**]. A similar formation of blood clots, reaching up to 10 μm in diameter, was observed in pneumococcus infection of *Danio rerio* larvae (20). Based on these data, we suppose that the VWF-mediated bacterial aggregate formation in the blood circulation of the zebrafish cause a partial or complete occlusion of the larval microvasculature. Thus, in severe cases of staphylococcal and pneumococcal septicaemiae, the vascular occlusion of small blood vessels throughout the body represents a life-threatening disease symptom, which might lead to multi-organ failure, resulting in high mortality rates of up to 50% [(74–77), **Figure 1B**]. Bacterial aggregate formation in sepsis and

infective endocarditis, in particular, are also prime examples of the strong connection between the hemostatic system and innate immunity, which is referred to as immune thrombosis (78). It is coincidently proposed that the infection-induced coagulase activity mediates bacterial capture within a fibrin meshwork, which enables this pathogen to disseminate via thromboembolic lesions and to resist opsonophagocytic clearance by host immune cells (73). On the other hand, platelets are the crucial mediators of the innate defense against staphylococci by releasing microbicidal proteins from alpha granules that kill the bacteria (79). On the first view, it appears to be contradictory that bacteria induce a clotting mechanism, which is originally developed as an anti-bacterial immune defense mechanism of the host. However, the biochemical and physiological attributes of the fibrin meshwork formed by staphylocoagulases are thought to be distinct and less solid than those generated by thrombin (80). Therefore, instead of containing the infection, immune thrombosis might rather create the optimal environment for bacteria to survive and to evade the immune defense of the host (24).

It is supposed that the bacterial infection mechanism leading to vascular dysfunction and enhanced activation of inflammation might also be implicated in developing cardiovascular complications (**Figure 1C**). An increasing number of clinical studies solidify the observation that pneumococci induce vascular inflammation of the endothelial vessel wall, including the aorta (81), and that severe pneumococcal infections such as pneumoniae and septicemiae lead to a higher risk for major adverse cardiac effects (MACE) such as myocardial infarction, ischemic stroke, and arterial thrombosis (29–31).

Since elevated VWF plasma levels are known to be associated with an increased risk for MACE (15), the endothelial VWF release induced by pneumococcal attachment and by pneumolysin activity might be partially responsible for the pathologic effects on the cardio vasculature (45). As further explanation, functional variants of VWF have been identified, which elicit differences in the protein conformation and shear sensitivity. These variants are associated with increased platelet aggregate size and the occurrence of these VWF variants correlates with a higher risk of thromboembolisms including myocardial infarction and stroke (82). In line with these observations, it can be assumed that bacterial interaction with VWF might effect the hemostatic function in various ways, i.e., by sterical hindrance of the platelet binding site, by alteration of the VWF conformation, and by inhibition of dimerization and multimerization activities, thereby increasing the risk for cardiovascular complications.

CONCLUSIONS

VWF is a live-saving key component of coagulation and immune thrombosis in response to vascular injury and inflammation. Bacterial interaction with VWF is of high medical and scientific importance since this interaction is directly associated with specific clinical manifestations and long-term complications of infectious diseases. It has been demonstrated that binding of S. aureus and *S. pneumoniae* to VWF strings is controlled by hydrodynamic flow conditions. So far, at least three bacterial pathomechanisms involving host-derived VWF can be named: (i) binding to multimerized VWF strings mediates bacterial attachment to endothelial surfaces in blood flow–a major prerequisite of bacterial colonization, inflammation, and dissemination. (ii) VWF recruitment facilitates bacterial capture within clotted blood, thereby preventing bacterial clearance via immunothrombosis; (iii) recruitment of intravascular VWF induces bacterial aggregate formation, which leads to occlusion of microcapillaries and impaired blood supply. Although several sophisticated technologies such as microfluidic systems and binding force determinations already provided most valuable insights into the cell biological and biochemical details, the multifactorial complexity of the bacterial interaction with VWF still remains a challenging subject of ongoing scientific research.

AUTHOR CONTRIBUTIONS

SB and MS contributed to text conception and wrote the text. IR has generated the figure and critically revised the text. All authors contributed to manuscript revision, read, and approved the submitted version.

FUNDING

We acknowledge support by the German Research Foundation and the Open Access Publication Funds of the Technische Universität Braunschweig.

REFERENCES

1. Weibel ER, Palade GE. New cytoplasmic components in arterial endothelia. *J Cell Biol*. (1964) 23:101–12. doi: 10.1083/jcb.23.1.101
2. Rondaij MG, Sellink E, Gijzen KA, ten Klooster JP, Hordijk PL, van Mourik JA, et al. Small GTP-binding protein Ral is involved in cAMP-mediated release of von willebrand factor from endothelial cells. *Arterioscler Thromb Vasc Biol*. (2004) 24:1315–20. doi: 10.1161/01.ATV.0000131267.13425.45
3. Ruggeri ZM. Structure of von willebrand factor and its function in platelet adhesion and thrombus formation. *Best Pract Res Clin Haematol*. (2001) 14:257–79. doi: 10.1053/beha.2001.0133
4. Rondaij MG, Bierings R, Kragt A, van Mourik JA, Voorberg J. Dynamics and plasticity of weibel-palade bodies in endothelial cells. *Arterioscler Thromb Vasc Biol*. (2006) 26:1002–7. doi: 10.1161/01.ATV.0000209501.56852.6c
5. Randi AM, Laffan MA. Von Willebrand factor and angiogenesis: basic and applied issues. *J Thromb Haemost*. (2017) 15:13–20. doi: 10.1111/jth.13551
6. Spiel AO, Gilbert JC, Jilma B. Von willebrand factor in cardiovascular disease: focus on acute coronary syndromes. *Circulation*. (2008) 117:1449–59. doi: 10.1161/CIRCULATIONAHA.107.722827
7. Tischer A, Machha VR, Frontroth JP, Brehm MA, Obser T, Schneppenheim R, et al. Enhanced local disorder in a clinically elusive von willebrand factor provokes high-affinity platelet clumping. *J Mol Biol*. (2017) 429:2161–77. doi: 10.1016/j.jmb.2017.05.013
8. Vischer UM, Ingerslev J, Wollheim CB, Mestries JC, Tsakiris DA, Haefeli WE, et al. Acute von willebrand factor secretion from the endothelium *in vivo*: assessment through plasma propeptide (vWf:AgII) Levels. *Thromb Haemost*. (1997) 77:387–93. doi: 10.1055/s-0038-1655973

9. Kalagara T, Moutsis T, Yang Y, Pappelbaum KI, Farken A, Cladder-Micus L, et al. The endothelial glycocalyx anchors von willebrand factor fibers to the vascular endothelium. *Blood Adv*. (2018) 2:2347–57. doi: 10.1182/bloodadvances.2017013995
10. Hudlicka O, Brown MM. Adaptation of skeletal muscle microvasculatura to increased or decreased blood flow role of shear stress, nitric oxide and vascular endothelial growth factor. *J Vasc Res*. (2009) 46:504–12. doi: 10.1159/000226127
11. Springer TA. Von willebrand factor, jedi knight of the bloodstream. *Blood*. (2014) 124:1412–25. doi: 10.1182/blood-2014-05-378638
12. Löf A, König G, Schneppenheim S, Benoit M, Budde U, Müller JP, et al. Advancing multimer analysis of von willebrand factor by single-molecule AFM imaging. *PLoS ONE*. (2019) 14:e0210963. doi: 10.1371/journal.pone.0210963
13. Schneider SW, Nuschele S, Wixforth A, Gorzelanny C, Alexander-Katz A, Netz RR, et al. Shear-induced unfolding triggers adhesion of von willebrand factor fibers. *Proc Natl Acad Sci USA*. (2007) 104:7899–903. doi: 10.1073/pnas.0608422104
14. Flood VH, Gill JC, Christopherson PA, Bellissimo DB, Friedman KD, Haberichter SL, et al. Critical von willebrand factor A1 domain residues influence type VI collagen binding. *J Thromb Haemost*. (2012) 10:1417–24. doi: 10.1111/j.1538-7836.2012.04746.x
15. Jager A, van Hinsbergh VW, Kostense PJ, Emeis JJ, Yudkin JS, Nijpels G, et al. Von willebrand factor, C-reactive protein, and 5-year mortality in diabetic and nondiabetic subjects: the hoorn study. *Arterioscler Thromb Vasc Biol*. (1999) 19:3071–8. doi: 10.1161/01.ATV.19.12.3071
16. Massberg S, Brand K, Gruner S, Page S, Muller E, Muller I, et al. A critical role of platelet adhesion in the initiation of atherosclerotic lesion formation. *J Exp Med*. (2002) 196:887–96. doi: 10.1084/jem.20012044
17. Vischer UM. Von willebrand factor, endothelial dysfunction, and cardiovascular disease. *J Thromb Haemost*. (2006) 4:1186–93. doi: 10.1111/j.1538-7836.2006.01949.x
18. Ruggeri ZM. Von Willebrand factor, platelets and endothelial cell interactions. *J Thromb Haemost*. (2003) 1:1335–42. doi: 10.1046/j.1538-7836.2003.00260.x
19. Pappelbaum KI, Gorzelanny C, Grassle S, Suckau J, Laschke MW, Bischoff M, et al. Ultralarge von willebrand factor fibers mediate luminal *Staphylococcus aureus* adhesion to an intact endothelial cell layer under shear stress. *Circulation*. (2013) 128:50–9. doi: 10.1161/CIRCULATIONAHA.113.002008
20. Jagau H, Behrens IK, Lahme K, Lorz G, Koster RW, Schneppenheim R, et al. Von Willebrand factor mediates pneumococcal aggregation and adhesion in blood flow. *Front Microbiol*. (2019) 10:511. doi: 10.3389/fmicb.2019.00511
21. Moreillon P, Que YA. Infective endocarditis. *Lancet*. (2004) 363:139–49. doi: 10.1016/S0140-6736(03)15266-X
22. Fowler RA, Gupta S. Subacute and acute infective endocarditis. *Lancet*. (2005) 366:1964. doi: 10.1016/S0140-6736(05)67788-4
23. Liesenborghs L, Meyers S, Lox M, Criel M, Claes J, Peetermans M, et al. *Staphylococcus aureus* endocarditis: distinct mechanisms of bacterial adhesion to damaged and inflamed heart valves. *Eur Heart J*. (2019) 40:3248–59. doi: 10.1093/eurheartj/ehz175
24. Liesenborghs L, Meyers S, Vanassche T, Verhamme P. Coagulation: At the heart of infective endocarditis. *J Thromb Haemost*. (2020) 18:995–1008. doi: 10.1111/jth.14736
25. Cartwright K. Pneumococcal disease in western Europe: burden of disease, antibiotic resistance and management. *Eur J Pediatr*. (2002) 161:188–95. doi: 10.1007/s00431-001-0907-3
26. Weiser JN, Ferreira DM, Paton JC. *Streptococcus pneumoniae*: transmission, colonization and invasion. *Nat Rev Microbiol*. (2018) 16:355–67. doi: 10.1038/s41579-018-0001-8
27. Aronin SI, Mukherjee SK, West JC, Cooney EL. Review of pneumococcal endocarditis in adults in the penicillin era. *Clin Infect Dis*. (1998) 26:165–71. doi: 10.1086/516279
28. de Egea V, Munoz P, Valerio M, de Alarcon A, Lepe JA, Miro JM, et al. Characteristics and outcome of *Streptococcus pneumoniae* endocarditis in the XXI century: a systematic review of 111 cases (2000-2013). *Medicine*. (2015) 94:e1562. doi: 10.1097/MD.0000000000001562
29. Musher DM, Rueda AM, Kaka AS, Mapara SM. The association between pneumococcal pneumonia and acute cardiac events. *Clin Infect Dis*. (2007) 45:158–65. doi: 10.1086/518849
30. Corrales-Medina VF, Alvarez KN, Weissfeld LA, Angus DC, Chirinos JA, Chang CC, et al. Association between hospitalization for pneumonia and subsequent risk of cardiovascular disease. *JAMA*. (2015) 313:264–74. doi: 10.1001/jama.2014.18229
31. Rae N, Finch S, Chalmers JD. Cardiovascular disease as a complication of community-acquired pneumonia. *Curr Opin Pulm Med*. (2016) 22:212–8. doi: 10.1097/MCP.0000000000000261
32. van Mourik JA, Romani de Wit T, Voorberg J. Biogenesis and exocytosis of weibel-palade bodies. *Histochem Cell Biol*. (2002) 117:113–22. doi: 10.1007/s00418-001-0368-9
33. Sporn LA, Shi RJ, Lawrence SO, Silverman DJ, Marder VJ. *Rickettsia rickettsii* infection of cultured endothelial cells induces release of large von willebrand factor multimers from weibel-palade bodies. *Blood*. (1991) 78:2595–602. doi: 10.1182/blood.V78.10.2595.bloodjournal78102595
34. Mascari LM, Ross JM. Quantification of staphylococcal-collagen binding interactions in whole blood by use of a confocal microscopy shear-adhesion assay. *J Infect Dis*. (2003) 188:98–107. doi: 10.1086/375826
35. Hartleib J, Kohler N, Dickinson RB, Chhatwal GS, Sixma JJ, Hartford OM, et al. Protein A is the von willebrand factor binding protein on *Staphylococcus aureus*. *Blood*. (2000) 96:2149–56.
36. Viela F, Prystopiuk V, Leprince A, Mahillon J, Speziale P, Pietrocola G, et al. Binding of *Staphylococcus aureus* protein A to von willebrand factor is regulated by mechanical force. *MBio*. (2019) 10:e00555–19. doi: 10.1128/mBio.00555-19
37. Bjerketorp J, Nilsson M, Ljungh A, Flock JI, Jacobsson K, Frykberg L. A novel von willebrand factor binding protein expressed by *Staphylococcus aureus*. *Microbiology*. (2002) 148:2037–44. doi: 10.1099/00221287-148-7-2037
38. Bjerketorp J, Jacobsson K, Frykberg L. The von willebrand factor-binding protein (vWbp) of *Staphylococcus aureus* is a coagulase. *FEMS Microbiol Lett*. (2004) 234:309–14. doi: 10.1111/j.1574-6968.2004.tb09549.x
39. Cheng AG, McAdow M, Kim HK, Bae T, Missiakas DM, Schneewind O. Contribution of coagulases towards *Staphylococcus aureus* disease and protective immunity. *PLoS Pathog*. (2010) 6:e1001036. doi: 10.1371/journal.ppat.1001036
40. Li DQ, Lundberg F, Ljungh A. Binding of von willebrand factor by coagulase-negative staphylococci. *J Med Microbiol*. (2000) 49:217–25. doi: 10.1099/0022-1317-49-3-217
41. Liesenborghs L, Peetermans M, Claes J, Veloso TR, Vandenbriele C, Criel M, et al. Shear-resistant binding to von willebrand factor Allows *Staphylococcus lugdunensis* to adhere to the cardiac valves and initiate endocarditis. *J Infect Dis*. (2016) 213:1148–56. doi: 10.1093/infdis/jiv773
42. Nilsson M, Bjerketorp J, Wiebensjo A, Ljungh A, Frykberg L, Guss B. A von willebrand factor-binding protein from *Staphylococcus lugdunensis*. *FEMS Microbiol Lett*. (2004) 234:155–61. doi: 10.1111/j.1574-6968.2004.tb09527.x
43. Carter AM, Moayyedi P, Catto A, Heppell RM, Axon AT, Grant PJ. The influence of *Helicobacter pylori* status on circulating levels of the coagulation factors fibrinogen, von willebrand factor, factor VII, and factor VIII. *Helicobacter*. (1996) 1:65–9. doi: 10.1111/j.1523-5378.1996.tb00011.x
44. Byrne MF, Kerrigan SW, Corcoran PA, Atherton JC, Murray FE, Fitzgerald DJ, et al. *Helicobacter pylori* binds von willebrand factor and interacts with GPIb to induce platelet aggregation. *Gastroenterology*. (2003) 124:1846–54. doi: 10.1016/S0016-5085(03)00397-4
45. Luttge M, Fulde M, Talay SR, Nerlich A, Rohde M, Preissner KT, et al. *Streptococcus pneumoniae* induces exocytosis of weibel-palade bodies in pulmonary endothelial cells. *Cell Microbiol*. (2012) 14:210–25. doi: 10.1111/j.1462-5822.2011.01712.x
46. Herrmann M, Hartleib J, Kehrel B, Montgomery RR, Sixma JJ, Peters G. Interaction of von willebrand factor with *Staphylococcus aureus*. *J Infect Dis*. (1997) 176:984–91. doi: 10.1086/516502
47. Bergmann S, Steinert M. From single cells to engineered and explanted tissues: new perspectives in bacterial infection biology. *Int Rev Cell Mol Biol*. (2015) 319:1–44. doi: 10.1016/bs.ircmb.2015.06.003
48. Goto S, Salomon DR, Ikeda Y, Ruggeri ZM. Characterization of the unique mechanism mediating the shear-dependent binding of soluble von willebrand factor to platelets. *J Biol Chem*. (1995) 270:23352–61. doi: 10.1074/jbc.270.40.23352

49. Just S. Laboratory testing for von willebrand disease: the past, present, and future state of play for von willebrand factor assays that measure platelet binding activity, with or without ristocetin. *Semin Thromb Hemost*. (2017) 43:75–91. doi: 10.1055/s-0036-1592164
50. Mascari L, Ymele-Leki P, Eggleton CD, Speziale P, Ross JM. Fluid shear contributions to bacteria cell detachment initiated by a monoclonal antibody. *Biotechnol Bioeng*. (2003) 83:65–74. doi: 10.1002/bit.10650
51. Claes J, Vanassche T, Peetermans M, Liesenborghs L, Vandenbriele C, Vanhoorelbeke K, et al. Adhesion of *Staphylococcus aureus* to the vessel wall under flow is mediated by von willebrand factor-binding protein. *Blood*. (2014) 124:1669–76. doi: 10.1182/blood-2014-02-558890
52. Kamei M, Saunders WB, Bayless KJ, Dye L, Davis GE, Weinstein BM. Endothelial tubes assemble from intracellular vacuoles *in vivo*. *Nature*. (2006) 442:453–6. doi: 10.1038/nature04923
53. Hanumanthaiah R, Day K, Jagadeeswaran P. Comprehensive analysis of blood coagulation pathways in teleostei: evolution of coagulation factor genes and identification of zebrafish factor VIIi. *Blood Cells Mol Dis*. (2002) 29:57–68. doi: 10.1006/bcmd.2002.0534
54. Weyand AC, Shavit JA. Zebrafish as a model system for the study of hemostasis and thrombosis. *Curr Opin Hematol*. (2014) 21:418–22. doi: 10.1097/MOH.0000000000000075
55. O'Seaghdha M, van Schooten CJ, Kerrigan SW, Emsley J, Silverman GJ, Cox D, et al. *Staphylococcus aureus* protein A binding to von willebrand factor A1 domain is mediated by conserved IgG binding regions. *FEBS J*. (2006) 273:4831–41. doi: 10.1111/j.1742-4658.2006.05482.x
56. Viela F, Speziale P, Pietrocola G, Dufrene YF. Bacterial pathogens under high-tension: *Staphylococcus aureus* adhesion to von willebrand factor is activated by force. *Microb Cell*. (2019) 6:321–3. doi: 10.15698/mic2019.07.684
57. Herman-Bausier P, Labate C, Towell AM, Derclaye S, Geoghegan JA, Dufrene YF. *Staphylococcus aureus* clumping factor A is a force-sensitive molecular switch that activates bacterial adhesion. *Proc Natl Acad Sci USA*. (2018) 115:5564–9. doi: 10.1073/pnas.1718104115
58. Thomer L, Schneewind O, Missiakas D. Multiple ligands of von willebrand factor-binding protein (vWbp) promote *Staphylococcus aureus* clot formation in human plasma. *J Biol Chem*. (2013) 288:28283–92. doi: 10.1074/jbc.M113.493122
59. Zakrzewicz D, Bergmann S, Didiasova M, Giaimo BD, Borggrefe T, Mieth M, et al. Host-derived extracellular RNA promotes adhesion of *Streptococcus pneumoniae* to endothelial and epithelial cells. *Sci Rep*. (2016) 6:37758. doi: 10.1038/srep37758
60. Claes J, Liesenborghs L, Peetermans M, Veloso TR, Missiakas D, Schneewind O, et al. Clumping factor A, von willebrand factor-binding protein and von willebrand factor anchor *Staphylococcus aureus* to the vessel wall. *J Thromb Haemost*. (2017) 15:1009–19. doi: 10.1111/jth.13653
61. Jagau H, Behrens IK, Steinert M, Bergmann S. Pneumococcus infection of primary human endothelial cells in constant flow. *J Vis Exp*. (2019) 152:e60323. doi: 10.3791/60323
62. Guerrero ML, Aldamiz G, Bayon J, Cohen VA, Fraile J. Long-term survival of salvage cardiac transplantation for infective endocarditis. *Ann Thorac Surg*. (2011) 92:e93–94. doi: 10.1016/j.athoracsur.2011.05.048
63. Thiene G, Basso C. Pathology and pathogenesis of infective endocarditis in native heart valves. *Cardiovasc Pathol*. (2006) 15:256–63. doi: 10.1016/j.carpath.2006.05.009
64. Yap CH, Saikrishnan N, Tamilselvan G, Yoganathan AP. Experimental measurement of dynamic fluid shear stress on the aortic surface of the aortic valve leaflet. *Biomech Model Mechanobiol*. (2012) 11:171–82. doi: 10.1007/s10237-011-0301-7
65. Yap CH, Saikrishnan N, Yoganathan AP. Experimental measurement of dynamic fluid shear stress on the ventricular surface of the aortic valve leaflet. *Biomech Model Mechanobiol*. (2012) 11:231–44. doi: 10.1007/s10237-011-0306-2
66. Gálvez-Santisteban M, Chen D, Zhang R, Serrano R, Nguyen C, Zhao L, et al. Hemodynamic-mediated endocardial signaling controls *in vivo* myocardial reprogramming. *Elife*. (2019) 8:e44816. doi: 10.7554/eLife.44816
67. Que YA, Haefliger JA, Piroth L, Francois P, Widmer E, Entenza JM, et al. Fibrinogen and fibronectin binding cooperate for valve infection and invasion in *Staphylococcus aureus* experimental endocarditis. *J Exp Med*. (2005) 201:1627–35. doi: 10.1084/jem.20050125
68. Kerdudou S, Laschke MW, Sinha B, Preissner KT, Menger MD, Herrmann M. Fibronectin binding proteins contribute to the adherence of *Staphylococcus aureus* to intact endothelium *in vivo*. *Thromb Haemost*. (2006) 96:183–9. doi: 10.1160/TH06-02-0116
69. Levi M, Ten Cate H. Disseminated intravascular coagulation. *N Engl J Med*. (1999) 341:586–92. doi: 10.1056/NEJM199908193410807
70. Cheng AG, Kim HK, Burts ML, Krausz T, Schneewind O, Missiakas DM. Genetic requirements for *Staphylococcus aureus* abscess formation and persistence in host tissues. *FASEB J*. (2009) 23:3393–404. doi: 10.1096/fj.09-135467
71. Friedrich R, Panizzi P, Fuentes-Prior P, Richter K, Verhamme I, Anderson PJ, et al. Staphylocoagulase is a prototype for the mechanism of cofactor-induced zymogen activation. *Nature*. (2003) 425:535–9. doi: 10.1038/nature01962
72. Kroh HK, Panizzi P, Bock PE. Von willebrand factor-binding protein is a hysteretic conformational activator of prothrombin. *Proc Natl Acad Sci USA*. (2009) 106:7786–91. doi: 10.1073/pnas.0811750106
73. McAdow M, Kim HK, Dedent AC, Hendrickx AP, Schneewind O, Missiakas DM. Preventing *Staphylococcus aureus* sepsis through the inhibition of its agglutination in blood. *PLoS Pathog*. (2011) 7:e1002307. doi: 10.1371/journal.ppat.1002307
74. van der Poll T, Opal SM. Host-pathogen interactions in sepsis. *Lancet Infect Dis*. (2008) 8:32–43. doi: 10.1016/S1473-3099(07)70265-7
75. van der Poll T, Opal SM. Should all septic patients be given systemic anticoagulation? No. *Intensive Care Med*. (2017) 43:455–7. doi: 10.1007/s00134-016-4607-x
76. Charalambous BM, Leung MH. Pneumococcal sepsis and nasopharyngeal carriage. *Curr Opin Pulm Med*. (2012) 18:222–7. doi: 10.1097/MCP.0b013e328352103b
77. van der Linden M, Reinert RR. Serotype distribution in pneumococcal acute otitis media with ruptured tympanic membrane or sepsis in Germany. *Eur J Clin Microbiol Infect Dis*. (2010) 29:749–54. doi: 10.1007/s10096-010-0945-8
78. Verhamme P, Hoylaerts MF. Hemostasis and inflammation: two of a kind? *Thromb J*. (2009) 7:15. doi: 10.1186/1477-9560-7-15
79. Yeaman MR, Norman DC, Bayer AS. Platelet microbicidal protein enhances antibiotic-induced killing of and postantibiotic effect in *Staphylococcus aureus*. *Antimicrob Agents Chemother*. (1992) 36:1665–70. doi: 10.1128/AAC.36.8.1665
80. Kopec M, Wegrzynowicz Z, Budzynski AZ, Jeljaszewicz J, Latallo ZS, Lipinski B, et al. Formation and properties of fibrin clots resulting from staphylocoagulase (SC) action. *Thromb Diath Haemorrh*. (1967) 18:475–86. doi: 10.1055/s-0038-1655057
81. Maclennan AC, Doyle DL, Sacks SL. Infectious aortitis due to penicillin-resistant *Streptococcus pneumoniae*. *Ann Vasc Surg*. (1997) 11:533–5. doi: 10.1007/s100169900086
82. Schneppenheim R, Hellermann N, Brehm MA, Klemm U, Obser T, Huck V, et al. The von willebrand factor Tyr2561 allele is a gain-of-function variant and a risk factor for early myocardial infarction. (2019) 133:356–65. doi: 10.1182/blood-2018-04-843425

Conflict of Interest: The authors declare that the research was conducted in the absence of any commercial or financial relationships that could be construed as a potential conflict of interest.

frontiers in Cell and Developmental Biology

REVIEW
published: 04 September 2020
doi: 10.3389/fcell.2020.576491

Endothelial Ribonuclease 1 in Cardiovascular and Systemic Inflammation

Katrin Bedenbender[1] *and Bernd T. Schmeck*[1,2,3,4]*

[1] Institute for Lung Research, Universities of Giessen and Marburg Lung Center, Marburg, Germany, [2] Department of Pulmonary and Critical Care Medicine, Department of Medicine, University Medical Center Giessen and Marburg, Philipps-University Marburg, Marburg, Germany, [3] Member of the German Center for Lung Research, Member of the German Center for Infectious Disease Research, Marburg, Germany, [4] Center for Synthetic Microbiology, Philipps-University Marburg, Marburg, Germany

The vascular endothelial cell layer forms the inner lining of all blood vessels to maintain proper functioning of the vascular system. However, dysfunction of the endothelium depicts a major issue in context of vascular pathologies, such as atherosclerosis or thrombosis that cause several million deaths per year worldwide. In recent years, the endothelial extracellular endonuclease Ribonuclease 1 (RNase1) was described as a key player in regulation of vascular homeostasis by protecting endothelial cells from detrimental effects of the damage-associated molecular pattern extracellular RNA upon acute inflammation. Despite this protective function, massive dysregulation of RNase1 was observed during prolonged endothelial cell inflammation resulting in progression of several vascular diseases. For the first time, this review article outlines the current knowledge on endothelial RNase1 and its role in function and dysfunction of the endothelium, thereby focusing on the intensive research from recent years: Uncovering the underlying mechanisms of RNase1 function and regulation in response to acute as well as long-term inflammation, the role of RNase1 in context of vascular, inflammatory and infectious diseases and the potential to develop novel therapeutic options to treat these pathologies against the background of RNase1 function in endothelial cells.

Keywords: ribonuclease 1, endothelial cells, inflammation, extracellular RNA, vascular diseases

OPEN ACCESS

Edited by:
Ritva Tikkanen,
University of Giessen, Germany

Reviewed by:
Anil Chauhan,
Saint Louis University, United States
Xinghui Sun,
University of Nebraska System, United States
Karima Ait-Aissa,
The University of Iowa, United States

***Correspondence:**
Bernd T. Schmeck
bernd.schmeck@uni-marburg.de

Specialty section:
This article was submitted to Molecular Medicine, a section of the journal Frontiers in Cell and Developmental Biology

Received: *26 June 2020*
Accepted: *14 August 2020*
Published: *04 September 2020*

Citation:
Bedenbender K and Schmeck BT (2020) Endothelial Ribonuclease 1 in Cardiovascular and Systemic Inflammation. Front. Cell Dev. Biol. 8:576491. doi: 10.3389/fcell.2020.576491

INTRODUCTION

Endothelial cells (ECs) form the inner lining of all blood vessels and act as anatomical and active physiological barrier to separate the blood from the surrounding tissue (Baldwin and Thurston, 2001; Michiels, 2003). Thereby, these cells highly contribute to control and maintenance of vascular homeostasis and integrity (Pober and Sessa, 2007; Rajendran et al., 2013). Under physiological conditions, the endothelium is the central component of vessel permeability and participates in the regulation of coagulation as well as the communication with band recruitment of circulating leukocytes from the blood stream (Arnout et al., 2006; Ley and Reutershan, 2006;

Abbreviations: Asn, asparagine; EC, endothelial cell; eRNA, extracellular RNA; HDAC, histone deacetylase; HUVEC, human umbilical vein endothelial cells; I/R, ischemic/reperfusion; IL, interleukin; MI, myocardial infarction; poly I:C, polyinosinic polycytidylic acid; RA, rheumatoid arthritis; RNase1, Ribonuclease 1; TNF-α, tumor necrosis factor alpha.

Minshall and Malik, 2006; Pober and Sessa, 2007). In this regard, ECs sequester leukocyte interactive proteins, such as chemokines or adhesion molecules within their storage vesicles, the Weibel-Palade Bodies (WPBs), and additionally repress the transcription of membrane bound adhesion molecules or proinflammatory cytokines (De Caterina et al., 1995; Rondaij et al., 2006; Pober and Sessa, 2007; Rajendran et al., 2013). Upon inflammation, ECs get rapidly activated, which goes along with decisive changes in gene expression, e.g., cytokines and adhesion molecules, WPB exocytosis to promote the release proinflammatory agents into the extracellular space, and exposure of adhesion molecules at the cell surface. Consequently, these processes support recruitment and interaction with circulating leukocytes, finally resulting in infiltration of inflammatory cells into the underlying tissue and secretion of proinflammatory mediators such as tumor necrosis factor alpha (TNF-α) or interleukin (IL)-1β into the blood stream. Altogether, these processes act in concert to eradicate the triggering inflammatory stimulus and restore vascular and tissue integrity (Pober and Sessa, 2007). However, persistent vascular inflammation can drastically affect the homeostatic function of the endothelium, followed by EC dysfunction and progression of vascular diseases, such as atherosclerosis, thrombosis, or consequential disorders like myocardial infarction or cerebral ischemia (Poredos, 2002; Sitia et al., 2010; Zernecke and Preissner, 2016). Such vascular diseases depict one of the leading causes of death worldwide with approximately 18 million deaths per year[1]. In recent decades, investigation of the underlying mechanisms of EC dysfunction in inflammation-associated vascular diseases and the development of novel therapeutic approaches to treat these pathologies was of great importance. In this context, Ribonuclease (RNase) 1 has been newly recognized as a vessel-protective factor in EC inflammation that is tightly associated to inflammation induced vascular dysfunction and subsequent pathologies (Zernecke and Preissner, 2016).

This review article summarizes the current knowledge of endothelial RNase1 and its regulation and function in vascular ECs under physiological and inflammatory conditions. Moreover, we outline the impact of RNase1 regulation in progression of diverse vascular diseases, as well as other inflammation-associated disorders, and the resulting potential to develop novel therapeutic strategies to treat pathological EC inflammation by preserving RNase1 function.

ENDOTHELIAL RNASE1

RNase1 belongs to the Ribonuclease A superfamily, consisting of in total 13 described enzymes (Sorrentino, 2010; Koczera et al., 2016). The biological function of this enzyme family varies from host defense and immune cell regulation [e.g., RNase2, RNase5, RNase7; (Hooper et al., 2003; Yang et al., 2004; Bedoya et al., 2006; Huang et al., 2007)] to tissue repair and remodeling, such as angiogenesis [e.g., RNase4, RNase5, RNase7; (Fett et al., 1985; Li et al., 2013; Schwartz et al., 2018)], as well as RNA cleavage [e.g., RNase5; (Lee and Vallee, 1989; Russo et al., 1994)]. Nevertheless, the precise physiological functions of the diverse members of the Ribonuclease A superfamily need to be further investigated (Koczera et al., 2016). The RNase1 endonuclease is described as one of eight secreteable and enzymatically active members of this protein family, also known as canonical RNases (Koczera et al., 2016). Thermostable RNase1 depicts the most prevalent human homolog of the well-described bovine pancreatic RNase A and was shown to be produced in numerous tissues of the whole body, such as pancreas, testis, ovary, and brain (Beintema et al., 1988; Futami et al., 1997; Landre et al., 2002; Sorrentino, 2010; Koczera et al., 2016). Moreover, human RNase1 mRNA and protein expression data from high-throughput analysis provided by the "proteinatlas" platform[2] is summarized in **Table 1**. Thereby, high levels of active RNase1 can be detected in different body fluids, e.g., plasma or serum, with concentrations up to 0.5 μg/ml, suggesting an endothelial origin of this enzyme (Weickmann et al., 1984; Morita et al., 1986; Futami et al., 1997; Petrova et al., 2002; Su et al., 2004). Indeed, RNase1 expression and release is predominantly observed in various types of vascular ECs for instance in primary human ECs from pulmonary arteries, cerebral microvasculature, or especially human umbilical vein ECs (HUVEC), that secrete highest amounts of RNase1 (Landre et al., 2002; Fischer et al., 2011). Thereby, these cells offer an ideal model system to study RNase1 function and regulation in human ECs and are widely used for further investigations.

RNase1 Glycosylation and Its Storage in WPBs

Secreted RNase1 molecules vary in size from approximately 18–26 kDa, depending on its glycosylation pattern (Landre et al., 2002; Koczera et al., 2016; Ressler and Raines, 2019). Investigation of RNase1 isolates from human serum identified exclusively three different N-glycosylation sites at secreted proteins with varying abundance and differential expression depending on tissue and cell type: Asparagine (Asn) 34, Asn76 and Asn88, with Asn34 presumably being the most important glycosylation sites resulting in significantly improved overall protein stability and robust catalytic activity (Beintema et al., 1988; Ribo et al., 1994; Barrabes et al., 2007; Ressler and Raines, 2019). Despite the function of RNase1 protein glycosylation in respect to stability and catalytic activity, further consequences of RNase1 glycosylation are still unknown (Ressler and Raines, 2019). In general, glycosylation is already intensively studied, for instance in context of protein stability, dictation of immune cell movement, or discrimination between self and non-self (Marth and Grewal, 2008; Reily et al., 2019; Ressler and Raines, 2019). Since, studies of the Ribonuclease A superfamily members RNase2 and RNase3 indicated a crucial role of their N-glycosylation in host-defense (Sorrentino, 2010; Lu et al., 2018), a comparable feature for RNase1 glycosylation in this context can be suggested. As protein glycosylation is a common co-translational modification originated from the endoplasmatic reticulum and the Golgi apparatus, it is hardly surprising that secreted RNase1 is partially stored and released from WPBs

[1]https://www.who.int/news-room/fact-sheets/detail/cardiovascular-diseases-(cvds)

[2]https://www.proteinatlas.org/ENSG00000129538-RNASE1/

(Marth and Grewal, 2008; Fischer et al., 2011; Reily et al., 2019). WPBs are small storage granules of vascular ECs and are known to be the "first aid kit" of the endothelial cell layer. These granules consist of several proinflammatory mediators such as adhesion molecules (e.g., P-selectin) or chemo - and cytokines (e.g., IL-8, monocyte chemoattractant protein 1) as well as the potent coagulation factor von Willebrand factor, which guides manufacturing and loading of mature WPBs at the trans-Golgi network (Valentijn et al., 2011; Schillemans et al., 2019). In respect to RNase1, Fischer and colleagues demonstrated that constitutively expressed endothelial RNase1 can be stored, and released from WPBs, where it co-localizes with factors like von Willebrand factor or P-selectin (Fischer et al., 2011; Koczera et al., 2016). Although the knowledge about WPB-assembly and loading has considerably increased in the past years, the exact mechanism by which RNase1 enters these vesicles is still unclear. Nevertheless, once packed with cargo, WPBs travel to the cell periphery and can release their content, including RNase1, to the extracellular space under physiological as well as inflammatory conditions (Fischer et al., 2011; Valentijn et al., 2011; Schillemans et al., 2019).

RNase1 Ribonuclease Function and Inhibition

According to its secretory phenotype, RNase1 comprises the ability to act in many body fluids, which is tightly associated to its neutral pH optimum to provide enhanced capacity to cleave single- as well as double-stranded RNA species in the extracellular space (Sorrentino et al., 2003; Koczera et al., 2016; Lomax et al., 2017). The catalytic mechanism is based on the interaction of cationic enzymatic residues with the anionic phosphoryl groups of RNA substrates and the formation of disulfide bonds (Klink et al., 2000; Ressler and Raines, 2019).

Thereby, RNase1 can act as an RNA scavenger to modulate and remove the heterogeneous content of extracellular RNA

TABLE 1 | RNase1 mRNA and protein expression in human tissue https://www.proteinatlas.org/ENSG00000129538-RNASE1/tissue.

Tissue		mRNA	Protein
Brain	Olfactory region, amygdala, hypothalamus, thalamus, midbrain, pons and medulla, corpus callosum, spinal cord	yes	n/a
	Cerebral cortex, hippocampal formation, basal ganglia	yes	Neuronal cells
	Cerebellum	yes	Purkinje cells
Eye	Retina	yes	n/a
Endocrine tissue	Thyroid gland, parathyroid gland, adrenal gland	yes	n/d
	Pituitary gland	yes	n/a
Lung	Nasopharynx	n/a	n/d
	Bronchus	yes	Respiratory epithelial cells
	Lung	yes	n/d
Proximal digestive tract	Tongue	yes	n/a
	Oral mucosa	n/a	Squamos epithelial cells
	Salivary gland	yes	Glandular cells
	Esophagus	yes	n/d
Gastrointestinal tract	Stomach, duodenum, small intestine, colon, rectum	yes	Glandular cells
Liver and gallbladder	Liver, gallbladder	yes	n/d
Pancreas	Pancreas	yes	Exocrine glandular cells
Kidney and urinary bladder	Kidney	yes	Cells in tubules
	Urinary bladder	yes	n/d
Male tissues	Ductus deferens	yes	n/a
	Testis	yes	Cells in seminiferous duct
	Epididymis, seminal vesicle	yes	Glandular cells
	Prostate	yes	n/d
Female tissues	Vagina, ovary, fallopian tube, endometrium, cervix, uterine, placenta, breast	yes	n/d
Muscle tissues	Heart muscle, smooth muscle, skeletal muscle	yes	n/d
Adipose and soft tissue	Adipose tissue	yes	n/d
	Soft tissue	n/a	Chondrocytes
Skin	Skin	yes	n/d
Bone marrow and lymphoid tissues	Thymus	yes	n/a
	Appendix	yes	Glandular cells
	Spleen, lymph node, tonsil	yes	n/d
Blood	Bone marrow	yes	n/d
	Granulocytes, monocytes, dendritic cells, total PBMCs	yes	n/a

n/a, not applicable, n/d, not detected, PBMCs, peripheral blood derived mononuclear cells; Data provided by www.proteinatlas.org.

(eRNA) that is highly associated to vascular inflammation (Koczera et al., 2016; Zernecke and Preissner, 2016; Lu et al., 2018). With respect to the high affinity of RNase1 to diverse RNA species, it is necessary to prevent intracellular self-RNA degradation, as well as excessive degradation of damage-associated RNA species in the extracellular space to maintain cellular responsibility. Intracellularly, RNases, including RNase1, can be efficiently bound by the human RNase inhibitor to prevent cytotoxicity by blocking the catalytic activity of the RNase via formation of a tight RNase-inhibitor complex. Thereby, the 50 kDa, cytosolic and anionic RNase inhibitor effectively binds the cationic surface of the enzyme via formation of several intermolecular hydrogen bonds to provide an extremely stable complex and protect intracellular RNA species from degradation (Dickson et al., 2005; Johnson et al., 2007). In terms of RNase1 clearance from the extracellular space, RNases can be taken up and removed from the extracellular space via the endocytic pathway by neighboring cells, however, the precise mechanisms need to be further investigated (Chao and Raines, 2011; Lomax et al., 2017).

RNASE1 REGULATION UPON EC INFLAMMATION

The release of glycosylated RNase1 from WPBs of vascular ECs, its high secretory levels into body-fluids, and its catalytic activity to diverse eRNA species pointed toward a regulatory impact of RNase1 on maintenance and integrity of vascular homeostasis (Landre et al., 2002; Sorrentino et al., 2003; Kannemeier et al., 2007; Fischer et al., 2011; Lomax et al., 2017). Accordingly, in 2014, Gansler and colleagues analyzed the regulation of RNase1 in context of acute and long-term EC inflammation, thereby revealing its importance as regulator of vascular function (Gansler et al., 2014).

The RNase1-eRNA System in ECs

In response to inflammation, infection or tissue injury, ECs get activated and initiate the release of leukocyte interactive molecules as well as large amounts of free damage-associated molecular patterns such as eRNA, e.g., via apoptosis or necrosis (Pober and Sessa, 2007; Fischer and Preissner, 2013; Fischer et al., 2013; Zernecke and Preissner, 2016). Once released to the extracellular space, free eRNA can act as potent inducer of the immune response, for instance via signaling through pattern-recognition receptors such as endosomal Toll-like receptors (reviewed by Fischer and Preissner, 2013; Fischer et al., 2014; Zernecke and Preissner, 2016; Lu et al., 2019), and the secretion of WPB-content from the EC layer (Fischer et al., 2013, 2014; Gansler et al., 2014; Zernecke and Preissner, 2016). These processes subsequently result in the release of the proinflammatory content of WPBs, including RNase1. Here, RNase1 protects the endothelium from an overwhelming eRNA-mediated inflammatory response by acting as natural counterpart to eRNA via degradation and generation of eRNA cleavage-products that are unable to disturb the EC-barrier function (Fischer et al., 2007, 2014; Cabrera-Fuentes et al., 2014; Gansler et al., 2014). However, upon prolonged EC inflammation, the balance of the RNase1-eRNA system is compromised due to accumulation of eRNA in the extracellular space. Thereby, eRNA facilitates various processes affecting the integrity of the endothelium: eRNA exposure of several types of vascular ECs increased vessel permeability via disorganization of cell-junctional proteins, like occludin or vascular endothelial cadherin. These processes are mediated via enhanced activation of vascular endothelial growth factor and vascular endothelial growth factor receptor two signaling (Fischer et al., 2007, 2009; Gansler et al., 2014). Additionally, augmented secretion of proinflammatory cytokines by circulating immune cells (e.g., monocytes, macrophages) is induced via eRNA-mediated signaling through pattern recognition receptors or cytokine shedding (Fischer and Preissner, 2013; Fischer et al., 2013, 2014; Gansler et al., 2014; Zernecke and Preissner, 2016; Lu et al., 2019), phospholipase C function, and intracellular Ca^{2+} release (Fischer et al., 2009). All these processes culminate in a highly proinflammatory state of the endothelium that is associated to a vast increase in cytokine levels in the extracellular space, especially TNF-α or IL-β. These cytokines further act on ECs via massive repression of RNase1 expression, as demonstrated by Gansler and colleagues in HUVEC (Gansler et al., 2014). Consequently, RNase1 protein generation, storage, and release from WPBs, as well as its eRNA-degrading function is impaired, followed by additional eRNA accumulation in the extracellular space and subsequent EC dysfunction (Gansler et al., 2014).

Molecular Mechanisms of Proinflammatory RNase1 Repression

In recent years, the identification of the molecular mechanisms of inflammation-mediated RNase1 regulation was intensively studied, yielding in a substantial increase in knowledge. In 2014, Gansler and colleagues implicated a regulatory mechanism for RNase1 repression, dependent on histone deacetylases (HDACs) rather than Nuclear factor κ B-mediated signaling by using specific pharmaceutical inhibitors (Gansler et al., 2014). Based on these findings, we further investigated the precise molecular mechanisms of RNase1 regulation: The promoter region of *RNASE1* was identified to examine the HDAC-mediated changes of *RNASE1* at chromatin level (Bedenbender et al., 2019). Thereby, proinflammatory stimulation of HUVEC resulted in the loss of different markers associated to active transcription, specific deacetylation of the *RNASE1* promoter at histone 4 and histone 3 lysine 27, along with the loss of RNA polymerase II transcription machinery binding (Kouzarides, 2007; Wang et al., 2008; Bedenbender et al., 2019). Additionally, administration of the specific HDAC inhibitor MS275, targeting the class I HDACs HDAC1–3, successfully recovered RNase1 mRNA expression upon inflammation (via TNF-α) as consequence of restored histone acetylation and RNA polymerase II recruitment (Bedenbender et al., 2019). The HDAC enzyme responsible for this regulatory process was further identified as HDAC2, demonstrated by its accumulation and deacetylation of the *RNASE1* promoter upon proinflammatory stimulation. However, the results also implicated that the highly similar class I family member HDAC1 might act redundantly to HDAC2

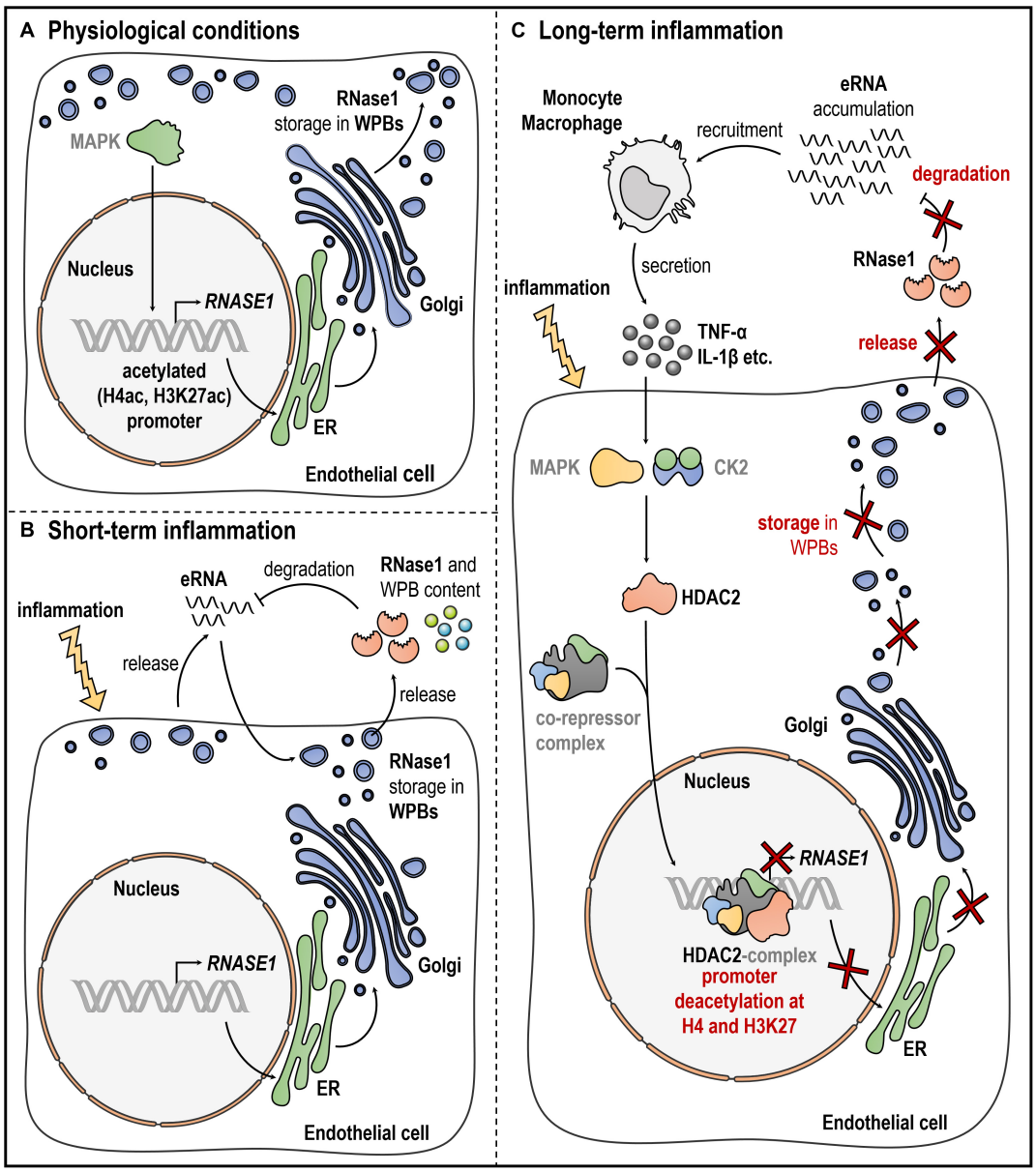

FIGURE 1 | Endothelial RNase1 regulation. Schematic overview of RNase1 regulation under **(A)** physiological conditions, **(B)**, short-term, or **(C)** long-term inflammation of ECs. **(A)** Under physiological conditions, RNase1 expression might be facilitated through MAPK signaling, *RNASE1* promoter H4ac and H3K27ac along with polymerase II transcription machinery binding. RNase1 protein and other proinflammatory/prothrombotic agents are stored in WPBs that are generated at the ER-Golgi network and located at the cell membrane. **(B)** Upon short-term inflammation, ECs get activated resulting in eRNA release to induce the immune response. eRNA initiates exocytosis of WPBs, releasing their content, including RNase1, into the extracellular space. RNase1 acts as counterpart to eRNA by degradation to protect the cells from detrimental eRNA-mediated effects. **(C)** Upon long-term inflammation, eRNA accumulates in the extracellular space, recruiting inflammatory cells (e.g., monocytes, macrophages) that secrete high amounts of proinflammatory agents like TNF-α or IL-1β. These cytokines act on RNase1 expression presumably via activation MAPK signaling and CK2-mediated signaling, mounting HDAC2 binding to so far unknown co-repressor complex(es), accumulation at the *RNASE1* promoter, H4 and H3K27 deacetylation and subsequent gene repression. CK2: casein kinase two, EC: endothelial cell, ER: endoplasmatic reticulum, eRNA: extracellular RNA, HDAC2: histone deacetylase 2, H4ac: histone four acetylation, H3K27ac: histone three lysine 27 acetylation, IL-1β: interleukin 1 beta, MAPK: mitogen-activated protein kinase, RNase1: Ribonuclease 1, TNF-α: tumor necrosis factor alpha, WPBs: Weibel-Palade Bodies. Gray writing depicts presumably involved molecules. This figure was created with the help of smart Servier Medical Art https://smart.servier.com/.

in this context (Sengupta and Seto, 2004; Yang and Seto, 2008; Bedenbender et al., 2019). In respect to the underlying signaling cascade, only little is known from literature. It was demonstrated that Nuclear factor kappa B-mediated signaling did not directly influence RNase1 expression upon proinflammatory stimulation (Gansler et al., 2014). However, it is worth to mention that the described proinflammatory agents have the potential to induce an inflammatory loop of cytokine production via Nuclear

factor kappa B signaling (Wajant and Scheurich, 2011), which in turn might increase the negative impact of proinflammatory conditions on RNase1. Nevertheless, several intermediate steps in the RNase1 regulatory signaling cascade in human ECs can be speculated: RNase1 regulation in HUVEC was identified as a specific proinflammatory reaction mediated via e.g., TNF-α, IL-1β or polyinosinic polycytidylic acid (poly I:C) signaling (Gansler et al., 2014; Bedenbender et al., 2019). These results assume a regulatory mechanism by common signaling cascade(s) that is independent from Nuclear factor kappa B. Here, TNF-α, IL-1β, or poly I:C are described as potent regulators of the inflammatory response via activation of the mitogen activated protein kinase pathways, for instance via c-Jun N-terminal kinase or p38 (Kawai and Akira, 2006; Weber et al., 2010; Brenner et al., 2015). These findings support the hypothesis of a mitogen activated protein kinase-dependent RNase1 regulation in human ECs. Despite the signaling cascade, it is still unclear how HDAC2 is recruited to the *RNASE1* promoter to conduct its deacetylase function. Based on the literature HDAC2 activity might be regulated by casein kinase two via phosphorylation (Tsai and Seto, 2002; Litchfield, 2003; Brandl et al., 2009; Segre and Chiocca, 2011). This further supports HDAC2 association into multiprotein co-repressor complexes (e.g., REST co-repressor complex, SIN3 complex and Nucleosome Remodeling and Deacetylase complex) and recruitment to the *RNASE1* promoter (Zhang et al., 1997; Tong et al., 1998; You et al., 2001; Sengupta and Seto, 2004; Sun et al., 2007; Yang and Seto, 2008). An overview of the current knowledge of RNase1 regulation, also including potential intermediate steps, in EC inflammation is depicted in **Figure 1**.

Other RNase1 Regulating Factors

Although the current literature mainly focuses on proinflammatory agents like TNF-α or IL-1β, it is worth mentioned that also other stimuli were investigated in respect to RNase1 regulation. The aforementioned proinflammatory stimuli as well as the double-stranded RNA analog poly I:C or prothrombotic factors like eRNA, thrombin or vasopressin, initiated RNase1 release from WPBs upon short term stimulation (Fischer et al., 2011; Gansler et al., 2014). However, upon long-term treatment, thrombin as well as a ligand for the endosomal Toll-like receptor-3, poly I:C, significantly mediated RNase1 repression in HUVEC, like TNF-α or IL-1β (Akira and Takeda, 2004; Gansler et al., 2014; Bedenbender et al., 2019). Compared to that, other proinflammatory agents like the Toll-like receptor-4 ligand lipopolysaccharide or IL-13 failed to do so, indicating a specific proinflammatory regulation of endothelial RNase1 upon certain treatments (Akira and Takeda, 2004; Bedenbender et al., 2019). Additionally, there is also indication that treatment of HUVEC with interferon gamma comprises the ability to promote RNase1 expression (Bedenbender et al., 2019). Based on these findings, it will be of future interest to not only investigate RNase1 repressive mechanisms but also RNase1 promoting factors that might offer potential new strategies to promote RNase1 restoration during resolution phase of inflammation and protect vascular integrity upon inflammation.

PROTECTIVE RNASE1 FUNCTION IN DISEASES

RNase1 Function in Cardiovascular Pathologies

In recent years, researchers provided strong evidence that imbalance of the RNase1-eRNA system and accumulation of nucleic acids species like eRNA contribute to development and progression of several vascular pathologies such as atherosclerosis or thrombosis. Thereby, eRNA acts not only as inducer of defense reactions by functioning as novel danger signal, but also acts as potent cofactor in context of vascular inflammation, finally counteracting RNase1 function and therewith misbalancing the RNase1-eRNA system (Zernecke and Preissner, 2016). In this context, previous studies demonstrated a protective role of RNase1 in diverse vascular as well as inflammatory disorders, focusing on the means of RNase1 administration as new therapeutic strategy to prevent disease progression.

Atherosclerosis and Thrombosis

Atherosclerosis is characterized by the formation of fibrous, fatty plaques in vascular walls, resulting in limited blood flow and tissue ischemia. These atherosclerotic lesions can further disrupt to provoke thrombus formation (Libby et al., 2019). Healthy ECs contribute to the regulation of coagulation and thrombus formation to maintain vascular homeostasis by secretion of both pro- and antithrombotic factors (Bochenek and Schafer, 2019). However, prolonged vessel injury and inflammation result in EC dysfunction, causing a pathological outcome of this process by complete vessel occlusion and development of consequential pathologies like myocardial infarction (MI) or stroke (Bochenek and Schafer, 2019; Libby et al., 2019). In this context, eRNA was identified to be enriched at sites of vascular injury, acting as a prothrombotic and proinflammatory factor (Zernecke and Preissner, 2016). Here, eRNA acts as a cofactor for contact phase proteins to induce the intrinsic blood coagulation cascade via factor XII/XI and promotes thrombus formation (Kannemeier et al., 2007; Fischer and Preissner, 2013). Therefore, several studies investigated the vessel protective function of RNase1 administration as a new potential therapeutic option to prevent plaque formation and vessel occlusion. Simsekyilmaz and colleagues described the accumulation of eRNA and proinflammatory mediators in atherosclerotic lesions or plasma of low-density lipoprotein receptor or Apolipoprotein E deficient mice that promote disease progression and reduction of RNase1 activity. Interestingly, administration of RNase1 decreased eRNA levels, inflammatory cell recruitment, proinflammatory mediators, and plaque formation in these animals (Simsekyilmaz et al., 2014). Additionally, prothrombotic eRNA was also associated to fibrin-rich thrombi in an arterial thrombosis mouse model and pretreatment of mice with RNase1 considerably reduced eRNA containing thrombi and delayed vessel occlusion (Kannemeier et al., 2007). These findings are in line with the phenotype of recently described RNase1 deficient mice that showed increased eRNA plasma levels and more rapid blood

clotting, indicating a crucial role for RNase1 in regulation of blood coagulation (Garnett et al., 2019).

Myocardial Infarction and I/R Injury

As consequential disorders of atherosclerosis and thrombosis, MI and ischemia/reperfusion (I/R) injury are of great importance. In MI, damaged cardiac tissue was shown to release proinflammatory and prothrombotic mediators, like TNF-α or eRNA, contributing to I/R injury (Cabrera-Fuentes et al., 2014; Chen et al., 2014). Several *in vivo* models implicated an important function of RNase1 administration in prevention and severity reduction of MI and I/R injury. Increased release of eRNA from injured cardiomyocytes was associated to a robust cytokine response in coronary artery occlusion mouse models followed by I/R. Here, eRNA levels, myocardial cytokines, leukocyte infiltration and myocyte apoptosis were diminished upon RNase1 administration, resulting in cardiac protection (Chen et al., 2014). Moreover, similar results were obtained in mice or isolated I/R Langendorff-perfused rat heart models. eRNA and TNF-α-induced cardiomyocyte death was prevented by RNase1 administration, resulting in reduced MI size and recovery of cardiac tissue (Cabrera-Fuentes et al., 2014). Additionally, RNase1 application also reduced eRNA-mediated myocardial edema formation, infarction size, improved artery perfusion, and conclusively increased survival rates of tested animals (Stieger et al., 2017). Finally, these findings have been utilized to study the RNase1-eRNA system in context of cardiac remote ischemic preconditioning in humans to prevent acute I/R injury during cardiac surgery. These findings revealed that remote ischemic preconditioning prior to surgery increased endogenous plasma RNase1 levels to reduce circulating eRNA and TNF-α and improve surgery outcome (Cabrera-Fuentes et al., 2015).

Hepatic Ischemia

Besides the heart, also other organs can be affected by thrombosis and I/R injury, e.g., the liver (Ma et al., 2017). In a mouse model of hepatic ischemia reperfusion, Ma and colleagues revealed increased serum and hippocampus proinflammatory cytokines (e.g., IL-1β, IL-6) and eRNA levels, along with cognitive impairment of treated animals in a liver ischemia reperfusion model. Interestingly, also these processes were markedly decreased by RNase1 administration (Ma et al., 2017).

Cerebral Edema and Stroke

Additionally, thrombus formation often results in progression of cerebral edema and stroke. In this context, different RNA species e.g., eRNA, poly I:C or single-stranded RNA, have been found to be associated to impaired blood-brain-barrier function (Fischer et al., 2007; Walberer et al., 2009). *In vivo* rodent animal models of sinus saggitalis thrombosis or middle cerebral artery occlusion to induce stroke and edema formation revealed that RNase1 administration considerably diminished vessel occlusion, infarct size, and edema formation (Fischer et al., 2007; Walberer et al., 2009).

RNase1 Function in Infectious and Inflammatory Disorders

Although studies addressing RNase1-eRNA related pathologies mainly focused on vascular diseases, there is also indication for an important function of RNase1 in several other disorders. For instance, RNase1 participated in recruitment of immune cells, in particular dendritic cells (Yang et al., 2004). These findings also suggested an important role for RNase1 in context of inflammatory or infectious diseases, thereby expanding the vessel-protective function of RNase1 beyond classical cardiovascular disorders.

Infectious Diseases

Human RNases are tightly associated to infectious diseases as already described for several members of the RNase A superfamily, e.g., the antiviral RNase2 (Koczera et al., 2016; Lu et al., 2018). Although less is known in this field about RNase1, there are a few publications addressing the function of RNase1 on different pathogens. In this context Bedoya as well as Rugeles and colleagues revealed an HIV inhibitory effect of RNase1 in infected lymphocytes (Rugeles et al., 2003; Bedoya et al., 2006). Additionally, the induction of RNase1 by interferon gamma (Bedenbender et al., 2019) also points toward a potential antiviral function of this enzyme that might be comparable to another RNase A superfamily member, RNaseL (also known as RNase4), that acts as an essential component of the interferon-mediated antiviral immune response (Li et al., 1998; Liang et al., 2006). Moreover, RNase1 was demonstrated to be involved in fighting *Streptococcus pneumoniae* infection of alveolar epithelial cells. Here, eRNA increased *S. pneumoniae* invasion of alveolar epithelial cells through its bacterial cell wall binding properties, while RNase1 treatment prevented this eRNA-pneumococcal interaction and subsequent infection (Zakrzewicz et al., 2016). Finally, RNase1expression was suppressed in context of other bacterial infections like *Francisella tularensis* or *Mycobacterium tuberculosis*, indicating RNase1 administration as potential therapeutic option to fight such pathogens (Lu et al., 2018). Thus, it can be speculated that RNase1 administration might be beneficial in diverse infectious contexts and should be in focus of future investigations.

Sepsis

Sepsis can induce dangerous organ dysfunctions and tissue injury that is associated with high levels of damage-associated molecular patterns, such as diverse types of eRNA that signal via pattern-recognition receptors, as well as severe dysregulation of cytokine production ("cytokine storm"), including TNF-α (Bianchi, 2007; Chan et al., 2012; Zechendorf et al., 2020). In context of septic cardiomyopathy, RNase1-counteracting molecules like eRNA were demonstrated to be significantly increased during sepsis and associated to cardiomyocyte apoptosis. Recent findings demonstrated that administration of RNase1 to septic mice considerably attenuated cardiac apoptosis, cytokine secretion and finally cardiomyopathy (Zechendorf et al., 2020).

Rheumatoid Arthritis

Chronic inflammatory rheumatoid arthritis (RA) is associated with chronic inflammation, synovial hyperplasia, and local hypoxia, resulting in synovial cell activation and massive tissue damage (Neumann et al., 2018). Within this context, activated RA synovial fibroblasts secreted high amounts of proinflammatory agents as well as eRNA, which was associated to RA fibroblast invasion into cartilage and tissue destruction (Zimmermann-Geller et al., 2016; Neumann et al., 2018). In an *in vivo* RA mouse model system, RNase1 application successfully prevented synovial fibroblast invasion, indicating that the RNase1-eRNA system contributes to RA pathophysiology (Zimmermann-Geller et al., 2016).

Cancer

The function of Ribonucleases as potential cancer therapy is already widely studied, due to their RNA-degrading ability and the associated potential to block protein biosynthesis, as well as the release of circulating eRNA species by tumor cells (Kopreski et al., 2001; Ardelt et al., 2009). Since, RNases are subsequently bound by RNase inhibitor upon entering the cytoplasm to prevent cytotoxicity, ongoing research focuses on development of artificial RNase variants to target cancer cells as chemotherapeutic options by increasing their cytotoxic potential (Lomax et al., 2017). Thereby, artificial RNase1 variants were designed that evade cytosolic RNase inhibitor binding to evoke cytotoxic effects (Psarras et al., 1998; Yagi et al., 2006). For instance, genetic insertion of human basic fibroblast growth factor into the RNase inhibitor binding site of RNase1 resulted in *in vivo* growth inhibition of squamous cell carcinoma in mice (Yagi et al., 2006). Additionally, previous research by Fischer and colleagues indicated a substantial role of eRNA in tumor cell migration through human cerebral microvascular ECs, including TNF-α secretion from tumor-infiltrating immune cells. Here, tumor volume and weight can be diminished by RNase1 treatment in a human subcutaneous xenograft cancer model (Fischer et al., 2013). These findings further demonstrate the potential of RNase1 as anti-cancer treatment. Besides the described ability to act as an anti-cancer drug, RNase1 is also suggested to operate as a tumor marker for pancreatic cancer, since tumor cells and cancer-associated ECs secreted a differently glycosylated form of RNase1 compared to healthy cells (Peracaula et al., 2003; Barrabes et al., 2007).

TARGETING RNASE1 REPRESSION AS NOVEL THERAPEUTIC STRATEGY IN DISEASES

Endothelial RNase1 was demonstrated as promising target for the development of novel treatment strategies in context of diverse pathologies, ranging from cardiovascular diseases over inflammatory and infectious pathologies to cancer. The current literature already describes several approaches that clearly define the protective function of RNase1 administration in different *in vitro* and *in vivo* models, also including at least one clinical approach in humans. However, these studies mainly focus on recovering RNase1 levels by enzyme addition instead of targeting the responsible repressive signaling cascades and molecules. Recent work revealed many aspects of the RNase1 repressive signaling pathway that is initiated by eRNA and high proinflammatory cytokine levels, like TNF-α or IL-1β. Unraveling these signaling pathways provides several potential access points for therapy. These targets might include mitogen-activated protein kinases like p38, casein kinase two, as well as HDAC2 and responsible co-repressor complex(es), which directly bind the *RNASE1* promoter to repress gene expression by chromatin remodeling. In this regard, several studies already focused on the usage of distinct pharmaceutical substances to block the function of these molecules in diverse pathologies. For instance, mitogen-activated protein kinase p38 as well as casein kinase two inhibitors have been applied in studies analyzing atherosclerosis, MI and I/R injury, or stroke (Barone et al., 2001; Zhao et al., 2002; Kaiser et al., 2004, 2005; Harvey et al., 2007), and both are used in clinical trials for diverse cancers and inflammatory disorders, e.g., RA (Kumar et al., 2003; Lee and Dominguez, 2005; Buontempo et al., 2018). Additionally, universal as well as specific HDAC inhibitors are already under clinical investigation or used for cancer therapy, by directly targeting the chromatin remodeling function of these enzymes (Yoon and Eom, 2016). Moreover, HDAC inhibitors were also described to be beneficial in context of cardiovascular diseases, like atherosclerosis or MI (Mann et al., 2007; Granger et al., 2008; Findeisen et al., 2011; Yoon and Eom, 2016). Based on these findings, further investigation of alternative strategies to prevent RNase1 repression is of great importance. Additionally, future investigations to develop novel therapeutic approaches should also include the analysis of physiological and RNase1 promoting signaling cascades and factors, such as interferon γ, to further expand and improve novel therapeutic options to preserve the vessel protective function of RNase1 in context of vascular inflammation.

CLOSING REMARKS AND FUTURE PERSPECTIVES

Endothelial RNase1 acts as potent vessel protective factor in context of vascular inflammation by counteracting damage-associated eRNA that is released upon vascular injury. However, long-term inflammation represses RNase1 expression and function by a mechanism where eRNA and high pro-inflammatory cytokine levels induce a molecular signaling cascade presumably via mitogen-activated protein kinase(s), casein kinase two and HDAC2-containing co-repressor complex(es) that finally ends up in histone deacetylation and transcriptional repression of RNase1. Although a large part of the RNase1 repressive signaling cascade as well as RNase1 structure and function have already been described extensively, several aspects remain unknown. Thus, it is of great importance to further define the molecular mechanism of RNase1 regulation (e.g., involved signaling pathways, HDAC2 activation, co-repressor complex(es), transcription factors, or RNase1 promoting factors), the precise

function of RNase1 glycosylation (e.g., in respect to vessel protection or infectious diseases), the uptake of RNase1 by neighboring cells via endocytosis, and also include the opportunity to use RNase1 knockout mice in prospective studies. Consequently, these future perspectives in concert with the current knowledge about RNase1 might improve and expand the development of potential therapeutic options to preserve RNase1 function and vascular integrity in context of pathologic EC inflammation.

AUTHOR CONTRIBUTIONS

KB designed the review, summarized current literature and progress, wrote the manuscript, and created the figure. BS provided constructive advice and scientific input. Both authors contributed to revision and finalization of the manuscript.

FUNDING

This work was supported by the Von-Behring Röntgen-Stiftung (61-0040 and 62-0002, Marburg, Germany) and ERACoSySMed SySMed-COPD (031L0140, Berlin, Germany) to BS.

ACKNOWLEDGMENTS

We thank all lab members of the Institute for Lung Research for support and discussion.

REFERENCES

Akira, S., and Takeda, K. (2004). Toll-like receptor signalling. *Nat. Rev. Immunol.* 4, 499–511.

Ardelt, W., Ardelt, B., and Darzynkiewicz, Z. (2009). Ribonucleases as potential modalities in anticancer therapy. *Eur. J. Pharmacol.* 625, 181–189. doi: 10.1016/j.ejphar.2009.06.067

Arnout, J., Hoylaerts, M. F., and Lijnen, H. R. (2006). "Haemostasis," in *The Vascular Endothelium II. Handbook of Experimental Pharmacology*, Vol. 176/II, eds S. Moncada and A. Higgs (Berlin: Springer), 1–41.

Baldwin, A. L., and Thurston, G. (2001). Mechanics of endothelial cell architecture and vascular permeability. *Crit. Rev. Biomed. Eng.* 29, 247–278. doi: 10.1615/critrevbiomedeng.v29.i2.20

Barone, F. C., Irving, E. A., Ray, A. M., Lee, J. C., Kassis, S., Kumar, S., et al. (2001). Inhibition of p38 mitogen-activated protein kinase provides neuroprotection in cerebral focal ischemia. *Med. Res. Rev.* 21, 129–145. doi: 10.1002/1098-1128(200103)21:2<129::aid-med1003>3.0.co;2-h

Barrabes, S., Pages-Pons, L., Radcliffe, C. M., Tabares, G., Fort, E., Royle, L., et al. (2007). Glycosylation of serum ribonuclease 1 indicates a major endothelial origin and reveals an increase in core fucosylation in pancreatic cancer. *Glycobiology* 17, 388–400. doi: 10.1093/glycob/cwm002

Bedenbender, K., Scheller, N., Fischer, S., Leiting, S., Preissner, K. T., Schmeck, B. T., et al. (2019). Inflammation-mediated deacetylation of the ribonuclease 1 promoter via histone deacetylase 2 in endothelial cells. *FASEB J.* 33, 9017–9029. doi: 10.1096/fj.201900451r

Bedoya, V. I., Boasso, A., Hardy, A. W., Rybak, S., Shearer, G. M., and Rugeles, M. T. (2006). Ribonucleases in HIV type 1 inhibition: effect of recombinant RNases on infection of primary T cells and immune activation-induced RNase gene and protein expression. *AIDS Res. Hum. Retrovirus.* 22, 897–907. doi: 10.1089/aid.2006.22.897

Beintema, J. J., Blank, A., Schieven, G. L., Dekker, C. A., Sorrentino, S., and Libonati, M. (1988). Differences in glycosylation pattern of human secretory ribonucleases. *Biochem. J.* 255, 501–505.

Bianchi, M. E. (2007). DAMPs, PAMPs and alarmins: all we need to know about danger. *J. Leukoc. Biol.* 81, 1–5. doi: 10.1189/jlb.0306164

Bochenek, M. L., and Schafer, K. (2019). Role of endothelial cells in acute and chronic thrombosis. *Hamostaseologie* 39, 128–139. doi: 10.1055/s-0038-1675614

Brandl, A., Heinzel, T., and Kramer, O. H. (2009). Histone deacetylases: salesmen and customers in the post-translational modification market. *Biol. Cell* 101, 193–205. doi: 10.1042/bc20080158

Brenner, D., Blaser, H., and Mak, T. W. (2015). Regulation of tumour necrosis factor signalling: live or let die. *Nat. Rev. Immunol.* 15, 362–374. doi: 10.1038/nri3834

Buontempo, F., Mccubrey, J. A., Orsini, E., Ruzzene, M., Cappellini, A., Lonetti, A., et al. (2018). Therapeutic targeting of CK2 in acute and chronic leukemias. *Leukemia* 32, 1–10. doi: 10.1038/leu.2017.301

Cabrera-Fuentes, H. A., Niemann, B., Grieshaber, P., Wollbrueck, M., Gehron, J., Preissner, K. T., et al. (2015). RNase1 as a potential mediator of remote ischaemic preconditioning for cardioprotectiondagger. *Eur. J. Cardiothorac. Surg.* 48, 732–737. doi: 10.1093/ejcts/ezu519

Cabrera-Fuentes, H. A., Ruiz-Meana, M., Simsekyilmaz, S., Kostin, S., Inserte, J., Saffarzadeh, M., et al. (2014). RNase1 prevents the damaging interplay between extracellular RNA and tumour necrosis factor-alpha in cardiac ischaemia/reperfusion injury. *Thromb. Haemost.* 112, 1110–1119. doi: 10.1160/th14-08-0703

Chan, J. K., Roth, J., Oppenheim, J. J., Tracey, K. J., Vogl, T., Feldmann, M., et al. (2012). Alarmins: awaiting a clinical response. *J. Clin. Invest.* 122, 2711–2719. doi: 10.1172/jci62423

Chao, T. Y., and Raines, R. T. (2011). Mechanism of ribonuclease A endocytosis: analogies to cell-penetrating peptides. *Biochemistry* 50, 8374–8382. doi: 10.1021/bi2009079

Chen, C., Feng, Y., Zou, L., Wang, L., Chen, H. H., Cai, J. Y., et al. (2014). Role of extracellular RNA and TLR3-Trif signaling in myocardial ischemia-reperfusion injury. *J. Am. Heart Assoc.* 3:e000683.

De Caterina, R., Libby, P., Peng, H. B., Thannickal, V. J., Rajavashisth, T. B., Gimbrone, M. A. Jr., et al. (1995). Nitric oxide decreases cytokine-induced endothelial activation. Nitric oxide selectively reduces endothelial expression of adhesion molecules and proinflammatory cytokines. *J. Clin. Invest.* 96, 60–68. doi: 10.1172/jci118074

Dickson, K. A., Haigis, M. C., and Raines, R. T. (2005). Ribonuclease inhibitor: structure and function. *Prog. Nucleic Acid Res. Mol. Biol.* 80, 349–374.

Fett, J. W., Strydom, D. J., Lobb, R. R., Alderman, E. M., Bethune, J. L., Riordan, J. F., et al. (1985). Isolation and characterization of angiogenin, an angiogenic protein from human carcinoma-cells. *Biochemistry* 24, 5480–5486. doi: 10.1021/bi00341a030

Findeisen, H. M., Gizard, F., Zhao, Y., Qing, H., Heywood, E. B., Jones, K. L., et al. (2011). Epigenetic regulation of vascular smooth muscle cell proliferation and neointima formation by histone deacetylase inhibition. *Arterioscler. Thromb. Vasc. Biol.* 31, 851–860. doi: 10.1161/atvbaha.110.221952

Fischer, S., Cabrera-Fuentes, H. A., Noll, T., and Preissner, K. T. (2014). Impact of extracellular RNA on endothelial barrier function. *Cell Tissue Res.* 355, 635–645. doi: 10.1007/s00441-014-1850-8

Fischer, S., Gerriets, T., Wessels, C., Walberer, M., Kostin, S., Stolz, E., et al. (2007). Extracellular RNA mediates endothelial-cell permeability via vascular endothelial growth factor. *Blood* 110, 2457–2465. doi: 10.1182/blood-2006-08-040691

Fischer, S., Gesierich, S., Griemert, B., Schanzer, A., Acker, T., Augustin, H. G., et al. (2013). Extracellular RNA liberates tumor necrosis factor-alpha to promote tumor cell trafficking and progression. *Cancer Res.* 73, 5080–5089. doi: 10.1158/0008-5472.can-12-4657

Fischer, S., Nishio, M., Dadkhahi, S., Gansler, J., Saffarzadeh, M., Shibamiyama, A., et al. (2011). Expression and localisation of vascular ribonucleases in

endothelial cells. *Thromb. Haemost.* 105, 345–355. doi: 10.1160/th10-06-0345

Fischer, S., Nishio, M., Peters, S. C., Tschernatsch, M., Walberer, M., Weidemann, S., et al. (2009). Signaling mechanism of extracellular RNA in endothelial cells. *FASEB J.* 23, 2100–2109. doi: 10.1096/fj.08-121608

Fischer, S., and Preissner, K. T. (2013). Extracellular nucleic acids as novel alarm signals in the vascular system mediators of defence and disease. *Hamostaseologie* 33, 37–42. doi: 10.5482/hamo-13-01-0001

Futami, J., Tsushima, Y., Murato, Y., Tada, H., Sasaki, J., Seno, M., et al. (1997). Tissue-specific expression of pancreatic-type RNases and RNase inhibitor in humans. *DNA Cell Biol.* 16, 413–419. doi: 10.1089/dna.1997.16.413

Gansler, J., Preissner, K. T., and Fischer, S. (2014). Influence of proinflammatory stimuli on the expression of vascular ribonuclease 1 in endothelial cells. *FASEB J.* 28, 752–760. doi: 10.1096/fj.13-238600

Garnett, E. R., Lomax, J. E., Mohammed, B. M., Gailani, D., Sheehan, J. P., and Raines, R. T. (2019). Phenotype of ribonuclease 1 deficiency in mice. *RNA* 25, 921–934. doi: 10.1261/rna.070433.119

Granger, A., Abdullah, I., Huebner, F., Stout, A., Wang, T., Huebner, T., et al. (2008). Histone deacetylase inhibition reduces myocardial ischemia-reperfusion injury in mice. *FASEB J.* 22, 3549–3560. doi: 10.1096/fj.08-108548

Harvey, E. J., Li, N., and Ramji, D. P. (2007). Critical role for casein kinase 2 and phosphoinositide-3-kinase in the interferon-gamma-induced expression of monocyte chemoattractant protein-1 and other key genes implicated in atherosclerosis. *Arterioscler. Thromb. Vasc. Biol.* 27, 806–812. doi: 10.1161/01.atv.0000258867.79411.96

Hooper, L. V., Stappenbeck, T. S., Hong, C. V., and Gordon, J. I. (2003). Angiogenins: a new class of microbicidal proteins involved in innate immunity. *Nat. Immunol.* 4, 269–273. doi: 10.1038/ni888

Huang, Y. C., Lin, Y. M., Chang, T. W., Wu, S. J., Lee, Y. S., Chang, M. D. T., et al. (2007). The flexible and clustered lysine residues of human ribonuclease 7 are critical for membrane permeability and antimicrobial activity. *J. Biol. Chem.* 282, 4626–4633. doi: 10.1074/jbc.m607321200

Johnson, R. J., Mccoy, J. G., Bingman, C. A., Phillips, G. N. Jr., and Raines, R. T. (2007). Inhibition of human pancreatic ribonuclease by the human ribonuclease inhibitor protein. *J. Mol. Biol.* 368, 434–449. doi: 10.1016/j.jmb.2007.02.005

Kaiser, R. A., Bueno, O. F., Lips, D. J., Doevendans, P. A., Jones, F., Kimball, T. F., et al. (2004). Targeted inhibition of p38 mitogen-activated protein kinase antagonizes cardiac injury and cell death following ischemia-reperfusion in vivo. *J. Biol. Chem.* 279, 15524–15530. doi: 10.1074/jbc.m313717200

Kaiser, R. A., Lyons, J. M., Duffy, J. Y., Wagner, C. J., Mclean, K. M., O'neill, T. P., et al. (2005). Inhibition of p38 reduces myocardial infarction injury in the mouse but not pig after ischemia-reperfusion. *Am. J. Physiol. Heart Circ. Physiol.* 289, H2747–H2751.

Kannemeier, C., Shibamiya, A., Nakazawa, F., Trusheim, H., Ruppert, C., Markart, P., et al. (2007). Extracellular RNA constitutes a natural procoagulant cofactor in blood coagulation. *Proc. Natl. Acad. Sci. U.S.A.* 104, 6388–6393. doi: 10.1073/pnas.0608647104

Kawai, T., and Akira, S. (2006). TLR signaling. *Cell Death. Differ.* 13, 816–825.

Klink, T. A., Woycechowsky, K. J., Taylor, K. M., and Raines, R. T. (2000). Contribution of disulfide bonds to the conformational stability and catalytic activity of ribonuclease A. *Eur. J. Biochem.* 267, 566–572. doi: 10.1046/j.1432-1327.2000.01037.x

Koczera, P., Martin, L., Marx, G., and Schuerholz, T. (2016). The ribonuclease A superfamily in humans: canonical RNases as the buttress of innate immunity. *Int. J. Mol. Sci.* 17:1278. doi: 10.3390/ijms17081278

Kopreski, M. S., Benko, F. A., and Gocke, C. D. (2001). Circulating RNA as a tumor marker - Detection of 5T4 mRNA in breast and lung cancer patient serum. *Circ. Nucleic Acids Plasma Serum Ii* 945, 172–178. doi: 10.1111/j.1749-6632.2001.tb03882.x

Kouzarides, T. (2007). Chromatin modifications and their function. *Cell* 128, 693–705. doi: 10.1016/j.cell.2007.02.005

Kumar, S., Boehm, J., and Lee, J. C. (2003). p38 map kinases: key signalling molecules as therapeutic targets for inflammatory diseases. *Nat. Rev. Drug Discov.* 2, 717–726. doi: 10.1038/nrd1177

Landre, J. B., Hewett, P. W., Olivot, J. M., Friedl, P., Ko, Y., Sachinidis, A., et al. (2002). Human endothelial cells selectively express large amounts of pancreatic-type ribonuclease (RNase 1). *J. Cell. Biochem.* 86, 540–552. doi: 10.1002/jcb.10234

Lee, F. S., and Vallee, B. L. (1989). Characterization of ribonucleolytic activity of angiogenin towards tRNA. *Biochem. Biophys. Res. Commun.* 161, 121–126. doi: 10.1016/0006-291x(89)91569-6

Lee, M. R., and Dominguez, C. (2005). MAP kinase p38 inhibitors: clinical results and an intimate look at their interactions with p38alpha protein. *Curr. Med. Chem.* 12, 2979–2994. doi: 10.2174/092986705774462914

Ley, K., and Reutershan, J. (2006). "Leucocyte-endothelial interactions in health and disease," in *The Vascular Endothelium II. Handbook of Experimental Pharmacology*, Vol. 176/II, eds S. Moncada and A. Higgs (Berlin: Springer), 97–133. doi: 10.1007/3-540-36028-x_4

Li, S. P., Sheng, J. H., Hu, J. K., Yu, W. H., Kishikawa, H., Hu, M. F. G., et al. (2013). Ribonuclease 4 protects neuron degeneration by promoting angiogenesis, neurogenesis, and neuronal survival under stress. *Angiogenesis* 16, 387–404. doi: 10.1007/s10456-012-9322-9

Li, X. L., Blackford, J. A., and Hassel, B. A. (1998). RNase L mediates the antiviral effect of interferon through a selective reduction in viral RNA during encephalomyocarditis virus infection. *J. Virol.* 72, 2752–2759. doi: 10.1128/jvi.72.4.2752-2759.1998

Liang, S. L., Quirk, D., and Zhou, A. M. (2006). RNase L: its biological roles and regulation. *IUBMB Life* 58, 508–514. doi: 10.1080/15216540600838232

Libby, P., Buring, J. E., Badimon, L., Hansson, G. K., Deanfield, J., Bittencourt, M. S., et al. (2019). Atherosclerosis. *Nat Rev Dis Prim.* 5:56.

Litchfield, D. W. (2003). Protein kinase CK2: structure, regulation and role in cellular decisions of life and death. *Biochem. J.* 369, 1–15. doi: 10.1042/bj20021469

Lomax, J. E., Eller, C. H., and Raines, R. T. (2017). Comparative functional analysis of ribonuclease 1 homologs: molecular insights into evolving vertebrate physiology. *Biochem. J.* 474, 2219–2233. doi: 10.1042/bcj20170173

Lu, K.-C., Zhang, Y., and Song, E. (2019). Extracellular RNA: mechanisms of it's transporting into target cells. *ExRNA* 1:22.

Lu, L., Li, J., Moussaoui, M., and Boix, E. (2018). Immune modulation by human secreted rnases at the extracellular space. *Front. Immunol.* 9:1012. doi: 10.3389/fimmu.2018.01012

Ma, G., Chen, C., Jiang, H. X., Qiu, Y. H., Li, Y. S., Li, X. Q., et al. (2017). Ribonuclease attenuates hepatic ischemia reperfusion induced cognitive impairment through the inhibition of inflammatory cytokines in aged mice. *Biomed. Pharmacother.* 90, 62–68. doi: 10.1016/j.biopha.2017.02.094

Mann, B. S., Johnson, J. R., Cohen, M. H., Justice, R., and Pazdur, R. (2007). FDA approval summary: vorinostat for treatment of advanced primary cutaneous T-cell lymphoma. *Oncologist* 12, 1247–1252. doi: 10.1634/theoncologist.12-10-1247

Marth, J. D., and Grewal, P. K. (2008). Mammalian glycosylation in immunity. *Nat. Rev. Immunol.* 8, 874–887. doi: 10.1038/nri2417

Michiels, C. (2003). Endothelial cell functions. *J. Cell. Physiol.* 196, 430–443.

Minshall, R. D., and Malik, A. B. (2006). Transport across the endothelium: regulation of endothelial permeability. *Handb. Exp. Pharmacol.* 176(176 Pt 1), 107–144. doi: 10.1007/3-540-32967-6_4

Morita, T., Niwata, Y., Ohgi, K., Ogawa, M., and Irie, M. (1986). Distribution of two urinary ribonuclease-like enzymes in human organs and body fluids. *J. Biochem.* 99, 17–25. doi: 10.1093/oxfordjournals.jbchem.a135456

Neumann, E., Hasseli, R., Lange, U., and Muller-Ladner, U. (2018). The role of extracellular nucleic acids in rheumatoid arthritis. *Curr. Pharm. Biotechnol.* 19, 1182–1188. doi: 10.2174/1389201020666190102150216

Peracaula, R., Royle, L., Tabares, G., Mallorqui-Fernandez, G., Barrabes, S., Harvey, D. J., et al. (2003). Glycosylation of human pancreatic ribonuclease: differences between normal and tumor states. *Glycobiology* 13, 227–244. doi: 10.1093/glycob/cwg019

Petrova, T. V., Makinen, T., Makela, T. P., Saarela, J., Virtanen, I., Ferrell, R. E., et al. (2002). Lymphatic endothelial reprogramming of vascular endothelial cells by the Prox-1 homeobox transcription factor. *EMBO J.* 21, 4593–4599. doi: 10.1093/emboj/cdf470

Pober, J. S., and Sessa, W. C. (2007). Evolving functions of endothelial cells in inflammation. *Nat. Rev. Immunol.* 7, 803–815. doi: 10.1038/nri2171

Poredos, P. (2002). Endothelial dysfunction and cardiovascular disease. *Pathophysiol. Haemost. Thromb.* 32, 274–277.

Psarras, K., Ueda, M., Yamamura, T., Ozawa, S., Kitajima, M., Aiso, S., et al. (1998). Human pancreatic RNase1-human epidermal growth factor fusion: an entirely

human 'immunotoxin analog' with cytotoxic properties against squamous cell carcinomas. *Protein Eng.* 11, 1285–1292. doi: 10.1093/protein/11.12.1285

Rajendran, P., Rengarajan, T., Thangavel, J., Nishigaki, Y., Sakthisekaran, D., Sethi, G., et al. (2013). The vascular endothelium and human diseases. *Int. J. Biol. Sci.* 9, 1057–1069.

Reily, C., Stewart, T. J., Renfrow, M. B., and Novak, J. (2019). Glycosylation in health and disease. *Nat. Rev. Nephrol.* 15, 346–366.

Ressler, V. T., and Raines, R. T. (2019). Consequences of the endogenous N-Glycosylation of human ribonuclease 1. *Biochemistry* 58, 987–996. doi: 10.1021/acs.biochem.8b01246

Ribo, M., Beintema, J. J., Osset, M., Fernandez, E., Bravo, J., De Llorens, R., et al. (1994). Heterogeneity in the glycosylation pattern of human pancreatic ribonuclease. *Biol. Chem. Hoppe Seyler.* 375, 357–363.

Rondaij, M. G., Bierings, R., Kragt, A., Van Mourik, J. A., and Voorberg, J. (2006). Dynamics and plasticity of Weibel-Palade bodies in endothelial cells. *Arterioscler. Thromb. Vasc. Biol.* 26, 1002–1007. doi: 10.1161/01.atv.0000209501.56852.6c

Rugeles, M. T., Trubey, C. A., Bedoya, V. I., Pinto, L. A., Oppenheim, J. J., Rybak, S. A., et al. (2003). Ribonuclease is partly responsible for the HIV-1 inhibitory effect activated by HLA alloantigen recognition. *Aids* 17, 481–486. doi: 10.1097/00002030-200303070-00002

Russo, N., Shapiro, R., Acharya, K. R., Riordan, J. F., and Vallee, B. L. (1994). Role of glutamine-117 in the ribonucleolytic activity of human angiogenin. *Proc. Natl. Acad. Sci. U.S.A.* 91, 2920–2924. doi: 10.1073/pnas.91.8.2920

Schillemans, M., Karampini, E., Kat, M., and Bierings, R. (2019). Exocytosis of Weibel-Palade bodies: how to unpack a vascular emergency kit. *J. Thromb. Haemost.* 17, 6–18. doi: 10.1111/jth.14322

Schwartz, L., Cohen, A., Thomas, J., and Spencer, J. D. (2018). The immunomodulatory and antimicrobial properties of the vertebrate ribonuclease A superfamily. *Vaccines* 6:76. doi: 10.3390/vaccines6040076

Segre, C. V., and Chiocca, S. (2011). Regulating the regulators: the post-translational code of class I HDAC1 and HDAC2. *J. Biomed. Biotechnol.* 2011:690848.

Sengupta, N., and Seto, E. (2004). Regulation of histone deacetylase activities. *J. Cell. Biochem.* 93, 57–67. doi: 10.1002/jcb.20179

Simsekyilmaz, S., Cabrera-Fuentes, H. A., Meiler, S., Kostin, S., Baumer, Y., Liehn, E. A., et al. (2014). Role of extracellular RNA in atherosclerotic plaque formation in mice. *Circulation* 129, 598–606. doi: 10.1161/circulationaha.113.002562

Sitia, S., Tomasoni, L., Atzeni, F., Ambrosio, G., Cordiano, C., Catapano, A., et al. (2010). From endothelial dysfunction to atherosclerosis. *Autoimmun. Rev.* 9, 830–834.

Sorrentino, S. (2010). The eight human "canonical" ribonucleases: molecular diversity, catalytic properties, and special biological actions of the enzyme proteins. *FEBS Lett.* 584, 2194–2200. doi: 10.1016/j.febslet.2010.04.018

Sorrentino, S., Naddeo, M., Russo, A., and D'alessio, G. (2003). Degradation of double-stranded RNA by human pancreatic ribonuclease: crucial role of noncatalytic basic amino acid residues. *Biochemistry* 42, 10182–10190. doi: 10.1021/bi030040q

Stieger, P., Daniel, J. M., Tholen, C., Dutzmann, J., Knopp, K., Gunduz, D., et al. (2017). Targeting of Extracellular RNA reduces edema formation and infarct size and improves survival after myocardial infarction in mice. *J. Am. Heart Assoc.* 6:e004541.

Su, A. I., Wiltshire, T., Batalov, S., Lapp, H., Ching, K. A., Block, D., et al. (2004). A gene atlas of the mouse and human protein-encoding transcriptomes. *Proc. Natl. Acad. Sci. U.S.A.* 101, 6062–6067. doi: 10.1073/pnas.0400782101

Sun, J. M., Chen, H. Y., and Davie, J. R. (2007). Differential distribution of unmodified and phosphorylated histone deacetylase 2 in chromatin. *J. Biol. Chem.* 282, 33227–33236. doi: 10.1074/jbc.m703549200

Tong, J. K., Hassig, C. A., Schnitzler, G. R., Kingston, R. E., and Schreiber, S. L. (1998). Chromatin deacetylation by an ATP-dependent nucleosome remodelling complex. *Nature* 395, 917–921. doi: 10.1038/27699

Tsai, S. C., and Seto, E. (2002). Regulation of histone deacetylase 2 by protein kinase CK2. *J. Biol. Chem.* 277, 31826–31833. doi: 10.1074/jbc.m204149200

Valentijn, K. M., Sadler, J. E., Valentijn, J. A., Voorberg, J., and Eikenboom, J. (2011). Functional architecture of Weibel-palade bodies. *Blood* 117, 5033–5043. doi: 10.1182/blood-2010-09-267492

Wajant, H., and Scheurich, P. (2011). TNFR1-induced activation of the classical NF-kappaB pathway. *FEBS J.* 278, 862–876. doi: 10.1111/j.1742-4658.2011.08015.x

Walberer, M., Tschernatsch, M., Fischer, S., Ritschel, N., Volk, K., Friedrich, C., et al. (2009). RNase therapy assessed by magnetic resonance imaging reduces cerebral edema and infarction size in acute stroke. *Curr. Neurovasc. Res.* 6, 12–19. doi: 10.2174/156720209787466037

Wang, Z., Zang, C., Rosenfeld, J. A., Schones, D. E., Barski, A., Cuddapah, S., et al. (2008). Combinatorial patterns of histone acetylations and methylations in the human genome. *Nat. Genet.* 40, 897–903. doi: 10.1038/ng.154

Weber, A., Wasiliew, P., and Kracht, M. (2010). Interleukin-1 (IL-1) pathway. *Sci. Signal.* 3:cm1. doi: 10.1126/scisignal.3105cm1

Weickmann, J. L., Olson, E. M., and Glitz, D. G. (1984). Immunological assay of pancreatic ribonuclease in serum as an indicator of pancreatic-cancer. *Cancer Res.* 44, 1682–1687.

Yagi, H., Ueda, M., Jinno, H., Aiura, K., Mikami, S., Tada, H., et al. (2006). Anti-tumor effect in an in vivo model by human-derived pancreatic RNase with basic fibroblast growth factor insertional fusion protein through antiangiogenic properties. *Cancer Sci.* 97, 1315–1320. doi: 10.1111/j.1349-7006.2006.00336.x

Yang, D., Chen, Q., Rosenberg, H. F., Rybak, S. M., Newton, D. L., Wang, Z. Y., et al. (2004). Human ribonuclease A superfamily members, eosinophil-derived neurotoxin and pancreatic ribonuclease, induce dendritic cell maturation and activation. *J. Immunol.* 173, 6134–6142. doi: 10.4049/jimmunol.173.10.6134

Yang, X. J., and Seto, E. (2008). The Rpd3/Hda1 family of lysine deacetylases: from bacteria and yeast to mice and men. *Nat. Rev. Mol. Cell Biol.* 9, 206–218. doi: 10.1038/nrm2346

Yoon, S., and Eom, G. H. (2016). HDAC and HDAC inhibitor: from cancer to cardiovascular diseases. *Chonnam. Med. J.* 52, 1–11. doi: 10.4068/cmj.2016.52.1.1

You, A., Tong, J. K., Grozinger, C. M., and Schreiber, S. L. (2001). CoREST is an integral component of the CoREST- human histone deacetylase complex. *Proc. Natl. Acad. Sci. U.S.A.* 98, 1454–1458. doi: 10.1073/pnas.98.4.1454

Zakrzewicz, D., Bergmann, S., Didiasova, M., Giaimo, B. D., Borggrefe, T., Mieth, M., et al. (2016). Host-derived extracellular RNA promotes adhesion of *Streptococcus pneumoniae* to endothelial and epithelial cells. *Sci. Rep.* 6:37758.

Zechendorf, E., O'riordan, C. E., Stiehler, L., Wischmeyer, N., Chiazza, F., Collotta, D., et al. (2020). Ribonuclease 1 attenuates septic cardiomyopathy and cardiac apoptosis in a murine model of polymicrobial sepsis. *JCI Insight* 5:e131571.

Zernecke, A., and Preissner, K. T. (2016). Extracellular ribonucleic acids (RNA) enter the stage in cardiovascular disease. *Circ. Res.* 118, 469–479. doi: 10.1161/circresaha.115.307961

Zhang, Y., Iratni, R., Erdjument-Bromage, H., Tempst, P., and Reinberg, D. (1997). Histone deacetylases and SAP18, a novel polypeptide, are components of a human Sin3 complex. *Cell* 89, 357–364. doi: 10.1016/s0092-8674(00)80216-0

Zhao, M., Liu, Y. W., Wang, X. F., New, L. G., Han, J. H., and Brunk, U. T. (2002). Activation of the p38 MAP kinase pathway is required for foam cell formation from macrophages exposed to oxidized LDL. *APMIS* 110, 458–468. doi: 10.1034/j.1600-0463.2002.100604.x

Zimmermann-Geller, B., Koppert, S., Fischer, S., Cabrera-Fuentes, H. A., Lefevre, S., Rickert, M., et al. (2016). Influence of Extracellular RNAs, released by rheumatoid arthritis synovial fibroblasts, on their adhesive and invasive properties. *J. Immunol.* 197, 2589–2597. doi: 10.4049/jimmunol.1501580

Conflict of Interest: The authors declare that the research was conducted in the absence of any commercial or financial relationships that could be construed as a potential conflict of interest.

frontiers in Cell and Developmental Biology

ORIGINAL RESEARCH
published: 15 October 2020
doi: 10.3389/fcell.2020.563604

p38 and Casein Kinase 2 Mediate Ribonuclease 1 Repression in Inflamed Human Endothelial Cells via Promoter Remodeling Through Nucleosome Remodeling and Deacetylase Complex

*Katrin Bedenbender[1], Isabell Beinborn[1], Evelyn Vollmeister[1] and Bernd Schmeck[1,2,3,4]**

[1] *Institute for Lung Research, Universities of Giessen and Marburg Lung Center, Philipps-University Marburg, Marburg, Germany,* [2] *Department of Pulmonary and Critical Care Medicine, Department of Medicine, University Medical Center Giessen and Marburg, Philipps-University Marburg, Marburg, Germany,* [3] *Member of the German Center for Lung Research, Member of the German Center for Infectious Disease Research, Marburg, Germany,* [4] *Center for Synthetic Microbiology, Philipps-University Marburg, Marburg, Germany*

OPEN ACCESS

Edited by:
Ritva Tikkanen, University of Giessen, Germany

Reviewed by:
Chunhua Song, Pennsylvania State University, United States
James Hagman, National Jewish Health, United States

***Correspondence:**
Bernd Schmeck
bernd.schmeck@uni-marburg.de

Specialty section:
This article was submitted to Molecular Medicine, a section of the journal Frontiers in Cell and Developmental Biology

Received: *19 May 2020*
Accepted: *28 September 2020*
Published: *15 October 2020*

Citation:
Bedenbender K, Beinborn I, Vollmeister E and Schmeck B (2020) p38 and Casein Kinase 2 Mediate Ribonuclease 1 Repression in Inflamed Human Endothelial Cells via Promoter Remodeling Through Nucleosome Remodeling and Deacetylase Complex. Front. Cell Dev. Biol. 8:563604. doi: 10.3389/fcell.2020.563604

Vascular pathologies, such as thrombosis or atherosclerosis, are leading causes of death worldwide and are strongly associated with the dysfunction of vascular endothelial cells. In this context, the extracellular endonuclease Ribonuclease 1 (RNase1) acts as an essential protective factor in regulation and maintenance of vascular homeostasis. However, long-term inflammation causes strong repression of RNase1 expression, thereby promoting endothelial cell dysfunction. This inflammation-mediated downregulation of RNase1 in human endothelial cells is facilitated via histone deacetylase (HDAC) 2, although the underlying molecular mechanisms are still unknown. Here, we report that inhibition of c-Jun N-terminal kinase by small chemical compounds in primary human endothelial cells decreased physiological RNase1 mRNA abundance, while p38 kinase inhibition restored repressed RNase1 expression upon proinflammatory stimulation with tumor necrosis factor alpha (TNF-α) and poly I:C. Moreover, blocking of the p38 kinase- and HDAC2-associated kinase casein kinase 2 (CK2) by inhibitor as well as small interfering RNA (siRNA)-knockdown restored RNase1 expression upon inflammation of human endothelial cells. Further downstream, siRNA-knockdown of chromodomain helicase DNA binding protein (CHD) 3 and 4 of the nucleosome remodeling and deacetylase (NuRD) complex restored RNase1 repression in TNF-α treated endothelial cells implicating its role in the HDAC2-containing repressor complex involved in RNase1 repression. Finally, chromatin immunoprecipitation in primary human endothelial cells confirmed recruitment of the CHD4-containing NuRD complex and subsequent promoter remodeling via histone deacetylation at the *RNASE1* promoter in a

p38-dependent manner upon human endothelial cell inflammation. Altogether, our results suggest that endothelial RNase1 repression in chronic vascular inflammation is regulated by a p38 kinase-, CK2-, and NuRD complex-dependent pathway resulting in complex recruitment to the *RNASE1* promoter and subsequent promoter remodeling.

Keywords: ribonuclease 1, endothelium, inflammation, p38 kinase, casein kinase 2, nucleosome remodeling and deacetylase complex, histone deacetylation, CHD4

INTRODUCTION

Endothelial cells (ECs) significantly participate in regulation and control of vascular homeostasis and are rapidly activated upon inflammation to support the immune system. Thereby, ECs promote the inflammatory response via interaction with circulating leukocytes that infiltrate into the underlying tissue to secrete high amounts of proinflammatory compounds (Pober and Sessa, 2007). Despite the necessity of these processes to ensure a sufficient immune response, prolonged inflammation may also destruct the homeostatic functions of the endothelium. This further promotes progression of vascular diseases, like thrombosis or atherosclerosis (Poredos, 2002; Sitia et al., 2010; Zernecke and Preissner, 2016). In context of vascular inflammation, the endothelial extracellular RNA (eRNA)–Ribonuclease 1 (RNase1) system is known as a major key player to induce the immune response and likewise protect the EC layer (Zernecke and Preissner, 2016). Upon acute inflammation, ECs release eRNA as danger signal to initiate the immune response at the site of vascular injury. Simultaneously, vessel-protective RNase1 is released by vascular ECs to protect the endothelium from an overwhelming inflammatory response via degradation of eRNA (Landre et al., 2002; Cabrera-Fuentes et al., 2014; Gansler et al., 2014). However, upon long-term inflammation, accumulating eRNA enhances immune cell recruitment to the vascular wall and secretion of proinflammatory cytokines like tumor necrosis factor (TNF)-α or interleukin (IL)-1β. These cytokines further act on the EC layer via recruitment of histone deacetylase (HDAC) 2 to the *RNASE1* promoter, resulting in massive RNase1 repression (Gansler et al., 2014; Bedenbender et al., 2019). Here, HDAC2 specifically reduces acetylation (ac) of the transcriptional activation markers histone 4 (H4) and histone 3 lysine 27 (H3K27) to induce chromatin remodeling and subsequent gene repression (Kouzarides, 2007; Wang et al., 2008; Bedenbender et al., 2019). However, the precise molecular mechanism by which HDAC2 is recruited to the *RNASE1* promoter in inflamed human ECs remains unknown. This study aims to investigate the underlying signaling cascade involved in RNase1 regulation via analysis of responsible signaling pathway(s), modulators of HDAC2 activity, and chromatin remodeling complexes upon EC inflammation.

Inflammation-mediated RNase1 repression is assumed to be a specific inflammatory reaction in human ECs, mediated via stimulation with the proinflammatory cytokines TNF-α and IL-1β, as well as the toll-like receptor 3 ligand polyinosinic polycytidylic acid (poly I:C) (Gansler et al., 2014; Bedenbender et al., 2019). Thus, RNase1 regulation by common signaling pathway(s) activated by the afore-mentioned stimuli is suggested. TNF-α, IL-1β, and poly I:C are potent regulators of gene expression, tightly associated to inflammation-mediated cellular responses. Thereby, they conduct their functions primarily via two distinct signaling cascades through nuclear factor kappa B (NF-κB) or mitogen-activated protein kinase (MAPK) signaling, such as c-Jun N-terminal kinase (JNK) or p38 MAPK (Kawai and Akira, 2006; Weber et al., 2010; Brenner et al., 2015). Gansler et al. (2014) already demonstrated an NF-κB-independent signaling mechanism for inflammation-mediated RNase1 repression, supporting the hypothesis of a MAPK-dependent RNase1 regulation.

Apart from signaling cascade(s), it is still unclear how HDAC2 is recruited to the *RNASE1* promoter. Enzymatic activity of class I HDACs, including HDAC2, is regulated through three different stages, subcellular localization, association with multiprotein complexes and post-translational modifications, e.g., serine phosphorylation (Segre and Chiocca, 2011). Especially, phosphorylation of HDAC2 is associated with its enzymatic activity and conducted by the highly conserved, constitutively active serine/threonine kinase casein kinase 2 (CK2) (Tsai and Seto, 2002; Litchfield, 2003; Brandl et al., 2009). Thereby, CK2 comprises the ability to regulate several hundred target proteins and is therewith involved in diverse cellular processes, including inflammation (Litchfield, 2003; Singh and Ramji, 2008). Additionally, CK2-mediated HDAC2 phosphorylation is also described to support its association with several multiprotein complexes (Segre and Chiocca, 2011). A prerequisite for sufficient enzymatic function and recruitment to the chromatin, as HDACs do not comprise any DNA-binding ability (Sengupta and Seto, 2004). The most abundant HDAC2-associated repressor complexes are the REST co-repressor (CoREST) complex, the SIN3 complex and the nucleosome remodeling and deacetylase (NuRD) complex, which in part also coexist together with CK2 (Zhang et al., 1997; Tong et al., 1998; You et al., 2001; Sengupta and Seto, 2004; Sun et al., 2007; Yang and Seto, 2008).

In this study, we investigated the underlying signaling cascade of inflammation-mediated RNase1 regulation in human

Abbreviations: Ac, acetylation; CK2, casein kinase 2; CHD, chromodomain helicase DNA binding protein; ChIP, chromatin immunoprecipitation; CoREST, REST co-repressor; COX-2, cyclo-oxygenase 2; CSNK2, casein kinase 2 subunit; CTRL, control; EC, endothelial cell; eRNA, extracellular RNA; H3K27, histone 3 lysine 27; H4, histone 4; HDAC, histone deacetylase; HUVEC, human umbilical vein endothelial cells; IL, interleukin; JNK, c-Jun N-terminal kinase; MAPK, mitogen-activated protein kinase; NF-κB, Nuclear factor kappa B; NuRD, nucleosome remodeling and deacetylase; poly I:C, polyinosinic polycytidylic acid; qPCR, quantitative PCR; qRT-PCR, quantitative reverse transcription PCR; RCOR1, REST co-repressor 1; RNase1, ribonuclease 1; SIN3, SIN3 transcription regulator family member; siRNA, small interfering RNA; TNF-α tumor necrosis factor alpha.

ECs: First, we addressed the impact of common signaling pathways involved in RNase1 regulation. Second, we investigated how HDAC2 can be regulated during EC inflammation, and third, which co-repressor complex is involved in chromatin remodeling of the *RNASE1* promoter. Our findings provide evidence that RNase1 expression is mediated via JNK signaling under physiological conditions, while its reduction during prolonged EC inflammation is regulated via p38 MAPK. We further provide evidence that the HDAC2-regulating kinase CK2, as well as the NuRD co-repressor complex acted as crucial regulators of inflammation-mediated RNase1 repression, on mRNA as well as chromatin level, respectively. Thereby, the NuRD complex component chromodomain helicase DNA binding protein (CHD) 4 accumulates at the *RNASE1* promoter along with reduction of H4ac and H3K27ac in a p38-dependent manner. These findings indicate a complex regulatory network involved in endothelial RNase1 regulation.

MATERIALS AND METHODS

Ethics Statement

All umbilical cords were donated from healthy individuals who were fully informed and consented to donation. Donated tissue was handled in accordance with the local ethics regulations of the Philipps-University Marburg (permit number: AZ 20/16).

Cell Culture

Cells used in this study were cultivated in a humidified incubator at 37°C with 5% CO_2. Human umbilical vein endothelial cells (HUVEC) were isolated and cultured in EC growth medium from PromoCell (Heidelberg, BW, Germany) supplemented with 1% penicillin and streptomycin (Thermo Fisher Scientific, Waltham, MA, United States) as described previously (Bedenbender et al., 2019) and cultured up to passage 4 for all indicated experiments. For stimulation experiments 3.8×10^4 cells/cm^2 were seeded overnight. Cells were stimulated with human recombinant TNF-α [10 ng/ml] (R&D Systems, Inc., Minneapolis, MN, United States) or poly I:C [10 μg/ml] (InvivoGen, San Diego, CA, United States) as indicated. For inhibitor assays, HUVEC were pretreated for 1 h with the NF-κB inhibitor BAY11-7082 [1 μM, 5 μM], the JNK inhibitor JNK inhibitor II [10 μM, 30 μM], the p38 inhibitor SB202190 [10 μM, 20 μM] (Merck KGaA, Sigma Aldrich, Darmstadt, HE, Germany) prior to indicated stimulation for 24 h. Dimethyl sulfoxide (DMSO) (Carl Roth GmbH & Co., KG, Karlsruhe, BW, Germany) was used as solvent control. For chromatin immunoprecipitation (ChIP) assays, HUVEC were stimulated with 10 ng/ml TNF-α (R&D Systems, Inc.) for 10 min. For p38 inhibitor ChIP assays, HUVEC were treated for 2 h with 20 μM p38 inhibitor SB202190 (Sigma Aldrich) or DMSO (Carl Roth GmbH & Co., KG) as solvent control prior to 10 ng/ml TNF-α treatment (R&D Systems, Inc.) for 10 min.

The hybrid EC line EA.hy926 (American Type Culture Collection (ATCC), Manassas, VA, United States) was cultured in Dulbecco's Modified Eagle's Medium with high glucose (DMEM) supplemented with 10% fetal calf serum (Gibco™, Thermo Fisher Scientific) for stimulation experiments. Cells were cultured up to passage 25 for all indicated experiments. Cells were seeded with 3.8×10^4 cells/cm^2 overnight followed by indicated treatments: For casein kinase 2 (CK2) inhibitor assays, EA.hy926 were pretreated for 30 min with 10 μM CK2 inhibitor TBB (4,5,6,7-Tetrabromobenzotriazole, Merck KGaA) or DMSO (Carl Roth GmbH & Co., KG) as solvent control prior to 24 h TNF-α [10 ng/ml] (R&D Systems, Inc.) or poly I:C [10 μg/ml] (InvivoGen) stimulation.

siRNA Knockdown

EA.hy926 (3.8×10^4 cells/cm^2) were seeded overnight and transfected for 24 h with ON-TARGETplus small interfering (si) RNA SMARTpools (Dharmacon™, Horizon Discovery Group Company, Lafayette, CO, United States) against CK2 alpha subunit 1 (CSNK2A1), CK2 alpha subunit 2 (CSNK2A2), CK2 beta subunit (CSNK2B), REST co-repressor 1 (RCOR1), SIN3 transcription regulator family member (SIN3) A, SIN3B, CHD3, CHD4 or an ON-TARGETplus Non-targeting Control Pool (siCTRL) as transfection control (50 pmol for single- or 25 pmol for double-transfection) using Lipofectamine™ RNAiMAX (Invitrogen™, Thermo Fisher Scientific) in Opti-MEM™ I reduced serum medium and DMEM with 10% fetal calf serum (Gibco™, Thermo Fisher Scientific). After transfection, fresh medium was added, and cells were stimulated for additional 24 h with 10 ng/ml TNF-α (R&D Systems, Inc.) or left untreated as control.

RNA-Isolation and Quantitative Reverse Transcription PCR

Total RNA was isolated from HUVEC or EA.hy926 and cDNA was generated as described previously (Bedenbender et al., 2019). Transcript expression of RNase1, IL-8, cyclo-oxygenase 2 (COX-2), CSNK2A1, CSNK2A2, CSNK2B, RCOR1, SIN3A, SIN3B, CHD3, CHD4, and RPS18 as internal control was analyzed by quantitative reverse transcription PCR (qRT-PCR) with respective primer pairs (**Table 1**, metabion international AG Planegg/Steinkirchen, BY, Germany), using LUNA® Universal quantitative PCR (qPCR) Master Mix (New England Biolabs, Ipswich, MA, United States) and the QuantStudio™ System and QuantStudio™ Design and Analysis Software v1.3.1 (Thermo Fisher Scientific) according to manufacturer's instructions. The fold-induction was calculated using the $2^{-\Delta\Delta ct}$ method and qRT-PCR results were normalized to the corresponding control cells (Livak and Schmittgen, 2001).

Chromatin Immunoprecipitation

Chemicals used for ChIP were purchased from Carl Roth GmbH & Co., KG, unless otherwise stated. Confluent cells were stimulated as indicated and ChIP assay was performed as described previously (Bedenbender et al., 2019). In brief, cells were fixed for 5 min with 1 % formaldehyde (methanol-free; Polysciences, Inc., Warrington, PA, United States) at room temperature. Fixation was stopped with glycine (0.125 M) for 5 min at room temperature. Cells were washed and scraped with ice cold 1× PBS (without magnesium and calcium; HyClone™, GE Healthcare, Solingen, NW, Germany) and centrifuged at

TABLE 1 | Primer sequences.

	Primer sequence 5′→3′		
Primer	**Forward**	**Reverse**	**Application**
RPS18	GCGGCGGAAAATAGCCTTTG	GATCACACGTTCCACCTCATC	mRNA analysis
RNase1	GCTGCAGATCCAGGCTTTTCTGGG	AATTTCTTGGCCCGGGATTC	mRNA analysis
COX-2	TCCCTTGGGTGTCAAAGGTAAA	TGGCCCTCGCTTATGATCTG	mRNA analysis
IL-8	ACTGAGAGTGATTGAGAGTGGAC	AACCCTCTGCACCCAGTTTTC	mRNA analysis
CSNK2A1	GAGATTCTGAAGGCCCTGGATT	ACTCAGCCAAACCCCAGTCT	mRNA analysis
CSNK2A2	CAACTATGACCAGCTTGTTCGC	TTTCCCAGCGTTTCCGTGA	mRNA analysis
CSNK2B	GCAGGTCCCTCACTATCGAC	ACTTTTCCAACATCTGGGCG	mRNA analysis
RCOR1	TCGCCGTACAAGCCATCAGG	ACCATGTTCTGCCTCCCATTC	mRNA analysis
SIN3A	GCTCCAGCTATCGAGCCTTA	ACATCAAGCTCAAAGCGTTC	mRNA analysis
SIN3B	TGCTTCAAGGTGATGTTCCTG	CATACTGCTCCACGTACCGA	mRNA analysis
CHD3	CAGCCACGGTTTATCACAGC	ACCTTTTGTGTGGCCCTCC	mRNA analysis
CHD4	CCCCGAGAGGTTCCACAAT	CTCGGGCATTGAGTGCTTCA	mRNA analysis
Region A	TGAGGAAGGAGTGGTGAATC	TTTCTCTGCTGCTCCTTGTG	ChIP
Region B	CATTAGATCGCCCTGTTG	TTTACACGACACGGGAGCCTTC	ChIP
Region C	CTGGCCCTAGGAATCCTGAAAC	CTGCAGTAAGGGCTTCTGATGG	ChIP

300 × *g* for 10 min at 4°C. Scraping and washing was repeated twice. Chemical lysis was performed using lysis buffer I [20 min at 4°C; 5 mM piperazine-N,N′-bis-(2 ethane sulfonic acid) pH 8, 85 mM potassium chloride, 0.5% Nonidet P40 (AppliChem GmbH, Darmstadt, HE, Germany)] and II [10 min at 4°C; 10 mM Tris–hydrochloride pH 7.5, 150 mM sodium chloride, 1% sodium deoxycholate, 0.1% sodium dodecyl sulfate, 1% Nonidet P40 (AppliChem GmbH)]. Chromatin was sheared by sonication, 20 cycles, each 30 s on/off using Bioruptor Plus (Diagenode SA, Seraing, LG, Belgium). Sepharose A (GE Healthcare) beads were blocked overnight at 4°C with 1 mg/ml bovine serum albumin (BSA) (Carl Roth GmbH & Co., KG) and 400 µg sonicated salmon sperm DNA (AppliChem GmbH). Sonicated chromatin was pre-cleared by incubation with blocked beads, and 10–20 µg pre-cleared chromatin were used for immunoprecipitation overnight at 4°C, using the following protein specific antibodies: anti-H4ac that recognizes acetylated histone 4 at lysine 5, 8, 12, and 16 as indicated by the manufacturer (06-598, Merck KGaA), anti-H3K27ac (ab4729), anti-CHD4 (ab72418), and anti-Rabbit IgG (ab171870; Abcam, Cambridge, United Kingdom) as indicated. Fresh beads were added to each IP for 2 h followed by diverse washing steps using washing buffer I-III (I: 20 mM Tris–hydrochloride pH 8.0, 150 mM sodium chloride, 2 mM Ethylenediaminetetraacetic acid (EDTA), 0.1% sodium dodecyl sulfate, 1% Triton X100; II: 20 mM Tris–hydrochloride pH 8.0, 500 mM sodium chloride, 2 mM EDTA, 0.1% sodium dodecyl sulfate, 1% Triton X100; III: 10 mM Tris–hydrochloride pH 8.0, 1% Nonidet P40, 1% sodium deoxycholate, 1 mM EDTA, 0.25 M Lithium chloride) and 1× Tris–EDTA buffer (10 mM Tris pH8.0, 1 mM EDTA). Chromatin-antibody complexes were chemically eluted (1% SDS, 0.1 M sodium hydrogen carbonate) and reversion of crosslinking was conducted over night by Proteinase K digestion (AppliChem GmbH) prior to DNA purification using the QIAquick PCR purification kit (QIAGEN GmbH) according to manufacturer's instructions. Purified chromatin was eluted in H_2O and analyzed by qPCR using indicated ChIP-primers (**Table 1**, metabion international AG) for human *RNASE1* promoter regions *Region A*, *Region B*, *Region C*. Results of ChIP experiments were normalized to the input control (depicted as % of input) and the respective CTRL samples with the specific antibody (CTRL or CTRL DMSO) were set to 1.

Statistical Analyses

Statistical analyses were performed using GraphPad Prism Version 6.05 (GraphPad Software, La Jolla, CA, United States). Results are expressed as mean ± standard deviation (SD) of linear data. Statistical analyses of mRNA data were conducted on log2-transformed data. One-way or two-way ANOVA and subsequent multiple comparison using Sidak post-test or Holm-Sidak post-test, respectively, were performed as indicated. Results were considered significant at $p < 0.05$.

RESULTS

p38 MAPK Signaling Mediates RNase1 mRNA Repression in Inflamed Human ECs

To investigate the underlying molecular mechanisms of RNase1 regulation in inflamed human ECs, we first aimed to identify relevant signaling pathways for this process. Besides TNF-α or IL-1β stimulation of primary human ECs, treatment with the toll-like receptor 3 ligand poly I:C for 24 h also resulted in downregulation of RNase1 mRNA (Bedenbender et al., 2019). Here, poly I:C stimulation kinetics in HUVEC from 0.5 to 24 h resulted in a significant downregulation of RNase1 mRNA abundance after 9 h of treatment that further intensified over time until 24 h (**Supplementary Figure 1A**). These findings are comparable to the previously observed RNase1 regulation in TNF-α or IL-1β stimulation kinetics (Bedenbender et al., 2019).

Based on these findings, common signaling cascades induced upon all three RNase1 repressive stimuli were investigated: NF-κB signaling or MAPK signaling via JNK and p38 kinases (Kawai and Akira, 2006; Weber et al., 2010; Brenner et al., 2015). HUVEC were pre-stimulated for 1 h with indicated concentrations of the signaling pathway inhibitors BAY11-7082 (NF-κB inhibitor) as negative control (Gansler et al., 2014), JNK inhibitor II (JNK MAPK inhibitor), SB202190 (p38 MAPK inhibitor) or DMSO as solvent control prior to 24 h TNF-α (white bars; **Figure 1A**) or poly I:C (gray bars; **Figure 1B**) stimulation, or left untreated as control (CTRL; black bars). In accordance with previous reports (Gansler et al., 2014), RNase1 mRNA expression was not affected by NF-κB inhibitor treatment in CTRL as well as TNF-α stimulated cells, compared to the DMSO control (**Figure 1A**, left panel). In respect to JNK inhibitor treatment, significantly diminished RNase1 mRNA expression was detected in CTRL cells compared to DMSO in a dose-dependent manner, while TNF-α-mediated RNase1 repression was even stronger after JNK inhibition (**Figure 1A**, middle panel). In contrast to these results, pretreatment of HUVEC with the p38 inhibitor slightly increased RNase1 mRNA abundance in CTRL cells compared to DMSO treatment. Moreover, TNF-α-mediated downregulation of RNase1 compared to the solvent control was completely restored dose-dependently by p38 inhibition (**Figure 1A**, right panel). In addition, comparable results to TNF-α treatment were obtained for RNase1 mRNA abundance by stimulation with the toll-like receptor 3 ligand poly I:C following NF-κB, JNK and p38 inhibitor stimulation compared to the solvent control DMSO as well as CTRL treated cells (**Figure 1B**). However, NF-κB inhibitor treatment slightly increased RNase1 expression in CTRL treated cells, compared to DMSO (**Figure 1B**, left panel). To validate the obtained results with the p38 inhibitor, we also investigated the expression of the p38-dependent gene COX-2, which is known to be upregulated upon proinflammatory stimulation of HUVEC (Viemann et al., 2004). Here, COX-2 was significantly upregulated upon TNF-α as well as poly I:C stimulation in DMSO treated samples, while p38 inhibition considerably blocked COX-2 induction upon proinflammatory treatment (**Supplementary Figure 1B**, left panel). Accordingly, physiological RNase1 expression seemed to be regulated via JNK signaling pathway, while inflammation-mediated RNase1 repression was mediated in a p38 MAPK-dependent manner in human ECs.

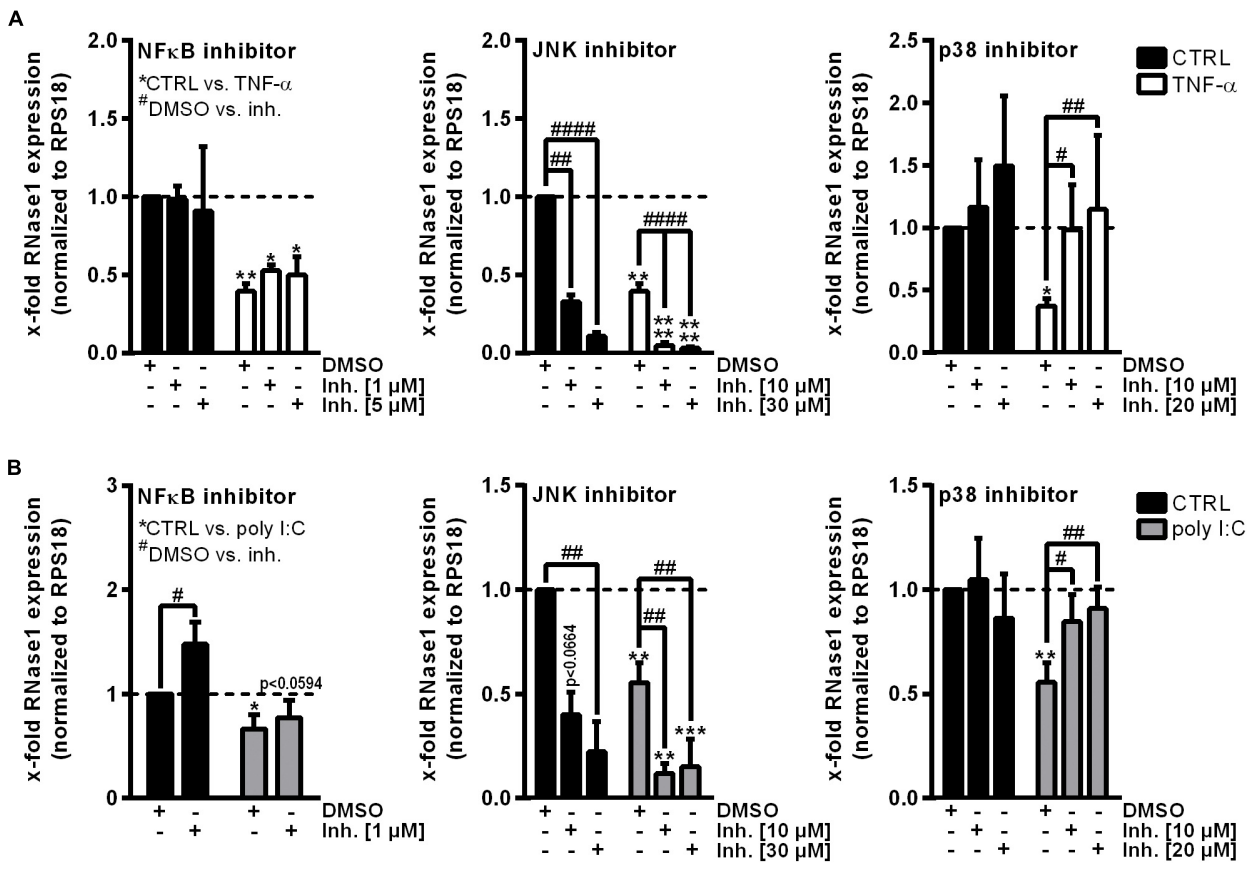

FIGURE 1 | p38 inhibitor treatment restores RNase1 mRNA expression in inflamed human ECs. HUVEC were pretreated for 1 h with indicated signaling pathway inhibitors or DMSO as solvent control prior to **(A)** TNF-α [10 ng/ml] (white bars) or **(B)** poly I:C [10 μg/ml] (gray bars) stimulation for 24 h or left untreated as control (black bars). Expression of RNase1 mRNA was analyzed by qRT-PCR. Results were normalized to RPS18 and the respective CTRL samples; $n = 3–4$; mean ± standard deviation (SD); Statistics were performed on log2-transformed data. Two-way ANOVA was performed using Holm-Sidak post-test. *CTRL vs. stimulus: $^{*}p < 0.05$, $^{**}p < 0.01$, $^{***}p < 0.001$, $^{****}p < 0.0001$; $^{\#}$DMSO vs. inhibitor (inh.): $^{\#}p < 0.05$, $^{\#\#}p < 0.01$, $^{\#\#\#\#}p < 0.0001$.

Inflammation-Mediated Repression of RNase1 in Human ECs Is Conducted by CK2 Kinase

Ribonuclease 1 repression upon EC inflammation is mainly attributed to the function of HDAC2, however, it is still unknown how HDAC2 activity is regulated in this context (Bedenbender et al., 2019). HDAC2 activity highly depends on its phosphorylation state and the association with multiprotein complexes, both described to be regulated by CK2 kinase (Tsai and Seto, 2002; Brandl et al., 2009). Thus, we investigated whether CK2 functions as intermediate step in the TNF-α-mediated signaling cascade to facilitate RNase1 repression. The human EC line EA.hy926 was pretreated for 30 min with 10 μM CK2 inhibitor TBB (white bars) or DMSO (black bars) as solvent control, followed by 24 h control (CTRL), TNF-α or poly I:C stimulation (**Figures 2A,B**). The experimental setup was validated by mRNA expression analysis of the proinflammatory marker IL-8 (for TNF-α) or CXCL10 (for poly I:C) that have been described to be partially regulated via CK2 signaling, respectively (Du et al., 2015; Li et al., 2019). IL-8 and CXCL10 mRNA were significantly upregulated in TNF-α (**Figure 2A**, left panel) or poly I:C (**Figure 2A**, right panel) treated EA.hy926 in DMSO pre-stimulated cells. Consistent with the literature, this effect was significantly reduced for IL-8 mRNA by TBB treatment upon TNF-α stimulation (**Figure 2A**, left panel), while CXCL10 expression upon poly I:C stimulation was further increased by TBB pretreatment (**Figure 2A**, right panel), both compared to the solvent control. *Vice versa*, RNase1 mRNA abundance was significantly elevated by TBB pretreatment in CTRL cells compared to the solvent control, and TNF-α-mediated reduction of RNase1 was completely recovered by TBB in contrast to DMSO (**Figure 2B**, left panel). Similar results were obtained

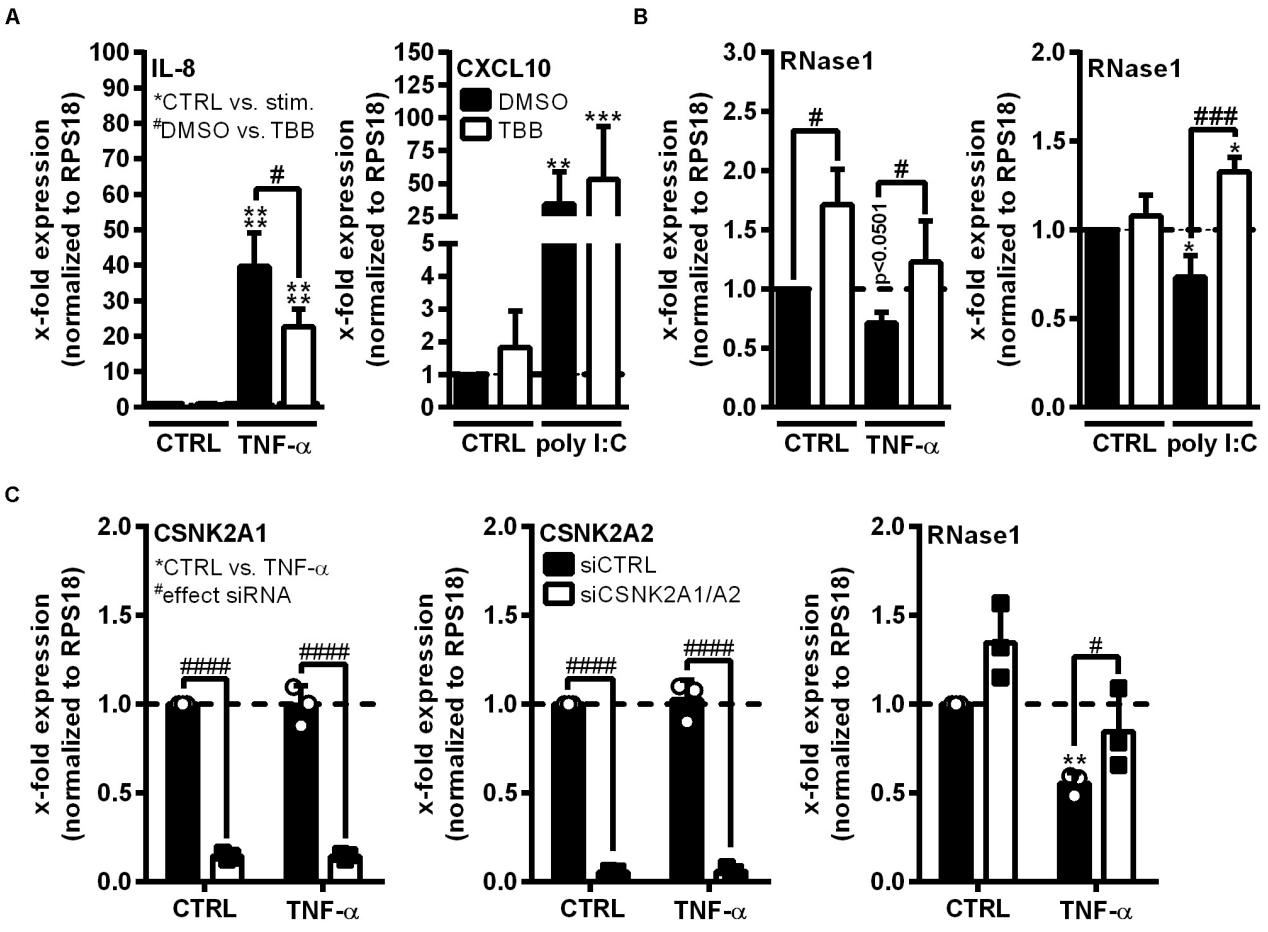

FIGURE 2 | CK2 function is required for RNase1 repression in inflamed human ECs. **(A,B)** EA.hy926 were pretreated for 30 min with CK2 inhibitor TBB [10 μM] (white bars) or DMSO as solvent control (black bars), prior to TNF-α [10 ng/ml] or poly I:C [10 μg/ml] stimulation for 24 h or left untreated as control (CTRL). **(C)** EA.hy926 were transfected with siRNA pools against both CSNK2A1 and CSNK2A2 (each 25 pmol; siCSNK2A1/A2; white bars) or 50 pmol scrambled siRNA control pool (siCTRL; black bars) for 24 h followed by additional 24 h stimulation with 10 ng/ml TNF-α or left untreated as control (CTRL). mRNA expression of **(A)** IL-8 (left panel) or CXCL10 (right panel), **(B)** RNase1, **(C)** CSNK2A1 (left panel), CSNK2A2 (middle panel) or RNase1 (right panel) was analyzed by qRT-PCR. Results were normalized to endogenous RPS18 and respective CTRL samples. $n = 3$–4; mean ± SD; Statistics were performed on log2-transformed data. Two-way ANOVA was performed using Holm-Sidak post-test. *effect of TNF-α or poly I:C: $^{*}p < 0.05$, $^{**}p < 0.01$, $^{***}p < 0.001$ $^{****}p < 0.0001$; $^{\#}$effect of TBB or siRNA: $^{\#}p < 0.05$, $^{\#\#\#}p < 0.001$, $^{\#\#\#\#}p < 0.0001$.

for TBB and poly I:C stimulation compared to DMSO, also considerably recovering RNase1 mRNA upon inflammation (**Figure 2B**, right panel).

To confirm the obtained results, the influence of small interfering RNA (siRNA)-mediated CK2 knockdown on RNase1 mRNA expression was investigated. CK2 is described as an tetrameric complex of two identical or non-identical catalytic subunits (CSNK2A1/A2) and two identical regulatory subunits (CSNK2B) in humans (Litchfield, 2003). EA.hy926 were transfected for 24 h with siRNA pools against both CSNK2A1 and A2 (**Figure 2B**; white bars), CSNK2B (**Supplementary Figures 2A,B**) or an unspecific siRNA control pool (siCTRL; black bars), prior to 24 h control (CTRL) or TNF-α stimulation. Knockdown was validated by significant downregulation of respective mRNAs of CSNK2A1 (**Figure 2B**, left panel) and CSNK2A2 (middle panel) upon specific siRNA treatment in both control and TNF-α stimulated cells. Interestingly, double-knockdown of the catalytic subunits CSNK2A1 and A2 slightly increased RNase1 expression in unstimulated cells, compared to siCTRL. Additionally, RNase1 mRNA was significantly repressed upon TNF-α treatment in control transfected cells, while CSNK2A1/2 double-knockdown considerably recovered RNase1 expression (**Figure 2B**, right panel). In respect to the regulatory subunit CSNK2B, successful knockdown was validated by significant downregulation of CSNK2B mRNA (**Supplementary Figure 2A**) upon specific siRNA treatment in both control and TNF-α stimulated cells. In contrast to CSNK2A1/A2 double-knockdown, significant downregulation of RNase1 was obtained upon TNF-α treatment compared to CTRL, for both, siCTRL and CSNK2B transfected cells (**Supplementary Figure 2B**). Altogether, TBB inhibitor treatment and CSNK2A1/A2 double-knockdown indicated an important role of CK2 kinase in TNF-α-mediated RNase1 repression in inflamed human ECs.

NuRD Co-repressor Complex Components CHD3 and 4 Are Required for RNase1 Repression in Inflamed Human ECs

HDAC2 enzymatic activity requires the association with multiprotein co-repressor complexes to get access to the chromatin (Tsai and Seto, 2002; Segre and Chiocca, 2011). To identify such complexes involved in RNase1 regulation, siRNA knockdown of crucial protein components of the most abundant HDAC-associated repressor complexes was performed in EA.hy926 (Zhang et al., 1997; Tong et al., 1998; You et al., 2001; Sengupta and Seto, 2004; Yang and Seto, 2008). siRNA pools against RCOR1 (CoREST complex), SIN3A and B (double-knockdown, SIN3 complex), CHD3 and 4 (double-knockdown, NuRD complex; white bars) or an unspecific siRNA control pool (siCTRL, black bars) were transfected in EA.hy926 for 24 h, followed by additional 24 h TNF-α stimulation or left untreated as control (CTRL; **Figure 3**). Knockdown of distinct complex components was validated by respective mRNA analysis, resulting in significant downregulation of RCOR1 (**Figure 3A**, left panel), SIN3A/B (**Figure 3B**, left and middle panel) and CHD3/4 (**Figure 3C**, left and middle panel) compared to siCTRL transfection upon the tested stimuli. In respect to RNase1, no effect of RCOR1 knockdown was detected upon both treatments (**Figure 3A**, right panel), while SIN3A/B double-knockdown increased RNase1 mRNA levels in unstimulated cells compared to siCTRL, but rather augmented the repressive effect of TNF-α on RNase1 mRNA (**Figure 3B**, right panel). Remarkably, double-knockdown of the NuRD co-repressor components CHD3 and 4 significantly increased RNase1 expression in control cells as well as considerably recovered TNF-α-mediated RNase1 repression compared to siCTRL (**Figure 3C**, right panel). Both CHD3 and 4, alone or in combination can associate in the NuRD complex to achieve either equal or individual functions (Denslow and Wade, 2007; Hoffmeister et al., 2017). To investigate whether only one of these proteins or both are essential for the RNase1 recovering effect, we performed single-knockdown of CHD3 (**Supplementary Figures 2C,D**) and CHD4 (**Supplementary Figures 2E,F**). In respect to knockdown efficiency, comparable results were obtained by single knockdown of CHD3 or 4 as for the double-knockdown (**Supplementary Figures 2C–E**), as well as for RNase1 recovery (**Supplementary Figures 2D–F**). In conclusion, these findings suggest an essential role for both, the CHD3- and the CHD4-containing NuRD co-repressor complex in RNase1 repression upon EC inflammation, presumably promoting HDAC2 recruitment to the *RNASE1* promoter.

CHD4 Accumulates at the RNASE1 Promoter Along With Histone Deacetylation Upon Proinflammatory Stimulation of Human ECs

To confirm the participation of the CHD3/4 containing NuRD complex in RNase1 repression, we investigated *RNASE1* promoter remodeling by histone deacetylation and recruitment of NuRD complex in inflamed human ECs by analyzing the acetylation state of H4 and H3K27 as well as accumulation of the NuRD component CHD4. ChIP was performed with HUVEC stimulated for 10 min with TNF-α (+), the time of HDAC2 promoter accumulation (Bedenbender et al., 2019), or left untreated as control (−). The histone acetylation state as well as CHD4 recruitment to the previously described *RNASE1* promoter regions, *Region A* (the core promoter) and the more upstream regions *Region B* (the proximal promoter) and *Region C* (the distal promoter) (Bedenbender et al., 2019), were analyzed by qPCR. In unstimulated cells, H4 as well as H3K27 were acetylated at promoter *Region A* of *RNASE1*, while 10 min TNF-α stimulation resulted in significant deacetylation of H4 and H3K27 at the same site (**Figure 4A**, left and middle panel). Along with these findings, CHD4 accumulation was significantly elevated at *Region A* upon TNF-α treatment compared to untreated cells (**Figure 4A**, right panel). In respect to *Region B* (**Figure 4B**) and *C* (**Figure 4C**), similar results were obtained for H4ac (left panels) and H3K27ac (middle panels), while almost no or equal CHD4 accumulation was detected in control and TNF-α treated cells (**Figures 4B,C**, right panels). Consequently, *RNASE1* promoter *Region A–C* is markedly deacetylated after 10 min of TNF-α stimulation. This effect went along with specific recruitment of CHD4 to *Region A* of *RNASE1*, indicating a role of the

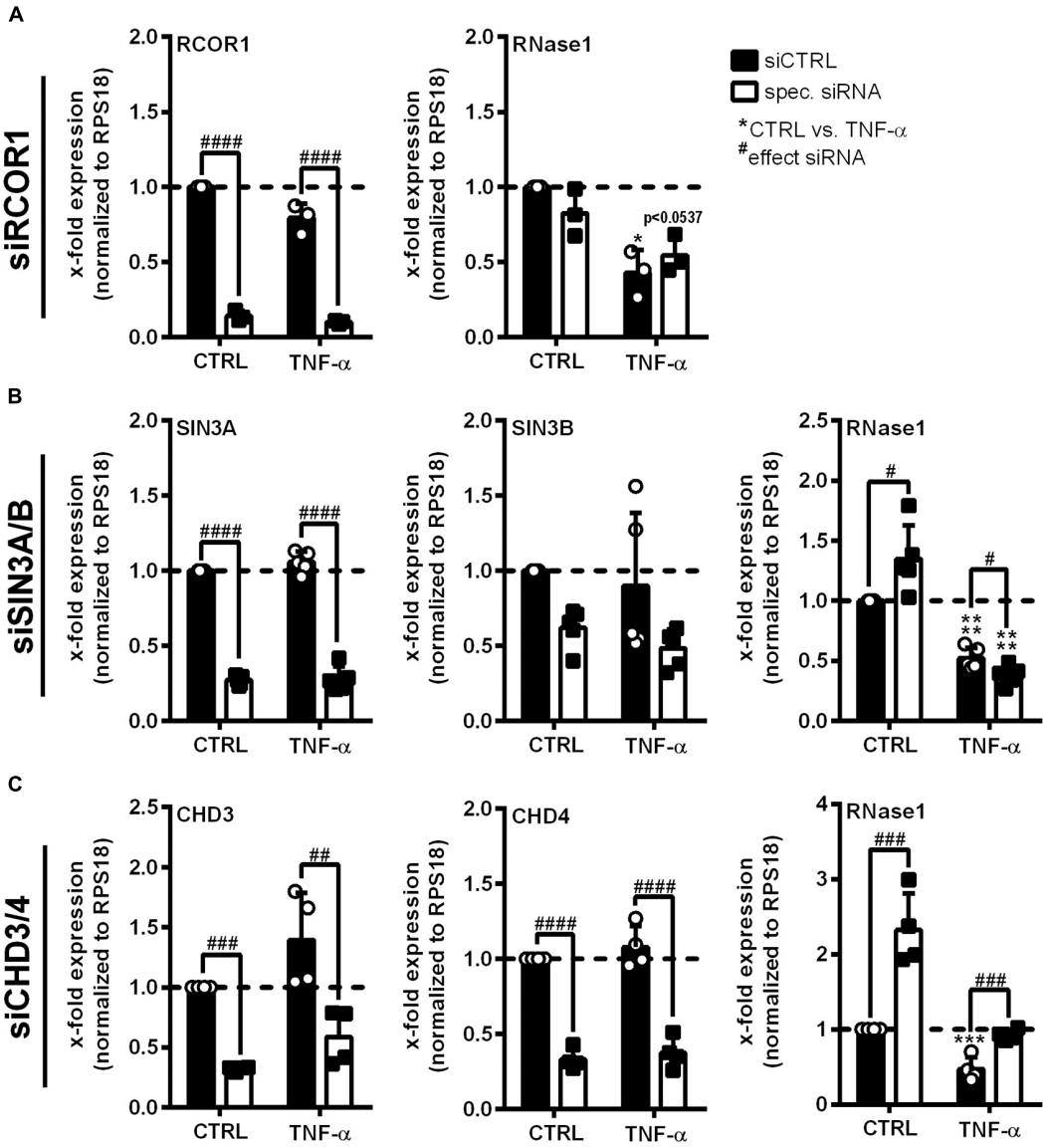

FIGURE 3 | Co-repressor complex NuRD is crucial for RNase1 downregulation upon human EC inflammation. EA.hy926 were transfected with siRNA pools (50 pmol for single- or 25 pmol each for double-transfection) against **(A)** RCOR1 (siRCOR1; CoREST complex), **(B)** a combination of SIN3A and SIN3B (siSIN3A/B; SIN3 complex), **(C)** CHD3 and CHD4 (siCHD3/4; NuRD complex; white bars) or scrambled siRNA control pool (siCTRL; black bars) for 24 h followed by additional 24 h stimulation with 10 ng/ml TNF-α or left untreated as control (CTRL). mRNA expression of **(A)** RCOR1, **(B)** SIN3A and SIN3B, **(C)** CHD3 and CHD4 as well as **(A–C)** RNase1 was analyzed by qRT-PCR. Results were normalized to endogenous RPS18 and CTRL treated siCTRL samples. $n = 3$–4; mean ± SD; Statistics were performed on log2-transformed data; Two-way ANOVA was performed using Holm-Sidak post-test. *effect of TNF-α: $^{*}p < 0.05$, $^{***}p < 0.001$, $^{****}p < 0.0001$; $^{\#}$effect of siRNA: $^{\#}p < 0.05$, $^{\#\#}p < 0.01$, $^{\#\#\#}p < 0.001$, $^{\#\#\#\#}p < 0.0001$.

CHD4 containing NuRD complex in *RNASE1* regulation in inflamed human ECs.

Inhibition of p38 MAPK Signaling Restores Histone Acetylation at the RNASE1 Promoter and Prevents CHD4 Accumulation

To investigate whether the described *RNASE1* promoter remodeling and CHD4 accumulation depend on p38 MAPK signaling, ChIP assays with p38 inhibition were performed. Therefore, HUVEC were pretreated for 2 h with 20 μM p38 inhibitor SB202190 (+) or DMSO (−) as solvent control, followed by 10 min stimulation with 10 ng/ml TNF-α (white bars) or left untreated as control (CTRL; black bars). Acetylation of H4 or H3K27, and the recruitment of NuRD co-repressor complex component CHD4 (right panels) were investigated by immunoprecipitation and analyzed by qPCR using respective promoter primers. Compared to inhibitor and DMSO treatment in CTRL cells, TNF-α stimulation resulted in significant

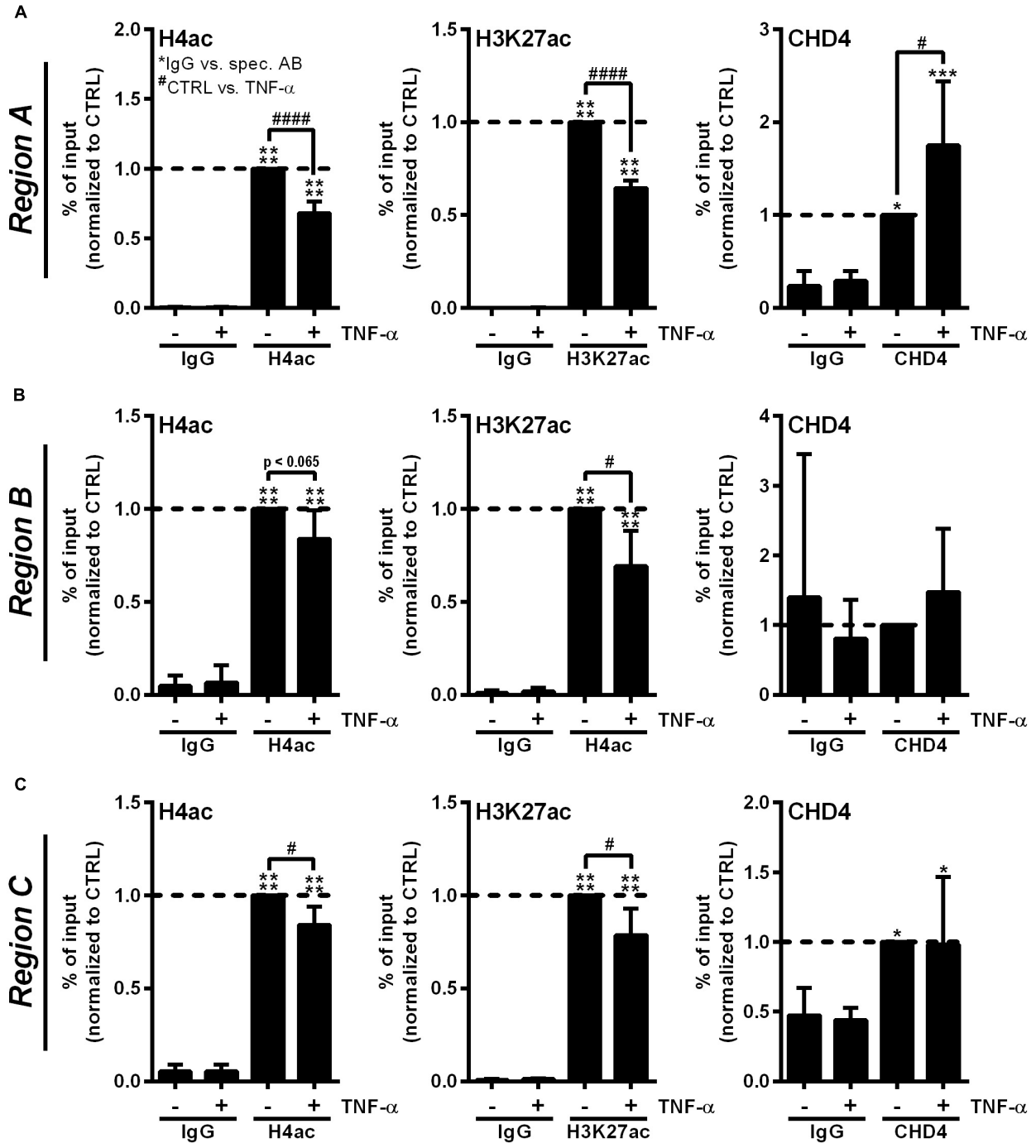

FIGURE 4 | Proinflammatory stimulation of human ECs induces *RNASE1* promoter deacetylation in concert with CHD4 recruitment. HUVEC were stimulated with 10 ng/ml TNF-α for 10 min (+) or left untreated as control (–). Immunoprecipitation using specific antibodies against histone 4 acetylation (H4ac; left panels), histone 3 lysine 27 acetylation (H3K27ac; middle panels), chromodomain helicase DNA binding protein 4 (CHD4; right panels) or an unspecific IgG control was performed. **(A)** *Region A*, **(B)** *Region B*, **(C)** *Region C* of the *RNASE1* promoter were pulled down by the respective antibodies and analyzed by qPCR using respective primers. Results were depicted as % input and the respective control sample with the specific antibody was set to 1. $n = 3$–4; mean ± SD; One-way ANOVA was performed using Sidak post-test, *IgG vs. specific (spec.) antibody (AB): $^{*}p < 0.05$, $^{***}p < 0.001$, $^{****}p < 0.0001$; $^{\#}$CTRL vs. TNF-α: $^{\#}p < 0.05$, $^{\#\#\#\#}p < 0.0001$.

deacetylation of H4 in DMSO treated samples at *Region A* of the *RNASE1* promoter. This effect was considerably restored by p38 inhibition upon TNF-α stimulation, resulting in comparable H4 acetylation as in untreated cells (**Figure 5A**, left panel). Similar effects were obtained for H4ac in *Region B* and *C* of the *RNASE1* promoter, although not significantly (**Figures 5B,C**,

left panel). With respect to H3K27, reduced acetylation at *Region A–C* was observed after proinflammatory stimulation of HUVEC compared to DMSO treated CTRL cells. Although no significant recovery of H3K27ac by p38 inhibition was detected after 10 min TNF-α stimulation, an increasing trend toward restoration of acetylation was observed in *Region A–C* (**Figures 5A-C**, middle panel). In context of CHD4, TNF-α treatment tented to increase recruitment to the *RNASE1* promoter *Region A* compared to the DMSO treated CTRL, while p38 inhibition inclined to reverse this effect to only basal CHD4 levels (**Figure 5A**, right panel). At the upstream promoter *Region B*, a similar trend can be observed for CHD4 upon TNF-α stimulation, indicated by an increase in CHD4 accumulation in solvent control treated cells and its prevention upon p38 inhibition (**Figure 5B**, right panel). Compared to that, CHD4 was almost absent from *Region C* upon all indicated treatments

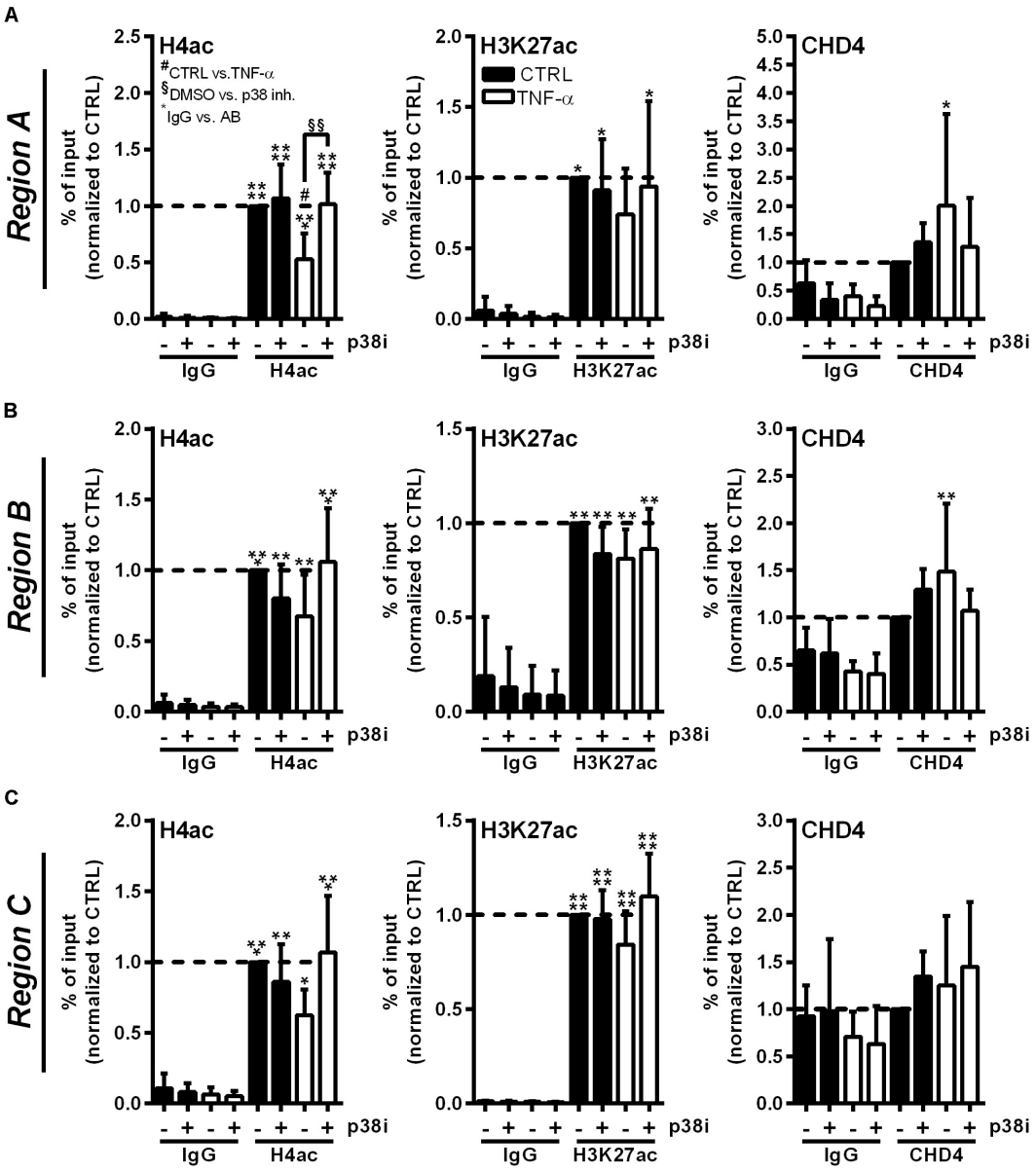

FIGURE 5 | p38 inhibitor treatment reverses *RNASE1* promoter deacetylation and CHD4 recruitment in inflamed human ECs. HUVEC were pretreated with 20 μM p38 inhibitor (inh.) SB202190 (+) or DMSO as solvent control (–) for 2 h, followed by 10 min TNF-α stimulation [10 ng/ml] (white bars) or left untreated as control (CTRL; black bars). Immunoprecipitation using specific antibodies against histone 4 acetylation (H4ac; left panels), histone 3 lysine 27 acetylation (H3K27ac; middle panels), chromodomain helicase DNA binding protein 4 (CHD4; right panels) or an unspecific IgG control was performed. **(A)** *Region A*, **(B)** *Region B*, **(C)** *Region C* of the *RNASE1* promoter were pulled down by the respective antibodies and analyzed by qPCR using respective primers. Results were depicted as % input and the respective control sample with the specific antibody was set to 1. $n = 3–4$; mean ± SD; Two-way ANOVA was performed using Holm-Sidak post-test. *IgG vs. specific (spec.) antibody (AB): $^{*}p < 0.05$, $^{**}p < 0.01$, $^{***}p < 0.001$, $^{****}p < 0.0001$; $^{\#}$CTRL vs. TNF-α: $^{\#}p < 0.05$; $^{\$}$DMSO vs. p38 inh.: $^{\$\$}p < 0.01$.

(**Figure 5C**, right panel). These findings provide evidence that proinflammatory stimulation of HUVEC with TNF-α induced deacetylation of H4 and H3K27 at the *RNASE1* promoter as well as recruitment of the NuRD/CHD4 co-repressor complex. Interestingly, these effects can be reversed by p38 inhibition, underlining the importance of p38 signaling in *RNASE1* promoter remodeling and repression.

DISCUSSION

Cardiovascular disease, such as atherosclerosis, thrombosis, or myocardial infarction, that are associated with endothelial dysfunction represent a global health issue, causing approximately 18 million deaths per year worldwide[1]. Thereby, disease development and progression tightly associate to the loss of vascular function, homeostasis, and integrity in consequence to inflammation, infection, or injury of the endothelium (Poredos, 2002; Sitia et al., 2010; Zernecke and Preissner, 2016). Thus, investigation of the underlying mechanisms of endothelial dysfunction upon vascular inflammation is an important need. In this study, we investigated the underlying mechanisms of repression of vasoprotective RNase1 in context of vascular inflammation (Gansler et al., 2014; Zernecke and Preissner, 2016). We identified a regulatory mechanism by which proinflammatory stimulation, such as TNF-α or poly I:C, activated p38 MAPK, CK2 kinase, and subsequent recruitment of the HDAC2 containing NuRD/CHD4 co-repressor complex to the *RNASE1* promoter. This resulted in chromatin remodeling via histone deacetylation and subsequent RNase1 repression. In recent years, the RNase1-eRNA system was identified as crucial factor in diverse pathologies, ranging from cardiovascular diseases, such as thrombosis, atherosclerosis or myocardial infarction, to inflammatory and infectious disorders like sepsis or bacterial infections (Kannemeier et al., 2007; Cabrera-Fuentes et al., 2014; Simsekyilmaz et al., 2014; Zakrzewicz et al., 2016; Zernecke and Preissner, 2016; Zechendorf et al., 2020). In this context, RNase1 has been demonstrated as potent regulator and protective factor of vascular homeostasis by counteracting the danger-associated molecule eRNA to compensate changes in the eRNA-RNase1 system (Zernecke and Preissner, 2016). Thereby, RNase1 protects the endothelium from overwhelming inflammation by e.g., decreasing myocardial infarction size or thrombus formation, mainly via reduction of circulating eRNA levels, inflammatory cells and cytokines to recover physiological organ functions (Fischer et al., 2007; Kannemeier et al., 2007; Cabrera-Fuentes et al., 2014, 2015; Chen et al., 2014). However, RNase1 function is significantly impaired upon long-term vascular inflammation due to increased extracellular eRNA levels that further result in loss of vascular integrity (Gansler et al., 2014). These processes were shown to be mainly regulated by an HDAC-dependent mechanism by which HDAC2 is recruited to the *RNASE1* promoter region to conduct histone deacetylation, resulting in a condensed chromatin structure, loss of Polymerase II transcription machinery binding and subsequent gene repression (Bedenbender et al., 2019). Therefore, unraveling the underlying molecular mechanisms of RNase1 repression in inflamed human ECs is of great importance, to offer new therapeutic options and treatment strategies to preserve RNase1 function upon vascular inflammation.

In this study, we identified the well-known MAPK phosphorylation cascades via JNK and p38 as potent regulators of RNase1 expression in human ECs under physiological as well as proinflammatory conditions. MAPK signaling via JNK and p38 is directly associated to the RNase1 repressive proinflammatory stimuli TNF-α, IL-1β, and poly I:C (Ashwell, 2006; Kawai and Akira, 2006; Weber et al., 2010; Brenner et al., 2015; Bedenbender et al., 2019). As blocking of JNK signaling strongly repressed RNase1 expression in untreated ECs, this signaling cascade seems to be essential for physiological RNase1 expression. These findings are supported by publications, demonstrating JNK as potent regulator of EC gene expression not only upon inflammation, for instance during thrombin induced intercellular adhesion molecule 1 expression (Miho et al., 2005), but also under physiological conditions, e.g., in context of EC motility (Shin et al., 2001). However, our findings indicate that JNK inhibition upon TNF-α and poly I:C treatment potentiates the negative effect of these stimuli on RNase1 mRNA. Thus, it can be speculated that the JNK cascade might still conduct residual RNase1 mRNA expression even upon inflammation. In addition, our results confirmed an p38-dependent regulatory mechanism for RNase1 repression upon inflammation of human ECs, as demonstrated by clear recovery of RNase1 expression after TNF-α and poly I:C treatment by p38 inhibition. These findings are comparable to previous results using the HDAC1-3 inhibitor MS275 that also fully recovered RNase1 expression upon inflammation (Bedenbender et al., 2019). p38 MAPK is generally associated to inflammatory events, as it was firstly described in context of proinflammatory cytokine synthesis in endotoxin stimulated macrophages (Lee et al., 1994). Besides its crucial role in induction of proinflammatory mediators, e.g., reduced IL-6 production in p38α-deficient embryonic stem cells, or p38-dependent COX-2 expression in TNF-α stimulated HUVEC (Allen et al., 2000; Viemann et al., 2004), also repressive functions of p38 signaling, such as the reduction of certain myogenic genes during muscle differentiation in myeloid cells, are described (Suelves et al., 2004). These findings support our results that inflammation-mediated RNase1 repression is primarily associated to p38 MAPK-dependent signaling in human ECs.

To unravel further intermediated steps in the RNase1 repression cascade upon EC inflammation, we analyzed the regulation of HDAC2 activity in this context. Previous findings by our group indicated that HDAC2 activity might be regulated independent of HDAC2 mRNA or protein levels (Bedenbender et al., 2019 and unpublished data), suggesting an alternative regulatory mechanism. Class I HDAC activity, including HDAC2, can be regulated through subcellular localization, association in protein complexes and post-translational modifications. Since HDAC2 is mainly located in the nucleus due to its nuclear localization sequence and the missing export sequence

[1]https://www.who.int/news-room/fact-sheets/detail/cardiovascular-diseases-(cvds)

(Micelli and Rastelli, 2015), we focused on its post-translational modification and association into multiprotein co-repressor complexes. Both processes can be regulated via phosphorylation of HDAC2 C-terminal serine residues by the highly conserved and constitutively active protein kinase CK2 (Tsai and Seto, 2002; Litchfield, 2003; Segre and Chiocca, 2011). CK2 function is directly associated with TNF-α and p38 signaling to mediate inflammatory processes as demonstrated in context of stress-induced human cervical carcinoma cells and diabetic retinopathy in retinal ECs (Sayed et al., 2000; Litchfield, 2003; Meggio and Pinna, 2003; Zhang and Steinle, 2014). Here, we investigated the impact of CK2 on RNase1 expression by CK2 inhibition and siRNA knockdown in the human EC line EA.hy926. Blocking of CK2 function by the inhibitor TBB as well as knockdown of the two catalytic subunits CSNK2A1/A2 significantly recovered RNase1 mRNA abundance upon TNF-α (or poly I:C) treatment, demonstrating an important role of CK2 kinase in the inflammation-mediated repression of RNase1. These findings are further supported by previously described functions of CK2 in context of inflammation, e.g., regulation of leukocyte interactive proteins, like endothelial selectin upon TNF-α-mediated EC activation or HDAC2 phosphorylation in hypoxia-associated tumors (Pluemsampant et al., 2008; Ampofo et al., 2015). To further test for a direct impact of CK2 on HDAC2 phosphorylation in inflamed ECs we performed Western Blot analysis upon CK2 inhibitor (TBB) treatment and proinflammatory stimulation of human ECs (data not shown). Although we found high HDAC2 phosphorylation levels in general, we did not observe any significant regulation. This suggests that HDAC2 activity might not be regulated exclusively by CK2-mediated phosphorylation but rather includes additional mechanisms like assembly of co-repressor complexes or cross-talk between post-translational modifications, as demonstrated for acetylation or ubiquitination. Within such complexes, HDAC2 activity has been shown to be influenced by formation of HDAC1:HDAC2 heterodimers, in which acetylated HDAC1 can control HDAC2 activity, or by combinations of HDAC2 modifications like phospho-acetylation (Adenuga and Rahman, 2010; Segre and Chiocca, 2011). In respect to a potential HDAC1:2 heterodimer formation and a possible functional redundancy of these enzymes, we already analyzed the impact of HDAC1 on RNase1 regulation in our previous publication (Bedenbender et al., 2019). Although, only HDAC2 accumulated at the *RNASE1* promoter, only siRNA double knockdown of both HDAC1 and HDAC2 recovers RNase1 mRNA expression. These findings implicate that HDAC2 is the most relevant enzyme in inflammation-mediated RNase1 regulation, however, HDAC1 might take over its function redundantly, once HDAC2 is missing (Bedenbender et al., 2019). Based on the literature, both enzymes, HDAC1 and HDAC2, can be regulated by CK2, while HDAC1 can also be regulated by other kinases (e.g., cAMP-dependent protein kinase; Tsai and Seto, 2002; Khan et al., 2013). In conclusion, our findings provide evidence that CK2 kinase is involved in regulation of RNase1 upon EC inflammation, presumably via regulation of HDAC2 activity. The interaction between CK2 and HDACs for *RNASE1* promoter remodeling remains to be clarified in detail.

As mentioned before, HDAC2 function and recruitment to promoter sites are associated with the formation of multiprotein co-repressor complexes, which in turn might also co-localize with CK2 (Grozinger and Schreiber, 2002; De Ruijter et al., 2003; Sengupta and Seto, 2004; Sun et al., 2007). Therefore, we investigated the impact of the three major HDAC2-associated repressor complexes on RNase1 mRNA expression upon EC inflammation via siRNA-mediated knockdown of essential co-repressor complex components: RCOR1 for CoREST, SIN3A/B for SIN3 and CHD3/4 (also known as Mi2α/β) for NuRD (Zhang et al., 1997; Tong et al., 1998; Humphrey et al., 2001; You et al., 2001). Only single- or double-knockdown of the NuRD repressor complex components CHD3 and 4 significantly restored RNase1 mRNA abundance upon TNF-α treatment in our experimental setting. Hence, our findings imply an important involvement of NuRD-associated CHD3 and CHD4 in RNase1 repression in inflamed human ECs. These findings are supported by the essential roles of NuRD in context of inflammation, e.g., in regulation of T- and B-cell development or macrophage immune responses (Fujita et al., 2004; Shimizu-Hirota et al., 2012; Shen et al., 2018). The great impact of NuRD co-repressor complex in RNase1 regulation is further confirmed by recruitment of CHD4 to the *RNASE1* promoter *Region A* upon 10 min TNF-α treatment. Additionally, this recruitment goes along with deacetylation of H4 and H3K27, two well-known markers of actively transcribed chromatin, that are already associated to regulation of *RNASE1* (Kouzarides, 2007; Wang et al., 2008; Bedenbender et al., 2019). Among the diverse types of co-repressor complexes, the NuRD chromatin-remodeling complex is unique due to the combination of chromatin-remodeling enzymes, like the DNA helicase-like ATPases CHD3 and CHD4, and histone modifying subunits, such as HDAC2 (Tong et al., 1998; Denslow and Wade, 2007). Hence, the obtained results for CHD4 are in accordance with the previously described accumulation of HDAC2 at the *RNASE1* promoter *Region A* after 10 min of TNF-α treatment (Bedenbender et al., 2019). Although HDAC2 also accumulated at *Region B* of the *RNASE1* promoter in previous experiments (Bedenbender et al., 2019), CHD4 seemed to be absent in this region under the same conditions. In this context, however, we are aware that ChIP analysis using primary ECs can be highly susceptible to donor variances of self-isolated primary cells. These effects might yield in high standard deviations and therewith potentially masking small differences in CHD4 recruitment to this region. Despite these small discrepancies, our current data indicate that HDAC2 recruitment to the *RNASE1* promoter is mainly mediated via the CHD3/4 containing NuRD complex upon inflammation of human ECs. To further strengthen these findings, the impact of NuRD knockdown or inhibition on HDAC2 recruitment and subsequent chromatin remodeling at the *RNASE1* promoter should be considered for future investigations. Although there are only few publications regarding NuRD functions in vascular ECs, the impact of this complex in context of vascular integrity seems to be crucial. Ingram et al. (2013) demonstrated a preventive function of NuRD/CHD4 on excessive extracellular matrix proteolysis, while Colijn et al. (2020) observed protection of vascular

integrity by NuRD/CHD4-mediated histone deacetylation and gene repression upon hypoxia in embryonic ECs. Altogether, the presented data and previous findings of our group suggest that simultaneous recruitment of HDAC2 and CHD4 within the NuRD complex induces chromatin remodeling like deacetylation of H4 and H3K27 that finally result in a condensed chromatin structure, loss of polymerase transcription machinery binding and subsequent *RNASE1* repression in inflamed human ECs (Bedenbender et al., 2019).

Since p38 inhibition in HUVEC illustrated the involvement of this signaling cascade in inflammation-mediated RNase1 repression, we wondered whether p38 inhibition was also able to reverse *RNASE1* chromatin remodeling with respect to histone acetylation and CHD4 recruitment. Using ChIP analysis in primary human ECs, we found that H4ac was restored by p38 inhibitor treatment at the *RNASE1* promoter despite TNF-α stimulation. With respect to H3K27ac, a trend toward recovery of acetylation was also induced upon p38 inhibition. However, the weak effect on H3K27ac could be due to kinetics, as H4 acetylation might be recovered prior to H3K27ac. These findings are in line with previous studies from our group that demonstrated that inhibition of HDAC1, HDAC2 and HDAC3 with the class I HDAC inhibitor MS275 significantly recovered histone acetylation after 30 min of TNF-α treatment (Bedenbender et al., 2019). Comparing the current findings with our previous work, stronger effects in respect to histone acetylation upon p38 inhibitor treatment might be obtained after 30 min of TNF-α stimulation. In general, these findings illustrate the role of p38 inhibition for the recovery of histone acetylation at the *RNASE1* promoter, especially at H4, and presumably also at H3K27. Additionally, p38 inhibition reduced inflammation-induced accumulation of CHD4 at *RNASE1* promoter *Region A* and *Region B*. Compared to the presented data from **Figure 4**, these findings also suggest accumulation of CHD4 at the upstream promoter *Region B* which would correspond to the recruitment of HDAC2 at the same site (Bedenbender et al., 2019). Thus, CHD4 as part of the NuRD co-repressor complex was recruited to the *RNASE1* promoter in a p38-dependent manner. MAPK signaling cascades are known to be highly involved in chromatin remodeling and subsequent gene regulation, for instance via phosphorylation of transcription factors that further influence recruitment of the polymerase II transcription machinery, histone acetyl transferase complexes, as well as chromatin remodeling and HDAC complexes (Suganuma and Workman, 2011). In this context, TNF-α-induced p38 signaling was shown to promote the interaction of transcription factor YY1 and the polycomb repressive complex 2 to induce repressive chromatin structures at target gene promoters (Palacios et al., 2010), while tumor suppressor SALL1 induces p38-dependent NuRD recruitment to promote cancer cell senescence (Ma et al., 2018). Although transcription factors involved in RNase1 repression are still unknown, these findings are in line with the presented observations that TNF-α-induced p38 signaling is critical for recruitment of the NuRD/CHD4 complex to the *RNASE1* promoter to conduct H4 and H3K27 deacetylation and *RNASE1* repression.

Finally, with respect to RNase1 recovery by inhibition of CK2 and p38, our study may pave the way to new strategies to maintain vascular homeostasis in context of vascular pathologies by preserving the protective factor RNase1. Previous studies already indicated an essential role of both CK and p38 in context of vascular diseases that can be also related to studies addressing RNase1 function in the same context. For instance, both CK2 and p38 kinase have been implicated in the regulation of foam cell formation during atherosclerosis, which can be blocked by either CK2 or p38 inhibition (Zhao et al., 2002; Harvey et al., 2007). Interestingly, the macrophage content in atherosclerotic lesions can be also associated to accumulating eRNA, which can be blocked by RNase1 administration (Simsekyilmaz et al., 2014). Additionally, p38 inhibition also protects cardiomyocytes from cellular injury upon myocardial ischemia and reperfusion, or reduces excessive inflammatory cytokine expression (e.g., TNF-α) and infarct size during stroke (Barone et al., 2001; Kaiser et al., 2004, 2005). Remarkably, RNase1 administration reduces myocardial as well as cerebral infarction size and preserves cellular function in the same pathological context (Walberer et al., 2009; Cabrera-Fuentes et al., 2014, 2015). Based on these findings, a close association between p38 signaling, CK2, TNF-α, eRNA and reduced RNase1 levels is likely in diverse vascular pathologies. In this context CK2, as well as p38 inhibitors are already used in clinical trials for treatment of hematological and solid cancers or chronic inflammatory diseases, like rheumatoid arthritis or diabetes mellitus, respectively (Kumar et al., 2003; Lee and Dominguez, 2005; Buontempo et al., 2018), indicating their use as promising targets also for treatment of vascular diseases.

In conclusion, we found evidence for a regulatory mechanism of RNase1 repression in inflamed human ECs by which proinflammatory stimulation induces p38 signaling to activate CK2 kinase which further promotes HDAC2 activation and association into the NuRD co-repressor complex. Consequently, NuRD/CHD4 as well as HDAC2 are recruited to the *RNASE1* promoter to facilitate chromatin remodeling via histone deacetylation, followed by chromatin condensation and transcriptional repression. Hence, identification of associated molecules in inflammation-mediated repression of the vessel-protective factor RNase1 may provide new potential targets, such as p38 MAPK, CK2 kinase, or the NuRD/CHD4 repressor complex, for treatment of cardiovascular pathologies.

DATA AVAILABILITY STATEMENT

The raw data supporting the conclusions of this article will be made available by the authors, without undue reservation.

ETHICS STATEMENT

The studies involving human participants were reviewed and approved by the local ethics regulations of the Philipps-University Marburg (permit number: AZ 20/16). The patients/participants provided their written informed consent to participate in this study.

AUTHOR CONTRIBUTIONS

KB, EV, and BS contributed to conception and design of the study. KB and IB performed the research and analyzed the data. KB wrote the manuscript. IB, EV, and BS contributed to manuscript revision, read and approved the submitted version. All authors contributed to the article and approved the submitted version.

FUNDING

This work was supported by the von Behring-Röntgen-Stiftung (61-0040 and 62-0002, Marburg, Germany) and ERACoSysMed SysMed-COPD (031L0140, Berlin, Germany) to BS.

ACKNOWLEDGMENTS

We thank Siegmund Köhler and the Department of Obstetrics of the Philipps-University Marburg as well as all participants for providing umbilical cords for HUVEC isolation. We also thank Uta Maria Bauer for technical advice, as well as Lukas Jerrentrup for contribution to the ethical approval application, Anna Lena Jung and all other lab members for support and discussion.

SUPPLEMENTARY MATERIAL

The Supplementary Material for this article can be found online at: https://www.frontiersin.org/articles/10.3389/fcell.2020.563604/full#supplementary-material

REFERENCES

Adenuga, D., and Rahman, I. (2010). Protein kinase CK2-mediated phosphorylation of HDAC2 regulates co-repressor formation, deacetylase activity and acetylation of HDAC2 by cigarette smoke and aldehydes. *Arch. Biochem. Biophys.* 498, 62–73. doi: 10.1016/j.abb.2010.04.002

Allen, M., Svensson, L., Roach, M., Hambor, J., Mcneish, J., and Gabel, C. A. (2000). Deficiency of the stress kinase p38alpha results in embryonic lethality: characterization of the kinase dependence of stress responses of enzyme-deficient embryonic stem cells. *J. Exp. Med.* 191, 859–870. doi: 10.1084/jem.191.5.859

Ampofo, E., Rudzitis-Auth, J., Dahmke, I. N., Rossler, O. G., Thiel, G., Montenarh, M., et al. (2015). Inhibition of protein kinase CK2 suppresses tumor necrosis factor (TNF)-alpha-induced leukocyte-endothelial cell interaction. *Biochim. Biophys. Acta* 1852, 2123–2136. doi: 10.1016/j.bbadis.2015.07.013

Ashwell, J. D. (2006). The many paths to p38 mitogen-activated protein kinase activation in the immune system. *Nat. Rev. Immunol.* 6, 532–540. doi: 10.1038/nri1865

Barone, F. C., Irving, E. A., Ray, A. M., Lee, J. C., Kassis, S., Kumar, S., et al. (2001). Inhibition of p38 mitogen-activated protein kinase provides neuroprotection in cerebral focal ischemia. *Med. Res. Rev.* 21, 129–145. doi: 10.1002/1098-1128(200103)21:2<129::aid-med1003>3.0.co;2-h

Bedenbender, K., Scheller, N., Fischer, S., Leiting, S., Preissner, K. T., Schmeck, B. T., et al. (2019). Inflammation-mediated deacetylation of the ribonuclease 1 promoter via histone deacetylase 2 in endothelial cells. *FASEB J.* 33, 9017–9029. doi: 10.1096/fj.201900451r

Brandl, A., Heinzel, T., and Kramer, O. H. (2009). Histone deacetylases: salesmen and customers in the post-translational modification market. *Biol. Cell* 101, 193–205. doi: 10.1042/bc20080158

Brenner, D., Blaser, H., and Mak, T. W. (2015). Regulation of tumour necrosis factor signalling: live or let die. *Nat. Rev. Immunol.* 15, 362–374. doi: 10.1038/nri3834

Buontempo, F., Mccubrey, J. A., Orsini, E., Ruzzene, M., Cappellini, A., Lonetti, A., et al. (2018). Therapeutic targeting of CK2 in acute and chronic leukemias. *Leukemia* 32, 1–10. doi: 10.1038/leu.2017.301

Cabrera-Fuentes, H. A., Niemann, B., Grieshaber, P., Wollbrueck, M., Gehron, J., Preissner, K. T., et al. (2015). RNase1 as a potential mediator of remote ischaemic preconditioning for cardioprotectiondagger. *Eur. J. Cardiothorac. Surg.* 48, 732–737. doi: 10.1093/ejcts/ezu519

Cabrera-Fuentes, H. A., Ruiz-Meana, M., Simsekyilmaz, S., Kostin, S., Inserte, J., Saffarzadeh, M., et al. (2014). RNase1 prevents the damaging interplay between extracellular RNA and tumour necrosis factor-alpha in cardiac ischaemia/reperfusion injury. *Thromb. Haemost.* 112, 1110–1119. doi: 10.1160/th14-08-0703

Chen, C., Feng, Y., Zou, L., Wang, L., Chen, H. H., Cai, J. Y., et al. (2014). Role of extracellular RNA and TLR3-Trif signaling in myocardial ischemia-reperfusion injury. *J. Am. Heart Assoc.* 3:e000683.

Colijn, S., Gao, S., Ingram, K. G., Menendez, M., Muthukumar, V., Silasi-Mansat, R., et al. (2020). The NuRD chromatin-remodeling complex enzyme CHD4 prevents hypoxia-induced endothelial Ripk3 transcription and murine embryonic vascular rupture. *Cell Death Differ.* 27, 618–631. doi: 10.1038/s41418-019-0376-8

De Ruijter, A. J., Van Gennip, A. H., Caron, H. N., Kemp, S., and Van Kuilenburg, A. B. (2003). Histone deacetylases (HDACs): characterization of the classical HDAC family. *Biochem. J.* 370, 737–749. doi: 10.1042/bj20021321

Denslow, S. A., and Wade, P. A. (2007). The human Mi-2/NuRD complex and gene regulation. *Oncogene* 26, 5433–5438. doi: 10.1038/sj.onc.1210611

Du, M., Liu, J., Chen, X., Xie, Y., Yuan, C., Xiang, Y., et al. (2015). Casein kinase II controls TBK1/IRF3 activation in IFN response against viral infection. *J. Immunol.* 194, 4477–4488. doi: 10.4049/jimmunol.1402777

Fischer, S., Gerriets, T., Wessels, C., Walberer, M., Kostin, S., Stolz, E., et al. (2007). Extracellular RNA mediates endothelial-cell permeability via vascular endothelial growth factor. *Blood* 110, 2457–2465. doi: 10.1182/blood-2006-08-040691

Fujita, N., Jaye, D. L., Geigerman, C., Akyildiz, A., Mooney, M. R., Boss, J. M., et al. (2004). MTA3 and the Mi-2/NuRD complex regulate cell fate during B lymphocyte differentiation. *Cell* 119, 75–86. doi: 10.1016/j.cell.2004.09.014

Gansler, J., Preissner, K. T., and Fischer, S. (2014). Influence of proinflammatory stimuli on the expression of vascular ribonuclease 1 in endothelial cells. *FASEB J.* 28, 752–760. doi: 10.1096/fj.13-238600

Grozinger, C. M., and Schreiber, S. L. (2002). Deacetylase enzymes: biological functions and the use of small-molecule inhibitors. *Chem. Biol.* 9, 3–16.

Harvey, E. J., Li, N., and Ramji, D. P. (2007). Critical role for casein kinase 2 and phosphoinositide-3-kinase in the interferon-gamma-induced expression of monocyte chemoattractant protein-1 and other key genes implicated in atherosclerosis. *Arterioscler Thromb. Vasc. Biol.* 27, 806–812. doi: 10.1161/01.atv.0000258867.79411.96

Hoffmeister, H., Fuchs, A., Erdel, F., Pinz, S., Grobner-Ferreira, R., Bruckmann, A., et al. (2017). CHD3 and CHD4 form distinct NuRD complexes with different yet overlapping functionality. *Nucl. Acids Res.* 45, 10534–10554. doi: 10.1093/nar/gkx711

Humphrey, G. W., Wang, Y., Russanova, V. R., Hirai, T., Qin, J., Nakatani, Y., et al. (2001). Stable histone deacetylase complexes distinguished by the presence of SANT domain proteins CoREST/kiaa0071 and Mta-L1. *J. Biol. Chem.* 276, 6817–6824. doi: 10.1074/jbc.m007372200

Ingram, K. G., Curtis, C. D., Silasi-Mansat, R., Lupu, F., and Griffin, C. T. (2013). The NuRD chromatin-remodeling enzyme CHD4 promotes embryonic vascular integrity by transcriptionally regulating extracellular matrix proteolysis. *PLoS Genet* 9:e1004031. doi: 10.1371/journal.pgen.1004031

Kaiser, R. A., Bueno, O. F., Lips, D. J., Doevendans, P. A., Jones, F., Kimball, T. F., et al. (2004). Targeted inhibition of p38 mitogen-activated

protein kinase antagonizes cardiac injury and cell death following ischemia-reperfusion in vivo. *J. Biol. Chem.* 279, 15524–15530. doi: 10.1074/jbc.m313717200

Kaiser, R. A., Lyons, J. M., Duffy, J. Y., Wagner, C. J., Mclean, K. M., O'neill, T. P., et al. (2005). Inhibition of p38 reduces myocardial infarction injury in the mouse but not pig after ischemia-reperfusion. *Am. J. Physiol. Heart Circ. Physiol.* 289, H2747–H2751.

Kannemeier, C., Shibamiya, A., Nakazawa, F., Trusheim, H., Ruppert, C., Markart, P., et al. (2007). Extracellular RNA constitutes a natural procoagulant cofactor in blood coagulation. *Proc. Natl. Acad. Sci. U S A.* 104, 6388–6393. doi: 10.1073/pnas.0608647104

Kawai, T., and Akira, S. (2006). TLR signaling. *Cell Death Differ.* 13, 816–825.

Khan, D. H., He, S., Yu, J., Winter, S., Cao, W., Seiser, C., et al. (2013). Protein kinase CK2 regulates the dimerization of histone deacetylase 1 (HDAC1) and HDAC2 during mitosis. *J. Biol. Chem.* 288, 16518–16528. doi: 10.1074/jbc.m112.440446

Kouzarides, T. (2007). Chromatin modifications and their function. *Cell* 128, 693–705. doi: 10.1016/j.cell.2007.02.005

Kumar, S., Boehm, J., and Lee, J. C. (2003). p38 map kinases: Key signalling molecules as therapeutic targets for inflammatory diseases. *Nat. Rev. Drug Discov.* 2, 717–726. doi: 10.1038/nrd1177

Landre, J. B., Hewett, P. W., Olivot, J. M., Friedl, P., Ko, Y., Sachinidis, A., et al. (2002). Human endothelial cells selectively express large amounts of pancreatic-type ribonuclease (RNase 1). *J. Cell Biochem.* 86, 540–552. doi: 10.1002/jcb.10234

Lee, J. C., Laydon, J. T., Mcdonnell, P. C., Gallagher, T. F., Kumar, S., Green, D., et al. (1994). A protein kinase involved in the regulation of inflammatory cytokine biosynthesis. *Nature* 372, 739–746. doi: 10.1038/372739a0

Lee, M. R., and Dominguez, C. (2005). MAP kinase p38 inhibitors: clinical results and an intimate look at their interactions with p38alpha protein. *Curr. Med. Chem.* 12, 2979–2994. doi: 10.2174/092986705774462914

Li, Q., Zong, Y., Li, K., Jie, X., Hong, J., Zhou, X., et al. (2019). Involvement of endothelial CK2 in the radiation induced perivascular resistant niche (PVRN) and the induction of radioresistance for non-small cell lung cancer (NSCLC) cells. *Biol. Res.* 52, 22.

Litchfield, D. W. (2003). Protein kinase CK2: structure, regulation and role in cellular decisions of life and death. *Biochem. J.* 369, 1–15. doi: 10.1042/bj20021469

Livak, K. J., and Schmittgen, T. D. (2001). Analysis of relative gene expression data using real-time quantitative PCR and the 2(T)(-Delta Delta C) method. *Methods* 25, 402–408. doi: 10.1006/meth.2001.1262

Ma, C. L., Wang, F., Han, B., Zhong, X. L., Si, F. S., Ye, J., et al. (2018). SALL1 functions as a tumor suppressor in breast cancer by regulating cancer cell senescence and metastasis through the NuRD complex. *Mole. Cancer* 17:78.

Meggio, F., and Pinna, L. A. (2003). One-thousand-and-one substrates of protein kinase CK2? *FASEB J.* 17, 349–368. doi: 10.1096/fj.02-0473rev

Micelli, C., and Rastelli, G. (2015). Histone deacetylases: structural determinants of inhibitor selectivity. *Drug Discov. Today* 20, 718–735. doi: 10.1016/j.drudis.2015.01.007

Miho, N., Ishida, T., Kuwaba, N., Ishida, M., Shimote-Abe, K., Tabuchi, K., et al. (2005). Role of the JNK pathway in thrombin-induced ICAM-1 expression in endothelial cells. *Cardiovasc. Res.* 68, 289–298. doi: 10.1016/j.cardiores.2005.05.029

Palacios, D., Mozzetta, C., Consalvi, S., Caretti, G., Saccone, V., Proserpio, V., et al. (2010). TNF/p38alpha/polycomb signaling to Pax7 locus in satellite cells links inflammation to the epigenetic control of muscle regeneration. *Cell Stem Cell* 7, 455–469. doi: 10.1016/j.stem.2010.08.013

Pluemsampant, S., Safronova, O. S., Nakahama, K., and Morita, I. (2008). Protein kinase CK2 is a key activator of histone deacetylase in hypoxia-associated tumors. *Int. J. Cancer* 122, 333–341. doi: 10.1002/ijc.23094

Pober, J. S., and Sessa, W. C. (2007). Evolving functions of endothelial cells in inflammation. *Nat. Rev. Immunol.* 7, 803–815. doi: 10.1038/nri2171

Poredos, P. (2002). Endothelial dysfunction and cardiovascular disease. *Pathophysiol. Haemost Thromb.* 32, 274–277.

Sayed, M., Kim, S. O., Salh, B. S., Issinger, O. G., and Pelech, S. L. (2000). Stress-induced activation of protein kinase CK2 by direct interaction with p38 mitogen-activated protein kinase. *J. Biol. Chem.* 275, 16569–16573. doi: 10.1074/jbc.m000312200

Segre, C. V., and Chiocca, S. (2011). Regulating the regulators: the post-translational code of class I HDAC1 and HDAC2. *J. Biomed. Biotechnol.* 2011:690848.

Sengupta, N., and Seto, E. (2004). Regulation of histone deacetylase activities. *J. Cell Biochem.* 93, 57–67. doi: 10.1002/jcb.20179

Shen, E., Wang, Q., Rabe, H., Liu, W., Cantor, H., and Leavenworth, J. W. (2018). Chromatin remodeling by the NuRD complex regulates development of follicular helper and regulatory T cells. *Proc. Natl. Acad. Sci. U S A.* 115, 6780–6785. doi: 10.1073/pnas.1805239115

Shimizu-Hirota, R., Xiong, W., Baxter, B. T., Kunkel, S. L., Maillard, I., Chen, X. W., et al. (2012). MT1-MMP regulates the PI3Kdelta.M*i*-2/NuRD-dependent control of macrophage immune function. *Genes Dev.* 26, 395–413. doi: 10.1101/gad.178749.111

Shin, E. Y., Kim, S. Y., and Kim, E. G. (2001). c-Jun N-terminal kinase is involved in motility of endothelial cell. *Exp. Mol. Med.* 33, 276–283. doi: 10.1038/emm.2001.45

Simsekyilmaz, S., Cabrera-Fuentes, H. A., Meiler, S., Kostin, S., Baumer, Y., Liehn, E. A., et al. (2014). Role of extracellular RNA in atherosclerotic plaque formation in mice. *Circulation* 129, 598–606. doi: 10.1161/circulationaha.113.002562

Singh, N. N., and Ramji, D. P. (2008). Protein kinase CK2, an important regulator of the inflammatory response? *J. Mol. Med.* 86, 887–897. doi: 10.1007/s00109-008-0352-0

Sitia, S., Tomasoni, L., Atzeni, F., Ambrosio, G., Cordiano, C., Catapano, A., et al. (2010). From endothelial dysfunction to atherosclerosis. *Autoimmun. Rev.* 9, 830–834.

Suelves, M., Lluis, F., Ruiz, V., Nebreda, A. R., and Munoz-Canoves, P. (2004). Phosphorylation of MRF4 transactivation domain by p38 mediates repression of specific myogenic genes. *EMBO J.* 23, 365–375. doi: 10.1038/sj.emboj.7600056

Suganuma, T., and Workman, J. L. (2011). Signals and combinatorial functions of histone modifications. *Annu. Rev. Biochem.* 80, 473–499. doi: 10.1146/annurev-biochem-061809-175347

Sun, J. M., Chen, H. Y., and Davie, J. R. (2007). Differential distribution of unmodified and phosphorylated histone deacetylase 2 in chromatin. *J. Biol. Chem.* 282, 33227–33236. doi: 10.1074/jbc.m703549200

Tong, J. K., Hassig, C. A., Schnitzler, G. R., Kingston, R. E., and Schreiber, S. L. (1998). Chromatin deacetylation by an ATP-dependent nucleosome remodelling complex. *Nature* 395, 917–921. doi: 10.1038/27699

Tsai, S. C., and Seto, E. (2002). Regulation of histone deacetylase 2 by protein kinase CK2. *J. Biol. Chem.* 277, 31826–31833. doi: 10.1074/jbc.m204149200

Viemann, D., Goebeler, M., Schmid, S., Klimmek, K., Sorg, C., Ludwig, S., et al. (2004). Transcriptional profiling of IKK2/NF-kappa B- and p38 MAP kinase-dependent gene expression in TNF-alpha-stimulated primary human endothelial cells. *Blood* 103, 3365–3373. doi: 10.1182/blood-2003-09-3296

Walberer, M., Tschernatsch, M., Fischer, S., Ritschel, N., Volk, K., Friedrich, C., et al. (2009). RNase therapy assessed by magnetic resonance imaging reduces cerebral edema and infarction size in acute stroke. *Curr. Neurovasc. Res.* 6, 12–19. doi: 10.2174/156720209787466037

Wang, Z., Zang, C., Rosenfeld, J. A., Schones, D. E., Barski, A., Cuddapah, S., et al. (2008). Combinatorial patterns of histone acetylations and methylations in the human genome. *Nat. Genet* 40, 897–903. doi: 10.1038/ng.154

Weber, A., Wasiliew, P., and Kracht, M. (2010). Interleukin-1 (IL-1) pathway. *Sci. Signal.* 3:cm1. doi: 10.1126/scisignal.3105cm1

Yang, X. J., and Seto, E. (2008). The Rpd3/Hda1 family of lysine deacetylases: from bacteria and yeast to mice and men. *Nat. Rev. Mol. Cell Biol.* 9, 206–218. doi: 10.1038/nrm2346

You, A., Tong, J. K., Grozinger, C. M., and Schreiber, S. L. (2001). CoREST is an integral component of the CoREST- human histone deacetylase complex. *Proc. Natl. Acad. Sci. U S A.* 98, 1454–1458. doi: 10.1073/pnas.98.4.1454

Zakrzewicz, D., Bergmann, S., Didiasova, M., Giaimo, B. D., Borggrefe, T., Mieth, M., et al. (2016). Host-derived extracellular RNA promotes adhesion of Streptococcus pneumoniae to endothelial and epithelial cells. *Sci. Rep.* 6:37758.

Zechendorf, E., O'riordan, C. E., Stiehler, L., Wischmeyer, N., Chiazza, F., Collotta, D., et al. (2020). Ribonuclease 1 attenuates septic cardiomyopathy and cardiac apoptosis in a murine model of polymicrobial sepsis. *JCI Insig.* 5:e131571.

Zernecke, A., and Preissner, K. T. (2016). Extracellular Ribonucleic Acids (RNA) Enter the Stage in Cardiovascular Disease. *Circ. Res.* 118, 469–479. doi: 10.1161/circresaha.115.307961

Zhang, Q., and Steinle, J. J. (2014). IGFBP-3 inhibits TNF-alpha production and TNFR-2 signaling to protect against retinal endothelial cell apoptosis. *Microvasc. Res.* 95, 76–81. doi: 10.1016/j.mvr.2014.07.009

Zhang, Y., Iratni, R., Erdjument-Bromage, H., Tempst, P., and Reinberg, D. (1997). Histone deacetylases and SAP18, a novel polypeptide, are components of a human Sin3 complex. *Cell* 89, 357–364. doi: 10.1016/s0092-8674(00)80216-0

Zhao, M., Liu, Y. W., Wang, X. F., New, L. G., Han, J. H., and Brunk, U. T. (2002). Activation of the p38 MAP kinase pathway is required for foam cell formation from macrophages exposed to oxidized LDL. *APMIS* 110, 458–468. doi: 10.1034/j.1600-0463.2002.100604.x

Conflict of Interest: The authors declare that the research was conducted in the absence of any commercial or financial relationships that could be construed as a potential conflict of interest.

frontiers in Physiology

ORIGINAL RESEARCH
published: 06 November 2020
doi: 10.3389/fphys.2020.576736

RNase A Treatment Interferes With Leukocyte Recruitment, Neutrophil Extracellular Trap Formation, and Angiogenesis in Ischemic Muscle Tissue

Manuel Lasch[1,2,3], Konda Kumaraswami[1,2], Simona Nasiscionyte[1], Susanna Kircher[1,2], Dominic van den Heuvel[1], Sarah Meister[4], Hellen Ishikawa-Ankerhold[1,5†] and Elisabeth Deindl[1,2†]*

[1]Walter-Brendel-Centre of Experimental Medicine, University Hospital, Ludwig-Maximilians-Universität München, Munich, Germany, [2]Biomedical Center, Institute of Cardiovascular Physiology and Pathophysiology, Ludwig-Maximilians-Universität München, Munich, Germany, [3]Department of Otorhinolaryngology, Head and Neck Surgery, University Hospital, Ludwig-Maximilians-Universität München, Munich, Germany, [4]Department of Obstetrics and Gynaecology, University Hospital, Ludwig-Maximilians-Universität München, Munich, Germany, [5]Department of Internal Medicine I, Faculty of Medicine, University Hospital, Ludwig-Maximilians-Universität München, Munich, Germany

OPEN ACCESS

Edited by:
Ritva Tikkanen, University of Giessen, Germany

Reviewed by:
Oliver Baum, Charité – Universitätsmedizin Berlin, Germany
Ebba Brakenhielm, Institut National de la Santé et de la Recherche Médicale (INSERM), France

***Correspondence:**
Elisabeth Deindl
elisabeth.deindl@med.uni-muenchen.de

[†]These authors have contributed equally to this work

Specialty section:
This article was submitted to Vascular Physiology, a section of the journal Frontiers in Physiology

Received: *26 June 2020*
Accepted: *16 October 2020*
Published: *06 November 2020*

Citation:
Lasch M, Kumaraswami K, Nasiscionyte S, Kircher S, van den Heuvel D, Meister S, Ishikawa-Ankerhold H and Deindl E (2020) RNase A Treatment Interferes With Leukocyte Recruitment, Neutrophil Extracellular Trap Formation, and Angiogenesis in Ischemic Muscle Tissue. Front. Physiol. 11:576736. doi: 10.3389/fphys.2020.576736

Background: RNase A (the bovine equivalent to human RNase 1) and RNase 5 (angiogenin) are two closely related ribonucleases. RNase 5 is described as a powerful angiogenic factor. Whether RNase A shares the same angiogenic characteristic, or interferes with vessel growth as demonstrated for arteriogenesis, has never been investigated and is the topic of this present study.

Methods and Results: To investigate whether RNase A shows a pro- or anti-angiogenic effect, we employed a murine hindlimb model, in which femoral artery ligation (FAL) results in arteriogenesis in the upper leg, and, due to provoked ischemia, in angiogenesis in the lower leg. C57BL/6J male mice underwent unilateral FAL, whereas the contralateral leg was sham operated. Two and seven days after the surgery and intravenous injection of RNase A (50 μg/kg dissolved in saline) or saline (control), the gastrocnemius muscles of mice were isolated from the lower legs for (immuno-) histological analyses. Hematoxylin and Eosin staining evidenced that RNase A treatment resulted in a higher degree of ischemic tissue damage. This was, however, associated with reduced angiogenesis, as evidenced by a reduced capillary/muscle fiber ratio. Moreover, RNase A treatment was associated with a significant reduction in leukocyte infiltration as shown by $CD45^+$ (pan-leukocyte marker), $Ly6G^+$ or MPO^+ (neutrophils), $MPO^+/CitH_3^+$ [neutrophil extracellular traps (NETs)], and $CD68^+$ (macrophages) staining. CD68/MRC1 double staining revealed that RNase A treated mice showed a reduced percentage of M1-like polarized ($CD68^+/MRC1^-$) macrophages whereas the percentage of M2-like polarized ($CD68^+/MRC1^+$) macrophages was increased.

Conclusion: In contrast to RNase 5, RNase A interferes with angiogenesis, which is linked to reduced leukocyte infiltration and NET formation.

Keywords: angiogenesis, capillary sprouting, RNase A, RNase 5, extracellular RNA, leukocyte recruitment, ischemia, neutrophil extracellular traps

INTRODUCTION

The human superfamily of ribonucleases (RNases) consists of eight members of secreted proteins, which share the ability to degrade RNA (Koczera et al., 2016). RNase A (the bovine equivalent to the human RNase 1) is one of the best-characterized mammalian proteins (Raines, 1998). According to their structural and biological or catalytic characteristics, the RNases have been grouped into four RNase types, whereby RNase 1, 4, and 5 have been grouped together (Sorrentino, 2010). RNase 5 shows high similarities to RNase A in its crystal structure and contains several identical catalytic residues, although its ribonucleolytic activity is much lower (Acharya et al., 1994; Leonidas et al., 1999; Leland et al., 2002).

Studies on their molecular evolution indicated that ancestral RNases were involved in host defense (zebrafish) or angiogenesis-related processes (birds and mammals; Sorrentino, 2010; Koczera et al., 2016). Interestingly, RNase 1 has been suggested to be involved in the regulation of vascular homeostasis (Landre et al., 2002; Fischer et al., 2011) and has been demonstrated to negatively influence coagulation and vascular permeability (Fischer et al., 2007; Kannemeier et al., 2007). Both, RNase 1 and RNase 5 are expressed and released from various types of endothelial cells (from arteries, veins, and capillaries; Landre et al., 2002; Fischer et al., 2011), and RNase 5, also termed angiogenin, is well described for its angiogenic activity (Fett et al., 1985; Strydom et al., 1985) as reviewed in detail by Gao and Xu (2008) as well as Sorrentino (2010). By complex formation with the cell surface protein actin, RNase 5 promotes basement membrane and extracellular matrix degradation, thus enabling endothelial cells to penetrate and migrate into the perivascular tissue (Soncin, 1992). Following translocation to the nucleus, the nuclear fraction of RNase 5 binds to the promoter of ribosomal RNA (rRNA), thereby enhancing its transcription and promoting endothelial cell proliferation (Kishimoto et al., 2005). In addition to its function to enhance angiogenesis, RNase 5 has also been reported to cleave transfer RNA (tRNA) to tRNA-derived small RNAs (tiRNAs) under conditions of stress, causing protein synthesis arrest, thus conserving energy for repair of damaged tissue (Fu et al., 2009; Yamasaki et al., 2009).

Angiogenesis is a complex process resulting in increased capillarity. This is either mediated by splitting of pre-existing capillaries (Egginton et al., 2001) or by sprouting of capillaries from pre-existing vasculature involving endothelial cell proliferation and migration (Carmeliet, 2000). Hypoxia and ischemia are well described as driving force for sprouting angiogenesis, however, there are also data available pointing to shear stress as stimulus for splitting angiogenesis (Egginton et al., 2001). In general, angiogenesis is designed to locally satisfy the oxygen and nutrient demand of tissue under various (patho-)physiological conditions (Adams and Alitalo, 2007; Potente and Carmeliet, 2017) such as embryonic development (Carmeliet, 2005), tumor growth (Folkman, 1995), wound healing (Tonnesen et al., 2000), or skeletal or cardiac muscle hypertrophy (Hudlicka et al., 1992). However, in damaged ischemic tissue, it is also engaged in removal of cell debris (Weckbach et al., 2018).

Vascular endothelial growth factor (VEGF) is one of the strongest and best characterized angiogenetic factors (Folkman, 1971; Folkman et al., 1971; Ferrara and Henzel, 1989; Neufeld et al., 1999). It has been demonstrated that administration of VEGF is a powerful tool to promote sprouting angiogenesis *in vivo* and even results in angioma formation (Isner et al., 1996; Tsurumi et al., 1997; Schwarz et al., 2000). Arteriogenesis, the growth of a natural bypass from pre-existing arteriolar connections (Deindl and Schaper, 2005), however, could hardly if at all be promoted by VEGF administration (Jazwa et al., 2016). On the other hand, blocking the tyrosine kinase (TK) VEGF receptor 2 (VEGFR2) strongly interfered with both, the process of angiogenesis and arteriogenesis (Jazwa et al., 2016). In both types of vessel growth, VEGF is supplied by leukocytes, i.e., neutrophils and monocytes (Deindl et al., 2001; Scapini et al., 2004; Morrison et al., 2014; Lautz et al., 2018; Zhang et al., 2020). But in contrast to angiogenesis, in arteriogenesis, an amplified and sustained local activation of VEGFR2 is necessary to promote endothelial cell proliferation by high levels of ERK activation (Kofler and Simons, 2015). The sustained activation of VEGFR2 is mediated by the non-TK VEGF receptor neuropilin 1 (NRP1; Koch et al., 2011; Lanahan et al., 2013; Kofler and Simons, 2015). Recently, it was demonstrated by Fischer et al. (2009) *in vitro* that the interaction of VEGF with VEGFR2 and NRP1 is mediated by extracellular RNA. For angiogenesis, it is described that the interaction of VEGF with VEGFR2 and NRP1 is essential for tip cell formation to allow a sprouting of endothelial cells (Kofler and Simons, 2015).

RNA, which is mainly composed of rRNA is released under various conditions, such as tissue damage, stress, and accordingly also increased shear stress from (endothelial-) cells (Lasch et al., 2019a). Recently, we demonstrated that arteriogenesis, which is triggered by increased shear stress (Pipp et al., 2004; Lasch et al., 2019b), is initiated by extracellular RNA, which is released from endothelial cells due to increased shear stress (Lasch et al., 2019a). In arteriogenesis, extracellular RNA induces a sustained activation of VEGFR2 provoking the release of von Willebrand factor (vWF) from endothelial cells. This initiates a cascade of signaling events, which involves an activation of platelets and mast cells. As a result, neutrophils and monocytes are recruited, which promote vessel growth by supplying growth factor and cytokines (Chandraratne et al., 2015; Chillo et al., 2016; Kluever et al., 2019; Lasch et al., 2019a). Interestingly, administration of bovine RNase A as well as recombinant human RNase 1 significantly interfered with the process of arteriogenesis and leukocyte recruitment, whereas the administration of inactive human recombinant RNase or DNase had no effect pointing to the relevance of extracellular RNA in arteriogenesis (Lasch et al., 2019a).

RNase A and RNase 5 are two closely related ribonucleases (Gao and Xu, 2008; Sorrentino, 2010). Accordingly, we were interested to investigate whether RNase A shows a similar pro-angiogenic effect as previously described for RNase 5 (Gao and Xu, 2008), or whether it interferes with the process of angiogenesis as demonstrated for arteriogenesis (Lasch et al., 2019a). For our purpose, we used the same mouse model, which we employed to investigate the effect of RNase A treatment on arteriogenesis (Lasch et al., 2019a). In that model, femoral

artery ligation (FAL) results due to increased shear stress in arteriogenesis in the upper leg and due to ischemia in angiogenesis in the lower leg (**Figure 1**). Whether shear stress is also involved in promoting angiogenesis in that particular animal model has never been investigated but cannot be excluded.

MATERIALS AND METHODS

Animals and Treatments

All experimental procedures were permitted by the Bavarian Animal Care and Use Committee (ethical approval code: ROB-55.2Vet-2532.Vet_02-17-99) and were done in strict accordance with the German animal legislation guidelines. To degrade extracellular RNA, wild type C57BL/6J mice (Charles River Laboratories, Sulzfeld, Germany) were injected i.v. with bovine RNase A (Thermo Fisher Scientific, Waltham, MA, United States) with a dose of 50 μg/kg dissolved in saline starting 30 min before the surgical procedure and followed every other day until tissue sampling. The control group received saline alone.

Femoral Artery Ligation and Tissue Sampling

To induce angiogenesis, 8–10 weeks old mice were initially anesthetized with a combination of fentanyl (0.05 mg/kg, CuraMED Pharma, Karlsruhe, Germany), midazolam (5.0 mg/kg, Ratiopharm GmbH, Ulm, Germany), and medetomidine (0.5 mg/kg, Pfister Pharma, Berlin, Germany). Once anesthetized, the mice were submitted to an unilateral FAL of the right hindlimb, while the left hindlimb was sham operated as previously described (Limbourg et al., 2009; Lasch et al., 2019b). For tissue sampling 2 or 7 days after the surgical procedure, mice were anesthetized as described above and were perfused with adenosine buffer [1% adenosine (Sigma-Aldrich, St. Louis, MO, United States), 5% bovine serum albumin (BSA, Sigma-Aldrich), dissolved in phosphate buffered saline (PBS, PAN Biotech, Aidenbach, Germany, pH 7.4)] followed by a perfusion with 3% paraformaldehyde (PFA, Merck, Darmstadt, Germany; for cryopreservation), or 4% PFA (for paraffin embedding) in PBS, pH 7.4. After the perfusion, the gastrocnemius muscles were carefully isolated and stored for further processing.

Histology and Immunohistology

Mice ($n \geq 3$ per group) were injected (i.p.) daily with BrdU (Sigma-Aldrich; 1.25 mg dissolved in 100 μl PBS) starting directly after FAL. BrdU-treated tissue isolated at day 7 after the surgical procedure was cut in 8–10 μm thick cryosections and was processed with 1 N HCl for 30 min at 37°C, blocked with 10% goat serum in 1x PBS/0.1% Tween-20 for 1 h at room temperature (RT), followed by an overnight incubation

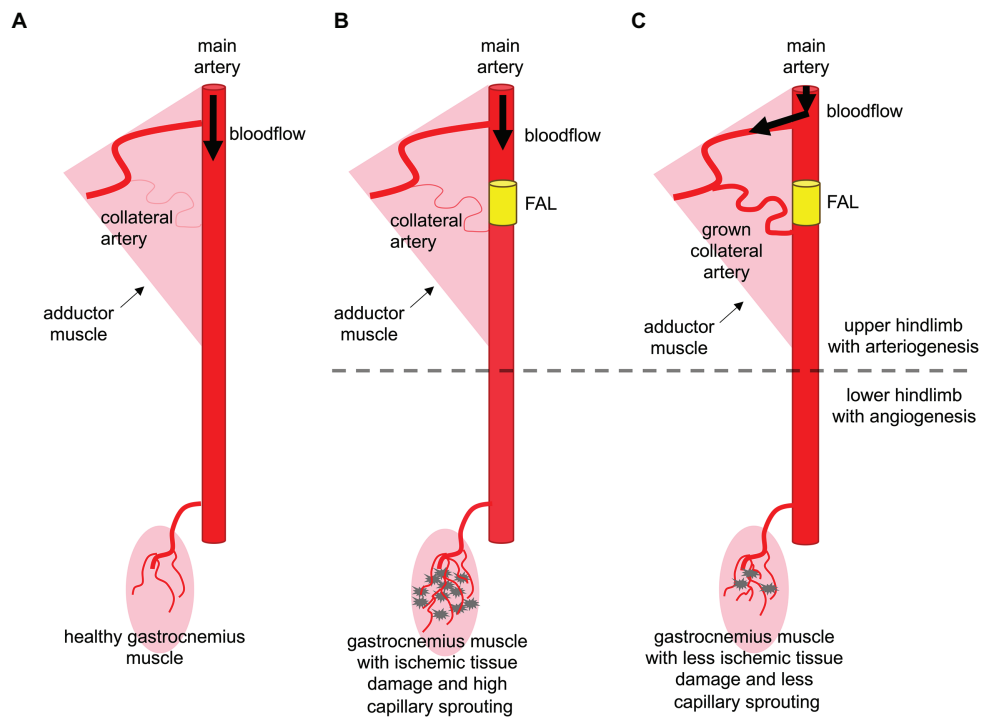

FIGURE 1 | Arteriogenesis in the thigh protects the gastrocnemius muscle from serve ischemic damage. **(A)** Arterial blood vessels have the function to supply organs and muscle tissue with oxygen and nutrients. In the murine hindlimb, the femoral artery supplies blood to the lower leg. **(B)** Upon arterial obstruction due to stenosis or artificial femoral artery ligation (FAL), muscles of the lower leg, such as the gastrocnemius muscle, suffer from ischemia, which leads to tissue damage and capillary sprouting (angiogenesis). **(C)** Effective collateral artery growth (arteriogenesis) in the thigh compensating the occluded (femoral) artery prevents severe ischemic tissue damage in the lower leg and makes capillary sprouting redundant.

with an anti-BrdU antibody (Abcam, ab6326; dilution 1:50 in 10% goat serum in 1x PBS/0.1% Tween-20) at 4°C. Secondary staining was performed with a goat anti-rat Alexa Fluor®-546 antibody or an Alexa Fluor®-647 antibody (both Invitrogen, Thermo Fisher Scientific, dilution 1:100) for 1 h at RT. Further, the tissues were stained with an anti-CD31-Alexa Fluor®-647 antibody (1:50; clone MEC13.3, Biolegend, 102,516) or an anti-CD45-Alexa Fluor®-488 antibody (clone 30-F11, BioLegend, 11-0451-85; dilution 1:100, both in 1x PBS/0.1% Tween-20) for 3 h at RT to stain endothelial cells and leukocytes, respectively. Pericytes were stained with an anti-ACTA2-Alexa Fluor®-488 antibody (Sigma-Aldrich, F3777) 1:400 dilution in 1x PBS/0.1% Tween-20. For neutrophil labeling, a rat anti-Ly6G antibody (Abcam, ab25377; 1:100) was added overnight at 4°C and a secondary Alexa Fluor®-488 goat anti-rat antibody (Invitrogen, Thermo Fisher Scientific) 1:200 in 1x PBS for 1 h. We have also followed this staining with an anti-Ly6G-PE antibody (eBioscience, 12-9668-82, Thermo Fisher Scientific) to eliminate any unspecific labeling. Macrophages were labeled with an anti-CD68-Alexa Fluor®-488 antibody (Abcam ab201844; dilution 1:50) together with an anti-MRC1 antibody (Abcam, ab64693; dilution 1:50) overnight 4°C, followed by the secondary antibodies: Alexa Fluor®-488 goat anti-rat and Alexa-Fluor®-594 goat anti-rabbit, respectively (both Invitrogen, Thermo Fisher Scientific). Neutrophil extracellular traps (NETs) of day 2 post-FAL tissues were labeled with an anti-myeloperoxidase (MPO) antibody (R and D Systems, AF3667) and an anti-citrullinated histone H3 antibody [Cit-H3; polyclonal rabbit anti-Histone H3 antibody (citrulline R2 + R8 + R17), Abcam, ab5103] by an overnight incubation at 4°C. This was followed by a secondary donkey anti-goat Alexa Fluor®-594 antibody (1:100) and Alexa Fluor®-488 antibody (1:200; both Invitrogen, Thermo Fisher Scientific) for 1 h at RT. Additionally, to label nucleic DNA, tissues were incubated with 1 µg/ml Hoechst 33342 (Invitrogen) for 15 min at RT. For mounting the samples, an antifade mounting medium (Dako) was used. Tissue muscle sections from saline and RNase A treated mice (3x saline treated non-ischemic, 3x saline treated ischemic, 3x RNase A treated non-ischemic, and 3x RNaseA treated ischemic) were stained for different leukocyte populations (neutrophils and macrophages) and NETs. We counted cells, muscle fibers, and NETs in 10 defined fields of view with a 20x objective (415 × 415 µm), resulting in a total area of 172,225 mm^2. To investigate angiogenesis (**Figure 2C**), the capillary to muscle fiber ratio for each group was calculated as previously described (Olfert et al., 2016), whereby $CD31^+$/$ACTA2^-$ were considered as endothelial cells. The images were acquired with a confocal laser scanning microscope LSM 880 from (Carl Zeiss AG) and analyzed by ZEN Blue software (Carl Zeiss AG).

Hematoxylin and Eosin (H and E) staining on slices of 5 µm thick paraffin embedded gastrocnemius muscles isolated from RNase A and saline treated mice ($n = 5$) at day 7 after surgery was done according to standard procedures. The necrotic area (%) of the whole tissue slices was analyzed using an Axioscope 40 (Carl Zeiss AG) with the AxioVision software (Carl Zeiss AG).

Statistical Analyses

Statistical analyses were carried out using GraphPad Prism 6 (GraphPad Software, La Jolla, CA, United States). Data are means ± standard error of the mean (S.E.M.). Statistical analyses were performed as indicated in the figure legends and considered as statistically significant at $p < 0.05$.

RESULTS

In order to investigate the impact of RNase A on angiogenesis, we used a murine hindlimb model, in which FAL results in arteriogenesis in the upper leg (adductor muscle) and due to provoked ischemia in angiogenesis in the lower leg (gastrocnemius muscle; **Figure 1**; Lasch et al., 2019a). Mice were treated intravenously before and then after the surgical procedure every other day with RNase A or saline (control). At day 2 and 7 after the surgical procedure, the gastrocnemius muscles of femoral artery ligated and contralateral sham operated legs were isolated for (immuno-) histological analyses.

Hematoxylin and Eosin staining demonstrated ischemic damage in gastrocnemius muscles of RNase A and of saline treated mice at day 7 after FAL. However, compared to the saline-treated controls, the ischemic tissue damage in gastrocnemius muscles was significantly increased in RNase A treated mice (**Figures 2A,B** and **Supplementary Table 1**).

To investigate whether RNase A treatment has an impact on angiogenesis, we performed immunofluorescence staining using an anti-CD31 antibody as a marker for endothelial cells, in combination with an antibody against ACTA2 to exclude $CD31^+$ pericytes. Calculating the capillary/muscle fiber ratio as index for angiogenesis, we found a significant reduction of the capillary/muscle fiber ratio in gastrocnemius muscles of RNase A treated mice at day 7 after the surgical intervention when compared to saline treated control mice (**Figures 2C,D** and **Supplementary Table 2**). The number of proliferating endothelial cells per muscle fiber was also strongly reduced in RNase A treated mice as shown by $CD31^+$/$BrdU^+$/$ACTA2^-$/$Hoechst^+$ quadruple staining (**Figure 2D**; **Supplementary Figure 1** and **Supplementary Table 2**).

Leukocytes, such as neutrophils and macrophages, are well described for their relevance to remove cell debris and to promote angiogenesis by supplying growth factors, and particularly VEGF (Scapini et al., 2004; Zhang et al., 2020). To investigate the influence of RNase A treatment on leukocyte recruitment, we performed CD45 (pan-leukocyte marker) staining. Our results demonstrated that RNase A treated mice have a significant decreased number of $CD45^+$ cells in ischemic tissue compared to saline treated control mice at day 7 after the surgical intervention (**Figures 3A,B** and **Supplementary Table 2**). In both treatments, only minor numbers of $CD45^+$/$BrdU^+$ double positive cells were found (**Supplementary Figure 2**).

Ly6G stain used to identify neutrophils and CD68 to identify macrophages showed moreover that both subsets of leukocytes were significantly decreased in ischemic muscle tissue of mice treated with RNase A compared to saline

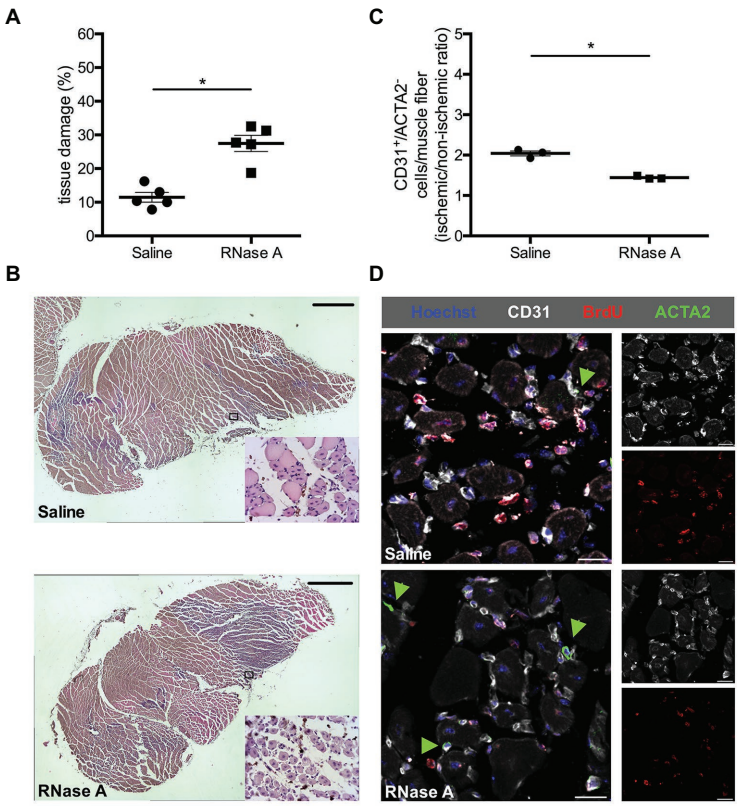

FIGURE 2 | RNase A treatment results in decreased angiogenesis and increased tissue damage. **(A)** The scatter plot shows the percentage of tissue damage in the gastrocnemius muscle of mice treated with RNase A or saline (control group) 7 days after FAL. Data are means ± S.E.M., $n = 5$ per group, the whole cross-sectional area of the gastrocnemius muscle was analyzed per mouse. *$p < 0.05$ (RNase A vs. saline treated group) by unpaired student's t-test. **(B)** Representative pictures of analyzed H and E stained gastrocnemius muscle of saline- (upper picture) or RNase A (lower picture) treated mice 7 days after FAL. After treatment with bovine RNase A, significant increased tissue damage can be seen becoming evident e.g., by skeletal muscle cells showing centralized nuclei (small magnifications right bottom). Scale bars 100 μm. **(C)** The scatter plot shows the $CD31^+/ACTA2^-$ cells per muscle fiber (ischemic vs. non-ischemic tissue ratio, respectively) in the gastrocnemius muscle of RNase A or saline treated mice 7 days after the surgical procedure. Data are means ± S.E.M., $n = 3$ per group, 10 cross-sectional areas (450 μm × 450 μm each) of the gastrocnemius muscle were analyzed per mouse per leg. *$p < 0.05$ (RNase A vs. saline treated group) by unpaired student's t-test. **(D)** Representative immunofluorescence pictures of analyzed gastrocnemius muscle tissue of saline- (upper picture) or RNase A treatment (lower picture) 7 days after FAL. Endothelial cells were labeled with anti-CD31 (gray), with anti-BrdU 546 (red), and Hoechst (blue). Pericytes, in addition, were labeled with anti-ACTA2 (green, and indicated by green arrowheads). Scale bars 20 μm.

treated control mice at day 7 after the surgery (**Figures 3C,D, 4A** and **Supplementary Table 2**).

To investigate whether RNase A treatment influences macrophage activation in ischemic tissue in terms of M1-like and M2-like polarization, we performed CD68/MRC1 double staining. Our immuno-histological analyses showed that the percentage of classically activated inflammatory $CD68^+/MRC1^-$ macrophages (M1-like) in gastrocnemius muscles of RNase A treated mice was significantly decreased, while the percentage of alternatively activated regenerative $CD68^+/MRC1^+$ macrophages (M2-like) was significantly increased compared to saline treated control mice (**Figures 4B–D** and **Supplementary Table 2**).

In gastrocnemius muscle samples isolated at day 2 after the surgery and RNase A or saline treatment, we have used MPO staining for neutrophil identification combined with CitH3 for NETs. As a criteria for NETs, we have considered three aspects: (i) the presence of extracellular DNA filamentary structure, (ii) the DNA should originate from MPO positive cells, and (iii) these filamentary structures have to be decorated with a marker for neutrophil granule proteins like Cit-H3 (**Figures 5C,D**). As shown in **Figure 5**, the numbers of neutrophils (MPO^+ cells) and NETs ($MPO^+/CitH3^+/Hoechst^+$ cells) are reduced in ischemic gastrocnemius muscles from RNase A treated mice compared to saline treated mice (**Figures 5A,B** and **Supplementary Table 2**).

DISCUSSION

In the current study, we investigated the impact of RNase A, an enzyme closely related to RNase 5, on angiogenesis. Our results demonstrate that RNase A, in contrast to RNase 5, shows anti-angiogenic effects, which is related to reduced leukocyte recruitment and NET formation.

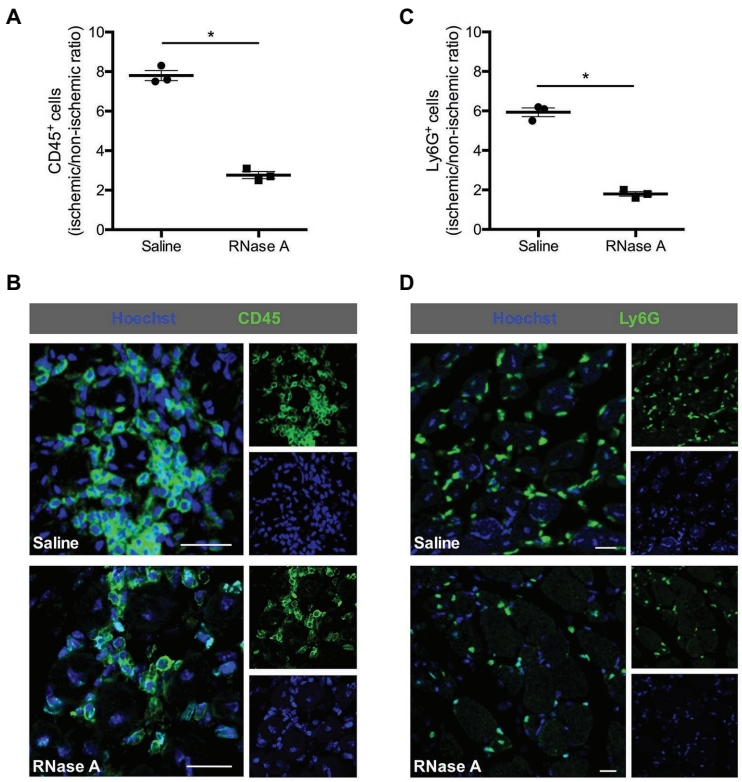

FIGURE 3 | RNase A treatment interferes with leukocyte recruitment. The scatter plots show the ratio of **(A)** total CD45$^+$ cells or **(C)** total Ly6G$^+$ cells (neutrophils; FAL vs. sham operation or ischemic vs. non-ischemic tissue, respectively) in the gastrocnemius muscle of RNase A or saline treated mice 7 days after the surgery. Data are means ± S.E.M., $n = 3$ per group, 10 cross-sectional areas (450 μm × 450 μm each) of the gastrocnemius muscle were analyzed per mouse per leg. *$p < 0.05$ (RNase A vs. saline treated group) by unpaired student's t-test. **(B,D)** Representative immunofluorescence pictures of analyzed gastrocnemius tissue of saline- (upper picture) or RNase A (lower picture) treated mice 7 days after FAL. Leukocytes were labeled with **(B)** anti-CD45 (pan-leukocyte marker) or **(D)** anti-Ly6G (marker for neutrophils; both green) and Hoechst (blue). Scale bars 20 μm.

RNase A, like its human counterpart RNase 1 as well as RNase 5 belongs to the RNase A superfamily (Beintema, 1998). RNase 5 shows about 35% homology to the human RNase 1 with conserved amino acid residues relevant for the RNase activity (Kurachi et al., 1985). However, the ribonucleic activity of RNase 5 is about 10^5–10^6 lower than that of the pancreatic RNase A (Gao and Xu, 2008). It has previously been shown that RNase 5, also known as angiogenin, is a potent angiogenic factor (Kurachi et al., 1985). Whether RNase A shows similar functions in terms of promoting angiogenesis as RNase 5, or whether it interferes with vessel growth as we have recently demonstrated for the process of arteriogenesis (Lasch et al., 2019a), has never been investigated.

To analyze the impact of RNase A on angiogenesis, we employed the same murine hindlimb model, in which we have previously demonstrated that the administration of RNase A interferes with arteriogenesis by degrading extracellular RNA. Extracellular RNA is a ribonucleic acid, which is essential for initiating the process of natural bypass growth (Lasch et al., 2019a). As depicted in **Figure 1**, ligation of the femoral artery results in reduced blood supply and consequently causes tissue fibrosis and gangrene formation in the lower leg. This is associated with angiogenesis and a pronounced infiltration of leukocytes (Scapini et al., 2004; Jaipersad et al., 2014; Chillo et al., 2016; Zhang et al., 2020). In case of effective collateral artery growth, creating a natural bypass, a less severe ischemic tissue damage is observed in muscle tissue of the lower leg. However, in the case of impaired arteriogenesis, as shown before as an effect of RNase A (Lasch et al., 2019a), ischemic tissue damage is expected to increase. This was confirmed by our present histological studies, which demonstrate increased ischemic damage in the gastrocnemius muscle of mice treated with RNase A. Pancreatic RNase 1 has no cytotoxic side-effects (Gaur et al., 2001), and, although no receptors for RNases have been identified up to now (Schirrmann et al., 2009), these enzymes may indeed enter cells by endocytosis (Haigis and Raines, 2003). RNases, however, are quickly inactivated by the cytosolic RNase Inhibitor (Leland et al., 1998; Haigis et al., 2003), which binds extremely tightly to mammalian RNases and, thereby, blocks their catalytic activity (Leland et al., 1998; Leland and Raines, 2001; Haigis et al., 2003; Arnold and Ulbrich-Hofmann, 2006; Schirrmann et al., 2009). Moreover, we have recently demonstrated that RNase A application is not

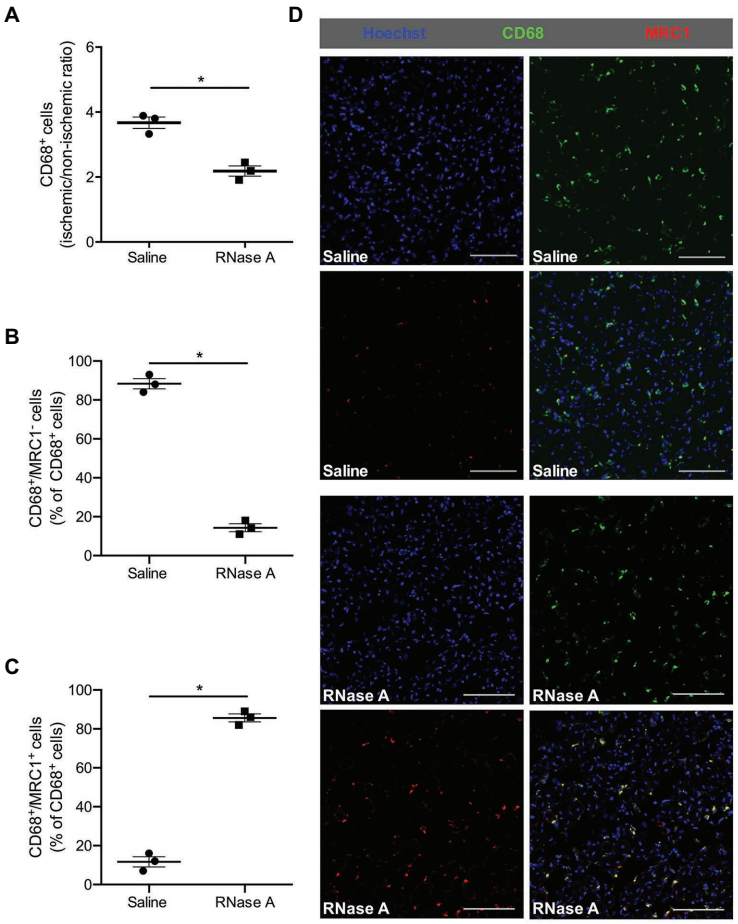

FIGURE 4 | The effect of bovine RNase A on macrophage recruitment and polarization. The scatter plots show the ratio (ischemic vs. non-ischemic tissue) of **(A)** total CD68⁺ cells and the percentage of **(B)** CD68⁺/MRC1⁻ and of **(C)** CD68⁺/MRC1⁺ cells of all CD68⁺ cells in the gastrocnemius muscle of RNase A or saline treated mice 7 days after the surgical procedure. Data are means ± S.E.M., $n = 3$ per group, 10 cross-sectional areas (450 μm × 450 μm each) of the gastrocnemius muscle were analyzed per mouse per leg. $^*p < 0.05$ (RNase A vs. saline treated group) by unpaired student's *t*-test. **(D)** Representative immunofluorescence pictures of analyzed gastrocnemius tissue of saline- (upper picture) or RNase A (lower picture) treated mice 7 days after FAL. Scale bars 100 μm.

associated with any toxic side effects, even when 20-fold overdosed (Kleinert et al., 2016).

Increased ischemic damage is expected to be associated with increased angiogenesis (Chillo et al., 2016). However, our immuno-histological analyses showed that ischemic tissue damage in RNase A treated mice is associated with reduced angiogenesis along with reduced endothelial cell proliferation. Leukocytes, particularly neutrophils and monocytes, which are recruited to ischemic tissue, are an important source of VEGF, which is one of the most powerful angiogenic factors (Gong and Koh, 2010; Seignez and Phillipson, 2017; Zhang et al., 2020). In our study, we found a high number of leukocytes in ischemic damaged tissue, however, the number of BrdU positive and thus proliferating leukocytes was very low in saline as well as RNase A treated mice. This is in accordance with a recent study in a murine hindlimb model showing that not resident, proliferating leukocytes, but recruited leukocytes are responsible for increased numbers of immune cells in ischemic muscle tissue (Zhang et al., 2020). We show that in RNase A treated mice the number of leukocytes was significantly reduced in ischemic tissue when compared to saline treated mice indicating that RNase A treatment interferes with leukocyte recruitment to ischemic tissue, and thus may affect VEGF bioavailability.

Using a murine cremaster model of inflammation, we have recently shown by means of intravital microscopy analyses that extracellular RNA acts as pro-inflammatory factor by promoting leukocyte recruitment (Fischer et al., 2012). In the same model as well as in the murine hindlimb model of arteriogenesis, which we used for our current study on angiogenesis, we have demonstrated that extracellular RNA mediated leukocyte recruitment is dependent on VEGFR2 activation (Lasch et al., 2019a). In detail, extracellular RNA promotes the interaction of VEGF with NRP1 and VEGFR2, thus inducing a sustained local activation of VEGFR2, which results in vWF release from endothelial cells (Fischer et al., 2009;

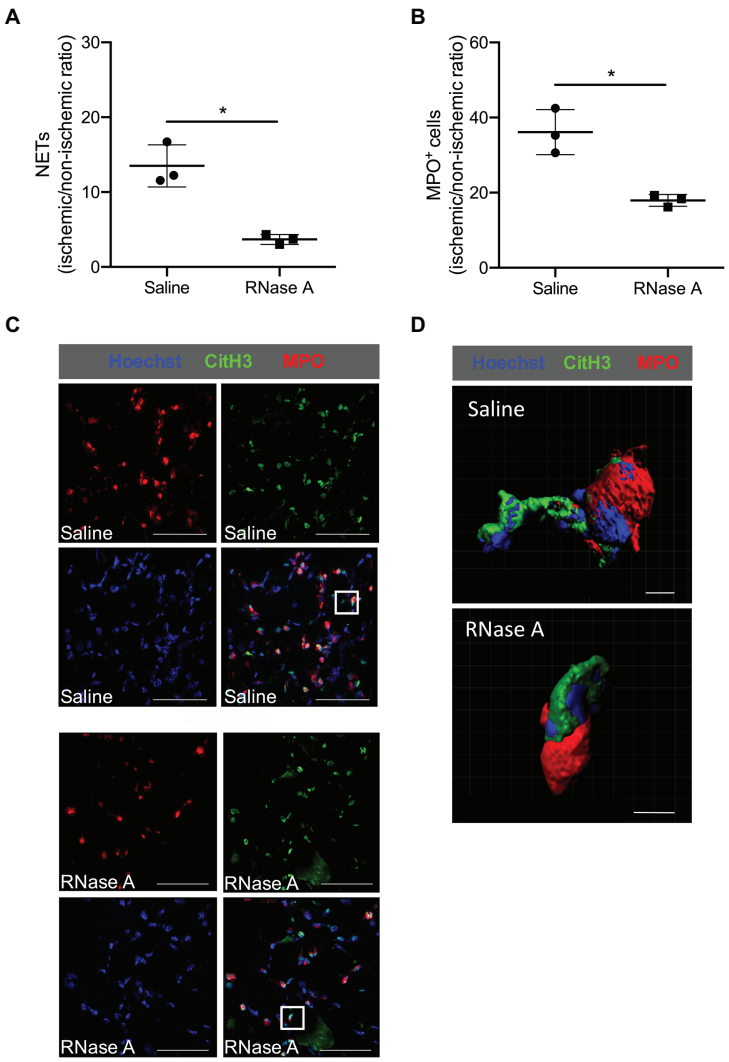

FIGURE 5 | RNase A treatment results in reduced numbers of neutrophil extracellular traps (NETs). **(A,B)** The scatter plots show the ratio (ischemic vs. non-ischemic tissue) of NETs expression **(A)** or total MPO⁺ (myeloperoxidase) cells **(B)** of RNase A or saline treated mice 2 days after surgery. Data are means ± S.E.M., $n = 3$ per group, 10 cross-sectional areas (450 μm × 450 μm each) of the gastrocnemius muscle were analyzed per mouse per leg. $^*p < 0.05$ (RNase A vs. saline treated group) by unpaired student's *t*-test. **(C)** Representative immunofluorescence pictures of analyzed gastrocnemius muscle tissue of saline- (upper picture) or RNase A (lower picture) treated mice 2 days after the surgery. NETs were stained with anti-MPO (red) and anti-CitH3 (green) and Hoechst (blue) for DNA staining. Scale bars 50 μm. **(D)** Representative immunofluorescence 3D reconstruction of a neutrophil with NET formation [magnification of white rectangle in **(C)**] of saline- (upper picture) or RNase A (lower picture) treated mice 2 days after FAL. Scale bars 4 μm.

Lasch et al., 2019a). Subsequent platelet-neutrophil aggregate (PNA) formation promotes mast cell activation, which in turn results in neutrophil and monocyte recruitment (Chillo et al., 2016; Lasch et al., 2019a). Treatment of mice with RNase A, the natural counterpart of extracellular RNA, however, significantly interfered with leukocyte recruitment (Lasch et al., 2019a). In the current study, we found that RNase A treatment also impaired neutrophil and monocyte recruitment strongly suggesting that this was due to the degradation of extracellular RNA, which is released from cells due to ischemic tissue damage. Whether extracellular RNA mediated leukocyte recruitment in angiogenesis is dependent on the axis of VEGFR2-PNA mediated mast cell activation, or due to the previously described function of extracellular RNA to induce tumor necrosis factor (TNF)α release from monocytic cells involving TNF-α-converting enzyme (TACE) activation (Fischer et al., 2012), remains to be elucidated. However, the idea that extracellular RNA might activate mast cells *via* the VEGFR2 pathway in angiogenesis is intriguing, since mast cells are not only relevant for leukocyte recruitment but are also local sources of the angiogenic factors VEGF and RNase 5 (Hiromatsu and Toda, 2003; Kulka et al., 2009). Interestingly, it has recently been published that mast cells are important players

in angiogenesis *in vivo*, as shown in a murine hindlimb model of ischemia (Bot et al., 2020).

The reduced accumulation of leukocytes in ischemic tissue of RNase A treated mice may, however, not only be a function of reduced leukocyte recruitment but also of reduced leukocyte extravasation. The expression of intracellular adhesion molecule 1 (ICAM1) on endothelial cells of post-capillary veins, which is a prerequisite for leukocyte transmigration and extravasation (Ley et al., 2007), is also a function of the VEGF/VEGFR2 system and thus might be dependent on the availability of extracellular RNA (Kluever et al., 2019).

Whether extracellular RNA might also be involved in VEGF induced NRP1-VEGFR2 mediated tip cell formation, thereby controlling capillary sprouting (Kofler and Simons, 2015) is another open question and remains to be addressed in further studies.

In a recent study, it has been shown that extracellular RNA is abundant in NETs in psoriatic skin and promotes in complex with LL37 further NET formation (Herster et al., 2020). In our study, we found that RNase A treatment was associated with reduced NET formation in ischemic tissue samples. However, this seems to be a direct consequence of reduced neutrophil infiltration, and not due to degradation of neutrophil-derived and LL37 complexed extracellular RNA, as LL37 protects extracellular RNA from degradation by RNase A (Tepekoylu et al., 2017; Herster et al., 2020). Interestingly, it has been demonstrated by another study that NETs promote capillary sprouting *in vitro* and *in vivo* (Aldabbous et al., 2016) and are relevant for reparative vascular regeneration in ischemic retina *in vivo* (Binet et al., 2020). Accordingly, RNase A treatment might interfere with angiogenesis by reducing the number of NETs.

Tissue ischemia is associated with an infiltration of monocytes, which mature to macrophages. Classically activated inflammatory M1-like ($CD68^+/MRC1^-$) macrophages are present in the beginning inflammatory phase and are involved in phagocytosis and further leukocyte recruitment. After the removal of necrotic tissue, M1-like macrophages repolarize toward alternatively activated regenerative M2-like ($CD68^+/MRC1^+$) macrophages and participate in tissue remodeling (Dort et al., 2019; Zhang et al., 2020). Our immuno-histochemical analyses evidenced that the percentage of regenerative M2 polarized macrophages in relation to the total number of macrophages was much higher in RNase A than in saline treated control mice. Saline treated mice on the other hand showed a very high percentage of inflammatory M1-like macrophages. *In vitro* studies have demonstrated that bone marrow-derived macrophages upon treatment with extracellular RNA are skewed toward M1-like macrophages and express increased levels of inflammatory cytokines such as TNFα and interleukin 6 (IL-6; Cabrera-Fuentes et al., 2015). Accordingly, RNase A treatment should interfere with the polarization of macrophages toward the M1-like phenotype and favor the switch toward M2-like polarization, as observed in the current study. In our study on arteriogenesis, using the same animal model, however, we found reduced numbers of $CD68^+/MRC1^-$ as well as $CD68^+/MRC1^+$ macrophages around growing collateral arteries in RNase A treated mice when compared to saline treated controls (Lasch et al., 2019a). Together, these data indicate that not only extracellular RNA but further micro-environmental conditions and factors control macrophage polarization. Interestingly, a recent study on a murine hindlimb model showed that lactate, a metabolite which is not found in increased amounts in tissue harboring growing collaterals (Deindl et al., 2001), is a major determinant of M2-like polarization of macrophages in ischemic muscle tissue (Zhang et al., 2020).

In summary, we show that RNase A counteracts angiogenesis, which might be due to reduced NRP1-VEGFR2 mediated tip cell formation, or reduced leukocyte recruitment along with reduced growth factor supply and NET formation. As RNase A shows no signs of toxicity, but a high ribonucleolytic activity, it is reasonable to deduce that RNase A interferes with angiogenesis by degrading extracellular RNA. Together, this implicates a yet unrecognized role for extracellular RNA in angiogenesis. However, further studies are necessary to confirm this assumption as well as the proposed molecular mechanisms.

DATA AVAILABILITY STATEMENT

The original contributions presented in the study are included in the article/**Supplementary Material** and further inquiries can be directed to the corresponding author.

ETHICS STATEMENT

The animal study was reviewed and approved by Bavarian Animal Care and Use Committee (Regierung Oberbayern; ethical approval code: ROB-55.2Vet-2532.Vet_02-17-99).

AUTHOR'S NOTE

This article is dedicated to Klaus T. Preissner, a mentor, colleague, and meanwhile friend. Klaus is a liberal-minded and enthusiastic scientist always coming up with a lot of very fruitful and excellent ideas how to proceed in research. Klaus ich danke dir für all die herzerfrischenden Diskussionen. Es ist eine Freude mit dir zu arbeiten.
Lisa

AUTHOR CONTRIBUTIONS

ML and KK performed surgery. ML, KK, SK, SN, DH, and HI-A performed histological analyses. SM participated in

scientific discussions. ML, HI-A, and ED wrote and revised the manuscript, designed the experiments, and analyzed the data. All authors contributed to the article and approved the submitted version.

FUNDING

The study was funded by the Lehre@LMU program from the LMU, Munich, Germany and the SFB 914 (HI-A/SM, project Z01).

ACKNOWLEDGMENTS

We thank the technical support of Filip Prica for the microscopy imaging support.

SUPPLEMENTARY MATERIAL

The Supplementary Material for this article can be found online at: https://www.frontiersin.org/articles/10.3389/fphys.2020.576736/full#supplementary-material

REFERENCES

Acharya, K. R., Shapiro, R., Allen, S. C., Riordan, J. F., and Vallee, B. L. (1994). Crystal structure of human angiogenin reveals the structural basis for its functional divergence from ribonuclease. *Proc. Natl. Acad. Sci. U. S. A.* 91, 2915–2919. doi: 10.1073/pnas.91.8.2915

Adams, R. H., and Alitalo, K. (2007). Molecular regulation of angiogenesis and lymphangiogenesis. *Nat. Rev. Mol. Cell Biol.* 8, 464–478. doi: 10.1038/nrm2183

Aldabbous, L., Abdul-Salam, V., McKinnon, T., Duluc, L., Pepke-Zaba, J., Southwood, M., et al. (2016). Neutrophil extracellular traps promote angiogenesis: evidence from vascular pathology in pulmonary hypertension. *Arterioscler. Thromb. Vasc. Biol.* 36, 2078–2087. doi: 10.1161/ATVBAHA.116.307634

Arnold, U., and Ulbrich-Hofmann, R. (2006). Natural and engineered ribonucleases as potential cancer therapeutics. *Biotechnol. Lett.* 28, 1615–1622. doi: 10.1007/s10529-006-9145-0

Beintema, J. J. (1998). Introduction: the ribonuclease A superfamily. *Cell. Mol. Life Sci.* 54, 763–765. doi: 10.1007/s000180050204

Binet, F., Cagnone, G., Crespo-Garcia, S., Hata, M., Neault, M., Dejda, A., et al. (2020). Neutrophil extracellular traps target senescent vasculature for tissue remodeling in retinopathy. *Science* 369:eaay5356. doi: 10.1126/science.aay5356

Bot, I., Velden, D. V., Bouwman, M., Kroner, M. J., Kuiper, J., Quax, P. H. A., et al. (2020). Local mast cell activation promotes neovascularization. *Cell* 9:701. doi: 10.3390/cells9030701

Cabrera-Fuentes, H. A., Lopez, M. L., McCurdy, S., Fischer, S., Meiler, S., Baumer, Y., et al. (2015). Regulation of monocyte/macrophage polarisation by extracellular RNA. *Thromb. Haemost.* 113, 473–481. doi: 10.1160/TH14-06-0507

Carmeliet, P. (2000). Mechanisms of angiogenesis and arteriogenesis. *Nat. Med.* 6, 389–395. doi: 10.1038/74651

Carmeliet, P. (2005). VEGF as a key mediator of angiogenesis in cancer. *Oncology* 69(Suppl. 3), 4–10. doi: 10.1159/000088478

Chandraratne, S., von Bruehl, M. L., Pagel, J. I., Stark, K., Kleinert, E., Konrad, I., et al. (2015). Critical role of platelet glycoprotein ibalpha in arterial remodeling. *Arterioscler. Thromb. Vasc. Biol.* 35, 589–597. doi: 10.1161/ATVBAHA.114.304447

Chillo, O., Kleinert, E. C., Lautz, T., Lasch, M., Pagel, J. I., Heun, Y., et al. (2016). Perivascular mast cells govern shear stress-induced arteriogenesis by orchestrating leukocyte function. *Cell Rep.* 16, 2197–2207. doi: 10.1016/j.celrep.2016.07.040

Deindl, E., Buschmann, I., Hoefer, I. E., Podzuweit, T., Boengler, K., Vogel, S., et al. (2001). Role of ischemia and hypoxia-inducible genes in arteriogenesis after femoral artery occlusion in the rabbit. *Circ. Res.* 89, 779–786. doi: 10.1161/hh2101.098613

Deindl, E., and Schaper, W. (2005). The art of arteriogenesis. *Cell Biochem. Biophys.* 43, 1–15. doi: 10.1385/CBB:43:1:001

Dort, J., Fabre, P., Molina, T., and Dumont, N. A. (2019). Macrophages are key regulators of stem cells during skeletal muscle regeneration and diseases. *Stem Cells Int.* 2019:4761427. doi: 10.1155/2019/4761427

Egginton, S., Zhou, A. L., Brown, M. D., and Hudlicka, O. (2001). Unorthodox angiogenesis in skeletal muscle. *Cardiovasc. Res.* 49, 634–646. doi: 10.1016/s0008-6363(00)00282-0

Ferrara, N., and Henzel, W. J. (1989). Pituitary follicular cells secrete a novel heparin-binding growth factor specific for vascular endothelial cells. *Biochem. Biophys. Res. Commun.* 161, 851–858. doi: 10.1016/0006-291x(89)92678-8

Fett, J. W., Strydom, D. J., Lobb, R. R., Alderman, E. M., Bethune, J. L., Riordan, J. F., et al. (1985). Isolation and characterization of angiogenin, an angiogenic protein from human carcinoma cells. *Biochemistry* 24, 5480–5486. doi: 10.1021/bi00341a030

Fischer, S., Gerriets, T., Wessels, C., Walberer, M., Kostin, S., Stolz, E., et al. (2007). Extracellular RNA mediates endothelial-cell permeability via vascular endothelial growth factor. *Blood* 110, 2457–2465. doi: 10.1182/blood-2006-08-040691

Fischer, S., Grantzow, T., Pagel, J. I., Tschernatsch, M., Sperandio, M., Preissner, K. T., et al. (2012). Extracellular RNA promotes leukocyte recruitment in the vascular system by mobilising proinflammatory cytokines. *Thromb. Haemost.* 108, 730–741. doi: 10.1160/TH12-03-0186

Fischer, S., Nishio, M., Dadkhahi, S., Gansler, J., Saffarzadeh, M., Shibamiyama, A., et al. (2011). Expression and localisation of vascular ribonucleases in endothelial cells. *Thromb. Haemost.* 105, 345–355. doi: 10.1160/TH10-06-0345

Fischer, S., Nishio, M., Peters, S. C., Tschernatsch, M., Walberer, M., Weidemann, S., et al. (2009). Signaling mechanism of extracellular RNA in endothelial cells. *FASEB J.* 23, 2100–2109. doi: 10.1096/fj.08-121608

Folkman, J. (1971). Tumor angiogenesis: therapeutic implications. *N. Engl. J. Med.* 285, 1182–1186. doi: 10.1056/NEJM197111182852108

Folkman, J. (1995). Angiogenesis in cancer, vascular, rheumatoid and other disease. *Nat. Med.* 1, 27–30. doi: 10.1038/nm0195-27

Folkman, J., Merler, E., Abernathy, C., and Williams, G. (1971). Isolation of a tumor factor responsible for angiogenesis. *J. Exp. Med.* 133, 275–288. doi: 10.1084/jem.133.2.275

Fu, H., Feng, J., Liu, Q., Sun, F., Tie, Y., Zhu, J., et al. (2009). Stress induces tRNA cleavage by angiogenin in mammalian cells. *FEBS Lett.* 583, 437–442. doi: 10.1016/j.febslet.2008.12.043

Gao, X., and Xu, Z. (2008). Mechanisms of action of angiogenin. *Acta Biochim. Biophys. Sin.* 40, 619–624. doi: 10.1111/j.1745-7270.2008.00442.x

Gaur, D., Swaminathan, S., and Batra, J. K. (2001). Interaction of human pancreatic ribonuclease with human ribonuclease inhibitor. Generation of inhibitor-resistant cytotoxic variants. *J. Biol. Chem.* 276, 24978–24984. doi: 10.1074/jbc.M102440200

Gong, Y., and Koh, D. R. (2010). Neutrophils promote inflammatory angiogenesis via release of preformed VEGF in an in vivo corneal model. *Cell Tissue Res.* 339, 437–448. doi: 10.1007/s00441-009-0908-5

Haigis, M. C., Kurten, E. L., and Raines, R. T. (2003). Ribonuclease inhibitor as an intracellular sentry. *Nucleic Acids Res.* 31, 1024–1032. doi: 10.1093/nar/gkg163

Haigis, M. C., and Raines, R. T. (2003). Secretory ribonucleases are internalized by a dynamin-independent endocytic pathway. *J. Cell Sci.* 116, 313–324. doi: 10.1242/jcs.00214

Herster, F., Bittner, Z., Archer, N. K., Dickhofer, S., Eisel, D., Eigenbrod, T., et al. (2020). Neutrophil extracellular trap-associated RNA and LL37 enable self-amplifying inflammation in psoriasis. *Nat. Commun.* 11:105. doi: 10.1038/s41467-019-13756-4

Hiromatsu, Y., and Toda, S. (2003). Mast cells and angiogenesis. *Microsc. Res. Tech.* 60, 64–69. doi: 10.1002/jemt.10244

Hudlicka, O., Brown, M., and Egginton, S. (1992). Angiogenesis in skeletal and cardiac muscle. *Physiol. Rev.* 72, 369–417. doi: 10.1152/physrev.1992.72.2.369

Isner, J. M., Piezcek, A., Schainfeld, R., Blair, R., Haley, L., Asahara, T., et al. (1996). Clinical evidence of angiogenesis after arterial gene transfer of phVEGF165 in patients with ischaemic limb. *Lancet* 348, 370–374. doi: 10.1016/s0140-6736(96)03361-2

Jaipersad, A. S., Lip, G. Y., Silverman, S., and Shantsila, E. (2014). The role of monocytes in angiogenesis and atherosclerosis. *J. Am. Coll. Cardiol.* 63, 1–11. doi: 10.1016/j.jacc.2013.09.019

Jazwa, A., Florczyk, U., Grochot-Przeczek, A., Krist, B., Loboda, A., Jozkowicz, A., et al. (2016). Limb ischemia and vessel regeneration: is there a role for VEGF? *Vasc. Pharmacol.* 86, 18–30. doi: 10.1016/j.vph.2016.09.003

Kannemeier, C., Shibamiya, A., Nakazawa, F., Trusheim, H., Ruppert, C., Markart, P., et al. (2007). Extracellular RNA constitutes a natural procoagulant cofactor in blood coagulation. *Proc. Natl. Acad. Sci. U. S. A.* 104, 6388–6393. doi: 10.1073/pnas.0608647104

Kishimoto, K., Liu, S., Tsuji, T., Olson, K. A., and Hu, G. F. (2005). Endogenous angiogenin in endothelial cells is a general requirement for cell proliferation and angiogenesis. *Oncogene* 24, 445–456. doi: 10.1038/sj.onc.1208223

Kleinert, E., Langenmayer, M. C., Reichart, B., Kindermann, J., Griemert, B., Blutke, A., et al. (2016). Ribonuclease (RNase) prolongs survival of grafts in experimental heart transplantation. *J. Am. Heart Assoc.* 5:e003429. doi: 10.1161/JAHA.116.003429

Kluever, A. K., Braumandl, A., Fischer, S., Preissner, K. T., and Deindl, E. (2019). The extraordinary role of extracellular RNA in arteriogenesis, the growth of collateral arteries. *Int. J. Mol. Sci.* 20:6177. doi: 10.3390/ijms20246177

Koch, S., Tugues, S., Li, X., Gualandi, L., and Claesson-Welsh, L. (2011). Signal transduction by vascular endothelial growth factor receptors. *Biochem. J.* 437, 169–183. doi: 10.1042/BJ20110301

Koczera, P., Martin, L., Marx, G., and Schuerholz, T. (2016). The ribonuclease A superfamily in humans: canonical RNases as the buttress of innate immunity. *Int. J. Mol. Sci.* 17:1278. doi: 10.3390/ijms17081278

Kofler, N. M., and Simons, M. (2015). Angiogenesis versus arteriogenesis: neuropilin 1 modulation of VEGF signaling. *F1000Prime Rep.* 7:26. doi: 10.12703/P7-26

Kulka, M., Fukuishi, N., and Metcalfe, D. D. (2009). Human mast cells synthesize and release angiogenin, a member of the ribonuclease A (RNase A) superfamily. *J. Leukoc. Biol.* 86, 1217–1226. doi: 10.1189/jlb.0908517

Kurachi, K., Davie, E. W., Strydom, D. J., Riordan, J. F., and Vallee, B. L. (1985). Sequence of the cDNA and gene for angiogenin, a human angiogenesis factor. *Biochemistry* 24, 5494–5499. doi: 10.1021/bi00341a032

Lanahan, A., Zhang, X., Fantin, A., Zhuang, Z., Rivera-Molina, F., Speichinger, K., et al. (2013). The neuropilin 1 cytoplasmic domain is required for VEGF-A-dependent arteriogenesis. *Dev. Cell* 25, 156–168. doi: 10.1016/j.devcel.2013.03.019

Landre, J. B., Hewett, P. W., Olivot, J. M., Friedl, P., Ko, Y., Sachinidis, A., et al. (2002). Human endothelial cells selectively express large amounts of pancreatic-type ribonuclease (RNase 1). *J. Cell. Biochem.* 86, 540–552. doi: 10.1002/jcb.10234

Lasch, M., Kleinert, E. C., Meister, S., Kumaraswami, K., Buchheim, J. I., Grantzow, T., et al. (2019a). Extracellular RNA released due to shear stress controls natural bypass growth by mediating mechanotransduction in mice. *Blood* 134, 1469–1479. doi: 10.1182/blood.2019001392

Lasch, M., Nekolla, K., Klemm, A. H., Buchheim, J. I., Pohl, U., Dietzel, S., et al. (2019b). Estimating hemodynamic shear stress in murine peripheral collateral arteries by two-photon line scanning. *Mol. Cell. Biochem.* 453, 41–51. doi: 10.1007/s11010-018-3430-9

Lautz, T., Lasch, M., Borgolte, J., Troidl, K., Pagel, J. I., Caballero-Martinez, A., et al. (2018). Midkine controls arteriogenesis by regulating the bioavailability of vascular endothelial growth factor A and the expression of nitric oxide synthase 1 and 3. *EBioMedicine* 27, 237–246. doi: 10.1016/j.ebiom.2017.11.020

Leland, P. A., and Raines, R. T. (2001). Cancer chemotherapy—ribonucleases to the rescue. *Chem. Biol.* 8, 405–413. doi: 10.1016/s1074-5521(01)00030-8

Leland, P. A., Schultz, L. W., Kim, B. M., and Raines, R. T. (1998). Ribonuclease A variants with potent cytotoxic activity. *Proc. Natl. Acad. Sci. U. S. A.* 95, 10407–10412. doi: 10.1073/pnas.95.18.10407

Leland, P. A., Staniszewski, K. E., Park, C., Kelemen, B. R., and Raines, R. T. (2002). The ribonucleolytic activity of angiogenin. *Biochemistry* 41, 1343–1350. doi: 10.1021/bi0117899

Leonidas, D. D., Shapiro, R., Allen, S. C., Subbarao, G. V., Veluraja, K., and Acharya, K. R. (1999). Refined crystal structures of native human angiogenin and two active site variants: implications for the unique functional properties of an enzyme involved in neovascularisation during tumour growth. *J. Mol. Biol.* 285, 1209–1233. doi: 10.1006/jmbi.1998.2378

Ley, K., Laudanna, C., Cybulsky, M. I., and Nourshargh, S. (2007). Getting to the site of inflammation: the leukocyte adhesion cascade updated. *Nat. Rev. Immunol.* 7, 678–689. doi: 10.1038/nri2156

Limbourg, A., Korff, T., Napp, L. C., Schaper, W., Drexler, H., and Limbourg, F. P. (2009). Evaluation of postnatal arteriogenesis and angiogenesis in a mouse model of hind-limb ischemia. *Nat. Protoc.* 4:1737. doi: 10.1038/nprot.2009.185

Morrison, A. R., Yarovinsky, T. O., Young, B. D., Moraes, F., Ross, T. D., Ceneri, N., et al. (2014). Chemokine-coupled beta2 integrin-induced macrophage Rac2-Myosin IIA interaction regulates VEGF-A mRNA stability and arteriogenesis. *J. Exp. Med.* 211, 1957–1968. doi: 10.1084/jem.20132130

Neufeld, G., Cohen, T., Gengrinovitch, S., and Poltorak, Z. (1999). Vascular endothelial growth factor (VEGF) and its receptors. *FASEB J.* 13, 9–22. doi: 10.1096/fasebj.13.1.9

Olfert, I. M., Baum, O., Hellsten, Y., and Egginton, S. (2016). Advances and challenges in skeletal muscle angiogenesis. *Am. J. Physiol. Heart Circ. Physiol.* 310, H326–H336. doi: 10.1152/ajpheart.00635.2015

Pipp, F., Boehm, S., Cai, W. J., Adili, F., Ziegler, B., Karanovic, G., et al. (2004). Elevated fluid shear stress enhances postocclusive collateral artery growth and gene expression in the pig hind limb. *Arterioscler. Thromb. Vasc. Biol.* 24, 1664–1668. doi: 10.1161/01.ATV.0000138028.14390.e4

Potente, M., and Carmeliet, P. (2017). The link between angiogenesis and endothelial metabolism. *Annu. Rev. Physiol.* 79, 43–66. doi: 10.1146/annurev-physiol-021115-105134

Raines, R. T. (1998). Ribonuclease A. *Chem. Rev.* 98, 1045–1066. doi: 10.1021/cr960427h

Scapini, P., Morini, M., Tecchio, C., Minghelli, S., Di Carlo, E., Tanghetti, E., et al. (2004). CXCL1/macrophage inflammatory protein-2-induced angiogenesis in vivo is mediated by neutrophil-derived vascular endothelial growth factor-A. *J. Immunol.* 172, 5034–5040. doi: 10.4049/jimmunol.172.8.5034

Schirrmann, T., Krauss, J., Arndt, M. A., Rybak, S. M., and Dubel, S. (2009). Targeted therapeutic RNases (ImmunoRNases). *Expert. Opin. Biol. Ther.* 9, 79–95. doi: 10.1517/14712590802631862

Schwarz, E. R., Speakman, M. T., Patterson, M., Hale, S. S., Isner, J. M., Kedes, L. H., et al. (2000). Evaluation of the effects of intramyocardial injection of DNA expressing vascular endothelial growth factor (VEGF) in a myocardial model in the rat-angiogenesis and angioma formation. *J. Am. Coll. Cardiol.* 35, 1323–1330. doi: 10.1016/s0735-1097(00)00522-2

Seignez, C., and Phillipson, M. (2017). The multitasking neutrophils and their involvement in angiogenesis. *Curr. Opin. Hematol.* 24, 3–8. doi: 10.1097/moh.0000000000000300

Soncin, F. (1992). Angiogenin supports endothelial and fibroblast cell adhesion. *Proc. Natl. Acad. Sci. U. S. A.* 89, 2232–2236. doi: 10.1073/pnas.89.6.2232

Sorrentino, S. (2010). The eight human "canonical" ribonucleases: molecular diversity, catalytic properties, and special biological actions of the enzyme proteins. *FEBS Lett.* 584, 2194–2200. doi: 10.1016/j.febslet.2010.04.018

Strydom, D. J., Fett, J. W., Lobb, R. R., Alderman, E. M., Bethune, J. L., Riordan, J. F., et al. (1985). Amino acid sequence of human tumor derived angiogenin. *Biochemistry* 24, 5486–5494. doi: 10.1021/bi00341a031

Tepekoylu, C., Primessnig, U., Polzl, L., Graber, M., Lobenwein, D., Nagele, F., et al. (2017). Shockwaves prevent from heart failure after acute myocardial ischaemia via RNA/protein complexes. *J. Cell. Mol. Med.* 21, 791–801. doi: 10.1111/jcmm.13021

Tonnesen, M. G., Feng, X., and Clark, R. A. (2000). Angiogenesis in wound healing. *J. Investig. Dermatol. Symp. Proc.* 5, 40–46. doi: 10.1046/j.1087-0024.2000.00014.x

Tsurumi, Y., Kearney, M., Chen, D., Silver, M., Takeshita, S., Yang, J., et al. (1997). Treatment of acute limb ischemia by intramuscular injection of vascular endothelial growth factor gene. *Circulation* 96(Suppl. 9), 382–388.

Weckbach, L. T., Preissner, K. T., and Deindl, E. (2018). The role of midkine in arteriogenesis, involving mechanosensing, endothelial cell proliferation, and vasodilation. *Int. J. Mol. Sci.* 19:2559. doi: 10.3390/ijms19092559

Yamasaki, S., Ivanov, P., Hu, G. F., and Anderson, P. (2009). Angiogenin cleaves tRNA and promotes stress-induced translational repression. *J. Cell Biol.* 185, 35–42. doi: 10.1083/jcb.200811106

Zhang, J., Muri, J., Fitzgerald, G., Gorski, T., Gianni-Barrera, R., Masschelein, E., et al. (2020). Endothelial lactate controls muscle regeneration from ischemia by inducing M2-like macrophage polarization. *Cell Metab.* 31, 1136.e1137–1153.e1137. doi: 10.1016/j.cmet.2020.05.004

Conflict of Interest: The authors declare that the research was conducted in the absence of any commercial or financial relationships that could be construed as a potential conflict of interest.

frontiers in Cell and Developmental Biology

ORIGINAL RESEARCH
published: 09 November 2020
doi: 10.3389/fcell.2020.564169

Neutrophil Extracellular Traps Induce MCP-1 at the Culprit Site in ST-Segment Elevation Myocardial Infarction

Thomas M. Hofbauer[1†], Anna S. Ondracek[1†], Andreas Mangold[1], Thomas Scherz[2], Johanna Nechvile[1], Veronika Seidl[1], Christine Brostjan[3] and Irene M. Lang[1]*

[1] Department of Internal Medicine II, Division of Cardiology, Medical University of Vienna, Vienna, Austria, [2] Department of Dermatology and Venereology, Landesklinikum Wiener Neustadt, Wiener Neustadt, Austria, [3] Department of Surgery, Division of Vascular Surgery and Surgical Research Laboratories, Medical University of Vienna, Vienna, Austria

OPEN ACCESS

Edited by:
Silvia Fischer,
University of Giessen, Germany

Reviewed by:
Lidija Radenovic,
University of Belgrade, Serbia
Ekhtear Hossain,
Southern University and A&M College, United States

***Correspondence:**
Irene M. Lang
irene.lang@meduniwien.ac.at

[†] These authors have contributed equally to this work

Specialty section:
This article was submitted to Cell Adhesion and Migration, a section of the journal Frontiers in Cell and Developmental Biology

Received: 20 May 2020
Accepted: 08 October 2020
Published: 09 November 2020

Citation:
Hofbauer TM, Ondracek AS, Mangold A, Scherz T, Nechvile J, Seidl V, Brostjan C, Lang IM (2020) Neutrophil Extracellular Traps Induce MCP-1 at the Culprit Site in ST-Segment Elevation Myocardial Infarction. Front. Cell Dev. Biol. 8:564169. doi: 10.3389/fcell.2020.564169

Background: Leukocyte-mediated inflammation is crucial in ST-segment elevation myocardial infarction (STEMI). We recently observed that neutrophil extracellular traps (NETs) are increased at the culprit site, promoting activation and differentiation of fibrocytes, cells with mesenchymal and leukocytic properties. Fibrocyte migration is mediated by monocyte chemoattractant protein (MCP)-1 and C-C chemokine receptor type 2 (CCR2). We investigated the interplay between NETs, fibrocyte function, and MCP-1 in STEMI.

Methods: Culprit site and peripheral blood samples of STEMI patients were drawn during primary percutaneous coronary intervention. MCP-1 and the NET marker citrullinated histone H3 (citH3) were measured by ELISA while double-stranded DNA was stained with a fluorescent dye. The influence of MCP-1 on NET formation *in vitro* was assessed using isolated healthy donor neutrophils. Human coronary artery endothelial cells (hCAECs) were stimulated with isolated NETs, and MCP-1 gene expression was measured by ELISA and qPCR. CCR2 expression of culprit site and peripheral blood fibrocytes was characterized by flow cytometry. Healthy donor fibrocyte receptor expression and chemotaxis were investigated in response to stimulation with MCP-1 and NETs *in vitro.*

Results: NETs and concentrations of MCP-1 were increased at the culprit site of 50 consecutive STEMI patients. NET stimulation of hCAECs induced transcription of ICAM-1, IL-6, and MCP-1, and secretion of MCP-1. MCP-1 promoted NET formation of healthy donor neutrophils *in vitro*. An increasing MCP-1 gradient correlated with fibrocyte accumulation at the culprit site. Locally increased MCP-1 levels were negatively correlated with CCR2 expression on fibrocytes. MCP-1 and NETs induced CCR2 downregulation on fibrocytes *in vitro*. NETs did not function as a chemotactic stimulus for fibrocytes or monocytes and could block migration in response to MCP-1 for both cell populations.

Conclusion: NETs function as signaling scaffolds at the culprit site of STEMI. NETs assist MCP-1 and ICAM-1 release from culprit site coronary artery endothelial cells. MCP-1 facilitates further NETosis. Monocytes enter the culprit site along an MCP-1 gradient, to transdifferentiate into fibrocytes in the presence of NETs.

Keywords: neutrophil extracellular traps, monocyte chemoattractant protein-1, fibrocytes, CCR2, ST-segment elevation myocardial infarction

INTRODUCTION

ST-segment elevation myocardial infarction (STEMI) accounts for substantial health burden (Hartley et al., 2016; Ibanez et al., 2018) and is a consequence of thrombotic occlusion of coronary arteries (Libby, 2013). The mainstay of treatment today is primary percutaneous coronary intervention to open the coronary vessel and re-establish blood flow to the ischemic myocardium (Ibanez et al., 2018). The target for intervention is fresh thrombus on the surface of atherosclerotic plaques and erosions (Libby et al., 2011). Pathomechanisms of vascular occlusion remain incompletely elucidated. Several immune cell types and subpopulations contribute to coronary thrombosis and amplify ischemia/reperfusion injury and left ventricular remodeling (Maier et al., 2005; Libby et al., 2011; Libby, 2013).

Previously, we have shown accumulation of neutrophils at the culprit site, which was associated with local complement activation (Distelmaier et al., 2009) and could predict mortality (Distelmaier et al., 2014). Neutrophils have the ability to form so-called neutrophil extracellular traps (NETs) in a process different from apoptosis or necrosis, termed NETosis. Several stimulants of NETosis have been described such as Ca^{2+} ionophores, phorbol myristate acetate, IL-8, activated endothelium (Remijsen et al., 2011), oxidized epitopes (Awasthi et al., 2016), and bacteria (Brinkmann et al., 2004). While precise mechanisms are not yet fully understood, however, NET formation seems to be dependent on the presence of reactive oxygen species (ROS) (Fuchs et al., 2007), myeloperoxidase and neutrophil elastase (Metzler et al., 2014), and the calcium-dependent enzyme peptidyl arginine deiminase 4 (PAD-4) (Martinod et al., 2013). Decondensation of nuclear DNA is driven by PAD-4 citrullinating histones (Wang et al., 2004) in synergism with histone degradation by myeloperoxidase and neutrophil elastase (Metzler et al., 2014). The breakdown of intracellular membranes results in adsorption of granular proteins to chromatin before expulsion (Brinkmann et al., 2004). This meshwork of DNA and associated proteins was identified as a major constituent of coronary thrombi (de Boer et al., 2013; Mangold et al., 2015). NET burden was associated with microvascular obstruction, myocardial salvage index, and left ventricular ejection fraction in STEMI patients (Helseth et al., 2019).

Recently, we have reported an impact of NETs on monocytes and fibrocytes at the culprit site, possibly influencing outcome (Hofbauer et al., 2019; Mangold et al., 2019). Fibrocytes are bone marrow-derived cells with properties of mesenchymal cells and leukocytes (Bucala et al., 1994) that can differentiate from monocytes (Keeley et al., 2012). It was proposed that fibrocytes are involved in the pathogenesis of hypertensive (Keeley et al., 2011) and coronary (Medbury et al., 2008) heart disease, including myocardial infarction (Fang et al., 2012). We demonstrated that fibrocytes accumulate and are highly activated at the culprit site in STEMI (Hofbauer et al., 2019), which might be mediated by increased expression of cell adhesion markers and presence of chemoattractants such as monocyte chemoattractant protein (MCP)-1. MCP-1 is recognized by C-C chemokine receptor type 2 (CCR2) expressed on fibrocytes and monocytes and stimulates fibrocyte proliferation, migration, and collagen deposition (Ekert et al., 2011). Elevated MCP-1 was shown to predict all-cause mortality in patients after myocardial infarction (de Lemos et al., 2007). A mutation in the *mcp-1* gene resulting in elevated protein levels in response to inflammatory stimuli (Rovin et al., 1999) was associated with increased susceptibility to ischemic heart disease in a meta-analysis of 22 studies (Cai et al., 2015). Ischemia-triggered release of MCP-1 was reported as a key mechanism of left ventricular remodeling (Frangogiannis et al., 2007). MCP-1 deficiency reduced recruitment of monocytes and fibroblasts and attenuated remodeling, but prolonged the inflammatory phase (Dewald et al., 2005).

In this study, we investigated the role of NETs at the culprit site of STEMI.

MATERIALS AND METHODS

Detailed information on used reagents is provided in **Supplementary Table S3**.

Sample Collection From Patients and Healthy Controls

We recruited 50 patients with STEMI undergoing primary percutaneous intervention as previously described (Hofbauer et al., 2019). Blood from the culprit site and the arterial sheath was collected. Twenty-one healthy probands served as controls. Blood was immediately processed for flow cytometry and centrifuged at 2000 × *g* for 10 min to receive platelet-poor plasma. Plasma was frozen in aliquots at −80°C for subsequent

Abbreviations: ACTB, actin beta; AUC, area under the curve; BSA, bovine serum albumin; CCR2, C-C chemokine receptor type 2; CD, cluster of differentiation; Cq, cycle of quantification; citH3, citrullinated histone H3; CK-MB, creatinine phosphokinase isoform MB (CK-MB); DNase, Deoxyribonuclease; ELISA, enzyme-linked immunosorbent assay; FC, flow cytometry; FCS, fetal calf serum; FSC, forward scatter; hCAECs, human coronary artery endothelial cells; ICAM-1, intercellular adhesion molecule-1; IL-6, Interleukin-6; IQR, interquartile range; MCP-1, monocyte chemoattractant protein-1; MFI, mean fluorescence intensity; NETs, neutrophil extracellular traps; PBMCs, peripheral blood mononuclear cells; PBS, phosphate-buffered saline; ROS, reactive oxygen species; RT-qPCR, reverse transcriptase quantitative polymerase chain reaction; SSC, side scatter; SD, standard deviation; STEMI, ST-segment elevation myocardial infarction.

analysis. This study was approved by the Ethics Committee of the Medical University of Vienna, Austria (approval reference numbers 303/2005, 581/2006, 151/2008, and 114/2011). All participants gave informed written consent. All procedures were performed according to ethical standards of the Declaration of Helsinki 2013.

Enzymatic Infarct Size

Creatinine phosphokinase isoform MB (CK-MB) area under the curve (AUC) as a measure of enzymatic infarct size was calculated using the trapezoidal formula as previously described (Crimi et al., 2013). CK-MB AUC is indicated as arbitrary units.

Detection of MCP-1 in Plasma and Cell Culture Supernatants

MCP-1 concentration was measured using the human MCP-1 DuoSet enzyme-linked immunosorbent assay (ELISA, R&D Systems) according to the manufacturer's instructions. All samples were measured in duplicate. The lower detection limit was 15.6 pg/ml.

Measurement of NET Surrogate Markers

dsDNA was measured using Sytox® Green Nucleic Acid Stain (1 μM, Invitrogen) in plasma diluted 1:20 in phosphate-buffered saline (PBS) containing 5 mM ethylenediaminetetraacetic acid (EDTA) and 0.1% bovine serum albumin (BSA). Citrullinated histone H3 (citH3) was measured using an ELISA as previously described (Thalin et al., 2017; Hofbauer et al., 2019) by assaying undiluted samples in duplicates.

Flow Cytometry-Based Quantification of citH3-Positive Neutrophils

Blood collected into K3EDTA-coated tubes was mixed 3:10:5 with anticoagulant buffer (15 nM EDTA, 1% BSA in PBS) and 6% Hetastarch (B| Braun), respectively, and incubated for 40 min at 37°C to allow sedimentation of erythrocytes. The supernatant containing leukocytes was transferred to a new tube filled with PBS and centrifuged at 524 × *g* for 5 min. The pellet was resuspended in 2 ml of RPMI 1640 (Gibco) per 150 μl of blood used in the beginning. Two milliliters was used for stimulation in polystyrene round-bottom tubes. Cells were treated with recombinant human MCP-1 (BioLegend, 500 pg/ml) or left untreated for 2:30 h at 37°C. Tubes were gently vortexed before fixation with 1% formaldehyde. Two thirds of the suspension was transferred to a new tube and mixed with 500 μl of FC buffer (2% BSA in PBS) before centrifugation at 3200 × *g* for 15 min at 4°C. The pellet was resuspended in red blood cell lysis buffer (154 mM ammonium chloride, 10 mM potassium bicarbonate, and 0.1 mM disodium EDTA, pH 7.3) and incubated for 15 min. After centrifugation, unspecific binding sites were blocked with FC buffer. All antibodies were diluted in FC buffer and washing between incubations was done by centrifugation at 3200 × *g* for 15 min at 4°C. The primary antibody directed against citH3 (Abcam) was added for 20 min at a concentration of 5.5 μg/ml. Thereafter, the secondary antibody (goat anti-rabbit-Alexa Fluor 647, 1:10,000, Invitrogen) and CD66b-PacificBlue (BioLegend, 1:40) were added for 20 min. Cells were resuspended in FC buffer. Acquisition and analysis of 50,000 events was performed using the Attune NxT Flow cytometer (Life Technologies) and accompanying software. Neutrophils were defined as cells positive for CD66b. CitH3-positive neutrophils were gated with respect to unspecific binding of the secondary antibody and are given as percentage of total neutrophils.

Isolation of Neutrophils

Neutrophils were isolated as previously described (Brinkmann et al., 2010). 6 ml of whole blood was layered carefully on top of 6 ml of Histopaque 1119 (Sigma) and centrifuged at 800 × *g*, 20 min, brakes off. After harvesting the neutrophil layer, cells were washed once with sterile PBS. The neutrophil pellet was resuspended in PBS and layered on top of a Percoll gradient (Sigma). Therefore, 18 ml of Percoll was mixed with 2 ml of PBS (10 ×) and density gradients of 85, 80, 75, 70, and 65% were prepared with PBS (1 ×). The gradients were layered with decreasing density before resuspended cells were added on top and centrifuged as above. Purified neutrophils were harvested and washed with PBS, and resuspended in Hank's balanced salt solution (HBSS) without phenol red (Lonza) containing 1.26 mM $CaCl_2$. The purity of neutrophils was assessed using a XN-350 Hematology Analyzer (Sysmex) and was consistently above 95%.

DNA Release Assay to Detect NET Formation

NET formation of isolated healthy donor neutrophils was measured using Sytox® Green Nucleic Acid Stain (Invitrogen), which is cell-impermeable and exclusively stains extracellular DNA as previously described (Vong et al., 2013). Isolated neutrophils (1×10^5) were seeded in duplicates into a 96-well flat-bottom culture plate. As a positive control, a final concentration of 0.33% Triton X-100 was added to one duplicate leading to maximum release of DNA. After incubation with recombinant human MCP-1 (BioLegend, 125, 250, and 500 pg/ml) or vehicle control for 20 min, NET formation was induced with 1.3 μM ionomycin (Sigma) for 2:45 h at 37°C, 5% CO_2. Sytox Green (Invitrogen) was added to a final concentration of 5 μM for 15 min, and fluorescence was measured on a Promega GloMax Discover microplate reader (excitation 485 nm, emission 520 nm) to assess release of dsDNA into the supernatant.

Intracellular Calcium Mobilization by MCP-1

Intracellular calcium mobilization was monitored using the Fluo-8 No Wash Calcium Assay Kit (Abcam) according to the manufacturer's instructions for non-adherent cells. Healthy donor neutrophils isolated as described above were resuspended in equal amounts of HBSS supplemented with 1.26 mM $CaCl_2$ and 20 mM HEPES and Fluo-8 dye-loading solution. A total of 10^5 cells/well/100 μl were seeded into sterile, black, flat-bottom 96-well plates and incubated for 30 min. Pre-warmed HBSS supplemented with 1.26 mM $CaCl_2$ was added to a final assay volume of 270 μl. The plate was transferred into a fluorescence plate reader with a dual injector function (Varioskan

Flash, Thermo Scientific) and monitored at 37°C for 85 min reading fluorescence at an excitation wavelength of 490 nm and an emission wavelength of 525 nm. After baseline recording, MCP-1 was injected at medium speed (BioLegend, 0.5 ng/ml final concentration) and fluorescence was measured per well immediately afterward. The plate was scanned every minute for 20 min. Then, ionomycin was injected at medium speed (Sigma, 1.3 μM final concentration) and fluorescence was again measured per well immediately afterward. Calcium mobilization was monitored for 15 min every minute and then for 50 min every 5 min. Results are presented as fold change to baseline.

Intracellular Formation of ROS by MCP-1

Intracellular formation of ROS was monitored using the DCFDA Cellular ROS Detection Assay Kit (Abcam) according to the manufacturer's instructions for non-adherent cells. Healthy donor neutrophils isolated as described above were resuspended in 1 × assay buffer containing 20 μM DCFDA. A total of 10^5 cells/well/100 μl were seeded into sterile, black, flat-bottom 96-well plates and incubated for 30 min. Pre-warmed HBSS supplemented with 1.26 mM $CaCl_2$ was added to a final assay volume of 270 μl. The plate was transferred into a fluorescence plate reader with a dual injector function (Varioskan Flash, Thermo Scientific) and monitored at 37°C for 85 min reading fluorescence at an excitation wavelength of 490 nm and an emission wavelength of 525 nm. After baseline recording, MCP-1 was injected at medium speed (BioLegend, 0.5 ng/ml final concentration) and fluorescence was measured per well immediately afterward. The plate was scanned every minute for 20 min. Then, ionomycin was injected at medium speed (Sigma, 1.3 μM final concentration) and fluorescence was again measured per well immediately afterward. ROS formation was monitored for 15 min every minute and then for 50 min every 5 min. Results are presented as fold change to baseline.

NETs Generation and Harvest

NETs were isolated as previously described (Hofbauer et al., 2019), with modifications. Briefly, 5 × 10^6/ml neutrophils isolated from healthy donors as described above were seeded into 6-well flat-bottom cell culture plates in RPMI supplemented with 3% fetal calf serum (FCS) and stimulated with 500 nM phorbol myristate acetate (Sigma) for 4 h at 37°C, 5% CO_2. After discarding supernatant, generated NETs were incubated with PBS containing 10 U/ml of the restriction enzyme *Alu*I (Roche) for 30 min. The supernatant was collected and centrifuged at 300 × *g* for 5 min to remove cellular debris. Supernatant was again collected, and double-stranded DNA concentration was measured using the Quant-iT PicoGreen kit (Thermo Fisher) as previously described (Hofbauer et al., 2019).

Stimulation of Human Coronary Artery Endothelial Cells

Human coronary artery endothelial cells (hCAECs, Lonza) were seeded into flat-bottom 12-well plates at a concentration of 4 × 10^4/ml in M199 medium (Sigma) supplemented with 20% FCS (Merck), 25 mM HEPES (gibco), 2 mM L-glutamine (Lonza), 1% MEM non-essential amino acids (Sigma), 100 U/ml penicillin, 100 U/ml streptomycin, 2.5 ng/ml amphotericin B (Lonza), and endothelial cell growth supplement (bovine thalamus homogenate supplemented with sodium chloride, streptomycin, ammonium phosphate, and sodium phosphate). After reaching confluence, cells were stimulated using 500 ng/ml isolated NETs, 1 IE/ml deoxyribonuclease (DNase) 1 (Pulmozyme®, Roche), 250 ng/ml citH3 (Cayman Chemical), and 250 ng/ml lambda DNA (Thermo^{TM} Fisher) for 6 and 24 h. The supernatant was collected, centrifuged for 10 min at 10,000 × *g* to remove cellular debris, and stored at −80°C for subsequent analysis. Cells were lysed using 500 μl of TRIzol reagent (ThermoFisher) and stored at −80°C.

Isolation of RNA

RNA was isolated from cell lysates using the ReliaPrep^{TM} RNA Cell Miniprep System (Promega) with modifications. Samples were incubated 5:1 in chloroform for 3 min and centrifuged for 15 min, 12,000 × *g* at 4°C. The aqueous, RNA-containing phase was transferred to a minicolumn and centrifuged for 1 min, 14,000 × *g* at 21°C. After washing with RNA washing solution, aqueous phase was incubated with Yellow Core Buffer containing DNase 1 and $MnCl_2$ (both 1:10) for 15 min. After three further washing steps, isolated RNA was eluted in nuclease-free water. RNA concentration was assessed using a NanoDrop® ND-1000 Spectrophotometer (Peqlab).

cDNA Synthesis

cDNA was synthesized from RNA isolates using the GoScript® Reverse Transcription System (Promega) according to the manufacturer's instructions. The mix contained oligo(dT)15 as well as random primers. Five hundred nanograms of RNA was transcribed into cDNA in a volume of 20 μl, incubating the samples for 5 min at 25°C, 60 min at 42°C, and 15 min at 70°C followed by a cool down to 4°C in an Eppendorf Mastercycler ep Gradient S.

Real-Time Quantitative PCR Analysis

Reverse transcriptase quantitative polymerase chain reaction (RT-qPCR) analyses were performed using a GoTaq Probe 2-step RT-qPCR System (Promega) according to the manufacturer's instructions. All measurements were made on an ABI PRISM 7000 Sequence Detector (Applied Biosystems). Efficiency of primer probe pairs was measured by assaying a six-point 1:2 serial dilution of pooled hCAEC cDNAs, using the same instrument settings as for all other experiments. Amplification efficiency (E) was calculated using the formula $E = 2^{-1/-y}$, where y is the slope of the standard curve resulting from plotting Cq values against dilution (**Supplementary Figure S1**). Suitable endogenous controls were identified by analyzing expression of actin beta (ACTB), glyceraldehyde 3-phosphate dehydrogenase (GAPDH), and hypoxanthine phosphoribosyl transferase 1 (HPRT1) of one exemplary stimulation experiment according to published recommendations (Chervoneva et al., 2010; Kozera and Rapacz, 2013), using the same instrument settings as for all other experiments. ACTB and HPRT1 were identified to be adequate endogenous controls due to similarity of amplification

curves with experimental assays and lack of gene regulation by experimental conditions. Representative plots are given in **Supplementary Figure S2**. Relative expression levels were calculated using the Pfaffl method (Pfaffl, 2001). The following primers (all ThermoFisher) were used: ACTB (Hs99999903), GAPDH (Hs99999905), HPRT1 (Hs99999909), intercellular adhesion molecule-1 (ICAM-1, Hs00164932), interleukin-6 (IL-6, Hs00174131), and MCP-1 (Hs00234140).

Identification of Circulating Fibrocytes by Flow Cytometry

Fibrocytes were analyzed using flow cytometry as previously described (Hofbauer et al., 2019). EDTA whole blood samples were incubated with fluorochrome-labeled primary antibodies against collagen-I (1:200, Merck-Millipore), CD34 (1:40, BioLegend), CD45 (1:40, BioLegend), and CCR2 (1:40, BioLegend) for 15 min. After red blood cell lysis (BD), cells were washed twice with PBS and analyzed on a BD FACSCanto II and FACSDiva Software (BD). Debris was excluded using forward and side scatter. Fibrocytes were identified as cells triple-positive for the leukocyte marker CD45, the hematopoietic stem cell marker CD34, and collagen-I (Pilling et al., 2009). Expression levels are given as mean fluorescence intensity (MFI).

Isolation of Peripheral Blood Mononuclear Cells

For isolation of peripheral blood mononuclear cells (PBMCs), 20 ml of healthy control whole blood was mixed with 10 ml of PBS, layered onto 15 ml of Lymphocyte Separation Medium (PromoCell), and centrifuged for 30 min, 800 × *g* at 21°C, with brakes off. The PBMC layer was harvested and washed with PBS. The remaining red blood cells were lysed using 154 mM ammonium chloride, 10 mM potassium hydrogen carbonate, and 0.1 mM EDTA (pH 7.3); washed twice; and resuspended in RPMI-1640 medium (Sigma). PBMC purity was assessed using an XN-350 Hematology Analyzer (Sysmex).

In vitro Stimulation of Fibrocytes

Isolated PBMCs were resuspended at a concentration of 1×10^6 cells/ml in RPMI-1640 (Sigma), seeded into polystyrene tubes, and stimulated with recombinant MCP-1 (BioLegend, 0.125, 0.250, 0.500, and 5 ng/ml), isolated NETs of four healthy donors (500 ng/ml dsDNA content), and corresponding control supernatant of unstimulated neutrophils for 6 h at 37°C, 5% CO_2. Afterward, cells were washed twice with PBS and unspecific binding sites were blocked with Fc fragments (BD Biosciences). Samples were incubated with fluorochrome-labeled primary antibodies against collagen-I (1:100, Merck-Millipore), CD34 (1:100, BioLegend), CD45 (1:240, BioLegend), and CCR2 (1:50, BioLegend) for 15 min. Cells were fixed with BD FACS lysis (BD), washed twice with PBS, and analyzed with an Attune NxT flow cytometer (Life Technologies). Debris was excluded using forward and side scatter. Fibrocytes were identified as described above. CCR2 expression levels are given as MFI relative to baseline.

Cell Migration Experiments

Chemotaxis assays were carried out in 24-well plates with cell culture inserts separating the upper and lower compartment by a membrane of 8-μm pore size (Greiner Bio-One). Chemotactic stimuli were added to the wells in RPMI supplemented with 0.3% BSA (Sigma). FCS (20%) served as assay positive control of migration. Recombinant MCP-1 (BioLegend, 0.500 ng/ml), isolated NETs of four healthy donors (500 ng/ml dsDNA content), and corresponding volume of control supernatant of unstimulated neutrophils were used to stimulate chemotaxis. The PBMC suspension (2×10^6 cells) isolated from 10 corresponding donors was added to inserts with or without NETs and control

TABLE 1 | Patient characteristics.

Patient characteristics	***n* = 50**
Age, years ± SD	61 ± 12
Male sex, *n* (%)	39 (78)
BMI > 25 kg/m^2, *n* (%)	34 (68)
BMI > 30 kg/m^2, *n* (%)	9 (18)
Diabetes, *n* (%)	9 (18)
History of hypertension, *n* (%)	37 (74)
Dyslipidemia, *n* (%)	33 (66)
Ever smoker, *n* (%)	33 (66)
Family history of CAD, *n* (%)	24 (48)
Previous MI, *n* (%)	9 (18)
Culprit lesion, *n* (%)	
LAD	24 (48)
CX	8 (16)
RCA	16 (32)
Multiple	2 (4)
CAD, *n* (%)	
1-VD	23 (46)
2-VD	13 (26)
3-VD	14 (28)
Symptom to balloon time, min	194 [146–415]
CK-MB AUC	8533 [4049–15,570]
CRP, nmol/L (< 4.8)	3.62 [1.90–7.81]
TnT, μg/L (0–0.03)	0.05 [0.02–0.11]
Creatinine, μmol/L (50–100)	86.16 ± 29.74
Cholesterol, mmol/L (< 5.2)	4.99 ± 0.85
LDL, mmol/L (< 4.1)	2.74 ± 0.83
HDL, mmol/L (> 1.5)	1.22 ± 0.34
Triglycerides, mmol/L (< 1.7)	1.61 ± 1.12
Culprit site dsDNA, ng/ml	529.8 [428.9–739.8]
Peripheral dsDNA, ng/ml	403.7 [349.2–562.7]
Culprit site citH3, ng/ml	331.6 [122.6–810.5]
Peripheral citH3, ng/ml	235.3 [112.8–434.3]

Characteristics of patients with STEMI are indicated with respective units and reference values in parentheses thereafter. Data are presented as mean ± standard deviation (SD), median [interquartile range (IQR)], or number (percent) of patients. Culprit site and peripheral NET markers differ significantly (dsDNA, $p < 0.0001$; citH3, $p = 0.0027$; Wilcoxon matched-pairs signed rank test). ASA, acetylsalicylic acid; BMI, body mass index; CAD, coronary artery disease; CK-MB AUC, area under the curve of creatinine kinase isoform MB; CRP, C-reactive protein; CX, circumflex; HDL, high-density lipoprotein; LAD, left anterior descending; LDL, low-density lipoprotein; MI, myocardial infarction; RCA, right coronary artery; STEMI, ST-segment elevation myocardial infarction; TnT, troponin T; VD, vessel disease.

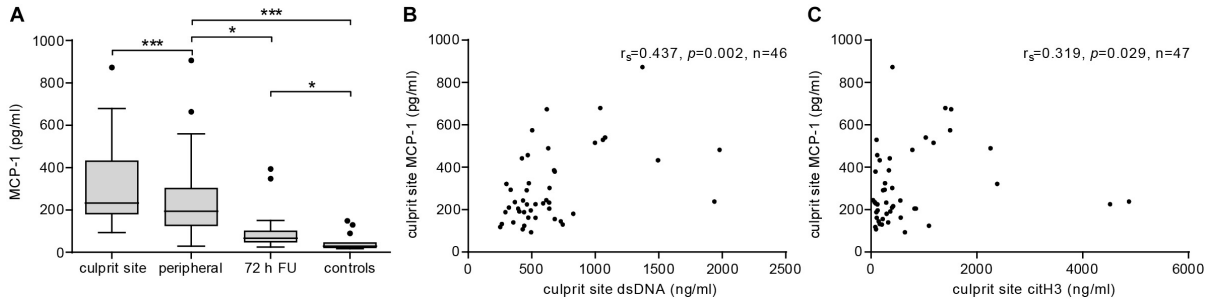

FIGURE 1 | MCP-1 and NETs are elevated at the culprit site in STEMI patients. **(A)** MCP-1 levels were measured in samples from culprit site (n = 47), peripheral site (n = 47), peripheral blood 72 h follow-up (n = 19), and healthy controls (n = 15) by ELISA. Statistical tests for respective pairwise comparisons and corrected and uncorrected p values are provided in **Supplementary Table S1**. Data are presented as boxplots with whiskers defined according to Tukey. Culprit site MCP-1 concentrations were positively correlated with **(B)** local dsDNA (Spearman signed-rank test, r_S = 0.437, n = 46) and **(C)** citH3 levels (Spearman signed-rank test, r_S = 0.319, n = 47). *$p < 0.05$, **$p < 0.01$, ***$p < 0.001$.

TABLE 2 | Determinants of enzymatic infarct size.

	β coefficient	[95% CI]	Standardized β	p-value
Age	186.2	[1.237; 371.1]	0.317	0.049
Female sex	−1842	[−7458; 3773]	−0.100	0.499
BMI	−847.7	[−1541; −153.7]	−0.358	0.019
Smoker	4796	[−306.4; 9898]	0.278	0.064
Anterior infarction	5272	[−186; 10732]	0.285	0.058
Symptom to balloon time	9.634	[2.685; 16.58]	0.424	0.009
Culprit lesion MCP-1	36.13	[18.74; 53.51]	0.647	<0.001

MCP-1 levels significantly add to enzymatic infarct size. A multiple linear regression model with CK-MB AUC as outcome variable was calculated (n = 26). The R^2 for the overall model was 0.667 (adjusted 0.538), which is indicative of a high goodness of fit. The model significantly predicts enzymatic infarct size $F(7, 18) = 5.157$, $p = 0.002$. CK-MB AUC, creatinine kinase isoform MB area under the curve.

supernatant. After 6 h at 37°C, the remaining cells were aspirated from the inner side of the insert and discarded, while cells from the lower chamber and the bottom side of the membrane were harvested using Trypsin EDTA for analysis by flow cytometry. Cells were washed twice with PBS and unspecific binding sites were blocked with Fc fragments (BD Biosciences). Samples were incubated with fluorochrome-labeled primary antibodies against collagen-I (1:100, Merck-Millipore), CD34 (1:100, BioLegend), CD45 (1:240, BioLegend), and CD14 (1:50, BioLegend) for 15 min. Cells were washed two times with PBS and analyzed with an Attune NxT flow cytometer (Life Technologies). Debris was excluded using forward and side scatter. Fibrocytes were identified as described above. Cells not characterized as fibrocytes and positive for CD45 and CD14 were identified as monocytes. Cell counts per microliter were recorded.

Statistics

Normality of data was analyzed via histograms and the Kolmogorov-Smirnov test (data not shown). In case of normal distribution, demographical data are presented as mean ± standard deviation (SD); otherwise, median and interquartile range (IQR) are given. Two groups were compared with respect to matching, normality, and variance, and multiple testing was corrected using the Bonferroni–Holm method. For patient data, all comparisons, uncorrected and corrected p values, as well as the specific tests employed are reported in **Supplementary Tables S1, S2**. Comparison of more groups was done with one-way ANOVA considering normality and repeated measures, if applicable, followed by Tukey's or Dunn's multiple comparisons test. Correlations were calculated using Spearman's rank correlation. Statistical tests used are specified in the respective figure legends. To identify determinants of enzymatic infarct size, we computed a multivariable linear regression model. Normality of residuals was verified using histograms and P–P and Q–Q plots. Heteroscedasticity was excluded by plotting the model residuals versus predicted values. Autocorrelation of residuals was assessed by Durbin–Watson statistics, which was inconclusive (1.812). Multicollinearity between predictors was excluded. Statistical analyses were performed using IBM SPSS 26.0 and GraphPad Prism 8.0 for Windows. Boxplots display the 25th and 75th percentile; whiskers are defined according to Tukey.

RESULTS

Culprit Site Milieu as Determinant of Enzymatic Infarct Size

We studied 50 patients presenting with STEMI. Patient characteristics are shown in **Table 1**.

Plasma MCP-1 levels were significantly elevated at the culprit site compared to the concentration at the peripheral femoral site (**Figure 1A**). Concentrations declined over the following 72 h but were still significantly higher than levels measured in samples from healthy controls. To assess the influence of MCP-1 levels on infarct size, a multiple linear regression model with CK-MB AUC as outcome variable was calculated (n = 26). The R^2 for the overall model was 0.667 (adjusted 0.538), which illustrates a high goodness of fit (**Table 2**). The model predicted enzymatic infarct size [$F(7,18) = 5.157$, $p = 0.002$] and culprit MCP-1 levels were significantly added to enzymatic infarct size, with a standardized β coefficient of 0.647. Culprit site MCP-1 correlated with local

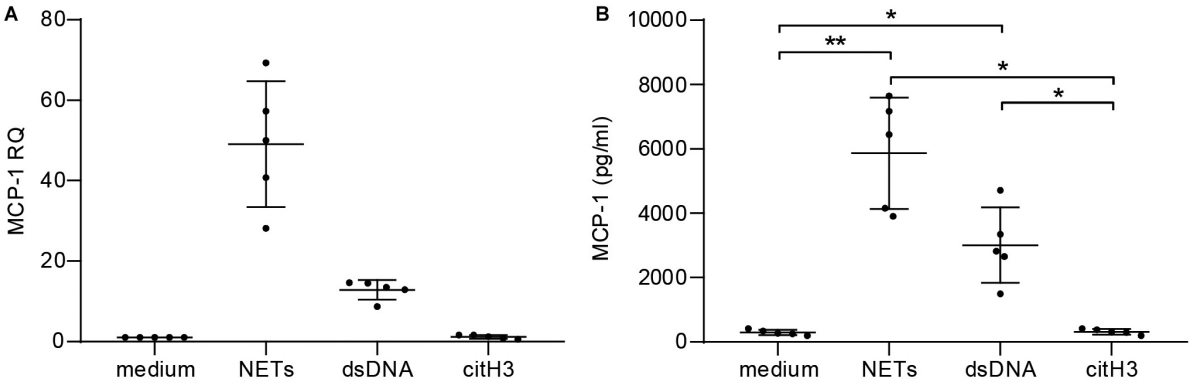

FIGURE 2 | Stimulation of human coronary artery endothelial cells with NETs. hCAECs were stimulated with isolated NETs, dsDNA, and citH3 for 6 and 24 h. MCP-1 gene expression was assessed **(A)** on mRNA levels by qPCR after 6 h and is presented as fold change over an unstimulated control after normalization to the mean of two endogenous controls. **(B)** Release of MCP-1 was measured in cell supernatants by ELISA after 24 h of stimulation. Data are presented as mean ± SD. Experiments were repeated five times and analyzed using one-way ANOVA followed by Tukey's multiple comparisons test. $*p < 0.05$, $**p < 0.01$.

levels of the NET markers dsDNA (**Figure 1B**, $r_s = 0.437$, $p = 0.002$) and citH3 (**Figure 1C**, $r_s = 0.319$, $p = 0.029$).

NETs Induce a Pro-inflammatory Phenotype in Human Coronary Endothelial Cells

To assess the pro-inflammatory effect of NETs *in vitro*, hCAECs were cultured and stimulated with NETs from healthy donors. Relative quantification by qPCR revealed that NETs (50-fold) and dsDNA (10-fold) induced MCP-1 expression on an mRNA level (**Figure 2A**) and led to significantly elevated protein levels in cell culture supernatants, as measured by ELISA (**Figure 2B**). Furthermore, NETs led to a more than 100-fold upregulation of the adhesion marker ICAM-1 in response to NETs (**Supplementary Figure S3**A), which was accompanied by an 8-fold increase of IL-6 mRNA (**Supplementary Figure S3**B). Expression of both markers was lower using dsDNA as a stimulant, but still led to a 20-fold increase of ICAM-1 and a 5-fold elevation of IL-6 mRNA, respectively. The addition of DNase did not antagonize the effects of NETs for any of the analyzed targets (data not shown), and citH3 alone did not confer any changes (**Figures 2A,B** and **Supplementary Figures S3A,B**).

MCP-1 Primes Neutrophils for NET Formation

To test whether MCP-1 primes neutrophils to undergo NETosis *in vitro*, we measured citH3 by flow cytometry. Stimulation with MCP-1 led to an increase in the percentage of citH3 positive neutrophils compared to untreated controls (**Figure 3A**). This observation did not directly translate into release of NETs as measured by dsDNA (**Supplementary Figure S4A**). We then assessed whether pre-treatment of isolated neutrophils with MCP-1 would modulate NET formation in response to a second stimulus. Release of dsDNA *in vitro* using ionomycin was significantly promoted by MCP-1 (**Figure 3B**). The highest level of NET formation occurred after pre-treatment with 250 pg/ml MCP-1, corresponding to levels measured at the culprit site in STEMI patients. Intracellular mobilization of Ca^{2+} and formation of ROS were not affected by MCP-1 in our setting (**Supplementary Figures S4B,C**).

Fibrocyte Influx Is Dependent on MCP-1 Gradient and CCR2 Trafficking

To evaluate the extent of the MCP-1 gradient between culprit site and peripheral site, the fold change between both sites was calculated. An increasing MCP-1 ratio was indicative of relative fibrocyte accumulation at the site of occlusion (**Figure 4A**, $r_s = 0.361$, $p = 0.013$). The MCP-1 receptor CCR2 was proportionally less detectable on culprit site fibrocytes as shown by a negative correlation with the MCP-1 gradient (**Figure 4B**, $r_s = -0.443$, $p = 0.030$). However, the relative increase of culprit site dsDNA and citH3 was not associated with fibrocyte counts or their CCR2 expression (**Supplementary Figure S5**). Peripheral fibrocytes expressed significantly more CCR2 than culprit site fibrocytes (**Figure 4C**). Peripheral intensity of CCR2 expression remained stable over 72 h and was overall elevated compared to healthy controls (**Figure 4C**). CCR2 receptor expression at the culprit site was at median levels of about 60% of peripheral control (**Figure 5A**). PBMCs incubated with culprit site concentrations of MCP-1 *in vitro* showed minimal downregulation of the receptor CCR2 and only an increase of the dose far above physiological levels matched the extent observed *in vivo* (**Figure 5B**). To investigate a potential role of NETs in CCR2 receptor downregulation on fibrocytes, PBMCs were incubated with NETs and analyzed by flow cytometry. Culprit site levels of NETs significantly decreased CCR2 on fibrocytes compared to control supernatant to a degree observed for high MCP-1 dosages (**Figure 5C**). Addition of MCP-1 and NETs was even more potent than NETs alone (**Figure 5C**).

In vitro Fibrocyte Migration Is Dependent on an MCP-1 Gradient

As NETs interfered with CCR2 receptor expression, we tested their influence on cell migration *in vitro* using cell culture inserts

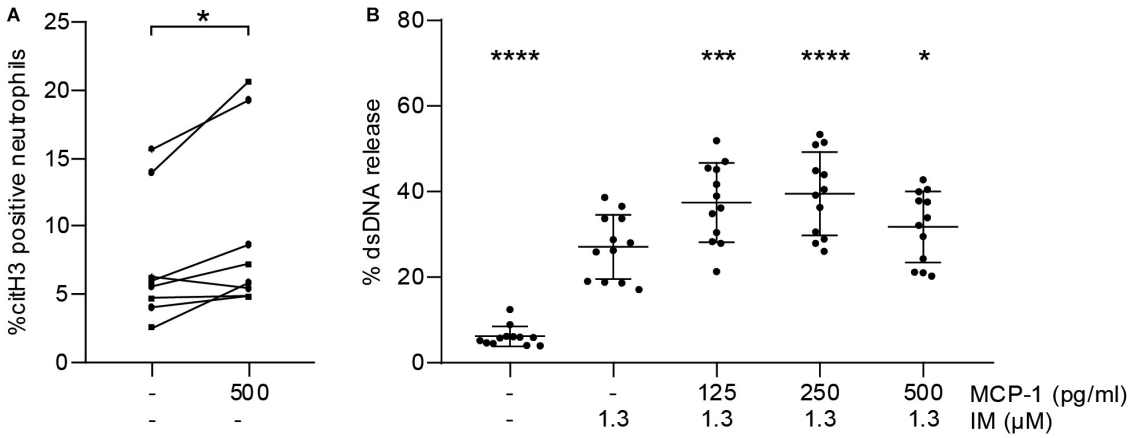

FIGURE 3 | MCP-1 primes neutrophils for NET formation. **(A)** Leukocytes of healthy donors (n = 8) were treated with 500 pg/ml of MCP-1 for 2:30 h and analyzed by flow cytometry. Data are presented as percentage of CD66b-positive cells staining for citH3. Groups were compared by Wilcoxon matched-pairs signed rank test. **(B)** Neutrophils of healthy donors (n = 12) were pre-treated with 125, 250, and 500 pg/ml MCP-1 and then stimulated with 1.3 μM ionomycin (IM) to induce formation of NETs. Data are provided in percent of positive control and are presented as mean ± SD. Experiments were analyzed by repeated measures ANOVA followed by Dunnett's multiple comparisons test using the group treated with 1.3 μM IM as single comparator. *$p < 0.05$, ***$p < 0.001$, ****$p < 0.0001$.

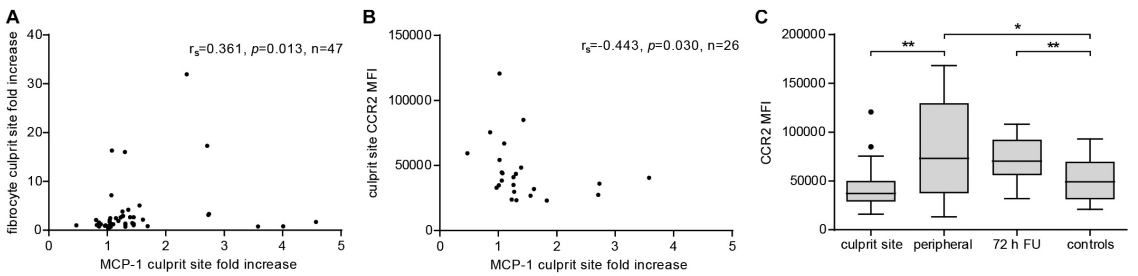

FIGURE 4 | Effect of MCP-1 on accumulation of fibrocytes and fibrocyte CCR2 expression at the culprit site. Fibrocyte counts in culprit and peripheral site blood, presented as influx ratio at the culprit site, and mean fluorescence intensity (MFI) of CCR2 expression were determined by flow cytometry; MCP-1 was measured by ELISA and presented as fold increase at the culprit site. **(A)** Correlation of relative fibrocyte count at the culprit site with MCP-1 fold increase (Spearman signed-rank test, r_S = 0.361, n = 47). **(B)** Correlation of fibrocyte CCR2 expression at the culprit site with MCP-1 fold increase (Spearman signed-rank test, r_S = –0.443, n = 26). **(C)** CCR2 receptor expression on fibrocytes of culprit site (n = 26), peripheral site (n = 26), 72 h follow-up (n = 14), and healthy control blood (n = 18). Statistical tests for respective pairwise comparisons, and corrected and uncorrected p values are provided in **Supplementary Table S2**. Data are presented as boxplots with whiskers defined according to Tukey. *$p < 0.05$, **$p < 0.01$.

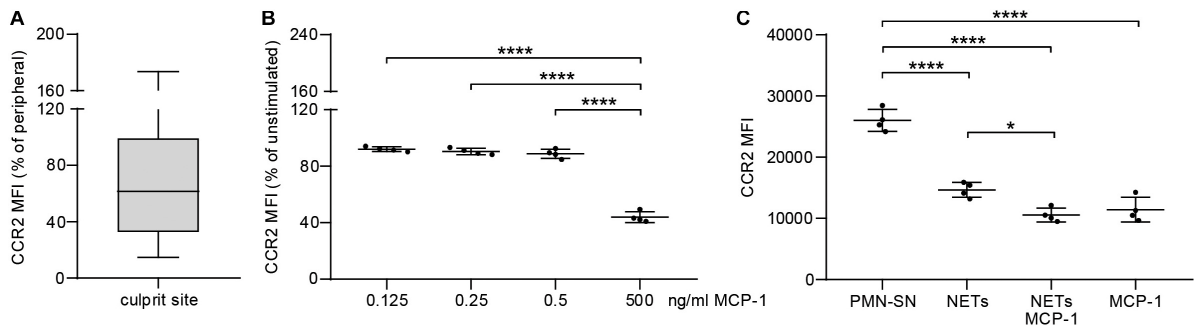

FIGURE 5 | Effect of MCP-1 and NET stimulation on fibrocyte CCR2 expression *in vivo* and *in vitro.* **(A)** Culprit site CCR2 expression on fibrocytes is presented relative to peripheral CCR2 expression. **(B)** PBMCs of healthy donors were stimulated for 6 h with 0.125, 0.250, 0.500, and 5 ng/ml recombinant MCP-1 and analyzed for CCR2 expression by flow cytometry. Data are presented relative to the unstimulated control as mean ± SD. **(C)** PBMCs of healthy donors were stimulated for 6 h with NETs (500 ng/ml dsDNA content), MCP-1 (5 ng/ml), NETs and MCP-1, and neutrophil control supernatant (PMN-SN) to investigate the effect on CCR2 expression as mean fluorescence intensity (MFI). Data are presented as mean ± SD. Experiments were repeated with four different donors and analyzed by repeated measures one-way ANOVA followed by Tukey's multiple comparisons test. **$p < 0.01$, ***$p < 0.001$, ****$p < 0.0001$.

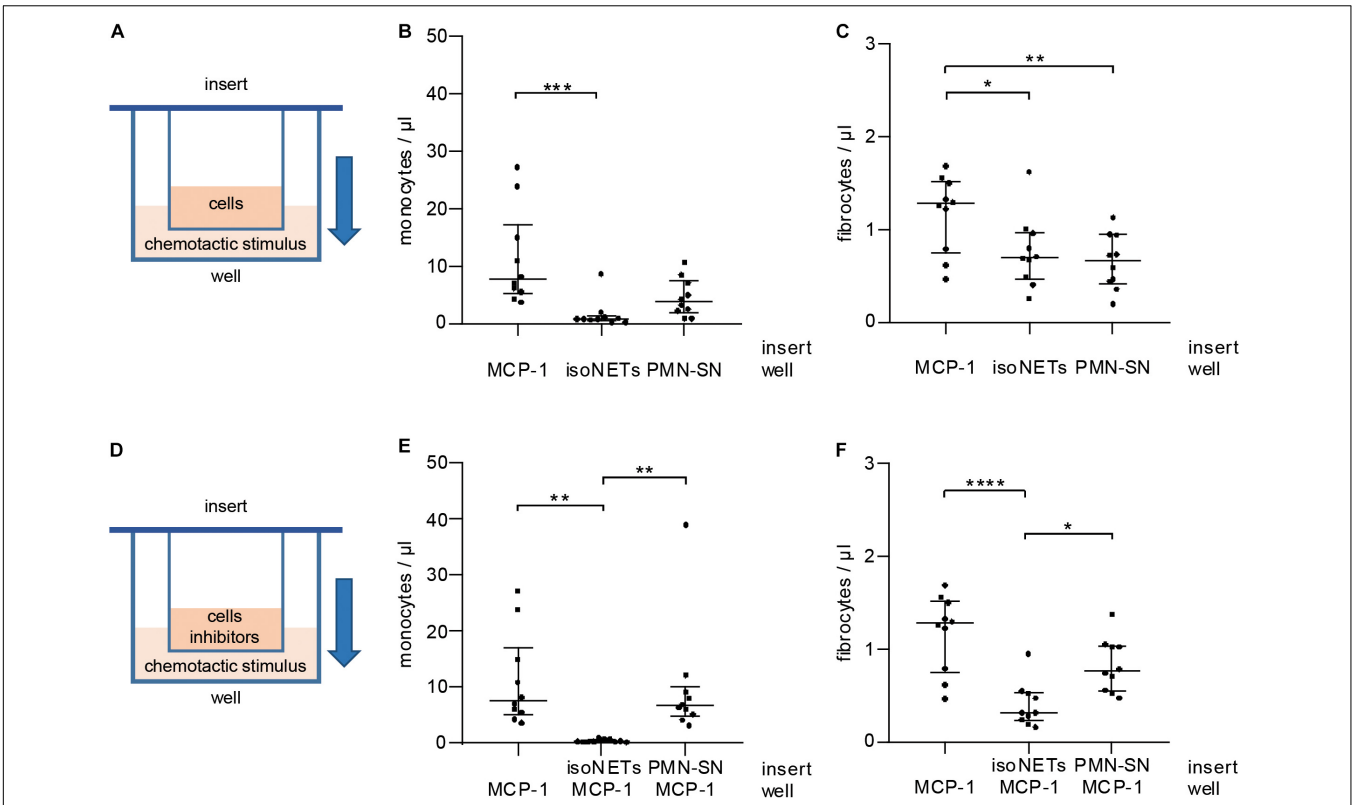

FIGURE 6 | Influence of MCP-1 and NETs on monocyte and fibrocyte migration *in vitro*. **(A)** PBMCs were subjected to chemotaxis assays using cell culture inserts. MCP-1 (500 pg/ml), NETs (500 ng/ml dsDNA content), and neutrophil control supernatant (PMN-SN) were compared as chemoattractants (well). Chemotaxis was assessed by flow cytometry recording of **(B)** monocyte and **(C)** fibrocyte cell counts/µl. **(D)** NETs (500 ng/ml dsDNA content) and neutrophil control supernatant were investigated as inhibitors of MCP-1-mediated migration. Migrated cells were stained and counted by flow cytometry recording **(E)** monocytes and **(F)** fibrocytes/µl. Experiments were repeated with PBMCs and NETs of 10 healthy donors. Monocyte counts of graphs **(B,E)** were compared with Friedman test followed by Dunn's multiple comparisons test, and fibrocyte counts of graphs **(C,D)** were analyzed by repeated measures ANOVA followed by Tukey's multiple comparisons test. $^{*}p < 0.05$, $^{**}p < 0.01$, $^{***}p < 0.001$, $^{****}p < 0.0001$.

separating cells from the chemotactic stimulus by a porous membrane (**Figure 6A**). NETs did not act as a chemotactic stimulus for monocytes (**Figure 6B**) and were significantly less potent chemoattractants for fibrocytes (**Figure 6C**) than MCP-1. Control supernatant of unstimulated neutrophils did not exhibit significantly enhanced chemotactic properties when compared to NETs. Next, NETs were tested as inhibitors of MCP-1-mediated chemotaxis (**Figure 6D**). While monocytes could still migrate in response to MCP-1 when incubated with neutrophil control supernatant, presence of NETs in the cell suspension abolished any directed chemotaxis (**Figure 6E**). Fibrocyte migration was significantly reduced by NETs, but not by neutrophil control supernatant (**Figure 6F**).

DISCUSSION

In this study, we investigated pro-inflammatory effects of NETs at the culprit site of STEMI patients. We observed a marked local increase of the chemoattractant MCP-1 and the NET surrogate markers dsDNA and citH3 at the culprit site. MCP-1 promoted NET formation *in vitro* and NETs prompted a pro-inflammatory phenotype in hCAECs, inducing MCP-1 transcription and release as well as elevation of ICAM-1 and IL-6 mRNA expression. MCP-1 and NETs downregulated CCR2 receptor expression on fibrocytes *in vitro* and *in vivo*. NETs did not act as a chemotactic stimulus *in vitro* and seem to even suppress MCP-1-mediated migration. A graphical abstract is provided as **Figure 7**.

NETs dominate the acute inflammatory setting of STEMI (Mangold et al., 2015; Helseth et al., 2019). We reported that besides their cytotoxic (Saffarzadeh et al., 2012) and pro-thrombotic (Fuchs et al., 2012) properties, the presence of NETs affects other cell types such as fibrocytes (Hofbauer et al., 2019) and monocytes (Mangold et al., 2019) that are recruited to the culprit site and the ischemic myocardium. An important chemotactic molecule orchestrating immune cell recruitment in STEMI is MCP-1 (Prabhu and Frangogiannis, 2016).

Marked elevations of systemic MCP-1 levels in STEMI (Benson et al., 2013), NSTEMI, and patients with unstable angina (Wang et al., 2007) compared to healthy controls have been reported. Adding to these observations, we found MCP-1 to be highly increased at the culprit site, exceeding peripheral levels in STEMI. The time course of inflammation is reflected by a decline of MCP-1 in serial blood draws 72 h after STEMI in

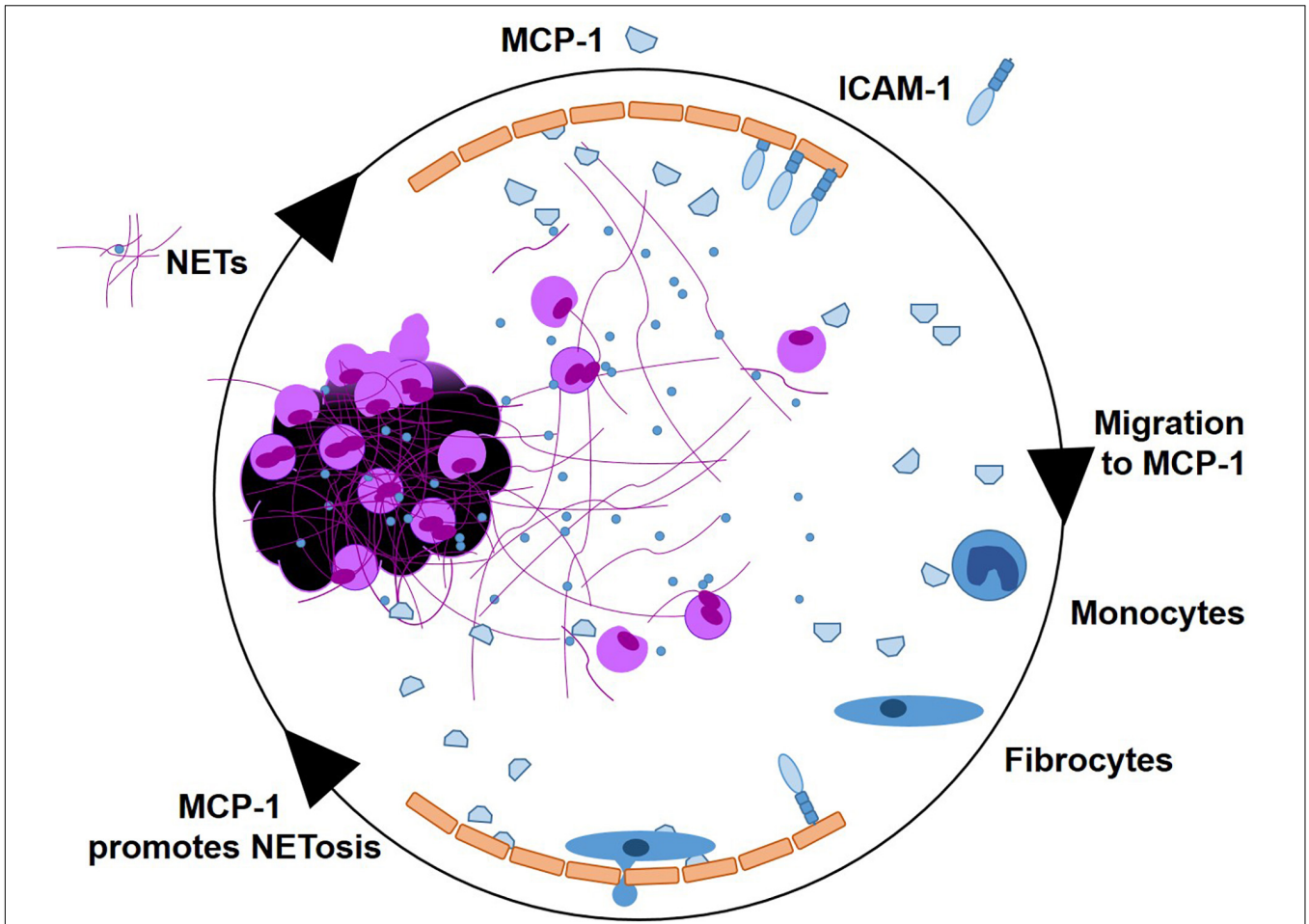

FIGURE 7 | Graphical abstract. NETs as signaling scaffolds at the culprit site of STEMI. MCP-1 and ICAM-1 are expressed by endothelial cells. MCP-1 stimulates further NETosis. Monocytes enter the culprit site along an MCP-1 gradient, to transdifferentiate into fibrocytes in the presence of NETs.

our study, which were still significantly higher than in healthy controls. Moreover, we could show that culprit site MCP-1 levels were significantly associated with infarct size in a multiple linear regression model complementing previous data on MCP-1 levels and patient survival after STEMI (de Lemos et al., 2007).

We found MCP-1 levels to be positively correlated with the NET markers dsDNA and citH3 at the culprit site; therefore, it was of interest to investigate potential causal relationships *in vitro*. MCP-1 is released by a variety of cell types such as smooth muscle cells, monocytes, and endothelial cells (Deshmane et al., 2009). As endothelium can be activated by neutrophil granule proteins (Soehnlein et al., 2009), we hypothesized that coronary artery endothelial cells would mount an inflammatory response in reaction to culprit site NETs. Indeed, we observed a potent manifold increase of MCP-1 mRNA and protein release by hCAECs when stimulated with culprit site levels of NETs. This effect seemed to be primarily mediated by neutrophil granule proteins attached to NETs, as we only observed an inferior impact of dsDNA and no effect by citH3. Moreover, treatment with human recombinant DNase 1 did not block MCP-1 release. In high concentrations, histones are cytotoxic for endothelial cells (Saffarzadeh et al., 2012). However, it is possible that signaling may require DNA and histones together as recently shown in monocytes (Tsourouktsoglou et al., 2020).

Our data suggest that MCP-1 is a component of the inflammatory cycle by enhancing and priming NET formation. As indicated by our *in vitro* data, MCP-1 promoted citrullination of histones and NET release upon a second stimulus. However, we were not able to link these observations to enhanced intracellular Ca^{2+} mobilization or ROS production in healthy donor neutrophils.

A mutual induction of NETs and MCP-1 is bound to attract other immune cells to the culprit site. Apart from previous reports on infarct-triggered infiltration of monocytes and macrophages (Dewald et al., 2005), we have recently shown accumulation of fibrocytes at the culprit site of STEMI with implications for ventricular dysfunction (Hofbauer et al., 2019). In this study, we report that relative fibrocyte influx seems dependent on the MCP-1 gradient between peripheral

and culprit site. As MCP-1 is recognized by the chemokine receptor CCR2 (Luster, 1998), we measured CCR2 on fibrocytes to investigate fibrocyte trafficking in STEMI. CCR2 receptor expression was decreased on culprit site fibrocytes compared to the peripheral control. Furthermore, excessive increases of MCP-1 at the culprit site were associated with decreased CCR2 expression levels. To enable effective chemotaxis, leukocytes adapt receptor expression levels by uncoupling or internalization of receptors in response to ligand binding (Franci et al., 1996). Therefore, we hypothesized that fibrocyte CCR2 was downregulated at the culprit site in response to high MCP-1 concentrations, a process already described in monocytes (Handel et al., 2008;Volpe et al., 2012). Indeed, fibrocytes dose-dependently downregulated CCR2 *in vitro* when stimulated with MCP-1, however, the extent observed *in vivo* could not be achieved with physiological doses. Accordingly, we also investigated the effect of NETs on CCR2 expression. Incubation with culprit site concentrations of NETs led to a marked decrease of CCR2 on fibrocytes. To investigate whether NETs would also influence monocyte or fibrocyte chemotaxis, we performed *in vitro* migration experiments. NETs did not exhibit significant chemotactic properties in comparison to MCP-1 for fibrocytes or their progenitors, monocytes. Migration toward MCP-1 was even repressed by NETs added to the cell suspension. Chemotaxis by CCR2 signaling was inhibited in monocytes and fibrocytes. This is especially interesting as macrophages were recently reported to digest and then engulf NETs via macropinocytosis as mechanism of clearing (Haider et al., 2020). Cardiac repair demands a timely transition from early inflammation to wound healing without disproportionally prolonged or excessively unbalanced immune responses (Prabhu and Frangogiannis, 2016). We speculate that blockade by NETs could limit MCP-1-mediated accumulation to a certain degree but at the same time ensures extravasation of inflammatory cells into inflamed tissue. In support of this theory, addition of isolated NETs to hCAECs *in vitro* led to increased transcription of the adhesion molecule ICAM-1, an effect described in response to CAP37, an anti-microbial neutrophil protein, on human umbilical vein endothelial cells (Lee et al., 2003). Expression of CAMs is expected to facilitate extravasation of cells for subsequent clearance of dead cells in infarcted tissue enabling tissue repair (Prabhu and Frangogiannis, 2016). Furthermore, we have previously reported that NETs also enhanced the adhesion marker CD11b on fibrocytes (Hofbauer et al., 2019). CD11b facilitates leukocyte adhesion to the endothelium (Diamond et al., 1990). Consequently, fibrocytes were found increased in infarcted sections compared to healthy myocardium (Hofbauer et al., 2019), raising the possibility that accumulated fibrocytes contribute to adverse remodeling and scar formation by production of extracellular matrix in cardiac tissue.

Unfortunately, *in vitro* studies of NETs and their effects on receptors and signaling cascades are subject to certain limitations. Proteomic analysis of NETs formed spontaneously compared with in response to ionomycin, phorbol myristate acetate, and LPS exhibited only 22% protein homology (Petretto et al., 2019). Attached granule proteins and chemokines and thus the inflammatory setting possibly differ between diseases (Bruschi et al., 2019). However, our protocol for NET preparation using phorbol myristate acetate was associated with proteins of the immune response, interleukin signaling, degranulation, and cytoskeleton organization (Petretto et al., 2019). Detection of NETs in the circulation typically relies on markers that are not specific for NETs. dsDNA, for example, is a general marker of cell death (Pisetsky, 2016). The exception is citH3, which is firmly established as a specific marker for NETs (Savchenko et al., 2014; Warnatsch et al., 2015; Laridan et al., 2017; Thalin et al., 2017, 2019).

Mutual induction of MCP-1 and NETs shapes the inflammatory milieu of the culprit site in STEMI. Both mediators contribute to the early phase of inflammation and synergistically transition to fibrocytes for vascular healing and scar formation.

DATA AVAILABILITY STATEMENT

The raw data supporting the conclusions of this article will be made available by the authors, without undue reservation.

ETHICS STATEMENT

The studies involving human participants were reviewed and approved by Ethics Committee of the Medical University of Vienna, Austria. The patients/participants provided their written informed consent to participate in this study.

AUTHOR CONTRIBUTIONS

TH, AO, and IL: conceptualization. TH, AO, AM, and CB: methodology. TH and AO: validation and TS formal analysis, writing—original draft preparation, and visualization. TH, AO, AM, TS, VS, and JN: investigation. AM, CB, and IL: resources. TH, AO, and VS: data curation. AM, TS, JN, VS, CB, and IL: writing—review and editing. AM and IL: supervision. IL: funding acquisition. All authors contributed to the article and approved the submitted version.

FUNDING

This study was supported by the Austrian Science Fund (FWF) projects SFB-F54 "Cellular Mediators Linking Inflammation and Thrombosis" and W 1205 Doktoratskollegs "Cell Communication in Health and Disease—CCHD".

SUPPLEMENTARY MATERIAL

The Supplementary Material for this article can be found online at: https://www.frontiersin.org/articles/10.3389/fcell.2020.564169/full#supplementary-material

REFERENCES

Awasthi, D., Nagarkoti, S., Kumar, A., Dubey, M., Singh, A. K., Pathak, P., et al. (2016). Oxidized LDL induced extracellular trap formation in human neutrophils via TLR-PKC-IRAK-MAPK and NADPH-oxidase activation. *Free Radic. Biol. Med.* 93, 190–203. doi: 10.1016/j.freeradbiomed.2016.01.004

Benson, V. L., Mcmahon, A. C., Khachigian, L. M., and Lowe, H. C. (2013). Acute local elevation in monocyte chemoattractant protein-1 (MCP-1), distal to the culprit lesion in acute ST elevation myocardial infarction. *Int. J. Cardiol.* 168, 1679–1680. doi: 10.1016/j.ijcard.2013.03.078

Brinkmann, V., Laube, B., Abu Abed, U., Goosmann, C., and Zychlinsky, A. (2010). Neutrophil extracellular traps: how to generate and visualize them. *J. Vis. Exp.* 24:1724.

Brinkmann, V., Reichard, U., Goosmann, C., Fauler, B., Uhlemann, Y., Weiss, D. S., et al. (2004). Neutrophil extracellular traps kill bacteria. *Science* 303, 1532–1535. doi: 10.1126/science.1092385

Bruschi, M., Petretto, A., Santucci, L., Vaglio, A., Pratesi, F., Migliorini, P., et al. (2019). Neutrophil Extracellular Traps protein composition is specific for patients with Lupus nephritis and includes methyl-oxidized alphaenolase (methionine sulfoxide 93). *Sci. Rep.* 9:7934.

Bucala, R., Spiegel, L. A., Chesney, J., Hogan, M., and Cerami, A. (1994). Circulating fibrocytes define a new leukocyte subpopulation that mediates tissue repair. *Mol. Med.* 1, 71–81. doi: 10.1007/bf03403533

Cai, G., Zhang, B., Weng, W., Shi, G., and Huang, Z. (2015). The associations between the MCP-1 -2518 A/G polymorphism and ischemic heart disease and ischemic stroke: a meta-analysis of 28 research studies involving 21,524 individuals. *Mol. Biol. Rep.* 42, 997–1012. doi: 10.1007/s11033-014-3836-8

Chervoneva, I., Li, Y., Schulz, S., Croker, S., Wilson, C., Waldman, S. A., et al. (2010). Selection of optimal reference genes for normalization in quantitative RT-PCR. *BMC Bioinform.* 11:253. doi: 10.1186/1471-2105-11-253

Crimi, G., Pica, S., Raineri, C., Bramucci, E., De Ferrari, G. M., Klersy, C., et al. (2013). Remote ischemic post-conditioning of the lower limb during primary percutaneous coronary intervention safely reduces enzymatic infarct size in anterior myocardial infarction: a randomized controlled trial. *JACC Cardiovasc. Interv.* 6, 1055–1063. doi: 10.1016/j.jcin.2013.05.011

de Boer, O. J., Li, X., Teeling, P., Mackaay, C., Ploegmakers, H. J., Van Der Loos, C. M., et al. (2013). Neutrophils, neutrophil extracellular traps and interleukin-17 associate with the organisation of thrombi in acute myocardial infarction. *Thromb. Haemost.* 109, 290–297. doi: 10.1160/th12-06-0425

de Lemos, J. A., Morrow, D. A., Blazing, M. A., Jarolim, P., Wiviott, S. D., Sabatine, M. S., et al. (2007). Serial measurement of monocyte chemoattractant protein-1 after acute coronary syndromes: results from the A to Z trial. *J. Am. Coll. Cardiol.* 50, 2117–2124. doi: 10.1016/j.jacc.2007.06.057

Deshmane, S. L., Kremlev, S., Amini, S., and Sawaya, B. E. (2009). Monocyte chemoattractant protein-1 (MCP-1): an overview. *J. Interf. Cytokine Res.* 29, 313–326.

Dewald, O., Zymek, P., Winkelmann, K., Koerting, A., Ren, G., Abou-Khamis, T., et al. (2005). CCL2/monocyte chemoattractant protein-1 regulates inflammatory responses critical to healing myocardial infarcts. *Circ. Res.* 96, 881–889. doi: 10.1161/01.res.0000163017.13772.3a

Diamond, M. S., Staunton, D. E., De Fougerolles, A. R., Stacker, S. A., Garcia-Aguilar, J., Hibbs, M. L., et al. (1990). ICAM-1 (CD54): a counter-receptor for Mac-1 (CD11b/CD18). *J. Cell Biol.* 111, 3129–3139. doi: 10.1083/jcb.111.6.3129

Distelmaier, K., Adlbrecht, C., Jakowitsch, J., Winkler, S., Dunkler, D., Gerner, C., et al. (2009). Local complement activation triggers neutrophil recruitment to the site of thrombus formation in acute myocardial infarction. *Thromb. Haemost.* 102, 564–572. doi: 10.1160/th09-02-0103

Distelmaier, K., Winter, M. P., Dragschitz, F., Redwan, B., Mangold, A., Gleiss, A., et al. (2014). Prognostic value of culprit site neutrophils in acute coronary syndrome. *Eur. J. Clin. Invest.* 44, 257–265. doi: 10.1111/eci.12228

Ekert, J. E., Murray, L. A., Das, A. M., Sheng, H., Giles-Komar, J., and Rycyzyn, M. A. (2011). Chemokine (C-C motif) ligand 2 mediates direct and indirect fibrotic responses in human and murine cultured fibrocytes. *Fibrogen. Tissue Repair* 4:23.

Fang, L., Moore, X. L., Chan, W., White, D. A., Chin-Dusting, J., and Dart, A. M. (2012). Decreased fibrocyte number is associated with atherosclerotic plaque instability in man. *Cardiovasc. Res.* 95, 124–133. doi: 10.1093/cvr/cvs156

Franci, C., Gosling, J., Tsou, C. L., Coughlin, S. R., and Charo, I. F. (1996). Phosphorylation by a G protein-coupled kinase inhibits signaling and promotes internalization of the monocyte chemoattractant protein-1 receptor. Critical role of carboxyl-tail serines/threonines in receptor function. *J. Immunol.* 157, 5606–5612.

Frangogiannis, N. G., Dewald, O., Xia, Y., Ren, G., Haudek, S., Leucker, T., et al. (2007). Critical role of monocyte chemoattractant protein-1/CC chemokine ligand 2 in the pathogenesis of ischemic cardiomyopathy. *Circulation* 115, 584–592. doi: 10.1161/circulationaha.106.646091

Fuchs, T. A., Abed, U., Goosmann, C., Hurwitz, R., Schulze, I., Wahn, V., et al. (2007). Novel cell death program leads to neutrophil extracellular traps. *J. Cell Biol.* 176, 231–241. doi: 10.1083/jcb.200606027

Fuchs, T. A., Brill, A., and Wagner, D. D. (2012). Neutrophil extracellular trap (NET) impact on deep vein thrombosis. *Arteriosc. Thromb. Vasc. Biol.* 32, 1777–1783. doi: 10.1161/atvbaha.111.242859

Haider, P., Kral-Pointner, J. B., Mayer, J., Richter, M., Kaun, C., Brostjan, C., et al. (2020). Neutrophil Extracellular trap degradation by differently polarized macrophage subsets. *Arteriosc. Thromb. Vasc. Biol.* 40, 2265–2278. doi: 10.1161/atvbaha.120.314883

Handel, T. M., Johnson, Z., Rodrigues, D. H., Dos Santos, A. C., Cirillo, R., Muzio, V., et al. (2008). An engineered monomer of CCL2 has anti-inflammatory properties emphasizing the importance of oligomerization for chemokine activity in vivo. *J. Leukoc. Biol.* 84, 1101–1108. doi: 10.1189/jlb.0108061

Hartley, A., Marshall, D. C., Salciccioli, J. D., Sikkel, M. B., Maruthappu, M., and Shalhoub, J. (2016). Trends in mortality from ischemic heart disease and cerebrovascular disease in Europe: 1980 to 2009. *Circulation* 133, 1916–1926. doi: 10.1161/circulationaha.115.018931

Helseth, R., Shetelig, C., Andersen, G. O., Langseth, M. S., Limalanathan, S., Opstad, T. B., et al. (2019). Neutrophil extracellular trap components associate with infarct size, ventricular function, and clinical outcome in STEMI. *Med. Inflamm.* 2019:7816491.

Hofbauer, T. M., Mangold, A., Scherz, T., Seidl, V., Panzenbock, A., Ondracek, A. S., et al. (2019). Neutrophil extracellular traps and fibrocytes in ST-segment elevation myocardial infarction. *Basic Res. Cardiol.* 114:33.

Ibanez, B., James, S., Agewall, S., Antunes, M. J., Bucciarelli-Ducci, C., Bueno, H., et al. (2018). 2017 ESC Guidelines for the management of acute myocardial infarction in patients presenting with ST-segment elevation: the Task Force for the management of acute myocardial infarction in patients presenting with ST-segment elevation of the European Society of Cardiology (ESC). *Eur. Heart J.* 39, 119–177.

Keeley, E. C., Mehrad, B., Janardhanan, R., Salerno, M., Hunter, J. R., Burdick, M. M., et al. (2012). Elevated circulating fibrocyte levels in patients with hypertensive heart disease. *J. Hypertens.* 30, 1856–1861. doi: 10.1097/hjh.0b013e32835639bb

Keeley, E. C., Mehrad, B., and Strieter, R. M. (2011). The role of fibrocytes in fibrotic diseases of the lungs and heart. *Fibrogen. Tissue Repair* 4:2. doi: 10.1186/1755-1536-4-2

Kozera, B., and Rapacz, M. (2013). Reference genes in real-time PCR. *J. Appl. Genet.* 54, 391–406.

Laridan, E., Denorme, F., Desender, L., François, O., Andersson, T., Deckmyn, H., et al. (2017). Neutrophil extracellular traps in ischemic stroke thrombi. *Ann. Neurol.* 82, 223–232. doi: 10.1002/ana.24993

Lee, T. D., Gonzalez, M. L., Kumar, P., Grammas, P., and Pereira, H. A. (2003). CAP37, a neutrophil-derived inflammatory mediator, augments leukocyte adhesion to endothelial monolayers. *Microvasc. Res.* 66, 38–48. doi: 10.1016/s0026-2862(03)00010-4

Libby, P. (2013). Mechanisms of acute coronary syndromes and their implications for therapy. *N. Engl. J. Med.* 368, 2004–2013. doi: 10.1056/nejmra1216063

Libby, P., Ridker, P. M., and Hansson, G. K. (2011). Progress and challenges in translating the biology of atherosclerosis. *Nature* 473, 317–325. doi: 10.1038/nature10146

Luster, A. D. (1998). Chemokines–chemotactic cytokines that mediate inflammation. *N. Engl. J. Med.* 338, 436–445. doi: 10.1056/nejm199802123380706

Maier, W., Altwegg, L. A., Corti, R., Gay, S., Hersberger, M., Maly, F. E., et al. (2005). Inflammatory markers at the site of ruptured plaque in acute myocardial infarction: locally increased interleukin-6 and serum amyloid A but

decreased C-reactive protein. *Circulation* 111, 1355–1361. doi: 10.1161/01.cir.0000158479.58589.0a

Mangold, A., Alias, S., Scherz, T., Hofbauer, T., Jakowitsch, J., Panzenbock, A., et al. (2015). Coronary neutrophil extracellular trap burden and deoxyribonuclease activity in ST-elevation acute coronary syndrome are predictors of ST-segment resolution and infarct size. *Circ. Res.* 116, 1182–1192. doi: 10.1161/circresaha.116.304944

Mangold, A., Hofbauer, T. M., Ondracek, A. S., Artner, T., Scherz, T., Speidl, W. S., et al. (2019). Neutrophil extracellular traps and monocyte subsets at the culprit lesion site of myocardial infarction patients. *Sci. Rep.* 9:16304.

Martinod, K., Demers, M., Fuchs, T. A., Wong, S. L., Brill, A., Gallant, M., et al. (2013). Neutrophil histone modification by peptidylarginine deiminase 4 is critical for deep vein thrombosis in mice. *Proc. Natl. Acad. Sci. U.S.A.* 110, 8674–8679. doi: 10.1073/pnas.1301059110

Medbury, H. J., Tarran, S. L., Guiffre, A. K., Williams, M. M., Lam, T. H., Vicaretti, M., et al. (2008). Monocytes contribute to the atherosclerotic cap by transformation into fibrocytes. *Int. Angiol.* 27, 114–123.

Metzler, K. D., Goosmann, C., Lubojemska, A., Zychlinsky, A., and Papayannopoulos, V. (2014). A myeloperoxidase-containing complex regulates neutrophil elastase release and actin dynamics during NETosis. *Cell Rep.* 8, 883–896. doi: 10.1016/j.celrep.2014.06.044

Petretto, A., Bruschi, M., Pratesi, F., Croia, C., Candiano, G., Ghiggeri, G., et al. (2019). Neutrophil extracellular traps (NET) induced by different stimuli: a comparative proteomic analysis. *PLoS One* 14:e0218946. doi: 10.1371/journal.pone.0218946

Pfaffl, M. W. (2001). A new mathematical model for relative quantification in real-time RT-PCR. *Nucleic Acids Res.* 29:e45.

Pilling, D., Fan, T., Huang, D., Kaul, B., and Gomer, R. H. (2009). Identification of markers that distinguish monocyte-derived fibrocytes from monocytes, macrophages, and fibroblasts. *PLoS One* 4:e7475. doi: 10.1371/journal.pone.0007475

Pisetsky, D. S. (2016). Anti-DNA antibodies–quintessential biomarkers of SLE. *Nat. Rev. Rheumatol.* 12, 102–110. doi: 10.1038/nrrheum.2015.151

Prabhu, S. D., and Frangogiannis, N. G. (2016). The biological basis for cardiac repair after myocardial infarction. *Circ. Res.* 119, 91–112. doi: 10.1161/circresaha.116.303577

Remijsen, Q., Kuijpers, T. W., Wirawan, E., Lippens, S., Vandenabeele, P., and Vanden Berghe, T. (2011). Dying for a cause: NETosis, mechanisms behind an antimicrobial cell death modality. *Cell Death Differ.* 18, 581–588. doi: 10.1038/cdd.2011.1

Rovin, B. H., Lu, L., and Saxena, R. (1999). A Novel Polymorphism in the MCP-1 gene regulatory region that influences MCP-1 expression. *Biochem. Biophys. Res. Commun.* 259, 344–348. doi: 10.1006/bbrc.1999.0796

Saffarzadeh, M., Juenemann, C., Queisser, M. A., Lochnit, G., Barreto, G., Galuska, S. P., et al. (2012). Neutrophil extracellular traps directly induce epithelial and endothelial cell death: a predominant role of histones. *PLoS One* 7:e32366. doi: 10.1371/journal.pone.0032366

Savchenko, A. S., Martinod, K., Seidman, M. A., Wong, S. L., Borissoff, J. I., Piazza, G., et al. (2014). Neutrophil extracellular traps form predominantly during the organizing stage of human venous thromboembolism development. *J. Thromb. Haemost.* 12, 860–870. doi: 10.1111/jth.12571

Soehnlein, O., Zernecke, A., and Weber, C. (2009). Neutrophils launch monocyte extravasation by release of granule proteins. *Thromb. Haemost.* 102, 198–205. doi: 10.1160/th08-11-0720

Thalin, C., Daleskog, M., Goransson, S. P., Schatzberg, D., Lasselin, J., Laska, A. C., et al. (2017). Validation of an enzyme-linked immunosorbent assay for the quantification of citrullinated histone H3 as a marker for neutrophil extracellular traps in human plasma. *Immunol. Res.* 65, 706–712. doi: 10.1007/s12026-017-8905-3

Thalin, C., Hisada, Y., Lundstrom, S., Mackman, N., and Wallen, H. (2019). Neutrophil extracellular traps: villains and targets in arterial, venous, and cancer-associated thrombosis. *Arteriosc. Thromb. Vasc. Biol.* 39, 1724–1738. doi: 10.1161/atvbaha.119.312463

Tsourouktsoglou, T. D., Warnatsch, A., Ioannou, M., Hoving, D., Wang, Q., and Papayannopoulos, V. (2020). Histones, DNA, and citrullination promote neutrophil extracellular trap inflammation by regulating the localization and activation of TLR4. *Cell Rep.* 31:107602. doi: 10.1016/j.celrep.2020.107602

Volpe, S., Cameroni, E., Moepps, B., Thelen, S., Apuzzo, T., and Thelen, M. (2012). CCR2 acts as scavenger for CCL2 during monocyte chemotaxis. *PLoS One* 7:e37208. doi: 10.1371/journal.pone.037208

Vong, L., Sherman, P. M., and Glogauer, M. (2013). Quantification and visualization of neutrophil extracellular traps (NETs) from murine bone marrow-derived neutrophils. *Methods Mol. Biol.* 1031, 41–50. doi: 10.1007/978-1-62703-481-4_5

Wang, J., Zhang, S., Jin, Y., Qin, G., Yu, L., and Zhang, J. (2007). Elevated levels of platelet-monocyte aggregates and related circulating biomarkers in patients with acute coronary syndrome. *Int. J. Cardiol.* 115, 361–365. doi: 10.1016/j.ijcard.2006.03.019

Wang, Y., Wysocka, J., Sayegh, J., Lee, Y. H., Perlin, J. R., Leonelli, L., et al. (2004). Human PAD4 regulates histone arginine methylation levels via demethylimination. *Science* 306, 279–283. doi: 10.1126/science.1101400

Warnatsch, A., Ioannou, M., Wang, Q., and Papayannopoulos, V. (2015). Inflammation. Neutrophil extracellular traps license macrophages for cytokine production in atherosclerosis. *Science* 349, 316–320. doi: 10.1126/science.aaa8064

Conflict of Interest: The authors declare that the research was conducted in the absence of any commercial or financial relationships that could be construed as a potential conflict of interest.

frontiers in Cell and Developmental Biology

ORIGINAL RESEARCH
published: 30 November 2020
doi: 10.3389/fcell.2020.578790

Brahma-Related Gene 1 Deficiency in Endothelial Cells Ameliorates Vascular Inflammatory Responses in Mice

Yuanyuan Zhang[2], Huidi Wang[1], Mingzi Song[3], Tongchang Xu[1], Xuyang Chen[1], Tianfa Li[2] and Teng Wu[1]**

[1] *Key Laboratory of Targeted Intervention of Cardiovascular Disease, Department of Pathophysiology, Collaborative Innovation Center for Cardiovascular Translational Medicine, Nanjing Medical University, Nanjing, China,* [2] *Department of Cardiology, The First Affiliated Hospital of Hainan Medical University, Haikou, China,* [3] *Laboratory Center for Experimental Medicine, Jiangsu Health Vocational College, Nanjing, China*

Endothelial dysfunction plays an important role in promoting the progression of disease genesis such as atherosclerosis and abdominal aortic aneurysm (AAA). The physiological unbalance of endothelial cells is a major pathological basis. In this present study, we investigated Brahma-related gene 1 (BRG1), a chromatin remodeling protein, was in mouse models of diabetic atherosclerosis and AAA, focusing on its role in endothelial dysfunction. We report that compared with their wild-type (WT, ApoE$^{-/-}$; BRG1$^{fl/fl}$) littermates, endothelium conditional BRG1 knockout mice (CKO, ApoE$^{-/-}$; BRG1$^{fl/fl}$; CDH5-*cre*) exhibited an alleviated phenotype of diabetic atherosclerosis. Immunohistochemically staining and real-time PCR analysis demonstrated fewer macrophages recruitment with a reduction of vascular inflammatory in CKO mice compared with WT mice. Further research in the Ang-II induced AAA model revealed that BRG1 deficiency had the protective effects on endothelium conditional BRG1 deletion, evidenced by the downregulation of pro-inflammatory mediators [interleukin (IL)-1β and IL-6, not tumor necrosis factor-α (TNF-α)] in the vessels of CKO mice compared with WT mice. In Ea.hy926 cell lines, anti-BRG1 small interfering RNA and PFI-3 treatment obviously alleviated tumor necrosis factor-α-induced IL-6 and CCL2 expression, and further research demonstrated that the BRG1 inhibition in endothelial cells not only decreased c-Fos expression but also blocked the c-Fos translocation into nuclei. In conclusion, our results suggest that endothelial BRG1 deficiency may protect the mice from diabetic atherosclerosis and AAA via inhibiting inflammatory response in vessels.

Keywords: BRG1, endothelium, diabetic atherosclerosis, abdominal aortic aneurysms, inflammation

OPEN ACCESS

Edited by:
Silvia Fischer,
University of Giessen, Germany

Reviewed by:
Xinyu Weng,
Fudan University, China
Gillian Douglas,
University of Oxford, United Kingdom

****Correspondence:***
Tianfa Li
litf79997@163.com
Teng Wu
tengwu@njmu.edu.cn

Specialty section:
This article was submitted to Molecular Medicine, a section of the journal Frontiers in Cell and Developmental Biology

Received: *01 July 2020*
Accepted: *27 October 2020*
Published: *30 November 2020*

Citation:
Zhang Y, Wang H, Song M, Xu T, Chen X, Li T and Wu T (2020) Brahma-Related Gene 1 Deficiency in Endothelial Cells Ameliorates Vascular Inflammatory Responses in Mice. Front. Cell Dev. Biol. 8:578790. doi: 10.3389/fcell.2020.578790

INTRODUCTION

Endothelium, a continuous monolayer of endothelial cells, separates the circulation and the vascular basal lamina under physiological conditions (Kruger-Genge et al., 2019). Endothelial injury, also called endothelial dysfunction, is a prominent feature in many cases and directly causes vascular injury. Endothelial injury is key to the initiation and progression of severe vascular diseases, including atherosclerosis and aneurysms (Czubryt, 2015). In these diseases,

injured endothelial cells mediate the inflammatory response, which further inducing recruitment of macrophages, proliferation and migration of smooth muscle cells, and expressing adhesion molecules, finally promoting the progression of the disease (Li H. et al., 2018; Maguire et al., 2019).

Diabetes mellitus affects more than 180 million people worldwide. Diabetic patients exhibit significantly higher risk for cardiovascular disease (CVD) (Boyle et al., 2001). Diabetes is often accompanied by synergistic risk factors such as hypertension, obesity, systemic inflammation, hypercoagulability, and dyslipidemia, which further increase CVD death rates (Stamler et al., 1993). For instance, there is a growth of evidence that also showed a higher prevalence of arteriosclerosis in people with diabetes. In addition, numerous observational studies have found increased levels of the mediators of inflammation, such as C-reactive protein, interleukin-6 (IL-6), and plasminogen activator inhibitor 1, to name only a few, as major associative findings between diabetes and atherosclerosis (La Sala et al., 2019). Insulin resistance, a prominent feature of type 2 diabetes mellitus, has been demonstrated as an important risk factor for inducing atherosclerosis among the patients diagnosed with diabetes even in the absence of hyperglycemia (DeFronzo, 2010). Interestingly, previous research also found the insulin receptors in vascular endothelial cells, which indicates the role of insulin in the regulation of vascular endothelial cells (Han et al., 2011; Pansuria et al., 2012). Further studies also proved that hyperglycemia induced excessive endothelial inflammatory response. It has been considered as the main reason for the endothelial injury, which further promotes diabetes mellitus-associated CVDs (Fadini et al., 2016). For instance, recent research proposed that inflammatory response induced by Nod-like receptor family pyrin domain containing 3 inflammasome or excessive reactive oxygen species (ROS) levels could induce endothelial injuries to promote atherosclerosis (Wang R. et al., 2017; Wan et al., 2019), a chronic inflammatory disease that can give rise to various CVDs. In this case, inflammatory cells and activated endothelial cells in atherosclerotic plaques upregulate adhesion molecules and release inflammatory cytokines such as tumor necrosis factor-α (TNF-α), IL-6, and IL-1β, promoting the progression of atherosclerosis (Siti et al., 2015). Statin therapy, traditional clinical therapeutic strategies for diabetes related atherosclerosis, was statistically significantly associated with reductions in the incidence of atherosclerotic CVD-caused mortality in the presence of diabetes. This effect decreased after age 85 years and disappeared in nonagenarians (Ramos et al., 2018). However, as the most frequently used drugs for atherosclerosis treatment, statin therapy may cause such adverse effects such as myopathy (Collins et al., 2016). Recently, preclinical research that suggested anti-inflammatory strategies such as metformin, berberine, or raising apolipoprotein AI levels were effective in atherosclerosis treatment for animal models (Barrett et al., 2019; Tang et al., 2019), which proved the effect of diabetic atherosclerosis treatment for anti-inflammatory strategy.

Pathologically, the features of abdominal aortic aneurysm (AAA) are complicated, including transmural inflammatory infiltration, noticeable breakdown of elastic lamellae, smooth muscle cell loss, and endothelial cell death and detachment (Moxon et al., 2010; Qin et al., 2013). The pathological changes of endothelial cells or endothelial dysfunction are possibly earlier than those of media and adventitia in the process of AAA formation. Heterogeneous research has shown that endothelial dysfunction promoted AAA pathogenesis via different factors, among which aberrant inflammation plays a key role (Dale et al., 2015). For example, ample evidence supports endothelial dysfunction, which enhanced the recruitment of circulating macrophages, finally leads to augment production and release of matrix metalloproteinases (MMPs), which in turn degrade elastin and disintegrate the medial layer (Samadzadeh et al., 2014). Inflammatory cytokines, such as IL-1β, IL-6, and TNF-α, have been reported to be significantly upregulated in patients with AAA (Lamblin et al., 2010; Golledge, 2019). These inflammatory mediators stimulate the expression of MMP-2 and MMP-9 in vessels, which lead to the damage of vascular wall integrity through inducing extracellular matrix degradation (Samadzadeh et al., 2014; Mallat, 2017). Anti-inflammatory treatment such as inhibition of the mammalian target of rapamycin pathway or genetic ablation of microRNA-33 attenuates inflammation and AAA (Li et al., 2017; Nakao et al., 2017), indicating that anti-inflammatory treatment should be the promising strategy for AAA treatment.

In the present investigation, we sought to determine the role of endothelial Brahma-related gene I (BRG1) in vascular inflammation in animal models of diabetes-related atherosclerosis or AAA. BRG1 is the catalytic subunit of the SWI/SNF chromatin remodeling complex and regulates gene expression via adenosine triphosphate hydrolysis-driven chromatin remodeling (Xu and Fang, 2012). Recent studies have found that BRG1 regulates heart muscle development in mice (Xiao et al., 2016). BRG1 can also regulate myocardial ischemia–reperfusion injury via inhibiting the inflammatory response and ROS production (Li Z. et al., 2018). Previous research demonstrated that endothelial-specific BRG1 knockout in mice could ameliorate the progression of atherosclerosis and AAA formation (Fang et al., 2013; Zhang et al., 2018a). However, the mechanism of BRG1 in regulating diabetes-related macrovascular cardiovascular atherosclerosis and Ang II induced AAA formation under *ApoE* gene knockout condition remain not to be proved. Here, we report that BRG1 deletion in endothelial cells blocked the progression of diabetes mellitus-related atherosclerosis and Ang II-induced AAA model under the *ApoE* gene knockout condition via inhibiting c-Fos expression as well as blocking c-Fos nucleic translocation, which further inhibits inflammatory response in endothelial cells. Our data hopefully may extend the current knowledge regarding the BRG1 function in CVDs.

MATERIALS AND METHODS

Ethics

The studies involving animals were reviewed and approved by the intramural Committee on Ethical Conduct of Animal Studies of Nanjing Medical University.

Reagents

Oil-red O powder was purchased from Sigma Aldrich (St. Louis, MO, United States, O0625). All the real-time polymerase chain reaction (PCR) primers were purchased from Sangon (Shanghai, China). Hematoxylin–eosin (H&E) stain kit was purchased from Beyotime Biotechnology Co. (Beijing, China, C0105). RNA extraction kit and real-time PCR kit were purchased from Vazyme Biotech Co., Ltd. (Nanjing, China, Q311). Streptozotocin (STZ) was purchased from Selleck Co. (Shanghai, China, S1312).

Animal Feeding

Homozygous apolipoprotein E-deficient mice (ApoE$^{-/-}$) were obtained from the Jackson Laboratory. According to the latest report, BRG1$^{fl/fl}$; CDH5-*cre* mice crossed by Brahma related gene 1-loxp (BRG1$^{fl/fl}$) mice and CDH5-*cre* mice were obtained from Nanjing Biomedical Research Institute of Nanjing University. ApoE$^{-/-}$ and BRG1*fl/fl*; CDH5-*cre* mice were crossed to obtain ApoE$^{-/-}$; BRG1$^{fl/fl}$; CDH5-cre mice. The F1 progeny of this mating (ApoE$^{\pm}$; BRG1$^{fl/+}$; CDH5^{-cre}) was crossed to obtain ApoE$^{-/-}$; BRG1$^{fl/fl}$; CDH5-*cre* [conditional knockout (CKO)] mice and their littermate control ApoE$^{-/-}$; BRG1$^{fl/fl}$ [wild-type (WT)] mice. All offspring were genotyped by PCR techniques and lived in specific pathogen-free conditions in accordance with the guidelines from the National Institutes of Health Guide for the Care and Use of Laboratory Animals in China.

Animal Model Construction

To induce diabetes-accelerated atherosclerosis, 8 weeks old male CKO and WT mice were intraperitoneally injected STZ for 5 days, then high-fat diets containing 40 kcal% fat, 1.25% cholesterol, 0.5% cholic acid (Research Diets, United States, D12109) bred for last 4 weeks. Ang II was utilized to induce mice AAA models; 8 weeks old male CKO and WT mice were randomly allocated to Ang II infusion or control, and mini-osmotic pumps (Alzet, Cupertino, CA) containing Ang II (1,000 ng/min per kg mice, Sigma, A9525) or saline were used by infusing Ang II or saline for 28 days using published protocols. Before killing, vessel diameter was determined by ultrasonography using a Vevo 660 imaging system (VisualSonics). Two-dimensional images (B mode) of the short-axis scan were acquired to determine the maximal diameters of suprarenal aortas. The abdominal aorta was immediately excised, photographed, and analyzed histologically.

Survival Rate, Body Weight, and Postprandial Blood Glucose Detection

The data of survival rate were collected after feeding up with high-fat diet. Before collecting mice tissue samples, we collected the data of mice's body weight, and postprandial blood glucose was measured directly from the tail tip with a glucometer.

Isolate Vascular Ring Function Experiment

Mice were killed using an overdose of ethyl ether and perfused with phosphate-buffered saline (PBS). The thoracic/abdominal aortas were separated from fat or other tissues. Then, the aortas were put into DMT 620M. Vasorelaxation of isolated aortic ring segments was determined in the oxygenated Krebs' solution. After an equilibration period of 60 min, aortic rings were stimulated to contract with contracted norepinephrine (10^{-7} M). Endothelium-dependent or independent relaxation was then assessed in response to a cumulation of acetylcholine (10^{-9}–10^{-5} M) or sodium nitroprusside (SNP, 10^{-9}–10^{-5} M). Relaxation at each concentration was measured and expressed as the percentage of force generated in response to norepinephrine.

Histology Staining

Mice abdominal artery were embedded in paraffin after fixed in 4% phosphate-buffered formalin, then achieved 4 μm thick tissue sections. For histological analysis, sections were stained with H&E or Verhoeff–Van Gieson.

Measurement of Atherosclerotic Lesions

Mice were killed using an overdose of ethyl ether and perfused with PBS. To assess the development of atherosclerosis, the thoracic/abdominal aortas separated from fat or other tissues were stained with Oil Red O (Sangon, Shanghai, China) for 90 min; aortic roots frozen sections by optimal cutting temperature embedding were stained with Oil Red O for 30 min. Imaging software (Image Pro Plus 6.0) was used to measure aortic lesions using the "en face" method, as previously described (Zheng et al., 2016).

Immunohistochemistry

For immunohistochemistry, dewaxed aortic root sections were fixed with cold acetone for 10 min, then incubated with mouse anti-CD68 (1:100, Abcam) at 4°C overnight. After washing three times with PBS, sections were incubated with goat anti-mouse secondary antibodies (Santa Cruz Biotechnology, United States) at 37°C for at least 1 h. Protein expression was visualized using 3,3′-diaminobenzidine (Vector Laboratories, CA) for 1.5 min, and hematoxylin was used to stain the nuclei.

For immunohistochemistry staining of aortic sections by anti-CD68 and α-smooth muscle actin (α-SMA), dewaxed aortic sections were boiled in 10 mM citrate (pH 6.0) for antigen retrieval, then incubated with mouse anti-CD68 (1:100, Abcam, Ab31630) and mouse anti-α-SMA antibody (1:200, Sigma, A2547) at 4°C overnight. After washing three times with PBS, sections were incubated with goat anti-mouse secondary antibodies (Santa Cruz Biotechnology, United States) at 37°C for at least 1 h. Protein expression was visualized using 3,3′-diaminobenzidine (Vector laboratories, CA) for 1.5 min, and hematoxylin was used to stain the nuclei.

RNA Extraction and Real-Time Polymerase Chain Reaction

RNA was extracted from mice aorta using an RNA extraction kit (HiScript II 1st strand cDNA Synthesis Kit) purchased from Vazyme Biotech Co., Ltd., according to the manufacturer's recommended protocol (Weng et al., 2019). A reverse transcription kit (Vazyme, ChamQ SYBR qPCR Master Mix) was used for reverse transcription. Complementary DNA was amplified

and measured using a StepOnePlus system (Applied Biosystems). Quantitative qPCR primer sequences were as follows: IL-6, forward 5′-TAGTCCTTCCTACCCCAATTTCC-3′ and reverse 5′-TTGGTCCTTAGCCACTCCTTC-3′; IL-1β forward 5′-TTAAAAACCTGGATCGGAACCAA-3′ and reverse 5′-GCATTAGCTTCAGATTTACGGGT-3′; TNF-α, forward 5′-ATGGGCTGTGATCGGAACTG-3′ and reverse 5′-GTCTTCCCAATAAGCATGTCTCC-3′. Ccl2 forward 5′-TTAAAAACCTGGATCGGAACCAA-3′ and reverse 5′-GCATTAGCTTCAGATTTACGGGT-3′; Ccl5 forward 5′-GCTGCTTTGCCTACCTCTCC-3′ and reverse 5′-TCGAGTGACAAACACGACTGC-3′; Ccl9 forward 5′-CCCTCTCCTTCCTCATTCTTACA-3′ and reverse 5′-AGTCTTGAAAGCCCATGTGAAA-3′; 18s rRNA forward 5′-CATTCGAACGTCTGCCCTATC-3′ and reverse 5′-CCTGCTGCCTTCCTTGGA-3′. Collagen I forward 5′-GCTCCTCTTAGGGGCCACT-3′ and reverse 5′-CCACGTCTCACCATTGGGG-3′; Collagen III forward 5′-CTGTAACATGGAAACTGGGGAAA-3′ and reverse 5′-CCATAGCTGAACTGAAAACCACC-3′. All PCR primers were purchased from Sangon. Quantitative measurements were obtained using the ΔCt method, using 18s rRNA as an internal control.

Cell Culture

Human endothelial cell line Ea.hy926 was cultured in Dulbecco's modified Eagle medium (DMEM) supplemented with 10% fetal bovine serum at 37°C in a 5% carbon dioxide incubator. Small interfering RNAs were purchased from Dharmacon. Transient transfection was performed with Lipofectamine 2000 (Invitrogen, United States, 11668019). Cells were harvested 48 h after transfection. TNF-α was purchased from Peprotech (United States, 300-01A-50). PFI-3 was purchased from Selleck (Shanghai, China, S7315). Ea.hy926 was seeded at 1×10^5 cells/p35 culture dish and starved in serum-free DMEM overnight. TNF-α (10 μg/L) was added the next day for another 12 or 24 h. In certain experiments, PFI-3 (2 μM) was added together with TNF-α.

Western Blot Technology

For Western blot, the total protein was extracted from Ea.hy926 cells receiving different treatments with radioimmunoprecipitation assay lysis (Beyotime, Shanghai, China) according to the recommended protocol (Li et al., 2020). Thirty micrograms of protein samples were separated on 10% sodium dodecyl sulfate-polyacrylamide gel electrophoresis and transferred to nitrocellulose filter membranes (Merck Millipore, Canada). After being blocked with 5% non-fat milk for 1 h at room temperature, the membranes were incubated with anti-TBP antibody (1:2,000 dilution, YIFEIXUE BIO TECH, A0055), anti-Poly II antibody (1:2,000 dilution, Proteintech, 20655-I-AP), anti-BRG1 antibody (1:2,000 dilution, Abcam, Ab110641), and anti-c-Jun and anti-c-Fos antibody (1:500 dilution, Santa Cruz, sc-1694 or sc-52) overnight at 4°C. The Anti-Poly II antibody or anti-TBP antibody was used as a standard internal protein for normalizing. Horseradish peroxidase-conjugated immunoglobulin G (YIFEIXUE BIO TECH, China) was used to amplify the signal. After treatment with the chemiluminescence kit (Thermo Fisher Scientific, United States), protein signals were detected by ChemiDoc RXC + (Bio-Rad, United States).

Immunofluorescence Staining

Briefly, cells were plated at a density of 2×10^4 cells per dish. After treatment with TNF-α, the cells were washed with PBS three times, fixed by 1% paraformaldehyde for 10 min, and stained with a c-Fos antibody (Sigma, United States A7811, 1:200) overnight at 4°C. The next day, the cells were incubated with AF488-labeled secondary antibody (Jackson ImmunoResearch) for 1 h. The nuclei were counterstained with 4',6-diamidino-2-phenylindole (Sigma, United States). Immunofluorescence was visualized on a confocal microscope (LSM 710, Zeiss).

Electrophoretic Mobility Shift Assay

Nuclear proteins for electrophoretic mobility shift assay (EMSA) were achieved according to the manufacturer's instruction. The nuclear proteins (5 μg) of each group were incubated with 1 × binding buffer (LightShift Chemiluminescent EMSA Kit, Pierce) in the presence of 50 ng/μl poly (dI/dC), 0.05% non-idet P-40, 5 mM $MgCl_2$, and 2.5% glycerol for 10 min and then incubated at room temperature for additional 20 min with 1 pmol of biotin-labeled Ap-1 oligonucleotide (Sangon Biotech Co., Ltd.). The reaction mixture was subjected to a 6% non-denaturing sodium dodecyl sulfate-polyacrylamide gel electrophoresis at 100 v for 50 min, transferred to polarity nylon hybridization transfer membrane (Beyotime, China) and DNA cross-linked for 2 min, and probed with peroxidase-conjugated streptavidin antibodies (1:1,500 dilution, Bytotime, China), then visualized with enhanced chemiluminescence and detected by ChemiDoc RXC + (Bio-Rad, United States). The sequences of Ap1 probe and mutant probe are listed: probe forward 5′-ATTTGTTCGGGGCGGGGCGAGC-3′; probe reverse 3′-TAAACAAGCCCCGCCCCGCTCG-5′.

Luciferase Report Assay

293T cells were transfected using Lipofectamine 2000 (Invitrogen, United States) in serum-free DMEM media with MCP-1-Luc plasmid (0.2 μg) and transfected with BRG1 overexpression adenoviruses. Six hours after transfection, the cells were culture in DMEM containing 10% fetal bovine serum for 24 h; the cells were lysed, and luciferase activity was determined by using the luciferase assay system according to the manufacturer's instruction (Promega Corp., United States). The MCP-1-Luc plasmid promoter fragments span the 2,000(−2,000) bp by region upstream of the transcription site. For controlling for differences in transfection efficiency, a plasmid that contained green fluorescent protein fluorescence was included in each transfection and used for normalization.

Statistical Analysis

Significant differences between the two groups were analyzed by unpaired Student's *t*-test (GraphPad Prism software, version 5.0; GraphPad Prism, United States). All experiments were performed with similar results, at least in triplicate repeat. Data are expressed as the mean ± SD. Statistical significance was set to $P < 0.05$.

RESULTS

Specific Deletion of Brahma-Related Gene 1 in Endothelial Cells Alleviated Diabetes Mellitus-Related Atherosclerosis

Diabetic atherosclerosis was induced in ApoE$^{-/-}$; BRG1$^{fl/fl}$; CDH5-*cre* mice (CKO) and their littermate control ApoE$^{-/-}$; BRG1$^{fl/fl}$ (WT) mice to evaluate the effects of endothelial-specific BRG1 deletion *in vivo*. As shown in **Figure 1A**, there was a significant mortality rate reduction in the ApoE$^{-/-}$; BRG1$^{fl/fl}$; CDH5-*cre* group compared with their littermate control group ($p < 0.001$), despite body weight and postprandial blood glucose did not obviously hang between the two groups. *In vitro* vascular tone experiment showed that endothelial BRG1 deletion ameliorated the vasodilation defect after acetylcholine treatment (**Figure 1B**, $P < 0.001$); vascular tone for SNP treatment were used as the positive control, and there was no difference of aortic relaxation in response to the nitric oxide donor SNP in the two groups. H&E staining of the aortic arteries showed that endothelial BRG1 deletion mitigated the atherosclerotic injuries in mice (**Figure 1C**). Meanwhile, Oil Red O staining, which allows the visualization of lipids, indicated over 30% reduction of atherosclerotic lesions ($p = 0.0263$) in the aortic trees (**Figures 1D,E**) and about 50% reduction ($p = 0.0453$) in the aortic roots (**Figures 1D,F**) in CKO mice compared to WT mice. These combined results suggest that endothelial-specific BRG1 deficiency may counteract the progression of diabetic atherosclerosis in mice.

Brahma-Related Gene 1 Deletion in Endothelial Cells Reduced Plaque Inflammatory Levels and Oxidative Stress in Diabetic Mice

Macrophage recruitment is one of the key characteristics during the development of atherosclerosis. As shown in **Figures 2A,B**, weaker CD68 immunohistochemistry staining was observed in the CKO plaques than in the WT plaques. Meanwhile, real-time quantitative PCR assay demonstrated that expression levels of a panel of pro-inflammatory mediators, including TNF-α (**Figure 2C**), IL-1β (**Figure 2D**), IL-6 (**Figure 2E**), CCL2 (**Figure 2F**), CCL5 (**Figure 2G**), and CCL9 (**Figure 2H**), were downregulated in the CKO mice compared with the WT mice. These data suggest that endothelial BRG1 may contribute to diabetic atherosclerosis by modulating vascular inflammation.

Endothelial Deletion of Brahma-Related Gene 1 Ameliorates Ang II-Induced Abdominal Aortic Aneurysm Progression in Mice

We next determined the role of endothelial BRG1 in Ang II-induced AAA model in CKO mice and WT mice. Of interest, 4 weeks after the Ang-II infusion, the gross anatomical evaluation revealed that the abdominal aortas in WT mice became overtly enlarged, indicative of AAA development (**Figure 3A**); by comparison, mice with endothelial conditional Brg1 knockout (CKO) exhibited an appreciable reduction in aortic enlargement. The ultrasonographic examination confirmed that Brg1 deficiency in endothelial cells led to an approximately 10% reduction in aortic diameter (**Figure 3B**). The incidence of AAA found on autopsy was 8/10 in the Ang II infusion WT group compared with 9/16 in the Ang II infusion KO group (**Figure 3B**). Morphometric analyses by Verhoeff–Van Gieson elastic staining showed significant dilation or breakage of the external and internal aortic walls in ApoE$^{-/-}$; BRG1$^{fl/fl}$ mice induced by Ang II (**Figure 3C**). α-SMA immunohistochemistry staining indicated an alleviation of elastin fragmentation in ApoE$^{-/-}$; BRG1$^{fl/fl}$; CDH5-*cre* mice treated by Ang II (**Figure 3C**). Meanwhile, CD68 immunohistochemistry staining also cues less macrophage recruitment in Ang II-infused CKO mice (**Figure 3C**). Further detection proved the significant upregulation of α-SMA (**Figure 3D**), collagen I (**Figure 3E**), and collagen III (**Figure 3F**) in the ApoE$^{-/-}$; BRG1$^{fl/fl}$; CDH5-*cre* mice, suggesting that endothelial cell deletion of BRG1 could ameliorate Ang II induced AAA progression in mice.

Pro-inflammatory factors participate in many important processes of AAA progression. To further determine the role of endothelial BRG1 in an aneurysm, pro-inflammatory cytokines, such as TNF-α, IL-1β, and IL-6, were measured by real-time qPCR. The data shown in **Figure 3** indicated that IL-1β and IL-6 messenger RNA (mRNA) levels significantly decreased in the ApoE$^{-/-}$; BRG1$^{fl/fl}$; CDH5-*cre* mice group (**Figures 3G,H**). However, there seemed to be no significant alteration of TNF-α (**Figure 3I**) between the two groups, indicating that endothelial BRG1 deletion could alleviate AAA progression via regulating IL-1β and IL-6 levels.

Inhibition of Brahma-Related Gene 1 Reduced Inflammatory Response and c-Fos Expression in Endothelial Cells

Regarding an inflammatory factor, TNF-α would increase inflammatory response in endothelial cells *in vitro*. In this work, exposure of Ea.hy926 cells to TNF-α increases the mild but obvious BRG1 upregulation. Interestingly, BRG1 inhibition significantly reduced BRG1 expression, which downregulates together with IL-1β and CCL2 in Ea.hy926 cells after anti-SiBRG1 RNAi treatment (**Figure 4A**). Despite not altering BRG1 mRNA levels, a molecular inhibitor of BRG1, PFI-3 treatment significantly decreased IL-1β and CCL2 expression after TNF-α treatment (**Figure 4B**). Transcription factor AP-1 is a menagerie of dimeric basic region leucine zipper proteins, consisting of homodimers of Jun or heterodimers of c-Fos and c-Jun. To explore the potential involvement of AP-1 in decreasing inflammatory factors by BRG1 inhibition, **Figures 4C,D** show significantly decreased c-Fos protein levels by anti-SiBRG1 RNAi or PFI-3 treatment in TNF-α-inducing endothelial cells *in vitro*. These data strongly suggest that blocked BRG1 functions obviously alleviated TNF-α-induced inflammatory response.

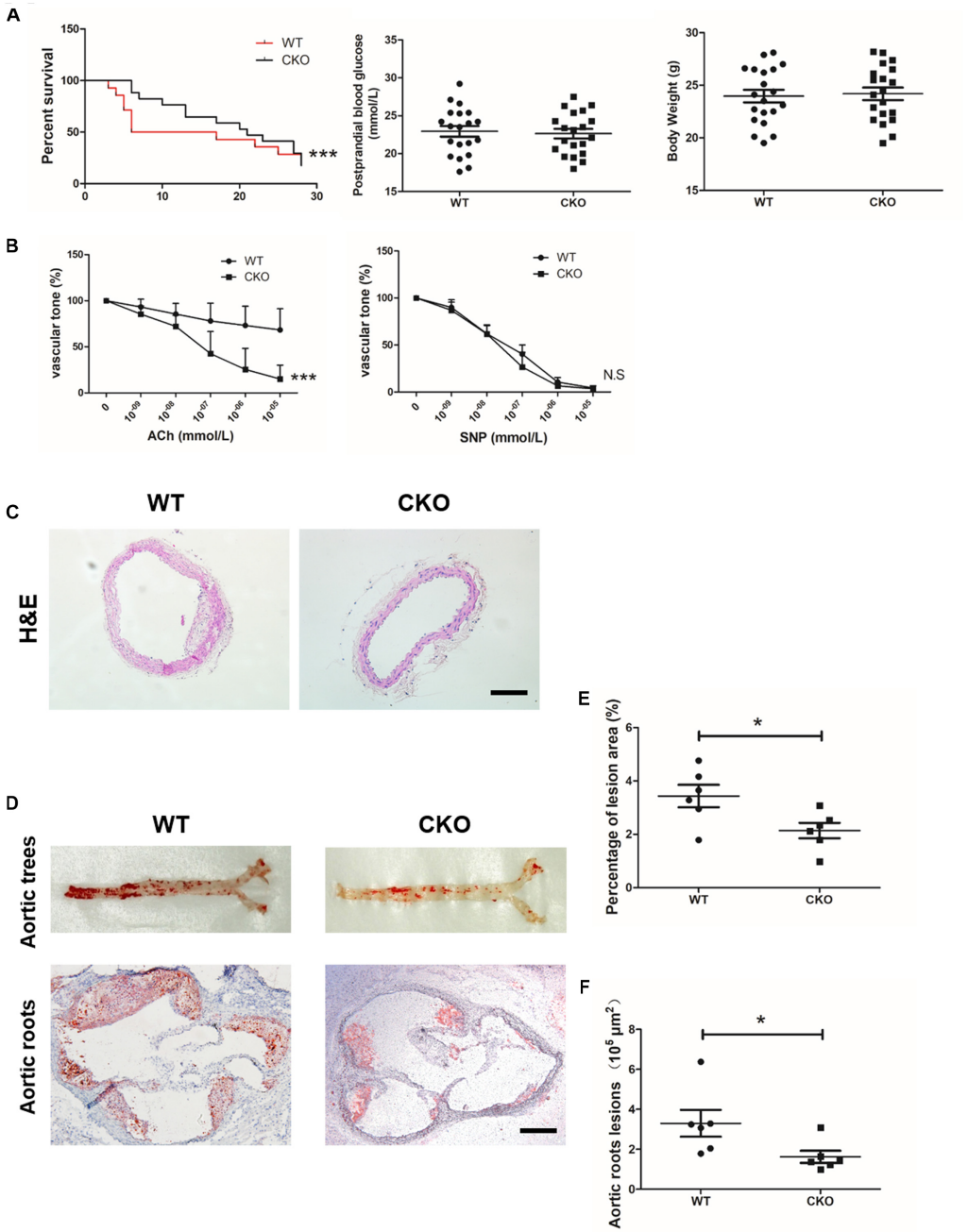

FIGURE 1 | Endothelial cell-specific deletion of BRG1 alleviated diabetes mellitus-related atherosclerosis. **(A)** Survival rate, body weight, and postprandial blood glucose for STZ and Western diet-induced mice diabetic atherosclerosis (n = 20). **(B)** Vascular tone experiment to detect the vasodilation effect of aortic after acetylcholine or SNP treatment. **(C)** H&E staining for abdominal aortic. **(D)** Oil-red O staining for aortic trees and aortic roots. **(E,F)** Statistics for Oil-Red O staining (scale bar: 200 μm, $^{*}P < 0.05$ and $^{***}P < 0.001$).

Inhibition of Brahma-Related Gene 1 Blocked c-Fos Translocation in Endothelial Cells

We measured the effect of c-Fos translocation into nuclear by Western blot, as shown in **Figures 5A,B**. c-Fos translocation into nuclear was significantly reduced by TNF-α induction after anti-SiBRG1 RNAi or PFI-3 treatment. In accordance, immunofluorescent staining of c-Fos showed that both siRNA-mediated depletion of BRG1 and PFI-3-mediated inhibition of BRG1 (**Figure 5C**) reduced TNF-α-induced c-Fos nucleic translocation of EA.Hy926 cells. AP-1 activation is also involved in increased DNA binding activity. We performed EMSA using a biotin-labeled double-strand robe corresponding to AP-1

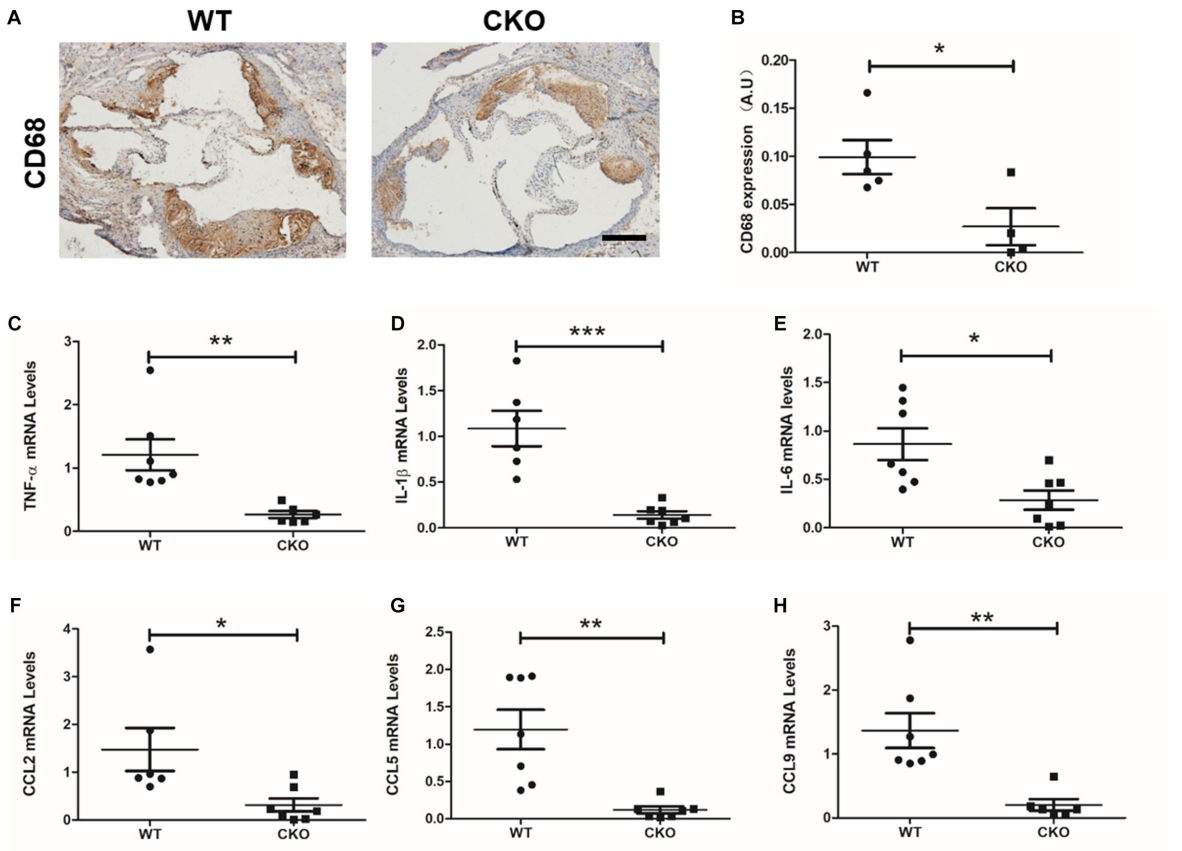

FIGURE 2 | BRG1 deletion in endothelial cells reduced plaque inflammatory levels and oxidative stress in diabetic mice. **(A)** CD68 immunohistochemistry staining for aortic roots and **(B)** statistics. **(C)** TNF-α, **(D)** IL-1β and **(E)** IL-6 mRNA levels detected by real-time PCR in abdominal/thoracic aortic. **(F–H)** Real-time PCR results for CCL2, CCL5, and CCL9 in abdominal/thoracic aortic (Scale bar: 200 μm, $^{*}P < 0.05$, $^{**}P < 0.01$, and $^{***}P < 0.001$).

and its flanking sequence. The DNA-AP-1 complex formation was induced obviously by TNF-α treatment, and the complex induced by TNF-α was significantly reduced when the cells were treated with anti-SiBRG1 RNAi or PFI-3 (**Figures 5D,E**). Luciferase report assay results in **Figure 5F** proved that the effect of MCP-1 promoter activation was induced by BRG1 overexpression in 293T cells. In **Figure 5F**, the induction of luciferase activity of MCP-1 also increased after BRG1 overexpression adenovirus transfection.

DISCUSSION

BRG1, encoded by the *SMARCA4* gene, is a member of the SWI/SNF family and shares significant homology with the Drosophila Brahma protein. BRG1 possesses an intrinsic ATPase activity and participates in regulating gene transcription by altering the chromatin structure. Recent research indicates that genetic interference of BRG1 expression in the adult mouse may bring beneficial effects in the models of CVD. For instance, it has been reported that BRG1 interference protected the mice against cardiac ischemia–reperfusion (Li Z. et al., 2018; Zhang et al., 2018b) and atherosclerosis (Fang et al., 2013). In contrast, endothelial cell-specific deletion of BRG1, achieved by lentivirus-mediated delivery of short hairpin RNA, resulted in anti-inflammatory effects via inhibiting inflammatory factors such as TNF-α in mice, which further ameliorated atherosclerosis in mice models (Fang et al., 2013). In the present study, we aimed to explore the role of endothelial BRG1 in diabetic atherosclerosis and AAA, and the results demonstrated the deletion of BRG1 in endothelial cells, which contributed to improved survival rate and amelioration of vascular function in a model of diabetic atherosclerosis. In addition, endothelial cell conditional BRG1 deletion also blocked the progression of AAA in mice.

Among the diabetic complications, vascular damage contributes to the major burden of morbidity and mortality associated with diabetes. In this research, we reported the deletion of endothelial BRG1 that ameliorated the survival rate in a model of diabetic-related atherosclerosis. Hyperglycemia is a risk factor for atherosclerotic disease. In this model, STZ has been utilized to induce mice hyperglycemia. According to previous studies, mice containing atherogenic mutations in $ApoE^{-/-}$ mice develop either spontaneous or high fat diet-induced coronary artery atherosclerosis, myocardial infarction, and dramatically reduced survival. This reduced survival of

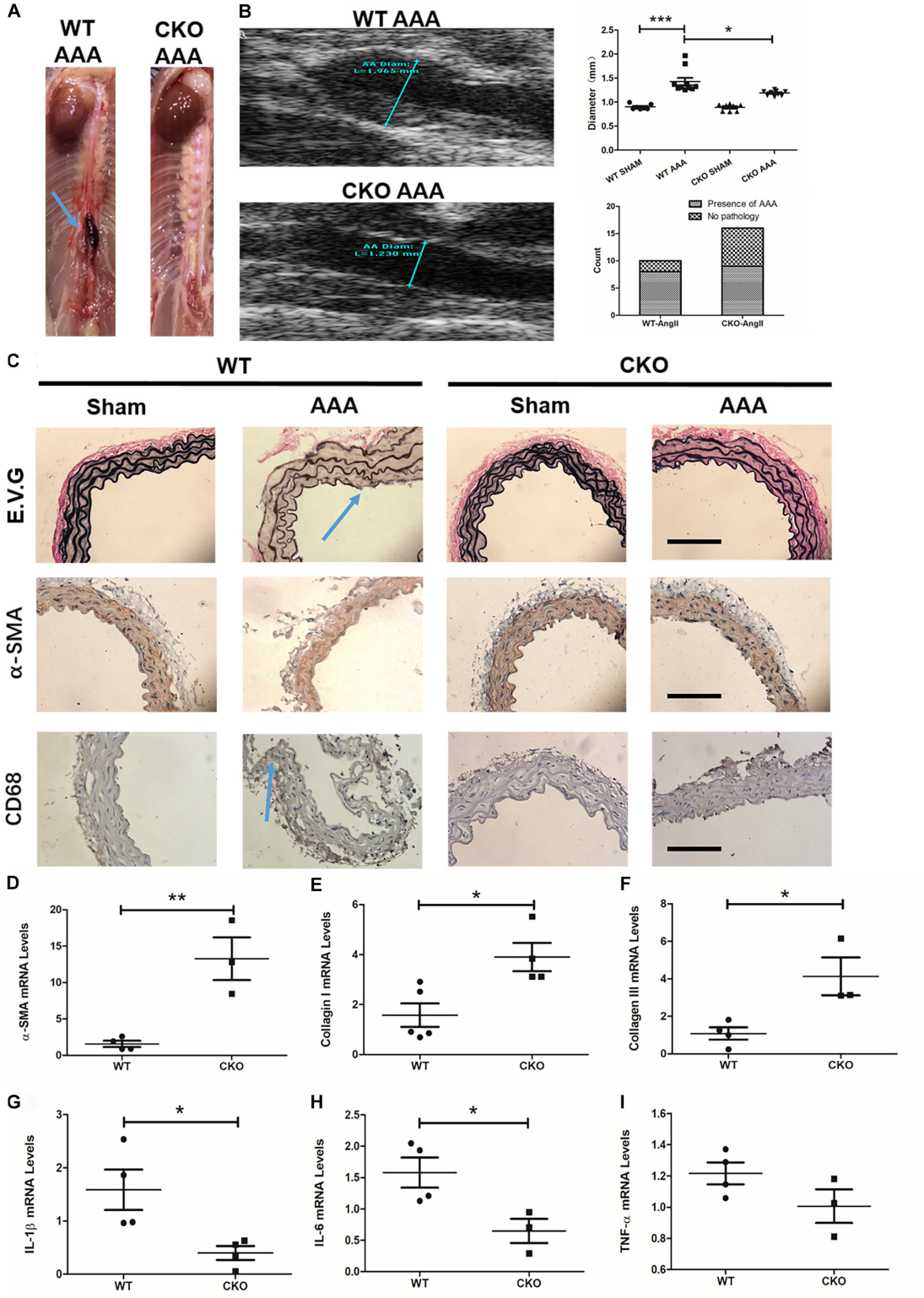

FIGURE 3 | Endothelial cell deletion of BRG1 ameliorates angiotensin II-induced AAA progression in mice. **(A)** Gross anatomy of abdominal aortas at 4 weeks. **(B)** Echocardiographic analysis of vessel diameters at 4 weeks. **(C)** Verhoeff–Van Gieson elastic staining, α-SMA staining, and CD68 staining in AAA, **(D)** α-SMA, **(E)** collagen-I, and **(F)** collagen-III mRNA levels in abdominal aortic. **(G)** IL-1β mRNA levels detected by real-time PCR in abdominal/thoracic aortic. **(H)** IL-6 mRNA levels detected by real-time PCR in abdominal/thoracic aortic. **(I)** TNF-α mRNA levels detected by real-time PCR in abdominal/thoracic aortic (Scale bar: 200 μm, $^{*}P < 0.05$, $^{**}P < 0.01$, and $^{***}P < 0.001$).

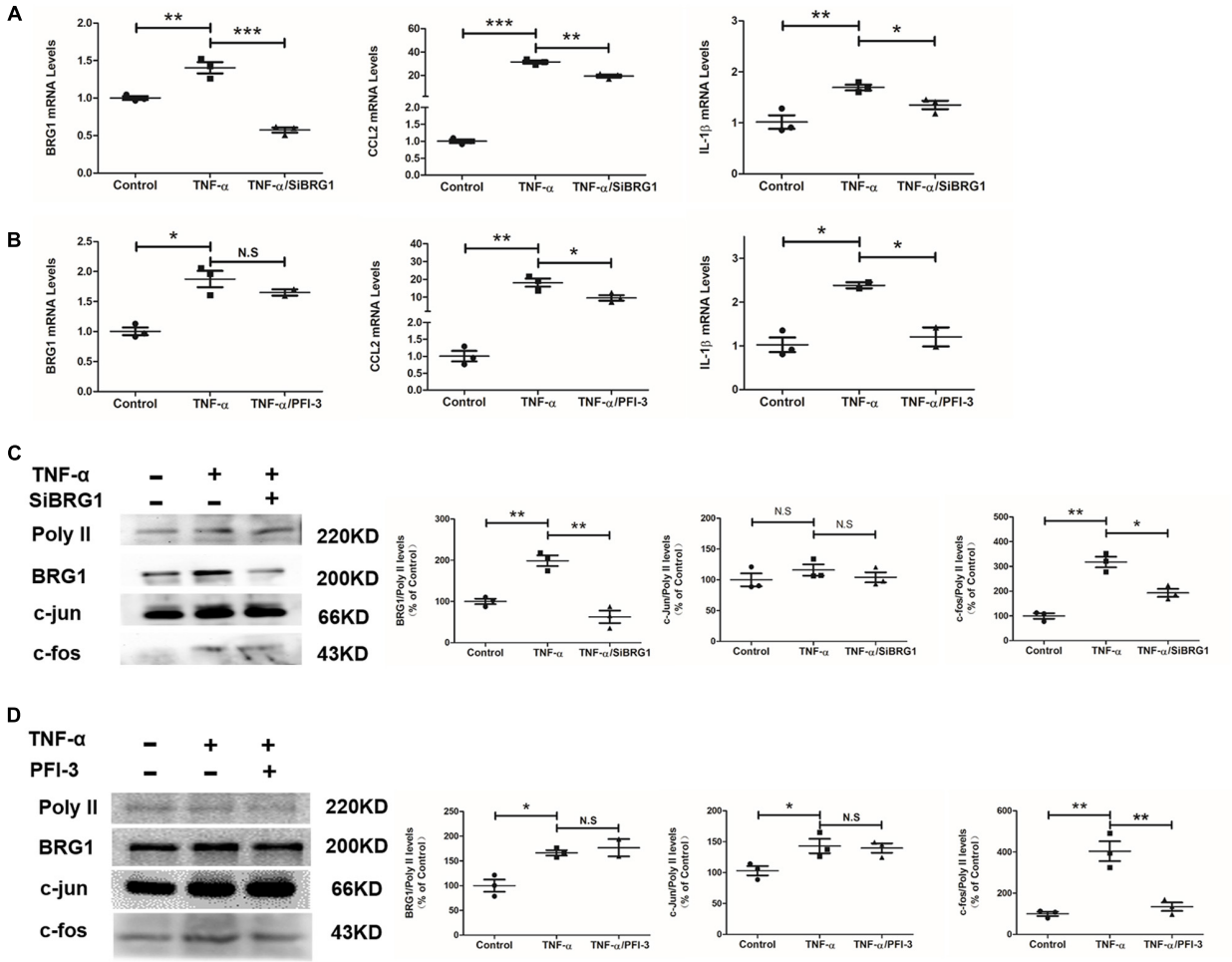

FIGURE 4 | Inhibition of BRG1 reduced inflammatory response and c-Fos expression in endothelial cells. **(A)** Ea.hy926 cells were transfected with siRNA targeting BRG1 or scrambled siRNA (SCR) followed by treatment with TNF-α (10 μg/L) for 24 h. Gene expression was examined by qPCR. **(B)** Ea.hy926 cells were transfected with PFI-3, followed by treatment with TNF-α (10 μg/L) for 24 h. Gene expression was examined by qPCR. **(C)** Ea.hy926 cells were transfected with siRNA targeting BRG1 or scrambled siRNA (SCR), followed by treatment with TNF-α (10 μg/L) for 24 h. Gene expression was examined by Western. **(D)** Ea.hy926 cells were transfected with PFI-3, followed by treatment with TNF-α (10 μg/L) for 24 h. Gene expression was examined by Western (*$P < 0.05$, **$P < 0.01$, and ***$P < 0.001$).

these mice seems to be associated with myocardial infarction and resulting cardiac conduction and functional abnormalities (Nakatsu et al., 2017; Wang Q. et al., 2017; Gonzalez et al., 2018). However, these associations still need to be further investigated. In many instances, the underlying pathology of diabetic atherosclerosis is observed in diabetic patients with myocardial infarction or thromboembolic stroke (Tillquist and Maddox, 2012). Along with heart failure and coronary artery disease, endothelial dysfunction has been considered as a key etiological factor for the progression of diabetic-induced atherosclerosis (Kovacic et al., 2014). Recent studies have suggested that attenuation of inflammation-related endothelial dysfunction could be considered as a reasonable therapeutic approach for diabetic atherosclerosis treatment. For instance, it is well known that inhibiting inflammatory factors such as IL-1β and IL-6 secreted by injured endothelium could protect atherosclerotic lesions (Alfaidi et al., 2018). Interestingly, dampened expression of C-C motif chemokine ligands helps diabetes-associated atherosclerosis (Cao et al., 2014; Xuan et al., 2017; Lin et al., 2018). BRG1 has been reported to participate in the regulation of inflammatory progression in many diseases progression. For instance, hepatocyte-specific Brg1 deletion alleviated the progression of steatohepatitis via regulating SREBP activity-related inflammatory response (Li N. et al., 2018). In cardiac ischemia–reperfusion injury mouse models, endothelial conditional Brg1 deficiency plays a protective role in ameliorating heart function through blocked neutrophil recruitment (Zhang et al., 2018b). This research indicated the promising effect of anti-inflammatory treatment by BRG1 deletion. The present study explores the anti-inflammatory effect of endothelial conditional BRG1 deletion in a diabetic atherosclerosis model in mice. We found that BRG1 deletion in endothelial cells reduced atherosclerotic plaques in thoracic/abdominal aortic and aortic roots in mice. Meanwhile, the deletion of BRG1 in endothelial cells reduced macrophage recruitment in plaques. Further research proved

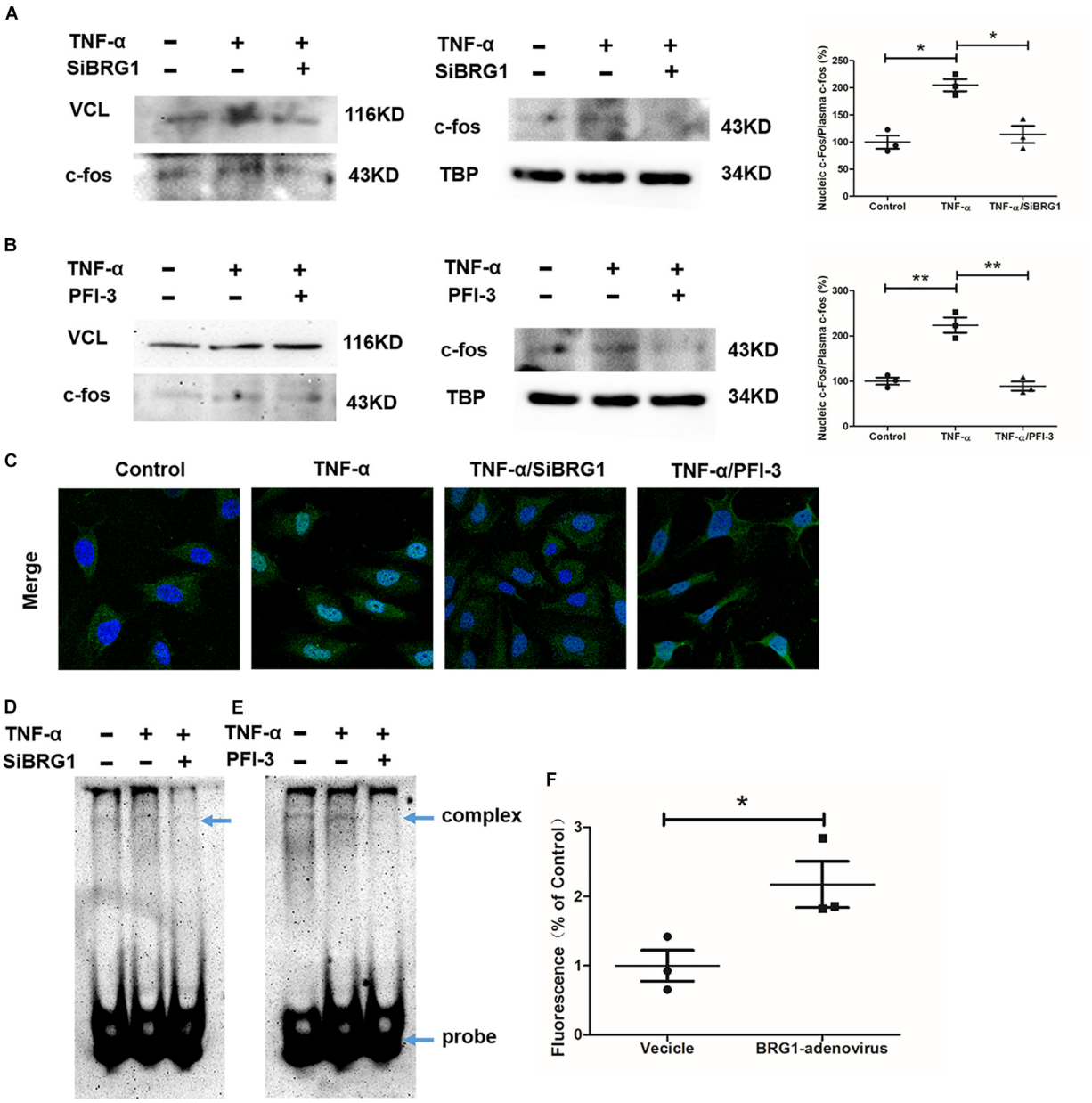

FIGURE 5 | BRG1 inhibition blocked c-Fos translocation in endothelial cells. **(A)** Ea.hy926 cells were transfected with siRNA targeting BRG1 or scrambled siRNA (SCR), followed by treatment with TNF-α (10 μg/L) for 24 h. C-Fos translocation levels were examined by Western. **(B)** Ea.hy926 cells were transfected with PFI-3, followed by treatment with TNF-α (10 μg/L) for 24 h. C-Fos translocation levels were examined by Western. **(C)** Immunofluorescence staining was performed with anti-c-Fos antibody. **(D)** Ea.hy926 cells were transfected with siRNA targeting BRG1 or scrambled siRNA (SCR), followed by treatment with TNF-α (10 μg/L) for 24 h. Alternatively, **(E)** Ea.hy926 cells were treated with TNF-α (10 μg/L) and PFI-3 for 24 h. Nuclear lysates were extracted, and EMSA was performed as described in section "Materials and Methods." **(F)** 293T cells were co-transfected with plasmid containing MCP-1-promoter-luc and overexpression Sp1 adenoviruses. Luciferase report assay was performed as described in section "Materials and Methods." (*$P < 0.05$ and **$P < 0.01$).

a reduction in IL-1β, IL-6, CCL2, CCL5, and CCL9 mRNA levels in BRG1 CKO mice. These findings provide novel insights that BRG1 is linked to diabetic atherosclerosis via a regulated inflammatory response in endothelial cells.

AAA is one of the most deadly cardiovascular pathologies. Although it is typically regarded as being a distinct entity, vascular inflammation also acts as a common pathogenic factor for AAA. Recent research indicated that a dysfunctional endothelium could increase ROS levels or secretion of chemokines and cytokines, which finally influence the progression of AAA (Siasos et al., 2015). Ameliorating endothelium function has been considered as a promising target for AAA treatment. The current report indicated that statins still seem very promising in animal AAA models

via improving endothelial function (de Sotomayor et al., 2005). In addition to their lipid-lowering capacity, statin can improve endothelial function via increasing endothelial nitric oxide synthase expression and BH4 bioavailability (Kosmidou et al., 2007; Wenzel et al., 2008). In contrast, statin treatment can also diminish IL-6 and MCP1 levels in AAA models (Kowalska et al., 2018). In this study, we focused on the protective effects of endothelium-specific BRG1 deletion in AAA, and our results demonstrated that BRG1 deletion in endothelial cells significantly inhibited Ang II-induced AAA development. Deletion of BRG1 in endothelial cells also augmented collagen I, collagen III, and α-SMA levels in mice. These findings collectively argue that BRG1 in endothelial cells could promote AAA pathological progression. Further studies showed a significant reduction of IL-1β and IL-6 but not TNF-α expression in mice, which indicated BRG1 might promote AAA by stimulating endothelial-derived pro-inflammatory mediators. Alternatively, the changes in expression levels of pro-inflammatory mediators could be secondary to a reduction in the recruitment of immune cells (e.g., macrophages).

Previous research reported endothelial-specific BRG1 knockout attenuated the progression of CVDs. For example, Weng et al. (2015) demonstrated endothelial-specific knockdown BRG1 ameliorating cardiac hypertrophy both *in vitro* and *in vivo*. Meanwhile, endothelial-specific BRG1 knockout had also been proved to ameliorate the $CaCl_2$-induced mice AAA progression via trans-activates endothelium-derived colony-stimulating factor (Zhang et al., 2018a). However, the mechanism of BRG1 in regulating Ang-II-induced AAA formation under *ApoE* gene knockout condition remains not to be proven. In this research, we reported endothelial-specific BRG1 knockout reduced AAA progression in mice Ang-II-induced AAA models.

We further reported that BRG1 regulated c-Fos expression and nucleic translocation in endothelial cells. In EA.hy926 cells, it obviously decreased c-Fos expression and blocked c-Fos translocation after anti-SiBRG1 RNAi or PFI-3 treatment. Protein c-Fos belongs to transcription factor AP-1, a menagerie of dimeric basic region—leucine zipper proteins, consisting of homodimers of Jun or heterodimers of Fos and Jun (Shaulian and Karin, 2001, 2002). Recent research reported the effects of regulating inflammatory-related gene expression by AP-1. A binding site of AP-1 in IL-1β and CCL2 promoter region has been identified in a variety of cell types, and AP-1 is an important transcription factor regulating inflammatory-related gene expression (Morse et al., 2003; Sutcliffe et al., 2009). AP-1 is a mediator of inflammatory responses and activated by TNF-α in endothelial cells, and TNF-α-induced endothelial inflammatory response is dependent on AP-1 activation (Morse et al., 2003; Hong et al., 2016). Together, these pieces of evidence suggest that activation of AP-1 enhances inflammatory response in endothelial cells under TNF-α treatment conditions. In this research, we further demonstrated endothelial conditional BRG1 knockout could not alter the c-Jun expression. Among these studies, we inched that the mechanism of BRG1 regulated inflammatory factors expression via mediated by c-Fos nucleic translocation, which could finally block the progression of diabetes-related atherosclerosis and Ang-II-induced mice AAA progression.

Adding to the understanding of the endothelial protective activity of PFI-3 in endothelial cells, we presented pieces of evidence that blocked the function of BRG1-inhibited IL-1β and CCL2 expression and decreasing BRG1 function also inhibiting the activity of AP-1 in endothelial cells. We showed that treatment with PFI-3 blocked the regulation of IL-1β and CCL2 by TNF-α through inhibition of the IL-1β and CCL2 gene promoter. Accompanying the suppression of c—Fos translocation, decreasing the BRG1 function also inhibited the DNA binding activity of AP-1 demonstrated by EMSA assays. Because the IL-1β and CCL2 promoter contains an AP-1—binding site (Morse et al., 2003; Sutcliffe et al., 2009), it is highly likely that the effect of PFI-3 on blocking TNF-α, which lead to induced IL-1β and CCL2 expression, is through the regulation of c-Fos promoter activity.

In summary, our results reveal a previously unrecognized protective role of endothelial cell-specific BRG1 deletion in alleviating diabetic atherosclerosis and Ang II-induced AAA progression via inhibiting the inflammatory responses. These findings indicated that BRG1 could be targeted to alleviate endothelial dysfunction, which helps diabetic atherosclerosis and AAA treatment.

DATA AVAILABILITY STATEMENT

The raw data supporting the conclusions of this article will be made available by the authors, without undue reservation.

ETHICS STATEMENT

The studies involving animals were reviewed and approved by the intramural Committee on Ethical Conduct of Animal Studies of Nanjing Medical University.

AUTHOR CONTRIBUTIONS

TL and TW conceived the project. YZ and TW designed the experiments. TW, YZ, TX, and XC performed the experiments and collected data. TW wrote the manuscript. YX and TL secured funding and provided supervision. HW, MS, and TW added the experiments in revised manuscript.

FUNDING

This work was supported by the Natural Science Foundation of Hainan Province of China (819QN366), the Program of Hainan Associate for Science and Technology Plans to Youth R&D Innovation (QCXM201901), grants from the National Natural Science Foundation of China (No. 81800426), grants from the Natural Science Foundation of the Jiangsu Higher Education Institutions of China (18KJB310009), and grants from Key Laboratory of Emergency and Trauma (Hainan Medical University), Ministry of Education (KLET-201916).

REFERENCES

Alfaidi, M. A., Chamberlain, J., Rothman, A., Crossman, D., Villa-Uriol, M. C., Hadoke, P., et al. (2018). Dietary docosahexaenoic acid reduces oscillatory wall shear stress, atherosclerosis, and hypertension, most likely mediated via an IL-1-mediated mechanism. *J. Am. Heart Assoc.* 7:e008757. doi: 10.1161/JAHA.118.008757

Barrett, T. J., Distel, E., Murphy, A. J., Hu, J., Garshick, M. S., Ogando, Y., et al. (2019). Apolipoprotein AI) promotes atherosclerosis regression in diabetic mice by suppressing myelopoiesis and plaque inflammation. *Circulation* 140, 1170–1184. doi: 10.1161/CIRCULATIONAHA.119.039476

Boyle, J. P., Honeycutt, A. A., Narayan, K. M., Hoerger, T. J., Geiss, L. S., Chen, H., et al. (2001). Projection of diabetes burden through 2050: impact of changing demography and disease prevalence in the U.S. *Diabetes Care* 24, 1936–1940. doi: 10.2337/diacare.24.11.1936

Cao, Q., Wang, X., Jia, L., Mondal, A. K., Diallo, A., Hawkins, G. A., et al. (2014). Inhibiting DNA Methylation by 5-Aza-2'-deoxycytidine ameliorates atherosclerosis through suppressing macrophage inflammation. *Endocrinology* 155, 4925–4938. doi: 10.1210/en.2014-1595

Collins, R., Reith, C., Emberson, J., Armitage, J., Baigent, C., Blackwell, L., et al. (2016). Interpretation of the evidence for the efficacy and safety of statin therapy. *Lancet* 388, 2532–2561. doi: 10.1016/S0140-6736(16)31357-5

Czubryt, M. P. (2015). Going the distance: epigenetic regulation of endothelial endothelin-1 controls cardiac hypertrophy. *J. Mol. Cell Cardiol.* 82, 60–62. doi: 10.1016/j.yjmcc.2015.02.028

Dale, M. A., Ruhlman, M. K., and Baxter, B. T. (2015). Inflammatory cell phenotypes in AAAs: their role and potential as targets for therapy. *Arterioscler. Thromb. Vasc. Biol.* 35, 1746–1755. doi: 10.1161/ATVBAHA.115.305269

de Sotomayor, M. A., Perez-Guerrero, C., Herrrera, M. D., Jimenez, L., Marin, R., Marhuenda, E., et al. (2005). Improvement of age-related endothelial dysfunction by simvastatin: effect on NO and COX pathways. *Br. J. Pharmacol.* 146, 1130–1138. doi: 10.1038/sj.bjp.0706420

DeFronzo, R. A. (2010). Insulin resistance, lipotoxicity, type 2 diabetes and atherosclerosis: the missing links. The Claude Bernard Lecture 2009. *Diabetologia* 53, 1270–1287. doi: 10.1007/s00125-010-1684-1

Fadini, G. P., Menegazzo, L., Scattolini, V., Gintoli, M., Albiero, M., and Avogaro, A. (2016). A perspective on NETosis in diabetes and cardiometabolic disorders. *Nutr. Metab. Cardiovasc. Dis.* 26, 1–8. doi: 10.1016/j.numecd.2015.11.008

Fang, F., Chen, D., Yu, L., Dai, X., Yang, Y., Tian, W., et al. (2013). Proinflammatory stimuli engage Brahma related gene 1 and Brahma in endothelial injury. *Circ. Res.* 113, 986–996. doi: 10.1161/CIRCRESAHA.113.301296

Golledge, J. (2019). Abdominal aortic aneurysm: update on pathogenesis and medical treatments. *Nat. Rev. Cardiol.* 16, 225–242. doi: 10.1038/s41569-018-0114-9

Gonzalez, L., MacDonald, M. E., Deng, Y. D., and Trigatti, B. L. (2018). Hyperglycemia aggravates diet-induced coronary artery disease and myocardial infarction in SR-B1-Knockout/ApoE-hypomorphic mice. *Front. Physiol.* 9:1398. doi: 10.3389/fphys.2018.01398

Han, K. A., Patel, Y., Lteif, A. A., Chisholm, R., and Mather, K. J. (2011). Contributions of dysglycaemia, obesity, and insulin resistance to impaired endothelium-dependent vasodilation in humans. *Diabetes Metab. Res. Rev.* 27, 354–361. doi: 10.1002/dmrr.1183

Hong, H., Jiang, L., Lin, Y., He, C., Zhu, G., Du, Q., et al. (2016). TNF-alpha promotes lymphangiogenesis and lymphatic metastasis of gallbladder cancer through the ERK1/2/AP-1/VEGF-D pathway. *BMC Cancer* 16:240. doi: 10.1186/s12885-016-2259-4

Kosmidou, I., Moore, J. P., Weber, M., and Searles, C. D. (2007). Statin treatment and 3' polyadenylation of eNOS mRNA. *Arterioscler. Thromb. Vasc. Biol.* 27, 2642–2649. doi: 10.1161/ATVBAHA.107.154492

Kovacic, J. C., Castellano, J. M., Farkouh, M. E., and Fuster, V. (2014). The relationships between cardiovascular disease and diabetes: focus on pathogenesis. *Endocrinol. Metab. Clin. North Am.* 43, 41–57. doi: 10.1016/j.ecl.2013.09.007

Kowalska, K., Habrowska-Gorczynska, D. E., Neumayer, C., Bolliger, M., Domenig, C., Piastowska-Ciesielska, A. W., et al. (2018). Lower levels of Caveolin-1 and higher levels of endothelial nitric oxide synthase are observed in abdominal aortic aneurysm patients treated with simvastatin. *Acta Biochim. Pol.* 65, 111–118. doi: 10.18388/abp.2017_2305

Kruger-Genge, A., Blocki, A., Franke, R. P., and Jung, F. (2019). Vascular endothelial cell biology: an update. *Int. J. Mol. Sci.* 20:4411. doi: 10.3390/ijms20184411

La Sala, L., Prattichizzo, F., and Ceriello, A. (2019). The link between diabetes and atherosclerosis. *Eur. J. Prev. Cardiol.* 26, 15–24. doi: 10.1177/2047487319878373

Lamblin, N., Ratajczak, P., Hot, D., Dubois, E., Chwastyniak, M., Beseme, O., et al. (2010). Profile of macrophages in human abdominal aortic aneurysms: a transcriptomic, proteomic, and antibody protein array study. *J. Proteome Res.* 9, 3720–3729. doi: 10.1021/pr100250s

Li, G., Qin, L., Wang, L., Li, X., Caulk, A. W., Zhang, J., et al. (2017). Inhibition of the mTOR pathway in abdominal aortic aneurysm: implications of smooth muscle cell contractile phenotype, inflammation, and aneurysm expansion. *Am. J. Physiol. Heart Circ. Physiol.* 312, H1110–H1119. doi: 10.1152/ajpheart.00677.2016

Li, H., Bai, S., Ao, Q., Wang, X., Tian, X., Li, X., et al. (2018). Modulation of immune-inflammatory responses in abdominal aortic aneurysm: emerging molecular targets. *J. Immunol. Res.* 2018:7213760. doi: 10.1155/2018/7213760

Li, N., Li, M., Hong, W., Shao, J., Xu, H., Shimano, H., et al. (2018). Brg1 regulates pro-lipogenic transcription by modulating SREBP activity in hepatocytes. *Biochim. Biophys. Acta Mol. Basis Dis.* 1864(9 Pt B), 2881–2889. doi: 10.1016/j.bbadis.2018.05.022

Li, Z., Zhang, X., Liu, S., Zeng, S., Yu, L., Yang, G., et al. (2018). BRG1 regulates NOX gene transcription in endothelial cells and contributes to cardiac ischemia-reperfusion injury. *Biochim. Biophys. Acta Mol. Basis Dis.* 1864, 3477–3486. doi: 10.1016/j.bbadis.2018.08.002

Li, Z., Zhang, Y., Zhang, Y., Yu, L., Xiao, B., Li, T., et al. (2020). BRG1 stimulates endothelial derived alarmin MRP8 to promote macrophage infiltration in an animal model of cardiac hypertrophy. *Front. Cell Dev. Biol.* 8:569. doi: 10.3389/fcell.2020.00569

Lin, C. S., Hsieh, P. S., Hwang, L. L., Lee, Y. H., Tsai, S. H., Tu, Y. C., et al. (2018). The CCL5/CCR5 axis promotes vascular smooth muscle cell proliferation and atherogenic phenotype switching. *Cell Physiol. Biochem.* 47, 707–720. doi: 10.1159/000490024

Maguire, E. M., Pearce, S. W. A., and Xiao, Q. (2019). Foam cell formation: a new target for fighting atherosclerosis and cardiovascular disease. *Vascul. Pharmacol.* 112, 54–71. doi: 10.1016/j.vph.2018.08.002

Mallat, Z. (2017). Macrophages. *Arterioscler. Thromb. Vasc. Biol.* 37, e92–e98. doi: 10.1161/ATVBAHA.117.309730

Morse, D., Pischke, S. E., Zhou, Z., Davis, R. J., Flavell, R. A., Loop, T., et al. (2003). Suppression of inflammatory cytokine production by carbon monoxide involves the JNK pathway and AP-1. *J. Biol. Chem.* 278, 36993–36998. doi: 10.1074/jbc.M302942200

Moxon, J. V., Parr, A., Emeto, T. I., Walker, P., Norman, P. E., and Golledge, J. (2010). Diagnosis and monitoring of abdominal aortic aneurysm: current status and future prospects. *Curr. Probl. Cardiol.* 35, 512–548. doi: 10.1016/j.cpcardiol.2010.08.004

Nakao, T., Horie, T., Baba, O., Nishiga, M., Nishino, T., Izuhara, M., et al. (2017). Genetic ablation of MicroRNA-33 attenuates inflammation and abdominal aortic aneurysm formation via several anti-inflammatory pathways. *Arterioscler. Thromb. Vasc. Biol.* 37, 2161–2170. doi: 10.1161/ATVBAHA.117.309768

Nakatsu, Y., Kokubo, H., Bumdelger, B., Yoshizumi, M., Yamamotoya, T., Matsunaga, Y., et al. (2017). The SGLT2 inhibitor luseogliflozin rapidly normalizes aortic mRNA levels of inflammation-related but not lipid-metabolism-related genes and suppresses atherosclerosis in diabetic ApoE KO mice. *Int. J. Mol. Sci.* 18:1704. doi: 10.3390/ijms18081704

Pansuria, M., Xi, H., Li, L., Yang, X. F., and Wang, H. (2012). Insulin resistance, metabolic stress, and atherosclerosis. *Front. Biosci.* 4, 916–931. doi: 10.2741/s308

Qin, Y., Yang, Y., Liu, R., Cao, X., Liu, O., Liu, J., et al. (2013). Combined Cathepsin S and hs-CRP predicting inflammation of abdominal aortic aneurysm. *Clin. Biochem.* 46, 1026–1029. doi: 10.1016/j.clinbiochem.2013.05.065

Ramos, R., Comas-Cufi, M., Marti-Lluch, R., Ballo, E., Ponjoan, A., Alves-Cabratosa, L., et al. (2018). Statins for primary prevention of cardiovascular events and mortality in old and very old adults with and without type 2 diabetes: retrospective cohort study. *BMJ* 362:k3359. doi: 10.1136/bmj.k3359

Samadzadeh, K. M., Chun, K. C., Nguyen, A. T., Baker, P. M., Bains, S., and Lee, E. S. (2014). Monocyte activity is linked with abdominal aortic aneurysm diameter. *J. Surg. Res.* 190, 328–334. doi: 10.1016/j.jss.2014.03.019

Shaulian, E., and Karin, M. (2001). AP-1 in cell proliferation and survival. *Oncogene* 20, 2390–2400. doi: 10.1038/sj.onc.1204383

Shaulian, E., and Karin, M. (2002). AP-1 as a regulator of cell life and death. *Nat. Cell Biol.* 4, E131–E136. doi: 10.1038/ncb0502-e131

Siasos, G., Mourouzis, K., Oikonomou, E., Tsalamandris, S., Tsigkou, V., Vlasis, K., et al. (2015). The role of endothelial dysfunction in aortic aneurysms. *Curr. Pharm. Des.* 21, 4016–4034. doi: 10.2174/1381612821666150826094156

Siti, H. N., Kamisah, Y., and Kamsiah, J. (2015). The role of oxidative stress, antioxidants and vascular inflammation in cardiovascular disease (a review). *Vascul. Pharmacol.* 71, 40–56. doi: 10.1016/j.vph.2015.03.005

Stamler, J., Vaccaro, O., Neaton, J. D., and Wentworth, D. (1993). Diabetes, other risk factors, and 12-yr cardiovascular mortality for men screened in the multiple risk factor intervention trial. *Diabetes Care* 16, 434–444. doi: 10.2337/diacare.16.2.434

Sutcliffe, A. M., Clarke, D. L., Bradbury, D. A., Corbett, L. M., Patel, J. A., and Knox, A. J. (2009). Transcriptional regulation of monocyte chemotactic protein-1 release by endothelin-1 in human airway smooth muscle cells involves NF-kappaB and AP-1. *Br. J. Pharmacol.* 157, 436–450. doi: 10.1111/j.1476-5381.2009.00143.x

Tang, G., Duan, F., Li, W., Wang, Y., Zeng, C., Hu, J., et al. (2019). Metformin inhibited Nod-like receptor protein 3 inflammasomes activation and suppressed diabetes-accelerated atherosclerosis in apoE(-/-) mice. *Biomed. Pharmacother.* 119:109410. doi: 10.1016/j.biopha.2019.109410

Tillquist, M. N., and Maddox, T. M. (2012). Update on diabetic cardiomyopathy: inches forward, miles to go. *Curr. Diab. Rep.* 12, 305–313. doi: 10.1007/s11892-012-0274-7

Wan, Z., Fan, Y., Liu, X., Xue, J., Han, Z., Zhu, C., et al. (2019). NLRP3 inflammasome promotes diabetes-induced endothelial inflammation and atherosclerosis. *Diabetes Metab. Syndr. Obes.* 12, 1931–1942. doi: 10.2147/DMSO.S222053

Wang, Q., Zhang, M., Torres, G., Wu, S., Ouyang, C., Xie, Z., et al. (2017). Metformin suppresses diabetes-accelerated atherosclerosis via the inhibition of Drp1-mediated mitochondrial fission. *Diabetes* 66, 193–205. doi: 10.2337/db16-0915

Wang, R., Wang, Y., Mu, N., Lou, X., Li, W., Chen, Y., et al. (2017). Activation of NLRP3 inflammasomes contributes to hyperhomocysteinemia-aggravated inflammation and atherosclerosis in apoE-deficient mice. *Lab. Invest.* 97, 922–934. doi: 10.1038/labinvest.2017.30

Weng, X., Yu, L., Liang, P., Li, L., Dai, X., Zhou, B., et al. (2015). A crosstalk between chromatin remodeling and histone H3K4 methyltransferase complexes in endothelial cells regulates angiotensin II-induced cardiac hypertrophy. *J. Mol. Cell Cardiol.* 82, 48–58. doi: 10.1016/j.yjmcc.2015.02.010

Weng, X., Zhang, Y., Li, Z., Yu, L., Xu, F., Fang, M., et al. (2019). Class II transactivator (CIITA) mediates IFN-gamma induced eNOS repression by enlisting SUV39H1. *Biochim. Biophys. Acta Gene Regul. Mech.* 1862, 163–172. doi: 10.1016/j.bbagrm.2019.01.005

Wenzel, P., Daiber, A., Oelze, M., Brandt, M., Closs, E., Xu, J., et al. (2008). Mechanisms underlying recoupling of eNOS by HMG-CoA reductase inhibition in a rat model of streptozotocin-induced diabetes mellitus. *Atherosclerosis* 198, 65–76. doi: 10.1016/j.atherosclerosis.2007.10.003

Xiao, C., Gao, L., Hou, Y., Xu, C., Chang, N., Wang, F., et al. (2016). Chromatin-remodelling factor Brg1 regulates myocardial proliferation and regeneration in zebrafish. *Nat. Commun.* 7:13787. doi: 10.1038/ncomms13787

Xu, Y., and Fang, F. (2012). Regulatory role of Brg1 and Brm in the vasculature: from organogenesis to stress-induced cardiovascular disease. *Cardiovasc. Hematol. Disord. Drug Targets* 12, 141–145. doi: 10.2174/1871529x11202020141

Xuan, Y., Gao, Y., Huang, H., Wang, X., Cai, Y., and Luan, Q. X. (2017). Tanshinone IIA attenuates atherosclerosis in apolipoprotein E knockout mice infected with *Porphyromonas gingivalis*. *Inflammation* 40, 1631–1642. doi: 10.1007/s10753-017-0603-8

Zhang, X., Liu, S., Weng, X., Wu, T., Yu, L., Xu, Y., et al. (2018a). Brg1 transactivates endothelium-derived colony stimulating factor to promote calcium chloride induced abdominal aortic aneurysm in mice. *J. Mol. Cell Cardiol.* 125, 6–17. doi: 10.1016/j.yjmcc.2018.10.012

Zhang, X., Liu, S., Weng, X., Zeng, S., Yu, L., Guo, J., et al. (2018b). Brg1 deficiency in vascular endothelial cells blocks neutrophil recruitment and ameliorates cardiac ischemia-reperfusion injury in mice. *Int. J. Cardiol.* 269, 250–258. doi: 10.1016/j.ijcard.2018.07.105

Zheng, L., Wu, T., Zeng, C., Li, X., Li, X., Wen, D., et al. (2016). SAP deficiency mitigated atherosclerotic lesions in ApoE(-/-) mice. *Atherosclerosis* 244, 179–187. doi: 10.1016/j.atherosclerosis.2015.11.009

Conflict of Interest: The authors declare that the research was conducted in the absence of any commercial or financial relationships that could be construed as a potential conflict of interest.

frontiers in Cell and Developmental Biology

MINI REVIEW
published: 23 December 2020
doi: 10.3389/fcell.2020.606407

The Role of Complement in Myocardial Infarction Reperfusion Injury: An Underappreciated Therapeutic Target

*Carl-Wilhelm Vogel**

University of Hawaii Cancer Center and Department of Pathology, John A. Burns School of Medicine, University of Hawaii at Manoa, Honolulu, HI, United States

This article reviews the pathogenetic role of the complement system in myocardial infarction reperfusion injury. The complement activation pathways involved in myocardial tissue injury are identified, as are the complement-derived effector molecules. The results of past anti-complement therapies are reviewed; as the more recent therapeutic concept of complement depletion with humanized CVF described.

Keywords: myocardial infarction, reperfusion injury, complement, complement depletion, cobra venom factor, humanized cobra venom factor

OPEN ACCESS

Edited by:
Silvia Fischer,
University of Giessen, Germany

Reviewed by:
Elisabeth Deindl,
Ludwig-Maximilians-University, Germany
Ienglam Lei,
University of Michigan, United States

***Correspondence:**
Carl-Wilhelm Vogel
cvogel@cc.hawaii.edu

Specialty section:
This article was submitted to Molecular Medicine, a section of the journal Frontiers in Cell and Developmental Biology

Received: *03 October 2020*
Accepted: *03 December 2020*
Published: *23 December 2020*

Citation:
Vogel C-W (2020) The Role of Complement in Myocardial Infarction Reperfusion Injury: An Underappreciated Therapeutic Target. Front. Cell Dev. Biol. 8:606407. doi: 10.3389/fcell.2020.606407

INTRODUCTION

The Complement System

The complement system is an important component of the immune system, with multiple roles in both the innate and adaptive immune response. The complement system is made up of approximately 20 plasma proteins and numerous receptors and regulatory proteins in the cell membranes of host cells. There are three pathways through which activation of the complement system can occur, referred to as classical pathway, lectin pathway, and alternative pathway, all of which share the same molecular architecture: an initial recognition event is amplified by a succession of proteolytic enzymes in a cascade-like fashion, merging at the step of C3 activation and resulting in the generation of multiple biologically active complement activation products (**Figure 1**).

The Three Pathways of Complement Activation

The activation of the classical pathway usually involves binding of an antibody to its antigen with subsequent recognition by C1q. The alternative pathway is continuously activated in plasma at a slow rate. Activation is usually restricted by regulatory mechanisms, but activation can proceed on certain cell surfaces. Mostly, the alternative pathway activation loop enhances complement activation by the classical and lectin pathways. The lectin pathway is typically activated by mannose binding lectin (MBL) which recognizes certain carbohydrate structures rarely present on normal cells, but frequently present on pathogens and dying host cells.

Complement Activation-Derived Effector Molecules

Complement activation by any of the three activation pathways leads to the generation of complement-derived effector molecules. Foremost, there are the two anaphylatoxins C3a and C5a. They are potent biologically active peptides released by the cleavage of C3 and C5, respectively,

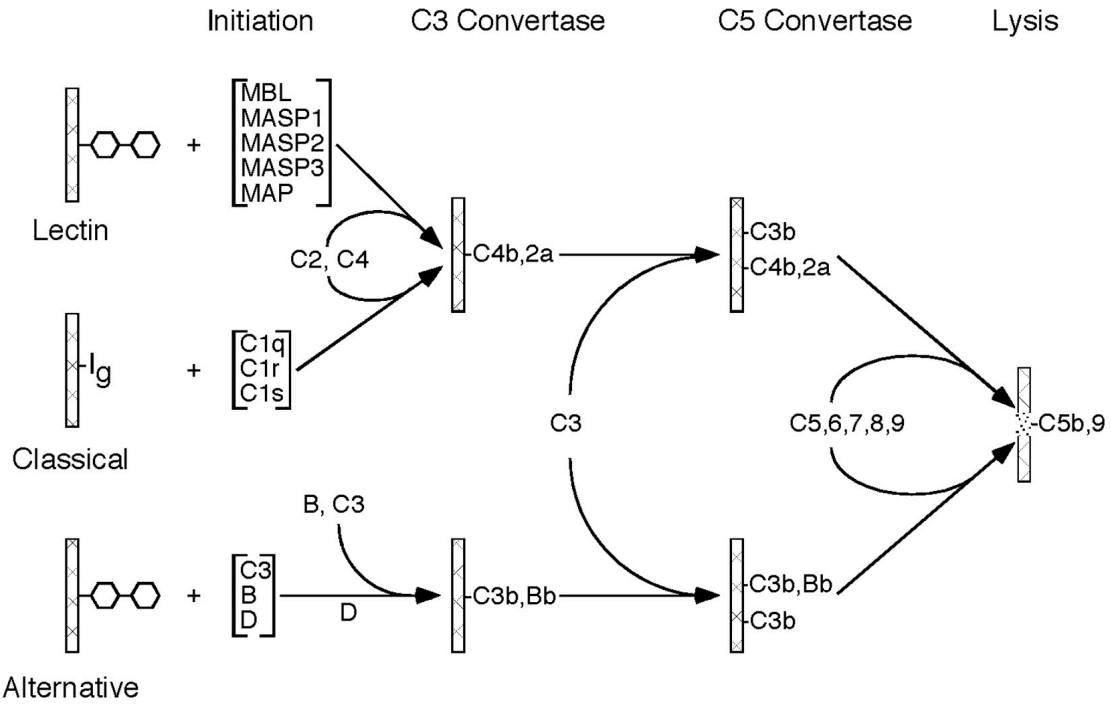

FIGURE 1 | Schematic drawing showing the molecular organization of the three complement activation pathways (lectin, classical, alternative). Please note that all three pathways merge at the stage of C3 activation and, after forming a C5 convertase, initiate the formation of the C5b-9 complex (MAC).

during complement activation through any of the three pathways. Both exhibit chemotaxis for important pro-inflammatory cells, and activate, in particular the strongly pro-inflammatory C5a, macrophages, eosinophils, and neutrophils. Carboxypeptidase N is the major regulator of anaphylatoxin activity, removing the C-terminal arginine residue from C3a to C5a. Both anaphylatoxins are rapidly inactivated by the removal of the C-terminal arginine residue. The resulting peptide after removal of the C-terminal arginine from C5a is referred to as C5a-des-arg. However, C5a-des-Arg still exhibits activity for neutrophils, making C5a a particularly powerful pro-inflammatory peptide.

Another important complement-derived effector is the macromolecular C5b-9 complex, also referred to as the membrane attack complex (MAC). It is generated by the cleavage of C5, with the activation product C5b serving as the nucleus for the assembly of the high molecular weight MAC, consisting of the complement proteins C5b, C6, C7, C8, and several C9. The MAC inserts itself into target membranes, leading to impairment of membrane function, physical destruction of targets cells, and ultimately cell death.

Another potent complement activation product is C3b. As the enzyme that cleaves C3 into C3a and C3b is typically located on a surface, nascent C3b can attach itself covalently to that surface through transesterification. The process of covalently binding of C3b molecules to a target (e.g., an immune complex, a microorganism, a cell), referred to as opsonization, has several biological consequences. C3b is recognized by the C3b receptor (CR1, CD35) on neutrophils, leading to cellular influx, nucleophile activation, inflammation, as well as ingestion and killing of target cells. Secondly, continuing deposition of C3b causes the creation of C5 convertases, leading to C5a generation and enhanced inflammation as well C5b generation and MAC formation as described above. Lastly, the covalently bound C3b is degraded in a step-wise fashion by Factor I to iC3b, C3dg, and eventually to C3d. The degradation products remain bound to their target surface. B cells express complement receptor 2 (CR2, CD21) which recognizes C3d. C3d bound to its antigen also binds to CR2 on follicular dendritic cells, eventually leading to antigen-specific IgG production.

This short overview of the complement system summarizes its important roles in host defense and immune response. Multiple excellent reviews of the complement system have been published (Walport, 2001a,b; Merle et al., 2015a,b).

Complement, a Pathogenetic Factor in Many Diseases

Inappropriate complement activation leads damage of host cells and tissues. Accordingly, the complement system is also an important pathogenetic factor in numerous diseases including, but not limited to, rheumatoid arthritis, lupus erythematosus, myasthenia gravis, age-related macular degeneration (AMD), ischemia reperfusion injury, transplant rejection, paroxysmal nocturnal hemoglobinuria, (PNH), bullous pemphigoid, asthma, anti-phospholipid syndrome, autoimmune hemolytic anemia, and atypical hemolytic uremic syndrome (Vogel and Fritzinger, 2010; Vogel et al., 2014).

THE ROLE OF COMPLEMENT IN MYOCARDIAL REPERFUSION INJURY

Complement activation has long been known to be an important factor for inflammation and injury of ischemic and infarcted myocardial tissue. The first report implicating the complement system demonstrated the generation of a C3-derived chemotactic activity resulting in intense accumulation of neutrophils in ischemic rat heart tissue (Hill and Ward, 1971) that could be suppressed by complement depletion with cobra venom factor (CVF) (Hill and Ward, 1971). Multiple authors demonstrated complement activation products such as C3d and C5b-9 in ischemic heart tissue (Mathey et al., 1994; Nijmeijer et al., 2004).

Reperfusion of infarcted myocardial tissue resulted, paradoxically, in significantly increased myocardial tissue damage of 50% or more (Ferreira, 2010), a phenomenon referred to as reperfusion injury. Several investigators demonstrated the significant role of complement activation in reperfusion injury of myocardial tissue in rats (MacLean et al., 1978), dogs (Maroko et al., 1978), and baboons (Pinckard et al., 1980). Complement depletion with CVF resulted in greatly reduced myocardial tissue damage and preservation of large areas of normal ventricular myocardium. The effect of complement depletion was demonstrated histologically, and by increased creatine phosphokinase (CPK) activity. There was also greatly reduced infiltration with neutrophils, and a virtual absence of deposited C3 in infarcted areas in CVF-treated animals. The extent of C3 and C5b-9 deposition is significantly increased in the myocardial tissue of humans after reperfusion (Nijmeijer et al., 2004).

Complement Pathways Activated in Myocardial Reperfusion Injury

Of the three complement pathways, the most important one for inducing tissue damage in myocardial reperfusion injury is the lectin pathway (Jordan et al., 2001; Walsh et al., 2005; Panagiotou et al., 2018). Mice lacking MBL, and therefore a functional lectin pathway, do not develop cardiac reperfusion injury (Walsh et al., 2005); and an anti-MBL monoclonal antibody greatly reduced infarct size, C3 deposition, and neutrophil infiltration. There is also a role for the alternative pathway. Although there is no evidence that the alternative pathway is activated on altered surfaces in the myocardial tissue after ischemic damage, the alternative pathway has been shown to significantly contribute to the tissue damage by lectin pathway activation, as Factor B knock-out mice exhibited significantly reduced necrosis and diminished deposition of C3 (Chun et al., 2017). There has been some question about the role of the classical pathway in myocardial reperfusion injury (McMullen et al., 2006; Gorsuch et al., 2012). In other organ systems such as intestinal reperfusion, a role of the classical pathway has been described (Williams et al., 1999). In myocardial reperfusion injury, it has been shown that both MBL and natural IgM are required for complement activation (Busche et al., 2009). IgM appears to bind MBL, and leads to lectin pathway activation without involvement of C1q (Gorsuch et al., 2012). Mice deficient in B-cells, and therefore natural IgM, are protected from myocardial reperfusion injury (Zhang et al., 2006; Linfert et al., 2009). However, activation of the classical pathway by natural IgM antibodies to neoepitopes in injured heart tissue after ischemia cannot be excluded, as has been shown in other tissues (Narang et al., 2017).

Complement Effector Molecules in Myocardial Reperfusion Injury

All complement-derived effector molecules as described above are involved in producing the inflammation, tissue injury, and necrosis of the heart tissue during reperfusion. C3 activation leads to covalent attachment of C3b to myocardial tissue. The concomitant release of the C3a anaphylatoxin causes influx and activation of neutrophils. C3b and its subsequent degradation products iC3b, C3dg, and C3d become covalently bound and durable signals of tissue inflammation. They are readily detected in infarcted tissue (Pinckard et al., 1980; Jordan et al., 2001; Stahl et al., 2003; Gorsuch et al., 2009). As a matter of fact, soluble radioactively labeled CR2 receptor (complement receptor type 2), recognizing the covalently bound C3d, was used to quantify the severity of myocardial tissue reperfusion injury (Sharif-Paghaleh et al., 2017).

Continued C3b deposition leads to the formation of C5 convertase activity. C5 activation leads to the release of the C5a anaphylatoxin with its strong pro-inflammatory activity for neutrophils. Moreover, C5 activation generates C5b and the subsequent formation of the membrane attack complex which can be detected in the injured myocardial tissue (Weisman et al., 1990; Mathey et al., 1994; Nijmeijer et al., 2004).

Activated neutrophils are important for myocardial inflammation and injury through release of reactive oxygen species (ROS) and pro-inflammatory cytokines. Activated neutrophils have also been shown to induce tissue damage in myocardial reperfusion injury through the formation of neutrophil extracellular traps (NETs) (Savchenko et al., 2014; Ge et al., 2015; Papayannopoulos, 2018). Whereas these neutrophil-derived cytotoxic activities are important mechanisms in myocardial reperfusion injury, they are only indirect consequences of complement activation.

ANTI-COMPLEMENT THERAPY IN MYOCARDIAL REPERFUSION

Soluble Complement Receptor Type 1 (CR1)

Several studies using anti-complement therapeutics have been reported in animal models of myocardial reperfusion injury as well as in patients. In a rat model of myocardial reperfusion, treatment with a soluble form of complement receptor type 1 (CR1), a cofactor for C3b inactivation by Factor I, reduced the infarct size by 44% (Weisman et al., 1990). Similarly, a membrane-targeted version of soluble CR1 decreased infarct size and myocardial apoptosis, and resulted in an improved ejection fraction in pigs (Banz et al., 2007). However, clinical trials with soluble CR1 in cardiopulmonary bypass failed to meet clinical endpoints (Lazar et al., 2004; Li et al., 2004). Surprisingly, there

was some therapeutic benefit seen in male patients, but not in female patients (Lazar et al., 2004).

C1 Esterase Inhibitor

Another complement inhibitor that has been used in myocardial reperfusion injury is the C1 esterase inhibitor (C1INH). C1INH inhibits both the classical and lectin pathways of complement. Use of C1INH has shown beneficial effects in multiple animal models of myocardial reperfusion injury (Panagiotou et al., 2018). There have been a few studies in patients, well over a decade ago, with no impressive results (Panagiotou et al., 2018); and C1INH is currently not used in the treatment of myocardial reperfusion injury.

Anti-C5 Antibodies

Antibodies to C5 have been employed in the therapy of myocardial reperfusion injury, based on the rationale that inhibition at the stage of C5 activation will prevent the generation of the pro-inflammatory C5a anaphylatoxin as well as the formation of the cytotoxic C5b-9 complex. Studies in animals (Vakeva et al., 1998; Pischke et al., 2017) and patients (Fitch et al., 1999; Granger et al., 2003; Armstrong et al., 2006) usually demonstrated beneficial effects, but failed to meet endpoints; and anti-C5 therapy is currently not in use to treat myocardial reperfusion injury. As appropriately pointed out, it is important to inhibit complement activation as far upstream as possible (Panagiotou et al., 2018).

Complement Depletion With Humanized CVF (hCVF)

Cobra venom factor (CVF) is a structural and functional analog of complement component C3 (Fritzinger et al., 2009; Vogel and Fritzinger, 2010, 2017; Vogel et al., 2020). CVF forms a bimolecular enzyme with Factor B that is resistant to inactivation, leading to continuous C3 cleavage and complement depletion. As mentioned above, CVF was instrumental 40 years ago demonstrating the important role of complement in myocardial infarction reperfusion injury (MacLean et al., 1978; Maroko et al., 1978; Pinckard et al., 1980). Similarly, CVF had been used in animals, from mice to baboons, for over 50 years to demonstrate the role of complement in many diseases. CVF was never used in patients because CVF is immunogenic, and cobra venom is obviously an impractical source for a therapeutic agent. But we know that CVF depletes humans of their complement just like other mammals. Studies in cobra bite victims demonstrated complement depletion mirroring depletion in animals with CVF, with no indication of depletion-related toxicity (Warrell et al., 1976; Vogel and Fritzinger, 2017). Although recombinant CVF became available (Kock et al., 2004; Vogel et al., 2004), its immunogenicity prevented clinical application.

Given the high degree of structural homology between human C3 and CVF, humanized CVF was created by exchanging about 10% at the C-terminal end of human C3 with the homologous sequences from CVF. And even in this C-terminal

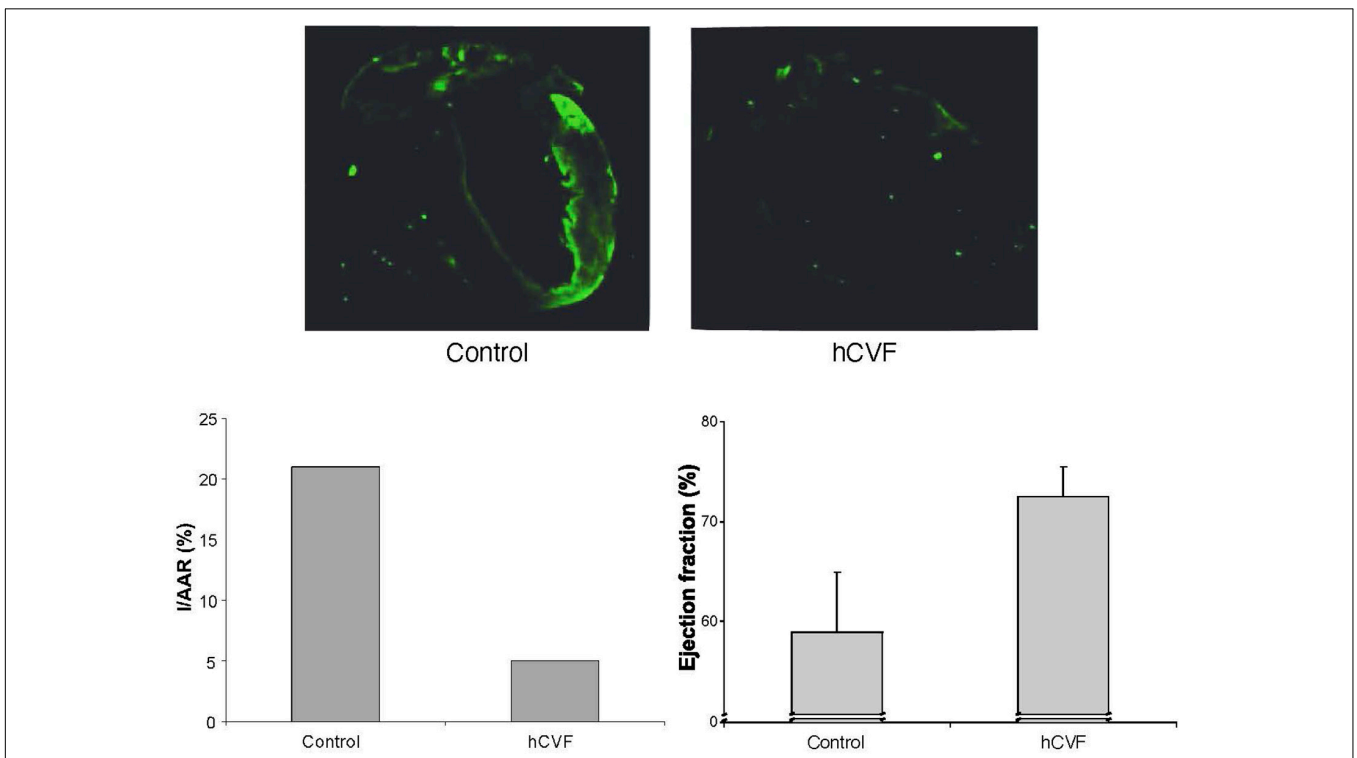

FIGURE 2 | Effect of complement depletion with humanized CVF in a murine model of myocardial ischemia reperfusion injury. The upper panel shows immunohistochemical staining for C3 deposition. The lower left panel shows the size of the infarcted area as a percentage of the area at risk. The lower right panel shows the ejection fraction as a measure of left ventricular function (Gorsuch et al., 2009).

FIGURE 3 | Dr. Klaus T. Preissner (left) and the author (right) at Windansea Beach, La Jolla, California (ca. 1980).

end, approximately 43% of amino acid residues are identical to human C3. Accordingly, these humanized CVF molecules are human C3 derivatives in which only less than 6% of all amino acid residues differ from human C3. Moreover, the three-dimensional structure at the C-terminal end of humanized CVF is essentially indistinguishable from human C3 (Vogel et al., 2014; Vogel and Fritzinger, 2017). Humanized CVF exhibits complement depletion activity just like CVF in serum from multiple species, including human. Its complement depletion activity has also been shown *in vivo* in multiple species, from mouse to non-human primates (Vogel and Fritzinger, 2010). Moreover, for reasons not understood, humanized CVF only leads to C3 activation but not C5 activation, thereby not releasing the pro-inflammatory C5a anaphylatoxin.

Humanized CVF was able to greatly reduce the tissue damage in multiple murine models of disease with complement pathology (Vogel et al., 2014). Significantly, no toxicity has been observed with complement depletion with humanized CVF, including non-human primates (Vogel and Fritzinger, 2010, 2017). Moreover, humanized CVF does not induce a neutralizing antibody response, allowing for repeated administration (Ing et al., 2018).

Complement Depletion With Humanized CVF in a Murine Model of Myocardial Infarction Reperfusion Injury

In a mouse model of myocardial infarction reperfusion injury, the mice were intubated, ventilated, and anesthesia was maintained with isoflurane. A suture was placed around the left anterior descending artery. After 30 min of ischemia, the ligation was loosened, and the myocardium reperfused for 4 h (Gorsuch et al., 2009). Both infarct size and area at risk were subsequently determined histologically with Evans Blue and triphenyl-tetrazolium chloride (TTC) (Walsh et al., 2005), demonstrating an approximately 75% reduction in size by treatment with humanized CVF (**Figure 2**; Gorsuch et al., 2009). C3 deposition was determined using an anti-mouse C3 antibody. The low extent of C3 deposition in animals depleted with humanized CVF reflects remaining C3. The ejection fraction was determined by transthoracic echocardiography (Gorsuch et al., 2009). Both parameters were dramatically improved by complement depletion with humanized CVF (**Figure 2**; Gorsuch et al., 2009). Collectively, these data demonstrate a significant reduction of myocardial injury by pathology, immunohistochemistry, and function.

In summary, complement depletion with humanized CVF appears to be a promising therapeutic approach for preventing or reducing myocardial ischemia reperfusion injury.

AUTHOR CONTRIBUTIONS

The author confirms being the sole contributor of this work and has approved it for publication.

FUNDING

This work was supported by the University of Hawai'i Cancer Center.

DEDICATION

I am dedicating this article to Prof. Klaus T. Preissner, Professor Emeritus at the Justus-Liebig-University in Giessen, Germany, who has made many important contributions throughout his career to our knowledge of vascular biology. I had the pleasure and privilege of overlapping with Klaus as postdoctoral fellows from 1979 to 1982 at the Research Institute of Scripps Clinic, La Jolla, CA (**Figure 3**). We remained close personal and professional friends ever since.

REFERENCES

Armstrong, P. W., Mahaffey, K. W., Chang, W.-C., Weaver, W. D., Hochmann, J. S., Theroux, P., et al. (2006). Concerning the mechanism of pexelizumab's benefit in acute myocardial infarction. *Amer. Heart J.* 151, 787–790.

Banz, Y., Hess, O. M., Robson, S. C., Csizmadia, E., Mettler, D., Meier, P., et al. (2007). Attenuation of myocardial reperfusion injury in pigs by Microcept, a membrane-targeted complement inhibitor derived from human CR1. *Cardiovasc. Res.* 76, 482–493. doi: 10.1016/j.cardiores.2007.07.016

Busche, M. N., Pavlov, V., Takahashi, K., and Stahl, G. L. (2009). Myocardial ischemia nd reperfusion injury is dependent on both IgM and mannose-binding lectin. *Amer. J. Physiol. Heart Circ. Physiol.* 297, H1853–H1859.

Chun, N., Haddadin, A. S., Liu, J., Hou, Y., Wong, K. A., Lee, D., et al. (2017). Activation of complement factor B contributes to murine and human myocardial ischemia/reperfusion injury. *PLoS One* 12:e0179450. doi: 10.1371/journal.pone.0179450

Ferreira, R. (2010). The reduction of infarct size – forty years of research. *Rev. Port. Cardiol.* 29, 1037–1053.

Fitch, J. C. K., Rollins, S., Matis, L., Alford, B., Aranki, S., Collatrd, C. D., et al. (1999). Pharmacology and biological efficiency of a recombinant, humanized single-chain antibody C5 complement inhibitor in patients undergoing coronary artery bypass graft surgery with cardiopulmonary bypass. *Circulation* 100, 2499–2506. doi: 10.1161/01.cir.100.25.2499

Fritzinger, D. C., Hew, B. E., Thorne, M., Pangburn, M. K., Janssen, B. J. C., Gross, P., et al. (2009). Functional characterization of human C 3/cobra venom factor hybrid proteins for therapeutic complement depletion. *Dev. Comp. Immunol.* 33, 105–116. doi: 10.1016/j.dci.2008.07.006

Ge, L., Zhou, X., Ji, W.-J., Lu, R.-Y., Zhang, Y., Zhang, Y.-D., et al. (2015). Neutrophil extracellular traps in ischemia-reperfusion injury-induced myocardial no-reflow: therapeutic potential of DNase-based reperfusion strategy. *Am. J. Physiol. Heart Circ. Physiol.* 308, H500–H509.

Gorsuch, W. B., Chrysanthou, E., Schwaeble, W. J., and Stahl, G. L. (2012). The complement system in ischemia-reperfusion injuries. *Immunobiology* 217, 1026–1033. doi: 10.1016/j.imbio.2012.07.024

Gorsuch, W. B., Guikema, B. J., Fritzinger, D. F., Vogel, C.-W., and Stahl, G. L. (2009). Humanized cobra venom factor decreases myocardial ischemia-reperfusion injury. *Mol. Immunol.* 47, 506–510. doi: 10.1016/j.molimm.2009.08.017

Granger, C. B., Mahaffey, K. W., Weaver, D., Theroux, P., Hochmann, J. S., Filloon, T. G., et al. (2003). Pexelizumab, an anti-C5 complement antibody, as adjunctive therapy to percutaneous coronary intervention in acute myocardial infarction. *Circulation* 108, 1184–1190. doi: 10.1161/01.cir.0000087447.12918.85

Hill, J. H., and Ward, P. A. (1971). The phlogistic role of C3 leukotactic fragments in myocardial infarcts of rats. *J. Exp. Med.* 133, 885–900. doi: 10.1084/jem.133.4.885

Ing, M., Hew, B. E., Fritzinger, D. C., Delignat, S., Lacroix-Desmazes, S., Vogel, C.-W., et al. (2018). Absence of a neutralizing antibody response to humanized cobra venom factor in mice. *Mol. Immunol.* 97, 1–7. doi: 10.1016/j.molimm.2018.02.018

Jordan, J. E., Montalto, M. C., and Stahl, G. L. (2001). Inhibition of mannose-binding lectin reduces postischemic myocardial reperfusion injury. *Circulation* 104, 1413–1418. doi: 10.1161/hc3601.095578

Kock, M. A., Hew, B. E., Bammert, H., Fritzinger, D. C., and Vogel, C.-W. (2004). Structure and function of recombinant cobra venom factor. *J. Biol. Chem.* 279, 30836–30843. doi: 10.1074/jbc.m403196200

Lazar, H. L., Bokesch, P. M., van Lenta, F., Fitzgerald, C., Emmett, C., Marsh, H. C. Jr., et al. (2004). Soluble human complement receptor 1 limits ischemic in cardiac surgery patients at high risk requiring cardiopulmonary bypass. *Circulation* 110, 11274–11279.

Li, J. S., Sanders, S. P., Perry, A. E., Stinnett, S. S., Jaggers, J., Bokesch, P., et al. (2004). Pharmacokinetics and safety of TP10, soluble complement receptor 1, in infants undergoing cardiopulmonary bypass. *Am. Heart J.* 147, 173–180. doi: 10.1016/j.ahj.2003.07.004

Linfert, D., Chowdhry, T., and Rabb, H. (2009). Lymphocytes and ischemia-reperfusion injury. *Transplant. Rev.* 23, 1–10. doi: 10.1016/j.trre.2008.08.003

MacLean, D., Fishbein, M. C., Braunwald, E., and Maroko, P. R. (1978). Long-term preservation of ischemic myocardium after experimental coronary artery occlusion. *J. Clin. Invest.* 61, 541–551.

Maroko, P. R., Carpenter, C. B., Chiariello, M., Fishbein, M. C., Radvany, P., Knostman, J. D., et al. (1978). Reduction by cobra venom factor of myocardial necrosis after coronary artery occlusion. *J. Clin. Invest.* 61, 661–670. doi: 10.1172/jci108978

Mathey, D., Schofer, J., Schäfer, H. J., Hamdoch, T., Joachim, H. C., Ritgen, A., et al. (1994). Early accumulation of the terminal complement-complex in ischemic myocardium after reperfusion. *Eur. Heart J.* 15, 418–423. doi: 10.1093/oxfordjournals.eurheartj.a060516

McMullen, M. E., Hart, M. L., Walsh, M. C., Buras, J., Takahashi, K., and Stahl, G. L. (2006). Mannose-binding lectin binds IgM to activate the lectin complement pathway in vitro and in vivo. *Immunobiology* 211, 759–766. doi: 10.1016/j.imbio.2006.06.011

Merle, N. S., Church, S. E., Fremeaux-Bacchi, V., and Roumenina, L. T. (2015a). Complement system part I – molecular mechanisms of activation and regulation. *Front. Immunol.* 6:262. doi: 10.3389/fimmu.2015.00262

Merle, N. S., Noe, R., Halbwachs-Mecarelli, L., Fremeaux-Bacchi, V., and Roumenina, L. T. (2015b). Complement system part II: role in immunity. *Front. Immunol.* 6:257. doi: 10.3389/fimmu.2015.00257

Narang, A., Qiao, F., Atkinson, C., Zhu, H., Yang, X., Kulik, L., et al. (2017). Natural IgM antibodies that bind neoepitopes exposed as a result of spinal cord injury, drive secondary injury by activating complement. *J. Neuroinflamm.* 14:120. doi: 10.1186/s12974-017-0894-6

Nijmeijer, R., Krijnen, P. A. J., Assink, J., Klaarenbeek, M. A. R., Lagrand, W. K., Veerhuis, R., et al. (2004). C-reactive protein and complement depositions in human infarcted myocardium are more extensive in patients with reinfarction or upon treatment with reperfusion. *Eur. J. Clin. Invest.* 34, 803–810. doi: 10.1111/j.1365-2362.2004.01425.x

Panagiotou, A., Trendelenburg, M., and Osthoff, M. (2018). The lectin pathway of complement in myocardial ischemia/reperfusion injury – Review of its significance and the potential impact of therapeutic interference by C1 esterase inhibitor. *Front. Immunol.* 9:1151. doi: 10.3389/fimmu.201801151

Papayannopoulos, V. (2018). Neutrophil extracellular traps in immunity and disease. *Nat. Rev. Immunol.* 18, 134–147. doi: 10.1038/nri.2017.105

Pinckard, R. N., O'Rourke, R. A., Crawford, M. H., Grover, F. S., McManus, L. M., Ghidoni, J. J., et al. (1980). Complement localization and mediation of ischemic injury in baboon myocardium. *J. Clin. Invest.* 66, 1050–1056. doi: 10.1172/jci109933

Pischke, S. E., Gustavsen, A., Orrem, H. L., Egge, K. H., Cpourivaud, F., Fontenelle, H., et al. (2017). Complement factor 5 blockade reduces porcinde myocardial infarction size and improves immediate cardiac function. *Basic Res. Cadiol.* 122:20. doi: 10.1007/s00395-017-0610-9

Savchenko, A. S., Borissoff, J. I., Martinod, K., De Meyer, S. F., Gallant, M., Erpenbeck, L., et al. (2014). VWF-mediated leukocyte recruitment with chromatin decondensation by PAD4 increases myocardial ischemia/reperfusion injury in mice. *Blood* 123, 141–148. doi: 10.1182/blood-2013-07-514992

Sharif-Paghaleh, E., Yap, M. L., Puhl, S.-L., Badar, A., Torres, J. B., Chuamsaamarkkee, K., et al. (2017). Non-invasive whole-body detetion of complement activation using radionuclide imaging in a mouse model of myocardil ischemia-reperfusion injury. *Sci. Rep.* 7:16009. doi: 10.1038/s41598-017-16387-1

Stahl, G. L., Xu, Y., Hao, L., Miller, M., Buras, J. A., Fung, M., et al. (2003). Role for the alternative complement pathway in ischemia/reperfusion injury. *Am. J. Pathol.* 162, 449–455.

Vakeva, A. P., Agah, A., Rollins, S. A., Matis, L. A., Li, L., and Stahl, G. L. (1998). Myocardial infarction and apoptosis after myocardial ischemia and reperfusion: Role of the terminal complement components and inhibition by anti-C5 therapy. *Circulation* 97, 2259–2267. doi: 10.1161/01.cir.97.22.2259

Vogel, C.-W., Finnegan, P. W., and Fritzinger, D. C. (2014). Humanized cobra venom factor: structure, activity, and therapeutic efficiency in preclinical disease models. *Mol. Immunol.* 61, 191–203. doi: 10.1016/j.molimm.2014.06.035

Vogel, C.-W., and Fritzinger, D. C. (2010). Cobra venom factor: structure, function, and humanization for therapeutic complement depletion. *Toxicon* 56, 1198–1222. doi: 10.1016/j.toxicon.2010.04.007

Vogel, C.-W., and Fritzinger, D. C. (2017). "Cobra venom factor: the unique component of cobra venom that activates the complement system," in *Snake Venoms*, eds P. Gopalakrishnakone, H. Inagaki, A. K. Mukherjee, T. R. Rahmy, and C.-W. Vogel (Dordrecht: Springer Nature), 345–404. doi: 10.1007/978-94-007-6410-1_4

Vogel, C.-W., Fritzinger, D. C., Hew, B. E., Thorne, M., and Bammert, H. (2004). Recombinant cobra venom factor. *Mol. Immunol.* 41, 191–199. doi: 10.1016/j.molimm.2004.03.011

Vogel, C.-W., Hew, B. E., and Fritzinger, D. C. (2020). "Cobra venom factor: structure, function, biology, research tool, and drug lead," in *Handbook of Venoms and Toxins of Reptiles*, 2nd Edn, ed. S. P. Mackessy (Boca Raton, FL: CRC Press/Taylor and Francis).

Walport, M. J. (2001a). Complement. First of two parts. *N. Engl. J. Med.* 344, 1058–1066.

Walport, M. J. (2001b). Complement. Second of two parts. *N. Engl. J. Med.* 344, 1134–1144.

Walsh, M. C., Bourcier, T., Takahashi, K., Shi, L., Busche, M. N., Rother, R. P., et al. (2005). Mannose-binding lectin is a regulator of inflammation that accompanies myocardial ischemia reperfusion injury. *J. Immunol.* 175, 541–546. doi: 10.4049/jimmunol.175.1.541

Warrell, D. A., Greenwood, B. M., Davidson, N. M., Ormerod, L. D., and Prentice, C. R. (1976). Necrosis, haemorrhage, and complement depletion following bites by the spitting cobra (Naja nigricollis). *Q. J. Med.* 45, 1–22.

Weisman, H. F., Bartow, T., Leppo, M. K., Marsh, H. C. Jr., Carson, G. R., Concino, M. F., et al. (1990). Soluble human complement receptor type 1: In vivo inhibitor of complement suppressing post-0ischemic myocardial inflammation and necrosis. *Science* 2549, 146–151. doi: 10.1126/science.2371562

Williams, J. P., Pechet, T. T., Weiser, M. R., Reid, R., Kobzik, L., Moore, F. D. Jr., et al. (1999). Intestinal reperfusion injury is mediated by IgM and complement. *J. Appl. Physiol.* 86, 938–942. doi: 10.1152/jappl.1999.86.3.938

Zhang, M., Michael, L. H., Grosjean, S. A., Kelly, R. A., Carroll, M. C., and Entman, M. L. (2006). The role of natural IgM in myocardial ischemia-reperfusion injury. *J. Mol. Cell. Cardiol.* 41, 62–67.

Conflict of Interest: The author has a financial interest in iC3 LLC of Sunnyvale, CA, a company that develops therapeutics for complement depletion.

frontiers in Physiology

REVIEW
published: 06 January 2021
doi: 10.3389/fphys.2020.586921

Autoregulatory "Multitasking" at Endothelial Cell Junctions by Junction-Associated Intermittent Lamellipodia Controls Barrier Properties

*Jochen Seebach, Nadine Klusmeier and Hans Schnittler**

Institute of Anatomy and Vascular Biology, Westfälische Wilhelms-Universität Münster, Münster, Germany

OPEN ACCESS

Edited by:
Silvia Fischer, Justus Liebig University Giessen, Germany

Reviewed by:
Britta Engelhardt, University of Bern, Switzerland
Jerome Breslin, University of South Florida, United States

***Correspondence:**
Hans Schnittler
hans.schnittler@uni-muenster.de

Specialty section:
This article was submitted to Vascular Physiology, a section of the journal Frontiers in Physiology

Received: *24 July 2020*
Accepted: *30 November 2020*
Published: *06 January 2021*

Citation:
Seebach J, Klusmeier N and Schnittler H (2021) Autoregulatory "Multitasking" at Endothelial Cell Junctions by Junction-Associated Intermittent Lamellipodia Controls Barrier Properties. Front. Physiol. 11:586921. doi: 10.3389/fphys.2020.586921

Vascular endothelial cell (EC) junctions are key structures controlling tissue homeostasis in physiology. In the last three decades, excellent studies have addressed many aspects of this complex and highly dynamic regulation, including cell signaling, remodeling processes of the proteins of tight junctions, adherens junctions, and gap junctions, the cytoskeleton, and post-transcriptional modifications, transcriptional activation, and gene silencing. In this dynamic process, vascular endothelial cadherin (VE-cadherin) provides the core structure of EC junctions mediating the physical adhesion of cells as well as the control of barrier function and monolayer integrity via remodeling processes, regulation of protein expression and post-translational modifications. In recent years, research teams have documented locally restricted dynamics of EC junctions in which actin-driven protrusions in plasma membranes play a central role. In this regard, our research group showed that the dynamics of VE-cadherin is driven by small (1–5 μm) actin-mediated protrusions in plasma membranes that, due to this specific function, were named "junction-associated intermittent lamellipodia" (JAIL). JAIL form at overlapping, adjacent cells, and exactly at this site new VE-cadherin interactions occur, leading to new VE-cadherin adhesion sites, a process that restores weak or lost VE-cadherin adhesion. Mechanistically, JAIL formation occurs locally restricted (1–5 μm) and underlies autoregulation in which the local VE-cadherin concentration is an important parameter. A decrease in the local concentration of VE-cadherin stimulates JAIL formation, whereas an increase in the concentration of VE-cadherin blocks it. JAIL mediated VE-cadherin remodeling at the subjunctional level have been shown to be of crucial importance in angiogenesis, wound healing, and changes in permeability during inflammation. The concept of subjunctional regulation of EC junctions is strongly supported by permeability assays, which can be employed to quantify actin-driven subjunctional changes. In this brief review, we summarize and discuss the current knowledge and concepts of subjunctional regulation in the endothelium.

Keywords: VE-cadherin, JAIL, actin, permeability, junction dynamics, ARP2/3 complex

INTRODUCTION

The inner surface of blood vessels is covered by a thin monolayer of endothelial cells (ECs) whose total area in the human body is estimated to be 4000–7000 m^2 (Aird, 2007). The vascular endothelium features organ- and vascular segment-specific phenotypes as verified in the pioneering work of Simionescu et al. (1975, 1976b). A central task of the endothelium is, apart from regulating blood pressure and organ perfusion, the control of exchange of water, gas, and solutes between the blood and the interstitium (regulated permeability). These functions are essential for the maintenance of tissue homeostasis and physiological adaptation processes. Control of permeability occurs by two mechanisms: a *transcellular pathway* controlled by transporters, transcytosis, or channels, and a *paracellular pathway* regulated by the dynamic opening and closing of cell junctions. Importantly, endothelial cell junctions have a key function during remodeling processes such as in the control of inflammatory responses, angiogenesis, wound healing, and tumor extravasation (Lampugnani et al., 2017; Duong and Vestweber, 2020). Tens of thousands of papers have been published on the vascular endothelium over the last few decades that have contributed to a fundamental understanding of the structure and regulation of endothelial cells and the endothelial cell junctions. However, most studies were performed on cell collectives that do not take into account locally restricted cell junction regulation and dynamics, both of which seems to be important for adaptational or remodeling processes of the junctions whose underlying mechanisms are not yet understood. The locally restricted transmigration of leukocytes and the relative movement of cells within a cell monolayer or in sheet migration are examples of the requirement for locally restricted dynamic junction regulation, as the overall monolayer integrity remains intact (see below). Those local phenomena cannot be adequately explained by general cell signaling mechanisms targeting the entire junctions. However, subcellular control of cell junctions and cell junction dynamics has remained an unsolved problem in cell biology for a long time, which was mostly due to inappropriate experimental and analytical techniques.

A significant improvement in live-cell microscopy techniques, the establishment of viral vectors for gene transduction in endothelial cells, and appropriate analytical software programs have contributed to a significant gain in knowledge with respect to cell junction dynamics, its local regulation, and the functional consequences for permeability. At this point the term *subjunctional* should be introduced: adjective refers to small, locally restricted areas of a few microns in length at the cell junction that can be locally opened or closed or undergo dynamic remodeling. It is therefore reasonable to assume that restricted local molecular interactions and signals at the cell contacts control this process. Indeed, work in recent years has revealed the first dynamic subjunctional structure, which were termed *junction-associated intermittent lamellipodia* (JAIL). JAIL are small, actin-driven plasma membrane protrusions of 1–5 μm in size that, in turn, directly drive the dynamics and remodeling of vascular endothelial cell adhesion molecules (VE-cadherin) via repeated formation of new VE-cadherin adhesions. A critical parameter controlling JAIL formation is the relative local VE-cadherin concentration (see below, under section "Subjunctional Regulation by JAIL Allows Multitasking Control of Endothelial Cell Junctions"). A local decrease in VE-cadherin facilitates JAIL formation while increasing amounts has inhibitory effects (Abu Taha et al., 2014; Cao et al., 2017). Since many different JAIL are constantly formed at the cell junctions, which also occur temporarily and at irregular intervals in time and space, we have postulated an autoregulatory mechanism for this phenomenon. Shortly, the discovery of this mechanism provides an extended concept of endothelial cell junction regulation that is able to explain subjunctional regulations required for inflammation, wound healing, angiogenesis, and shear stress adaptation. The functional impact of JAIL and the underlying mechanistic aspects are discussed in the following overview together with novel permeability assays that are able to detect local small differences in barrier function along endothelial cell junctions.

ADHERENS JUNCTIONS IN VASCULAR ENDOTHELIUM

In contrast to the apicobasal order of tight, adherens, and gap junctions in the epithelium (Takeichi, 2014; Yonemura, 2017), the respective cell junctions in the endothelium are interwoven (Simionescu et al., 1976a). Regardless of the organ-specific diversity of endothelial cells and their cell contacts, adherens junctions are common to all endothelial phenotypes. They are characterized by the presence of endothelium-specific VE-cadherin (Suzuki et al., 1991; Lampugnani et al., 1995) and also by their close structural and functional association with the actin filament cytoskeleton via linker proteins such as catenins and others, as numerous studies on the physiology and pathophysiology of the endothelium have shown (Marcos-Ramiro et al., 2014; Schnittler et al., 2014; Taha and Schnittler, 2014; Garcia-Ponce et al., 2015; Schnoor, 2015; Zankov and Ogita, 2015; Alon and van Buul, 2017; Schnoor et al., 2017; Belvitch et al., 2018). VE-cadherin is a type-II calcium-dependent (Brasch et al., 2011) adhesion molecule that forms the backbone of adherens junctions and is thus expressed in all endothelial cells (Aird, 2006, 2007). The critical influence of VE-cadherin in endothelial cell biology has been demonstrated by studies in mice using blocking antibodies and genetic ablation of VE-cadherin that observed as a consequence an increase in vascular permeability and leukocyte transmigration but also an organ-specific heterogeneity (Corada et al., 2001; Frye et al., 2015). Furthermore, knockout of VE-cadherin expression in mice is lethal, which further underlines the important role of VE-cadherin in vascular development and homeostasis (Vittet et al., 1997; Carmeliet et al., 1999).

Vascular endothelial-cadherin is a single-spanning transmembrane protein with five extracellular repeats (EC1–EC5) at the amino terminus and a short cytosolic carboxy terminus that has binding sites for β-catenin associated with α-catenin. The extracellular domain of VE-cadherin connects adjacent cells by a homophilic, calcium ion-dependent interaction *via* the EC1/EC2 domains (Brasch et al., 2011),

whereas the juxtamembrane region of the VE-cadherin-carboxy terminus binds p120 catenin, which is essential for the stabilization, internalization, and turnover of VE-cadherin (Reynolds, 2007; Vaughan et al., 2007; Komarova et al., 2017). The supramolecular organization of VE-cadherin at endothelial cell junctions has been sparsely studied. Investigations employing Stimulated Emission Depletion (STED) microscopy, however, showed clear evidence of a cluster-like structure. The VE-cadherin clusters were detected in several sizes and in two arrangements at the endothelial cell contacts: a linear arrangement of the clusters and a more planar arrangement, which was particularly visible at the overlapping cell junction areas. The size and number of clusters changed in response to external stimulation such as shear stress, which was accompanied by a functional modulation of the barrier function (Seebach et al., 2007).

There is a general consensus that the interdependent interaction between VE-cadherin and actin filaments is key in controlling endothelial permeability, barrier function, cell migration, and monolayer integrity, which are of critical importance in angiogenesis, inflammation, and wound healing. Either the β-catenin/α-catenin complex (Dejana and Vestweber, 2013) or, alternatively, the β-catenin/α-catenin/EPLIN complex are directly involved in connecting VE-cadherin to actin filaments. EPLIN (epithelial protein lost in neoplasm), which is an actin- and α-catenin-binding protein (Maul and Chang, 1999), has been shown to link actin filaments to adherens junctions in both epithelium and endothelium. In endothelium, EPLIN isoforms were shown to control actin dynamics in an isotype-specific manner, which directly impacts adherens junction dynamics and function (Abe and Takeichi, 2008; Chervin-Pétinot et al., 2012; Taha et al., 2019). It should also be mentioned that VE-cadherin is further associated with vimentin intermediary filaments via association with plakoglobin (γ-catenin); however, the functional role γ-catenin plays in this association is not completely understood. The few available studies on intermediate filaments and γ-catenin in endothelium indicate a role in junction stability, particularly during mechanical challenge by fluid shear stress of blood flow and leukocyte transmigration (Schnittler et al., 1997; Nottebaum et al., 2008; Muramatsu et al., 2017).

JUNCTION ASSOCIATED INTERMITTENT LAMELLIPODIA (JAIL)

As outlined above, current issue in research into the regulation of EC junctions concerns the observation that the maintenance and restoration of monolayer integrity requires cellular junction dynamics that are limited to *subjunctional,* small cell contact areas of 1–5 μm rather than a central signal that triggers a uniform junction response (Cao and Schnittler, 2019). The currently best-understood subjunctional dynamics relate to actin-driven plasma membrane protrusions (comparable to classical lamellipodia) at EC junctions, which have been described independently by different authors (Doggett and Breslin, 2011; Hoelzle and Svitkina, 2012; Martinelli et al., 2013; Abu Taha et al., 2014; Adderley et al., 2015). The importance of these small (1–5 μm), actin-driven plasma membrane protrusions for the barrier function and monolayer integrity of ECs was elucidated by our research team. We showed that these transiently occurring membrane protrusions, which we named "junction-associated intermittent lamellipodia" (JAIL), led directly to new VE-cadherin adhesion sites (Abu Taha et al., 2014; Cao and Schnittler, 2019). There is evidence that JAIL-mediated VE-cadherin dynamics is autoregulated, which allows "multitasking activity" for recovery at different subjunctional sites at the same time.

Investigation of such a sophisticated dynamic mechanism requires advanced methodologies. In this case, we combined virus-mediated gene transfer of fluorescence-tagged proteins and fluorescence spinning-disk microscopy for time-lapse recordings and utilized divers software packages for the analyses. By expression of actin-binding and cell junction molecules such as VE-cadherin-mCherry or -EGFP, subunits of the ARP2/3 complex (EGFP-p20) or LifeAct-EGFP in ECs, our research team documented that the actin-driven protrusions lead directly to new VE-cadherin adhesions. This process occurs at a junction size between 1 and 5 μm in time frames of 5 min (Abu Taha et al., 2014; Seebach et al., 2015; Cao et al., 2017; Taha et al., 2019). Since JAIL formation is a continuous process that leads to new VE-cadherin adhesions, VE-cadherin dynamics is also subject to permanent remodeling. This process is the reason for the different VE-cadherin patterns observed along the endothelial cell junctions. Significant insight into this VE-cadherin remodeling by JAIL was also gained by studying and correlating cell density dependent cell motility/migration with JAIL-mediated VE-cadherin dynamics. Growing endothelial cultures show a very heterogeneous VE-cadherin pattern that is caused by the extended cell junction length. The different VE-cadherin patterns, which can be described as interrupted, linear or reticular, show different local concentrations of VE-cadherin. Accordingly, JAIL occur at sites where the Rel-VEcad-C is low, which is common in growing cultures with long cell contacts. Increasing cell density of up to 10^5 cells/cm^2 decreases the cell junction length and thus increases the number of areas with high Rel-VEcad-C. This leads to a decrease in JAIL frequency, JAIL size, and VE-cadherin dynamics occurs (Abu Taha et al., 2014). This shows that the JAIL activity depends on the local VE-cadherin pattern and the local VE-cadherin concentration, which is directly related to the length of the cell boundaries. The actin driven VE-cadherin dynamics showing this relationship is shown in the video annotated taken from Abu Taha et al. (2014) (herein Supplementary Movie 8). Documentation and interpretation of this mechanism is difficult using snapshots of fixed and immune-labeled cells, since the rapid spatiotemporal dynamics permanently changes the observed protein pattern. The best setup for investigating cellular dynamics is time-lapse recording setups using fluorescence and phase-contrast microscopy, since it allows visualization of rapidly occurring events. For time-lapse recordings the image acquisition frequency and the timeframe should be carefully selected. The reader is encouraged to view the accompanying video of JAIL-dependent VE-cadherin dynamics, taken from Cao et al. (2017) (herein Supplementary Movie 4).

SUBJUNCTIONAL REGULATION BY JAIL ALLOWS MULTITASKING CONTROL OF ENDOTHELIAL CELL JUNCTIONS

One of the first examples of subjunctional regulation was described for leukocyte transmigration by actin-driven protrusions in plasma membranes, denoted "lateral lamellipodia." Those lamellipodia have also been indicated to seal pores upon transcellular leukocytes transmigration. This occurs in a Rac- and actin-related protein (ARP)2/3 complex-dependent manner (Martinelli et al., 2013) and appears to be dependent on actin/myosin-mediated contractility (Heemskerk et al., 2016). While leukocyte transmigration is restricted to one subjunctional site, a more complex problem is related to subjunctional activity during cell growth and sheet migration. In particular, in a monolayer-forming cell sheet, each individual cell of the monolayer is surrounded by several adjacent cells and accordingly requires at least the same number of bilateral cell interconnections. In growing cell cultures, each of the individual cells within the monolayer displays an individual cell migration path, leading to displacement of cells relative to each other. Relative cell displacements and migration become more complex during endothelial sheet migration, as occurs in angiogenesis and wound healing. Under these conditions, some cells even migrate in opposite directions (Cao et al., 2017; Taha et al., 2019); however, the entire monolayer remains intact. In particular, the interaction of two adjacent cells in a monolayer, might appear to occur at a length of several dozen microns. Therefore, it becomes obvious that a further reduction of junction remodeling is required to allow a relative cell displacement. The high resolution of phase-contrast microscopy with time-lapse recording reveals that a cell monolayer remains almost intact irrespective of the dynamics, which is obviously due to high membrane activities at the cell borders. Protrusions corresponding to JAIL occur simultaneously or with different time delays at different cell junction locations of the same cell. The presence of JAIL at EC junctions was also confirmed by other authors in mammalian ECs (Neto et al., 2018; Chrifi et al., 2019; Gomez-Escudero et al., 2019). Structures with dynamics comparable to that of JAIL were demonstrated in the developing vasculature of fish and were described as "junction-based lamellipodia" (Paatero et al., 2018). Mechanistically, the subjunctional decrease in the amount of VE-cadherin at distinct junction sites (e.g., by gap formation or change in cell shape) leads to activation of the Rac/Wave/WASP/ARP2/3 complex. This activation causes the formation of branched actin filaments that promote locally restricted protrusions of the plasma membrane (Abu Taha et al., 2014). These JAIL overlap adjacent cells and it is only in this area that interactions of VE-cadherin molecules can occur, which diffuse freely in the plasma membrane and form a structure known as a "VE-cadherin plaque (**Figure 1**)." Subsequently, after actin filaments have been depolymerized at the protrusion front [e.g., by EPLIN-a-mediated blockade of the ARP2/3 complex (Taha et al., 2019)], JAIL retract and VE-cadherin molecules of the plaques cluster together and become incorporated into junctions, thereby closing gaps or restoring insufficient/weak areas of cell junctions (Abu Taha et al., 2014).

Numerous JAIL arise simultaneously or form with overlapping timeframes, so knowing which regulatory principles underlie the formation of an individual JAIL is important. There is strong evidence that subjunctional JAIL-mediated VE-cadherin dynamics follow an autoregulatory mechanism, which, for the first time, demonstrates the possibility that endothelial contacts are controlled at different sites independently. Local formation of JAIL is dependent upon the subjunctional concentration of VE-cadherin, whereby a low level increases and a high level blocks JAIL formation, as demonstrated by overexpression of VE-cadherin in EC cultures (Abu Taha et al., 2014; Cao et al., 2017). For quantitative analyses of local JAIL formation, it is helpful to calculate the relative VE-cadherin concentration (Rel-VEcad-C), which is defined as the ratio between the local

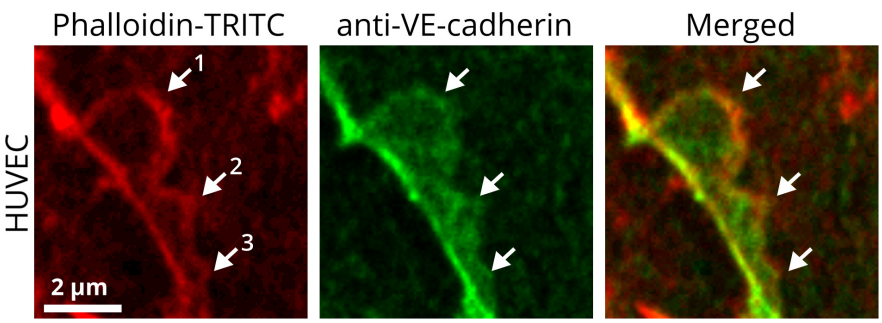

FIGURE 1 | JAIL are subjunctional structures forming new VE-cadherin adhesion sites in the vascular endothelium. HUVEC cultures were treated with phalloidin-TRITC to label actin filaments and with anti-VE-cadherin to label cell junctions. JAIL of different sizes (1, 2, 3) are visible at EC junctions. Actin-driven JAIL induce VE-cadherin plaques directly, visible in the JAIL area that overlaps adjacent cells (merged). JAIL-mediated VE-cadherin dynamics occurs continuously and leads directly to new VE-cadherin adhesions. JAIL are formed at junctions where a local decrease in VE-cadherin-mediated adhesion appears, which may be spontaneous or caused by stimuli. The decrease in VE-cadherin is then a direct stimulus for JAIL formation to compensate for weak or absent VE-cadherin adhesion due to an increase in JAIL frequency and, thus, VE-cadherin-mediated cell adhesion. This interdependence is most likely of an autoregulatory nature. This mechanism also allows individual migration of cells within a cell monolayer while maintaining monolayer integrity. The dynamics of JAIL formation can be followed in the two movies.

concentration of VE-cadherin (e.g., measured fluorescence intensity) along a given cell border and the corresponding length of the cell junction (Cao and Schnittler, 2019). This is where the cell shape comes into play. After application of vascular endothelial growth factor (VEGF) to confluent cell cultures, or under wound-healing conditions, or during angiogenesis in the developing retina, ECs change shape, which leads to an increase in cell-cell contact length within sheets of ECs. VE-cadherin expression in these cells remains unchanged, so cell elongation dilutes the given amount of VE-cadherin and leads to a decrease in Rel-VEcad-C at cell contacts. A decrease in the VE-cadherin concentration stimulates JAIL formation, which increases both cell junction and overall dynamics of the cells.

The mechanism of JAIL-induced VE-cadherin dynamics has been shown to be essential in randomized and polarized cell migration and to be observed in growing cell cultures, angiogenesis, wound healing, and during shear stress-induced morphologic adaptation of ECs (Cao et al., 2017; Taha et al., 2019). These studies showed that, during directed polarized cell migration, large JAIL occur at the migration front, whereas only small JAIL develop at the lateral borders to neighboring cells. Analyses of VE-cadherin dynamics by spinning-disk live-cell imaging in cultured ECs revealed the intermittent appearance of an interrupted VE-cadherin alternating with large JAIL-mediated VE-cadherin plaques, whereas the overall appearance of VE-cadherin at lateral junctions was faint but linear, which explained the formation of small JAIL at this site. Functionally, large JAIL developing at the leading cell pole direct and drive polarized cell migration whereas JAIL at the lateral junctions allow relative displacement of adjacent cells. This observation suggests that asymmetric JAIL dynamics are also involved in establishing cell polarity, although the underlying mechanisms of JAIL polarization are incompletely understood.

As shown for actin-mediated closure of micro-wounds (Martinelli et al., 2013), JAIL-mediated VE-cadherin dynamics close mediator-induced or spontaneously appearing intercellular gaps (Abu Taha et al., 2014; Seebach et al., 2015; Neto et al., 2018; Gomez-Escudero et al., 2019). This feature is relevant to maintaining overall endothelial integrity under resting conditions as well as during inflammation with increased permeability and leukocyte transmigration (Martinelli et al., 2013; Breslin et al., 2015; Seebach et al., 2015; Heemskerk et al., 2016). Junction remodeling under physiologic and pathologic conditions has been shown to involve several mechanisms, including activation of Rho-GTPases, PI 3-kinase, Src, PKC, actin/myosin contractility, myosin light-chain kinases and phosphatases, and the vascular endothelial phosphotyrosine phosphatase (VE-PTP) (Kuppers et al., 2014; Komarova et al., 2017; Duong and Vestweber, 2020).

The concept of junction control by subjunctional dynamics is in accordance with work that revealed N-WASP as an important regulator in the recovery of barrier function after thrombin stimulation (Rajput et al., 2013; Abu Taha et al., 2014; Seebach et al., 2015; Belvitch et al., 2017; Cao et al., 2017). N-WASP is a nucleation-promoting factor that activates ARP2/3 and controls actin dynamics (Schnoor, 2015; Pollard, 2016; Steffen et al., 2017; Svitkina, 2018). Dynamic structures comparable to JAIL were later demonstrated in developing vessels of the zebrafish (Paatero et al., 2018), and as local lamellipodia in cell culture (Breslin et al., 2015). These structures, together with the immunofluorescence microscopic identification of JAIL in the developing retina and in the yolk sack of the mouse (Cao et al., 2017), strongly suggest a general subjunctional regulation of endothelial cell contacts in cultured endothelial cells and *in vivo*. Since the paracellular transendothelial migration (TEM) of leukocytes is accompanied by a local opening of cell junctions and most likely a restricted loss of VE-cadherin-mediated adhesion, it would be challenging to find out whether local inhibition of JAIL might play a role in TEM, as was demonstrated for the increase in permeability induced by thrombin (Breslin et al., 2015; Seebach et al., 2015). The dissociation of VE-cadherin during TEM, however, has been shown to include targeted trafficking of the so-called lateral border recycling compartment (LBRC), a reticulum of interconnecting vesicle-like structures along the endothelial cell border that contains a pool of PECAM-1 necessary for effective TEM (Mamdouh et al., 2003; Gonzalez et al., 2016). Intriguingly, the recruitment of the LBRC depends on kinesin and the microtubule cytoskeleton for independent regulation of actin-dependent VE-cadherin adhesion between neighboring endothelial cells on the one hand and PECAM-1-mediated adhesion between endothelial cells and the transmigrating leukocyte on the other hand. Since the dissociation of VE-cadherin occurs downstream of the trafficking event, it is intriguing to speculate that the LBRC might be associated with local JAIL activity. A link between YAP/TAZ signaling and JAIL has been reported, further indicating the critical impact of this mechanism in angiogenesis (Neto et al., 2018). In summary, these data strongly support our hypothesis on subjunctional cell-contact dynamics and further underline the functional importance of JAIL. However, there are still many questions to be answered regarding the coordination between actin-driven protrusions such as JAIL, dynamics of actin filaments, VE-cadherin remodeling, and cell adhesion.

SUBJUNCTIONAL CONTROL OF ENDOTHELIAL BARRIER FUNCTIONS

Quantifying the organ- and vascular bed-specific characteristics of the endothelial barrier allows mechanistic insights into physiologic and pathologic regulation. In recent decades, several *in vitro* and *in vivo* methods have been developed. The most frequently used and common parameters to describe the integrity of the endothelial barrier *in vitro* are the permeability to: (i) tracer molecules described by the permeability coefficient (PE); (ii) ions expressed as the transendothelial electrical resistance (TEER or TER); (iii) water quantified by the hydraulic conductivity (LP) (Wegener and Seebach, 2014). These assays have contributed significantly to the understanding of the mechanisms governing the function of the endothelial barrier. However, immunofluorescence microscopy using VE-cadherin antibodies of ECs treated with permeability-enhancing agents such as histamine, tumor necrosis factor-α, or thrombin show a heterogeneous distribution of VE-cadherin clusters at cell junctions described variously as "interrupted," "linear," "reticular," and "invaginated" [(Cao and Schnittler, 2019), and references

therein]. These data, together with results of fluorescence-based live-cell microscopic studies, led to the hypothesis that endothelial barrier function is related to dynamic changes at a subjunctional level (Cao and Schnittler, 2019). Knowledge about the dynamic reorganization of junctional proteins has benefited largely from the rapid development of innovative live-cell imaging methods in recent decades. However, knowledge about the resulting effects on local barrier function at cellular and subjunctional levels is still limited. The ability to determine local permeability, particularly in sheet-forming cell layers, would further enlighten many phenomena accompanying the transient loss of intercellular junctions as observed in cell division, apoptosis, or regenerative and repair processes. Indeed, permeability assays have been developed that can be used to obtain spatial resolution at the cellular (and even subjunctional) level, as smmarized in **Table 1** and describd in more detail below.

ASSAYS USED TO DETECT LOCAL PERMEABILITY ALONG CELL JUNCTIONS

For investigation of local permeability in cell layers, Frömter and Diamond established in the early 1970s a test of ionic conductivity based on microelectrodes that were used to scan the cell layer with a resolution of ∼1.5 μm. Improvements of these methods then provided the possibility to determine permeability kinetics after single-cell defects caused by, for example, apoptosis or mechanical manipulation (Gitter et al., 2000; Florian et al., 2002). These studies were the first to describe local changes in permeability in EC layers. In recent decades, fluorescence-labeled macromolecules of different sizes have been used as tracers to determine quantitatively local permeability in epithelial and EC layers by various methods. In particular, Phelps and DePaola (2000) established an assay for the quantification of local flow-induced permeability at EC monolayers. For this assay, cells are cultured on a filter membrane and transferred to an agarose layer. Fluorescein isothiocyanate (FITC)-dextran molecules passing through the cell layer accumulate topically in the agarose layer and can be measured quantitatively. Even though this assay recognizes permeability of cell collectives in a lateral resolution of 1 mm, it is able to detect local differences in endothelial barrier function in response to disturbed flow profiles.

Development of the XPerT assay offered a significant increase in spatial resolution (Dubrovskyi et al., 2013). In this assay, ECs are grown on biotin-labeled solid substrates. FITC-labeled avidin is used as a tracer, which binds with high affinity to the immobilized biotin. After washing and fixing the samples, local differences in permeability are detected by fluorescence microscopy with a resolution of a few micrometers. Application of this assay revealed subjunctional changes in permeability triggered by mechanical stimulation or pro-inflammatory agonists (Dubrovskyi et al., 2013). This assay is based on endpoint measurement, so analyses of dynamics are not possible. Other assays also use fluorescence-coupled molecules as tracers which, after passing through a cell layer, accumulate in a macroporous silicon chip composed of circular pores of diameter 1.3 μm (Michaelis et al., 2012). Pores are arranged so close together that one cell covers many pores, which determines the local resolution. Thus, paracellular permeability and transcellular transport through the cell body can be detected. In addition to determination of local paracellular permeability, the method is very well suited for characterization of the basic transport routes of substances through a cell monolayer provided that the transport substance is fluorescence labeled.

With the discovery of subjunctional dynamics, we aimed to establish a permeability assay that could detect permeability dynamics at the subjunctional level in the vascular endothelium. Therefore, the Seebach research team at the Institute of Anatomy and Vascular Biology (Münster, Germany) developed the "dynamic measurement of local endothelial barrier function in living endothelial cells" (DyMEB) assay. Fluorescence-tagged tracers of different molecular weight pass an EC layer at particular subjunctional sites and are detected by total internal reflection fluorescence (TIRF) microscopy. In TIRF mode, an evanescent field of ≤100 nm in the z-plane is established and fluorescence can be detected in this field only. The assay achieves a subjunctional lateral resolution of ∼15 μm with a high temporal resolution of 1 min (Klusmeier et al., 2019). More details of the DyMEB assay are illustrated in **Figure 2**.

Application of this assay has already shown the extraordinary heterogeneity and dynamics of subjunctional permeability in cultures of resting confluent ECs. Furthermore, evaluation

TABLE 1 | Assays for the detection of local permeability in sheet-forming cell layers.

Assay	Method	Applied to	Spatial Resolution	Living Cells	Time Resolution	References
Ion Conductivity	Microelectrodes	Epithelium	μm	Yes	ms to sec	Frömter and Diamond, 1972; Gitter et al., 2000; Florian et al., 2002
Transport Assay	Immobilized Fluorescence Tracer	Endothelium	mm	No	n.a.	Phelps and DePaola, 2000
Macroporous Assay	Collection of Tracer in Pores	Epithelium	μm	Yes	n.d.	Michaelis et al., 2012
XPerT	Fluorescent Avidin/Biotin	Endothelium, Epithelium	μm	No	n.a.	Dubrovskyi et al., 2013; Song et al., 2016
DyMEB	TIRF Microscopy	Endothelium	μm	Yes	1 min	Klusmeier et al., 2019

n.a., not available; n.d., not determined.

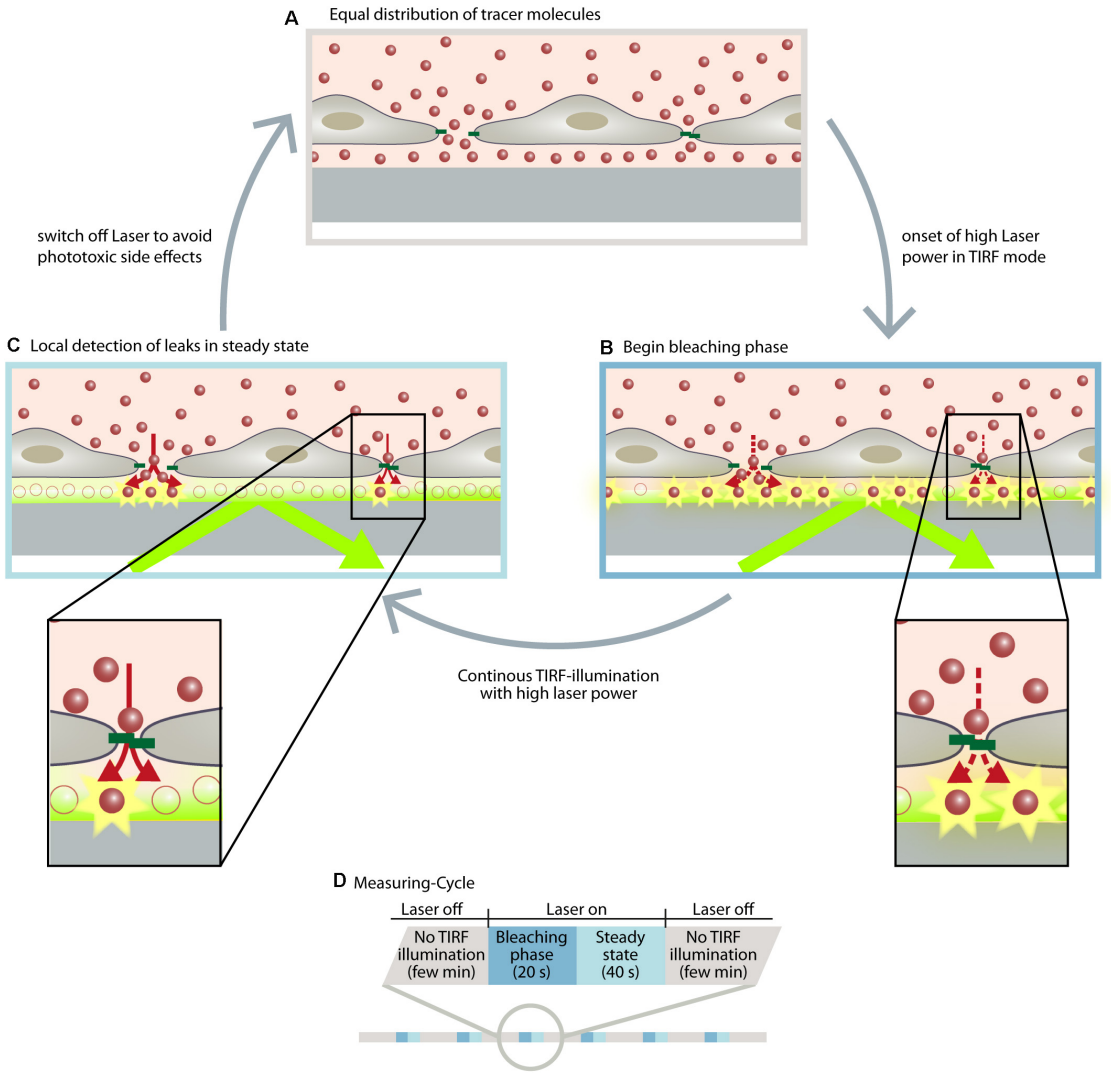

FIGURE 2 | The DyMEB assay was designed to analyze the dynamics of barrier function at the subjunctional level in cultures of confluent endothelial cells. **(A)** Endothelial cells were cultured on glass-bottomed dishes suitable for TIRF microscopy, and a fluorescence-labeled marker molecule (e.g., Atto565-Dextran) was added to the culture medium. Due to the small volume of the basal compartment, an equal distribution between apical and basal sides of the cell is reached within a few minutes, even in confluent cell layers. **(B)** Due to TIRF illumination, fluorescence-labeled molecules are bleached at the glass/medium interface due to the high power of the laser. This generates a concentration gradient of fluorescent-labeled molecules between the apical and basal compartment, which continues the diffusion (dotted arrows). **(C)** The diffusion rate and the bleaching rate reach a steady state in which regions with higher permeability show a greater fluorescence intensity than regions with lesser permeability. **(D)** Illustration of the measuring cycles to avoid phototoxic effects. Furthermore antioxidants are added to the medium and the measurements are carried out at intervals of ∼2 min so that the reactive oxygen species formed by the TIRF illumination can be inactivated or degraded. During this interval other microscopic techniques (DIC, phase contrast, LSM) can be applied to analyze structural parameters of the cells. For further detailed information, see Klusmeier et al. (2019).

of subjunctional changes in permeability due to the proinflammatory agonist histamine (Moy et al., 1993; Di Lorenzo et al., 2009; Wessel et al., 2014) indeed displayed heterogeneous subjunctional permeability between different cells and, remarkably, even along the junctions of one EC (**Figure 3**). Close evaluation revealed that some subjunctional sections remained unaffected, whereas other areas displayed rapidly increased fluorescence in the TIRF mode (**Figure 3**). This subjunctional activity was consistent with studies showing subjunctional RhoA activity (Szulcek et al., 2013), and regulation of gap closure has also been proposed for Rac1 (Martinelli et al., 2013; Timmerman et al., 2015; Cao et al., 2017). Furthermore, histamine induced a change in barrier function that was suggested to be dependent upon activation of Rac1 and RhoA (Wojciak-Stothard et al., 2001).

In summary, the spatiotemporal heterogeneity of endothelial permeability at rest and under stimulation strongly support the concept of subjunctional dynamics of cell junction proteins, as demonstrated for JAIL-mediated VE-cadherin. In addition, dynamic measurements of subjunctional permeability combined

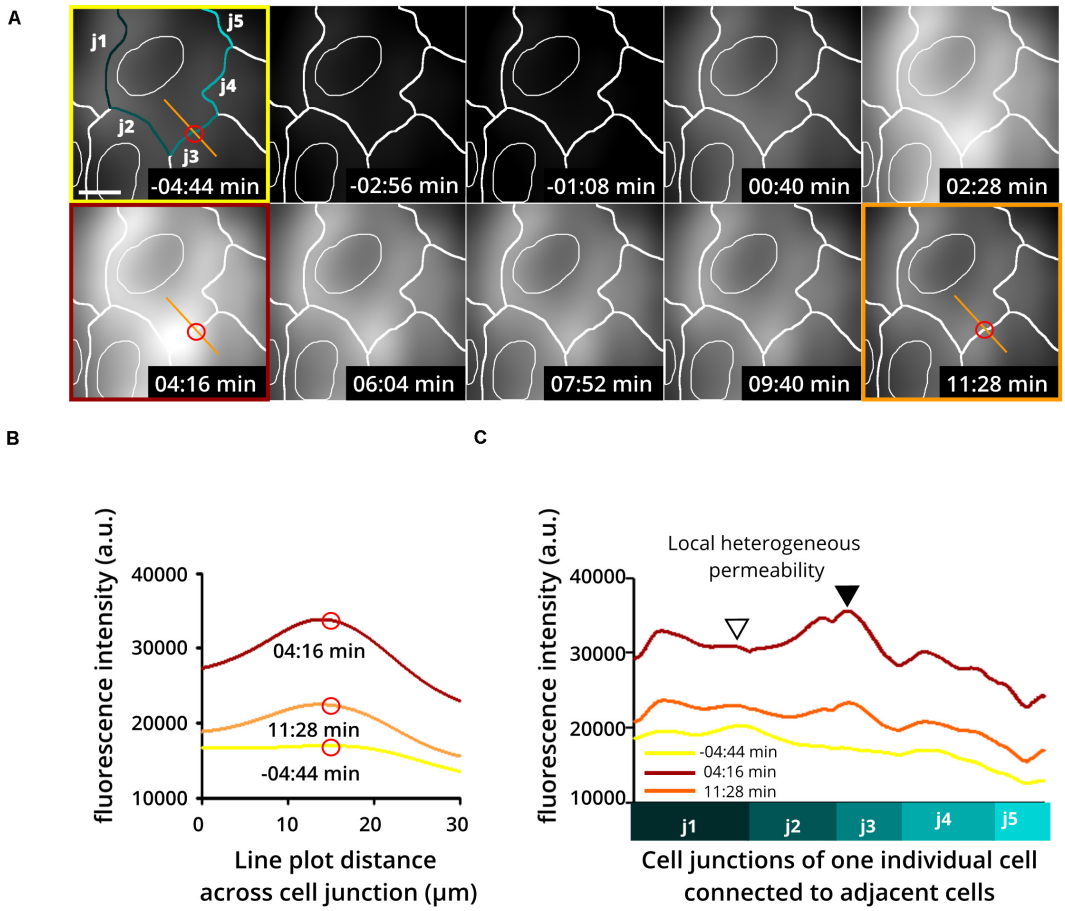

FIGURE 3 | Heterogeneous and dynamic change in barrier function at the subjunctional level as shown upon histamine application to confluent endothelial cell cultures. Histamine is a proinflammatory product of mast cells and basophils known to increase endothelial permeability. Here, human umbilical vein endothelial cells (HUVEC) were treated with histamine to determine changes in endothelial permeability. **(A)** Time-lapse recording using the DyMEB assay combined with DIC images (not shown) taken alternately with TIRF microscopy allow an estimation of cell junctions (white lines). (Upper 3 left-hand images) Prior to histamine application, background fluorescence was low. Application of histamine (100 µM) increased the detectable fluorescence in a transient and heterogeneous pattern corresponding to the indicated cell junctions as a result of a heterogeneous increase in permeability. Scale bar, 10 µm. **(B)** Line plots taken from images shown in **(A)** at different time points as indicated by the red circle and orange line. **(C)** Line plots of junction-related fluorescence intensity at different time points for locations j1 to j5 in **(A)**. The different levels of brightness document the heterogeneous local permeability.

with differential interference contrast microscopy time-lapse imaging can be used to analyze cellular morphodynamics. Laser scanning live-cell microscopy of fluorescence-labeled molecules can be used to visualize protein dynamics. Application of both of these methods allows analysis and correlation of structural and functional changes at cell contacts. The mechanistic concept of subjunctional regulation of cell junctions opens up the possibility of "fine tuning" and autoregulating permeability during dynamic remodeling of a cell layer.

CONCLUSION AND FUTURE PERSPECTIVES

The discovery of the subjunctional control of EC contacts explains several phenomena that were difficult to understand previously. One of the challenging questions relates to migration of individual cells within a confluent cell layer, such as that occurring in angiogenesis and in wound healing where, surprisingly, monolayer integrity remains largely intact. This phenomenon cannot be explained exclusively by the classical models of signaling mechanisms and pathways. The extended model of subjunctional autoregulatory control of cell contacts within the range of 1–5 µm has been demonstrated convincingly in recent years, at least for ECs. This model meets all requirements to explain migration of individual cells within a cell layer while maintaining monolayer integrity, and it also provides a concept for the mechanism of opening and closing of cell junctions due to transmigration of leukocytes or tumor cells. For dynamic analyses, combined application of morphologic methods involving optogenetic tools (Gautier et al., 2014; Karunarathne et al., 2015), such

as light-sensitive kinases or GTPases (Guglielmi et al., 2016; Leopold et al., 2018), together with a permeability assay to analyze subjunctional dynamics opens further possibilities to investigate mechanisms of local regulation of the function of endothelial barriers. Challenging work in the future will be to determine how classical signaling mechanisms can interfere and target particular cell-junction sites to control the permeability of cell monolayers.

AUTHOR CONTRIBUTIONS

All authors listed have made a substantial, direct and intellectual contribution to the work, and approved it for publication.

FUNDING

This work was supported by grants from the German Research Council (DFG grants SCHN 430/6-2, and SCHN 430/9-1 as well as DFG INST 2105/24–1) and the BMBF (03ZZ0902D) to HS. Support by the Excellence Cluster Cells-In-Motion flexible fund to JS (FF-2016-15) as well as to HS (FF-2014-15) is also gratefully acknowledged.

ACKNOWLEDGMENTS

We are grateful to Nina Knubel for drawing **Figure 2**.

REFERENCES

Abe, K., and Takeichi, M. (2008). EPLIN mediates linkage of the cadherin-catenin complex to F-actin and stabilizes the circumferential actin belt. *Proc. Natl. Acad. Sci. U.S.A.* 105, 13–19. doi: 10.1073/pnas.0710504105

Abu Taha, A., Taha, M., Seebach, J., and Schnittler, H. J. (2014). ARP2/3-mediated junction-associated lamellipodia control VE-cadherin-based cell junction dynamics and maintain monolayer integrity. *Mol. Biol. Cell* 25, 245–256. doi: 10.1091/mbc.e13-07-0404

Adderley, S. P., Lawrence, C., Madonia, E., Olubadewo, J. O., and Breslin, J. W. (2015). Histamine activates p38 MAP kinase and alters local lamellipodia dynamics, reducing endothelial barrier integrity and eliciting central movement of actin fibers. *Am. J. Physiol. Cell Physiol.* 309, C51–C59.

Aird, W. C. (2006). Mechanisms of endothelial cell heterogeneity in health and disease. *Circ. Res.* 98, 159–162. doi: 10.1161/01.res.0000204553.32549.a7

Aird, W. C. (2007). Phenotypic heterogeneity of the endothelium: II. Representative vascular beds. *Circ. Res.* 100, 174–190. doi: 10.1161/01.res.0000255690.03436.ae

Alon, R., and van Buul, J. D. (2017). Leukocyte breaching of endothelial barriers: the actin link. *Trends Immunol.* 38, 606–615. doi: 10.1016/j.it.2017.05.002

Belvitch, P., Brown, M. E., Brinley, B. N., Letsiou, E., Rizzo, A. N., Garcia, J. G. N., et al. (2017). The ARP 2/3 complex mediates endothelial barrier function and recovery. *Pulm. Circ.* 7, 200–210. doi: 10.1086/690307

Belvitch, P., Htwe, Y. M., Brown, M. E., and Dudek, S. (2018). Cortical actin dynamics in endothelial permeability. *Curr. Top. Membr.* 82, 141–195. doi: 10.1016/bs.ctm.2018.09.003

Brasch, J., Harrison, O. J., Ahlsen, G., Carnally, S. M., Henderson, R. M., Honig, B., et al. (2011). Structure and binding mechanism of vascular endothelial cadherin: a divergent classical cadherin. *J. Mol. Biol.* 408, 57–73. doi: 10.1016/j.jmb.2011.01.031

Breslin, J. W., Zhang, X. E., Worthylake, R. A., and Souza-Smith, F. M. (2015). Involvement of local lamellipodia in endothelial barrier function. *PLoS One* 10:e0117970. doi: 10.1371/journal.pone.0117970

Cao, J., Ehling, M., Marz, S., Seebach, J., Tarbashevich, K., Sixta, T., et al. (2017). Polarized actin and VE-cadherin dynamics regulate junctional remodelling and cell migration during sprouting angiogenesis. *Nat. Commun.* 8:2210.

Cao, J., and Schnittler, H. (2019). Putting VE-cadherin into JAIL for junction remodeling. *J. Cell Sci.* 132:jcs222893. doi: 10.1242/jcs.222893

Carmeliet, P., Lampugnani, M. G., Moons, L., Breviario, F., Compernolle, V., Bono, F., et al. (1999). Targeted deficiency or cytosolic truncation of the VE-cadherin gene in mice impairs VEGF-mediated endothelial survival and angiogenesis. *Cell* 98, 147–157. doi: 10.1016/s0092-8674(00)81010-7

Chervin-Pétinot, A., Courçon, M., Almagro, S., Nicolas, A., Grichine, A., Grunwald, D., et al. (2012). Epithelial protein lost in neoplasm (EPLIN) interacts with α-catenin and actin filaments in endothelial cells and stabilizes vascular capillary network in vitro. *J. Biol. Chem.* 287, 7556–7572. doi: 10.1074/jbc.M111.328682

Chrifi, I., Louzao-Martinez, L., Brandt, M. M., Van Dijk, C. G. M., Burgisser, P. E., Zhu, C., et al. (2019). CMTM4 regulates angiogenesis by promoting cell surface recycling of VE-cadherin to endothelial adherens junctions. *Angiogenesis* 22, 75–93. doi: 10.1007/s10456-018-9638-1

Corada, M., Liao, F., Lindgren, M., Lampugnani, M. G., Breviario, F., Frank, R., et al. (2001). Monoclonal antibodies directed to different regions of vascular endothelial cadherin extracellular domain affect adhesion and clustering of the protein and modulate endothelial permeability. *Blood* 97, 1679–1684. doi: 10.1182/blood.v97.6.1679

Dejana, E., and Vestweber, D. (2013). The role of VE-cadherin in vascular morphogenesis and permeability control. *Prog. Mol. Biol. Transl. Sci.* 116, 119–144. doi: 10.1016/b978-0-12-394311-8.00006-6

Di Lorenzo, A., Fernández-Hernando, C., Cirino, G., and Sessa, W. C. (2009). Akt1 is critical for acute inflammation and histamine-mediated vascular leakage. *Proc. Natl. Acad. Sci. U.S.A.* 106, 14552–14557. doi: 10.1073/pnas.0904073106

Doggett, T. M., and Breslin, J. W. (2011). Study of the actin cytoskeleton in live endothelial cells expressing GFP-actin. *J. Vis. Exp.* 57:3187.

Dubrovskyi, O., Birukova, A. A., and Birukov, K. G. (2013). Measurement of local permeability at subcellular level in cell models of agonist- and ventilator-induced lung injury. *Lab. Invest.* 93, 254–263. doi: 10.1038/labinvest.2012.159

Duong, C. N., and Vestweber, D. (2020). Mechanisms ensuring endothelial junction integrity beyond VE-Cadherin. *Front. Physiol.* 11:519. doi: 10.3389/fphys.2020.00519

Florian, P., Schoneberg, T., Schulzke, J. D., Fromm, M., and Gitter, A. H. (2002). Single-cell epithelial defects close rapidly by an actinomyosin purse string mechanism with functional tight junctions. *J. Physiol.* 545, 485–499. doi: 10.1113/jphysiol.2002.031161

Frömter, E., and Diamond, J. (1972). Route of passive ion permeation in epithelia. *Nat. New Biol.* 235, 9–13. doi: 10.1038/newbio235009a0

Frye, M., Dierkes, M., Kuppers, V., Vockel, M., Tomm, J., Zeuschner, D., et al. (2015). Interfering with VE-PTP stabilizes endothelial junctions in vivo via Tie-2 in the absence of VE-cadherin. *J. Exp. Med.* 212, 2267–2287. doi: 10.1084/jem.20150718

Garcia-Ponce, A., Citalan-Madrid, A. F., Velazquez-Avila, M., Vargas-Robles, H., and Schnoor, M. (2015). The role of actin-binding proteins in the control of endothelial barrier integrity. *Thromb. Haemost.* 113, 20–36. doi: 10.1160/th14-04-0298

Gautier, A., Gauron, C., Volovitch, M., Bensimon, D., Jullien, L., and Vriz, S. (2014). How to control proteins with light in living systems. *Nat. Chem. Biol.* 10, 533–541. doi: 10.1038/nchembio.1534

Gitter, A. H., Bendfeldt, K., Schulzke, J. D., and Fromm, M. (2000). Leaks in the epithelial barrier caused by spontaneous and TNF-alpha-induced single-cell apoptosis. *FASEB J.* 14, 1749–1753. doi: 10.1096/fj.99-0898com

Gomez-Escudero, J., Clemente, C., Garcia-Weber, D., Acin-Perez, R., Millan, J., Enriquez, J. A., et al. (2019). PKM2 regulates endothelial cell junction dynamics and angiogenesis via ATP production. *Sci. Rep.* 9:15022.

Gonzalez, A. M., Cyrus, B. F., and Muller, W. A. (2016). Targeted recycling of the lateral border recycling compartment precedes adherens junction dissociation during transendothelial migration. *Am. J. Pathol.* 186, 1387–1402. doi: 10.1016/j.ajpath.2016.01.010

Guglielmi, G., Falk, H. J., and De Renzis, S. (2016). Optogenetic control of protein function: from intracellular processes to tissue morphogenesis. *Trends Cell Biol.* 26, 864–874. doi: 10.1016/j.tcb.2016.09.006

Heemskerk, N., Schimmel, L., Oort, C., Van Rijssel, J., Yin, T., Ma, B., et al. (2016). F-actin-rich contractile endothelial pores prevent vascular leakage during leukocyte diapedesis through local RhoA signalling. *Nat. Commun.* 7:10493.

Hoelzle, M. K., and Svitkina, T. (2012). The cytoskeletal mechanisms of cell-cell junction formation in endothelial cells. *Mol. Biol. Cell* 23, 310–323. doi: 10.1091/mbc.e11-08-0719

Karunarathne, W. K. A., O'Neill, P. R., and Gautam, N. (2015). Subcellular optogenetics – controlling signaling and single-cell behavior. *J. Cell Sci.* 128, 15–25. doi: 10.1242/jcs.154435

Klusmeier, N., Schnittler, H., and Seebach, J. (2019). A novel microscopic assay reveals heterogeneous regulation of local endothelial barrier function. *Biophys. J.* 116, 1547–1559. doi: 10.1016/j.bpj.2019.02.008

Komarova, Y. A., Kruse, K., Mehta, D., and Malik, A. B. (2017). Protein interactions at endothelial junctions and signaling mechanisms regulating endothelial permeability. *Circ. Res.* 120, 179–206. doi: 10.1161/circresaha.116.306534

Kuppers, V., Vockel, M., Nottebaum, A. F., and Vestweber, D. (2014). Phosphatases and kinases as regulators of the endothelial barrier function. *Cell Tissue Res.* 355, 577–586.0.

Lampugnani, M. G., Corada, M., Caveda, L., Breviario, F., Ayalon, O., Geiger, B., et al. (1995). The molecular organization of endothelial cell to cell junctions: differential association of plakoglobin, beta-catenin, and alpha- catenin with vascular endothelial cadherin (VE-cadherin). *J. Cell Biol.* 129, 203–217. doi: 10.1083/jcb.129.1.203

Lampugnani, M. G., Dejana, E., and Giampietro, C. (2017). Vascular endothelial (VE)-cadherin, endothelial adherens junctions, and vascular disease. *Cold Spring Harb. Perspect. Biol.* 10:a029322. doi: 10.1101/cshperspect.a029322

Leopold, A. V., Chernov, K. G., and Verkhusha, V. V. (2018). Optogenetically controlled protein kinases for regulation of cellular signaling. *Chem. Soc. Rev.* 47, 2454–2484. doi: 10.1039/c7cs00404d

Mamdouh, Z., Chen, X., Pierini, L. M., Maxfield, F. R., and Muller, W. A. (2003). Targeted recycling of PECAM from endothelial surface-connected compartments during diapedesis. *Nature* 421, 748–753. doi: 10.1038/nature01300

Marcos-Ramiro, B., Garcia-Weber, D., and Millan, J. (2014). TNF-induced endothelial barrier disruption: beyond actin and Rho. *Thromb. Haemost.* 112, 1088–1102. doi: 10.1160/th14-04-0299

Martinelli, R., Kamei, M., Sage, P. T., Massol, R., Varghese, L., Sciuto, T., et al. (2013). Release of cellular tension signals self-restorative ventral lamellipodia to heal barrier micro-wounds. *J. Cell Biol.* 201, 449–465. doi: 10.1083/jcb.201209077

Maul, R. S., and Chang, D. D. (1999). EPLIN, epithelial protein lost in neoplasm. *Oncogene* 18, 7838–7841. doi: 10.1038/sj.onc.1203206

Michaelis, S., Rommel, C. E., Endell, J., Goring, P., Wehrspohn, R., Steinem, C., et al. (2012). Macroporous silicon chips for laterally resolved, multi-parametric analysis of epithelial barrier function. *Lab. Chip.* 12, 2329–2336. doi: 10.1039/c2lc00026a

Moy, A. B., Shasby, S. S., Scott, B. D., and Shasby, D. M. (1993). The effect of histamine and cyclic adenosine monophosphate on myosin light chain phosphorylation in human umbilical vein endothelial cells. *J. Clin. Invest.* 92, 1198–1206. doi: 10.1172/JCI116690

Muramatsu, F., Kidoya, H., Naito, H., Hayashi, Y., Iba, T., and Takakura, N. (2017). Plakoglobin maintains the integrity of vascular endothelial cell junctions and regulates VEGF-induced phosphorylation of VE-cadherin. *J. Biochem.* 162, 55–62. doi: 10.1093/jb/mvx001

Neto, F., Klaus-Bergmann, A., Ong, Y. T., Alt, S., Vion, A. C., Szymborska, A., et al. (2018). YAP and TAZ regulate adherens junction dynamics and endothelial cell distribution during vascular development. *eLife* 7:e31037.

Nottebaum, A. F., Cagna, G., Winderlich, M., Gamp, A. C., Linnepe, R., Polaschegg, C., et al. (2008). VE-PTP maintains the endothelial barrier via plakoglobin and becomes dissociated from VE-cadherin by leukocytes and by VEGF. *J. Exp. Med.* 205, 2929–2945. doi: 10.1084/jem.20080406

Paatero, I., Sauteur, L., Lee, M., Lagendijk, A. K., Heutschi, D., Wiesner, C., et al. (2018). Junction-based lamellipodia drive endothelial cell rearrangements in vivo via a VE-cadherin-F-actin based oscillatory cell-cell interaction. *Nat. Commun.* 9:3545.

Phelps, J. E., and DePaola, N. (2000). Spatial variations in endothelial barrier function in disturbed flows in vitro. *Am. J. Physiol. Heart Circ. Physiol.* 278, H469–H476.

Pollard, T. D. (2016). Actin and actin-binding proteins. *Cold Spring Harb. Perspect. Biol.* 8:a018226.

Rajput, C., Kini, V., Smith, M., Yazbeck, P., Chavez, A., Schmidt, T., et al. (2013). Neural Wiskott-Aldrich syndrome protein (N-WASP)-mediated p120-catenin interaction with Arp2-Actin complex stabilizes endothelial adherens junctions. *J. Biol. Chem.* 288, 4241–4250. doi: 10.1074/jbc.m112.440396

Reynolds, A. B. (2007). p120-catenin: past and present. *Biochim. Biophys. Acta* 1773, 2–7. doi: 10.1016/j.bbamcr.2006.09.019

Schnittler, H., Taha, M., Schnittler, M. O., Taha, A. A., Lindemann, N., and Seebach, J. (2014). Actin filament dynamics and endothelial cell junctions: the Ying and Yang between stabilization and motion. *Cell Tissue Res.* 355, 529–543. doi: 10.1007/s00441-014-1856-2

Schnittler, H. J., Puschel, B., and Drenckhahn, D. (1997). Role of cadherins and plakoglobin in interendothelial adhesion under resting conditions and shear stress. *Am. J. Physiol.* 273, H2396–H2405.

Schnoor, M. (2015). Endothelial actin-binding proteins and actin dynamics in leukocyte transendothelial migration. *J. Immunol.* 194, 3535–3541. doi: 10.4049/jimmunol.1403250

Schnoor, M., Garcia Ponce, A., Vadillo, E., Pelayo, R., Rossaint, J., and Zarbock, A. (2017). Actin dynamics in the regulation of endothelial barrier functions and neutrophil recruitment during endotoxemia and sepsis. *Cell Mol. Life Sci.* 74, 1985–1997. doi: 10.1007/s00018-016-2449-x

Seebach, J., Donnert, G., Kronstein, R., Werth, S., Wojciak-Stothard, B., Falzarano, D., et al. (2007). Regulation of endothelial barrier function during flow-induced conversion to an arterial phenotype. *Cardiovasc. Res.* 75, 596–607. doi: 10.1016/j.cardiores.2007.04.017

Seebach, J., Taha, A. A., Lenk, J., Lindemann, N., Jiang, X., Brinkmann, K., et al. (2015). The CellBorderTracker, a novel tool to quantitatively analyze spatiotemporal endothelial junction dynamics at the subcellular level. *Histochem. Cell Biol.* 144, 517–532. doi: 10.1007/s00418-015-1357-8

Simionescu, M., Simionescu, N., and Palade, G. E. (1975). Segmental differentiations of cell junctions in the vascular endothelium. The microvasculature. *J. Cell Biol.* 67, 863–885. doi: 10.1083/jcb.67.3.863

Simionescu, M., Simionescu, N., and Palade, G. E. (1976a). Characteristic endothelial junctions in different segments of the vascular system. *Thromb. Res.* 8, 247–256. doi: 10.1016/0049-3848(76)90067-0

Simionescu, M., Simionescu, N., and Palade, G. E. (1976b). Segmental differentiations of cell junctions in the vascular endothelium. Arteries and veins. *J. Cell Biol.* 68, 705–723. doi: 10.1083/jcb.68.3.705

Song, M. J., Davis, C. I., Lawrence, G. G., and Margulies, S. S. (2016). Local influence of cell viability on stretch-induced permeability of alveolar epithelial cell monolayers. *Cell. Mol. Bioeng.* 9, 65–72. doi: 10.1007/s12195-015-0405-8

Steffen, A., Stradal, T. E., and Rottner, K. (2017). Signalling pathways controlling cellular actin organization. *Handb. Exp. Pharmacol.* 235, 153–178. doi: 10.1007/164_2016_35

Suzuki, S., Sano, K., and Tanihara, H. (1991). Diversity of the cadherin family: evidence for eight new cadherins in nervous tissue. *Cell Regul* 2, 261–270. doi: 10.1091/mbc.2.4.261

Svitkina, T. (2018). The actin cytoskeleton and actin-based motility. *Cold Spring Harb. Perspect. Biol.* 10:a018267. doi: 10.1101/cshperspect.a018267

Szulcek, R., Beckers, C. M., Hodzic, J., De Wit, J., Chen, Z., Grob, T., et al. (2013). Localized RhoA GTPase activity regulates dynamics of endothelial monolayer integrity. *Cardiovasc. Res.* 99, 471–482. doi: 10.1093/cvr/cvt075

Taha, A. A., and Schnittler, H. J. (2014). Dynamics between actin and the VE-cadherin/catenin complex: novel aspects of the ARP2/3 complex in regulation of endothelial junctions. *Cell Adh. Migr.* 8, 125–135. doi: 10.4161/cam.28243

Taha, M., Aldirawi, M., Marz, S., Seebach, J., Odenthal-Schnittler, M., Bondareva, O., et al. (2019). EPLIN-alpha and -beta isoforms modulate endothelial cell dynamics through a spatiotemporally differentiated interaction with actin. *Cell Rep.* 29, 1010–1026.e6.

Takeichi, M. (2014). Dynamic contacts: rearranging adherens junctions to drive epithelial remodelling. *Nat. Rev. Mol. Cell Biol.* 15, 397–410. doi: 10.1038/nrm3802

Timmerman, I., Heemskerk, N., Kroon, J., Schaefer, A., Van Rijssel, J., Hoogenboezem, M., et al. (2015). A local VE-cadherin and Trio-based signaling complex stabilizes endothelial junctions through Rac1 (vol 128, pg 3041, 2015). *J. Cell Sci.* 128, 3514–3514. doi: 10.1242/jcs.179424

Vaughan, M. H., Xia, X., Wang, X., Chronopoulou, E., Gao, G. J., Campos-Gonzalez, R., et al. (2007). Generation and characterization of a novel phospho-specific monoclonal antibody to p120-catenin serine 879. *Hybridoma* 26, 407–415. doi: 10.1089/hyb.2007.0527

Vittet, D., Buchou, T., Schweitzer, A., Dejana, E., and Huber, P. (1997). Targeted null-mutation in the vascular endothelial-cadherin gene impairs the organization of vascular-like structures in embryoid bodies. *Proc. Natl. Acad. Sci. U.S.A.* 94, 6273–6278. doi: 10.1073/pnas.94.12.6273

Wegener, J., and Seebach, J. (2014). Experimental tools to monitor the dynamics of endothelial barrier function: a survey of in vitro approaches. *Cell Tissue Res.* 355, 485–514. doi: 10.1007/s00441-014-1810-3

Wessel, F., Winderlich, M., Holm, M., Frye, M., Rivera-Galdos, R., Vockel, M., et al. (2014). Leukocyte extravasation and vascular permeability are each controlled in vivo by different tyrosine residues of VE-cadherin. *Nat. Immunol.* 15, 223–230. doi: 10.1038/ni.2824

Wojciak-Stothard, B., Potempa, S., Eichholtz, T., and Ridley, A. J. (2001). Rho and Rac but not Cdc42 regulate endothelial cell permeability. *J. Cell Sci.* 114, 1343–1355.

Yonemura, S. (2017). Actin filament association at adherens junctions. *J. Med. Investig.* 64, 14–19. doi: 10.2152/jmi.64.14

Zankov, D. P., and Ogita, H. (2015). Actin-tethered junctional complexes in angiogenesis and lymphangiogenesis in association with vascular endothelial growth factor. *Biomed. Res. Int.* 2015:314178.

Conflict of Interest: The authors declare that the research was conducted in the absence of any commercial or financial relationships that could be construed as a potential conflict of interest.

frontiers in Physiology

ORIGINAL RESEARCH
published: 16 September 2021
doi: 10.3389/fphys.2021.724611

RNase A Inhibits Formation of Neutrophil Extracellular Traps in Subarachnoid Hemorrhage

Anton Früh[1†], Katharina Tielking[1†], Felix Schoknecht[1], Shuheng Liu[1], Ulf C. Schneider[1], Silvia Fischer[2], Peter Vajkoczy[1] and Ran Xu[1]*

[1]Department of Neurosurgery, Charité – Universitätsmedizin Berlin, Corporate Member of Freie Universität Berlin, Humboldt-Universität zu Berlin, and Berlin Institute of Health, Berlin, Germany, [2]Department of Biochemistry, Giessen University, Giessen, Germany

OPEN ACCESS

Edited by:
Jean-Luc Morel,
Centre National de la Recherche Scientifique (CNRS), France

Reviewed by:
Erik Josef Behringer,
Loma Linda University, United States
Md. A. Hakim,
Loma Linda University, United States
Jose Javier Provencio,
University of Virginia Hospital, United States

***Correspondence:**
Peter Vajkoczy
peter.vajkoczy@charite.de

[†]These authors have contributed equally to this work

Specialty section:
This article was submitted to Vascular Physiology, a section of the journal Frontiers in Physiology

Received: 13 June 2021
Accepted: 10 August 2021
Published: 16 September 2021

Citation:
Früh A, Tielking K, Schoknecht F, Liu S, Schneider UC, Fischer S, Vajkoczy P and Xu R (2021) RNase A Inhibits Formation of Neutrophil Extracellular Traps in Subarachnoid Hemorrhage. Front. Physiol. 12:724611. doi: 10.3389/fphys.2021.724611

Background: Subarachnoid hemorrhage (SAH) caused by rupture of an intracranial aneurysm, is a life-threatening emergency that is associated with substantial morbidity and mortality. Emerging evidence suggests involvement of the innate immune response in secondary brain injury, and a potential role of neutrophil extracellular traps (NETs) for SAH-associated neuroinflammation. In this study, we investigated the spatiotemporal patterns of NETs in SAH and the potential role of the RNase A (the bovine equivalent to human RNase 1) application on NET burden.

Methods: A total number of $n = 81$ male C57Bl/6 mice were operated utilizing a filament perforation model to induce SAH, and Sham operation was performed for the corresponding control groups. To confirm the bleeding and exclude stroke and intracerebral hemorrhage, the animals received MRI after 24 h. Mice were treated with intravenous injection of RNase A (42 μg/kg body weight) or saline solution for the control groups, respectively. Quadruple-immunofluorescence (IF) staining for cell nuclei (DAPI), F-actin (phalloidin), citrullinated H3, and neurons (NeuN) was analyzed by confocal imaging and used to quantify NET abundance in the subarachnoid space (SAS) and brain parenchyma. To quantify NETs in human SAH patients, cerebrospinal spinal fluid (CSF) and blood samples from day 1, 2, 7, and 14 after bleeding onset were analyzed for double-stranded DNA (dsDNA) *via* Sytox Green.

Results: Neutrophil extracellular traps are released upon subarachnoid hemorrhage in the SAS on the ipsilateral bleeding site 24 h after ictus. Over time, NETs showed progressive increase in the parenchyma on both ipsi- and contralateral site, peaking on day 14 in periventricular localization. In CSF and blood samples of patients with aneurysmal SAH, NETs also increased gradually over time with a peak on day 7. RNase application significantly reduced NET accumulation in basal, cortical, and periventricular areas.

Conclusion: Neutrophil extracellular trap formation following SAH originates in the ipsilateral SAS of the bleeding site and spreads gradually over time to basal, cortical, and periventricular areas in the parenchyma within 14 days. Intravenous RNase application abrogates NET burden significantly in the brain parenchyma, underpinning a potential role in modulation of the innate immune activation after SAH.

Keywords: neutrophil extracellular traps, neutrophils, subarachnoid hemorrhage, hemorrhagic stroke, neuroinflammation, innate immune response, innate immune reaction

INTRODUCTION

Subarachnoid hemorrhage (SAH) caused by rupture of an intracranial aneurysm, is a life-threatening emergency that is associated with substantial morbidity and mortality (Lawton and Vates, 2017; Van Lieshout et al., 2018). Approximately 5% of all strokes are caused by SAH and the incidence is estimated to be nine per 100.000 person years (Etminan et al., 2019). Women are about 1.24 times more likely to be affected by the disease, and the incidence of SAH increases from the age > 50 years and is higher in Japan and Finland compared to other industrialized countries (Macdonald and Schweizer, 2017). Around one-third of SAH patients die within the first 30 days after the initial bleeding event (Schertz et al., 2016). Among survivors, secondary brain injury is described as the main cause of morbidity (Macdonald, 2014). Thereby, emerging evidence points toward involvement of inflammatory processes (Gris et al., 2019), particularly of innate immune cells (Schneider et al., 2015; Lucke-Wold et al., 2016; Zhang et al., 2020).

Among these immune reactions, recent studies suggest that neutrophils play a particular role in SAH induced inflammation (Atangana et al., 2017). Neutrophil granulocytes are the first line of the innate immune system to fight pathogens (Borregaard, 2010). During infectious processes, they exit blood vessel systems, migrate to the site of infection and accumulate in high numbers (Niemiec et al., 2015). Neutrophil infiltration into damaged brain tissues has been shown after SAH, stroke, and traumatic brain injury (Liu et al., 2018; García-Culebras et al., 2019; Zeng et al., 2021). Upon stimulation, neutrophils release DNA, granule proteins, and histones (Brinkmann et al., 2004). These fibril matrixes are coined as neutrophil extracellular traps (NETs). NETs are involved in various immune reactions and the pathophysiology of diverse diseases (Papayannopoulos, 2018), including central nervous system pathologies (Zhang et al., 2020). The impact of NET formation in SAH has not yet been studied extensively, but recent evidence suggests that they may promote aneurysm rupture, and pharmacological removal of NETs can reduce the rate of aneurysm rupture (Korai et al., 2021). Moreover, there is growing evidence that NETs aggravate the inflammatory events after SAH, and impair revascularization and increase blood brain barrier (BBB) damage after stroke (Kang et al., 2020).

Next to extracellular DNA, other alarmins or so-called danger-associated molecular pattern (DAMP) signals such as extracellular RNA (exRNA) have been described as a key player in the involvement of central system pathologies, including hemorrhagic stroke (Tielking et al., 2019). In this context, RNase is a natural enzyme involved in the regulation of vascular homeostasis that can counteract exRNA when applied exogenously (Fischer et al., 2011; Lasch et al., 2020; Preissner et al., 2020). Recent studies have shown that NET-associated RNA is a relevant NET component and its formation can occur also independently of DNA, which opened the hypothetical avenue that RNase A (the bovine equivalent to human RNAse1) may also modify NET formation *in vivo* SAH models (Herster et al., 2020). Moreover, preliminary data from our laboratory show that RNase A modulates exRNA accumulation in SAH and the microglia-specific immune reaction after SAH.

In this study, with regard to the migratory characteristics of neutrophils, we investigated the spatial and temporal pattern of NET formation in an *in vivo* model of SAH. We report that NET accumulation begins in the ipsilateral side of bleeding, and spreads over time to the parenchyma on both hemispheres, peaking on day 14 after SAH. To confirm these findings in the human system, we also measured NET burden in cerebrospinal spinal fluid (CSF) and blood samples in SAH patients and show that NET accumulation occurs in both compartments significantly. Furthermore, we report that RNase significantly reduces NET formation in the parenchyma, thus being an attractive mediator for evaluation in subsequent studies.

MATERIALS AND METHODS

Study Approval

The analysis on human samples was approved by the local ethics committee of Charité University Hospital (ethical approval number: EA2/134/18). All patients or their authorized individuals gave written consent to the collection of blood and CSF samples. All animal experiments were approved by the Regional Office for Health and Social Affairs (Landesamt für Gesundheit und Soziales; approval number: TVA 0063/18) and were performed in conformity with the German law of animal protection and the National Institute of Health Guidelines for care and use of laboratory animals.

Human Data

Measurement of NET Surrogate Markers in CSF and Peripheral Blood in SAH Patients

Peripheral blood and CSF samples were collected from patients with aneurysmal SAH on day 1, 2, 7, and 14 after SAH onset. For each time point, 2 ml peripheral blood was drawn using Ethylene Diaminetetraacetic acid (EDTA) tubes, and 2 ml CSF was collected from the initial placement of an extraventricular drain (EVD) at onset of SAH, and then further collected from the existing EVD. Some patients also had additional lumbar

drainage, but in this study only ventricular CSF was used. Blood and CSF samples were immediately placed on ice and spun down twice at 4°C at 500 g for 5 min, and supernatant was frozen at −80°C before further analysis. Double-stranded DNA (dsDNA) was quantified in CSF and plasma samples as previously published (Ondracek et al., 2020). In detail, samples were incubated with Sytox Green (Thermo Fisher), a fluorescent dsDNA-binding dye, in a concentration of 1 µM for 5 min. Fluorescence intensities (excitation 480 nm, emission 520 nm) were measured in 96-well microplates using a Tecan Infinite M200 reader. Values were normalized to a standard curve of dsDNA (Lambda DNA, Thermo Fisher).

Animal Experiments

Male C57BL/6-mice were kept at the animal facility at the Neuroscience Research Center at Charité University (NWFZ, Berlin). Their age ranged from 8 to 12 weeks and with a weight range of 18–28 g. Animals underwent SAH operation, and sham operation (as the control condition), and were sacrificed at three different time points (1, 7, and 14 days) after operation. A total number of $n = 81$ mice were included in this study.

Mouse Model of Subarachnoid Hemorrhage

Subarachnoid hemorrhage was induced with a filament perforation model as described previously (Schneider et al., 2015). Briefly, mice were anesthetized with an intraperitoneal ketamine/xylazine (70 mg resp. 16 mg/kg body weight) injection and placed in supine position. Starting with a midline neck incision, the carotid artery was exposed and a 5–0 non-absorbable monofilament polypropylene suture inserted into the external carotid artery in a retrograde manner and advanced into the common carotid artery. In a next step, the filament invaginated into the internal carotid artery (ICA) and pushed forward to perforate the intracranial arterial bifurcation. Mice were perfused intracardially with PBS.

MRI

All SAH mice received an MRI 24 h after surgery to confirm the bleeding and animals who had a stroke or intracranial hemorrhage (ICH) were excluded from the experiments (**Figure 1A**). The 1H magnetic resonance imaging was performed on a PharmaScan 70/16 U (Bruker Corporation) with a field strength of 7 Tesla by using the software Paravision 5.1 (Bruker Corporation). During the scans, mice received an O_2/N_2O + isoflurane gas anesthesia. The animals' respiration was observed with Small Animal Monitoring System (SA Instruments, Inc.), while their temperature was maintained *via* controlled warming blankets. The presence of SAH was validated from T2 weighted image. Here, SAH volume was estimated based on the formula $V = (A_1 + A_2 + \ldots + A_x) \cdot d$, by which A_n corresponds to the bleeding area on each coronal MRI and d corresponds to the MRI slide thickness.

RNase Treatment

Both groups (Sham and SAH animals) received treatment with RNase A (Thermoscientific EN0531), which was administered intravenously (42 µg/kg body weight) and intravenous application of saline solution was used as a control, as described previously (Walberer et al., 2009). The first injection was administered perioperatively to ensure penetration to the CNS due to breakdown of the BBB after SAH surgery. Due to anesthesia of mice during operation as well their supine positioning, the first injection was applied *via* the sublingual vein. The further injections were repeated every 3 days in the tail vein until scarification as previously reported (Fischer et al., 2013). The total volume of injection was 100 µl at a flow rate of 20 µl/s.

Preparation of the Subarachnoid Space for Immunohistochemistry

To preserve the SAS, whole skulls were harvested and kept in an ascending concentration series of sucrose for proper dehydration (4 days at 20%, 4 days at 30%, and 4 days at 40%) at 4°C and then snap frozen with isopentane. The skulls were then embedded in Tissue-Tek O.C.T. Compound (4583, Sakura Finetek) and carefully cut into 10 µm thin slices with Microm Sec35 blades (Termo APD Consumables) using a cryostat (Thermo Fisher Scientific Inc. Microm HM 560).

Immunofluorescence

Brain sections were blocked for 30 min with 5% bovine serum albumin (BSA) in Tris-Buffered Saline with 0.05% Tween (TBST) at room temperature. After that, primary antibodies against citrullinated H3 (rabbit, 1:30, ab5103, Abcam), NeuN (rabbit, 1:200, ABN78, Millipore), and F-actin (Alexa Fluor 488 Phalloidin, 1:200, A12379, Thermo Fisher Scientific) diluted in 5% BSA/TBST were added for incubation at 4°C over night. The next day, sections were washed three times in 5% BSA/TBST for 10 min, followed by 1.5 h of incubation with the secondary antibodies Rhodamine Red-X-conjugated Donkey IgG anti-Mouse (1:200, 715-295-151, Dianova) and Alexa Fluor 647-conjugated Donkey IgG anti-Rabbit IgG (1:200, 711-605-152, Dianova), diluted in 5% BSA/TBST. After secondary antibody incubation, specimens were washed three times in PBS for 5 min and mounted with DAPI Mounting Medium (SCR-038448, Dianova). The sections were then imaged with confocal microscopy (Leica DM 6000/SP5) and analyzed with ImageJ. Amount of NETs was determined by calculating the ratio area covered by citH3 over total area covered by phalloidin, NeuN, and DAPI (**Supplementary Figure S1**).

Statistical Analysis and Figures

Data were analyzed using GraphPad Prism for statistical analyses (Graphpad Software, Version 6.0). ANOVA analyses were used to compare multiple, unpaired *t*-tests for the comparison of two groups. The values are displayed as means ± SEs and values of $p < 0.05$ were considered statistically significant. Elements of **Figures 1A, 2A,B, 3A** were composed with BioRender.com.

RESULTS

NETs Are Released After Onset of Subarachnoid Bleeding in an *in vivo* Mouse Model of Subarachnoid Hemorrhage

To determine whether NETs are released upon subarachnoid hemorrhage *in vivo*, we utilized a filament perforation model

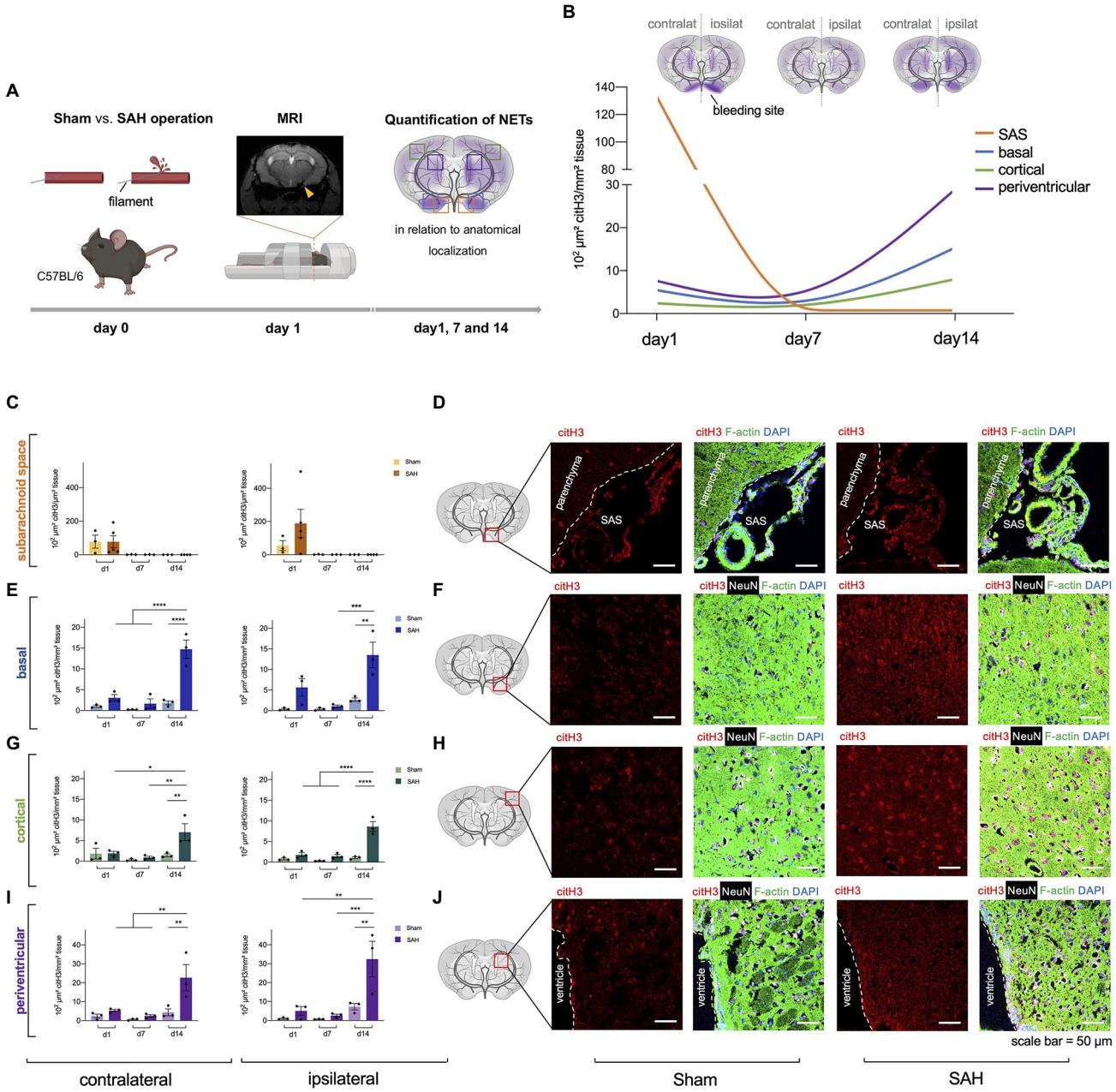

FIGURE 1 | Neutrophil extracellular traps (NETs) are increased in subarachnoid hemorrhage (SAH). **(A)** The filament perforation model was utilized to induce SAH in C57BL/6 mice. MRI was done 24 h after SAH onset to verify bleeding and exclude stroke or intracerebral hemorrhage, and NETs were quantified *via* immunofluorescence in relation to anatomical localization on three different time points (day 1, 7, and 14). **(B)** Cumulative data of NETs accumulation in SAH condition over time. **(C,D)** Quantification of NETs in subarachnoid space (SAS) with representative immunofluorescence staining of extracellular citH3 (exCitH3), F-actin, NeuN, and DAPI. Sham, $n = 3$ for each time point; SAH, $n = 5$ for each time point. **(E–J)** Quantification of NETs in basal, cortical, and periventricular parenchyma with representative immunofluorescence staining of citH3 (citrullinated H3), F-actin, NeuN, and DAPI on day 1, 7, and 14. Sham, $n = 3$ for each time point; SAH, $n = 3$ for each time point. contralat., contralateral; ipsilat., ipsilateral. Scale bar = 50 µm. $^{*}p < 0.05$, $^{**}p < 0.01$, $^{***}p < 0.001$, and $^{****}p < 0.0001$.

to induce subarachnoid hemorrhage in C57BL/6 mice, while Sham operation was performed as a control condition. MRI was conducted 24 h after bleeding to verify SAH and exclude other pathologies such as stroke or intracerebral hemorrhage (**Figure 1A**), and NETs quantified *via* immunofluorescence staining using citrullinated Histone (citH3), a known specific marker for NET remnants (Wang et al., 2009). Indeed, increased levels of NET formation were found in SAH with the highest amount in the SAS on the ipsilateral side (where bleeding was induced) on day 1 (**Figures 1C,D**), while after this time point they were essentially not detectable anymore in both control and SAH conditions (**Figure 1C**). In contrast, in the

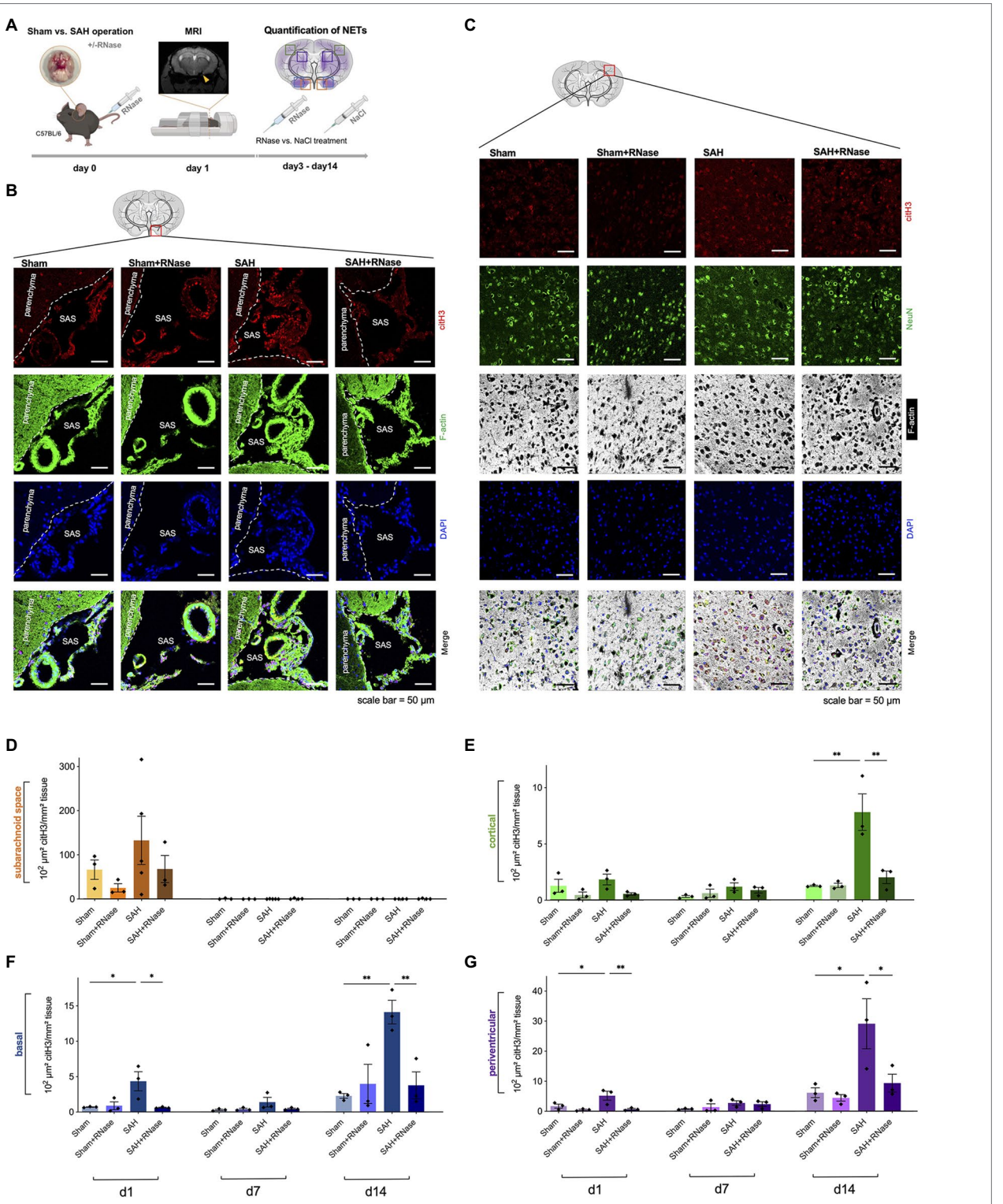

FIGURE 2 | RNase A treatment reduces accumulation of NETs. **(A)** Experimental setup for RNase treatment: during operative induction of SAH, mice were treated with RNase A (42 µg/kg body weight) or sodium chloride (NaCl) as a control condition, and MRI to confirm bleeding. RNase A treatment was repeated every 3 days. **(B)** Representative images of triple immunofluorescence staining with citH3, F-actin, and DAPI subarachnoid space of the four subgroups (Sham, $n = 3$; Sham + RNase, $n = 3$; SAH, $n = 3$; and SAH + RNase, $n = 3$) on day 1, scale bar = 50 µm. **(C)** Representative images of quadruple immunofluorescence staining with citH3, NeuN, F-actin, and DAPI of the corresponding four subgroups in cortical area on day 14, scale bar = 50 µm. **(D–G)** Quantification of NETs after RNase A treatment in relation to localization (subarachnoid space, basal, cortical, and periventricular parenchyma) and time course (day 1, 7, and 14). SAS, subarachnoid space. $^{*}p < 0.05$ and $^{**}p < 0.01$.

A

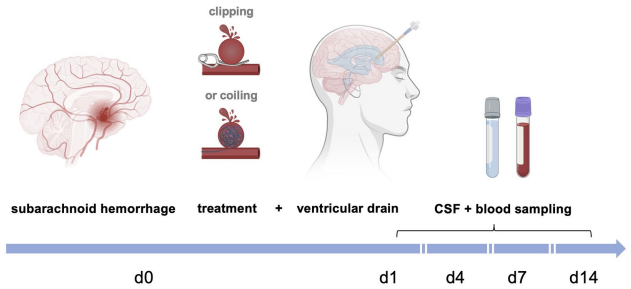

B

Patient characteristics *(n=20)*		
age	median (range)	58 (29 – 70)
female sex	no. (%)	11 (55%)
Hunt & Hess Score	median (range)	3 (1-5)
BNI Score	median (range)	3 (2-4)
mRS at discharge	median (range)	4 (0-6)
mRS at 90 days	median (range)	3 (0-6)
location of aneurysm	no. (%)	
- ICA/MCA		9 (45%)
- Acom or Pcom		8 (40%)
- Basilar/vertebral		3 (15%)
treatment modality	no. (%)	
- Clipping		12 (60%)
- Endovascular		8 (40%)

C

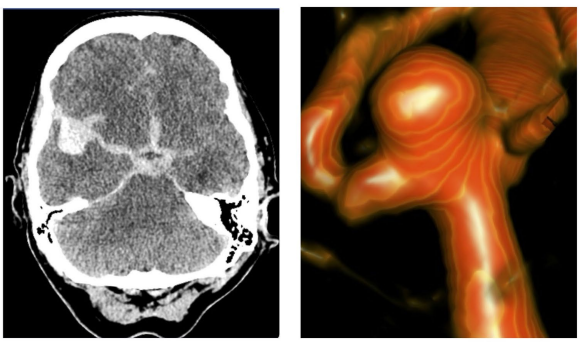

D

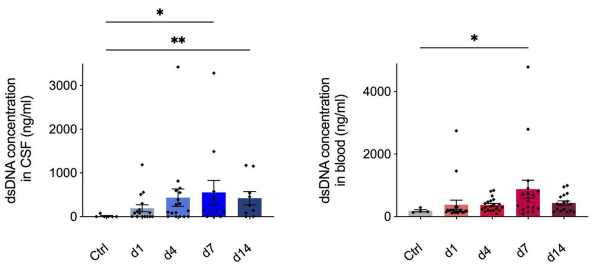

FIGURE 3 | Neutrophil extracellular traps are increased in human cerebrospinal spinal fluid (CSF) and peripheral blood after aneurysmal SAH. **(A)** Study protocol for collection of CSF and Ethylene Diaminetetraacetic acid (EDTA) blood; patients with aneurysmal SAH received either microsurgical clipping or endovascular intervention (coiling) with placement of an extraventricular drain (EVD). In the course of 14 days, CSF and peripheral blood were collected in a prospective manner. **(B)** Overview of patient characteristics. **(C)** Illustrative cases of SAH. CT imaging shows hyperdense blood collection in subarachnoid space and in the right sylvian fissure of a 55-year old patient who experienced SAH from a right-sided MCA aneurysm who underwent microsurgical clipping (left). 3D reconstruction of angiogram showing an ACom aneurysm of a 59-year old patient who was further treated *via* coiling. **(D)** Double-stranded DNA (dsDNA) concentration in CSF and peripheral blood of control patients and SAH patients shows peak on day 7 after bleeding onset. Acom, anterior communicating artery; BNI score, barrow neurological institute score; CSF, cerebrospinal fluid; ICA, internal carotid artery; MCA, middle cerebral artery; mRs, modified Rankin score; and Pcom, posterior communicating artery. $^{*}p<0.05$ and $^{**}p<0.01$.

parenchyma, the NETs showed a gradual increase over time with the highest density on day 14 in all localizations (**Figures 1E–J**). Interestingly, NET accumulation followed a spreading pattern within the parenchyma from basal to cortical over time, with the most significant increase in periventricular localization (**Figure 1B**).

Pharmacological Modulation With RNase A Reduces NET Formation

Since recent evidence suggests that NET-associated RNA is a physiologically relevant NET component and its formation can occur also independently of the canonical NET component DNA (Herster et al., 2020), we questioned whether RNase A application can modify NET burden in SAH *in vivo*. RNase A seemed a feasible therapeutic approach since previous studies in our group showed that RNase A can modulate other DAMPs including exRNA, and influence the microglia-specific immune reaction after SAH. Hence, we treated mice with intravenous application of RNase A and quantified NETs in both SAS and parenchyma (**Figure 2A**). In SAS, RNase A decreased NET accumulation on day 1, but this was not statistically significant. In contrast, in the parenchyma, RNase A reduced NET accumulation significantly, specifically on day 14, where accumulation of citH3 peaked in all localizations (**Figures 2B–G**).

NETs Are Increased in Both CSF and Blood of SAH Patients

Next, we questioned whether this observed NET accumulation after SAH is also relevant in the human system. To investigate this, CSF and blood samples were collected within the scope of a prospective observational study in aneurysmal SAH patients (**Figure 3A**), and NETs were measured *via* quantification of

dsDNA *via* Sytox Green. **Figure 3B** shows the baseline characteristics of the SAH patients included in the study. **Figure 3C** illustrates imaging from two exemplary cases of SAH patients: on the left side, a CT scan of a 55-year old female patient is shown with SAH (Hunt&Hess grade II) with a ruptured right-sided middle cerebral artery (MCA) aneurysm who underwent microsurgical clipping; on the right side, a three-dimensional reconstruction of a ruptured anterior communicating artery (ACom) aneurysm of a 59-year old female (Hunt & Hess grade II) is shown who was further treated with aneurysm coiling. The control patients comprised of patients in which lumbar puncture was done to rule out meningitis or SAH without evidence of any intracranial pathology. Interestingly, dsDNA was significantly increased in both CSF and peripheral blood of SAH patients compared to the control group, with a gradual increase over time, peaking in both compartments on day 7 (**Figure 3D**).

DISCUSSION

Aneurysmal SAH remains a devastating pathology with high morbidity and mortality, and attempts to reduce secondary brain damage have been made for decades, yet the exact pathomechanism contributing to the long-term damage is unclear (Black, 1986; Peterson et al., 1990; Mathiesen et al., 1997; Sheehan et al., 1999). Recent data suggests involvement of the immune system attributable to secondary brain damage, specifically through an outside-in activation of neutrophil recruitment to endothelium, contributing to microglia activation and neuronal apoptosis (Schneider et al., 2015; Atangana et al., 2017). Among the classical immune defense mechanisms of neutrophils, consisting of engulfment of microbes and secretion of anti-microbials, recent data pinpoints to a novel function of neutrophils as part of the innate immune response – the formation of NETs to kill extracellular pathogens (Brinkmann et al., 2004).

In this study, we sought to investigate the potential role of NET formation in SAH and describe the spatiotemporal patterns of NET accumulation after SAH. We demonstrate that in the acute setting, a direct flood of NET formation occurs in the ipsilateral subarachnoid space (SAS), while in the parenchyma, NET levels increase gradually over time in basal, cortical, and periventricular compartments distant to the region of bleeding. These findings are supported by a recent study reporting NET accumulation after SAH as well as their involvement in neuroinflammatory events, albeit the time point of the peak of NETs differed to some degree (Zeng et al., 2021). Interestingly, in the study by Zeng et al. (2021), inhibition of NET formation *via* the PAD4 antagonist GSK484 as well as DNase I inhibited NET-associated neuroinflammation. Our data show that the quantitatively most relevant NET formation occurred 14 days after SAH specifically in periventricular localizations. This is intriguing as it raises the question whether NETs may also be involved in CSF hydrodynamics after aneurysmal SAH, especially since post-hemorrhagic hydrocephalus is a common complication after SAH (Germanwala et al., 2010).

Moreover, while a direct inhibition of NETs *via* DNase has been postulated as a potential mechanistic treatment strategy to reduce NET burden (Ondracek et al., 2020; Korai et al., 2021), there is mounting evidence that NET-associated RNA is a relevant component of NET formation and can occur independently of DNA (Herster et al., 2020). Based on this finding and previously published data on the dampening effects of RNase A on immune cells (Lasch et al., 2020), we questioned whether RNase A also modifies NET formation. Indeed, our data show that RNase A significantly reduces NET formation in all compartments of the brain. This specific effect on the CNS may be explained by the blood brain barrier breakdown after SAH with permeability to also bigger proteins such as Evans Blue (70 kDa; Blecharz-Lang et al., 2018). In our experiments, we used a 13.7 kDa pancreatic RNase A for pre- and postoperative intravenous injections. These finding are particular compelling since RNAse therapeutics have already been used to some degree in clinical trials (Mikulski et al., 2002; Ardelt et al., 2007; Chang et al., 2010; Squiquera et al., 2017). Therefore, it is tempting to speculate that RNAse may be an accessible interesting potential therapeutic strategy for treatment of the underlying immune reaction after SAH. However, the influence of i.v. application of RNAse on physiological processes such as regulation of cerebral blood flow was not investigated in this study and should be addressed in further studies.

The exact molecular mechanisms of NET formation are not fully understood. SAH promotes generation of reactive oxygen species (ROS; Ayer and Zhang, 2008), that have also been described as triggers of NET formation (Erpenbeck and Schön, 2017). Therefore, one may pose the hypothesis that ROS-activation in the setting of SAH contributes NET accumulation, which then may promote microglial activation leading to the activation of neuroinflammatory cascades. Furthermore, recent studies have described that NET formation in the context of SAH increases levels of cytokines such as IL-1β, IL-6, and TNF-α (Zeng et al., 2021).

Furthermore, in order to investigate whether NET burden is also relevant in the human system, we measured circulating NET abundance *via* the surrogate marker dsDNA and show that increased levels are found in both CSF and peripheral blood of SAH patients. Here, we observed a peak of dsDNA 7 days after the bleeding event, supporting the *in vivo* data from our SAH mouse model. Our findings are in line a recent study of Zeng et al. (2021) showed that a significant increase of citH3 in patients suffering SAH after 24 h of the bleeding event, which correlated with the clinical Hunt and Hess score. Additionally, we showed for the first time the further temporal dynamics of NETs and their involvement in CSF in humans. The postponed peak of NET burden potentially indicates a therapeutic window after the bleeding event to attenuate secondary brain damage after SAH. The accumulation of NETs in the brain parenchyma also raises intriguing questions of its origin. Increasing levels of neutrophils in the CSF after SAH have also been associated with development of vasospasms (Provencio et al., 2010). Therefore, neutrophils may migrate in the brain parenchyma after SAH and produce NETs *in situ* as already described in other studies in a model of ischemic stroke (Kang et al., 2020).

Our study is limited by a small sample size, investigations on the association of NET burden and clinical characteristics, and exploratory studies on cell-specific mechanism by which

NETs may affect further inflammatory events in SAH. Albeit the range of the SAH patients in our small study cohort varies between 29 and 70, the median age of our study group in the patients is 58, which is fairly representative of typical age of aneurysm rupture in large cohorts (Rinkel et al., 1998; Shea et al., 2007; Jordan et al., 2009). In order to investigate potential aging effects, further subgroup analyses on young and old mice with larger study numbers are necessary. As we analyzed exclusively male mice, sex-related effects in the animal experiments cannot be excluded. This study also did not investigate the impact of RNAse treatment on humans. As potential neuroprotective effects of RNase in SAH patients are of pressing interest, a clinical study on the effect of RNase treatment in hemorrhagic stroke patients are planned for the future.

In summary, our data reveal the spatiotemporal dynamics of NET accumulation after SAH *in vivo* with evidence for a gradual increase of NET formation over time, both in a SAH mouse model as well as in patients suffering aneurysmal SAH. Intriguingly, intravenous RNase A application abrogates NET burden in the parenchyma, underpinning a potential role in of RNase in the innate immune response after SAH. Further studies are needed to fully elucidate the exact nature of NET formation and related immune cell-specific changes of RNase application after SAH.

DATA AVAILABILITY STATEMENT

The raw data supporting the conclusions of this article will be made available by the authors, without undue reservation.

ETHICS STATEMENT

The studies involving human participants were reviewed and approved by Ethikkommission Charité, Charité – Universitätsmedizin, Berlin (Germany). The patients/participants provided their written informed consent to participate in this study. The animal study was reviewed and approved by Landesamt für Gesundheit und Soziales (LaGeSo) Berlin (Germany).

AUTHOR CONTRIBUTIONS

KT, FS, AF, SL, and RX conducted the experiments and analyzed the data. RX, AF, and PV designed the study. All authors contributed to the article and approved the submitted version.

FUNDING

RX was supported by the BIH-Charité Clinician Scientist Program funded by the Charité – Universitätsmedizin Berlin and the Berlin Institute of Health. We acknowledge support from the German Research Foundation (DFG) and the Open Access Publication Fund of Charité – Universitätsmedizin Berlin. KT is supported by the Berlin Institute of Health (BIH) Research Stipend as well as the Sonnenfeld Foundation.

ACKNOWLEDGMENTS

This paper is dedicated to the work of our dear colleague and friend Klaus T. Preissner.

SUPPLEMENTARY MATERIAL

The Supplementary Material for this article can be found online at: https://www.frontiersin.org/articles/10.3389/fphys.2021.724611/full#supplementary-material

REFERENCES

Ardelt, B., Juan, G., Burfeind, P., Salomon, T., Wu, J. M., Hsieh, T. C., et al. (2007). Onconase, an anti-tumor ribonuclease suppresses intracellular oxidative stress. *Int. J. Oncol.* 31, 663–669. doi: 10.3892/ijo.31.3.663

Atangana, E., Schneider, U. C., Blecharz, K., Magrini, S., Wagner, J., Nieminen-Kelha, M., et al. (2017). Intravascular inflammation triggers intracerebral activated microglia and contributes to secondary brain injury after experimental subarachnoid hemorrhage (eSAH). *Transl. Stroke Res.* 8, 144–156. doi: 10.1007/s12975-016-0485-3

Ayer, R., and Zhang, J. (2008). "Oxidative stress in subarachnoid haemorrhage: significance in acute brain injury and vasospasm," in *Cerebral Vasospasm*. ed. T. Kiris (Springer), 33–41.

Black, P. M. (1986). Hydrocephalus and vasospasm after subarachnoid hemorrhage from ruptured intracranial aneurysms. *Neurosurgery* 18, 12–16. doi: 10.1227/00006123-198601000-00003

Blecharz-Lang, K. G., Wagner, J., Fries, A., Nieminen-Kelha, M., Rosner, J., Schneider, U. C., et al. (2018). Interleukin 6-mediated endothelial barrier disturbances can be attenuated by blockade of the IL6 receptor expressed in brain microvascular endothelial cells. *Transl. Stroke Res.* 9, 631–642. doi: 10.1007/s12975-018-0614-2

Borregaard, N. (2010). Neutrophils, from marrow to microbes. *Immunity* 33, 657–670. doi: 10.1016/j.immuni.2010.11.011

Brinkmann, V., Reichard, U., Goosmann, C., Fauler, B., Uhlemann, Y., Weiss, D. S., et al. (2004). Neutrophil extracellular traps kill bacteria. *Science* 303, 1532–1535. doi: 10.1126/science.1092385

Chang, C.-H., Gupta, P., Michel, R., Loo, M., Wang, Y., Cardillo, T. M., et al. (2010). Ranpirnase (frog rnase) targeted with a humanized, internalizing, anti–trop-2 antibody has potent cytotoxicity against diverse epithelial cancer cells. *Mol. Cancer Ther.* 9, 2276–2286. doi: 10.1158/1535-7163.MCT-10-0338

Erpenbeck, L., and Schön, M. (2017). Neutrophil extracellular traps: protagonists of cancer progression? *Oncogene* 36, 2483–2490. doi: 10.1038/onc.2016.406

Etminan, N., Chang, H.-S., Hackenberg, K., De Rooij, N. K., Vergouwen, M. D., Rinkel, G. J., et al. (2019). Worldwide incidence of aneurysmal subarachnoid hemorrhage according to region, time period, blood pressure, and smoking prevalence in the population: a systematic review and meta-analysis. *JAMA Neurol.* 76, 588–597. doi: 10.1001/jamaneurol.2019.0006

Fischer, S., Gesierich, S., Griemert, B., Schanzer, A., Acker, T., Augustin, H. G., et al. (2013). Extracellular RNA liberates tumor necrosis factor-alpha to promote tumor cell trafficking and progression. *Cancer Res.* 73, 5080–5089. doi: 10.1158/0008-5472.CAN-12-4657

Fischer, S., Nishio, M., Dadkhahi, S., Gansler, J., Saffarzadeh, M., Shibamiyama, A., et al. (2011). Expression and localisation of vascular ribonucleases in endothelial cells. *Thromb. Haemost.* 105, 345–355. doi: 10.1160/TH10-06-0345

García-Culebras, A., Durán-Laforet, V., Peña-Martínez, C., Moraga, A., Ballesteros, I., Cuartero, M. I., et al. (2019). Role of TLR4 (toll-like receptor 4) in N1/N2 neutrophil programming after stroke. *Stroke* 50, 2922–2932. doi: 10.1161/STROKEAHA.119.025085

Germanwala, A. V., Huang, J., and Tamargo, R. J. (2010). Hydrocephalus after aneurysmal subarachnoid hemorrhage. *Neurosurg. Clin. N. Am.* 21, 263–270. doi: 10.1016/j.nec.2009.10.013

Gris, T., Laplante, P., Thebault, P., Cayrol, R., Najjar, A., Joannette-Pilon, B., et al. (2019). Innate immunity activation in the early brain injury period following subarachnoid hemorrhage. *J. Neuroinflammation* 16:253. doi: 10.1186/s12974-019-1629-7

Herster, F., Bittner, Z., Archer, N. K., Dickhofer, S., Eisel, D., Eigenbrod, T., et al. (2020). Neutrophil extracellular trap-associated RNA and LL37 enable self-amplifying inflammation in psoriasis. *Nat. Commun.* 11:105. doi: 10.1038/s41467-019-13756-4

Jordan, L. C., Johnston, S. C., Wu, Y. W., Sidney, S., and Fullerton, H. J. (2009). The importance of cerebral aneurysms in childhood hemorrhagic stroke: a population-based study. *Stroke* 40, 400–405. doi: 10.1161/STROKEAHA.108.518761

Kang, L., Yu, H., Yang, X., Zhu, Y., Bai, X., Wang, R., et al. (2020). Neutrophil extracellular traps released by neutrophils impair revascularization and vascular remodeling after stroke. *Nat. Commun.* 11:2488. doi: 10.1038/s41467-020-16191-y

Korai, M., Purcell, J., Kamio, Y., Mitsui, K., Furukawa, H., Yokosuka, K., et al. (2021). Neutrophil extracellular traps promote the development of intracranial aneurysm rupture. *Hypertension* 77, 2084–2093. doi: 10.1161/HYPERTENSIONAHA.120.16252

Lasch, M., Kumaraswami, K., Nasiscionyte, S., Kircher, S., Van Den Heuvel, D., Meister, S., et al. (2020). RNase A treatment interferes with leukocyte recruitment, neutrophil extracellular trap formation, and angiogenesis in ischemic muscle tissue. *Front. Physiol.* 11:576736. doi: 10.3389/fphys.2020.576736

Lawton, M. T., and Vates, G. E. (2017). Subarachnoid hemorrhage. *N. Engl. J. Med.* 377, 257–266. doi: 10.1056/NEJMcp1605827

Liu, Y.-W., Li, S., and Dai, S.-S. (2018). Neutrophils in traumatic brain injury (TBI): friend or foe? *J. Neuroinflammation* 15:146. doi: 10.1186/s12974-018-1173-x

Lucke-Wold, B. P., Logsdon, A. F., Manoranjan, B., Turner, R. C., Mcconnell, E., Vates, G. E., et al. (2016). Aneurysmal subarachnoid hemorrhage and neuroinflammation: a comprehensive review. *Int. J. Mol. Sci.* 17:497. doi: 10.3390/ijms17040497

Macdonald, R. L. (2014). Delayed neurological deterioration after subarachnoid haemorrhage. *Nat. Rev. Neurol.* 10, 44–58. doi: 10.1038/nrneurol.2013.246

Macdonald, R. L., and Schweizer, T. A. (2017). Spontaneous subarachnoid haemorrhage. *Lancet* 389, 655–666. doi: 10.1016/S0140-6736(16)30668-7

Mathiesen, T., Edner, G., Ulfarsson, E., and Andersson, B. (1997). Cerebrospinal fluid interleukin-1 receptor antagonist and tumor necrosis factor-alpha following subarachnoid hemorrhage. *J. Neurosurg.* 87, 215–220. doi: 10.3171/jns.1997.87.2.0215

Mikulski, S. M., Costanzi, J. J., Vogelzang, N. J., Mccachren, S., Taub, R. N., Chun, H., et al. (2002). Phase II trial of a single weekly intravenous dose of ranpirnase in patients with unresectable malignant mesothelioma. *J. Clin. Oncol.* 20, 274–281. doi: 10.1200/JCO.2002.20.1.274

Niemiec, M. J., De Samber, B., Garrevoet, J., Vergucht, E., Vekemans, B., De Rycke, R., et al. (2015). Trace element landscape of resting and activated human neutrophils on the sub-micrometer level. *Metallomics* 7, 996–1010. doi: 10.1039/C4MT00346B

Ondracek, A., Hofbauer, T., Wurm, R., Arfsten, H., Seidl, V., Früh, A., et al. (2020). Imbalance between plasma double-stranded DNA and deoxyribonuclease activity predicts mortality after out-of-hospital cardiac arrest. *Resuscitation* 151, 26–32. doi: 10.1016/j.resuscitation.2020.03.006

Papayannopoulos, V. (2018). Neutrophil extracellular traps in immunity and disease. *Nat. Rev. Immunol.* 18, 134–147. doi: 10.1038/nri.2017.105

Peterson, J. W., Kwun, B. D., Hackett, J. D., and Zervas, N. T. (1990). The role of inflammation in experimental cerebral vasospasm. *J. Neurosurg.* 72, 767–774. doi: 10.3171/jns.1990.72.5.0767

Preissner, K. T., Fischer, S., and Deindl, E. (2020). Extracellular RNA as a versatile DAMP and alarm signal that influences leukocyte recruitment in inflammation and infection. *Front. Cell Dev. Biol.* 8:619221. doi: 10.3389/fcell.2020.619221

Provencio, J. J., Fu, X., Siu, A., Rasmussen, P. A., Hazen, S. L., and Ransohoff, R. M. (2010). CSF neutrophils are implicated in the development of vasospasm in subarachnoid hemorrhage. *Neurocrit. Care* 12, 244–251. doi: 10.1007/s12028-009-9308-7

Rinkel, G. J., Djibuti, M., Algra, A., and Van Gijn, J. (1998). Prevalence and risk of rupture of intracranial aneurysms: a systematic review. *Stroke* 29, 251–256. doi: 10.1161/01.STR.29.1.251

Schertz, M., Mehdaoui, H., Hamlat, A., Piotin, M., Banydeen, R., and Mejdoubi, M. (2016). Incidence and mortality of spontaneous subarachnoid hemorrhage in Martinique. *PLoS One* 11:e0155945. doi: 10.1371/journal.pone.0155945

Schneider, U. C., Davids, A. M., Brandenburg, S., Muller, A., Elke, A., Magrini, S., et al. (2015). Microglia inflict delayed brain injury after subarachnoid hemorrhage. *Acta Neuropathol.* 130, 215–231. doi: 10.1007/s00401-015-1440-1

Shea, A. M., Reed, S. D., Curtis, L. H., Alexander, M. J., Villani, J. J., and Schulman, K. A. (2007). Characteristics of nontraumatic subarachnoid hemorrhage in the United States in 2003. *Neurosurgery* 61, 1131–1138. doi: 10.1227/01.neu.0000306090.30517.ae

Sheehan, J. P., Polin, R. S., Sheehan, J. M., Baskaya, M. K., and Kassell, N. F. (1999). Factors associated with hydrocephalus after aneurysmal subarachnoid hemorrhage. *Neurosurgery* 45, 1120–1127. doi: 10.1097/00006123-199911000-00021

Squiquera, L., Taxman, D. J., Brendle, S. A., Torres, R., Sulley, J., Hodge, T., et al. (2017). Ranpirnase eradicates human papillomavirus in cultured cells and heals anogenital warts in a phase I study. *Antivir. Ther.* 22, 247–255. doi: 10.3851/IMP3133

Tielking, K., Fischer, S., Preissner, K. T., Vajkoczy, P., and Xu, R. (2019). Extracellular RNA in central nervous system pathologies. *Front. Mol. Neurosci.* 12:254. doi: 10.3389/fnmol.2019.00254

Van Lieshout, J. H., Dibué-Adjei, M., Cornelius, J. F., Slotty, P. J., Schneider, T., Restin, T., et al. (2018). An introduction to the pathophysiology of aneurysmal subarachnoid hemorrhage. *Neurosurg. Rev.* 41, 917–930. doi: 10.1007/s10143-017-0827-y

Walberer, M., Tschernatsch, M., Fischer, S., Ritschel, N., Volk, K., Friedrich, C., et al. (2009). RNase therapy assessed by magnetic resonance imaging reduces cerebral edema and infarction size in acute stroke. *Curr. Neurovasc. Res.* 6, 12–19. doi: 10.2174/156720209787466037

Wang, Y., Li, M., Stadler, S., Correll, S., Li, P., Wang, D., et al. (2009). Histone hypercitrullination mediates chromatin decondensation and neutrophil extracellular trap formation. *J. Cell Biol.* 184, 205–213. doi: 10.1083/jcb.200806072

Zeng, H., Fu, X., Cai, J., Sun, C., Yu, M., Peng, Y., et al. (2021). Neutrophil extracellular traps may be a potential target for treating early brain injury in subarachnoid hemorrhage. *Transl. Stroke Res.* doi: 10.1007/s12975-021-00909-1 [Epub ahead of print]

Zhang, Z., Fang, Y., Lenahan, C., and Chen, S. (2020). The role of immune inflammation in aneurysmal subarachnoid hemorrhage. *Exp. Neurol.* 336:113535. doi: 10.1016/j.expneurol.2020.113535

Conflict of Interest: The authors declare that the research was conducted in the absence of any commercial or financial relationships that could be construed as a potential conflict of interest.

Publisher's Note: All claims expressed in this article are solely those of the authors and do not necessarily represent those of their affiliated organizations, or those of the publisher, the editors and the reviewers. Any product that may be evaluated in this article, or claim that may be made by its manufacturer, is not guaranteed or endorsed by the publisher.

Advantages of publishing in Frontiers

OPEN ACCESS
Articles are free to read for greatest visibility and readership

FAST PUBLICATION
Around 90 days from submission to decision

HIGH QUALITY PEER-REVIEW
Rigorous, collaborative, and constructive peer-review

TRANSPARENT PEER-REVIEW
Editors and reviewers acknowledged by name on published articles

Frontiers
Avenue du Tribunal-Fédéral 34
1005 Lausanne | Switzerland

Visit us: www.frontiersin.org
Contact us: frontiersin.org/about/contact

REPRODUCIBILITY OF RESEARCH
Support open data and methods to enhance research reproducibility

DIGITAL PUBLISHING
Articles designed for optimal readership across devices

FOLLOW US
@frontiersin

IMPACT METRICS
Advanced article metrics track visibility across digital media

EXTENSIVE PROMOTION
Marketing and promotion of impactful research

LOOP RESEARCH NETWORK
Our network increases your article's readership